THE EFFECTS OF STEADY LAMINAR SHEAR STRESS ON AORTIC VALVE CELL BIOLOGY

A Dissertation

Presented to

The Academic Faculty

By

a. Jonathan Talbot Butcher

In Partial Fulfillment

Of the Requirements for the Degree

Doctor of Philosophy in Mechanical Engineering

Georgia Institute of Technology

December, 2004

THE EFFECTS OF STEADY OF LAMINAR SHEAR STRESS ON AORTIC VALVE CELL BIOLOGY

Approved by:

Dr. Robert M. Nerem

Dr. Andres J. Garcia

Dr. Ajit P. Yoganathan

Dr. Hanjoong Jo

Dr. Stephen Hilbert

October 19, 2004

for Christine

ACKNOWLEDGEMENTS

This thesis represents not only four years of my effort at Georgia Tech, but the culmination of the help and support of many people. First and foremost I would like to thank my thesis advisor, Dr. Robert Nerem, for his enthusiastic support and willingness to take a chance on mentoring me in a new field in which neither of us had any experience. Through his support I have had the opportunity to travel to several parts of the world, and interact with an international community I never imagined before arriving at Georgia Tech. His manner of mentoring me over these years has been a great model I hope to mimic in the future with my own students.

This work could not have been done without the help and support of the many people who have been in the Nerem lab during my time there. From learning cell culture from Greg Bowden and Jeff Guild, to critical early guidance from Joe, Jan, and Stephanie, and finally from bouncing ideas off of Tiffany, Ann, Kara, JoSette, Stacey and Taby, my progress was certainly not the sole result of my own efforts. Steve Woodard was also very helpful to me, even to the point of taking trips to the slaughterhouse (Holifield Farms) when I was unable to. He could always suggest a biological mechanism for anything that was going wrong with my cells, and was always willing to look into things with me. These people have been critical to my development and maturation as a researcher and as a person. I would like to think I have made some progress on at least one of those fronts.

I have also received extensive help and mentoring from Dr. Andrés García and the many people in his lab, as well as Dr. Hanjoong Jo and his lab. Dr. Yoganathan and Dr. Stephen Hilbert also participated in shaping the directions of my research, and for their input and collaboration I am truly grateful.

There are many other people at the Petit Institute for Bioengineering and Bioscience that were also very influential to me during my time here, academically and personally that are too numerous to list. I hope it is suffice to include all of the IBB staff together and thank them for their help in organizing GTEC Student Council events, the URS and REU programs, and dealing with my own needs to find Dr. Nerem wherever in the world he might be and fixing core lab equipment whenever it stopped working.

Last but certainly not least, I would like to give my wholehearted appreciation to my family for their continual love, support, and interest in my tenure at Georgia Tech, even if they were faking the interest every now and then. Primary among them is my wife, Christine. She has been a steady source of strength for me during all that I have been through since coming to Atlanta, and without her I would have never been able to cope with the stresses of research and school to the degree that I have. Hopefully in the next coming years I can repay some of that support as she begins to explore some of her own talents while I pay the bills for a change. I would also like to thank both our families for raising us and supporting us for this chapter in our lives, and the chapters to follow in the future.

Portions of the material presented in this Thesis have been previously published in scientific journals. Portions of Chapter 3 was published in the May 2004 issue of the *Journal of Heart valve Disease*, and Chapter 4 was published in the August 2004 issue of *Arteriosclerosis, Thrombosis, and Vascular Biology.* I have received permission from the publishers to reprint this information in this document.

TABLE OF CONTENTS

LIST OF TABLES

LIST OF FIGURES

LIST OF ABBREVIATIONS

PAVEC:	Porcine aortic valve endothelial cell
PAEC:	Porcine aortic endothelial cell
PAVIC:	Porcine aortic valve interstitial cell
PASMC:	Porcine aortic smooth muscle cell
LSS:	Laminar shear stress
TEVL:	Tissue engineered valve leaflet

SUMMARY

Aortic valve disease (AVD) affects millions of people of all ages around the world. Current treatment for AVD consists of valvular replacement with a non-living prosthetic valve, which is incapable of growth, self-repair, or remodeling. While tissue engineering has great promise to develop a living heart valve alternative, success in animal models has been limited. This may be attributed to the fact that understanding of valvular cell biology has not kept pace with advances in biomaterial development. Aortic valve leaflets are exposed to a complex and dynamic mechanical environment unlike any in the vasculature, and it is likely that native endothelial and interstitial cells respond to mechanical forces differently from other vascular cells. The objective of this thesis was to compare valvular cell phenotype to vascular cell phenotype, and assess the influence of steady shear stress on valvular cell biology. This thesis demonstrates that valvular endothelial cells respond differently to shear than vascular endothelial cells, by aligning perpendicular to the direction of steady shear stress, and by the differential regulation of hundreds of genes in both static and fluid flow environments. Valvular interstitial cells expressed a combination of contractile and synthetic phenotypes not mimicked by vascular smooth muscle cells. Two three-dimensional leaflet models were developed to assess cellular interactions and the influences of steady laminar shear stress. Valvular co-culture models exhibited a physiological response profile, while interstitial cell-only constructs behaved more pathologically. Steady shear stress enhanced physiological functions of valvular co-cultures, but increased pathological response of interstitial cell-only constructs. These results showed that valvular cells, whether cultured separately or together, behaved distinctly different from vascular cells. It was also determined that

shear stress alone cannot induce tissue remodeling to more resemble native valve leaflets. The leaflet models developed in this thesis can be used in future experiments to explore valvular cell biology, assess the progression of certain forms AVD, and develop targeted diagnostic and therapeutic strategies to hopefully eliminate the need for valvular replacement entirely.

CHAPTER 1

INTRODUCTION

Cardiovascular disease (CVD) is the leading cause of death in the United States and the developed world. CVD is an umbrella term that includes many more specific diseases and conditions, including coronary heart disease, stroke, and less common forms such as congenital heart defects and rheumatic heart disease (RHD). In the United States in 2001, over 61 million people were suffering from one or more CVD[5], with over $200 billion spent each year on hospitalizations and lost wages[5]. The United States has a relatively modest death rate for cardiovascular diseases, however, with Russia and Eastern Europe having the highest death rates. Approximately 1 million Americans are living with a congenital heart defect (CHD), and more than 40,000 babies are born each year (1-2% of all live births) with a CHD. Due to advances in the development and distribution of antibiotics, deaths from RHD has plummeted over 70% in the U.S., from 15,000 in 1950 to only about 4,000 in 1999[5].

While the prevalence of “western” style CVD in less developed countries is much rarer, some of the less common diseases in the U.S. are major issues. In India, for example, up to 130,000 babies are born with congenital heart defects and over 50,000 new cases of rheumatic fever each year[6]. In developing countries, rheumatic fever is the most frequent cause of heart disease in the 5-13 age group, causing 25-40% of all CVD, and 33-50% of all hospital admissions[5].

Many CVD are associated with pathologies of the aortic valve, due to its prominent position above the left ventricle and critical function of maintaining normal left

ventricular ejection. The aortic valve opens and closes approximately 3 billion times in a 70 year lifespan, a fatigue life virtually unreachable by nonliving materials. Any valvular impairment will lead to left ventricular dysfunction (a strong predictor of mortality[12]) if not corrected in a timely manner, and vice versa. Approximately 12,000 Americans died in 2002 from aortic valve related causes, and over 52,000 were hospitalized. That same year, approximately 96,000 valve replacement operations were conducted in the U.S., the majority for the aortic valve[5]. The prevalence of aortic valve disease in patients may be underestimated due to a "selection bias" that may occur at diagnosis or autopsy. Clinicians may only list the pathologies they consider most significant in a patient, and therefore neglect valve related diseases[9]. There are very few studies that have compared the relative prevalence of different types of aortic valve disease (AVD) within a patient population. A comparison between studies that do exist of countries of different stages of development is shown in Figure 1-1. The United States[7, 8] and Japan[9] represent two types of developed countries, while Pakistan[10] and Ethiopia[11] represent lesser developed countries. While it is difficult to compare medical information from multiple countries, because of differences in diagnostic techniques, experience of the medical technicians, and differences in patient populations, an analysis can be made to compare the relative prevalence of general disease classifications. It is clearly evident from Figure 1-1 that the prevalence of degenerative type diseases (calcification, senile valve) is associated with more developed countries, while inflammatory diseases (rheumatic heart disease) is associated with poorer countries. The lack of degenerative valve pathologies in lesser developed countries may reflect the shorter life span of these populations, as well as a lack of experience with this type of failure, not necessarily a lesser incidence. Clearly, aortic valve diseases are a global concern.

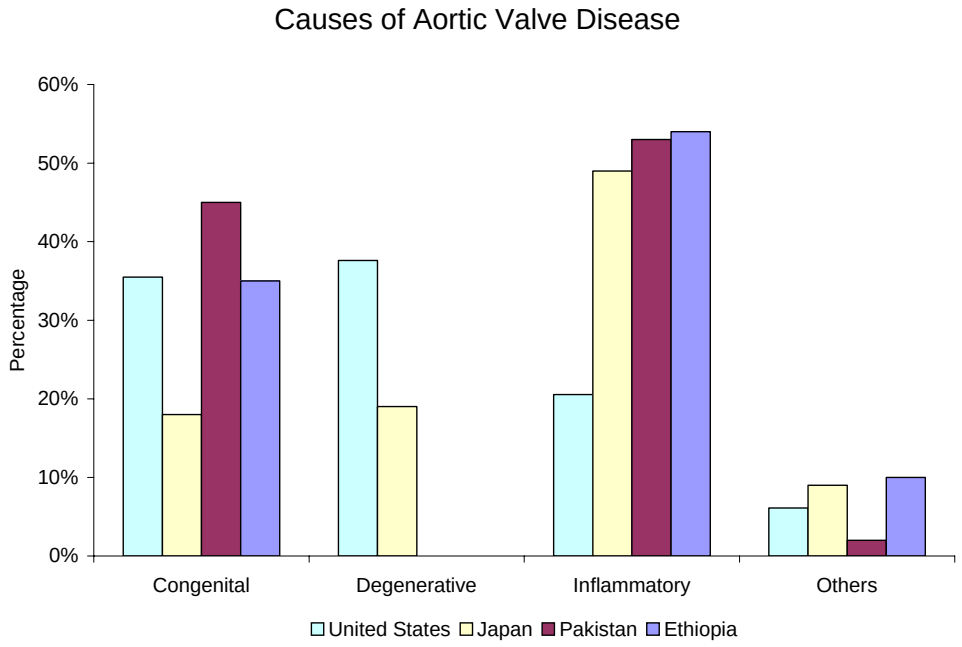

Figure 1-1: Distribution of aortic valve disease etiologies as classified by clinicians in different countries. Taken from[7-11].

1.1: Aortic Valve Physiology

Structure of the Aortic Root. The aortic valve is composed of three semilunar cusps attached to a fibrous annulus embedded in the fibers of the left ventricular septum (Figure 1-2A). The functional unit of the valve, however, includes both the cusp and its respective aortic sinus complex. The sinuses of Valsalva are three elliptical depressions in the aortic wall, from which the coronary ostia initiate. The aortic annulus is a coronet-like fibrous structure to which the aortic cusps, or leaflets, are attached. Figure 1-2B shows the arrangement of the components of the aortic valve. The cusps attach to the annulus with semi-elliptical profile, meeting at commissure points.

Aortic Valve Leaflet Structure. The valve leaflets are very thin, flexible structures, which come together to seal the valve when it closes. The bulk of the leaflet may be subdivided into three distinct layers: the *fibrosa*, *ventricularis*, and *spongiosa*[20],

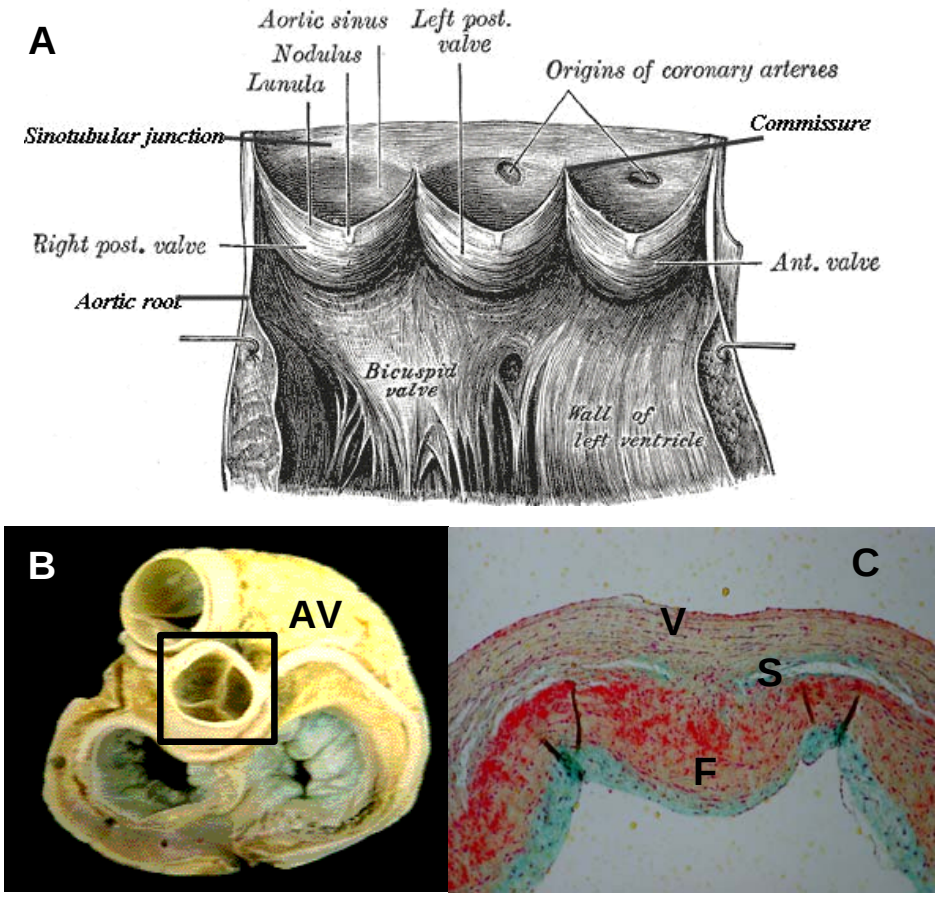

Figure 1-2: The aortic valve.; A: Identification of the major features of the aortic valve. Adapted from Gray's Anatomy; B: The location of the aortic valve (AV) on the heart (www.iun.edu) C: Leaflet structure (Movat's Pentachrome). V=ventricularis, S=spongiosa, F=fibrosa.

as shown in Figure 2C. The relative proportions of the thickness of these layers vary along the radial length of the leaflets, and the amount and organization of the fibrous components (collagen and elastin) are also different. The fibrosa is located on the aortic side of the leaflet, and is composed of collagen sheets and bundles arranged in the circumferential direction with very little elastin[21]. The thinner ventricularis covers the ventricular surface of the leaflet, and has considerably more elastin than the fibrosa, but both components are organized with somewhat less directionality than in the fibrosa when fully relaxed[21]. Between the fibrosa and the ventricularis is the spongiosa,

comprised of a large amount of glycosaminoglycans (GAGs) and a few loosely connected fibrous proteins[20]. It is thicker near the aortic wall, and thins to virtually absent at the free margin of the leaflet. It is unclear whether any vasculature is present in normal healthy human aortic valve leaflets. Diffusion limitations require capillaries spaced roughly every 250 μm to prevent hypoxia. Bovine aortic valve leaflets have vasculature, while porcine and ovine leaflets generally do not. Some cases of leaflet vascularity in humans has been documented, but this may be a result of pathological angiogenesis from thickening of the leaflets[22-24].

Function of the Aortic Valve Leaflets. The aortic valve leaflets function in concert with the aortic root to ensure smooth opening and closing, and therefore root mechanics should not be neglected when considering valve function. A schematic of aortic valve and root dynamics is shown in Figure 1-3. The leaflets are mutually

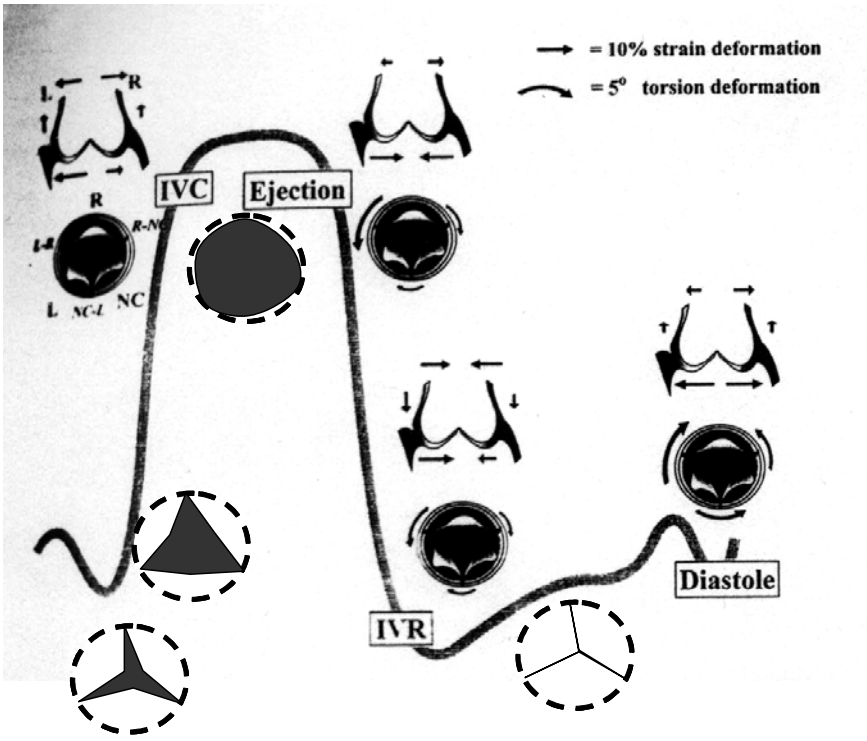

Figure 1-3: Schematic of aortic valve leaflet and root dynamics during the cardiac cycle. Line indicates relative blood velocity at the level of the valve. Taken from[4].

apposed during diastole, and a small overlap of leaflet tissue, called the lunula, ensures a closed volume for efficient filling of the left ventricle. The valve annulus expands during this time, pulling the leaflets taught to prevent prolapse[25]. Further increase in annular radius at end diastole and into the isovolumic contraction phase of the cardiac cycle pulls the leaflets from their commissures such that a small stellate orifice results, even without the presence of transvalvular flow[26]. The valve orifice changes quickly from stellate, to triangular, to finally a circular pattern as blood is ejected from the ventricle, opening the aortic valve in less than 1/60 of a second. The aortic root adjusts from a conical to a cylindrical shape during ejection, providing optimal hemodynamics at the larger flow volume[27]. The aortic valve closes much more gradually relative to opening, the dynamics depending on the transvalvular pressure and the parameters of the vortexes that develop within the sinuses of Valsalva. The reduction of forward blood velocity causes a bifurcation of the flow field to develop, and part of the flow circulates behind the leaflets, creating a vortex[28]. These vortexes help circulate oxygenated blood through the coronary arteries, as well as create a small pressure gradient across the leaflet, which help bring the leaflets to a smooth and efficient closure.

1.2: Aortic Valve Mechanics

Tissue Mechanics in Vivo. The majority of the stresses and strains experienced by the leaflets occur during diastole and early opening of the valve. Although an exact measurement of these stresses in vivo is very difficult to perform, a reasonable approximation can be made based on elementary mechanics. Thubrikar and colleagues approximated the stresses in vivo by assuming that the majority of the pressure load is supported by a combination of bending and membrane stretching [29].

Considering bending and stretching as independent components, they developed a model of the in vivo leaflet stresses, which was a function of the transvalvular pressure:

$$\text{Stress} = (PR/T) +/- E \times (T/2R)$$

where P is the transvalvular pressure, R is the radius of the leaflet, T is the thickness, E is the tissue modulus of elasticity, and the bending stresses are either tensile (+) or compressive (-) depending on the side of the leaflet. The relative contributions of the components changed as the leaflet changed curvature during the opening phase. They concluded that the total stresses in the leaflet in systole were on the order of 50 kPa in systole and 500 kPa in diastole. The aortic surface of the leaflet (fibrosa) bore the diastolic load, while the ventricular surface (ventricularis) bore the systolic load. From their calculations of membrane stress, they determined that the leaflet stretches approximately 10% circumferentially from systole to diastole. More careful considerations of the geometry of the load bearing surfaces during systole and diastole have generated estimates of maximum physiological leaflet stress between 200 - 400 kPa [20, 30]. Using similar methods, in vivo leaflet strains have been calculated to be 0.1 in the circumferential direction and 0.4 in the radial direction (Brewer, 1977; Thubrikar et al., 1980, Missirlis, 1973).

Material properties of the aortic valve leaflet. Characterization of these material properties has proven difficult because the physiological strain rate of leaflet tissue is as high as 2.5/s[31, 32], and instruments capable of applying physiological strain rates to leaflet tissues have only recently been developed. Both pseudoelastic and viscoelastic material property data is presented below.

Pseudoelastic properties: Although biaxial testing techniques are preferable for analyzing anisotropic tissues, the majority of published studies determining leaflet

material properties performed uniaxial tensile test at very low strain rates, and of those still fewer analyzed human leaflets. Both data on human and porcine aortic valve leaflets are presented for comparison. Figure 1-4A shows the representative pseudoelastic stress-strain response[33] of leaflet tissue in circumferential and radial directions. While the values of each of the components of the graph, shown in Figure 1-4B, differ between studies, the responses all show similar distinct features. First, an initial elastic phase, with a modulus E_e, a transition strain at an extensibility of ε_t, and an inelastic modulus E_i. These results indicate fairly good agreement between the material properties of human and porcine leaflet tissues, thus supporting the use of the porcine aortic valve as a model of human valve behavior. Material properties appear dependent on strain rate, and the ratio of circumferential to radial modulus increases with increasing strain rate. The biaxial test data mirrors that of the uniaxial tests with the exception of the higher radial extensibility. This data clearly demonstrates the biphasic nonlinear response of the leaflet tissue hypothesized earlier. The high compliance at low strains and high modulus at high strains enables the tissue to be optimally flexible and rigid during systole and diastole. Ultimate tensile stress loads of aortic valve leaflets range from 2.0 to 4.0 MPa [39], which is ten times greater than the physiological stresses that occur in vivo. This phenomenon is ideal for materials that must endure many loading cycles without fatigue.

Stress Relaxation Tests – The previously tabulated data, as well as other data by researchers[30, 32, 39] demonstrate a significant dependence of stress on strain rate, a hallmark of viscoelastic materials. Both linear and quasilinear viscoelastic (QLV) constitutive models[33] have been applied to aortic valve leaflet tissues, as well as more complex models[42]. Viscoelastic tests are difficult to apply tovalvular tissues, because it is impossible to apply an instantaneous step change in stress or strain, which is necessary for ideal creep and relaxation tests. Although no studies exist characterizing

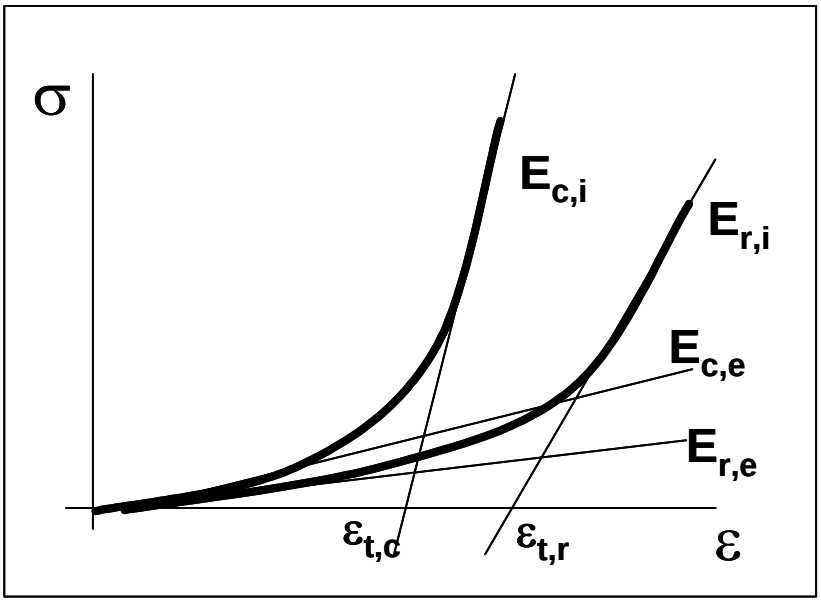

Study (Year)	Strain rate 1/s	E_e, rad kN/m^2	ε_t, rad	E_i, rad kN/m^2	E_e, circ kN/m^2	ε_t, circ	E_i, circ kN/m^2
Clark (1973)[34][1]	1.69E-3	11.03	0.24	1707	19.49	0.13	5866
Missirlis (1976)[35][1]	2.67E-3	---	0.28	2276	---	0.11	7092
Missirlis (1978)[31][2]	3.3E-3	---	0.60	1089	---	0.33	3355
Sauren (1983)[32][2]	2.5	167	0.07	1000	3333	0.03	25000
Rousseau (1983)[36][2]	1.0	---	---	---	133.33	0.10	14000
Lee (1984)[37][2]	0.833	---	0.37	1666	---	0.09	5000
Mavrilas (1991)[38][1]	2.5	---	0.07	1570	---	0.07	14600
Leeson-Dietrich (1995)[39][2]	4.0	---	0.33	1860	---	0.13	19640
Christie, 1992[20][2]	---	2.688	0.63	333.3	10.6	0.13	2333.3

Figure 1-4: Mechanical properties of aortic valve leaflets in the circumferential (c) and radial (r) direction. σ = stress, ε = strain, E = effective modulus, t = transition. [1]human leaflets, [2]porcine leaflets, --- not determined.

the stress relaxation of human aortic valve leaflets, several studies have defined early relaxation in porcine leaflets, and a summary of the early time constants of therelaxation responses in the literature is given in Table 1-1. Stress relaxation is important because it characterizes the ability of the leaflet to transmit diastolic stress to the aortic root. This property highlights the ability of the leaflet tissue to dynamically reorganize its microstructure. The level of stress remaining in the tissue prior to opening of the leaflets must be carried by the flexion of the leaflet base. Thus it is critical that adequate stress relaxation occur in diastole to ensure long-term function of the leaflets.

Table 1-1: Stress relaxation time constants for aortic valve leaflets in the radial and circumferential directions.

Study (year)	% Stress remaining/s Radial	% Stress remaining/s Circumferential
Lee et al. (1984)[30]	-2.94	-5.00
Leeson-Dietrich et al. (1995)[39]	-6.00	-5.90
Vesely et al (1995)[40]	-5.93	-4.62
Duncan et al. (1996)[41]	-4.0	-6.2

Internal Shear – Internal shear is a material property that assesses the ability for layers of leaflet tissue to slip relative to one another. Talman and Boughner found that the shear modulus within the leaflet is minimal through the physiological level of strain (~ 0 kPa for $|\varepsilon| < 0.2$), indicating low viscosity through the spongiosa, which allows for eff icient transmission of stress as the leaflet flexes[43].

Aortic Valve Function Related to Tissue Microstructure. The presented data supports the proposed hypothesis that there are two relatively distinct mechanical regimes in which the leaflets operate. The leaflet behaves relatively inelastically in diastole (supported by the fibrosa), while elastic in systole (supported by the

ventricularis). These responses can be related to the microstructure of the different tissue layers. Since collagen fibers offer minimal resistance to extension while in a highly crimped state, the elastin fibers of the ventricularis must dominate the elastic response of the leaflet at lower strains of the elastic phase in systole. The diastolic pressure loads, supported by the fibrosa, are then resisted by the now completely unfurled collagen fibers. These observations have been confirmed experimentally by tensile tests of normal and digested leaflets[21]. The increased radial leaflet extensibility observed in biaxial tests results from a planar reorganization of circumferentially orientation collagen fibers that would have been cut during radial sectioning[44, 45] in uniaxial tests.

1.3: Aortic Valve Cell Biology.

The principal cell types in aortic valve leaflets are interstitial cells and endothelial cells. Smaller populations of smooth muscle cells[46] and nerve cells have also been noted[5, 47, 48]. Few studies have been conducted to characterize these cells, save for in vitro studies of cytoskeletal[49] and surface marker expression[50] and histological analyses[51]. In vitro experimentation with valvular cells has been difficult because no commercially available source exists, and manual isolation of pure populations has proved difficult. Important studies that do exist relative to this introduction are summarized below.

Aortic Valve Interstitial Cells. Interstitial cells are responsible for organizing and remodeling matrix proteins to withstand the dynamic tissue strains mentioned previously. They appear as elongated cells in vivo, and are present in all of the leaflet layers with varying densities. They have been generally classified as myofibroblastic, possessing prominent stress fibers and some secretory vesicles[52]. It has been

suggested that two morphologically distinct interstitial phenotypes exist, one more contractile and the other secretory, but only in vitro experimental evidence exists[53]. Valve leaflets respond to a number of vasoactive agents, suggesting that interstitial cells share some active contractile responses with smooth muscle cells[54]. Schneider and Deck observed that normal aortic valve interstitial cells secrete proteins and glycosaminoglycans at a dramatically increased rate in comparison to other cell types in vivo, with a significantly higher index of proliferation[55]. These results suggest that interstitial cells phenotypically resemble more of a hybrid between fibroblasts and smooth muscle cells than either phenotype. In pathology, interstitial cells may respond to endothelial denuding injuries by increased proliferation, as has been reported with mitral valve interstitial cells[56]. Aortic valve interstitial cell dysfunction characterized by thymosin beta4 upregulation and secretion of TGFβ1 have been implicated in the pathogenesis of valvular calcification[57, 58] and serotonin (5-HT) disorders[59].

Aortic Valve Endothelial Cells. Aortic valve endothelial cells, like other endothelial cells, are responsible for maintaining a non-thrombogenic blood contact surface, as well as transmit nutrient and biochemical signals to the interstitial cells[60]. Aortic valve endothelial cells form single cell monolayers on leaflet surfaces, express von Willebrand factor[61], produce nitric oxide[62] and prostacyclin activity[50], and possess cell junctions similar to arterial endothelial cells[50]. Deck observed that valvular endothelial cells are oriented circumferentially across leaflets, perpendicular to the direction of blood flow, in contrast to vascular endothelium, which aligns parallel to flow[63]. Endothelial cells of the aortic valve arise from different sources than either arterial endothelial or ventricular endocardial cells in development, which suggests that these cells may be different in some respects from other endothelial cell types[64]. Dysfunction in aortic valve endothelial cells has been highlighted in some recent studies

as being an important initiator of inflammatory responses related to the initiation of valvular disorders[65-68].

From this cursory analysis, it is apparent that aortic valve cells are significant regulators of normal valve functions. It is currently unknown whether valvular cells are truly unique phenotypes of cardiovascular nature, or merely vascular cells in a different mechanical environment.

1.4: Aortic Valve Pathology/Etiology

A list of valvular disease etiology classifications and some examples is given in Table 1-2. While some have a genetic component either inherited or developed during cardiogenesis, others are acquired or completely epigenetic, developed later in life. Some valvular diseases are acquired as a consequence of other pathologies, such as in chronic renal failure[69] or AIDS[70]. Clinical evaluation of aortic valve disease is usually done through echocardiography, with a diagnosis of valve stenosis (constriction), regurgitation (retrograde flow), or both. The exact disease cause varies depending on the specific pathology classification, examples of which are explained below in greater detail.

Congenital Heart Defects. Many congenital heart defects have minimal long term consequences, while others are life threatening from birth. More deaths occur due to cardiac defects than any other birth defect. Some of the more prevalent defects to the aortic valve (shown in Figure 1-5) include *bicuspid aortic valve*, *ventricular septal defects*, *Tetralogy of Fallot*, and *coarctation of the aorta*. Each of these defects can compromise the function of the heart, particularly the aortic valve. A *bicuspid aortic valve (BAV)* has only two leaflets attached to the aortic root instead of three. BAV leaflets are larger and thicker than normal leaflets, and as a result distribute

Table 1-2: Sources of aortic valve stenosis and regurgitation.
Adapted from[1].

Heriatable – Congenital
Heritable disorders of the connective tissues (Marfan's, Ehlers Danlos)
Genetic mutations (Kir2.1, NKX2.5)
Congenital heart defects (bicuspid aortic valve, tetralogy of Fallot)
Inflammatory – Immunological
Rheumatic fever
Infective endocarditis
Acquired Immune Deficiency Syndrome (AIDS)
Cardiovascular syphilis
Non-bacterial thrombotic endocarditis
Myocardial Dysfunction
Ischemic heart disease
Dilated cardiomyopathy
Hypertrophic cardiomyopathy
Diseases and Disorders of Other Organ Systems
Polycystic kidney disease
Systemic lupus erythematosus
Rheumatoid arthritis
Chronic renal failure
Aging
Calcific aortic stenosis
Aortic sinus aneurysm
Post-Interventional Valvular Lesion
Valvulotomy
Valve reconstructive surgery
Valve replacement
Drugs and Physical Agents
Chronic use of ergotamine products
Radiation induced valvular disease
Trauma induced valvular disease

hemodynamic and mechanical stresses poorly [71]..

Ventricular septal defects (VSD) are imperfect closures of the ventricular wall during development, causing circulation shunts that severely impair normal unidirectional blood flow. Depending on the size and location of the defect, the aortic valve may be adversely affected[72]. *Tetralogy of Fallot* (ToF) has four components: a VSD, stenotic pulmonary root, increased muscular left ventricle, and an aortic valve above the VSD. Babies with ToF are often blue at birth because of the inability to supply oxygen rich blood to the rest of the body. Most of these patients require open heart surgery at a young age to repair the defects[73]. *Coarctation of the aorta* (CoA) is a severe narrowing of the aortic root (stenosis), causing dramatic increases in ventricular pressure, wall shear stresses, and impaired blood delivery to the lower body[74]. The aforementioned defects can occur separately or together. Relative percentages of

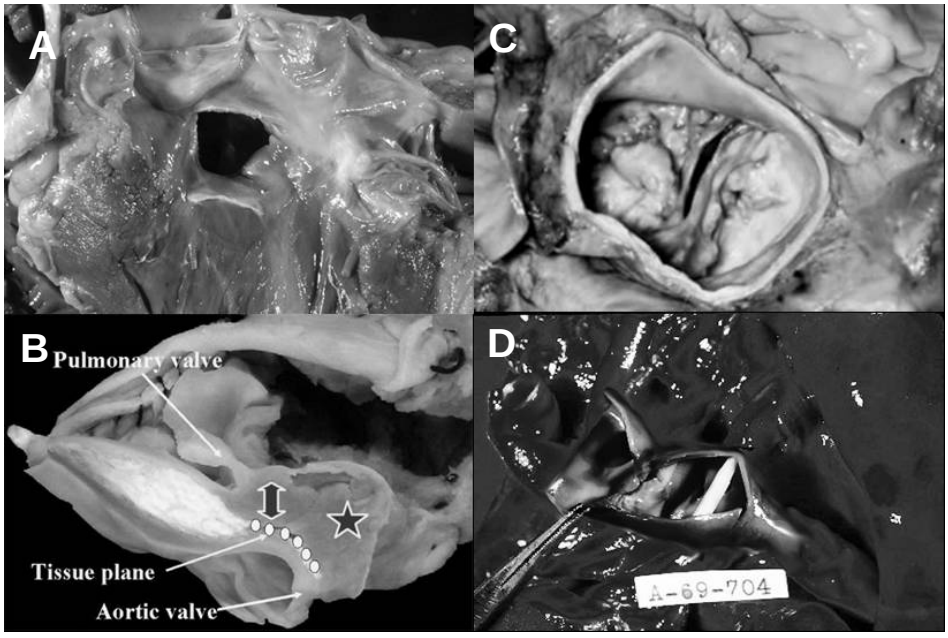

Figure 1-5: Congenital heart defects. A: Ventricular septal defect (medlib.med.utah.edu); B: Tetralogy of Fallot (www.acc.org); C: Bicuspid aortic valve (www.esp-inc.com); D: Coarctation of the aorta (www.som.tulane.edu).

congenital heart defect type are difficult to discern, owing to differences in diagnosis techniques, terminologies, and adequate case numbers. BAV is most often diagnosed, but this may be due to the fact that it does not present serious clinical complications at birth, is rather obvious morphologically, and can be detected later in life or at autopsy with relative ease. Other more serious defects can occur in concert, making diagnoses of the primary defect virtually impossible. In the United States, VSD occurs in 14-17 percent of defects, followed by ToF (9-12 percent) and CoA (8-11 percent)[5].

Heritable Disorders. Some congenital defects to the aortic valve are heritable. Many common connective tissue disorders, such as the Marfan Syndrome and Ehlers-Danlos Syndromes, also present aortic valve complications. Marfan Syndrome is an autosomal dominant connective tissue disorder that is caused by mutations in the fibrillin-1 gene, resulting in improper valve tissue development, in addition to eye and skeletal disorders[75]. Ehlers-Danlos syndromes are a group of heterogenic connective tissue disorders associated with mutations in genes coding for collagens and lysl-oxidases[76]. A rare autosomal recessive cardiac valvular form of Ehlers-Danlos Syndrome has been found by Schwarze and colleagues to be caused by mutations in the *COL1A2* gene, resulting in aortic insufficiency, mitral valve prolapse, and ventricular enlargement[77]. There is also evidence of heritability of bicuspid aortic valve[78]. Andelfinger traced the genetic locus of this trait to chromosome 17, encoding for an inwardly rectifying calcium channel *Kir2.1*. Further studies in frogs with the same *Kir2.1* mutation showed a dominant negative effect and lack of inward rectification[79]. Other heritable genetic mutations are associated with more heterotypic valvular pathologies. Benson and colleagues identified several mutations in the transcription factor *NKX2.5* in 26 individuals suffering with cardiac defects, including atrioventricular block, ventricular septal defect, and Tetralogy of Fallot[80]. This gene is also involved with Epstein's anomaly, which is heritable. Numerous studies conducted in animals have identified

putative genetic regulators of cardiac valve development, such as bone morphogenetic proteins[81], transcription factors[82], and growth factors[83]. Most of these types of studies involved gene knockout models that become embryonically lethal with severe cardiac defects and other complications. These studies are somewhat limited, however, in that this only identifies a particular gene as a critical component to valve development. Many human preterm miscarried pregnancies are the result of severely complicated defects with little chance of survival or intervention success[84]. Defects in live births, however, are usually much less severe than the complete loss of valves seen in some of these animal cases.

Acquired Pathologies. Several acquired diseases specifically affect heart valves, many of these are associated with bacterial infections that cause lesions preferentially on valve leaflets. Over time, leaflet tissues become remodeled pathologically, and can no longer respond appropriately to mechanical forces. Eventually, leaflets contract and the valve becomes severely regurgitant. Two major diagnoses of acquired valvular disease are infective endocarditis (IE) and rheumatic heart disease (RHD). Infective endocarditis is an inflammatory-like reaction caused by the presence of a variety of bacterial vegetations on valve leaflets, including staphylococci, streptococci, and enterococcus strains[85]. Many patients with a congenital heart defect have an increased propensity for bacterial infection from any vascular surgery, including routine dental work[86]. Rheumatic heart disease often results from rheumatic fever, which is defined as a poststreptococcal multisystem disease characterized by migratory arthritis, subcutaneous nodules, chorea, and other symptoms occurring separately or in concert[87]. The valvular pathology, however, is somewhat similar to that of IE. Bacterial lesions which envaginate the leaflets remodel the local matrix architecture, compromising its integrity, resulting in diseased valves[88]. It is not completely understood how these strains of bacteria specifically adhere to

valvular tissues, remodel the extracellular matrix, and interact with the native cell populations.

Epigenetic Causes. The majority of heart valve disease not diagnosed in childhood occurs later in life with no apparent etiology. Late-onset valvular heart disease is an umbrella term which encompasses a variety of symptoms, including aortic valve stenosis, regurgitation, tissue calcification and degeneration. Because there is no standard classification scheme (nosology), the incidences of specific types of tissue pathology are not well characterized, and many of the aforementioned symptoms occur in concert[1]. There has been increasing attention to, and evidence to support, the theory that many aspects of late onset valvular heart disease are really just extensions of vascular atherosclerosis. Researchers have identified atherosclerotic-like lesions in valves, as well as some potential inflammatory mediators[89, 90].

Disease Progression. While some valvular diseases are acute, such as from thoracic trauma[91, 92], disease progression in heart valves is more often slow, only compromising function at advanced stages. Early events include valvular endothelial dysfunction[65, 68, 93] and interstitial cell activation[94, 95]. Biochemical factors secreted by these cells then modify the local extracellular matrix and change cell proliferation rates[96, 97]. In some cases, lipid accumulation occurs leading to cell death and the nucleation of calcium deposits[98]. Eventually, valvular cells lose the ability to remodel the valve matrix, and constant mechanical insult leads to tissue microdamage. Left unchecked, this damage eventually propagates to gross tissue pathology resulting in aortic regurgitation and/or stenosis. A regurgitant valve (Figure 1-6A) does not close properly, allowing a percentage of blood to leak back into ventricle during diastolic filling. A stenotic aortic valve (Figure 1-6B) is constricted, restricting blood flow out of the left ventricle. Both of these conditions cause the ventricle to pump harder to supply enough blood to the rest of the body, leading to left ventricular pressure overload. Like any

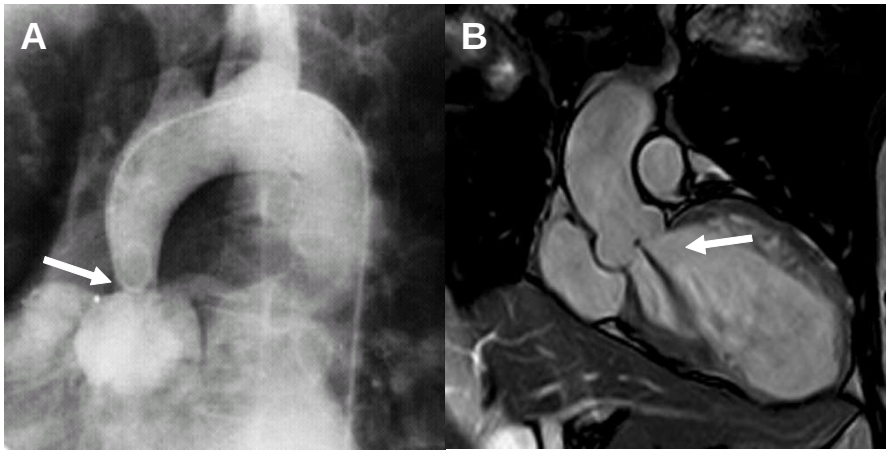

Figure 1-6: Diagnoses of aortic stenosis (A, www.circulation.or.kr) and regurgitation (B, www.medical.philips.com)

exercised muscle, the ventricular wall becomes thickened under the increased load, eventually impairing bioelectrical conduction, causing ventricular wall atrophy, and resulting in congestive heart failure[99].

1.5: Current Treatment Options

Treatment of heart valve pathology began as an operation to salvage left ventricle function, with little understanding or concern of valvular functions. The fact that many valvular pathologies progress slowly is both a blessing and a curse. Many patients do not know that they have a serious valvular complication until it is too late to treat without interventional surgery. Therapy for heart valve disease includes valve sparing surgery or prosthetic valve replacement, and in some cases both. As understanding of the complex functions of the aortic valve grew, so also did advances in surgical techniques and prosthetic designs to preserve valvular structure and prosthetic valve design to mimic valvular hemodynamics.

Valve Sparing Surgery. Because normal aortic root and valvular leaflet function is ideal, and in some cases leaflets are not affected by valvular pathology, preserving native valve leaflet and sinus tissue could dramatically benefit patients[3]. A number of aortic valve leaflet sparing and salvage surgeries have been developed specifically for cases of aortic regurgitation (insufficiency) caused by root dilatation or dissection, conditions that cannot accommodate a prosthetic replacement. Surgeries include valve reimplantation and aortic root remodeling techniques. The reimplantation technique (Figure 1-7A), first developed by Tirone David[100], involves dissecting the aortic valve intact, removing the diseased aortic root, and combining the healthy valve within a Dacron tube. The remodeling technique (Figure 1-7B) involves dissecting the diseased aorta while preserving aortic valve attachment to the left ventricle[101]. Post-operative mortality is reasonably low (0-6%), with long-term survival rates (72-78%) and freedom from reoperation (90-97%) acceptable, with recurrence of aortic dilatation and insufficiency is a common failure mode[102, 103]. The experience and expertise of the surgeon is of paramount importance for these complicated surgeries, and therefore valve sparing surgeries can only be done at a few centers around the world. Most valvular interventions therefore involve replacement with a prosthetic valve.

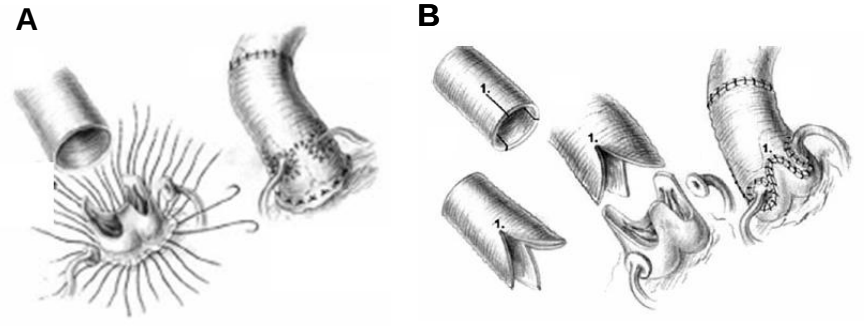

Figure 1-7: Aortic valve reimplantation (A) and remodeling (B) techniques. Adapted from[3].

Prosthetic Valve Replacement. Prosthetic aortic valve replacement has existed since the early 1960's, beginning with the successful implantation of a mechanical valve in the subcoronary sinus by Dr. Dwight Harken[104]. Over the last 40 years, there have been over 70 different types of mechanical and bioprosthetic valves used in hundreds of thousands of patients around the world[105]. Four main groups of options exist for surrogate valves: mechanical (Figure 1-8 Top), bioprosthetic (Figure 1-8 Bottom), homograft, and pulmonary autograft. Each of these valve groups has their advantages and limitations, and therefore surgeons try to match the valve choice with the patient's particular clinical condition.

The continuous and demanding requirements for aortic valve function lead engineers and surgeons to first try mechanical devices for valvular replacement. Figure 1-8A shows an approximate evolution of the mechanical valve since the early 1960's. The first generation valves were caged-ball valves, followed by disk valves, tilting disk

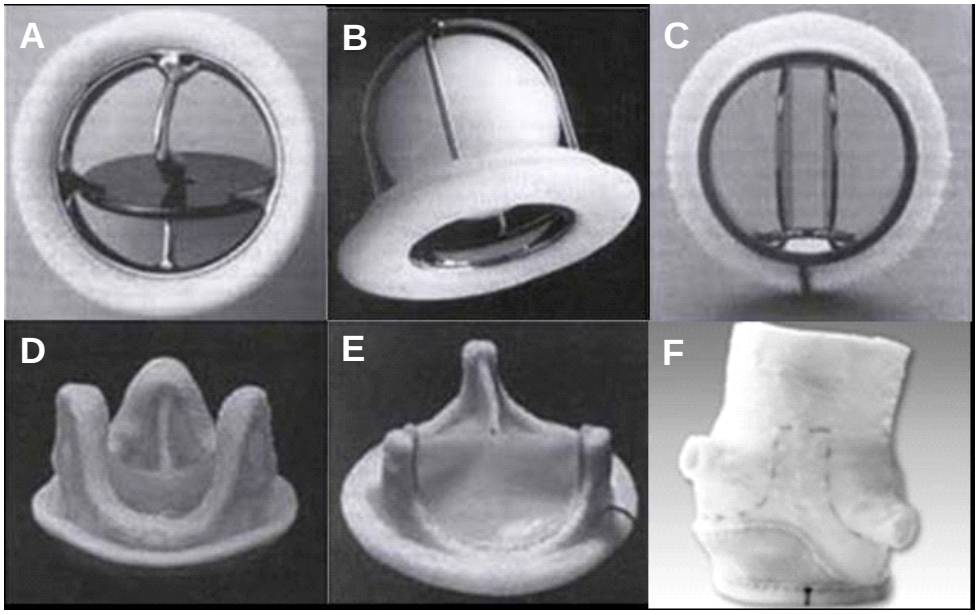

Figure 1-8: Mechanical (A-C) and bioprosthetic (D-F) valves (www.rjmatthewsmd.com). A: Tilting disk valve, B: Caged ball valve; C: Bileaflet valve; D: Porcine aortic valve (stented); E: Bovine pericardial valve (stented); F: Porcine aortic root (stentless).

valves, and more recently bileaflet valves[105]. While each valve design prevents regurgitation, differences in hemodynamic parameters exist between them. The ideal mechanical valve will restrict the least amount of blood flow out of the left ventricle, while minimizing fluid shear stresses and turbulent flow regimes, which can cause hemolysis and cell death[106]. The progression from caged ball to more leaflet-like valves represents an appreciation gained by engineers for the normal aortic valve function: each new design having a larger orifice area while guarding the hinge mechanisms from flow[105]. Early valves were constructed out of stainless steel, titanium, and silicone, and newer valves are constructed out of more biologically inert materials such as pyrolytic carbon. Currently, the tilting disk and bileaflet valves are predominantly used, each with well over 200,000 implantations in the aortic position. The major drawback for these valves is the need for continual anticoagulant therapy to prevent blood clot formation, which could spontaneously clog the valve and lead to instant death[16].

The use of bioprosthetic valves arose out of concern for the side effects accommodating anticoagulant therapy. Porcine aortic valves were considered an ideal substitute because of the similar hemodynamic and mechanical environment of that species. Once Carpentier and colleagues introduced the concept of glutaraldehyde fixation in 1968, that durable, non immunogenic xenograft valves became readily available[107]. Bioprosthetic valves come in two major forms: stented and stentless. Stented valves contain a rigid cassette to which the valve leaflets are sewn, while the stentless valves leaves the aortic root largely preserved. While stented valves are much easier to implant, stentless valves are more compliant, and can better accommodate normal leaflet function[2]. Additional bioprosthetic valve designs include bovine pericardial and complete porcine aortic root designs. These valves do not require the anticoagulation therapy needed in mechanical valves, but suffer instead from tissue

degeneration from mechanical wear[45], and calcification from glutaraldehyde and cell residues[98].

Homograft (or allograft) valves are human aortic or pulmonary valves that are obtained at autopsy, sterilized, and stored until needed for implantation. These valves are generally preferred over other valves because they are identical to the valve being replaced. The obvious drawback for these valves is that they are in extremely short supply. Advances in collection, sterilization and storage techniques have dramatically extended the “shelf life” of these valves, and with the advent of cryopreservation, have some cell viability at implantation[108].

Pulmonary Autograft – The Ross Procedure. It was recognized rather early on that the pulmonary valve is similar morphologically to the aortic valve, and may serve as a living replacement of a diseased aortic valve. The pulmonary circulation is the higher pressure side of the heart throughout cardiovascular development, so it was thought that this valve would function well in the high pressure aortic position in adults. The adult pulmonary circulation experiences pressures only on the order of 15 mmHg, and could therefore tolerate a prosthetic substitute much more readily. The first pulmonary autograft (same human) into the aortic position was performed by Dr. Ross in 1962, and since then the Ross procedure has received praise and concern throughout the world[109]. Some surgeons prefer it to other techniques because it provides a living valve in the critical aortic region, while other surgeons shun the procedure because it demands extreme technical expertise and failure would then result in two damaged valves. As a result, this surgery is performed in only a few centers around the world, yet with highly favorable results[110].

Current Treatment Limitations. While these valvular replacements help preserve other cardiac functions, they eventually fail due to a number of reasons. A comparison of long term survival and freedom from valve-related events for the different

types of valve replacements is shown in Figure 1-9. The pulmonary autograft (Ross Procedure) is clearly superior in terms of survival and freedom from operation (>80% at 10 years). Mechanical and homograft valves exhibit slightly higher survival rates than xenograft valves, but all three of these valves have equal incidences of valvular events requiring medical attention. Nevertheless, survival with any of the prosthetic valves is greater than 50% after 10 years (Figure 1-9A,B). An analysis of the failure modes incurred by each valve is given in Table 1-3. Mechanical valves are superior for durability, but suffer from bleeding events associated with the anticoagulation therapy and clotting from blood contact with the valve materials. Tissue valves are generally free from either bleeding events, but suffer instead from tissue degeneration and calcification. The aortic root and ascending aorta can be independently damaged secondary to aortic valve replacement, leading to root dilatation and aneurysm formation. All prosthetic valves pose an increased susceptibility to bacterial infection[111].

While 10-15 years of survival is generally acceptable for older patients (>70 yrs. old), this outcome is clearly not acceptable for younger adults. More active young adults subject the aortic valve to changing heart rates and blood pressures, limiting the options available to them for valvular replacement. This is best seen in statistics on heart valve replacement procedures with children, shown in Figure 1-9C,D. Few studies exist that compare valve replacement options in children, but it is apparent from these that tissue valves are far inferior to mechanical or autograft valves in terms of freedom from events. Over 50% of all tissue derived valves (xenograft, homograft) require reoperation before 10 years post operation. Even though these failed prosthetic valves can be operated on successfully (as evidenced by minimal differences in survival), repeat open heart surgeries severely impair the quality of life of the patient. Unfortunately, the remaining options are also severely limited. The more preferred Ross can only be performed in a

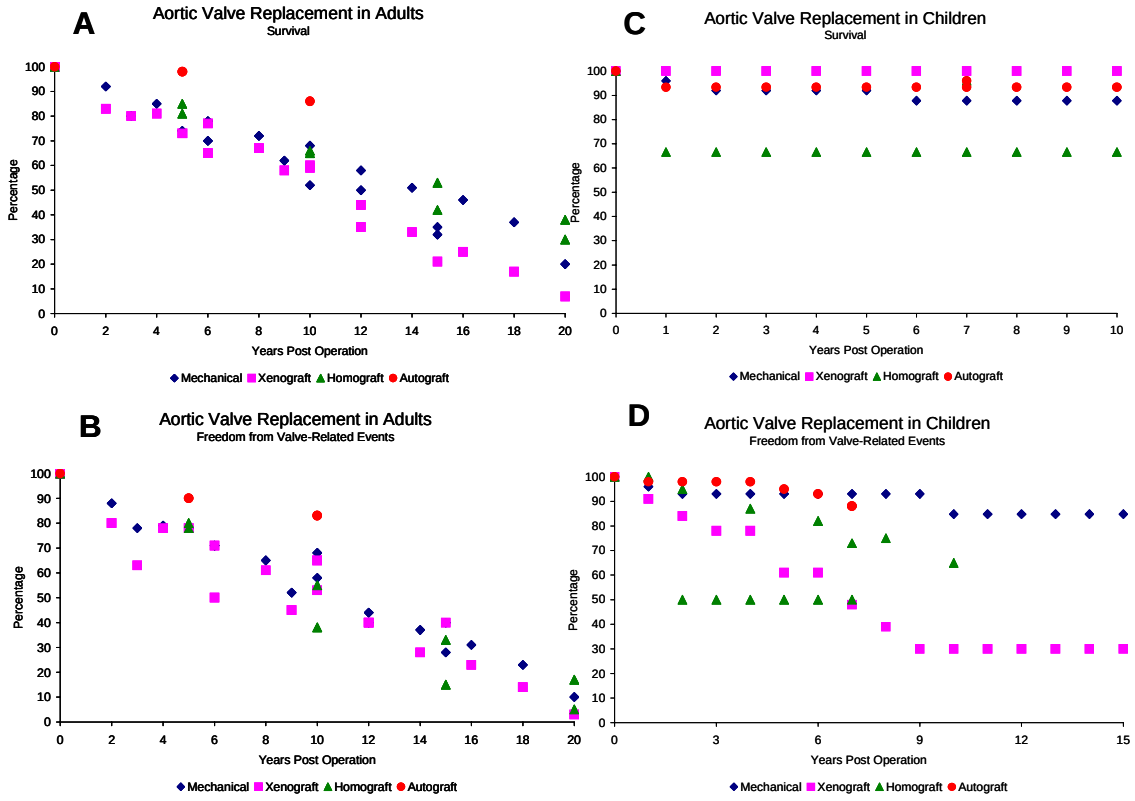

Figure 1-9: Survival and freedom from valve related events from aortic valve replacements in adults (A,B) and children (C,D). Data taken from[13-19].

Table 1-3: Prominent failure modes of mechanical and biological prosthetic heart valves.

Mechanical Prostheses	Biological Prostheses
Structural failure	Calcification
Thromboembolism formation	Cuspal tears
Uncontrollable bleeding	Paravalvular leak
Paravalvular leak	Tissue overgrowth
Tissue overgrowth	Endocarditis
Endocarditis	

limited number of facilities, and mechanical prostheses require constant anticoagulant therapy that again severely limits the activities a young child can engage in. Even if advances in non-coagulating materials were developed, several repeat open heart surgeries will still be required to accommodate the growth of the child and his/her aortic root. Patient/prosthesis mismatch can be a severe complication. Many cardio-thoracic surgeons attempt to create a system for the assignment of valvular substitutes that takes into consideration a patient's age and cardiovascular risk, an example of which is given in Figure 1-10[2]. The Ross procedure is preferred over other options until age 35, when use of other substitutes is more encouraged. Nevertheless, these statistics paint a dismal picture for most patients suffering from aortic valve disease, and the increasing life expectancy of Americans is only going to make better heart valve replacement options more critical for the future.

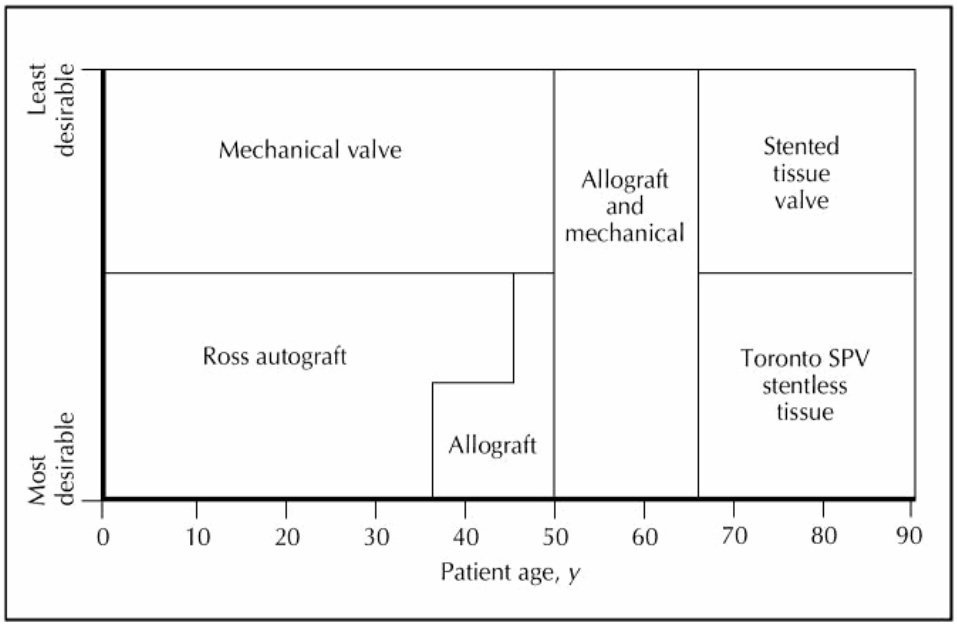

Figure 1-10: Strategy for choosing valve replacements. Taken from[2].

1.6: Heart Valve Tissue Engineering

The ideal valvular substitute on a surface level would be a tissue-like valve that is durable enough to thrive in the aortic position long term, is non-thrombogenic, and can grow and remodel according to the needs of the patient, eventually becoming identical to the valve it replaced[112]. Tissue engineering has emerged as a promising technology to respond to this demand. This field explores the combination of living cells, a matrix-like scaffold, and stimulation factors to create a living tissue that, once implanted, can remodel according to the body's needs and after time function normally[113, 114]. Tissue engineering is being applied to address concerns in orthopedics[115], secretory organs[116], neurological disorders[117], and cardiovascular pathologies[118]. Although not as advanced as cardiovascular tissue engineering, heart valve tissue engineering has progressed dramatically over the last decade[119]. The primary focus of heart valve tissue engineering has been the aortic valve, not only because of its significant clinical

importance, but also because of its near symmetry and single line of attachment to the aortic root. Most research has focused on the development of scaffold materials that can withstand the dynamic mechanical environment of the aortic valve, while accommodating cell ingrowth and remodeling. Three basic strategies have been employed: biodegradable polymeric scaffolds, decellularized valvular conduits, and completely biological matrix scaffolds.

Biodegradable Polymers. The most widely used strategy involves biodegradable synthetic polymers repopulated with autologous cell types. Over time, the polymer degrades by normal metabolic activity, and is replaced by biological matrix. The choice of polymer substrate varies according to the desired mechanical properties, melting temperatures, and degradation times. Some polymers that have been used include PGLA, PHO, and PHA, separately or in combination[120]. The initial successes in leaflet replacement studies in lambs using synthetic polymers [121] have spawned over a decade of research with this strategy, eventually culminating in landmark pulmonary valve implant studies in adult sheep[122]. After 20 weeks in the pulmonary circulation, these valves resembled normal leaflet morphology, had similar mechanical properties compared to normal leaflets, and no incidences of preterm death. While these results were exciting and promising, there still was significant transvalvular pressures (10-15 mmHg) associated with regurgitation due to leaflet shrinkage. Since these pressures are on the order of systemic pulmonary circulation pressures, these valves may have been mimicking valve motions without actually maintaining function. Ultimately, this strategy may be limited in that the end products from the degrading polymers may change local pH, causing undesired cell death and differentiation[123]. Nevertheless, a biodegradable polymer based valvular substitute has been successfully implanted in the pulmonary position in Europe, and short term followup indicates excellent pulmonary function[124].

Decellularized Valvular Conduits. Decellularized aortic valve conduits make an attractive choice of matrix scaffold because the complete native leaflet tissue ultrastructure may provide unique biochemical and matrix signals for invading cells to encourage differentiation into leaflet cells. In this method, excised porcine aortic roots are soaked with a series of chemicals to remove cellular fragments while preserving tissue ultrastructure, providing an ideal matrix structure for recellularization. The challenge is the washing the tissue to completely remove residual detergents without additional tissue destruction. This matrix can then be recellularized by invading cells, which then remodel the matrix according to local stimuli. This method was first presented by Bader and colleagues in 1998[125] and commercialized by Cryolife with the SynerGraft decellularized valve, which is a detergent decellularized porcine aortic valve fabricated into a stentless implant[126]. Results in animal trials showed promising hemodynamic parameters and evidence of host repopulation, which lead researchers to begin human clinical trials in Europe for pulmonary valve indications. Short term experience in adults (6 months) indicates reasonable leaflet coaptation and hemodynamic parameters in adults[127], but disastrous results were reported in children. Massive immune response and spontaneous failures directly relating to rapid SynerGraft tissue degeneration led to the deaths of three children early into the study, immediately prompting the halt of the trial[128]. Interestingly, no cellular ingrowth was found on any of the excised valves.

Biological Matrix Scaffolds. The least developed strategy involves creating a scaffold with completely biological matrix components. Some examples that have been explored in cardiovascular tissue engineering include collagen[129], fibrin[130], and small intestinal submucosa (SIS)[131]. The advantage is that these materials can be obtained in large supply from xenogenic sources, can readily accommodate cellular ingrowth, and do not have cytotoxic degradation products. While removing many of the

concerns of the previous options, this strategy is limited by mechanical fragility of the material[132], and the inability to create complex tissue geometries. No published results exist using completely biologically derived matrices in heart valve tissue engineering, but exciting advances have been reported in small diameter blood vessel construction using a cell sheet technology first developed by Nicholas L'Heureux in 1993[133]. Cells are grown in culture for several weeks, by which time they have secreted a considerable amount of matrix, forming a detachable cell sheet. Multiple layers of these sheets then form a laminate structure that can be rolled into tubular geometries. While these vessels exhibit improved mechanical properties compared to other biologically derived scaffolds, long term animal studies have not been published to date. Edwards Lifesciences was recently exploring the development of completely biological tissue engineered aortic valve using cell sheet technology and SIS biomaterials, capitalizing on sewing techniques used in their pericardial bioprosthetic valves.

Shi and colleagues have proposed the development of a composite approach[134]. They combine a biomimmetic hyaluronan gel with stacked collagen fiber bundles arranged in a layered structure similar to the native aortic valve. While they report relatively strong collagen bundles (> 1 MPa), and the production of elastin, they are formed using neonatal rat cells, which may not be mimicked by human cells. It is also unclear how these layers will be attached to each other while maintaining shear forces. Ultimately, the fact that this valve design contains a non-biodegradable polymer (hyaluronan gel) prevents it from possible use in pediatric applications.

Cell Sources. A number of cell sources have been used in heart valve tissue engineering applications. Early research focused on vascular cell sources, such as arterial smooth muscle and endothelial cells, which have been well characterized and easily isolated. Shinoka and colleagues conducted a series of leaflet replacement

studies in an ovine model investigating allogeneic and autologous cell sources for heart valve tissue engineering, and found that autologous arterial cells were preferable to allogeneic sources and dermal fibroblasts[121, 135, 136]. Heart valve tissue engineering may necessitate the use of some other cell type for reconstitution of tissue, because leaflet tissue is largely non-sacrificial. Maisch and colleagues have developed a protocol for isolating valvular interstitial cells from a tricuspid valve biopsy, and were able to generate sufficient cell numbers for seeding a valve substitute[137]. The risk of postoperative death and unclear long term prognosis of tricuspid valve function suggest caution for this technique, but it demonstrates the feasibility of producing large cell numbers from a biopsy. The authors were not able to generate tricuspid valve endothelial cells from this technique. Rabkin and colleagues investigated the evolution of cellular phenotype of their blood vessel cell populated polymeric valve substitute, and found that after 16-20 weeks in the lamb pulmonary circulation the blood vessel cells were very similar to native valvular cells in terms of marker expression[51]. While autologous blood vessel cells provide an immediate source for repopulation, stem cells may be superior in that they theoretically provide an unending source of cells that may be able to differentiate into mature valvular phenotypes. Preliminary experience using bone marrow derived stem cells suggests that these cells can differentiate according to mechanical signals and become more like valvular cells, but it is unclear that these cells are mature enough after in vitro stimulation for implantation[138]. The possibility of adipocyte transdifferentiation suggests the possibility of early leaflet calcification through lipid accumulation[139].

Mechanical Stimulation. It is well known that cells and tissues respond to mechanical forces by growth, strengthening, and remodeling responses. Cardiovascular tissues are situated in a continuously mechanical environment, the aortic valve being a prime example. The use of mechanical forces in the stimulation of engineered tissue

remodeling has been explored in bone[140], blood vessel[129], and heart valve applications. Pulse duplicator systems have been developed to expose engineered valvular tissues to gradually increasing pressures and flows to encourage accelerated scaffold remodeling in vitro prior to implantation[141-143]. Studies with these systems reported improved mechanical properties and extracellular matrix production during in vitro stimulation compared to static controls. Valvular conduits stimulated mechanically in vitro for two weeks before implantation demonstrated improved performance in vivo, leading researchers to conclude that in vitro preconditioning should be standard for heart valve tissue engineering[144].

While these systems recreate some aspects of heart valve fluid mechanics, virtually nothing can be learned about the roles of specific mechanical forces on tissue strengthening and remodeling from these coupled devices. It is possible that one particular mechanical or hemodynamic force plays a large role in shaping valvular tissue, while others are more deleterious. Creating devices to mechanically stimulate engineered tissue is a challenge because of difficulties stemming from their extreme fragility. Pulsatile stretch bioreactors have been developed for vascular applications, imposing predominantly circumferential strain through cyclic lumenal pressure changes[129]. Recently, a three-point bending apparatus was developed to expose tissue strips to uniform flexure[145]. Preliminary studies have tested biodegradable polymer meshes seeded with cells, and indicate some remodeling responses. It is unclear, however, how the flexure loads are distributed across the length of the strips. The observed responses may be localized to the region of the central bending pin, while the rest of the tissue acts like a hinge and remains statically cultured. Native valvular leaflets and biologically derived matrix scaffolds have virtually no buckling resistance, making three point bending bioreactor designs somewhat limited.

Tissue Engineering As a Model System. While the current clinical applicability of tissue engineered cardiovascular substitutes is limited, advances in the study of cardiovascular physiology can be made using tissue engineering in vitro. Indeed, the evolution of blood vessel cell biology study platforms has progressed from isolated cell populations cultured on coated rigid substrates to more physiological three dimensional substrates with relevant cell phenotypes in co-culture under well defined mechanical forces[146]. These tissue models have the advantage that well controlled mechanical and exogenous biochemical stimulation can be applied knowing all cellular and matrix components a priori[147]. This enables better induction of mechanistic pathways of biological response. Because tissue engineered models of vascular systems can be created in a matter of days, biological inquiry can then progress more quickly and less expensively than animal models, with less variability. Initial studies using vascular tissue engineering have demonstrated similar responses to what are observed in vivo, with the potential for greater understanding clearly evident[146, 148].

1.7: Objective of this Research

The data presented earlier indicate a significant clinical need for a solution to aortic valve disease. It is unclear how many of the causes of aortic stenosis and insufficiency progress undetected by current methods until they too require invasive surgery. This fact coupled with the limited success to date of tissue engineered valvular substitutes in vivo underscores a fundamental lack of understanding of valvular cell biology. It is becoming apparent that valvular physiology is distinct from vascular physiology, and therefore valvular cell biology may be different as well. It is unclear whether the vascular cell populated tissue engineered valves fail because of a fundamental biological attribute of valvular cells that is absent, or a pathological

biological response to the very different valvular mechanical environment, or both. If an understanding of normal valvular cell biology and the influence of mechanical forces can be developed, then perhaps an understanding of aortic valve disease initiation can be learned and therapies targeted before it progresses, removing all need for prosthetic valve implantation. Tissue engineering can be of great service to this end, as a relevant physiological model can be developed to perform well controlled mechanical and chemical stimulations, and assess biological response[149]. The objective of this thesis was to develop a valvular leaflet model using tissue engineering technologies, and investigate valvular cell response to a well defined mechanical force. To achieve this, several research goals were set, and the results of each are presented and discussed in separate chapters. They are summarized as follows:

Goal 1: Isolate and characterize pure populations of normal aortic valve cells: Native valvular cells are not easily obtained or commercially available, so techniques to isolate valvular cells were developed and applied to porcine aortic valve tissues. Cells were then characterized according to cytoskeletal marker expression, functional assays, and morphology. These results are located in Chapter 2.

Goal 2: Compare the phenotype of aortic valve interstitial cells and arterial smooth muscle cells in three dimensional culture: Since primarily arterial smooth muscle cells were used to populate tissue engineered heart valve scaffolds, contractile and synthetic phenotype comparison was conducted between these cells and aortic valve interstitial cells. Tissue compaction, contractile marker expression, and matrix production were assessed, and the results presented in Chapter 3.

Goal 3: Compare the biological response of aortic valve and arterial endothelial cells to steady laminar shear stress: Many vascular and valvular pathologies begin with endothelial dysfunction, and it is likely that differences may exist between these cells in how they respond to mechanical forces. Aortic valve endothelial cells and aortic endothelial cells were exposed to steady laminar shear stress, with static cultures serving as controls. Cell morphology, focal adhesion development, and initial signal pathway results are presented and discussed in Chapter 4.

Goal 4: Compare the genetic response of aortic valve and arterial endothelial cells to steady laminar shear stress: The complete phenotypic response of a cell population to a stimulus can be profiled using microarray technology. RNA profiles from shear conditioned and statically cultured endothelial cells were compared using cDNA microarrays and gene ontology software, and significant gene changes confirmed using real time PCR. The results are presented and discussed in Chapter 5.

Goal 5: Develop a three dimensional co-culture model of aortic valve cells and analyze the biological response to a well defined mechanical force: Collagen I hydrogels were used to develop a three dimensional co-culture model using aortic valve cells. Models with and without endothelial cells were exposed to steady laminar shear stress, with static cultures serving as controls. Cell proliferation, marker expression, and matrix synthesis results are presented and discussed in Chapter 6.

The significance and consequences of the results of these studies are presented in Chapter 7, followed by a concluding summary in Chapter 8.

1.8: References

1. Boudoulas, H., M. Vavuranakis, and C.F. Wooley, *Valvular heart disease: the influence of changing etiology on nosology.* J Heart Valve Dis, 1994. **3**(5): p. 516-26.

2. Park, S.Z. and M.J. Reardon, *Current status of stentless aortic xenografts.* Curr Opin Cardiol, 2000. **15**(2): p. 74-81.

3. Hopkins, R.A., *Aortic valve leaflet sparing and salvage surgery: evolution of techniques for aortic root reconstruction.* Eur J Cardiothorac Surg, 2003. **24**(6): p. 886-97.

4. Dagum, P., et al., *Deformational dynamics of the aortic root: modes and physiologic determinants.* Circulation, 1999. **100**(19 Suppl): p. II54-62.

5. *2002 Heart and Stroke Statistical Update*. 2001, Dallas, TX: American Heart Association. 19-21.

6. Choudhury, R., et al., *Active infective endocarditis observed in an Indian hospital 1981-1991.* Am J Cardiol, 1992. **70**(18): p. 1453-8.

7. Passik, C.S., et al., *Temporal changes in the causes of aortic stenosis: a surgical pathologic study of 646 cases.* Mayo Clin Proc, 1987. **62**(2): p. 119-23.

8. Dare, A.J., et al., *New observations on the etiology of aortic valve disease: a surgical pathologic study of 236 cases from 1990.* Hum Pathol, 1993. **24**(12): p. 1330-8.

9. Matsumura, T., et al., *Etiology of aortic valve disease and recent changes in Japan:a study of 600 valve replacement cases.* Int J Cardiol, 2002. **86**(2-3): p. 217-23.

10. Sadiq, M., M. Nazir, and S.A. Sheikh, *Infective endocarditis in children--incidence, pattern, diagnosis and management in a developing country.* Int J Cardiol, 2001. **78**(2): p. 175-82.

11. Ephrem, D., B. Abegaz, and L. Muhe, *Profile of cardiac diseases in Ethiopian children.* East Afr Med J, 1990. **67**(2): p. 113-7.

12. Noji, S., et al., *Different functional recovery of the left ventricle after valve replacement for aortic regurgitation: correlation between grade of ventricular arrhythmia and long-term mortality.* J Heart Valve Dis, 1995. **4**(3): p. 254-9.

13. Daly, R.C., et al., *Long-term results of aortic valve replacement with nonviable homografts.* Circulation, 1991. **84**(5 Suppl): p. III81-8.

14. Elkins, R.C., et al., *Pulmonary autograft root replacement: mid-term results.* J Heart Valve Dis, 1999. **8**(5): p. 499-503; discussion 503-6.

15. Grocott-Mason, R.M., et al., *Long-term results after aortic valve replacement in patients with congestive heart failure. Homografts vs prosthetic valves.* Eur Heart J, 2000. **21**(20): p. 1698-707.

16. Hammermeister, K., et al., *Outcomes 15 years after valve replacement with a mechanical versus a bioprosthetic valve: final report of the Veterans Affairs randomized trial.* J Am Coll Cardiol, 2000. **36**(4): p. 1152-8.

17. Lupinetti, F.M., et al., *Comparison of autograft and allograft aortic valve replacement in children.* J Thorac Cardiovasc Surg, 2003. **126**(1): p. 240-6.

18. Oxenham, H., et al., *Twenty year comparison of a Bjork-Shiley mechanical heart valve with porcine bioprostheses.* Heart, 2003. **89**(7): p. 715-21.

19. Turrentine, M.W., et al., *Biological versus mechanical aortic valve replacement in children.* Ann Thorac Surg, 2001. **71**(5 Suppl): p. S356-60.

20. Christie, G.W., *Anatomy of aortic heart valve leaflets: the influence of glutaraldehyde fixation on function.* Eur J Cardiothorac Surg, 1992. **6 Suppl 1**: p. S25-32; discussion S33.

21. Vesely, I., *The role of elastin in aortic valve mechanics.* J Biomech, 1998. **31**(2): p. 115-23.

22. Weind, K.L., C.G. Ellis, and D.R. Boughner, *The aortic valve blood supply.* J Heart Valve Dis, 2000. **9**(1): p. 1-7; discussion 7-8.

23. Weind, K.L., C.G. Ellis, and D.R. Boughner, *Aortic valve cusp vessel density: relationship with tissue thickness.* J Thorac Cardiovasc Surg, 2002. **123**(2): p. 333-40.

24. Weind, K.L., et al., *Oxygen diffusion and consumption of aortic valve cusps.* Am J Physiol Heart Circ Physiol, 2001. **281**(6): p. H2604-11.

25. Thubrikar, M., et al., *The cyclic changes and structure of the base of the aortic valve.* Am Heart J, 1980. **99**(2): p. 217-24.

26. Thubrikar, M., L.P. Bosher, and S.P. Nolan, *The mechanism of opening of the aortic valve.* J Thorac Cardiovasc Surg, 1979. **77**(6): p. 863-70.

27. Vesely, I., *Aortic root dilation prior to valve opening explained by passive hemodynamics.* J Heart Valve Dis, 2000. **9**(1): p. 16-20.

28. Bellhouse, B.J., F.H. Bellhouse, and K.G. Reid, *Fluid mechanics of the aortic root with application to coronary flow.* Nature, 1968. **219**(158): p. 1059-61.

29. Thubrikar, M., et al., *The elastic modulus of canine aortic valve leaflets in vivo and in vitro.* Circ Res, 1980. **47**(5): p. 792-800.

30. Lee, J.M., D.W. Courtman, and D.R. Boughner, *The glutaraldehyde-stabilized porcine aortic valve xenograft. I. Tensile viscoelastic properties of the fresh leaflet material.* J Biomed Mater Res, 1984. **18**(1): p. 61-77.

31. Missirlis, Y.F. and M. Chong, *Aortic valve mechanics--Part I: material properties of natural porcine aortic valves.* J Bioeng, 1978. **2**(3-4): p. 287-300.

32. Sauren, A.A., et al., *The mechanical properties of porcine aortic valve tissues.* J Biomech, 1983. **16**(5): p. 327-37.

33. Fung, Y.C., *Biomechanics: Mechanical Properties of Living Tissues*. Second ed. 1993, New York: Springer. 568.

34. Clark, R.E., *Stress-strain characteristics of fresh and frozen human aortic and mitral leaflets and chordae tendineae. Implications for clinical use.* J Thorac Cardiovasc Surg, 1973. **66**(2): p. 202-8.

35. Missirlis, Y.F., C.D. Armeniades, and J.H. Kennedy, *Mechanical and histological study of aortic valve tissue from a patient with Marfan's disease.* Atherosclerosis, 1976. **24**(1-2): p. 335-8.

36. Rousseau, E.P., et al., *Elastic and viscoelastic material behaviour of fresh and glutaraldehyde-treated porcine aortic valve tissue.* J Biomech, 1983. **16**(5): p. 339-48.

37. Lee, J.M., D.R. Boughner, and D.W. Courtman, *The glutaraldehyde-stabilized porcine aortic valve xenograft. II. Effect of fixation with or without pressure on the tensile viscoelastic properties of the leaflet material.* J Biomed Mater Res, 1984. **18**(1): p. 79-98.

38. Mavrilas, D. and Y. Missirlis, *An approach to the optimization of preparation of bioprosthetic heart valves.* J Biomech, 1991. **24**(5): p. 331-9.

39. Leeson-Dietrich, J., D. Boughner, and I. Vesely, *Porcine pulmonary and aortic valves: a comparison of their tensile viscoelastic properties at physiological strain rates.* J Heart Valve Dis, 1995. **4**(1): p. 88-94.

40. Vesely, I., D.R. Boughner, and J. Leeson-Dietrich, *Bioprosthetic valve tissue viscoelasticity: implications on accelerated pulse duplicator testing.* Ann Thorac Surg, 1995. **60**(2 Suppl): p. S379-82; discussion S383.

41. Duncan, A.C., D. Boughner, and I. Vesely, *Dynamic glutaraldehyde fixation of a porcine aortic valve xenograft. I. Effect of fixation conditions on the final tissue viscoelastic properties.* Biomaterials, 1996. **17**(19): p. 1849-56.

42. Billiar, K.L. and M.S. Sacks, *Biaxial mechanical properties of the native and glutaraldehyde-treated aortic valve cusp: Part II--A structural constitutive model.* J Biomech Eng, 2000. **122**(4): p. 327-35.

43. Talman, E.A. and D.R. Boughner, *Internal shear properties of fresh porcine aortic valve cusps: implications for normal valve function.* J Heart Valve Dis, 1996. **5**(2): p. 152-9.

44. Billiar, K.L. and M.S. Sacks, *Biaxial mechanical properties of the natural and glutaraldehyde treated aortic valve cusp--Part I: Experimental results.* J Biomech Eng, 2000. **122**(1): p. 23-30.

45. Sacks, M.S. and F.J. Schoen, *Collagen fiber disruption occurs independent of calcification in clinically explanted bioprosthetic heart valves.* J Biomed Mater Res, 2002. **62**(3): p. 359-71.

46. Cimini, M., K.A. Rogers, and D.R. Boughner, *Smoothelin-positive cells in human and porcine semilunar valves.* Histochem Cell Biol, 2003.

47. De Biasi, S. and L. Vitellaro-Zuccarello, *Intrinsic innervation of porcine semilunar heart valves.* Anat Embryol (Berl), 1982. **165**(1): p. 71-9.

48. Marron, K., et al., *Innervation of human atrioventricular and arterial valves.* Circulation, 1996. **94**(3): p. 368-75.

49. Taylor, P.M., S.P. Allen, and M.H. Yacoub, *Phenotypic and functional characterization of interstitial cells from human heart valves, pericardium and skin.* J Heart Valve Dis, 2000. **9**(1): p. 150-8.

50. Manduteanu, I., et al., *Calf cardiac valvular endothelial cells in culture: production of glycosaminoglycans, prostacyclin and fibronectin.* J Mol Cell Cardiol, 1988. **20**(2): p. 103-18.

51. Rabkin, E., et al., *Evolution of cell phenotype and extracellular matrix in tissue-engineered heart valves during in-vitro maturation and in-vivo remodeling.* J Heart Valve Dis, 2002. **11**(3): p. 308-14; discussion 314.

52. Filip, D.A., A. Radu, and M. Simionescu, *Interstitial cells of the heart valves possess characteristics similar to smooth muscle cells.* Circ Res, 1986. **59**(3): p. 310-20.

53. Messier, R.H., Jr., et al., *Dual structural and functional phenotypes of the porcine aortic valve interstitial population: characteristics of the leaflet myofibroblast.* J Surg Res, 1994. **57**(1): p. 1-21.

54. Hafizi, S., et al., *Mitogenic and secretory responses of human valve interstitial cells to vasoactive agents.* J Heart Valve Dis, 2000. **9**(3): p. 454-8.

55. Schneider, P.J. and J.D. Deck, *Tissue and cell renewal in the natural aortic valve of rats: an autoradiographic study.* Cardiovasc Res, 1981. **15**(4): p. 181-9.

56. Lester, W.M., et al., *Bovine mitral valve organ culture: role of interstitial cells in repair of valvular injury.* J Mol Cell Cardiol, 1992. **24**(1): p. 43-53.

57. Li, Q.Y., et al., *Thymosin beta4 regulation, expression and function in aortic valve interstitial cells.* J Heart Valve Dis, 2002. **11**(5): p. 726-35.

58. Jian, B., et al., *Progression of aortic valve stenosis: TGF-beta1 is present in calcified aortic valve cusps and promotes aortic valve interstitial cell calcification via apoptosis.* Ann Thorac Surg, 2003. **75**(2): p. 457-65; discussion 465-6.

59. Xu, J., et al., *Serotonin mechanisms in heart valve disease II: the 5-HT2 receptor and its signaling pathway in aortic valve interstitial cells.* Am J Pathol, 2002. **161**(6): p. 2209-18.

60. Frater, R.W., et al., *Endothelial covering of biological artificial heart valves.* Ann Thorac Surg, 1992. **53**(3): p. 371-2.

61. Lester, W.M., et al., *Interstitial cells from the atrial and ventricular sides of the bovine mitral valve respond differently to denuding endocardial injury.* In Vitro Cell Dev Biol, 1993. **29A**(1): p. 41-50.

62. Siney, L. and M.J. Lewis, *Nitric oxide release from porcine mitral valves.* Cardiovasc Res, 1993. **27**(9): p. 1657-61.

63. Deck, J.D., *Endothelial cell orientation on aortic valve leaflets.* Cardiovasc Res, 1986. **20**(10): p. 760-7.

64. Jaffee, O.C., *The development of the arterial outflow tract in the chick embryo heart.* Anat Rec, 1967. **158**(1): p. 35-42.

65. Poggianti, E., et al., *Aortic valve sclerosis is associated with systemic endothelial dysfunction.* J Am Coll Cardiol, 2003. **41**(1): p. 136-41.

66. Simon, A., et al., *Cardiac valve endothelial cells: relevance in the long-term function of biologic valve prostheses.* J Thorac Cardiovasc Surg, 1998. **116**(4): p. 609-16.

67. Hoekstra, F., et al., *Stimulation of immune-competent cells in vitro by human cardiac valve-derived endothelial cells.* Ann Thorac Surg, 1995. **60**(2 Suppl): p. S131-3; discussion S133-4.

68. Ghaisas, N.K., et al., *Adhesion molecules in nonrheumatic aortic valve disease: endothelial expression, serum levels and effects of valve replacement.* J Am Coll Cardiol, 2000. **36**(7): p. 2257-62.

69. Spies, C., J.R. Madison, and I.J. Schatz, *Infective endocarditis in patients with end-stage renal disease: clinical presentation and outcome.* Arch Intern Med, 2004. **164**(1): p. 71-5.

70. Miro, J.M., A. del Rio, and C.A. Mestres, *Infective endocarditis and cardiac surgery in intravenous drug abusers and HIV-1 infected patients.* Cardiol Clin, 2003. **21**(2): p. 167-84, v-vi.

71. Otto, C.M., *Calcification of bicuspid aortic valves.* Heart, 2002. **88**(4): p. 321-2.

72. Waller, B.F., J. Howard, and S. Fess, *Pathology of aortic valve stenosis and pure aortic regurgitation: a clinical morphologic assessment--Part II.* Clin Cardiol, 1994. **17**(3): p. 150-6.

73. Pigula, F.A., et al., *Repair of tetralogy of Fallot in neonates and young infants.* Circulation, 1999. **100**(19 Suppl): p. II157-61.

74. Tchervenkov, C.I., et al., *Single-stage repair of aortic arch obstruction and associated intracardiac defects with pulmonary homograft patch aortoplasty.* J Thorac Cardiovasc Surg, 1998. **116**(6): p. 897-904.

75. Giampietro, P.F., C. Raggio, and J.G. Davis, *Marfan syndrome: orthopedic and genetic review.* Curr Opin Pediatr, 2002. **14**(1): p. 35-41.

76. Yeowell, H.N. and S.R. Pinnell, *The Ehlers-Danlos syndromes.* Semin Dermatol, 1993. **12**(3): p. 229-40.

77. Schwarze, U., et al., *Rare autosomal recessive cardiac valvular form of Ehlers-Danlos syndrome results from mutations in the COL1A2 gene that activate the nonsense-mediated RNA decay pathway.* Am J Hum Genet, 2004. **74**(5): p. 917-30.

78. Cripe, L., et al., *Bicuspid aortic valve is heritable.* J Am Coll Cardiol, 2004. **44**(1): p. 138-43.

79. Andelfinger, G., et al., *KCNJ2 mutation results in Andersen syndrome with sex-specific cardiac and skeletal muscle phenotypes.* Am J Hum Genet, 2002. **71**(3): p. 663-8.

80. Benson, D.W., et al., *Mutations in the cardiac transcription factor NKX2.5 affect diverse cardiac developmental pathways.* J Clin Invest, 1999. **104**(11): p. 1567-73.

81. Delot, E.C., et al., *BMP signaling is required for septation of the outflow tract of the mammalian heart.* Development, 2003. **130**(1): p. 209-20.

82. de la Pompa, J.L., et al., *Role of the NF-ATc transcription factor in morphogenesis of cardiac valves and septum.* Nature, 1998. **392**(6672): p. 182-6.

83. Dor, Y., et al., *VEGF modulates early heart valve formation.* Anat Rec, 2003. **271A**(1): p. 202-8.

84. Tennstedt, C., et al., *Pathologic correlation of sonographic echogenic foci in the fetal heart.* Prenat Diagn, 2000. **20**(4): p. 287-92.

85. Francioli, P., *Antibiotic treatment of streptococcal and enterococcal endocarditis: an overview.* Eur Heart J, 1995. **16 Suppl B**: p. 75-9.

86. Nord, C.E. and A. Heimdahl, *Cardiovascular infections: bacterial endocarditis of oral origin. Pathogenesis and prophylaxis.* J Clin Periodontol, 1990. **17**(7 (Pt 2)): p. 494-6.

87. da Silva, N.A. and B.A. Pereira, *Acute rheumatic fever. Still a challenge.* Rheum Dis Clin North Am, 1997. **23**(3): p. 545-68.

88. Heper, G. and Y. Yorukoglu, *Clinical, bacteriologic and echocardiographic evaluation of infective endocarditis in Ankara, Turkey.* Angiology, 2002. **53**(2): p. 191-7.

89. Adler, Y., et al., *Mitral annulus calcification--a window to diffuse atherosclerosis of the vascular system.* Atherosclerosis, 2001. **155**(1): p. 1-8.

90. Wierzbicki, A. and C. Shetty, *Aortic stenosis: an atherosclerotic disease?* J Heart Valve Dis, 1999. **8**(4): p. 416-23.

91. Cohn, L.H. and V. Birjiniuk, *Therapy of acute aortic regurgitation.* Cardiol Clin, 1991. **9**(2): p. 339-52.

92. Blaszyk, H., A.J. Witkiewicz, and W.D. Edwards, *Acute aortic regurgitation due to spontaneous rupture of a fenestrated cusp: report in a 65-year-old man and review of seven additional cases.* Cardiovasc Pathol, 1999. **8**(4): p. 213-6.

93. Goldsmith, I.R., et al., *Plasma fibrinogen, soluble P-selectin, and von Willebrand factor in aortic valve disease: evidence for abnormal haemorheology, platelet activation, and endothelial dysfunction.* Heart, 2000. **83**(5): p. 577-8.

94. Jian, B., et al., *Serotonin mechanisms in heart valve disease I: serotonin-induced up-regulation of transforming growth factor-beta1 via G-protein signal transduction in aortic valve interstitial cells.* Am J Pathol, 2002. **161**(6): p. 2111-21.

95. Fitzgerald, L.W., et al., *Possible role of valvular serotonin 5-HT(2B) receptors in the cardiopathy associated with fenfluramine.* Mol Pharmacol, 2000. **57**(1): p. 75-81.

96. Rabkin, E., et al., *Activated interstitial myofibroblasts express catabolic enzymes and mediate matrix remodeling in myxomatous heart valves.* Circulation, 2001. **104**(21): p. 2525-32.

97. Decker, R.S. and J.T. Dingle, *Cardiac catabolic factors: the degradation of heart valve intercellular matrix.* Science, 1982. **215**(4535): p. 987-9.

98. Schoen, F.J. and R.J. Levy, *Founder's Award, 25th Annual Meeting of the Society for Biomaterials, perspectives. Providence, RI, April 28-May 2, 1999. Tissue heart valves: current challenges and future research perspectives.* J Biomed Mater Res, 1999. **47**(4): p. 439-65.

99. Ishii, K., et al., *Natural history and left ventricular response in chronic aortic regurgitation.* Am J Cardiol, 1996. **78**(3): p. 357-61.

100. David, T.E., C.M. Feindel, and J. Bos, *Repair of the aortic valve in patients with aortic insufficiency and aortic root aneurysm.* J Thorac Cardiovasc Surg, 1995. **109**(2): p. 345-51; discussion 351-2.

101. Sarsam, M.A. and M. Yacoub, *Remodeling of the aortic valve anulus.* J Thorac Cardiovasc Surg, 1993. **105**(3): p. 435-8.

102. David, T.E., et al., *Aortic valve-sparing operations in patients with aneurysms of the aortic root or ascending aorta.* Ann Thorac Surg, 2002. **74**(5): p. S1758-61; discussion S1792-9.

103. Kallenbach, K., et al., *Valve-sparing aortic root reconstruction in patients with significant aortic insufficiency.* Ann Thorac Surg, 2002. **74**(5): p. S1765-8; discussion S1792-9.

104. Harken, D.E., et al., *Aortic valve replacement with a caged ball valve.* Am J Cardiol, 1962. **9**: p. 292-9.

105. Gott, V.L., D.E. Alejo, and D.E. Cameron, *Mechanical heart valves: 50 years of evolution.* Ann Thorac Surg, 2003. **76**(6): p. S2230-9.

106. Yoganathan, A.P., et al., *Advances in prosthetic heart valves: fluid mechanics of aortic valve designs.* J Biomater Appl, 1988. **2**(4): p. 579-614.

107. Carpentier, A., et al., *Six-year follow-up of glutaraldehyde-preserved heterografts. With particular reference to the treatment of congenital valve malformations.* J Thorac Cardiovasc Surg, 1974. **68**(5): p. 771-82.

108. O'Brien, M.F., et al., *Allograft aortic valve replacement: long-term follow-up.* Ann Thorac Surg, 1995. **60**(2 Suppl): p. S65-70.

109. Ross, D.N., *Homograft replacement of the aortic valve.* Lancet, 1962. **2**: p. 487.

110. Oury, J.H., et al., *The Ross Procedure: current registry results.* Ann Thorac Surg, 1998. **66**(6 Suppl): p. S162-5.

111. Vlessis, A.A., et al., *Risk, diagnosis and management of prosthetic valve endocarditis: a review.* J Heart Valve Dis, 1997. **6**(5): p. 443-65.

112. Stock, U.A., et al., *Tissue engineering of heart valves -- current aspects.* Thorac Cardiovasc Surg, 2002. **50**(3): p. 184-93.

113. Langer, R. and J.P. Vacanti, *Tissue engineering.* Science, 1993. **260**(5110): p. 920-6.

114. Griffith, L.G. and G. Naughton, *Tissue engineering--current challenges and expanding opportunities.* Science, 2002. **295**(5557): p. 1009-14.

115. Case, N.D., et al., *Bone formation on tissue-engineered cartilage constructs in vivo: effects of chondrocyte viability and mechanical loading.* Tissue Eng, 2003. **9**(4): p. 587-96.

116. Sambanis, A., et al., *Towards the development of a bioartificial pancreas: immunoisolation and NMR monitoring of mouse insulinomas.* Cytotechnology, 1994. **15**(1-3): p. 351-63.

117. Bellamkonda, R., et al., *Hydrogel-based three-dimensional matrix for neural cells.* J Biomed Mater Res, 1995. **29**(5): p. 663-71.

118. Niklason, L.E., et al., *Functional arteries grown in vitro.* Science, 1999. **284**(5413): p. 489-93.

119. Flanagan, T.C. and A. Pandit, *Living artificial heart valve alternatives: a review.* Eur Cell Mater, 2003. **6**: p. 28-45; discussion 45.

120. Sodian, R., et al., *Fabrication of a trileaflet heart valve scaffold from a polyhydroxyalkanoate biopolyester for use in tissue engineering.* Tissue Eng, 2000. **6**(2): p. 183-8.

121. Shinoka, T., et al., *Tissue engineering heart valves: valve leaflet replacement study in a lamb model.* Ann Thorac Surg, 1995. **60**(6 Suppl): p. S513-6.

122. Hoerstrup, S.P., et al., *Functional living trileaflet heart valves grown in vitro.* Circulation, 2000. **102**(19 Suppl 3): p. III44-9.

123. Gunatillake, P.A. and R. Adhikari, *Biodegradable synthetic polymers for tissue engineering.* Eur Cell Mater, 2003. **5**: p. 1-16; discussion 16.

124. Dohmen, P.M., et al., *Ross operation with a tissue-engineered heart valve.* Ann Thorac Surg, 2002. **74**(5): p. 1438-42.

125. Bader, A., et al., *Tissue engineering of heart valves--human endothelial cell seeding of detergent acellularized porcine valves.* Eur J Cardiothorac Surg, 1998. **14**(3): p. 279-84.

126. O'Brien, M.F., et al., *The SynerGraft valve: a new acellular (nonglutaraldehyde-fixed) tissue heart valve for autologous recellularization first experimental studies before clinical implantation.* Semin Thorac Cardiovasc Surg, 1999. **11**(4 Suppl 1): p. 194-200.

127. Sievers, H.H., et al., *Decellularized pulmonary homograft (SynerGraft) for reconstruction of the right ventricular outflow tract: first clinical experience.* Z Kardiol, 2003. **92**(1): p. 53-9.

128. Simon, P., et al., *Early failure of the tissue engineered porcine heart valve SYNERGRAFT in pediatric patients.* Eur J Cardiothorac Surg, 2003. **23**(6): p. 1002-6; discussion 1006.

129. Seliktar, D., et al., *Dynamic mechanical conditioning of collagen-gel blood vessel constructs induces remodeling in vitro.* Ann Biomed Eng, 2000. **28**(4): p. 351-62.

130. Jockenhoevel, S., et al., *Tissue engineering: complete autologous valve conduit--a new moulding technique.* Thorac Cardiovasc Surg, 2001. **49**(5): p. 287-90.

131. Badylak, S.F., *Xenogeneic extracellular matrix as a scaffold for tissue reconstruction.* Transpl Immunol, 2004. **12**(3-4): p. 367-77.

132. Seliktar, D., R.M. Nerem, and Z.S. Galis, *The role of matrix metalloproteinase-2 in the remodeling of cell-seeded vascular constructs subjected to cyclic strain.* Ann Biomed Eng, 2001. **29**(11): p. 923-34.

133. L'Heureux, N., et al., *A completely biological tissue-engineered human blood vessel.* Faseb J, 1998. **12**(1): p. 47-56.

134. Shi, Y., A. Ramamurthi, and I. Vesely, *Towards tissue engineering of a composite aortic valve.* Biomed Sci Instrum, 2002. **38**: p. 35-40.

135. Shinoka, T., et al., *Tissue-engineered heart valve leaflets: does cell origin affect outcome?* Circulation, 1997. **96**(9 Suppl): p. II-102-7.

136. Shinoka, T., et al., *Tissue-engineered heart valves. Autologous valve leaflet replacement study in a lamb model.* Circulation, 1996. **94**(9 Suppl): p. II164-8.

137. Maish, M.S., et al., *Tricuspid valve biopsy: a potential source of cardiac myofibroblast cells for tissue-engineered cardiac valves.* J Heart Valve Dis, 2003. **12**(2): p. 264-9.

138. Perry, T.E., et al., *Thoracic Surgery Directors Association Award. Bone marrow as a cell source for tissue engineering heart valves.* Ann Thorac Surg, 2003. **75**(3): p. 761-7; discussion 767.

139. Demer, L.L., Y. Tintut, and F. Parhami, *Novel mechanisms in accelerated vascular calcification in renal disease patients.* Curr Opin Nephrol Hypertens, 2002. **11**(4): p. 437-43.

140. Mauney, J.R., et al., *Mechanical stimulation promotes osteogenic differentiation of human bone marrow stromal cells on 3-D partially demineralized bone scaffolds in vitro.* Calcif Tissue Int, 2004. **74**(5): p. 458-68.

141. Hoerstrup, S.P., et al., *New pulsatile bioreactor for in vitro formation of tissue engineered heart valves.* Tissue Eng, 2000. **6**(1): p. 75-9.

142. Dumont, K., et al., *Design of a new pulsatile bioreactor for tissue engineered aortic heart valve formation.* Artif Organs, 2002. **26**(8): p. 710-4.

143. Zeltinger, J., et al., *Development and characterization of tissue-engineered aortic valves.* Tissue Eng, 2001. **7**(1): p. 9-22.

144. Sodian, R., et al., *Tissue engineering of heart valves: in vitro experiences.* Ann Thorac Surg, 2000. **70**(1): p. 140-4.

145. Engelmayr, G.C., et al., *A novel bioreactor for the dynamic flexural stimulation of tissue engineered heart valve biomaterials.* Biomaterials, 2003. **24**(14): p. 2523-32.

146. Ziegler, T., R.W. Alexander, and R.M. Nerem, *An endothelial cell-smooth muscle cell co-culture model for use in the investigation of flow effects on vascular biology.* Ann Biomed Eng, 1995. **23**(3): p. 216-25.

147. Stegemann, J.P. and R.M. Nerem, *Phenotype modulation in vascular tissue engineering using biochemical and mechanical stimulation.* Ann Biomed Eng, 2003. **31**(4): p. 391-402.

148. Villaschi, S. and R.F. Nicosia, *Paracrine interactions between fibroblasts and endothelial cells in a serum-free coculture model. Modulation of angiogenesis and collagen gel contraction.* Lab Invest, 1994. **71**(2): p. 291-9.

149. Kladakis, S.M. and R.M. Nerem, *Endothelial cell monolayer formation: effect of substrate and fluid shear stress.* Endothelium, 2004. **11**(1): p. 29-44.

CHAPTER 2

ISOLATION AND CHARACTERIZATION OF PORCINE AORTIC VALVE CELLS

One of the challenges to in vitro experimentation is acquiring reliable and homogeneous cell populations. While cells isolated from animal tissues are assumed to be "normal" due to the fact that they were isolated from healthy animals. Cells isolated from human valves may be problematic because some of the other valves were diseased, the heart was removed for transplant, or the tissue was required at autopsy. Rabkin and colleagues analyzed the expression of various markers of normal and diseased (myxomatous) valves[1]. They found dramatic increases in the expression of contractile markers and proteases. Nevertheless, these sources are probably the only ones available for research purposes. In addition, to minimize variability between cell batches, it is important to obtain cells from the same population of species. Since valvular tissue is not sacrificial (as for a peripheral blood vessel) in humans, and may be compromised by old age and/or pathology, we focused on manually isolating cells from accessible animal tissues.

There is some heterogeneity between human and other animal valve tissues, mainly associated with the degree of vascularity and hemodynamics. Human aortic valve leaflets are normally avascular, as are porcine and ovine cusps, but bovine leaflets have a number of capillaries through them[2]. The presence of capillaries is generally associated with either diffusion requirements or pathological angiogenesis. Cells can only survive within about 250 μm of a capillary or blood contacting surface. The average thickness of aortic valve leaflets is on the order of 500 μm, but somewhat thicker at the

attachment region. Thicker leaflets tend to have some capillaries, mainly near the basal third of the leaflet. Pig heart circulation mechanics are most similar to humans, followed closely by sheep and dog. Additionally, the porcine aortic valve differs from the human valve only in the existence of a small muscle shelf under one of the leaflets, which has been attributed to the fact that pigs are quadrupeds. For these reasons, we decided to use porcine aortic valve tissue for cell isolation.

2.1: Valvular Endothelial Cell Isolation and Characterization

Isolation. Isolation of endothelial cells is by no means a trivial procedure. These cells are very fragile once removed from physiological conditions, and any disruption of the underlying matrix often liberates contaminating cells from the rest of the tissue. There are only a few reports of successful isolation and culture of valvular endothelial cells in the literature, the specifics of which are summarized in Table 2-1. Each technique involves either enzymatic digestion of the underlying basal matrix, or

Table 2-1: Literature reported protocols of valvular endothelial cell isolation.

Tissue	Storage Medium	Dissociation Agent	Dissociation Technique	Purification Technique	Culture Medium	Ref.
Porcine hearts with ascending aorta	EBSS w/ 100 U/ml Penicillin, 20 μg/ml Gentamicin	Collagenase (0.6 mg/ml) 5 mins. at 37C	Gently hand shaken in dish w/media	Plated in 96 well plates coated w/FN	M199, 10% FBS, 100 U/ml Pen. 20 μg/ml Gen.	[3]
Young calf hearts	PBS with 300 U/ml Penicillin-Streptomycin	3 mM EDTA w/o Calcium for 20 mins. at 37C	Centrifuged at 120g for 10 mins.	Plated onto dishes. EC colonies selected manually	DMEM or M199, 20% FCS, 100 U/ml Pen-Strep, supplemented with amino acids.	[4]
Ovine and Human pulmonary valves	Endothelial basal medium, 5% FBS, PSF, 2 mM L-glutamine, 100 μg/ml gentamicin	0.2% collagenase A, 5 mins. at 37C	Centrifugation at 200g	Ulex europeas I-coated Dynabeads, followed by clonal expansion	EBM, 10% FBS, 1XGPS, 2 ng/ml bFGF	[5]

chemical dissociation of the endothelial adhesive bonds. The resulting liberated cells are purified through additional processing, and cultured in vitro. The objective of these studies was to develop a method to isolate a pure population of endothelial cells from valvular tissue that would not require manual selection or clonal expansion. These techniques, while often necessary, compromise the ability to assume that the derived cells are representative of the whole population and reduce the number of passages obtainable in vitro prior to senescence or phenotype shift.

Preliminary isolation experiments were qualitatively assessed for three parameters: numbers of cells isolated, purity of the isolation, and propensity to become contaminated. It was determined early on that hearts needed to be thoroughly washed, transported, and stored in fresh sterile PBS on ice. The use of antibiotics or antifungal agents at this stage was probably killing the endothelium as well as any bacteria. The isolation protocols attempted and their results are briefly summarized in Table 2-2. During this process, several steps in these procedures were found to be optimal and therefore were made common to all dissociation techniques attempted. Prior to cell isolation serial rinses of the tissue in PBS with decreasing concentrations of Antibiotic/Antimycotic solution (5%, 2%, and 1%) were used to clean the tissue of any

Table 2-2: Results of preliminary valvular endothelial cell isolation protocols.

Dissociation Agent	Dissociation Technique	Cell Collection	Cell Quantity	Cell Purity	Contamination
EDTA (3 mM) without $CaCl_2$	5, 20, 60 min. before $CaCl_2$ addition	20, 60, 120 min. before collection	-	+/-	+++
EDTA (6 mM) without $CaCl_2$	5, 20, 60 min. before $CaCl_2$ addition	20, 60, 120 min. before collection	+/-	+	+++
Trypsin-EDTA (0.5 g/L	5, 10, 15 min. before deactivation	Medium collected immediately	+	+	++
Collagenase II (300 U/ml)	5, 10, 30 min. before deactivation	Medium collected immediately	-,+,++	-,++,+	+
Collagenase II (600 U/ml)	5, 10, 30 min. before deactivation	Medium collected immediately	+,++,+++	++,++,-	-

residual bacteria and/or blood material. Cell scrapers (Fisher), lifters (Corning), and sterile cotton swabs (Puritan) were evaluated for their ability to dislodge cells, and it was concluded that the cotton swabs were superior in this regard. Any resulting cell solutions were centrifuged (200 g, 5 mins.) into a pellet, which was then plated. Different base mediums were also assayed for cell growth, including M199 (Invitrogen), MCDB131 (VWR), and DMEM (Invitrogen). DMEM was found to be optimal for valvular cell growth when supplemented with 10% Fetal Bovine Serum (FBS, Hyclone), 1% Penicillin-Streptomycin (Hyclone), and 1% L-Glutamine (Mediatech), and this formulation was used as the standard medium for all the valvular cell culture presented.

The results of these experiments showed that EDTA (or Trypsin-EDTA) incubation for up to 60 minutes was unsuccessful at dislodging cells, and it is possible that cells were being killed during the process. Collagenase digestion was more successful at removing cells, but contaminating interstitial cells became a problem once the cells were adhered. From an evaluation of all the techniques, it was determined that a 10 minute digestion in 600 U/ml collagenase was best at retrieving a usable number of pure valvular endothelial cells.

The optimal protocol used in isolating valvular endothelial cells is summarized below and also included in detail in the Appendix. Intact porcine hearts or isolated aortic roots were obtained at a local slaughterhouse (Holifield farms, Porterdale, GA) and immediately placed in cold sterile phosphate buffered saline (PBS, Invitrogen). The aortic valve was excised within 12 hours post-mortem, and the leaflets were trimmed to 1/3 of their length away from their apposition to the base of the aortic root (Figure 2-1). Leaflets were then rinsed several times in a series of solutions containing gradually reduced amounts of antibiotic-antimycotic (A-A, Invitrogen, 5%, 3%, 1%, 10 min. each). The leaflets were moderately vortexed before each solution transfer. The leaflets were then placed in 30 mm dishes (3 leaflets per dish), and incubated with a collagenase II

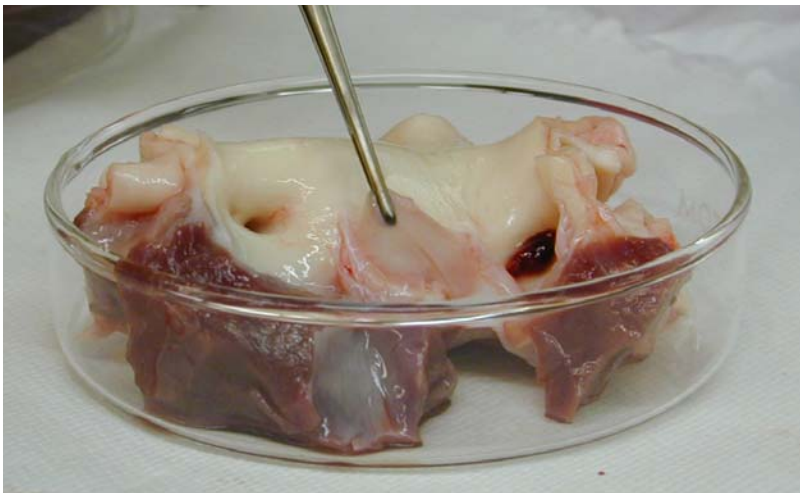

Figure 2-1: Porcine aortic valve leaflet isolation.

solution (Worthington, 600 U/mL in serum free medium) for approximately 10 minutes. The surfaces of the leaflets were then gently scraped with sterile cotton swabs, and the resulting cell solution pelleted in a bucket centrifuge at 200 g's for 5 minutes. The pelleted cells were then plated onto tissue culture flasks pre-coated with collagen type I (Becton-Dickenson, Rat tail, 50 μg/mL). Cells were cultured with Dulbecco's Modified Eagle's Medium (DMEM, Invitrogen) supplemented with 10% fetal bovine serum (FBS, Hyclone), 1% penicillin-streptomycin (Hyclone), and 1% L-Glutamine (Mediatech) at 37°C and 5% CO_2. Primary culture media was also briefly supplemented with 50 units/mL Heparin (Sigma) and 0.1% Mycoplasma Removal Agent (MRA, ICN). Medium was changed every 48 hours, and cells were split 1:3 upon confluence. Porcine aortic valve endothelial cells (PAVECs) required an adhesive protein for attachment and growth, unlike aortic endothelial cells (PAECs). Gelatin, collagen I, and fibronectin were all supportive of cell growth. The aforementioned procedure was also successful at isolating PAECs, and it was possible to isolate both PAVECs and PAECs from the same animal.

Characterization. Porcine aortic valve endothelial cells (PAVECs) exhibit a typical endothelial morphology (Figure 2-2). Cells are generally cobblestone with contact inhibited growth. Generally cells became confluent in about 4 days of culture, and could be cultured up to 8 passages using the aforementioned isolation technique. Valvular endothelial cell phenotype was assessed initially through typical endothelial marker expression, morphology, and functional characteristics. Several published reports have identified some aspects of valvular endothelial cell phenotype, which are summarized in Table 2-3. While most of these markers are common to many endothelial cell sources, it was unclear if there were any differences in the expression between the cell types. A preliminary panel of assays was then used to determine and compare endothelial phenotype between valvular and vascular endothelial cells. Endothelial cells from the porcine ascending aorta (PAECs) were similarly isolated from

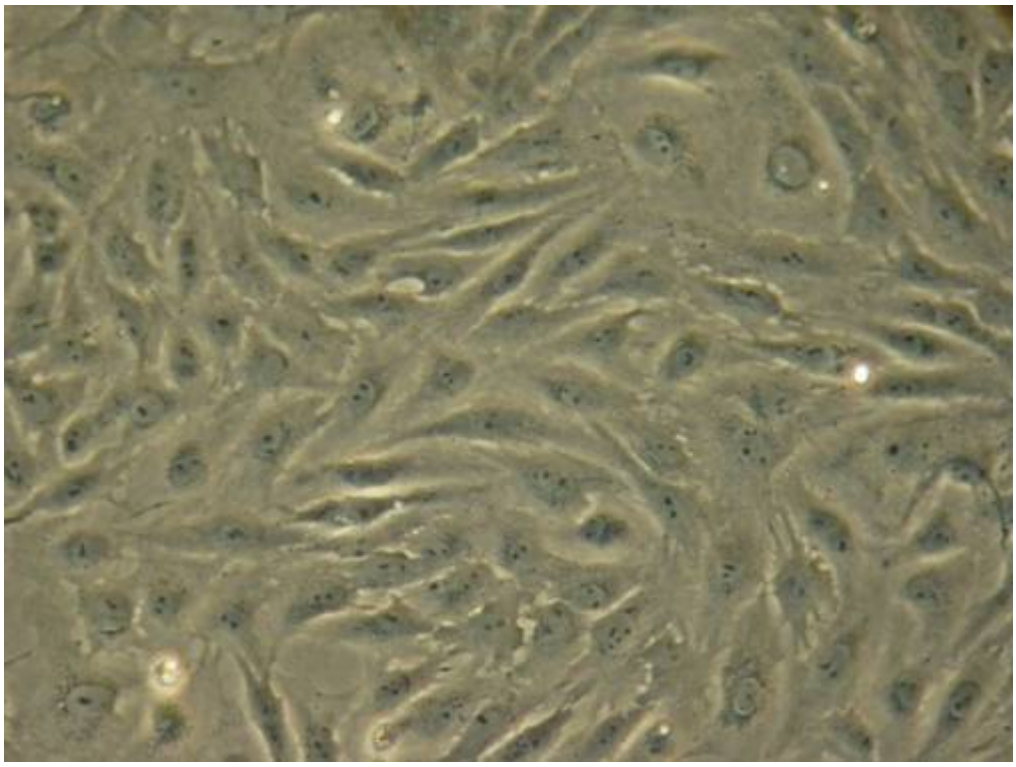

Figure 2-2: Porcine aortic valve endothelial cells in culture.

Table 2-3: Valvular endothelial cell characterization.

Cell Surface Proteins	Expression	Animal	Valve	Passage	Notes	Ref.
Griffonia Simplicifolia lectin	+	Rat	All			[6]
Panel of CD Markers	Varied	Human	Aortic	1	Compared to Aortic Endothelium, Explanted valves	[7]
PECAM (CD31)	+	Human	Pulmonary	Unkn.		[8]
Fibronectin surface labeling	-	Porcine	A/M/CoA	4 to 7	Only artery in vivo	[3]
Tight Junctions	+	Bovine	Mitral	4		[4]
Gap Junctions	+	Bovine	Mitral	4		[4]

Cytoplasmic Proteins	Expression	Animal	Valve	Passage	Notes	Ref.
Weibel-Palade bodies	Rare	Porcine	Aortic	3 to 4		[3]
von Willebrand Factor	+	Bovine	Mitral	Tissue	called endocardial	[9]
von Willebrand Factor	-	Porcine	Aortic	3 to 4		[3]
von Willebrand Factor	+	Human	Pulmonary	Unkn.		[8]
von Willebrand Factor	+	Bovine	Mitral	4		[9]
Factor VIII Antigen	-	Human	Aortic	1	Compared to Aortic Endothelium, Explanted valves	[7]

Stimulus - Response	Conc. [M]	Animal	Valve	Passage	Notes	Ref.
Acetylcholine - [Ca]i increase	2.00E-06	Rabbit	A/P	Leaflets	averaged to cells/camera field	[10]
Bradykinin - [Ca]i increase	2.00E-07	Rabbit	A/P	Leaflets	averaged to cells/camera field	[10]
Histamine - [Ca]i increase	1.00E-05	Rabbit	A/P	Leaflets	averaged to cells/camera field	[10]
ATP - [Ca]i increase	1.00E-05	Rabbit	A/P	Leaflets	averaged to cells/camera field	[10]

Table 2.3 continued:

Matrix/Factor Secretion	Expression	Animal	Valve	Passage	Notes	Ref.
Fibronectin	+	Bovine	Mitral	4		[4]
Fibronectin	-	Porcine	Aortic	3 to 4	Aortic EC 10 fold more	[3]
Gelatin-bound protein	+/-	Porcine	Aortic	3 to 4	Aortic EC 10-30 fold more	[3]
Prostacyclin	+	Bovine	Mitral	4	In medium	[4]
Angiotensin Converting Enzyme	+	Porcine	Aortic	3 to 4	aortic 0.034	[3]
Chondroitin Sulfate	+	Bovine	Mitral	4	In medium	[4]
Hyaluronic Acid	+	Bovine	Mitral	4	In cells and medium	[4]
Heparin	+	Bovine	Mitral	4	In cells	[4]
Heparin Sulfate	+	Bovine	Mitral	4	In cells	[4]

the same pig population and used as the control vascular endothelial cell for these studies. Endothelial phenotype was assessed through indirect immunofluorescent staining and acetylated LDL uptake (a-LDL). Endothelial cell phenotype is generally determined by aLDL uptake, positive von Willebrand factor (vWF) expression, and negative α-smooth muscle actin (α-SMA) expression. For a-LDL comparisons, PAECs and PAVECs were incubated with 10 mg/mL a-LDL (Biomedical Technologies #BT-902) in serum-free media for 4 hours. A detailed protocol for immunofluorescent staining is given in the appendix. For these experiments, PAVECs and PAECs were seeded onto coverslips coated with collagen I and grown to confluence, after which they were rinsed in PBS and fixed in 3.7% paraformaldehyde (Tousimis). Cells were then permeablized with 0.1% Triton X-100 (Sigma), and blocked with 1% neonatal goat serum (Sigma) for one hour. The coverslips were then incubated with either anti-α-smooth muscle actin

(Sigma #F3777, 1:100) or anti-von Willebrand factor (vWF, Sigma #F3520, 1:100) for one hour. These cells were then incubated with a fluorescently labeled secondary antibody for one hour. The coverslips were then flipped onto glass slides and sealed. The samples were imaged using laser confocal microscopy for qualitative expression of the aforementioned markers. Figure 2-3 shows the expression comparison between the PAECs and PAVECs. Both of these endothelial cell types were similarly positive for a-LDL uptake and von Willebrand Factor expression, but negative for α-Smooth Muscle Actin. This compared favorably with previous published reports, and led us to conclude that these cells were in fact endothelial cells. This degree of expression was maintained at least to passage 8. Later passage cells were not assayed for expression, because primary culture endothelial cells tended to enter senescent cell death at this point, and are no longer useful for any experiments.

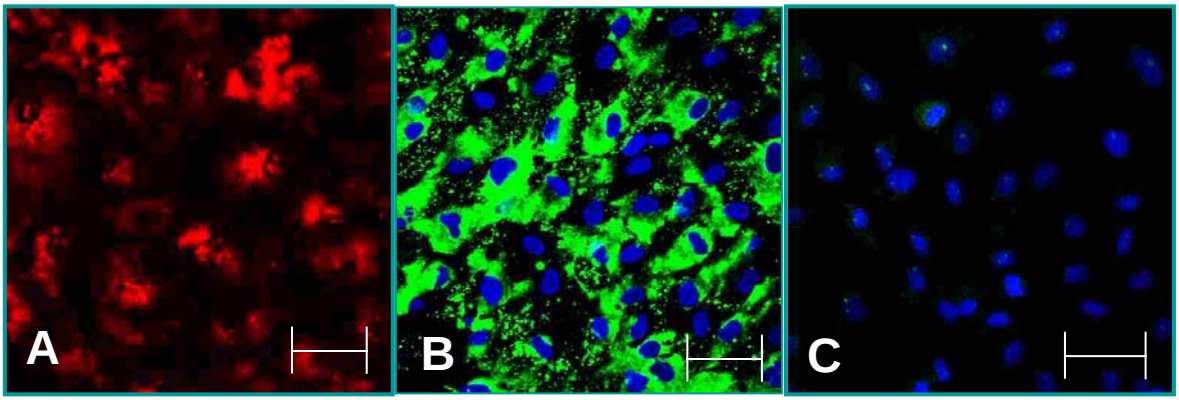

Figure 2-3. Aortic valve endothelial cell characterization. A: acetylated-LDL uptake. B: von Willebrand Factor expression. C: α-smooth muscle actin expression. Scale bar = 50 μm.

Endothelial Isolation from Different Sides of the Leaflet. The aforementioned isolation technique pools valvular endothelial cells isolated from both sides of the leaflet. To isolate cells from one side of the leaflet at a time, a system was developed to confine the collagenase digestion to a single surface, shown in Figure 2-4. It consists of a 150

mm glass dish with four smaller (60 mm) dishes inside, all lined with foil. Paraffin beads were placed inside the dishes, the outside dish covered, and the ensemble autoclaved. Once all of the paraffin was melted, the dish ensemble was allowed to cool on a flat surface. This created a thin layer that could support needle punctures. In this way, single sides of the leaflets could be held open by immobilizing them with sterile needles. Collagenase was then applied to the exposed surface using the same protocol described previously, with the process repeated to the other surface. Endothelial cell isolation from each side of the leaflet was successful using this system.

Figure 2-4: Device to isolate endothelial cells from both sides of an aortic valve leaflet.

2.2: Valvular Interstitial Cell Isolation and Characterization

Isolation. All of the cells underneath the surface of the leaflet are classified as interstitial cells, and they can therefore be easily isolated once the endothelial cells have been removed. Several reports of interstitial cell isolation exist in the literature, and the results are summarized in Table 2-4. These methods were basically divided into two categories: explant and digestion. Explant methods involve mincing the tissue into tiny pieces, and adhering them to a culture substrate. Cells then grow out of these tissue pieces over time. The tissue pieces are then removed, leaving just the cells to grow. The digestion method involves incubating the tissue in enzymes which degrade the principal matrix components, and the cells fall out of the matrix into solution. The resulting cell suspensions can then be plated normally. While both methods are equally effective at retrieving cells, some researchers have pointed out that explant methods may select for certain phenotypes. Migratory and chemotactic cells may move out of the tissue more abundantly than other cells, thus enriching the resulting cell population with those cells. Some researchers have found that there “may” be two types of valvular interstitial cells, denoted as “cuboidal” and “spindle-shaped”[11]. Cuboidal cells appear as contact inhibited monolayers, while spindle-shaped cells are elongated, have prominent stress fibers, and form multicellular layers. These classifications are given based on in vitro culture, however, and only appeared after several passages. It is possible that the “cuboidal” cells could be endothelial-like cells, although the cells did not take up acetylated-LDL to the same degree as aortic endothelial cells. Additionally, these interstitial cells were isolated using an explant technique, which selects for migratory cells, and may enrich for a certain cell phenotype that may otherwise not be noticed.

Because of the potential problems associated with explant mediated cell isolation, collagenase digestion was used to retrieve interstitial cells. The isolation protocol is briefly summarized below and is included in the Appendix. The protocol was designed so that interstitial cells could be isolated immediately following endothelial cell removal. Once the endothelium was removed, the remaining portions of the leaflets were then incubated for 24 hours in culture medium (as described previously) supplemented with 3% ABAM at 37°C under continuous gentle shaking. Cultures that were negative for any bacterial contamination were then digested overnight (15-18 hrs) in fresh collagenase (600 U/ml) at 37°C again under gentle shaking. The resulting cell suspension was pelleted in a bucket centrifuge (200 g, 5 mis.), and plated onto tissue culture treated flasks. The cells were fed the standard culture medium, which was changed every 48 hours, and split 1:3 upon confluence.

Valvular Interstitial Cell Characterization. Valvular interstitial cells grow and exhibit similar morphology to other myofibroblast cells: spindle shaped cells that are not

Table 2-4: Literature reports of valvular interstitial cell isolation and culture.

Tissue	Storage Medium	Isolation Method	Cell collection	Purification Technique	Culture Medium	Ref.
Porcine aortic valve	EBSS w/ 100 U/ml penicillin, 20 μg/ml gentamicin	Collagenase digestion for 60 min at 37°C	Vigorous vortexing for 2 min.	96 well plates, observed morphology	M199, 10% FBS, 100 U/ml Pen. 20 μg/ml Gen.	[12]
Porcine anterior mitral leaflet (middle third)	PBS w/o Calcium	Explant migration 4x5 mm pieces	Trypsin-EDTA collection at 3 weeks	Scraping of surfaces of leaflet	M199, 10% FBS, 100 U/ml Pen-Strep., 0.3 mg/L L-glutamine, 20 μg/ml amphotericin B.	[13]
Mouse, rat, and rabbit valves	Unknown	Explant migration	Trypsinization after 3 weeks	None	DMEM, 10-15% FBS	[14]

contact inhibited (Figure 2-5). Several studies have isolated interstitial cells from valves and analyzed phenotypic marker expression, agonist response, and matrix secretion during in vitro culture. The results of these studies are summarized in Table 2-5. Generally, valvular interstitial cells express markers similar to both smooth muscle cells and fibroblasts. Interstitial cells respond to contractile agents to a similar degree as smooth muscle cells, express some immature contractile cytoskeletal proteins, but also secrete matrix proteins. Taylor and colleagues compared the expression level of smooth muscle and fibroblast markers between different human valves, pericardium, and dermis[15]. They showed that a-smooth muscle actin expression was most prevalent in aortic valve interstitial cells, and least in dermal fibroblasts, whereas fibroblast surface antigen expression was consistent across cell types. There were some differences between valves, which could be associated with several factors, most prominently differences in hemodynamic environment and tissue mechanics. It appears that no one cell type studied could effectively mimic the expression trends of valvular interstitial cells.

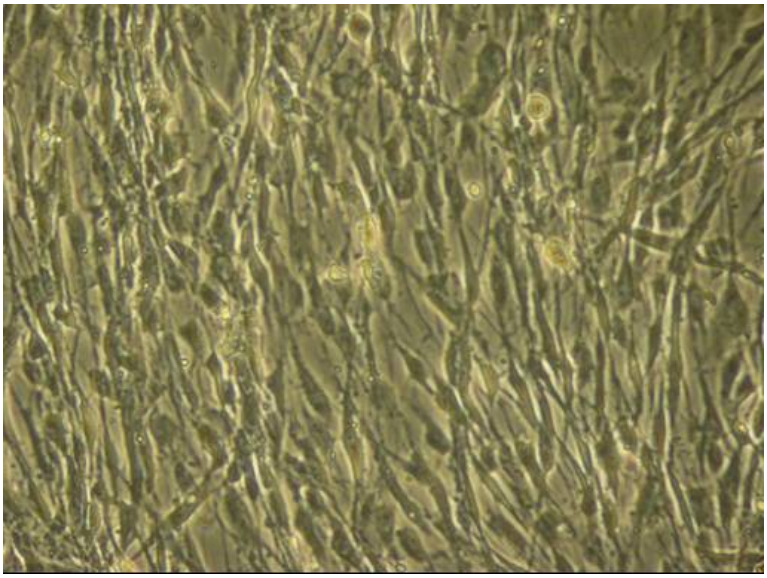

Figure 2-5: Porcine aortic valve interstitial cells in culture.

Table 2.5: Valvular interstitial cell characterization.

Cell Surface Markers	Expression	Species	Valve	Passage	Notes	Ref.
Griffonia simplicifolia lectin	-	Rat	All	Unkn.	Rat heart endo. Positive	[6]
PECAM (CD31)	-	Pig	Aortic	Tissue	Porcine aortic valve endothelial cells positive	[5]
Adherens junctions	+	Pig	Mitral	up to 22		[13]
Gap junctions	+/-	Pig	Mitral	up to 22		[13]
Basal lamina	Incomplete	Pig	Mitral	up to 22		[13]

Cytoskeletal Markers	Expression	Species	Valve	Passage	Notes	Ref.
Vimentin	+	Pig	Aortic	1 to 3	Not concentrated in any portion of the leaflet in vivo	[16]
Vimentin	+/-	Human	Mitral	Tissue	Myxomatous valves more positive	[1]
Desmin	+/-	Pig	Aortic	1 to 3		[16]
Desmin	-	Rat	All	Unkn.		[6]
Myosin light chain	+/-	Pig	Aortic	1 to 3		[16]
α-Smooth Muscle Actin	+ 78 +/- 28%	Human	Aortic	"Early"	lesser for other valves (50-60%)	[15]
α-Smooth muscle actin positive	+	Cow	Mitral	Tissue	Stronger for wound	[17]
α-Smooth muscle actin	+/-	Human	Mitral	Tissue	At ventricularis subendothelium	[1]
SM1	+/-	Human	Mitral	Tissue	At ventricularis subendothelium	[1]
SM2	+/-	Human	Mitral	Tissue	At ventricularis subendothelium	[1]

Stimulus-Response	Conc. (M)	Species	Valve	Passage	Notes	Ref.
Epinephrine – Contraction	1.00E-06	Pig	Aortic	1 to 3	PASMC also responded to this magnitude	[16]
Bradykinin – Contraction	3.20E-07	Pig	Aortic	1 to 3	PASMC also responded to this magnitude	[16]
Angiotensin II – Contraction	3.20E-07	Pig	Aortic	1 to 3	PASMC also responded to this magnitude	[16]
Carbachol – Contraction	1.10E-04	Pig	Aortic	1 to 3	PASMC also responded to this magnitude	[16]
Isoproterenol – Contraction	1.10E-04	Pig	Aortic	1 to 3	PASMC also responded to this magnitude	[16]
Potassium Chloride KCl) – Contraction	5.00E-02	Pig	Aortic	1 to 3	PASMC also responded to this magnitude	[16]
Endothelin I – Contraction	5.00E-09	Pig	Aortic	1 to 3	PASMC also responded to this magnitude	[16]
L-Epiniphrine – Contraction	1.00E-06	Rabbit	Various	1 to 2		[14]

Table 2.5 continued:

Matrix/Factor Secretion	Expression	Species	Valve	Passage	Notes	Ref.
Fibronectin	+	Pig	Aortic	1 to 3	Adjacent to IC in vivo	[16]
Chondroitin sulphate	+	Pig	Aortic	1 to 3	Diffuse through matrix in vivo	[16]
Prolyl-4-hydroxylase	+/-	Pig	Aortic	Unkn.	"Spindle" cells only	[12]
Prostacyclin	+	Pig	Aortic	Unkn.	Similar to PAEC secretion	[12]
Angiotensin I	+	Rat	Unkn.	3 to 6		[18]
Angiotensin II	+	Rat	Unkn.	3 to 6		[18]
Collagenases (MMP-1. MMP-13)	+/-	Human	Mitral	In Tissue	3X expression in Myxomatous valves	[1]
Gelatinases (MMP-2, MMP-9)	+/-	Human	Mitral	In Tissue	2X expression in Myxomatous valves	[1]
Cysteine Endoproteases (Cathepsin S, K)	+/-	Human	Mitral	In Tissue	Higher expression in Myxomatous valves	[1]

Porcine aortic valve interstitial cells (PAVICs) were differentiated from PAVECs by opposite expression of the aforementioned cell markers. Figure 2-6 shows that PAVICs are positive for α-smooth muscle actin, but negative for von Willebrand factor or a-LDL uptake. Given that aortic valve leaflets contain only endothelial or interstitial cells, we concluded that this technique isolated pure interstitial cells.

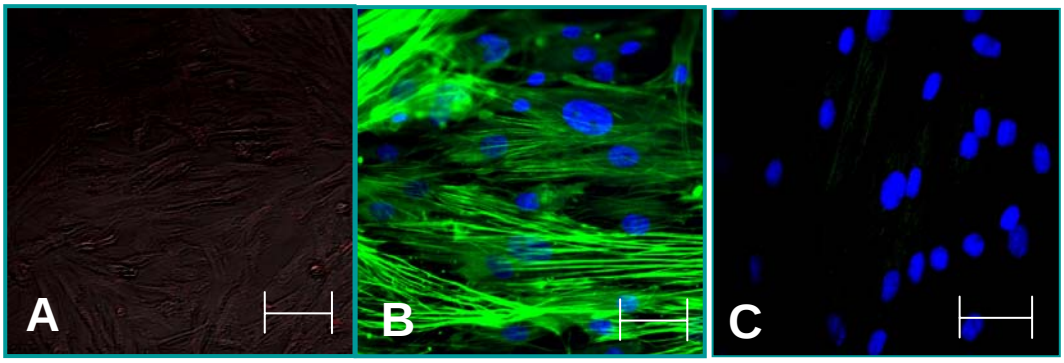

Figure 2-6: Characterization of porcine aortic valve interstitial cells. A: acetylated-LDL uptake. B: von Willebrand Factor expression. C: α-smooth muscle actin expression. Scale bar = 50 μm.

2.3: References

1. Rabkin, E., et al., *Activated interstitial myofibroblasts express catabolic enzymes and mediate matrix remodeling in myxomatous heart valves.* Circulation, 2001. **104**(21): p. 2525-32.

2. Weind, K.L., C.G. Ellis, and D.R. Boughner, *Aortic valve cusp vessel density: relationship with tissue thickness.* J Thorac Cardiovasc Surg, 2002. **123**(2): p. 333-40.

3. Johnson, C.M. and D.N. Fass, *Porcine cardiac valvular endothelial cells in culture. A relative deficiency of fibronectin synthesis in vitro.* Lab Invest, 1983. **49**(5): p. 589-98.

4. Manduteanu, I., et al., *Calf cardiac valvular endothelial cells in culture: production of glycosaminoglycans, prostacyclin and fibronectin.* J Mol Cell Cardiol, 1988. **20**(2): p. 103-18.

5. Paranya, G., et al., *Aortic valve endothelial cells undergo transforming growth factor-beta-mediated and non-transforming growth factor-beta-mediated transdifferentiation in vitro.* Am J Pathol, 2001. **159**(4): p. 1335-43.

6. Katwa, L.C., et al., *Angiotensin converting enzyme and kininase-II-like activities in cultured valvular interstitial cells of the rat heart.* Cardiovasc Res, 1995. **29**(1): p. 57-64.

7. Simon, A., et al., *Cardiac valve endothelial cells: relevance in the long-term function of biologic valve prostheses.* J Thorac Cardiovasc Surg, 1998. **116**(4): p. 609-16.

8. Johnson, E.N., et al., *NFATc1 mediates vascular endothelial growth factor-induced proliferation of human pulmonary valve endothelial cells.* J Biol Chem, 2003. **278**(3): p. 1686-92.

9. Lester, W.M., et al., *Interstitial cells from the atrial and ventricular sides of the bovine mitral valve respond differently to denuding endocardial injury.* In Vitro Cell Dev Biol, 1993. **29A**(1): p. 41-50.

10. Laskey, R.E., D.J. Adams, and C. van Breemen, *Cytosolic [Ca2+] measurements in endothelium of rabbit cardiac valves using imaging fluorescence microscopy.* Am J Physiol, 1994. **266**(5 Pt 2): p. H2130-5.

11. Zacks, S., et al., *Characterization of Cobblestone mitral valve interstitial cells.* Arch Pathol Lab Med, 1991. **115**(8): p. 774-9.

12. Johnson, C.M., M.N. Hanson, and S.C. Helgeson, *Porcine cardiac valvular subendothelial cells in culture: cell isolation and growth characteristics.* J Mol Cell Cardiol, 1987. **19**(12): p. 1185-93.

13. Lester, W., et al., *Porcine mitral valve interstitial cells in culture.* Lab Invest, 1988. **59**(5): p. 710-9.

14. Filip, D.A., A. Radu, and M. Simionescu, *Interstitial cells of the heart valves possess characteristics similar to smooth muscle cells.* Circ Res, 1986. **59**(3): p. 310-20.

15. Taylor, P.M., S.P. Allen, and M.H. Yacoub, *Phenotypic and functional characterization of interstitial cells from human heart valves, pericardium and skin.* J Heart Valve Dis, 2000. **9**(1): p. 150-8.

16. Messier, R.H., Jr., et al., *Dual structural and functional phenotypes of the porcine aortic valve interstitial population: characteristics of the leaflet myofibroblast.* J Surg Res, 1994. **57**(1): p. 1-21.

17. Lester, W.M., et al., *Bovine mitral valve organ culture: role of interstitial cells in repair of valvular injury.* J Mol Cell Cardiol, 1992. **24**(1): p. 43-53.

18. Katwa, L.C., et al., *Valvular interstitial cells express angiotensinogen and cathepsin D, and generate angiotensin peptides.* Int J Biochem Cell Biol, 1996. **28**(7): p. 807-21.

CHAPTER 3

COMPARISON OF PORCINE AORTIC VALVE INTERSTITIAL CELLS WITH AORTIC SMOOTH MUSCLE CELLS[1]

The focus in heart valve tissue engineering for the last 10 years has been to develop a scaffold material capable of withstanding the highly demanding hemodynamic and mechanical environment of the aortic valve. While this objective is certainly critical for success in this application, it is equally important that these scaffolds be populated with cells capable of performing functions of native valvular interstitial cells. Previous studies have used cells isolated from arterial[1], venous[2], and dermal tissues[3], both from autologous and allogeneic sources. In general, autologous arterial cells have performed superior to other differentiated cell types in animal studies[4]. Recently, efforts have focused on the use of stem cells as cell source for heart valve tissue engineering. Stem cells retain the potential to differentiate into all cell lineages, and theoretically can differentiate into valvular interstitial cells given appropriate stimuli. Preliminary results indicate these cells are capable of expressing contractile markers in vitro, populating polymeric valve molds, and thriving within a pulsatile bioreactor [5].

The previously mentioned studies focused on cells that could be isolated from autologous tissue that could be sacrificed. Autologous valvular tissue is generally not available for interstitial cell isolation. One study isolated interstitial cells from a tricuspid valve biopsy, and were able to culture the cells to 10 passages in vitro, while maintaining

[1] Portions of the material presented in this chapter were published in the May 2004 issue of the *Journal of Heart Valve Disease*.

expression of several markers [6]. Two of their animals died in the process, and it is probable that the culture period required for generation of enough cells for tissue repopulation is prohibitively long. Isolation of autologous mitral or aortic valve interstitial cells from excised tissue during prosthetic valve implant would probably also be unsuccessful, because these cells may already be compromised by pathology, and repeat open heart surgeries are severely demanding on patients.

While native valvular cells probably cannot be used as a cell source for human tissue engineered valves, there is surprisingly little known about their phenotype, mimicking which would be critical for the long term stability of the tissue. Autoradiographic studies done in rats have shown that valvular interstitial cells rapidly and actively secrete protein and glycosaminoglycans, with increased cell proliferation compared to arterial cells[7]. Studies with mitral valves have shown that valvular interstitial cells from different sides of the valve respond differently to endothelial denudation injury[8]. It is unclear whether those differences represent heterogeneity in the interstitial cell population, differences in signaling from matrix constituents, or differences in signal loss from heterogenic valvular endothelium.

One question not addressed by the aforementioned studies is how three dimensional cell culture, as in a biological scaffold, affects interstitial cell phenotype. Phenotypic differences have been shown in smooth muscle cells when cultured in two and three dimensional geometries[9]. While relatively small differences in cell phenotype may be masked in the short term, it is possible that over long-term culture, phenotypic differences may become more apparent. These differences may be further augmented in three dimensional culture or within animal models. A study by Rabkin and colleagues showed that the phenotype of isolated smooth muscle cells changed between culture conditions and over time, becoming more and more like valvular

interstitial cells[10]. The marker expression was semi-quantified, however, and it is not known how interstitial cells would behave in these changing conditions.

The objective of this study is to compare the phenotype of cultured aortic valve interstitial cells and aortic smooth muscle cells in two and three dimensional culture. This study will improve upon previous methods of comparison by quantitatively assessing phenotype marker expression using flow cytometry. Contractile marker expression, total protein, and sulfated glycosaminoglycan expression will be assessed and compared.

3.1: Methods

Cell Isolation and culture. Porcine aortic valve interstitial cells (PAVICs) and porcine aortic smooth muscle cells (PASMCs) were isolated as described in Chapter 2, using the protocol in Appendix A. Briefly, the endothelium was removed from the tissue surfaces by short collagenase digestion (Worthington, 600 U/ml) followed by scraping with cotton swabs. For PAVIC isolation, the leaflet tissue was digested in collagenase (Worthington, 600 U/ml) for 24 hours, and the resulting cell solution pelleted, resuspended, and plated onto tissue culture plastics. PASMCs were isolated by removing the adventitia layers of the aorta, mincing the tissue into 3x3 mm sections, and digesting in collagenase (600 U/ml) for 48 hours. Cells were then plated onto tissue culture plastic.

Both PAVICs and PASMCs were cultured in Dulbecco's Modified Eagle's Medium (DMEM, Invitrogen) supplemented with 10% fetal bovine serum (FBS, Hyclone), 1% penicilin/streptomyocin (PS, Hyclone) and 1% L-glutamine (LG, Mediatech). Cultures were fed every 48 hours, and split 1:3 at confluence. Cultures were used for experiments between passages 5 and 8.

Three dimensional construct creation. Three dimensional hydrogel constructs were created using either PAVICs or PAVICs as described previously [11] following the protocol included in the Appendix. Briefly, a suspension of $1x10^6$ cells/ml was created with 5X DMEM, 10% FBS, type I collagen (Coll I, rat tail, BD Biosciences), and enough 0.1 M NaOH to neutralize the solution. The resulting 2 mg/ml collagen I solution forms a fibrillar gel network at 37°C and neutral pH. Approximately 3 ml of solution was inoculated into wells of six-well plates and placed into a 37°C, 5% CO_2 incubator. After one hour, constructs were liberated from the walls and bottom of the wells and 5 ml of media was added to each well. The disks were allowed to compact freely, and media was changed every 48 hours.

Construct area measurement. Construct compaction was measured each time media was changed. Constructs were placed on a clear sterile dish, and circular diameter measured by sliding a ruler underneath. For constructs of non-circular shapes, constructs were photographed with the ruler underneath the dish, and areas digitally measured using Adobe Photoshop. For statistical analysis, one way ANOVAs were used to determine significant compaction differences across experimental conditions, and T tests for differences between cell types.

Phenotype analysis. Cell contractile phenotype was determined using fluorescent antibodies to the cytoskeletal markers α-smooth muscle actin (α-SMA, Sigma, 1:100), and desmin (Sigma, 1:100). The distribution of each marker within cells was assessed through confocal microscopy, and expression levels were determined through flow cytometry. It is difficult to quantitatively assess expression levels with confocal microscopy, while it is impossible to determine expression pattern (within the cell) by cytometric analysis. Marker expression was determined at day 10 for both 2D and 3D culture.

For flow cytometry, cells were detached from flasks with trypsin-EDTA (Gibco) at confluency, and spun into a pellet. Cells from three dimensional constructs (3D) were isolated using a 60 minute collagenase (600 U/ml) digestion, and the resulting suspension was spun into a pellet. The pellets were then washed twice by resuspending in PBS, followed by centrifugation and supernatant aspiration. Immunofluorescence antibody staining was performed according to the protocol given in the appendix. Briefly, cells were fixed in 3.7% paraformaldehyde (Tousimis) for 5 minutes, and permeablized with 0.1% Triton X-100 (Sigma) for 5 minutes. Cells were then incubated in blocking buffer (1% neonatal goat serum, NGS, Sigma) for 1 hour. Cells were then washed in PBS before incubation with the primary antibody for one hour. Cells were then washed twice, followed by incubation with a fluorescently conjugated secondary antibody (Anti-rabbit Alexaflour 488, Molecular Probes, 1:100) for one hour. Secondary antibody only incubations served as control. Cells were then washed twice, again, and approximately 200μl of solution was added to a cytometry tube. Flow cytometry was then performed to determine the marker expression distributions using a BD LSR Flow Cytometer (BD Biosciences). The negative control was used to calibrate the signal, and histograms were collected from the negative control and four samples from different experimental trials. Population statistics (algebraic mean, standard deviation) were determined and used for subsequent statistics as described previously[11]. Two factor Analysis of Variance was conducted with a significance level of $P = 0.005$. Pairwise comparisons were then conducted post hoc with $P < 0.005$ considered significant. The decreased P value was used as a more stringent requirement to conservatively account for the comparison of samples means instead of population distribution.

For confocal microscopy studies, cells were either seeded to confluence onto glass coverslips coated with collagen I (50 μg/ml), or in entombed in 2 mg/ml collagen

constructs. After 10 days of culture, cells were fixed and stained while adhered to the coverslip or in embedded in the constructs using the same procedure described above. Samples were also counterstained with Hoechst dye to reveal cell nuclei. Five representative pictures were taken of each sample for qualitative analysis.

Extracellular Matrix Synthesis. Total soluble protein and sulfated glycosaminoglycan content was measured at day two and day six. Total protein content was assessed using the BCA Total Protein Assay Kit (Pierce, Cat. No. 23225), while total sulfated glycosaminoglycan content was determined using the Blyscan sGAG Kit (Biocolor, Cat. No. B1000). Constructs were washed thoroughly of all residual media with room temperature PBS by gentle shaking, lyophilized with a vacuum centrifuge (Jouan RC 10.10), and dissolved in a Tris-HCL buffered Proteinase-K (Sigma) solution as detailed in the protocol included in the appendix. The Hoechst DNA assay was used to determine construct cell number to normalize protein and GAG content as previously described [11]. Briefly, 10 μl of lysate was incubated with Hoechst dye for 15 minutes at room temperature, and then measured using a UV Spectrophotometer (Biotech Powerwave 340) at 488 nm. The amount of EDTA in the sample lysis buffer was above the acceptable for the BCA assay, so 5 μl of sample was added to 50 ml 1:10 sample buffer in dH_20. The BCA reagents were added at a 50:2 (A:B) ratio for increased sample gain and absorbance measurements were read at 650nm. The Blyscan sGAG assay was performed according to the manufacturer's instructions, and samples analyzed at 560 nm. Statistical analyses were conducted using single factor Analysis of variance within a cell type followed by T tests between cell types. $P < 0.05$ was considered significant for these tests.

3.2: Results

Two-dimensional culture. Porcine aortic valve interstitial cells grow in a similar manner as porcine aortic smooth muscle cells, with similar growth rates and morphological appearance, as shown in Figure 3-1. Smooth muscle cells (A) tend to be slightly larger than interstitial cells (B), and form directional patterns in two dimensional culture. Interstitial cells show less pattern formation, and are somewhat less likely to form nodules common to super-confluent smooth muscle cells in flask culture.

Three-dimensional culture. Both smooth muscle and interstitial cells compacted the polymerized type I collage gel over the six day period, as shown in Figure 3-2A. Very slight differences in gel compaction were observed at day two ($P < 0.05$), but no differences in compaction were recorded at any other time point analyzed.

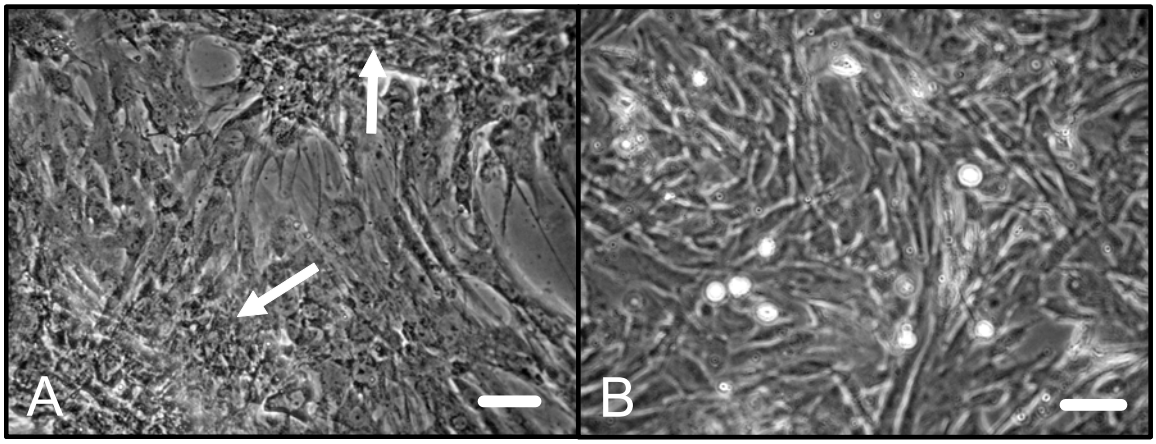

Figure 3-1: Porcine aortic smooth muscle cells (A) and porcine aortic valve interstitial cells (B) in culture. Scale bar = 50 μm.

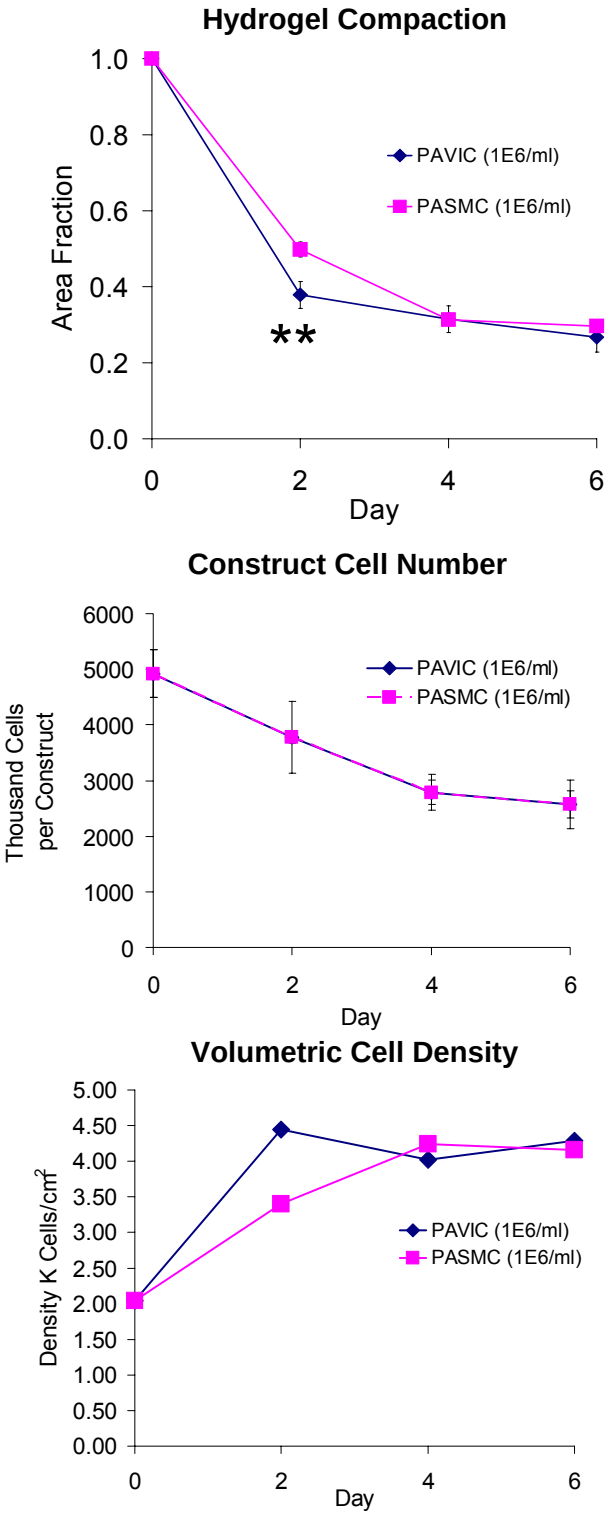

Figure 3-2: Construct compaction and cell number parameters.

The disks generally maintained a circular profile during compaction, indicating homogenous contractile properties and/or cell distribution. The constructs generally decreased in DNA content over the culture period, indicative of a reduction in cell number, but there was no difference between cell types (Figure 2B). Both the compaction and cell number of each construct stabilized at six days, and the constructs appear to maintain a specific cell density of approximately 4.2 million cells/cm^3 (Figure 2C). This could be due to specific cell mediated requirements, or limitations of nutrient diffusion.

Cell marker expression. Cell phenotype was determined through expression of cytoskeletal markers as previously described. Figure 3-3 shows confocal microscopy images of α-smooth muscle actin expression for the two cell types in the two different

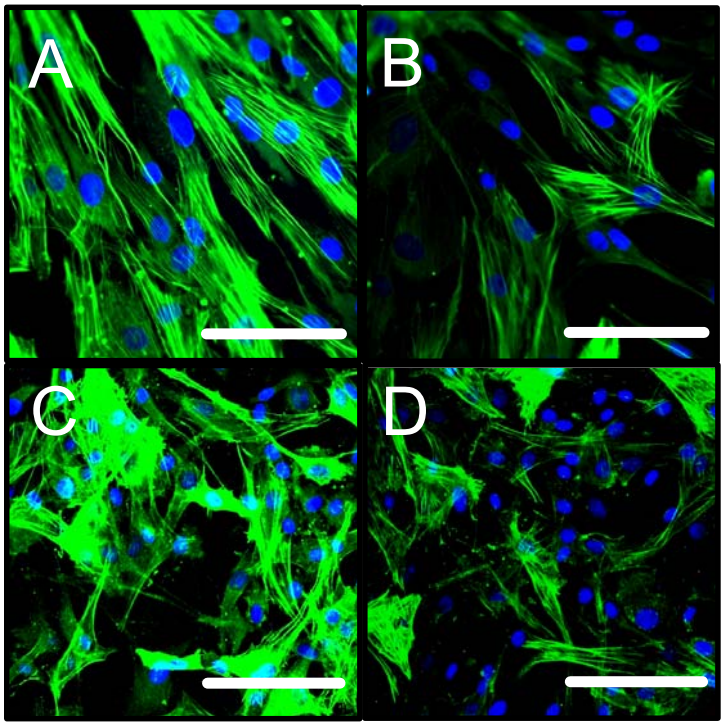

Figure 3-3: Confocal microscopy images of alpha-smooth muscle actin expression. Panels A and C – PASMC, Panels B and D – PAVIC. Panels A and B – 2D culture, Panels C and D – 3D culture. Scale bar = 50 μm.

culture conditions. Both cell types express the α-smooth muscle actin in both two and three dimensional culture, but to varying degrees. Flow cytometry results highlighting these differences is shown in Figure 3-4. No differences were observed between the cell types ($P > 0.005$), but differences were observed between culture conditions ($P < 0.005$). A reduction in α-smooth muscle actin expression occurs in three dimensional cultures for both cell types, but nearly all cells are still positive as compared to negative controls. The cytometry histograms indicate broad expression peaks, which indicate that these cells express α-smooth muscle actin in an inhomogeneous manner. There appears to be a small subpopulation of cells that do not express α-smooth muscle actin (arrow). Caution should therefore be taken when using mean values to quantify expression levels, and replicate experiments need to be conducted to ensure accuracy. Figure 3-5 shows desmin expression levels as determined by confocal microscopy and flow cytometry. Clearly, smooth muscle cells express desmin to a greater degree than interstitial cells, regardless of culture condition, in contrast to the α-smooth muscle actin expression.

Protein content. Constructs containing either interstitial or smooth muscle cells were assayed for protein content as described previously, and the results are shown in Figure 3-6. Over the course of construct compaction, between days two and six, there is a slight (but not significant $P > 0.05$) decrease in protein content in smooth muscle cell constructs, whereas there is a dramatic increase in protein content over the same period in interstitial cell constructs ($P < 0.05$). Differences in protein content between cell types at day two were insignificant ($P < 0.05$), but by day six interstitial cell constructs had more protein than smooth muscle constructs ($P < 0.05$). Taken together, these results

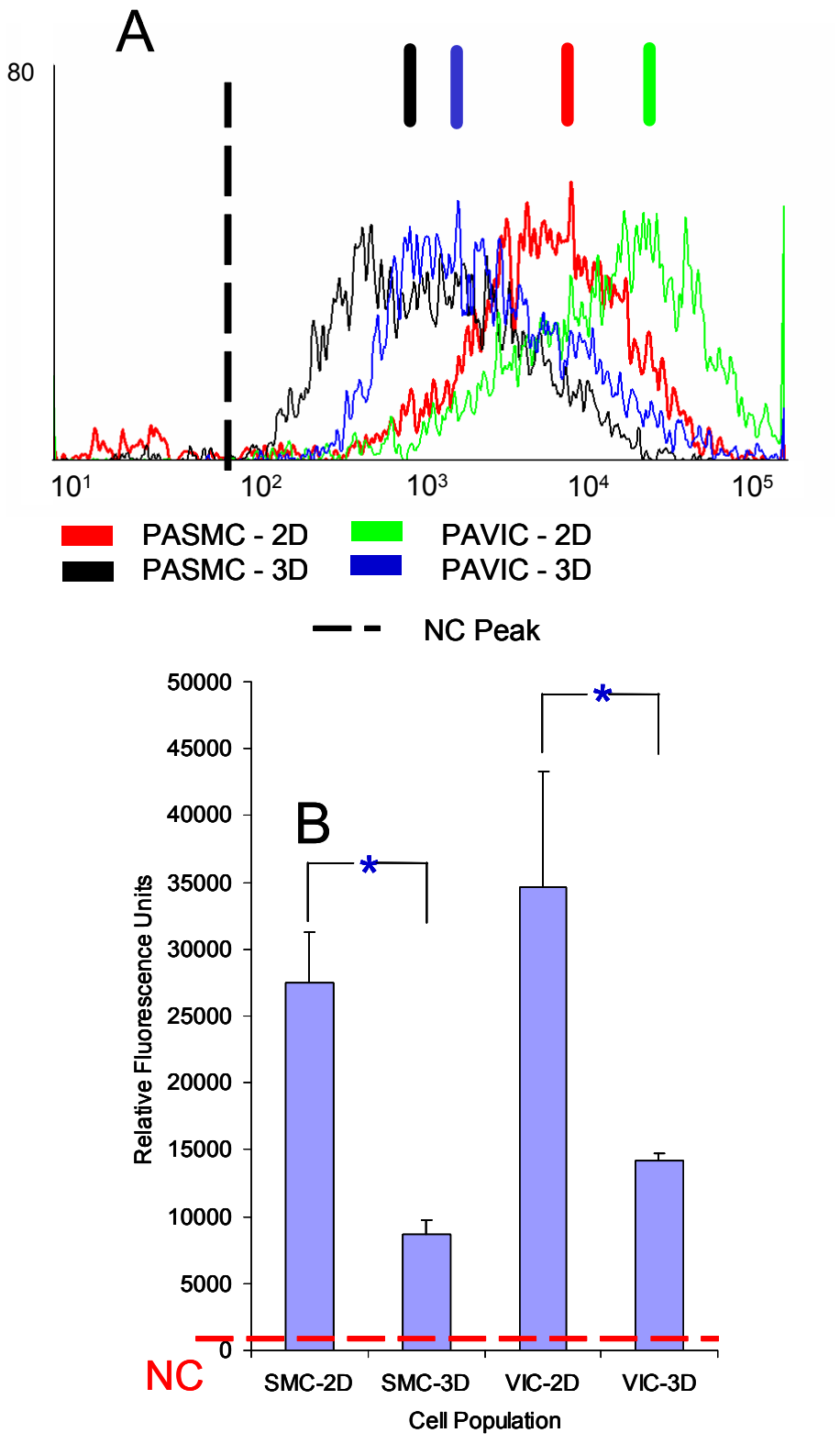

Figure 3-4: Quantification of alpha-smooth muscle actin expression using flow cytometry. Panel A – Expression histograms. Panel B – comparison of algebraic mean. * denotes significance (P<0.005). NC = negative control.

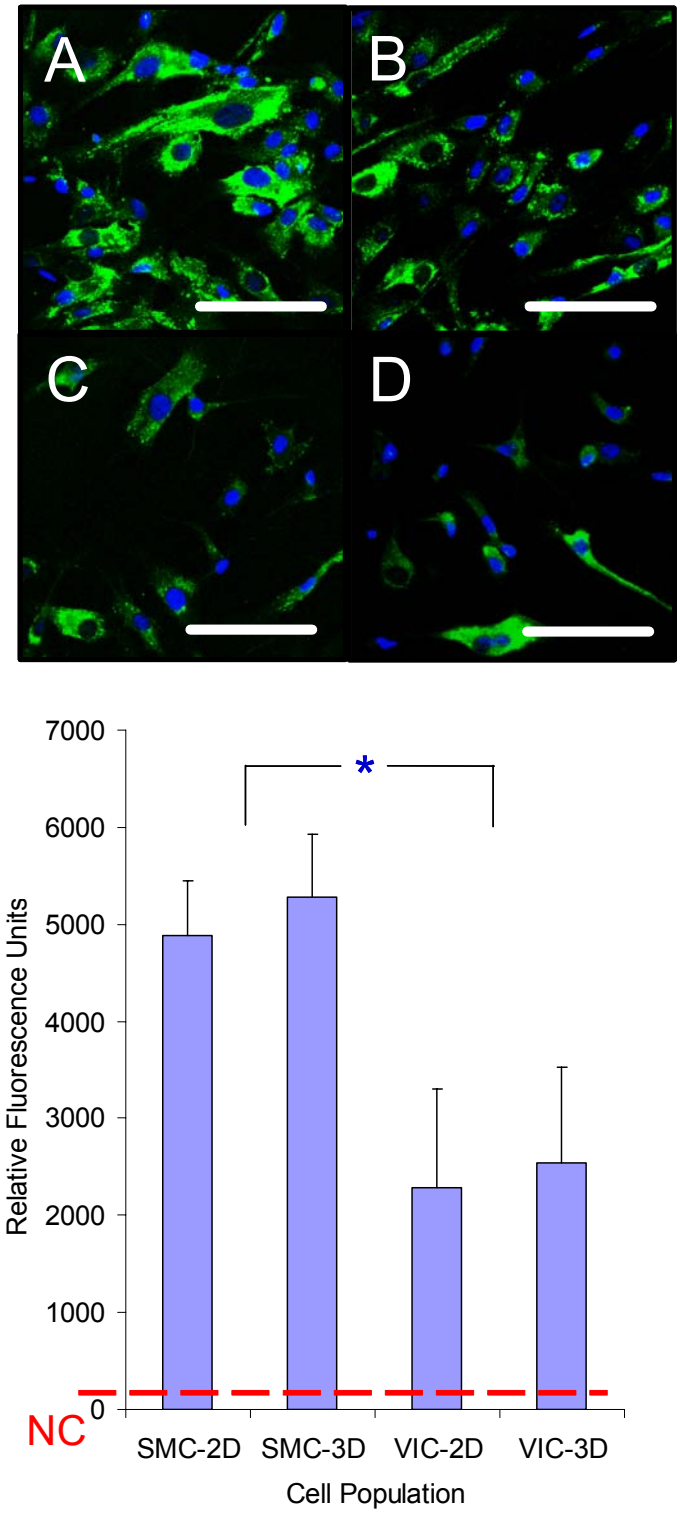

Figure 3-5: Desmin expression as determined by confocal microscopy (Top) and flow cytometry (Bottom). Panels A and C – PASMC, Panels B and D – PAVIC. Panels A and B – 2D culture, Panels C and D – 3D culture. Scale bar = 50 μm. NC = negative control.

suggest that the balance of protein synthesis and degradation is shifted towards synthesis in the interstitial cells, this in contrast to the degradation observed in smooth muscle cells in type I collagen gels. There may have been some difference in initial protein content because of the differences that may exist between the cellular protein levels.

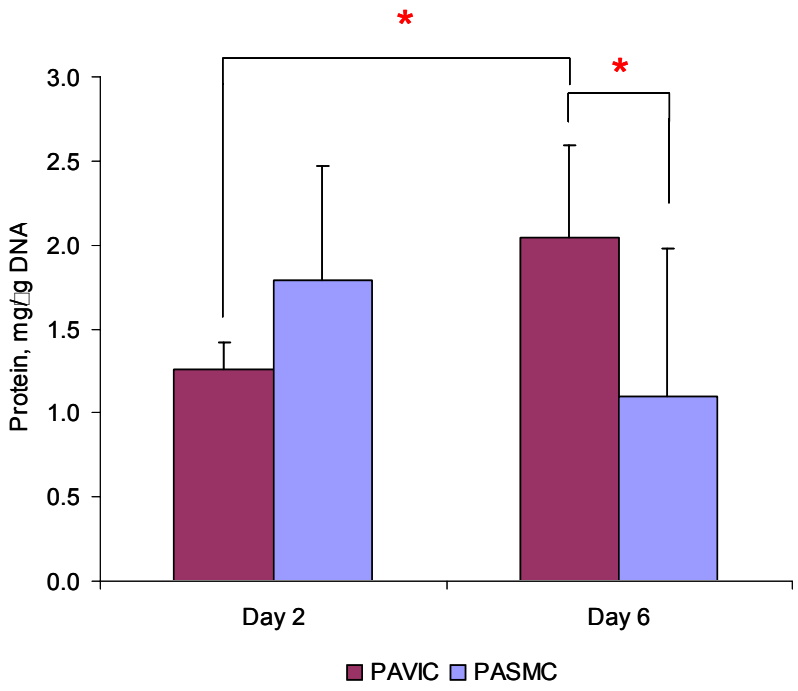

Figure 3-6: Construct total protein content normalized to DNA content.

Glycosaminoglycan content. Figure 3-7 shows the sulfated glycosaminoglycan content of interstitial and smooth muscle cell constructs. There are fewer glycosaminoglycans per DNA in the interstitial constructs at day two compared to the smooth muscle constructs ($P<0.05$). By day six, however, there is no difference in content between the two cell types ($P > 0.05$). The smooth muscle constructs do not increase in glycosaminoglycan content over the six day period ($P > 0.05$), whereas the interstitial cells do ($P < 0.05$). Differences in glycosaminoglycan content at day two may indicate differences in cellular GAG content between PAVICs and PASMCs. These results indicate that the balance between synthesis and degradation of glycosaminoglycans for interstitial cells is shifted towards synthesis, whereas for smooth muscle cells, such a shift was not observed.

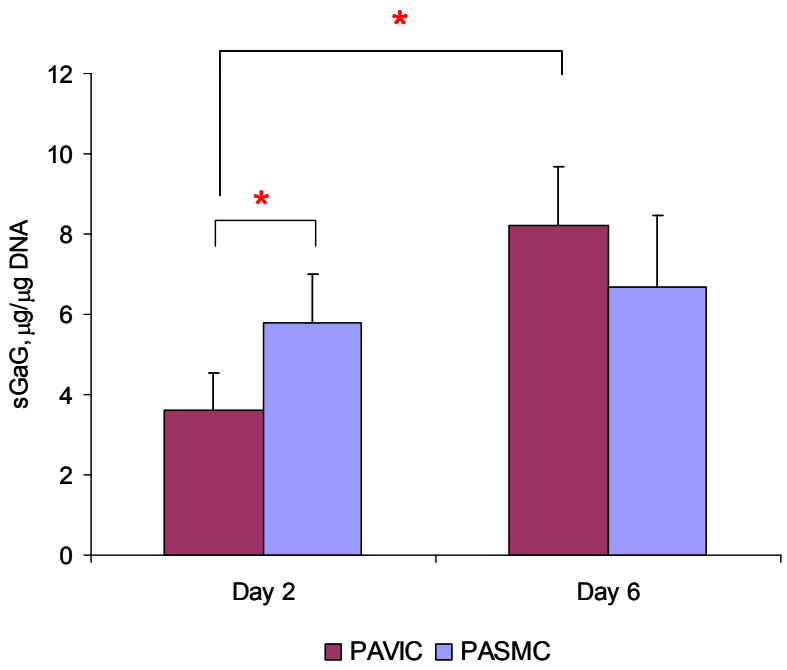

Figure 3-7: Total sulfated glycosaminoglycan content normalized to DNA content.

3.3: Discussion

The mechanical environment of the aortic valve is highly complex and demanding, and bioprosthetic valve substitutes eventually fail under the loads imposed. These non-living valves lack a viable cell component that can remodel and repair the tissue matrix as it develops microscale defects under stress, without these growing to macro tissue failure. Tissue engineering approaches to replacing a diseased aortic valve incorporate living cells and relevant matrix components to create a viable valve that theoretically can grow and remodel with the patient. This of course would be particularly beneficial for pediatric patients. While this technology shows promise, little is known about the biological functions these devices are intended to replace. Certainly adequate tissue mechanical properties are fundamentally critical to the success of these devices, but many biological functions may need to be present for long-tem implant success. Understanding these functions will certainly become important in the future.

The results from these studies demonstrate some similarities and some differences between the phenotypes of aortic valve interstitial cells and aortic smooth muscle cells. Interstitial cell-populated constructs and smooth muscle-cell populated constructs both compacted to similar degrees over the culture period, and both cell types expressed similar levels of α-smooth muscle actin. α-SMA is a structural protein present in smooth muscle, and its expression is correlated with gel compaction in other cell types [12], indicating contractile phenotype. Significant reduction in α-SMA expression was measured in three dimensional gel culture, highlighting the role that matrix interaction plays in modulating cell phenotype [9]. Desmin expression was different between the two cell types, with aortic smooth muscle cells expression greater than interstitial cell expression. Desmin is an intermediate filament that is involved in supplementing

contractile function [13]. From our studies, desmin expression is not correlated directly to gel compaction, but to cell type. The increased expression of desmin may be related to the differences in synthetic properties observed, which is discussed later. There are several reports of interstitial cell expression of fibroblast markers in situ, with limited expression of α-smooth muscle actin [14, 15]. Other researchers have shown that cell phenotype can be modulated through culture conditions. α-SMA expression can be enhanced through mechanical or biochemical stimulation, and matrix composition is also involved in this process [9, 11]. Rabkin et al. demonstrated that long term culture of tissue engineered valvular substitutes modulated smooth muscle expression of α-SMA similar to what is observed in vivo, but that expression levels of these molecules in vitro were initially different [10]. It is therefore probable that culture conditions and time in culture are also modulators of marker expression. It is also important to note the relatively broad expression peaks of the different markers, indicating a relatively wide range of expression between individual cells within these groups. There were no observations of multiple positive expression peaks in any experiment, suggesting that the expression range is associated with a single cell type, and not multiple cell types. Many factors can be associated with the range of expression between individual cells, which necessitates population statistics on distribution.

The marked differences in protein and glycosaminoglycan content indicate an ability of the valvular interstitial cell to synthesize matrix in three-dimensional culture apart from biochemical or mechanical stimulation. This was not evident for the smooth muscle cells studied in this investigation. It may be that the increased expression of desmin in conjunction with α-SMA may commit the smooth muscle cell to a more singularly contractile phenotype, and thus limit the synthetic capabilities. It should be understood that a combination of synthesis and degradation is likely occurring with these

cells, and content measures can only indicate the “net” results of this balance. As the gel constructs were created with cells and a collagen solution, limited conclusions can be made about initial protein content. There may also be more protein associated with the larger smooth muscle cells. The changes in protein content do provide a framework for more studies to further develop these effects.

The limited initial glycosaminoglycan content followed by dramatic increases in content of PAVIC constructs not apparent in PASMC constructs demonstrates different GAG synthesis capacity of PAVIC in three dimensional cultures. GAGs are an important component of valve leaflets, particularly the spongiosa layer, which is primarily responsible for lubrication between the two load bearing layers (ventricularis and fibrosa) and reducing internal shear between them [16]. A successful living valve substitute will require the ability to synthesize GAGs to maintain this important function.

Taken together, these results indicate that valvular interstitial cells possess the ability to contract tissue and synthesize matrix components in collagen gels. Normal smooth muscle cells have limited capacity to synthesize matrix, and dedifferentiated smooth muscle cells have limited ability to control matrix synthesis, as well as reduced contractile ability. This raises concern about the use of vascular smooth muscle for tissue engineered valvular substitutes. This concern, however, must be balanced with the ease of obtaining smooth muscle cells, e.g. from a peripheral vessel, compared to interstitial cells, where there is no readily available source.

Quantification of phenotypic marker expression levels between cell types is nontrivial. Flow cytometry is a more powerful method to assess expression level over epifluorescence or confocal microscopy, because a histogram is created with measurements unique to each cell in a sample. The challenge with this technique is comparing between different populations. In this study, algebraic mean was used to represent the populations for statistical purposes. This was more accurate than

arithmetic mean given the log scale X axis, but could be severely limited depending on the actual population distributions. Any deviations from a normal distribution, as would be seen in a heterogeneous population, will compromise the validity of using the mean value. Most of the sample distributions appeared normally distributed about the algebraic mean, but the sample variances were different. Statistical analysis of these curves would be improved by generating Gaussian curves that approximate the distributions, and then determining statistically significant distributions using these curves. Non-normal distributions could be approximated by exponential, binomial, or other distributions.

The BCA and Blyscan assays only measure a snapshot of sGAG and total protein content, and therefore represent net synthesis or degradation rate. To determine actual synthesis or degradation levels, timed radiolabeling studies can be conducted on constructs according to the method of Deck and colleagues [7].

One challenge in culturing three dimensional constructs is having viable cells throughout the engineered tissue. Most constructs are highly porous when first made, but as the cells contract and pull the matrix filaments together, the porosity reduces, and diffusion limits become a problem. Some cells are more sensitive to this than others, but constructs may have some nonviable cells within the tissue milieu. To investigate this issue in the constructs studied here, identical constructs were created using either PAVICs or PASMCs as described earlier, and cultured for either 4 or 10 days. They were then washed thoroughly in PBS, and incubated with 4 μM of calcein and 4 μM of ethidium homodimer (Live Dead, Molecular Probes) for 30 minutes at 37°C. Calcein becomes fluorescent when cleaved by enzymes in the cytoplasm (indicating cells are alive), and ethidium is a large fluorescent molecule that normally can't pass through a living cell membrane (indicating dead cells). These constructs were imaged using confocal microscopy, and the results are shown in figure 3-8. Homogeneous

distributions of cells are apparent, but the viability of the PASMCs appears somewhat reduced in comparison to PAVICs. This was somewhat surprising, given the avascular nature of aortic valve leaflets. Upon closer inspection, it appeared that some of the PASMCs were expressing both markers, which suggests some cell death occurred during the incubation and imaging process. Many PAVICs are in a matrix rich in glycosaminoglycans, in contrast to smooth muscle cells, which see mainly collagen and elastin. Matrix proteins have been shown to be important for cell survival and differentiation, and therefore some cells may thrive better in a collagen I matrix than others. More work to elucidate valvular cell behavior when interacting with other matrix materials needs to be done.

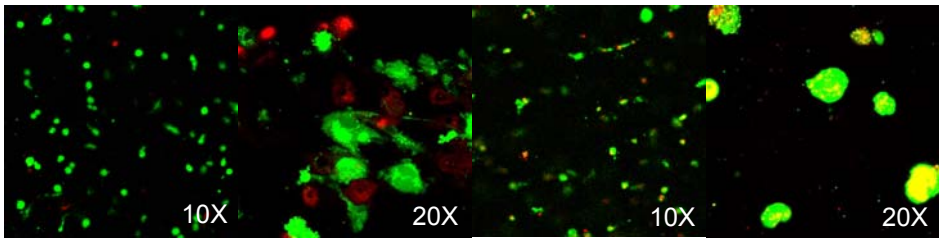

Figure 3-8: Confocal microscope images of cell viability. Number indicates objective magnification.

3.4: References

1. Stock, U.A., et al., *Tissue-engineered valved conduits in the pulmonary circulation.* J Thorac Cardiovasc Surg, 2000. **119**(4 Pt 1): p. 732-40.

2. Cebotari, S., et al., *Construction of autologous human heart valves based on an acellular allograft matrix.* Circulation, 2002. **106**(12 Suppl 1): p. I63-I68.

3. Zeltinger, J., et al., *Development and characterization of tissue-engineered aortic valves.* Tissue Eng, 2001. **7**(1): p. 9-22.

4. Shinoka, T., et al., *Tissue-engineered heart valve leaflets: does cell origin affect outcome?* Circulation, 1997. **96**(9 Suppl): p. II-102-7.

5. Perry, T.E., et al., *Thoracic Surgery Directors Association Award. Bone marrow as a cell source for tissue engineering heart valves.* Ann Thorac Surg, 2003. **75**(3): p. 761-7; discussion 767.

6. Maish, M.S., et al., *Tricuspid valve biopsy: a potential source of cardiac myofibroblast cells for tissue-engineered cardiac valves.* J Heart Valve Dis, 2003. **12**(2): p. 264-9.

7. Deck, J.D., et al., *Structure, stress, and tissue repair in aortic valve leaflets.* Cardiovasc Res, 1988. **22**(1): p. 7-16.

8. Lester, W.M., et al., *Interstitial cells from the atrial and ventricular sides of the bovine mitral valve respond differently to denuding endocardial injury.* In Vitro Cell Dev Biol, 1993. **29A**(1): p. 41-50.

9. Stegemann, J.P. and R.M. Nerem, *Phenotype modulation in vascular tissue engineering using biochemical and mechanical stimulation.* Ann Biomed Eng, 2003. **31**(4): p. 391-402.

10. Rabkin, E., et al., *Evolution of cell phenotype and extracellular matrix in tissue-engineered heart valves during in-vitro maturation and in-vivo remodeling.* J Heart Valve Dis, 2002. **11**(3): p. 308-14; discussion 314.

11. Stegemann, J.P. and R.M. Nerem, *Altered response of vascular smooth muscle cells to exogenous biochemical stimulation in two- and three-dimensional culture.* Exp Cell Res, 2003. **283**(2): p. 146-55.

12. Hinz, B., et al., *Alpha-smooth muscle actin expression upregulates fibroblast contractile activity.* Mol Biol Cell, 2001. **12**(9): p. 2730-41.

13. Rasmussen, H., Y. Takuwa, and S. Park, *Protein kinase C in the regulation of smooth muscle contraction.* Faseb J, 1987. **1**(3): p. 177-85.

14. Taylor, P.M., et al., *Human cardiac valve interstitial cells in collagen sponge: a biological three-dimensional matrix for tissue engineering.* J Heart Valve Dis, 2002. **11**(3): p. 298-306; discussion 306-7.

15. Vogt, P.R., et al., *Explanted cryopreserved allografts: a morphological and immunohistochemical comparison between arterial allografts and allograft heart valves from infants and adults.* Eur J Cardiothorac Surg, 1999. **15**(5): p. 639-44; discussion 644-5.

16. Talman, E.A. and D.R. Boughner, *Internal shear properties of fresh porcine aortic valve cusps: implications for normal valve function.* J Heart Valve Dis, 1996. **5**(2): p. 152-9.

CHAPTER 4

COMPARISON OF MORPHOLOGY AND FOCAL ADHESION DEVELOPMENT BETWEEN VALVULAR AND VASCULAR ENDOTHELIAL CELLS[1]

As vascular biology and tissue engineering advancements continue [1], heart valve therapy will become a new frontier for bioengineering research [2]. Heart valves perform a critical function in maintaining unidirectional flow through the vasculature, and as such the cells and tissue that comprise the leaflets of the valve may be uniquely suited to endure this demanding environment. Leaflet tissue is organized differently than vascular wall tissue, and evidence has emerged demonstrating that the interstitial cells of the leaflet milieu exhibit a different phenotype in comparison to vascular smooth muscle cells[3]. Like blood vessels, the surfaces of valve leaflets are lined with endothelial cells, which are critical in maintaining a non-thrombogenic surface[4], transport of nutrients, and transduction of mechanical and biochemical signals[5]. Valvular leaflet failure has been traced to endothelial dysfunction and denudation, and much pathology unique to the valve originates with the endothelium[6, 7].

In vitro research has been instrumental in the discovery of endothelial function in mechanical environments[8, 9]. Endothelial cells align parallel to the direction of unidirectional flow, through the reorganization of cytoskeletal filaments and focal adhesion complexes [10-12]. Fluid flow also induces secretion of vasoactive agents such as nitric oxide and prostaglandin to maintain vessel tone[13, 14], and these processes

[1] Portions of the material presented in this chapter were published in the August 2004 issue of *Arterioscelrosis Thrombosis and Vascular Biology.*

are regulated by complex signaling events[15-17]. Disruption of this signal process, through the oscillation of fluid flow direction [18, 19] or signal pathway blockade, inhibits cell alignment, focal adhesion reorganization, and agent release[20, 21]. The complete picture of this process is still incomplete, but is the focus of much research.

Valvular endothelial cells are much less understood. Similar to vascular endothelium, these cells exhibit contact inhibition and grow with cobblestone-like morphology in vitro [22]. Observations of cell morphology in vivo show alignment concomitant with leaflet collagen fibers, but perpendicular to fluid flow [23]. It is currently not known whether valvular endothelial cells are phenotypically similar to vascular endothelial cells. Preliminary observations indicate that subpopulations of valvular endothelial cells are capable of transdifferentiating into smooth-muscle like phenotypes [24]. Genes uniquely expressed in valvular endothelium are also critical for appropriate valve development [25]. Heart valve leaflets develop in the embryo by forming protrusions within the heart tube, which are then populated through specially differentiated mesenchymal cells [26]. The endothelium that eventually remains may therefore be distinct from vascular endothelial cells. Indeed, preliminary evidence indicates that valvular endothelial cells exhibit differences in transcriptional profiles in comparison to vascular endothelial cells, and valvular endothelial cells are more proliferative in vitro[27].

The objective of this work was to quantitatively compare the morphological responses of valvular and vascular endothelial cells to steady laminar fluid flow in vitro, and determine the changes in spatial arrangement of focal adhesion complexes. We report that the valvular endothelial cells align perpendicular to fluid flow, in contrast to vascular endothelial cells, which align parallel. The valvular cell alignment is

independent of PI 3-kinase, while this signaling pathway is critical for vascular endothelial alignment.

4.1: Methods

Cell isolation and culture. Porcine aortic valve endothelial cells (PAVECs) and porcine aortic endothelial cells (PAECs) were isolated from intact porcine hearts according to the protocol given in the appendix. Briefly, excised leaflets were incubated with 600 U/ml collagenase for 10 minutes at 37°C, followed by gentle scraping using cotton swabs. The resulting cell suspension was centrifuged and plated onto tissue culture plastic pre-coated with 50 μg/ml collagen I. Cells were cultured with DMEM supplemented with 10% FBS, 1% L-Glut, and 1% Pen-Strep, and split 1:3 upon confluence. Cells at passage 5 were used in all experiments. Cell phenotype was confirmed through expression of von Willebrand factor, acetylated LDL uptake, and non-expression of α-smooth muscle actin as shown previously in Chapter 2.

Shear Stress Experiments. Cells were detached using trypsin-EDTA solution, and seeded onto glass microscope slides precoated with Collagen I (50 μg/ml) at a density of 25,000 cells/cm^2. Cells were allowed to adhere and proliferate for 48 hours, by which time a confluent monolayer was present. The slides were then placed into a parallel plate flow chamber system[8], shown in Figure 4-1. The flow system consists of a polycarbonate block that has been machined to include inlet, outlet, and flow ports. A glass slide containing cultured cells is placed in an aluminum chamber, containing a rubber gasket, and secured with machine screws. This creates a rectangular chamber for fluid flow, the height of which can be changed with the use of polyester spacers. Therefore, a channel with defined geometry is created, and using Navier-Stokes

equations of fluid flow with constant density, the wall shear stress (τ) can be related to flow rate and channel geometry by the formula:

$$\tau = 6Q/\mu bh^2$$

where Q is the flow rate, μ is the fluid viscosity (0.012 poise), and b and h are channel width and height respectively (see Appendix for complete derivation). The flow chamber was connected to a peristaltic pump that controls the flow rate. A medium reservoir and a pulse dampener are also included into the flow circuit, as well as an air filter (Figure 4-1). The reservoirs were then filled with 125 mL of culture medium. Completed circuits were then placed in an incubator and attached to the pump. Steady, unidirectional laminar shear stress of 20 dynes/cm^2 was applied to monolayers of PAVECS or PAECS for either 24 or 48 hours, with static cultures serving as controls. Few morphological response differences have been reported with pulsatile versus steady flow [19], and steady shear therefore can serve as a first approximation of the flow environment for

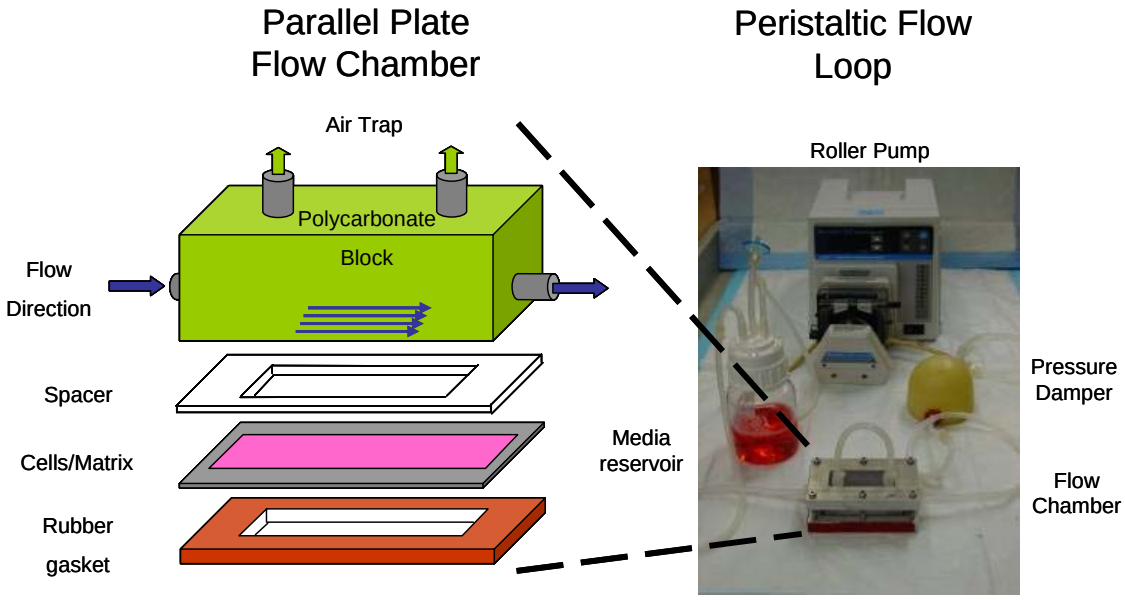

Figure 4-1: Parallel plate shear flow system, comprised of the parallel plate flow chamber and the peristaltic flow loop.

comparison in vitro.

Morphological analysis. Five representative images were taken of confluent monolayers at predetermined locations on the central region of the slides. The slides were aligned such that the image horizontal corresponded to the direction of flow. Image analysis software (LSM Image Browser, Zeiss Corp.) was used to overlay polygons delineating cell areas according to f-actin filaments. The angle between the horizontal (flow direction) and the majority of f-actin filaments was also determined. The software calculated the cell area, perimeter, and orientation angle (Figure 4-2). Two indices of cell alignment were used: cell shape index (SI) and orientation angle (OA) [8]. SI is a non-dimensional parameter that quantifies cell elongation on a scale of 0 to 1, with 0 denoting a straight line, and 1 a perfect circle. It is represented by the following equation:

$$SI = 4\pi A/P^2$$

where A is the cell area and P is the perimeter. Orientation angle was the deviation of the major actin filament axis from the slide horizontal, which was parallel to the flow direction. The shape index and cell orientation angle for at least 50 cells per slide were

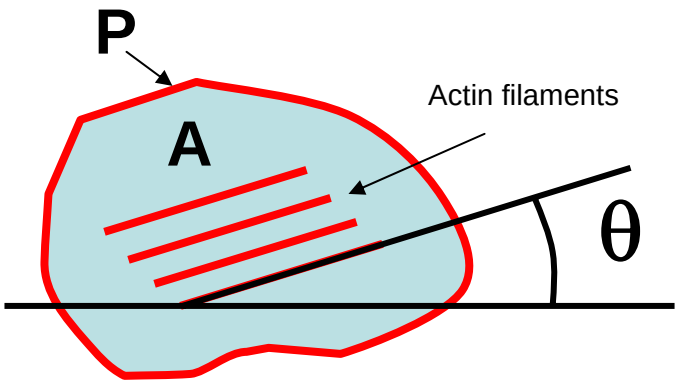

θ = Orientation angle from flow direction (horizontal)

Figure 4-2: Measurement of cell area, perimeter, and orientation angle.

tabulated for analysis. Two factor ANOVA statistics were employed with post hoc tests for interactions between conditions. $P<0.05$ was considered significant for these studies.

Focal Adhesion Development. Additional studies were conducted to determine differences in focal adhesion complex arrangement between valvular and vascular endothelial cells, and any influences of steady shear stress. Endothelial monolayers from shear and control experiments were stained for focal adhesion components as previously described[10] and explained in detail in the Appendix. Briefly, cells were fixed in 3.7% paraformaldehyde and permeablized in 0.1% Triton X-100, and blocked in 1% goat serlium. Cells were then incubated with antibodies to β1 integrin (Chemicon #MAB2000, 1:100), focal adhesion accessory molecules (vinculin, Upstate Biotech #05-386, 1:100) or signang complexes (focal adhesion kinase, Upstate Biotech #06-543, 1:100), and counterstained for f-actin (rhodamine phalloidin, Molecular Probes #R-415, 1:400) and cell nuclei (Hoechst, Sigma #33258, 1:100). At least five representative images were taken using confocal microscopy.

Western Blotting. Additional flow and static culture experiments were conducted to determine the levels of total focal adhesion protein between cell type and condition using Western blotting. A more detailed protocol is given in the appendix. Briefly, cells from shear and static control experiments were lysed in RIPA buffer containing protease inhibitors (aprotinin, leupeptin, PMSF, 25μg/ml each) and a phosphate analog (sodium orthovanadate, 25 μg/ml) to inhibit phosphatases. Lysate was quantified for total protein using a micro-BCA assay (Pierce), and equal quantities of protein were loaded into 7% polyacrylamide gels. Gels were run at 90V for 90 minutes, transferred to nitrocellulose paper, and blocked overnight in 5% nonfat milk. The samples were then incubated blocking buffer with either anti-b1 integrin (1:500), anti-vinculin (1:1000), or anti-FAK (1:500) antibody for one hour, followed by rinsing in TBS-

Tween buffer. Samples were then incubated in biotinylated anti-rabbit or anti-mouse antibodies for one hour, rinsed in TBS-Tween, incubated in alkaline phosphotase anti-biotin for one hour, and rinsed with TBS-Tween. Alkaline phosphatase was then visualized by ECF for 5 minutes, after which the samples were dried and imaged.

Signal pathway inhibition. Any differences in morphology and/or focal adhesion development may be related to differences in mechanotransduction pathways. Monolayers of PAVECS or PAECS were incubated with either Rho kinase inhibitor (Y-27632, Calbiochem #688000, 5 μM), PI-3 kinase inhibitor (Wortmannin, Calbiochem #681675, 1μM) or calpain inhibitor I (CI-1, Roche #1086090, 20 μM) for 30 minutes prior to flow and during 24 hours of flow (20 dynes/cm^2). Static cultures and vehicle-only incubation cultures served as controls. Inhibitor concentrations were determined from the literature and confirmed through serial dilution response assays.

4.2: Results

Valvular endothelial cells are similar to vascular endothelial cells in static culture. Porcine aortic valve endothelial cells grow similar to vascular endothelial cells in static culture (Figure 4-3 A-D), but some filamentous extensions appear to extend from the cytoplasm of one PAVECs and overlap the border of another cell (arrows). This morphology has also been reported with endocardial endothelial cells [28], perhaps indicating that valvular endothelial cells share some characteristics with those cells. Quantification of cell shape and angle of orientation for PAECs and PAVECs in static culture shows that both cell types are randomly oriented (Figure 4-4), with the angle of orientation ranging from 0 to 90 degrees. There is no correlation with shape index. The mean orientation angle for the PAECs in static culture is 41 +/- 21 degrees, while it is 40

+/- 25 degrees for PAVECs under static conditions (not significant). PAECs in static conditions have a shape index of 0.84 +/- 0.07, while for PAVECs it is 0.78 +/- 0.08. This lower shape index is due to the more stellate pattern the valvular cell presents. The shape index is a robust measurement of elongation in polarized cells, but less accurate for more stellate cells. This pattern changes somewhat over time in culture, presumably because the cells are spreading further without any influence of flow. The shape index of PAECS does not change because of their lack of extensions and a generally polygonal shape.

Valvular endothelial cells align differently under steady flow. As shown in Figure 4-3 E-H, porcine aortic endothelial cells align parallel to steady flow, as has been well documented. Porcine valvular endothelial cells, in contrast, align perpendicular to steady laminar flow in vitro. Biochemical staining shows that cytoplasmic actin filaments also align perpendicular to the flow direction. Quantification of these morphological changes demonstrates the extent of the alignment caused by shear stress in both cell types. The shape index vs. orientation data from the two cell populations, shown in Figure 4-5, clearly diverge after 48 hours of steady flow. The PAVECs clearly align towards 90 degrees, perpendicular to the fluid flow direction, while the PAECs align parallel to flow (0 degrees). The cells that are more elongated are also more oriented towards their preferred direction. The cell populations at 24 hours of flow begin to diverge in a similar manner, but the trends are not as pronounced as at 48 hours (online supplement). With laminar shear stress, PAECs orient parallel to the flow direction, and the orientation is also more pronounced with time. After 24 hours, the average angle of deviation from the flow direction for PAECs reduces to 25 +/- 22 degrees, and further decreases to 11 +/- 8 degrees by 48 hours, denoting nearly complete parallel orientation. PAVECs, in contrast, progress towards a near perpendicular orientation.

After 24 hours of flow, the orientation angle is 60 +/- 22.42 degrees, which further increases to 76 +/- 13 degrees after 48 hours of flow. The cell shape index also

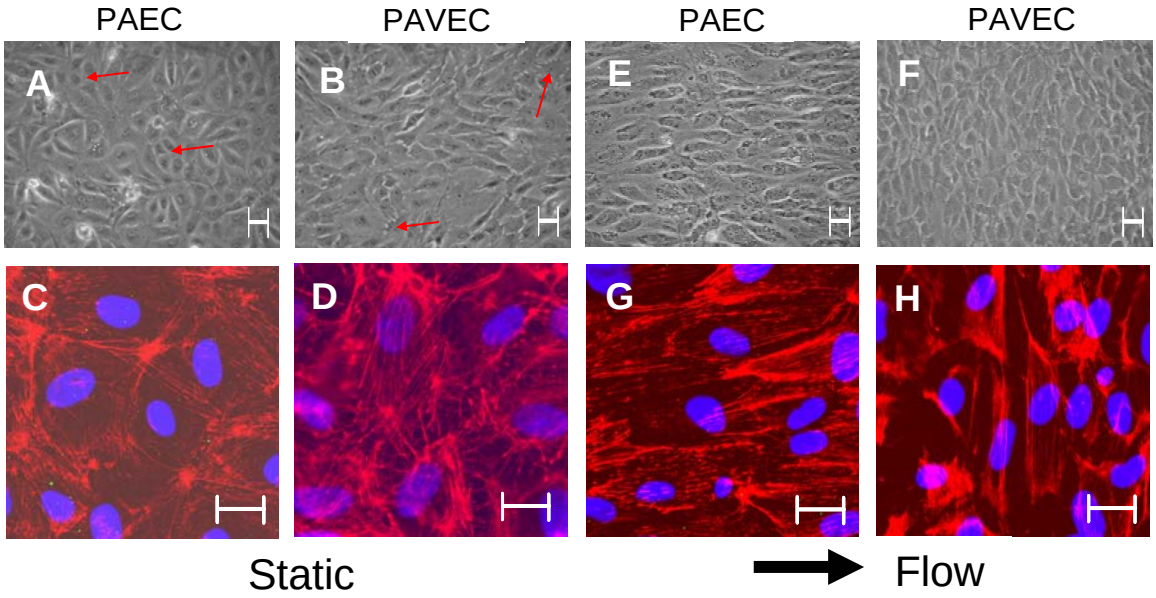

Figure 4-3: Images of PAECs and PAVECs in static and steady fluid flow environments. PAECs are presented panels A, C, E, and G, while PAVECs are in panels B, D, F, and H. Panels A-D are in static culture, while panels E-H are after 48 hours of 20 dynes/cm^2 steady laminar shear stress. Top panels are phase microscopy images, and bottom panels are laser confocal microscopy images. Cells are stained for f-actin (red) and cell nuclei (blue). Flow direction is horizontal left to right. Scale bar = 50 μm.

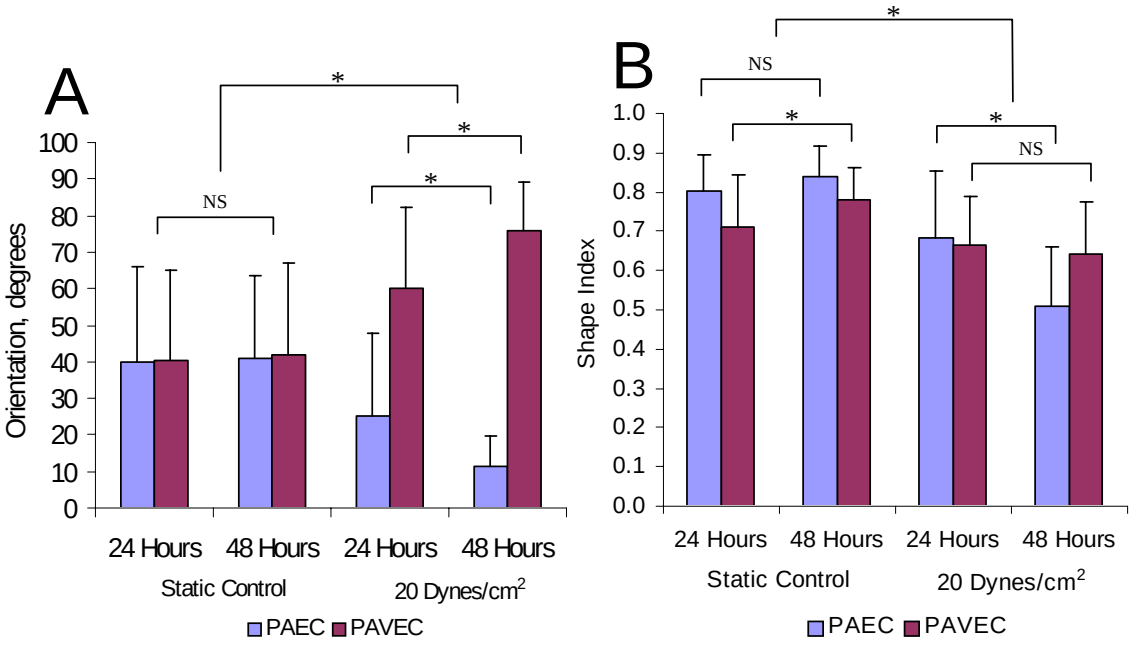

Figure 4-4: Cell Orientation changes with experimental condition (Panel A). Cell shape index changes with experimental condition (Panel B). Bars indicate standard deviation. (*) Indicates significance P<0.05, (NS) indicates no significance. Visually obvious significant differences not denoted for clarity.

changes with the application of steady flow, decreasing with time under flow, indicating that the cells are becoming more elongated. After 24 hours, the shape index for PAECs is 0.68 +/- 0.17, while for the PAVECs it is 0.67 +/- 0.12. After 48 hours of flow, these values reduce further to 0.51 +/- 0.15 and 0.64 +/- 0.14 respectively. These results indicate that the elongation of the PAECs continued beyond the 24 hour period, while the elongation of the PAVECs stabilized after 24 hours of flow.

Confirmation of alignment tendency. As an additional demonstration of the perpendicular alignment tendency of the valvular endothelial cells, a glass coverslip seeded to confluence with PAVECs was fixed to a microscope slide with vacuum grease (Figure 4-6). This combination was then exposed to 20 dynes/cm^2 for 24 hours, the coverslip rotated 90 degrees, and again subjected to flow for 24 hours. The PAVECs aligned perpendicular to flow after the first 24 hours, and then re-aligned perpendicular to flow after the second 24 hours (Figure 4-7), demonstrating their dynamic responses to fluid flow and a preference for a perpendicular alignment. The alignment after the second 24 hours is not as dramatic as after the first, probably due to the fact that the cells had to progress from an oppositely aligned state, instead of a more random orientation distribution.

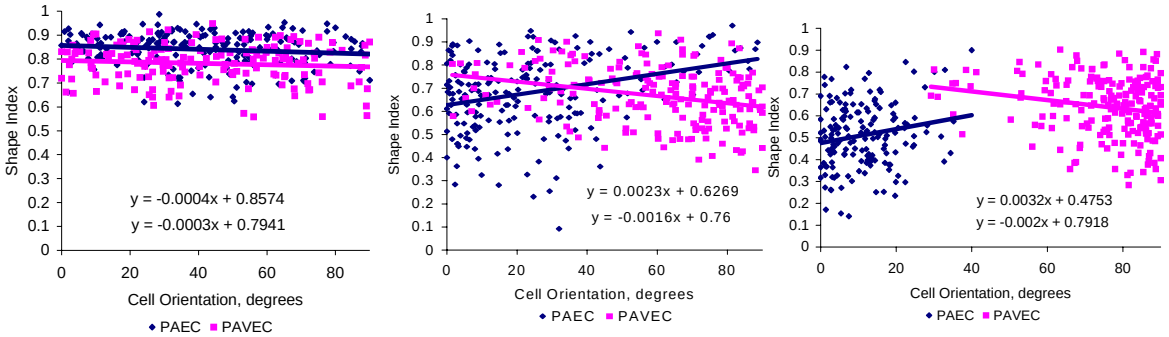

Figure 4-5: Cell alignment (Shape Index vs. Orientation) regressions. Static culture control vs.20 dynes/cm^2 for static culture (left), 24 hour flow (middle), or 48 hour flow condition (right).

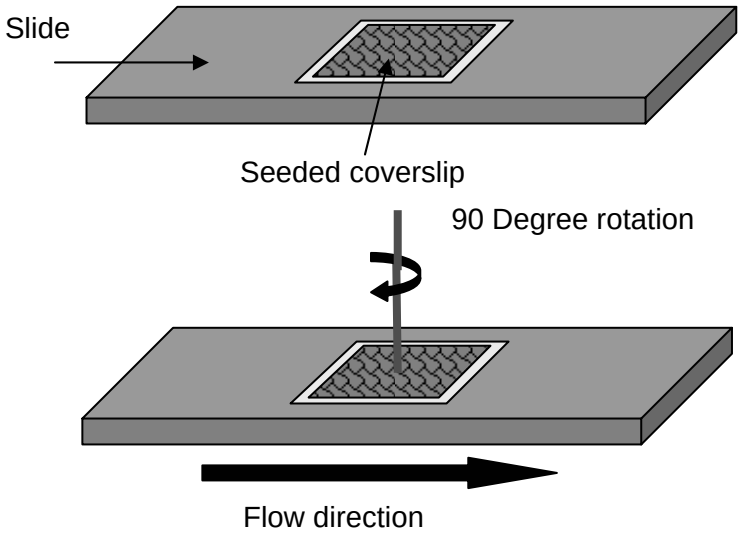

Figure 4-6: System to rotate cultured endothelial cells under aseptic conditions.

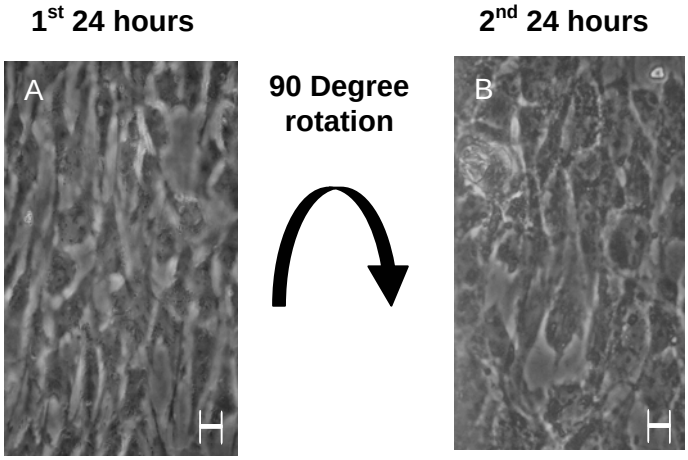

Figure 4-7: Re-orientation of valvular endothelial cells under flow. PAVECS were seeded on a coverslips coated with collagen I were adhered to a glass slide using vacuum grease. The ensemble was then placed in the flow system for 24 hours (A). The coverslip was then rotated 90 degrees, and subjected to flow for an additional 24 hours (B). PAVECs re-oriented perpendicular to flow, demonstrating their preference for this arrangement. Scale bar = 50 μm.

Cell alignment dependent on actin polymerization. Experiments were conducted to determine the mechanism for valvular endothelial alignment to flow. Valvular endothelial cells were incubated with Cytochalasin-D (CD, Sigma #30385, 0.1 μM) for one hour prior to exposure to flow, and identical concentrations of either chemical were included in the flow medium as well. Alignment was then determined as previously described after 48 hours, with static cultures serving as controls. The aforementioned concentrations were determined through 48 hour static culture titration assays. The alignment change of the valvular endothelial cells was found to be correlated with the reorganization of actin filaments. Disruption of actin filaments with CD inhibited the alignment changes observed previously (Figure 4-8). Fragmented actin filaments prohibited an accurate determination of alignment parameters, but no tendency of cell alignment was observed.

Different patterns of focal adhesion develop under flow. The development and reorganization of focal adhesions paralleled changes in morphology for both cell types, resulting in different patterns between the two cell types. The spatial arrangement of focal adhesion components, represented by the clustering of β1 integrins (Figure 4-9, arrows), accessory molecules (vinculin, Figure 4-10, arrows) and signaling molecules

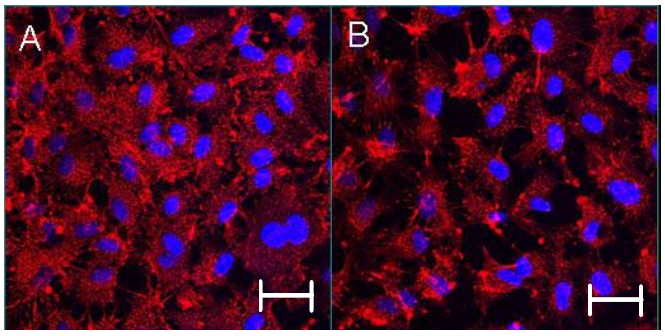

Figure 4-8: PAVECs with disrupted actin polymerization through Cytochalasin D failed to align under flow. Confocal images in 48 hour static (A) and 20 dynes/cm^2 shear stress for 48 hours (B). Cells stained for f-actin (red) and cell nuclei (blue). Scale bar = 50 μm.

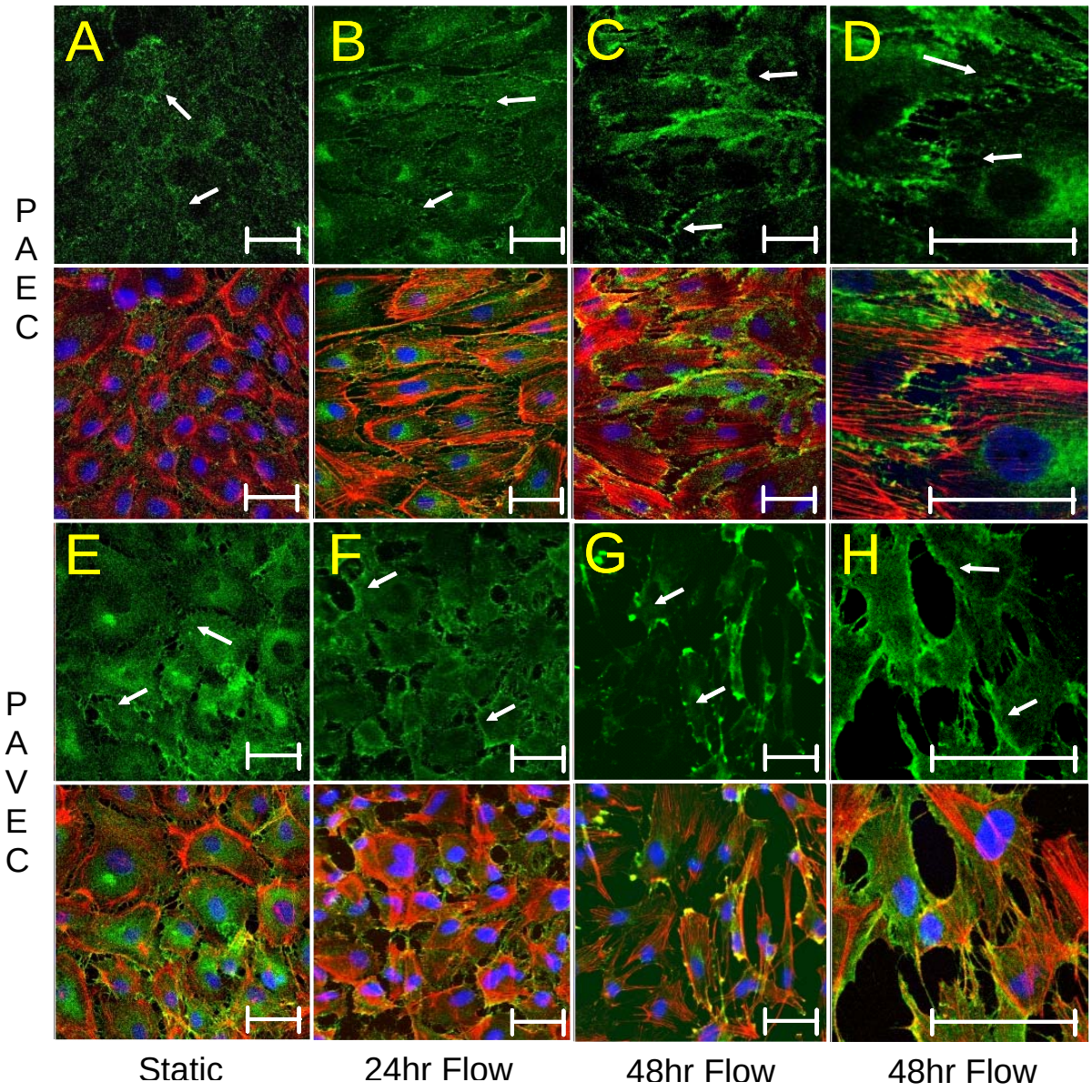

Figure 4-9: β1 integrin expression of PAECs and PAVECs. Cells stained for β1 integrin (green), f-actin (red) and cell nuclei (blue). Top portion of panels are β1 integrin expression only. Scale bar = 50 μm.

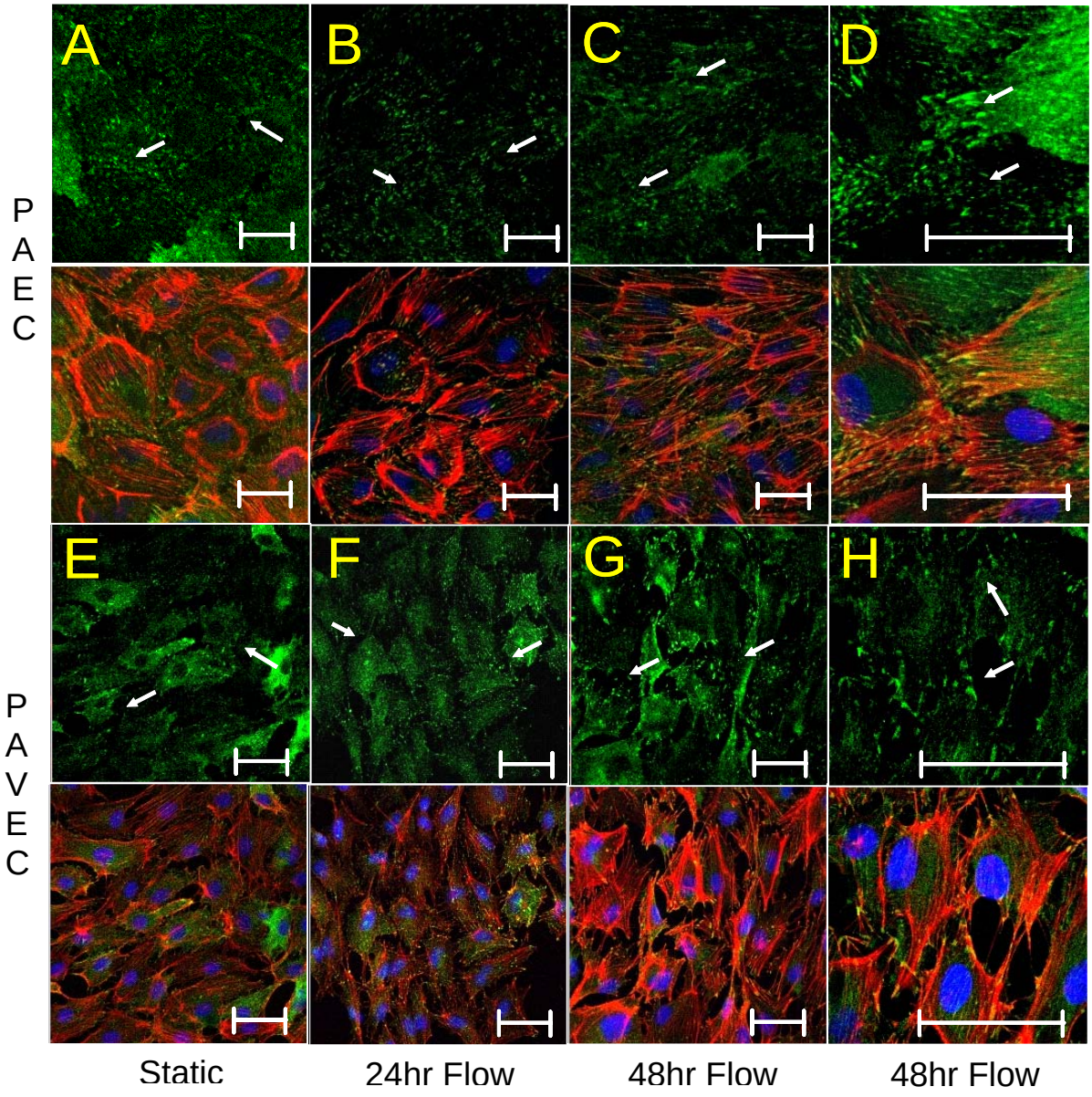

Figure 4-10: Vinculin expression of PAECs and PAVECs. Cells stained for vinculin (green), f-actin (red) and cell nuclei (blue). Top portion of panels are vinculin expression only. Scale bar = 50 μm.

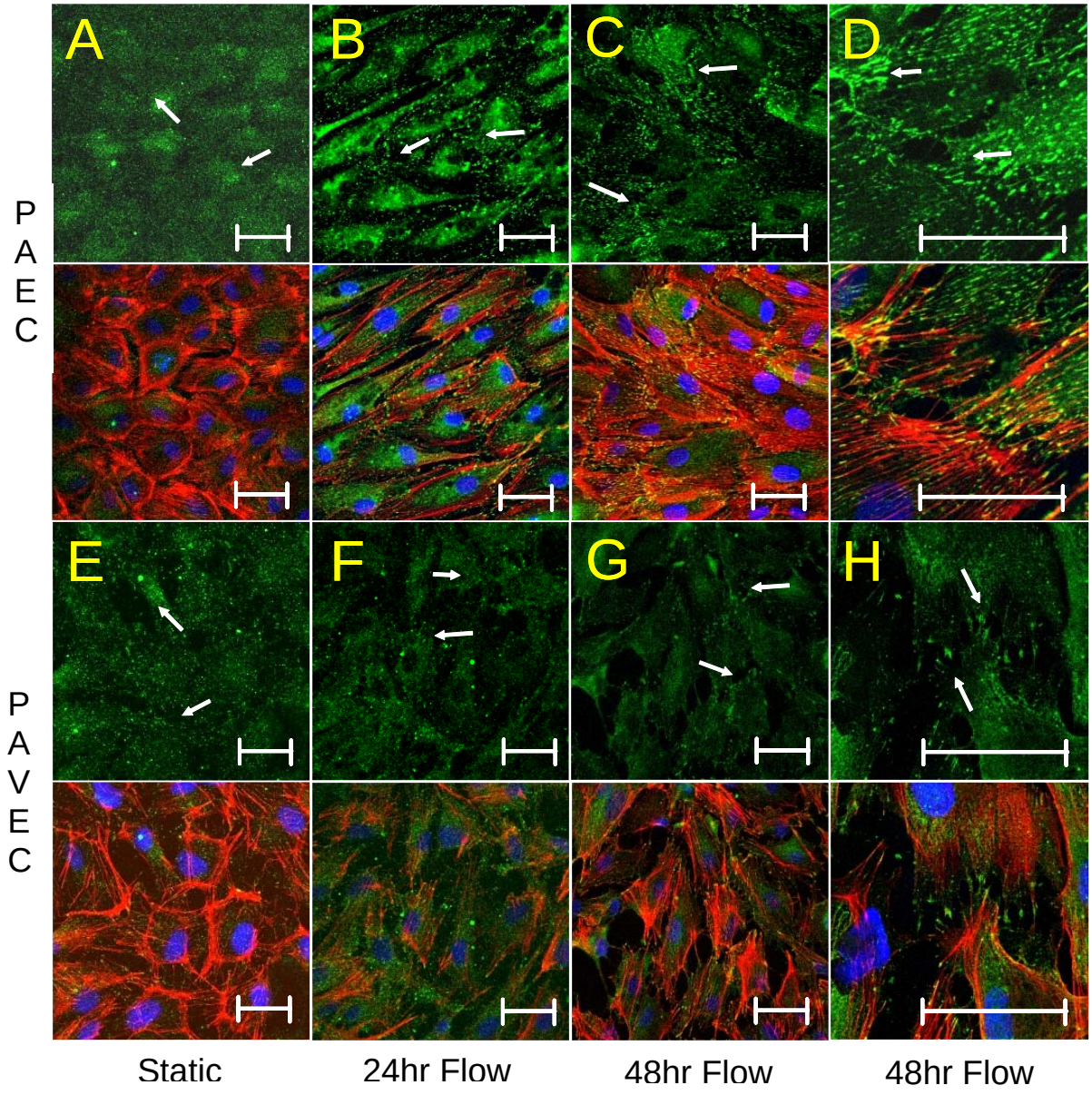

Figure 4-11: FAK expression of PAECs and PAVECs. Cells stained for FAK (green), f-actin (red) and cell nuclei (blue). Top portion of panels are FAK expression only. Scale bar = 50 μm.

(FAK, Figure 4-11, arrows), was concentrated at the upstream and downstream portions of flow in PAECs. The arrangement of focal adhesions in static cultures of PAECs was more homogeneous, with some tendency to concentrate at the cell periphery. All adhesion components were co-localized with f-actin termini, indicating they are directly involved in supporting the changing cytoskeletal tension under flow. The reorganization of adhesions in PAVECs under flow is not concentrated at the upstream and downstream portions of the flow, but rather at the ends of the long axis of the aligned cells. Focal adhesions of PAVECs in static culture are somewhat similar to PAECs, with a tendency to concentrate near the periphery of the cell and also within the cellular extensions. Vinculin and FAK co-localize with f-actin termini, along with β1 integrins, suggesting mechanical connectivity. Interestingly, there was significant presence of β1 integrin without vinculin or FAK at the upstream portion of PAVECs under flow, which was incompletely connected to f-actin (arrows). This suggests that there may be a partitioning of mechanical signal in PAVECs that is different in PAECs. There is most likely other focal adhesion components involved in the reorganization process than those examined in this study which may account for this.

No differences in total levels of focal adhesion proteins with cell type of flow condition. Figure 4-12 shows the results of the Western blots. It is evident that there are no significant differences in any of the focal adhesion complexes studied between the cell types, and no significant changes with flow. This confirms that the arrangement of focal adhesion proteins, and not the total amount of adhesion proteins, is important for the morphological differences see between these two cell types.

Signal pathway involvement in the regulation of cell morphology under flow. Figure 4-13 shows the changes in morphology of PAVECs and PAECs in static and flow environments when specific signal kinases or proteases are inhibited. The

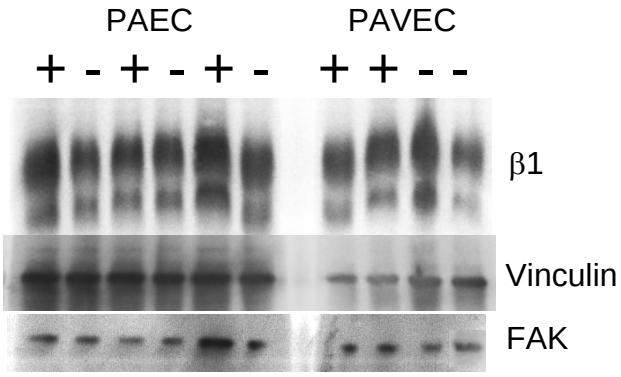

Figure 4-12: Western blots of β1 integrin, vinculin, and focal adhesion kinase. + or – indicates whether the samples were treated with 20 dynes/cm^2 steady laminar shear stress for 48 hours (+) or culture statically (-) for 48 hours.

cytoskeletal reorganization of PAECs under flow is blocked by the inhibition of Rho kinase, PI 3-kinase, and calpain. The alignment of PAVECs under flow was also disrupted through the inhibition of Rho kinase and calpain, but not PI 3-kinase. No differences in cell orientation were observed in static cultures. Additional studies were conducted to investigate the action of calpain inhibitor I (CI-1) on focal adhesion pattern development as represented by vinculin localization. CI-1 disrupted focal adhesion reorganization under flow, and adhesions remained diffuse and peripheral (Figure 4-14). The disruption was similar in both cell types, suggesting calpain acts similarly in both cells to enable focal adhesion reorganization.

4.3: Discussion

This study demonstrates that valvular endothelial cells align perpendicular to fluid flow in vitro, in contrast to vascular endothelial cells, and that this alignment is mediated by the reorganization of focal adhesions within the cell. Furthermore, the signaling

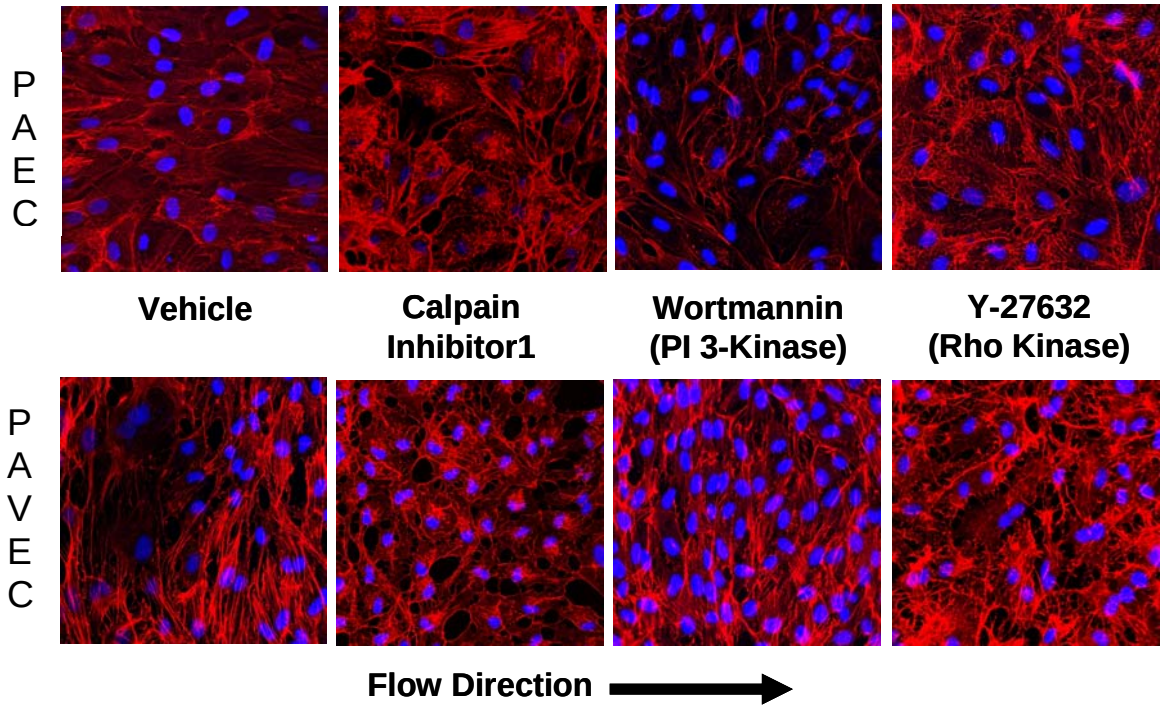

Figure 4-13: Effects of inhibitors on morphological response to flow. Cells exposed to 20 dynes/cm^2 steady laminar shear stress for 24 hours while in the presence of either Rho kinase inhibitor (Y-27632, 5μM), PI 3-kinase inhibitor (Wortmannin, 1 μM), or calpain inhibitor (calpain inhibitor I, 20 μM). Top row, PAECs. Bottom row PAVECs. Phase contrast microscopy images with confocal microscopy inserts. Cells stained for f-actin (red) and cell nuclei (blue). Flow direction is horizontal left to right. Scale bar = 50 μm.

pathways that mediate these responses are different for the two cell types. Vascular endothelial alignment is calpain, Rho kinase and PI 3-kinase dependent, while valvular endothelial cell alignment is calpain and Rho kinase dependent, but PI 3-kinase independent. To our knowledge, the only other cell type that aligns perpendicular to the direction of fluid flow is the vascular smooth muscle cell (SMC) [29]. Paranya et al. [24] found that some populations of ovine and human valve endothelial cells could be irreversibly induced to produce α-SMA through incubation with TGFβ-1. The most dramatic results were found with clonal expansions of individual cells that may have been more progenitor-like. However, they also found populations of valvular endothelial

cells that stained positive for both CD-31 and α-SMA in vivo, possibly indicating a differentiating phenotype. It is also known that vascular SMC secrete paracrine factors, such as TGFβ-1 in the presence of fluid flow [30]. These studies suggest that it may be possible that valvular endothelial cells differentiate in the presence of fluid flow to a more smooth muscle-like phenotype, and therefore align perpendicular to flow and express α-SMA. Additional monolayer studies were conducted to determine whether the PAVECs were transdifferentiating into a more smooth muscle-like (or valvular interstitial cell-like) phenotype. No expression of α-SMA was detected in static culture, or after 48 hours of flow (Figure 4-15), suggesting that these cells do not transdifferentiate under flow. There may be other markers, whose expressions describe an intermediate phenotype [31], and it may be possible that these cells may be encouraged through flow to exhibit the beginning stages of altered differentiation not observed in this study. It is also important to note that these experiments were conducted with early passage endothelial cells isolated from both sides of the aortic leaflets. There may be some differences between the endothelium from the aortic and ventricular sides of the leaflets, as has been observed with the interstitial cells of the mitral leaflet [32]. Such differences may be flow regulated, as seen in the vasculature. The complex fluid dynamics of the aortic valve may suggest a large plurality of different endothelial morphologies in vivo depending on location on the leaflet surface, not just between aortic and ventricular sides [33]. It would be difficult, however, to determine such differences through the types of studies presented here, as relatively large cell populations are required to achieve confidence in the results. Indeed, higher passage valvular endothelial cells (greater than P7) do not appear to exhibit this alignment tendency, and progress to a more non-aligned or even parallel-aligned state. Cells expanded in vitro from a very

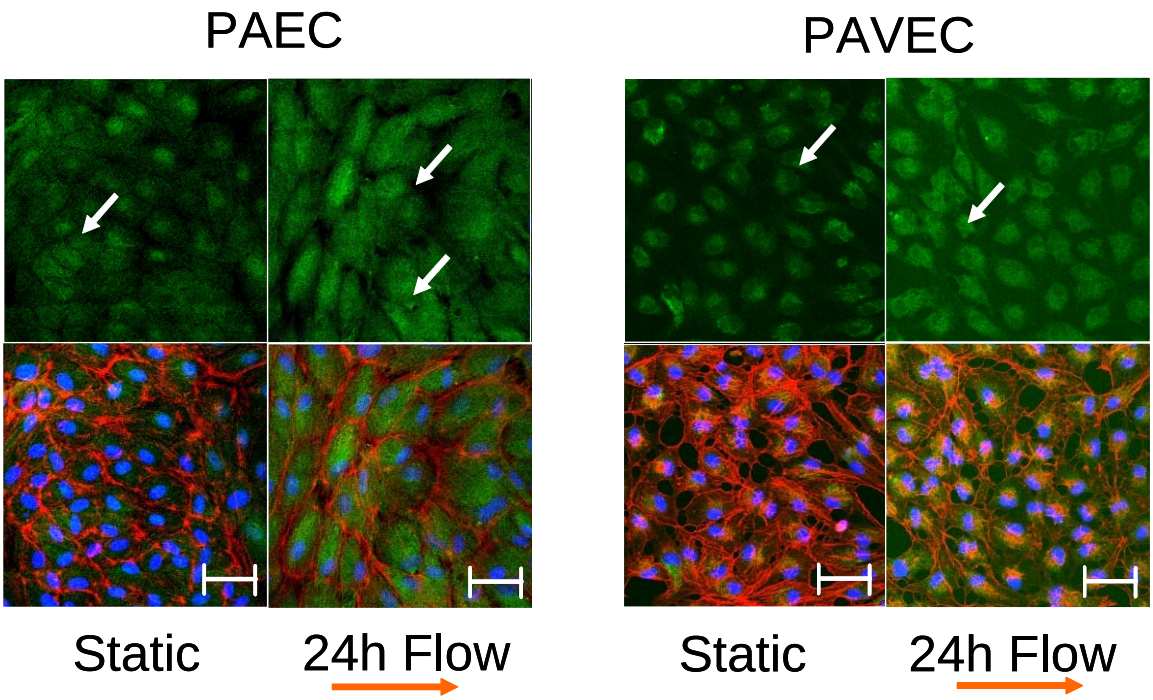

Figure 4-14: Effects of calpain inhibitor I on focal adhesion reorganization as determined by vinculin arrangement. Cells stained for vinculin (green), f-actin (red), and cell nuclei (blue). Scale bar = 50 μm.

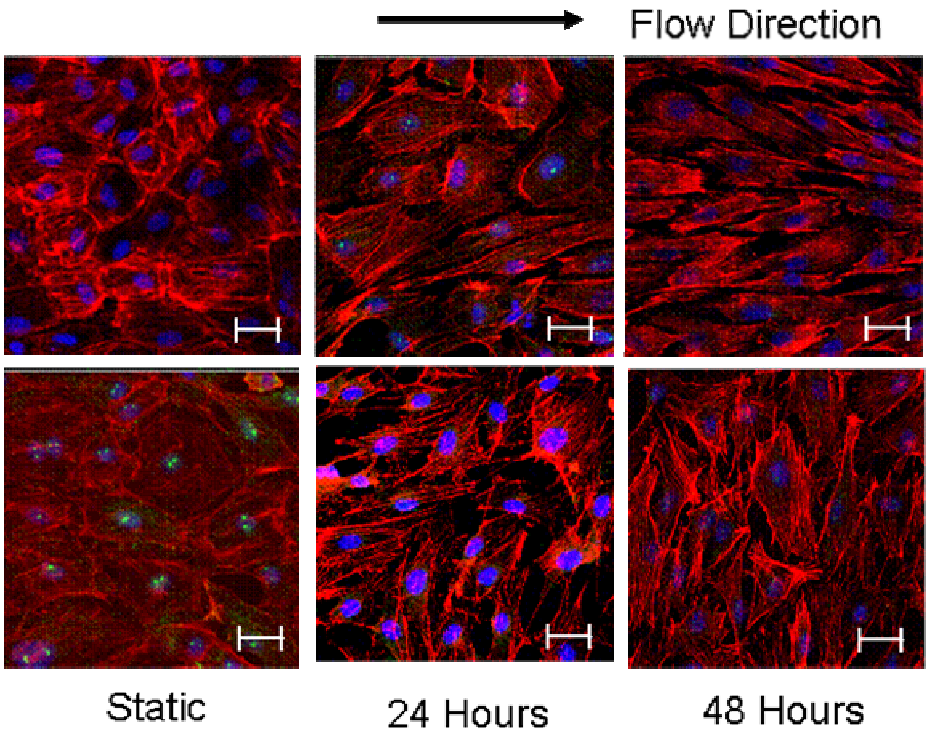

Figure 4-15: Confocal images of cell monolayers stained for α-SMA (Green), f-actin (red) and cell nuclei (blue). Top row is PAECS, while the bottom row is PAVECS. Scale bar = 50 μm.

small initial population of isolated cells may therefore not respond similarly to a defined flow environment.

Focal adhesion patterns are important indicators of cell function, as they provide sensory and response instruments for cells in contact with extracellular matrix. The predominant integrins for interaction with collagen involve β1 components, the integrin examined in these studies. Focal adhesions are centers for adhesion, migration, and signaling in response to mechanical forces such as shear flow. The differences in patterns observed between PAECs and PAVECs suggest differences in sensing of and adaptation to the external environment between the cell types. The resulting changes are consistent with in vivo observations, which strongly suggest that there may be differential mechanisms controlling responses to fluid flow.

To investigate these mechanisms further, molecules involved in signal pathways were independently inhibited to assess their effects on these two cell types. Important signal pathways that originate at cytoplasmic integrin terminals are Rho kinase and phosphatidylinositide 3-kinase (PI 3-kinase). These have established roles in regulating the actin cytoskeleton, cell growth, and migration, and are critical to the morphological changes in vascular endothelial cells. Rho kinase, PI 3-kinase, and calpain are involved in a myriad of cytoskeletal functions. Rho kinase (p160ROCK or ROCK1) is a downstream target of Rho, which is part of the Ras family of small GTPases [34]. Expression of constitutively active Rho inhibits parallel alignment of vascular endothelial cells, as does inhibition of the Rho kinase[35, 36]. Rho kinase is also important for biphasic migration of sparse endothelial cells in short term response to flow[37]. Y-27632 is a potent cell-permeable inhibitor of Rho kinase by competing with ATP for the binding catalytic site[38]. PI 3-kinase is critical for the modulation of endothelial production of nitric oxide in response to shear stress[39]. PI 3-kinase has been reported not to influence cell elongation in response to steady shear in sparse cultures[37], but its

effects on morphology in confluent cultures under long term (24 hour) shear has not been studied. Wortmannin is a fungal metabolite that irreversibly blocks the catalytic activity of PI 3-kinase. In addition to kinases, calpain I is a cysteine protease that has substrates for proteins in focal adhesion components such as talin [40, 41]and phosphorylated FAK [42]. It thus may be important in the reorganization of focal adhesion complexes and their initiation of signal cascades. Calpain inhibitor I has been shown to inhibit the morphological reorganization of lung epithelial cells after exposure to TPA [43]. The results of our study demonstrate that calpain function, and therefore the reorganization of focal adhesion complexes, are critical for cellular rearrangement in response to shear stress. Rho kinase inhibition of endothelial reorganization with shear is confirmed in aortic endothelial cells and now established with valvular endothelial cells. The differences in morphological response between the two cell types under shear with the inhibition of PI 3-kinase suggests a phenotypic difference between the two cell types. A schematic summarizing the major findings in this study is shown in Figure 4-16.

Coupled with the differences in focal adhesion patterns, valvular endothelial cells may compartmentalize mechanical signals in a different manner than vascular endothelial cells. This may be related to the differences in the native mechanical environment of the two cell types. Aortic valve leaflets experience up to 40% strains at a strain rate of 25/s, both much greater than the vessel wall [44, 45]. The circumferential alignment of endothelial cells observed on leaflet surfaces also corresponds to circumferential alignment of collagen fibers. The confirmation of the endothelial alignment in vitro without the confounding effects of underlying matrix alignment, coupled with the different signal pathways that have been implicated in the alignment process of the two endothelial types strongly suggests differences in the behavior of these two cell types, and elucidating these differences will require further study.

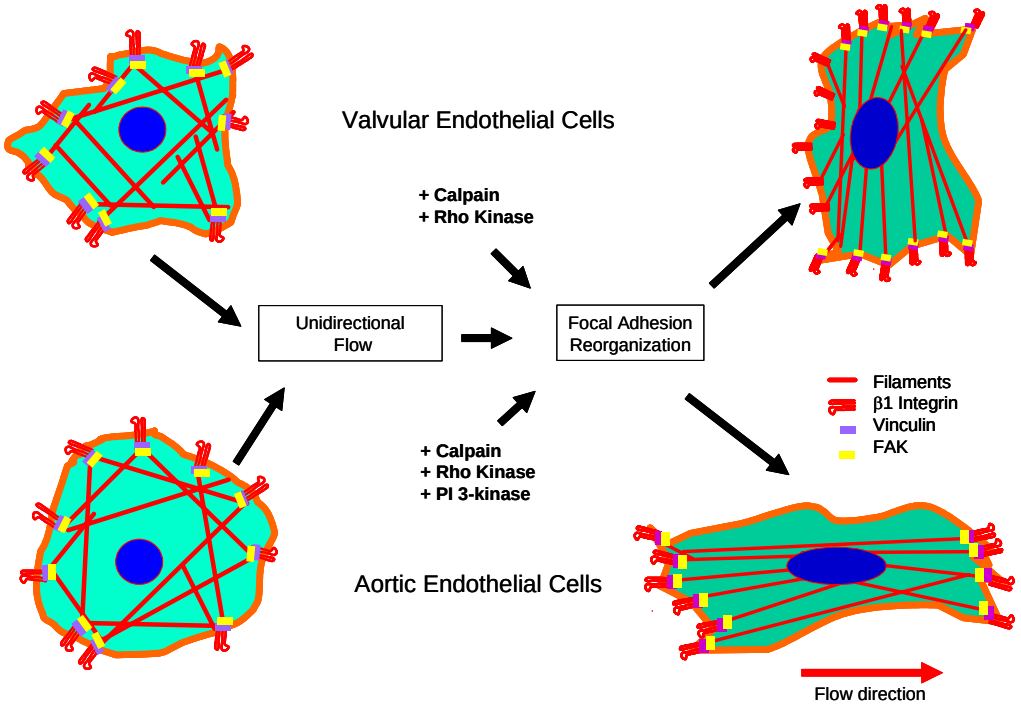

Figure 4-16: Schematic summarizing the differences in morphological response and focal adhesion arrangement between the endothelial cell types under flow.

These results highlight considerations for appropriate cell sourcing of tissue engineered valvular substitutes. Using non-valvular endothelial cells, at least for an aortic valve substitute, may sacrifice important functional behavior. It is currently unknown if the dissimilar responses of vascular and valvular endothelial cells to fluid flow has any effect on overall leaflet function, but different responses may imply altered paracrine signaling to surrounding cells [30]. Assuming that appropriate cell behavior is essential for the successful tissue-engineering of substitutes, then a better understanding of valvular cell behavior is critical to the development of living replacement heart valves.

The quantification of morphology was done using confocal microscopy images. While this method allowed accurate measurement of parameters, it was extremely labor intensive. Furthermore, only five images were used per slide analyzed. With about 12-

20 cells measurable per image, and therefore 50 – 100 cells per slide measured, this corresponds to less than 0.1% of the cells on the slide, which may not be a useful statistical sampling of the cell population. Furthermore, it was evident that some portions of slides contained localized cell alignment tendencies that were somewhat different from the rest of the slide. Given these difficulties, some modifications to the experiment protocol could be made to improve accuracy. First, a software program designed to measure and record cell morphology parameters would be written. This would be coordinated with a motorized stage on the confocal microscopy, so that the cells on the whole slide can be scanned for image parameters, and data tabulated in a spreadsheet form. Imaging software has been created for similar applications, but relied on external cell shape. Using cytoplasmic filaments is preferable, because it suggests the axis of cell traction, and hence orientation. It was observed not a few times that the major axis of the cell membrane and the axis of cytoplasmic filaments were at widely different angles.

4.4: References

1. Niklason, L.E., et al., *Functional arteries grown in vitro.* Science, 1999. **284**(5413): p. 489-93.

2. Hoerstrup, S.P., et al., *Functional living trileaflet heart valves grown in vitro.* Circulation, 2000. **102**(19 Suppl 3): p. III44-9.

3. Deck, J.D., et al., *Structure, stress, and tissue repair in aortic valve leaflets.* Cardiovasc Res, 1988. **22**(1): p. 7-16.

4. Risberg, B., *Pathophysiological mechanisms of thromboembolism.* Acta Chir Scand Suppl, 1989. **550**: p. 104-14.

5. Davies, P.F., et al., *Spatial relationships in early signaling events of flow-mediated endothelial mechanotransduction.* Annu Rev Physiol, 1997. **59**: p. 527-49.

6. Durbin, A.D. and A.I. Gotlieb, *Advances towards understanding heart valve response to injury.* Cardiovasc Pathol, 2002. **11**(2): p. 69-77.

7. Poggianti, E., et al., *Aortic valve sclerosis is associated with systemic endothelial dysfunction.* J Am Coll Cardiol, 2003. **41**(1): p. 136-41.

8. Levesque, M.J. and R.M. Nerem, *The elongation and orientation of cultured endothelial cells in response to shear stress.* J Biomech Eng, 1985. **107**(4): p. 341-7.

9. Levesque, M.J., et al., *Correlation of endothelial cell shape and wall shear stress in a stenosed dog aorta.* Arteriosclerosis, 1986. **6**(2): p. 220-9.

10. Girard, P.R. and R.M. Nerem, *Shear stress modulates endothelial cell morphology and F-actin organization through the regulation of focal adhesion-associated proteins.* J Cell Physiol, 1995. **163**(1): p. 179-93.

11. Cucina, A., et al., *Shear stress induces changes in the morphology and cytoskeleton organisation of arterial endothelial cells.* Eur J Vasc Endovasc Surg, 1995. **9**(1): p. 86-92.

12. Stamatas, G.N. and L.V. McIntire, *Rapid flow-induced responses in endothelial cells.* Biotechnol Prog, 2001. **17**(3): p. 383-402.

13. Gryglewski, R.J., R.M. Botting, and J.R. Vane, *Mediators produced by the endothelial cell.* Hypertension, 1988. **12**(6): p. 530-48.

14. Russo, G., J.A. Leopold, and J. Loscalzo, *Vasoactive substances: nitric oxide and endothelial dysfunction in atherosclerosis.* Vascul Pharmacol, 2002. **38**(5): p. 259-69.

15. Luscinskas, F.W. and J. Lawler, *Integrins as dynamic regulators of vascular function.* Faseb J, 1994. **8**(12): p. 929-38.

16. Helmlinger, G., B.C. Berk, and R.M. Nerem, *Calcium responses of endothelial cell monolayers subjected to pulsatile and steady laminar flow differ.* Am J Physiol, 1995. **269**(2 Pt 1): p. C367-75.

17. Prasad, A.R., et al., *Flow-related responses of intracellular inositol phosphate levels in cultured aortic endothelial cells.* Circ Res, 1993. **72**(4): p. 827-36.

18. Davies, P.F., et al., *Turbulent fluid shear stress induces vascular endothelial cell turnover in vitro.* Proc Natl Acad Sci U S A, 1986. **83**(7): p. 2114-7.

19. Helmlinger, G., et al., *Effects of pulsatile flow on cultured vascular endothelial cell morphology.* J Biomech Eng, 1991. **113**(2): p. 123-31.

20. Davies, P.F., et al., *Hemodynamics and the focal origin of atherosclerosis: a spatial approach to endothelial structure, gene expression, and function.* Ann N Y Acad Sci, 2001. **947**: p. 7-16; discussion 16-7.

21. Chappell, D.C., et al., *Oscillatory shear stress stimulates adhesion molecule expression in cultured human endothelium.* Circ Res, 1998. **82**(5): p. 532-9.

22. Johnson, C.M. and D.N. Fass, *Porcine cardiac valvular endothelial cells in culture. A relative deficiency of fibronectin synthesis in vitro.* Lab Invest, 1983. **49**(5): p. 589-98.

23. Deck, J.D., *Endothelial cell orientation on aortic valve leaflets.* Cardiovasc Res, 1986. **20**(10): p. 760-7.

24. Paranya, G., et al., *Aortic valve endothelial cells undergo transforming growth factor-beta-mediated and non-transforming growth factor-beta-mediated transdifferentiation in vitro.* Am J Pathol, 2001. **159**(4): p. 1335-43.

25. Johnson, E.N., et al., *NFATc1 mediates vascular endothelial growth factor-induced proliferation of human pulmonary valve endothelial cells.* J Biol Chem, 2003. **278**(3): p. 1686-92.

26. Sugi, Y. and R.R. Markwald, *Early endocardial formation originates from precardiac mesoderm as revealed by QH-1 antibody staining.* Ital J Anat Embryol, 1995. **100 Suppl 1**: p. 263-72.

27. Farivar, R.S., et al., *Transcriptional profiling and growth kinetics of endothelium reveals differences between cells derived from porcine aorta versus aortic valve.* Eur J Cardiothorac Surg, 2003. **24**(4): p. 527-34.

28. Andries, L. and D.L. Brutsaert, *Differences in structure between endocardial and vascular endothelium.* J Cardiovasc Pharmacol, 1991. **17**(Suppl. 3): p. S243-S246.

29. Lee, A.A., et al., *Fluid shear stress-induced alignment of cultured vascular smooth muscle cells.* J Biomech Eng, 2002. **124**(1): p. 37-43.

30. Rhoads, D., S. Eskin, and L. McIntire, *Fluid flow release fibroblast growth factor-2 from human aortic smooth muscle cells.* Arterioscler., Thromb., Vascular Biol., 2000. **20**: p. 416 - 421.

31. Mulholland, D.L. and A.I. Gotlieb, *Cell biology of valvular interstitial cells.* Can J Cardiol, 1996. **12**(3): p. 231-6.

32. Lester, W.M., et al., *Interstitial cells from the atrial and ventricular sides of the bovine mitral valve respond differently to denuding endocardial injury.* In Vitro Cell Dev Biol, 1993. **29A**(1): p. 41-50.

33. Davies, P.F., et al., *The convergence of haemodynamics, genomics, and endothelial structure in studies of the focal origin of atherosclerosis.* Biorheology, 2002. **39**(3-4): p. 299-306.

34. Riento, K. and A.J. Ridley, *Rocks: multifunctional kinases in cell behaviour.* Nat Rev Mol Cell Biol, 2003. **4**(6): p. 446-56.

35. Tzima, E., et al., *Activation of integrins in endothelial cells by fluid shear stress mediates Rho-dependent cytoskeletal alignment.* Embo J, 2001. **20**(17): p. 4639-47.

36. Li, S., et al., *Distinct roles for the small GTPases Cdc42 and Rho in endothelial responses to shear stress.* J Clin Invest, 1999. **103**(8): p. 1141-50.

37. Wojciak-Stothard, B. and A.J. Ridley, *Shear stress-induced endothelial cell polarization is mediated by Rho and Rac but not Cdc42 or PI 3-kinases.* J Cell Biol, 2003. **161**(2): p. 429-39.

38. Kaibuchi, K., S. Kuroda, and M. Amano, *Regulation of the cytoskeleton and cell adhesion by the Rho family GTPases in mammalian cells.* Annu Rev Biochem, 1999. **68**: p. 459-86.

39. Malek, A.M., et al., *Induction of nitric oxide synthase mRNA by shear stress requires intracellular calcium and G-protein signals and is modulated by PI 3 kinase.* Biochem Biophys Res Commun, 1999. **254**(1): p. 231-42.

40. Hemmings, L., et al., *Talin contains three actin-binding sites each of which is adjacent to a vinculin-binding site.* J Cell Sci, 1996. **109 (Pt 11)**: p. 2715-26.

41. Muguruma, M., et al., *Organization of the functional domains in membrane cytoskeletal protein talin.* J Biochem (Tokyo), 1995. **117**(5): p. 1036-42.

42. Cooray, P., et al., *Focal adhesion kinase (pp125FAK) cleavage and regulation by calpain.* Biochem J, 1996. **318 (Pt 1)**: p. 41-7.

43. Dwyer, L.D., et al., *Calpain-induced downregulation of activated protein kinase C-alpha affects lung epithelial cell morphology.* Am J Physiol, 1994. **266**(5 Pt 1): p. L569-76.

44. Thubrikar, M., et al., *Stresses of natural versus prosthetic aortic valve leaflets in vivo.* Ann Thorac Surg, 1980. **30**(3): p. 230-9.

45. Brewer, R., et al., *An in vivo study of the dimensional changes of the aortic valve leaflets during the cardiac cycle.* J Thorac Cardiovasc Surg, 1977. **74**: p. 645-650.

CHAPTER 5

COMPARISON OF GENE EXPRESSION PROFILES BETWEEN VALVULAR AND VASCULAR ENDOTHELIAL CELLS

One important factor in many cardiovascular pathologies is the additional presence of valvular deficiencies, particularly to the aortic valve. While valvular complications and vascular disorders are related, there are also diseases unique to valves, such as bacterial endocarditis and rheumatic heart disease. Many vascular pathologies, including atherosclerosis, originate at the endothelial surface, which highlights this cell layer as an important mediator of physiological and pathological functions[1]. The mechanisms as to why these pathologies are specific to valvular tissues are unclear, but it is possibly related to the differences in native cell populations and tissue structure. While blood vessels are comprised of endothelial cells, smooth muscle cells, and fibroblasts entombed in a lamellar collagen and elastin fiber matrix, aortic valve leaflets are much more complex. Leaflets have a highly organized, tri-layer structure composed of native endothelial and interstitial cells. While much work has been done to characterize the phenotype of interstitial cells as reported in Chapter 2, little is known about valvular endothelial cells. Endothelial cells perform many critical functions, including the maintenance of a non-thrombogenic surface, transduction of mechanical and biochemical signals to underlying cells, and transmission of nutrients through the tissue. The results from Chapter 4 have shown that valvular endothelial cells respond to fluid shear in a different manner than vascular endothelial cells. Valvular endothelial cells align perpendicular to flow, involving a PI 3-kinase independent signal pathway, with focal adhesions concentrating at the opposite ends of the major axis of cell alignment. This was in contrast to aortic endothelial cells, which aligned

parallel to flow in a PI 3-kinase dependent manner, with focal adhesions concentrating at the upstream and downstream portions of the cells. Valvular endothelial cells have also been shown to differentiate into a more smooth muscle cell-like phenotype[2], and proliferate more than vascular endothelial cells[3].

These phenotypic differences could be due in part to genetic differences between these two cell types. The profile of gene transcripts in a cell gives an assessment of what proteins cells are producing. Changes in gene expression in response to a stimulus precede actual protein changes, but predict cell behavior in short term experiments where protein accumulation cannot occur. Recently, gene arrays have become a standard tool to screen the genetic profiles of cells under a stimulus. Gene arrays enable the simultaneous investigation of the expression of thousands of proteins at the gene transcript level. They consist of an array of small islands of RNA fragment strands called “spots”, each representing a specific portion of a particular gene. Often these arrays contain complimentary DNA fragments (cDNA), which represent a portion of an RNA sample that has been amplified by Polymerase Chain Reaction (PCR). Gene arrays come in two basic forms: oligonucleotide arrays and cDNA microarrays. Oligonucleotide arrays are made by spotting small fragments (<50 bases) of RNA sequences onto a nylon felt, while cDNA microarrays prints larger fragments (200-400 bases) onto a glass substrate. Oligonucleotide arrays are typically analyzed through radiolabeling, while cDNA arrays utilize two fluorophores (Cy3 and Cy5). Each type has its own advantages and disadvantages, and selection of a specific platform is based on the type of experiments carried out. Oligonucleotide arrays are preferable for determining absolute transcript numbers, whereas cDNA arrays are better suited for cross-species analysis (i.e. porcine cells on a human array set) and give relative differences in expression between two sample pools. Several studies have used microarrays to profile the genetic response of vascular endothelial cells to shear

stress[4-6]. These studies have attempted to isolate genes that are sensitive to fluid forces in endothelial cells. While several genes previously identified as mechanosensitive genes, such as nitric oxide synthase (eNOS)[7], cyclo-oxygenase 2 (COX-2)[8], and vascular endothelial growth factor (VEGF)[9] have been confirmed using gene array techniques, many other genes have been identified as being flow regulated[5]. The format of gene arrays enables the development numerous research hypotheses from essentially "fishing expeditions", where little or none of the results are expected a priori. Improvements in image analysis software, gene array processing algorithms, and statistical packages have led to an information explosion that creates its own challenge: interpreting the data. While hundreds of genes may be differentially expressed in a gene array experiment, many of these may in fact be false positives. Statistical analyses require multiple data points for each sample, which can rapidly become prohibitively expensive. One aspect of this problem that has been little explored, however, is that experimental design is often not optimized to maximize statistical power to give high confidence in the results. It has been shown that two factor ANOVA greatly increases the predictive capability of microarrays, and reduces the probability of false positives[10]. In addition, further advances in post-processing have enabled the comparison of changes in gene categories. Many availably software packages can link genes with their ontological hierarchy, create categories at each level, and compare changes in the number of genes in these categories. This enables a multileveled approach in determining genetic phenotype change[11].

The objective of this study is to compare the genetic response of valvular and vascular endothelial cells to steady laminar shear stress, and characterize the genetic differences between the cell types in static and flow conditions. Statistically designed microarray analysis was integrated with new post-processing techniques, and hundreds of genes were differentially expressed between the cell types in both flow conditions.

Genes were grouped into relevant categories to facilitate new hypothesis generation. Real time PCR on was also conducted on selected genes as an independent method to confirm some of the microarray results.

5.1: Methods

Stress Experimental Setup. Porcine aortic valve endothelial cells (PAVECs) and porcine aortic endothelial cells (PAECs) were isolated from tissue obtained at a local slaughterhouse and cultured as previously described in Chapter 4 and explained in detail in the Appendix. Passage 5 monolayers of either PAVECs or PAECs were plated on glass slides coated with Collagen I (Becton-Dickenson, Rat tail, 50 μg/mL), and allowed to grow to confluence for 48 hours. Slides were then placed in a parallel plate flow system[12] shown in Chapter 4, and subjected to 20 dynes/cm^2 for 48 hours, with statically cultured slides serving as controls. While native heart valves experience a complex pulsatile shear flow, it is nearly impossible to replicate this environment in a controlled manner in vitro. The challenges in actually measuring the leaflet wall shear stress have resulted in a wide range of estimates (15-800 dynes/cm^2)[13-17]. Weston and colleagues determined a mean value of wall shear stress over the entire cardiac cycle of approximately 20 dynes/cm^2, which also compared well with laminar boundary layer theory for simplified geometries[18]. Because this purpose was to compare the response of both valvular and vascular endothelial cell to a mechanical force that could be considered physiological for both cell types, we concluded 20 dynes/cm^2 was a reasonable starting point. Much more data exists on endothelial cells in steady laminar shear than other velocity profiles, enabling a stronger comparison of our results to other work. It was demonstrated previously in Chapter 4 that morphological changes (and presumably other transient responses) under flow were completed by 48 hours for both

cell types, after which we postulate that reasonably stable genetic profiles would be present. Four experimental groups were created for comparison, and are summarized in Figure 5-1. One comparison was made with PAVECs in shear flow versus static (Group 1), one comparing PAECs in shear flow versus static, and two comparisons were made between cell types cultured statically (Group 3) or under flow (group 4). These groups comprise all paired comparisons relating endothelial cell types and fluid shear stress.

RNA Isolation. A detailed protocol for RNA isolation and quantification is given

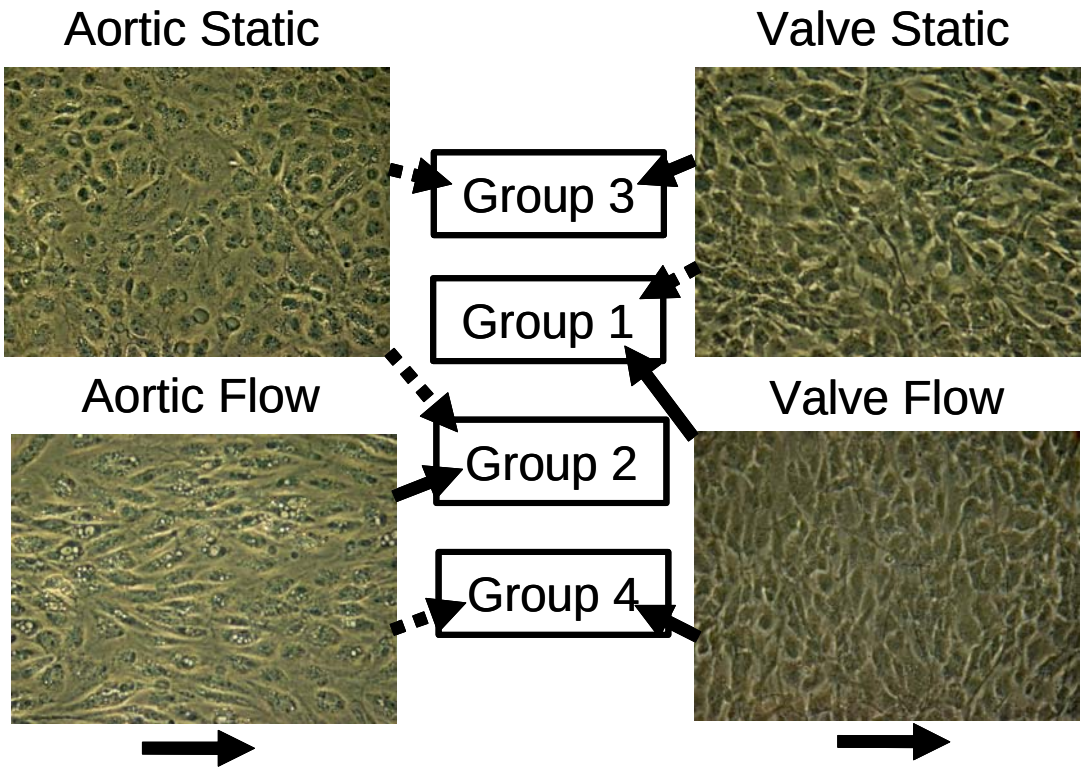

Figure 5-1: Schematic of comparison groups for microarray analysis. Solid line indicates "treated" condition. Dashed line indicates "control" condition.

in the Appendix. Briefly, upon completion of the experimental time points, the slides were removed from the flow systems (along with the non-sheared controls), trypsinized, and centrifuged at 1000 RPM in a bucket centrifuge. The supernatant was then

completely drained, the cells disrupted using a GITC-containing buffer, which inactivates RNases, and then homogenized by using a QIAshredder column (QIAGEN #79654). The resulting lysate was run through an RNeasy mini column (QIAGEN #74104), which enriches for mRNA by selectively binding RNA sequences longer than 200 nucleotides. The quantity and quality of the RNA was then checked by spectrophotometry and gel electrophoresis respectively. High quality RNA is determined by an absorbance ratio A_{260}/A_{280} of 1.8 – 2.1, with no other appreciable peaks, while the quantity of RNA is determined by measuring the absorbance at 260nm (A_{260}). Acceptable integrity of mRNA is alternatively quantified by sharp 28S and 18S bands in gel electrophoresis, with the intensity of the 28S band approximately twice that of the 18S band. The quality and quantity of the total RNA samples were determined in these experiments using the Agilent Bioanalyzer (Agilent #2100) and UV spectrometry. Only samples with greater than 10 μg total RNA and 28S/18S rRNA ratios between 1.8 and 2.1 were used for microarray hybridization. Preliminary experiments indicated that the amount of total RNA per experiment was approximately 5-7 μg, which was too low for optimal hybridization (10 μg.). While techniques exist for amplifying RNA quantities[19], it was decided early on to avoid any potential issues with biases that may exist in these processes. To achieve adequate sample quantities, two RNA samples from identical experiments were pooled together. This not only achieves an adequate RNA quantity, but also mitigates possible variation between samples.

RNA Labeling and Hybridization. Since no oligonucleotide array is available for porcine cells, a cDNA microarray platform was used. Porcine RNA has been shown to hybridize well with human probes in microarray experiments[20]. Total RNA pools from two different experimental conditions, each labeled differently, were hybridized together to an Agilent Human 1 cDNA microarray slide (Agilent #G4100A), which

contains 12,814 unique clones from Incyte's Unigene 1 and Human Drug Targets DNA clone sets. This is a competitive microarray platform, where two independently generated RNA samples are labeled with two different fluorophores (either Cy3 or Cy5) and hybridized competitively on a single probe array. This creates a comparative assessment of RNA levels between the two samples based on the color of the spot (red for one sample, green for another, and yellow for a mix), as well as an estimate of total mRNA levels per gene (intensity level). Total RNA from experiments and controls at identical time points were then directly labeled fluorescently (experimental RNA with Cy3, while control pools with Cy5), mixed together, and hybridized overnight to a cDNA microarray. The RNA labeling and hybridization process was performed at the Morehouse School of Medicine's Cardiovascular Research Institute, which had a core facility specializing in the Agilent cDNA microarray platform. It was important to have expert technicians handle these steps, as the chips used in these experiments cost over $1000 each, and optimized techniques and reagents are critical to the success of the experiments.

Image Analysis and Feature Extraction. Three slides were processed for each experimental condition, giving 6 arrays in an N = 3 (number of slides), n = 2 (replicates per slide) arrangement. High resolution images were taken of each array hybridization area using a microarray scanner (Agilent) and these images were analyzed to extract fluorescence intensities (Cy3 and Cy5) at each spot. The processing of these images involves several steps[21-23], and a more detailed description of the process can be found in Appendix C. First is the proper identification of spots on the array and their separation from the local background. This is especially important, because contaminating fragments can cause artificial spikes in genes, which confound analysis with small sample numbers. Misaligning the microarray in a scanner by as little as 10 μm can cause the false identification of every spot in the array. Local background levels,

rather than global background levels, must be determined for spot intensity normalization, because random differences in the hybridization process cause background to vary across the array. Next all spots which do not contain appreciable signal in either of the fluorescence channels, or are saturated, need to be removed from post analysis, because their digitized values are likely misleading. Finally each array needs to be analyzed to identify and adjust for any perceived bias in the expression of fluorophores[24], and non-specific hybridizations. Strategies for accomplishing this include difference to mean ratio thresholds, duplicate spotting, and anti-sense strand spotting[25]. Many array analysis software packages perform these functions, but it is important to know how the specific package employed handles these difficulties. The Agilent cDNA microarrays used in these experiments contain duplicate spots, sense and anti-sense strands, and a controlled ink jet spotting procedure that ensures consistent numbers of immobilized fragments at each location. In addition, the Feature Extraction Software (Agilent) used for these experiments identifies each array spot based on the alignment of specific reference spots that frame the array areas. Each feature is identified according to the preset spotting order. A detailed description of how the Agilent Feature Extraction Software was used in these experiments can be found in the Appendix C.

Statistical Analyses. Once fluorescent intensity measurements have been generated for each feature, representing the hybridization of each sample, statistical analyses must then be conducted to determine significant changes in expression between treatments. Because of the variation that is apparent between supposedly identical arrays (due to random differences in the spotting process, imperfections in the substrate, etc.), it is necessary to conduct multiple microarray hybridizations to achieve statistical significance[26]. Many feature extraction software packages have the capability to perform rudimentary statistical analyses on arrays, but only on one array at

a time. This is severely limiting for the aforementioned reasons. For instance, the Agilent Feature Extraction Software performs population statistics (Z-Tests) based on the green and red channel values of each pixel within a spot [27]. The significance test is therefore based on a large degree of freedom due to the over 200 pixels per spot. The variation between pixels in a single spot is much less than the variation between identical spots in different arrays and the degrees of freedom will be much lower between arrays. Therefore statistics must be conducted on multiple arrays using the average fluorescence intensity levels for each channel at a spot as the data points. Statistical analyses on data from multiple arrays have been conducted in several ways. Many microarray reports in the literature use a “fold expression” cutoff level to determine significant genes [28]. While this is a quick and simple method to identify genes of interest, there is no *statistical* basis for this method, and large but wild expression differences between samples would be improperly deemed significant, especially if only a small number of arrays are processed. Also, it is possible that many biological systems are highly sensitive to small changes in gene expression that would be less than a prescribed fold change limit. Statistical models, which are based on population distributions, are therefore much more useful tools for significance determination. Agilent microarray slides contain two identical array areas, which facilitate the use of highly robust statistical models to determine significant relationships across experimental conditions. Two factor mixed Analysis of Variance (ANOVA) was therefore used to determine significant changes in expression with treatment condition. This method isolates the variation associated with the treatment effect, thus dramatically improving sensitivity. A more detailed explanation can be found in Appendix C. The treatment condition (flow or cell type) was identified as the fixed effect, and the microarray slide as the random effect. The data for each array area served as the replicate measurements for the ANOVA. ANOVAS were performed on each comparison group shown in Figure

5-1. Because the statistical analysis requires that the number of measurements for each condition be equal, only genes for which an accepted spot was recorded in all six arrays were used in this analysis. The data from each useful feature of each array was overlapped to identify genes with measurements in all the arrays in the comparison. This reduced the number of comparable genes to approximately 5000 for each group, which was still greater than 50% of the genes with identified functions. To further improve statistical sensitivity, the mean squares of a particular gene ANOVA were pooled according to the rules of Sokal and Rohlf[29]. Basically, two variance estimators can be pooled together if they are not significantly different from each other (and thus estimators of the same quantity). While increasing the absolute value of the error variance in the ANOVA, pooling also increases the degrees of freedom for the significance test, thus reducing the threshold value needed for significance. However, because the actual population parameters estimated by the mean squares are unknown, strict rules must be followed, or incorrect conclusions could be drawn. Because of the improved sensitivity, $P<0.005$ was used as the significance threshold for these analyses.

Clustering and Ontological Characterization. Subsequent to statistical analysis *within* comparison groups, further characterization of differences *between* comparisons can be done using other software techniques. One helpful tool is called clustering. This involves grouping genes across arrays that are similarly expressed. Genes with upregulated expression in group 1, downregulated expression in group 2, etc., appear grouped together in a cluster. Free software to achieve this is available through Stanford University[30]. K-means clustering was performed on the data from all arrays together, and organized into 30 groups of similar expression trends. Because each comparison group had many genes that were either uniquely expressed in that group, or were significant only in that group, all genes for which readings existed in every array with a significant difference existed in at least one comparison, were

included in the clustering. While this method may confound statistically significant trends with non significant trends, it is helpful to visualize as many genes as possible to develop related cluster groups. The expression trends of the clusters were then visualized using software that bins the fold changes and renders them in a pseudocolor format, called a heatmap. Genes whose expression levels were significantly changed were also categorized using the GoMiner database engine[11]. This program links every known gene to its ontological hierarchy, creating multiple categories to which the gene is associated, an example of which is shown in Figure 5-2. This is done for every gene, and changes in the numbers of genes changing within a gene category can be assessed statistically. GoMiner uses a Fisher's Exact test to determine significance based on the numbers of significantly changed genes and total genes given by the user. In this manner, enrichment or depletion of genes in a category, as well as changes in expression of category members, can be assessed. A significance level of 0.05 was

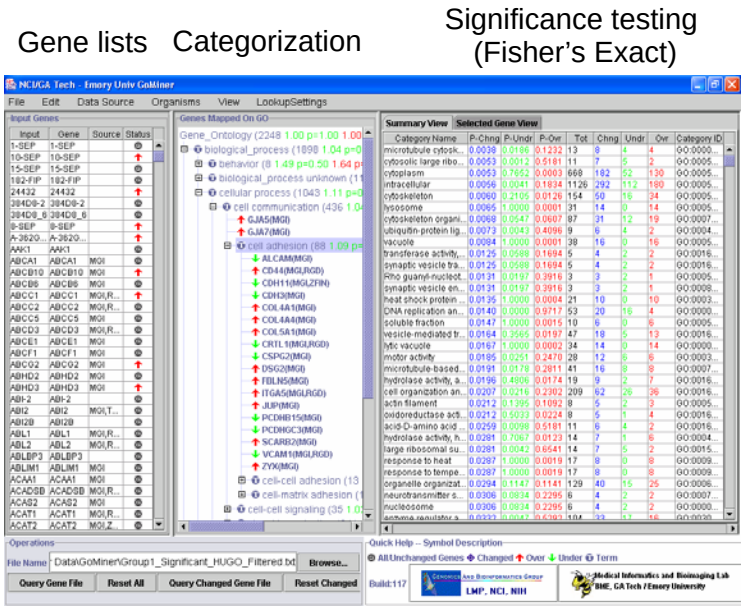

Figure 5-2: GoMiner gene categorization software. The example above shows significantly changing cell adhesion genes.

used in the Fisher's tests.

Real Time PCR Confirmation for Selected Genes. Additional shear flow and static experiments were carried out according to the aforementioned comparison scheme (Figure 5-1) to confirm the expression of relevant genes as determined by the microarray data. Briefly, 4 μg of total RNA (isolated as previously described) was reverse-transcribed by using random primers and a Superscript-II kit (Invitrogen) to synthesize first-strand cDNA. The cDNA was purified using a microbiospin 30 column (Bio-Rad) in Tris buffer and stored at –20 °C until used. PCR primers for *bone morphogenic protein 4* (*BMP-4*)[31], *cytochrome P450* (*CYP1A1)*[32], and *caveolin-1* (*Cav-1)*[33] were used to amplify the cDNA using a LightCycler (Roche Applied Science) RT-PCR machine. Similar amplification using universal *18S* primers (Ambion, 50 nM) were used as an internal control for the real-time PCR[31]. Each reaction was conducted a capillary (Roche Applied Sciences) containing 50 nM primers, 1 μg total RNA, PCR buffer (20 mM Tris-Cl, pH 8.4, at 25 °C, 4mM $MgCl_2$ to which was added 250 μg/ml bovine serum albumin, 200 μM deoxynucleotides) containing SYBR green (1:84,000 dilution), 0.05 unit/μl *Taq* DNA polymerase (Invitrogen), and Taq Start antibody (Clontech, 1:100 dilution). The mRNA copy numbers were determined based on standard curves generated with serial dilutions of the *BMP-4*, *CYP1A1*, *Cav-1* and 18 S templates. The primers used in these experiments, as well as the cycling temperatures, are listed in Table 5-1. To confirm the specific amplification of the RNA, DNA gel electrophoresis was conducted using the amplified samples. Briefly, 2% agarose gel containing 30 μL of ethidium bromide were created, and 20 uL of samples were inoculated into separate wells, followed by a well with a standard DNA ladder (100 – 400 bp). Gels were run for 1.5 hours at 80V, and imaged under UV light.

Table 5-1: Primers used for real time PCR confirmation of example genes.

Gene	Primers 5' – 3' +: Forward, -: Reverse	Transcript Length (bp)	Anneal Temp. °C	Extension Temp. °C	Extension Time s
BMP-4	+:CTGCGGGACTTCGAGGCGACACTTCT -:TCTTCCTCCTCCTCCTCCCCAGACTG	130	65	72	7
Cav-1	+:ACAAGCCCAACAACAAGGC -:TTGCCATTCTCTCCTTCCTG	250	68	72	13
CYP1A1	+:TGGAGAGGCAAGAGTAGTTGG -:GGCACAACGGAGTAGCTCATA-3	180	57	72	8

PCR - Microarray Comparison Across Microarray Groups. Expression comparison across these cDNA microarray groups requires relating data generated with two independent variables: treatment condition and array. The expression data for all four variable combinations (PAVEC shear, PAVEC static, PAEC shear, PAEC static) can be extracted from the microarray data. Because individual sample conditions are fluorescently labeled differently (either Cy3 or Cy5), a numerical intensity value proportional to copy number can be obtained for each sample pooled in the array. Comparisons can be made using each component of the shear-treated arrays (groups 1 and 2), or cell-treated arrays (groups 3 and 4). The results of the PCR were compared to the absolute expression levels of the hybridized RNA obtained from the microarray studies. For statistical purposes, one way ANOVA was used to determine significance within a methodology, and Students-t tests were employed for comparison between methodologies, with $P<0.05$ considered significant.

5.2: Results

Gene Expression Differences between Endothelial Cell Types. The goal of this study was to compare the genetic response of two different types of endothelial cells (PAVEC and PAEC) to steady laminar shear stress. To achieve this goal, the effects of steady shear stress were compared within each cell type (Group 1: PAVECs shear vs. PAVECs static, and Group 2: PAECs shear vs. PAECs static). Next, differences in gene expression between the two cell types were determined in either statically cultured cells (Group 3: PAVEC static vs. PAEC static) or cells under flow (Group 4: PAVEC flow vs. PAEC flow). Adequate quantities of high quality, pure total RNA were needed for the hybridizations. Figure 5-3 shows the results of several RNA isolation samples as determined by the Bioanalyzer. Two clear peaks representing the large amount of rRNA are seen, with virtually no other bands. The 28S/18S ratios were between 1.8 and 2.1,

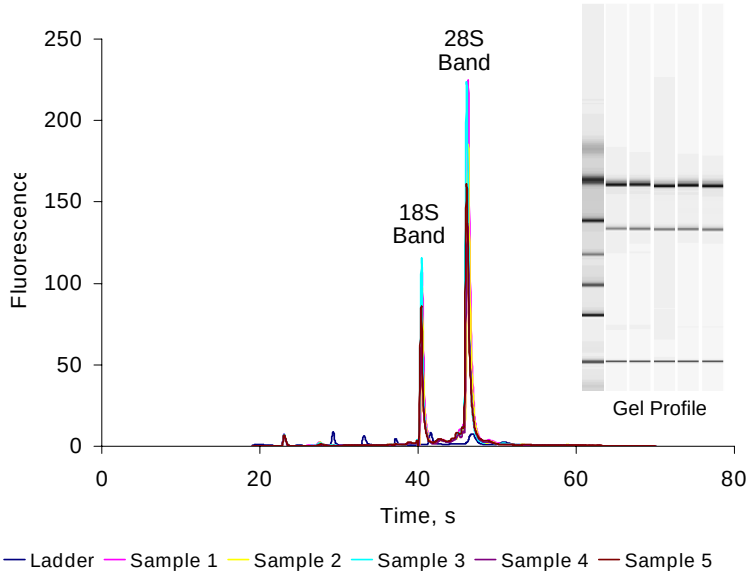

Figure 5-3: Confirmation of high quality pure RNA as evidenced by 28S/18S rRNA peaks with minimal contamination.

validating them as useful samples for hybridizations. Each sample used for hybridization was similarly characterized before use. The results of the cDNA microarray analysis are summarized in Table 5-2. Over 9000 spots were identified as reliable on each array, an example of which is shown in Figure 5-4, and approximately 4,700 genes were expressed above local background levels in all 6 arrays processed. Using the two factor mixed ANOVA model, over 1,200 genes in one sample were determined significantly changed relative to their co-hybridized sample at $P<0.05$, and over 400 at $P<0.005$. Further data processing was conducted on genes at $P<0.005$ because of the high false positive generation rate often seen in microarray data. As an example, microarray experiments that generate 200 significantly changed genes at $P<0.05$ with 1000 total genes analyzed, have a 25% chance that any particular gene is a false positive. The Positive Predictive Value (PPV) is an indication of the confidence one can place in the hypothesis rejection of one trial in a large number of trials[10]. The PPV for our dataset at $P<0.005$ was approximately 0.95 for each group, indicating a 95% “confidence” that

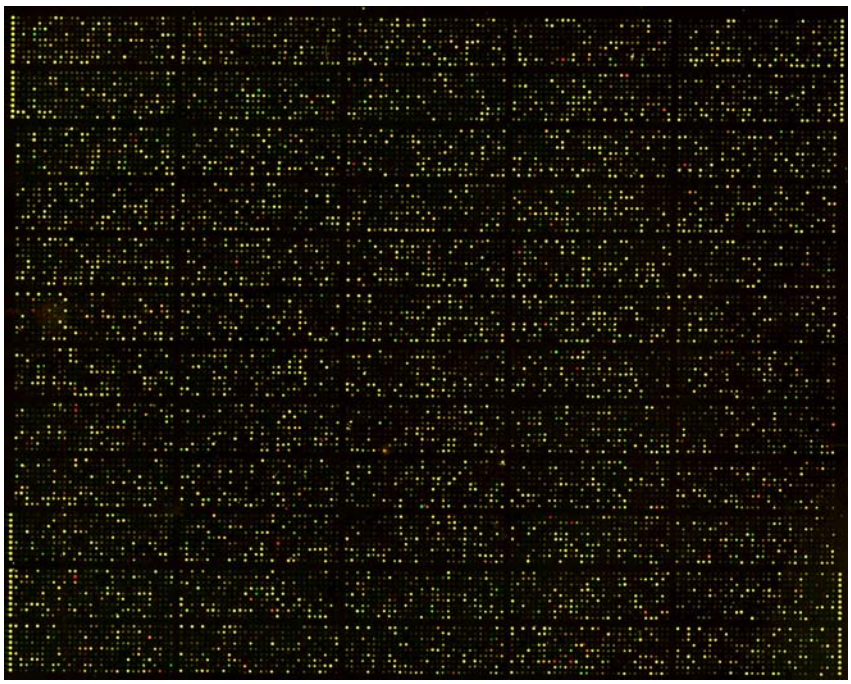

Figure 5-4: Example of microarray image generated by Agilent scanner.

any particular gene in the dataset is a true positive. In each microarray group, more genes were upregulated than downregulated in each group. This was not due to fluorescence bias, as the intensity signals for each array spot were normalized to internal dye controls on each array. The significantly changed genes from each group are listed in Appendix F. The improved sensitivity of the two factor ANOVA in comparison to other relevant statistical methods is highlighted in Appendix C.

As shown in Table 5-2, the two different endothelial cell types show quite distinct gene expression profiles under both static and shear exposed conditions. Shear exposure increased 545 and 324 genes in PAVEC and PAEC, respectively. Under static conditions, 236 genes were upregulated in PAVEC in comparison to PAEC. In contrast, 615 genes were upregulated in PAVEC in comparison to PAEC in response to shear

Table 5-2: Comparison of gene expression changes within experimental groups. V = Valvular EC, A = aortic EC, F = 20 dynes/cm^2 flow, S = static control.

Array Set Comparison type	Group1 PAVEC F vs. S	Group 2 PAEC F vs. S	Group 3 Static V vs. A	Group 4 Flow V vs. A
Total genes included	4297	4801	4786	5404
No. Significant Genes (P<0.05)	1586	1262	1213	2276
No. Significant Genes (P<0.005)	856	481	416	1152
PPV (P<0.005)	0.975	0.950	0.942	0.977
No. Upregulated (P<0.005)	545	324	236	615
No. Downregulated (P<0.005)	311	157	180	537
GoMiner categories enriched (P<0.05)	133	97	36	37
Gominer categories depleted (P<0.05)	66	20	25	12

stress. On the other hand, shear exposure downregulated expression of 311 and 157 genes in PAVEC and PAEC, respectively. The comparisons between the two cell types showed that 180 and 537 genes were downregulated in static and sheared PAVEC, respectively, in comparison to that of PAEC. As an initial comparison between experiment groups, the results of one array group were compared against another to note similarly and oppositely regulated genes, summarized in Table 5-3. This shows the number of genes that are registered in the compared categories (at $P<0.005$ significance level). While hundreds of genes were found significantly changed with flow in one cell type and unchanged with flow in another (compare groups 1 and 2), very few genes were actually oppositely regulated under flow. Due to the fact that approximately 75% of all genes on each microarray registered data, some important genes may be missed.

The relationships among changed genes between experimental comparisons were further analyzed through clustering, and the results are rendered in a Heatmap format (Figure 5-5). Four groups of columns represent the comparisons, and within in each row, six data points represent the results of the three microarrays in duplicate. The pseudo-color indicates a degree of fold change (red for increased expression, green for decreased). This schematic is helpful to isolate and highlight clusters of genes of interest, such as genes that are regulated differently between aortic and aortic valve origin. Inset A of Figure 5-5 highlights genes that are upregulated in PAVEC with shear, but downregulated in PAEC with shear. In contrast, inset B shows genes that are upregulated in PAEC with shear, but downregulated in PAVEC with shear. Inset C shows genes similarly regulated by flow in both cell types. The complete clustered data set is given in Appendix E. Analyzing the color changes within a group

Table 5-3: Numbers of genes regulated by overlapping the expression results of two comparison groups, as explained by row subheadings. (P<0.005). F=Flow, S=Static, V=Valve EC, A=Aortic EC, NC = No significant change.

Gene Expression Results for Each Independent Comparison Group							
Group 1: V-F vs. S		Group 2: A-F vs. S		Group 3: S-V vs. A		Group 4: F-V vs. A	
Up	545	Up	327	Up	121	Up	615
Down	311	Down	157	Down	126	Down	537
NC	3441	NC	4320	NC	4539	NC	4252

Comparisons of endothelial gene expression in response to flow (Groups 1 and 2)	**# Genes Up**	**# Genes Down**
Valvular and Aortic EC	119	45
Valvular EC not Aortic EC	260	184
Aortic EC not Valvular EC	69	37
Valvular EC UP Aortic EC DOWN	2	
Valvular EC DOWN Aortic EC UP	0	

Other Paired Group Comparisons from the Gene Data							
1 UP and 4 UP	**172**		1 UP and 3 UP	42		4 UP and 3 UP	101
1 UP and 4 DOWN	20		1 UP and 3 DOWN	22		4 UP and 3 DOWN	1
1 UP and 4 NC	258		1 UP and 3 NC	350		4 UP and 3 NC	337
1 DOWN and 4 UP	15		1 DOWN and 3 UP	8		4 DOWN and 3 UP	0
1 DOWN and 4 DOWN	**60**		1 DOWN and 3 DOWN	10		4 DOWN and 3 DOWN	85
1 DOWN and 4 NC	171		1 DOWN and 3 NC	204		4 DOWN and 3 NC	248
1 NC and 4 UP	219		1 NC and 3 UP	127		4 NC and 3 UP	32
1 NC and 4 DOWN	239		1 NC and 3 DOWN	98		4 NC and 3 DOWN	34
1 NC and 4 NC	2212		1 NC and 3 NC	2238		4 NC and 3 NC	2796
2 UP and 4 UP	92		2 UP and 3 UP	25		2 NC and 3 UP	132
2 UP and 4 DOWN	**11**		2 UP and 3 DOWN	14		2 NC and 3 DOWN	100
2 UP and 4 NC	135		2 UP and 3 NC	185		2 NC and 3 NC	2185
2 DOWN and 4 UP	**8**		2 DOWN and 3 UP	4		2 NC and 4 UP	310
2 DOWN and 4 DOWN	39		2 DOWN and 3 DOWN	15		2 NC and 4 DOWN	252
2 DOWN and 4 NC	66		2 DOWN and 3 NC	70		2 NC and 4 NC	2021

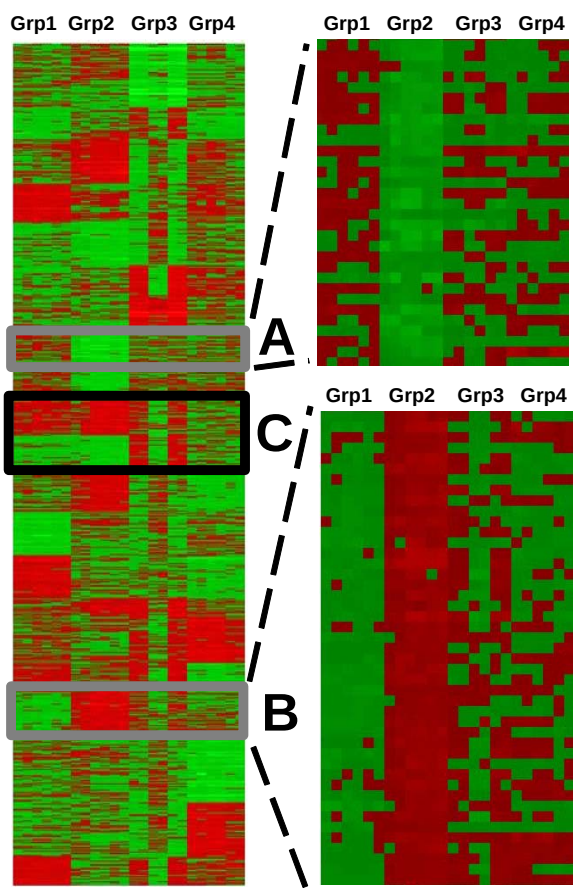

D

Gene ID	Description	G1 Ave	G2 Ave	G3 Ave	G4 Ave
AL524757	ARP1 (actin-related protein 1, yeast) homolog A (centractin alpha)	1.637	0.319	0.899	0.642
AF037447	Human ribosomal S6 protein kinase mRNA, complete cds.	1.681	0.349	0.823	0.880
BG424817	heat shock 70kD protein 9B (mortalin-2)	1.654	0.774	0.912	0.853
BG708735	ras homolog gene family, member C	2.286	0.753	1.030	1.017
AU139931	core promoter element binding protein	2.195	0.660	1.053	0.887
AB014606	kinesin family member 1C	1.660	0.754	0.841	0.724
AF009674	axin	1.558	0.794	0.956	1.133
BE787478	thioredoxin reductase 1	3.381	0.757	1.048	1.172

E

Gene ID	Description	G1 Ave	G2 Ave	G3 Ave	G4 Ave
BC011519	Human, angiotensinogen (serine (or cysteine) protease inhibitor, clade A	0.797	1.976	0.867	0.978
BI496977	protein phosphatase 2, regulatory subunit B	0.757	2.424	1.075	1.085
U67733	phosphodiesterase 2A, cGMP-stimulated	0.705	1.763	1.323	0.962
BC009200	Human, Rho GDP dissociation inhibitor (GDI) beta	0.767	4.369	1.148	0.934
AL526053	cAMP responsive element modulator	0.710	2.166	0.941	1.078
AL079635	RNA polymerase II transcriptional regulation mediator	0.767	1.580	0.930	0.938
BF676785	S-adenosylmethionine decarboxylase 1	0.747	2.042	1.129	0.889
BI756567	phosphodiesterase 3B, cGMP-inhibited	0.516	1.651	1.156	0.861

Figure 5-5: Heatmap rendition of global gene expression clusters. Gene expression levels were converted into a pseudocolor, with red indicating upregulation, and green downregulation. Insets A and B indicate groups of genes that are oppositely regulated by shear in PAVEC and PAEC. Inset C shows genes that are similarly regulated under shear in both cell types. Panels D and E list some of the genes that are included within Insets A and B, respectively.

indicates the high reproducibility of the data within each group. Group 1 (PAVECs) and Group 2 (PAECs) show the shear effects in comparison to static controls in each cell type. On the other hand, Group 3 shows the differential gene expression between the cell types in static culture (PAVECs vs. PAECs). Group 4 shows the genes expressed in sheared PAVECs vs. PAECs.

Categorization of changed genes. To determine which categories of genes change under different flow vs. static condition in the two different cell types, GoMiner was used. GoMiner displays significantly changed genes according to ontological hierarchy, as shown in figure 5-2. The gene categories created by the GoMiner database engine were assessed for enrichment and depletion, and the significantly changed gene categories were organized according to function, and are shown in Table 5-4, along with the direction of the change. As an example, the superoxide metabolism category is enriched (more upregulated genes than by chance) in PAECs under flow. The changes in gene categories therefore may provide additional mechanistic insights and suggest testable hypotheses of functional differences between the cell types[34-36]. For example, the GoMiner software indicated that valvular endothelial cells were more proliferative than vascular endothelium. To investigate this hypothesis, the effects of four different extracellular matrices (tissue culture plastic-TCP, collagen I, gelatin, and fibronectin) on endothelial cell proliferation were determined. While PAEC proliferate more than PAVEC on TCP, PAVEC proliferate more than PAEC when cultured on collagen I matrix (Figure 5-6). No differences in cell proliferation were observed with fibronectin or gelatin. A complete list of the changed gene categories for each array group is given in Appendix D.

Table 5-4: A profile of gene categories that were enriched or depleted within each array comparison as determined by GoMiner. The numbers in each box represent categories of related genes, a significant proportion ($P<0.05$) of which are similarly regulated under the imposed condition. V = Valvular EC, A = aortic EC, F = 20 dynes/cm^2 flow, S = static control. The category names can be found in Appendix D.

Biological Function		Group 1: V-F vs. S	Group 2: A-F vs. S	Group 3: S-V vs. A	Group 4: F-V vs. A
Oxioreductase Activity	Up	109,139,155, 169,177	8,29,51-53	3	13,28,41,5 7
	Down				
Cell Proliferation	Up			26,29,42, 54,58	12,21,22,3 6,42,44
	Down	28,30,49,52-54,65,66,112 +	73,87,88,93,12 4		
Cell Polarity	Up	16-20,71,73,77,2 21		50,57	
	Down				
Cell Migration	Up		12	1,6,11,17	
	Down		103		31
Extracellular Matrix	Up		1,2,5,9,25,106, 131		16,17,26
	Down		6		
Membrane Channel Activity	Up	145,238			
	Down			23,37,38, 46,47	
Synaptic Transmission	Up		55,102,132,133		
	Down	32,34		32,33	
Metal Ion Binding/Transport	Up	64	14,67,71		
	Down			2,10,39,5 2	1,22

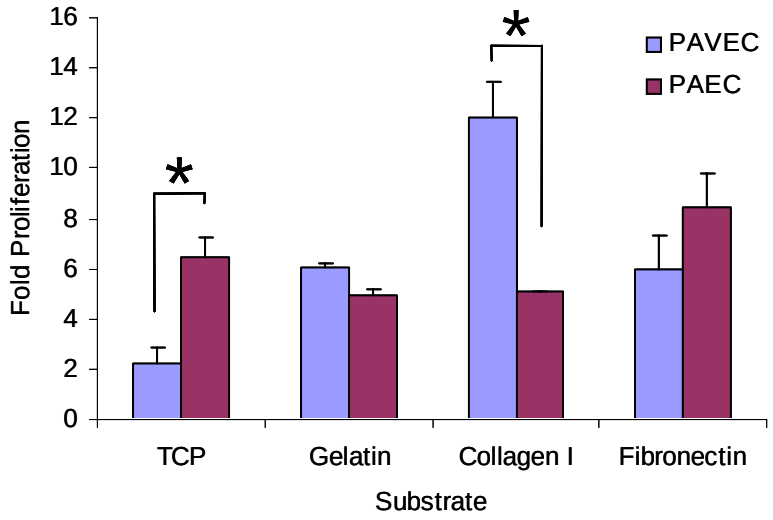

Figure 5-6: Comparison of cell proliferation between endothelial cell types cultured on different matrices. Cell number assessed at day 0 and day 5. * denotes significant ($P<0.05$).

While enrichment or depletion of genes within a category determined by GoMiner can provide an overall assessment of cell phenotype, different genes within a category also indicate phenotypic differences. For example, Table 5-5 shows the genes which are significantly changed in each comparison that are associated with extracellular proteins, whether they are cytokines, growth factors, or matrix proteins. Some genes are present in only one experimental comparison (e.g. *CLCA*, *CYR61* in Group 1), while some are present in all comparisons (e.g., *BMP-4*, *SST*). Within this particular category, somatostatin (*SST*) appears to be differentially regulated with flow between valvular and aortic endothelial cells. Extracellular-related proteins are important indicators of cell phenotype and biological response, and these results suggest important differences between these two cell types.

Table 5-5: Differentially expressed genes within the "extracellular" category as determined by GoMiner. V = Valvular EC, A = aortic EC, F = 20 dynes/cm^2 flow, S = static control.

G1: V- F vs. S		G2: A- F vs. S		G3: S- V vs. A		G4: F- V vs. A	
Gene	Reg.	Gene	Reg.	Gene	Reg.	Gene	Reg.
BMP4	Down	BMP4	Down	BMP4	Down	BMP4/BMP6	Down
						CRIM1	Up
IL13	Down	IL1A	Up	IL13	Down	IL1A	Down
		CSF2	Up	CXCL1	Down	CXCL14	Up
		SAA1	Down			SAA4	Up
						CCL2	Down
						CCL3	Up
IGF1	Down			IGFBP5	Up	IGFBP4	Up
						CTGF	Down
SST	Up	SST	Down	SST	Down	SST	Down
		NPY	Down			ADM	Down
		INHBA	Up			INHBA	Down
		FBLN2	Down			FBLN2	Up
DKK3	Up	DKK3	Up				
				MIA	Down	MIA	Down
PROC	Up	F2	Up			PRL	Down
SNK	Down	STC2	Down				
CALCA	Up						
CYR61	Up						

Real Time PCR confirmation of selected flow sensitive genes. Real time PCR was used to confirm some of the Microarray data. Each sample amplification was normalized to amplified 18S rRNA from the same sample. Figure 5-7 shows a comparison of real time PCR *BMP-4* expression and *18S* expression on an experiment-wide basis. The different color boxes indicate separate reverse transcriptions. Based on the trends within each box, it is clear that while *BMP-4* expression changes between cell type and flow conditions, the *18S* expression remains consistent. There will always be some differences between reverse transcriptions, because random factors in the reaction process will contribute to slight differences in transcription efficiency. Nevertheless, the use of *18S* as a control primer for these experiments was confirmed.

The expression of *BMP-4* across all four conditions as determined by the different methods (real time PCR and microarray) is shown in Figure 5-8A. The real time PCR data showed that *BMP-4* levels were downregulated in both PAVEC and PAEC and in response to flow. The PCR data indicates a much stronger expression of *BMP-4* in statically cultured PAVECs compared to PAECs (9.4 fold greater), and a much stronger sensitivity to shear stress (23.5-fold downregulation vs. 5.0 fold downregulation in PAECs). Although the fold stimulation was not identical to that of the microarray result, real time PCR data did confirm the trend. There was no significant differences between either rendering of the microarray data ($P>0.05$).

The upregulation of *CYP1A1* by flow in PAECs as shown by the microarray data was confirmed by real time PCR (Figure 5-8B). The sensitivity of *CYP1A1* to flow was more prominent with PCR (12.6-fold) than that of the microarray data (9.4-fold and 2.9-fold). The absolute expression of *CYP1A1* in PAVECs was greater than PAECs in both conditions according to PCR ($P<0.05$), but there was no significant difference in sensitivity to shear stress between the two cells (13.2-fold for PAVECs, 12.6-fold for PAECs, $P>0.05$). The data comparison of *Cav-1* is shown in Figure 5-8C. The PCR data indicates a downregulation of *Cav-1* with shear in PAECs, while the microarray datasets did not indicate a significant change in expression for PAECs. Both the microarray datasets and the PCR data indicated downregulation of *Cav-1* in PAVEC with shear. There was a greater expression of *Cav-1* in static PAVECs compared to static PAECs according to PCR ($P<0.05$), but no difference in expression between the cells under flow.

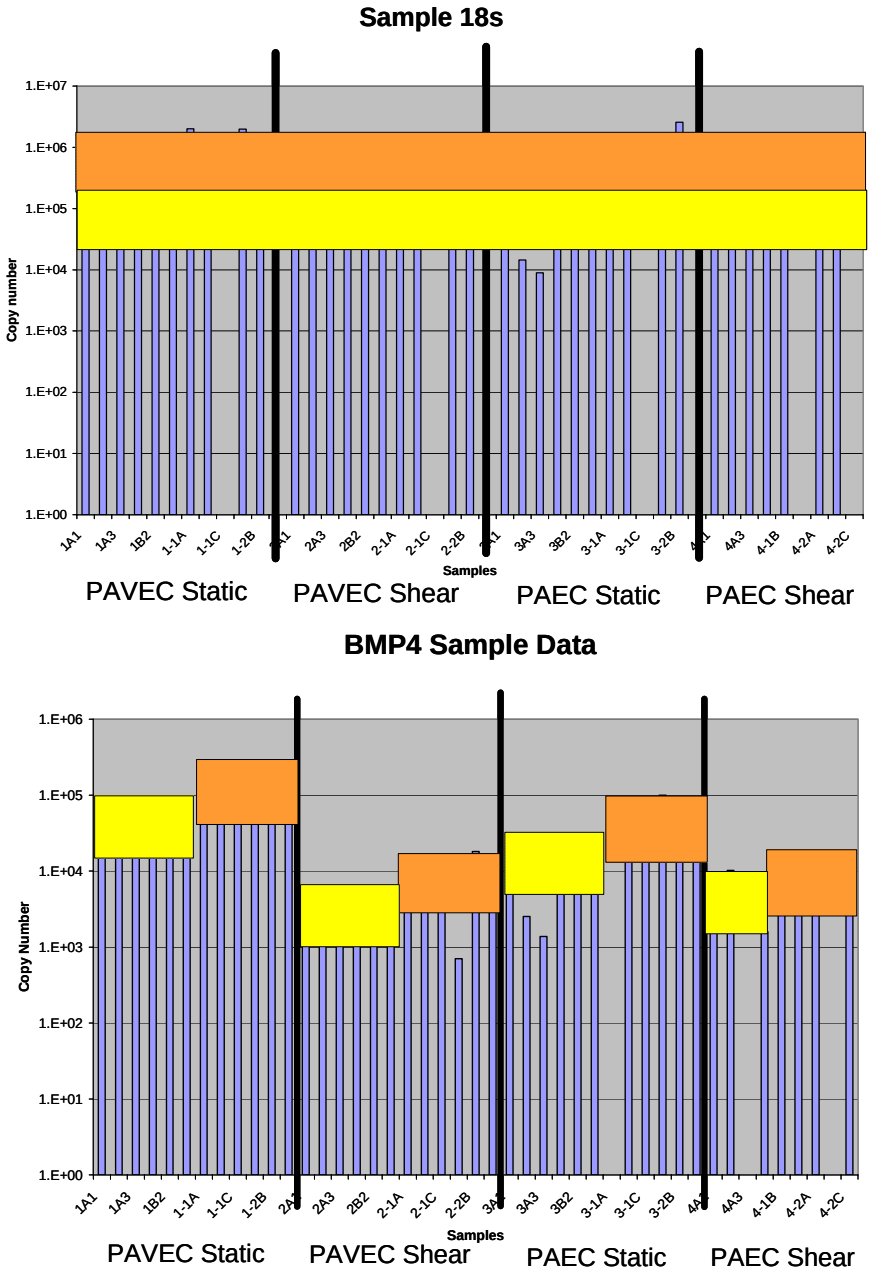

Figure 5-7: Individual sample expression of 18s and BMP-4 as determined by real time PCR. Each color bar represents a different reverse transcription of the original RNA.

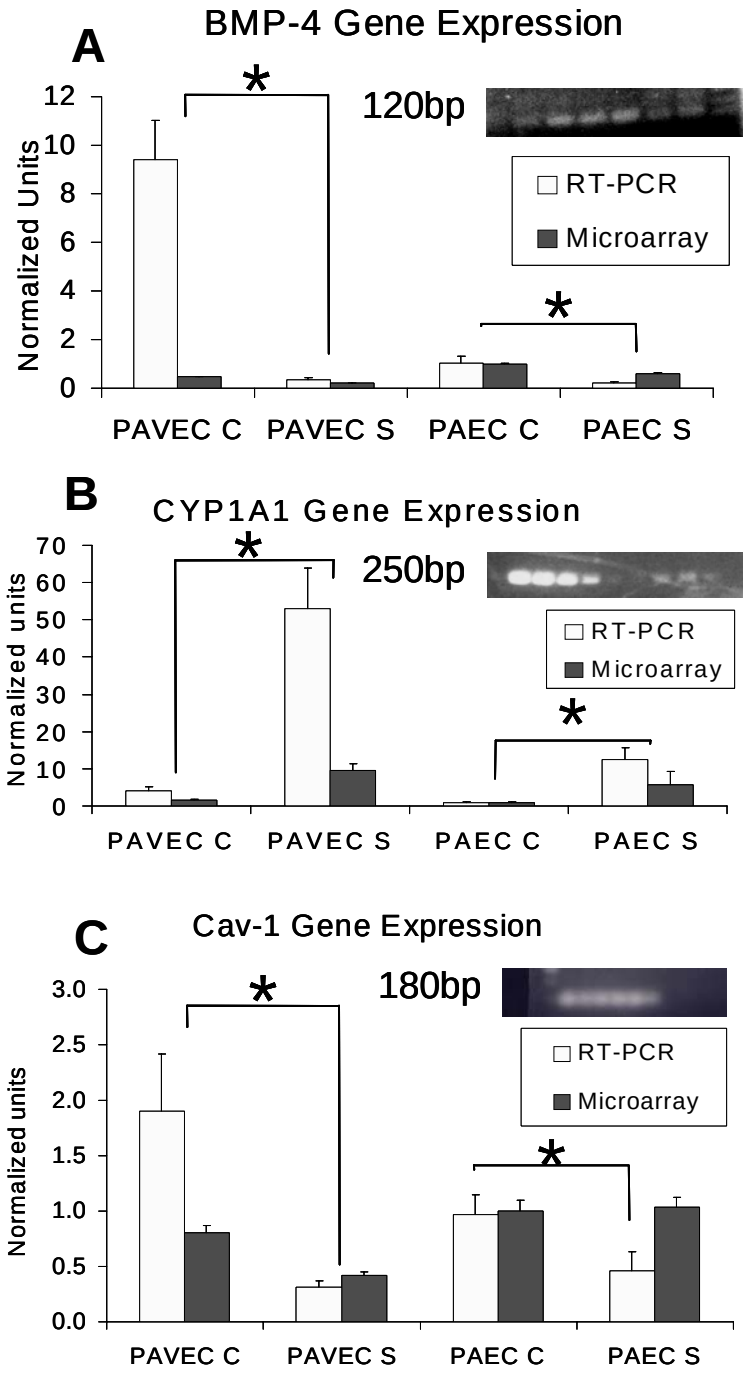

Figure 5-8: Verification of the expression of example genes by quantitative real time PCR. Microarray intensities were compared to PCR product normalized to 18S content. Data normalized to PAEC control for comparison. Inset shows gel confirmation of appropriate band. * denotes significance ($P<0.05$).

5.3: Discussion

It was determined in this study that endothelial cells derived from aortic and aortic valvular origins share several similarities, but present notable differences at the genomic level. As reported in Chapter 4, both cell types grow with contact inhibition and show a similar cobblestone shape in static culture. However, in response to shear PAVECs align perpendicular to flow whereas PAECs align with the flow direction[37]. The mechanisms underlying these different morphological responses may have a significant implication in understanding how they behave under *in vivo* hemodynamic conditions. The microarray results showed hundreds of genes that were significantly regulated in each comparison group. The genes that were significantly changed in one cell type but not in another and not may therefore provide more clues as to functions not present in both cell types. For example, more than 1,100 genes (615 up and 535 down in Group 4, Table 3) were differentially expressed in response to flow in PAVEC when compared to PAEC. At least a part of these differential genes may be responsible for the unique mechanoresponses including the morphological responses (Fig. 1) between the two cell types. Further comparison of this subset of genes with Groups 3 and 4 would then indicate flow regulated genes that are expressed significantly more or less in one cell type. The heat map analysis provides the simplest rendering of the results from all four Groups. Clusters of genes following the aforementioned patterns could be identified, and some genes from these groups were highlighted. While it is inappropriate to exhaustively discuss all of the possible combinations revealed by this analysis, the complete cluster database is presented in the online supplement. This cluster analysis is by no means complete, however, because any gene for which a spot was not

recorded on any of the 24 arrays studied could not be included in this profile. This reduced the number of genes analyzed to just over 1000, which is about 80% less than the 5000 that existed in each comparison group and significantly less than the 12,814 possible features on each array. While it would be expected that a large percentage of genes would not register on these arrays because of low expression in these cell types, experimental difficulties common to all microarray hybridization and processing may in addition corrupt array regions containing potentially important information. It is therefore critical to review the data from each stage in this analysis (microarray, pairwise comparison, K-means clustering, ontological hierarchy) to create a clearer picture of how these cells are similar and different.

Ontological profiling of the gene changes provided the fastest access to potential research hypotheses as to the unique and shared phenotypic properties of these cells, some of which have been verified by previous studies. The GoMiner engine indicated enrichment of many cell polarity genes in PAVECs in static and fluid flow environments (Table 5-4), and this supports the unique morphology reported for PAVECs. The enrichment of proliferation-related gene categories in PAVECs compared to PAECs and depletion of proliferation-related categories under flow also support the data reported in this study and others[3, 38, 39]. Many other categories were also enriched and depleted, and the database provided by this study in Table 5-4 and in the online supplement suggests other readily testable hypotheses of similarities and differences between these two cell types.

To begin to ascertain some of the similarities and differences between these two cell types while confirming the microarray data, real time PCR was conducted on selected genes which coded for important regulatory proteins in endothelial physiology and pathology. *BMP-4* was one of the most robustly inhibited genes by laminar shear in both PAEC and PAVEC. Consistent with this finding, it has been shown previously that

laminar shear stress inhibits and oscillatory shear stimulates *BMP-4* production[31]. *BMP-4*, induced by the pro-atherogenic oscillatory shear stress, is a potent inflammatory cytokine stimulating monocyte adhesion to endothelial cells, a critical early atherogenic step. BMP's are also critical for normal development of the aortic valve[40]. Given the additional importance of *BMP-4* in osteogenic differentiation, the dramatically high levels of *BMP-4* in statically cultured PAVEC suggests possible connections between shear environment and the initiation of calcification. The majority of valvular calcification originates on the aortic side of the valve leaflet, which experiences a circulating flow pattern with much lower wall shear stresses than the ventricular side. It is thus possible that unstable and low shear stress may initiate some endothelial dysfunctions resulting in the initiation of calcification through *BMP-4*. *CYP1A1* is a mechanosensitive protein that is part of the cytochrome P450 family of oxidants. It is an indicator of oxidative stress state, which is induced by pharmacological toxins[32, 41] and shear stress[42]. In our experiments, a similar large increase in *CYP1A1* expression under steady shear was observed in both cell types, but greater expression was observed with PAVECs. The ontological profiling suggested enrichment of oxioreductive gene categories in PAVECs in shear and over PAECs, suggesting that PAVECs are more sensitive to oxidative stress than PAECs. Indeed some pharmacological agents that increase oxidative stress have been shown to preferentially affect aortic valve function[43, 44]. *Cav-1* is another mechanosensitive gene hat has been shown to be downregulated by shear stress[33]. Cav-1 protein was shown to be reorganized into the luminal surface of the plasma membrane caveolae in valvular and vascular endothelial cells[45], altering the responsiveness of endothelial cells to subsequent shear changes[33]. *Cav-1* expression was one of the least significant determined in the microarray studies, and only for PAVECs. The expression of this gene therefore would be an appropriate check of the sensitivity of the array design. While real time PCR confirmed *Cav-1* downregulation

with shear in both cell types, the microarray indicated downregulation in valvular endothelial cells only. The exhaustive literature supporting *Cav-1* downregulation under flow in vascular endothelial cells coupled with the PCR data that indicates the same lead to the conclusion that the microarray was not sensitive to this effect, not that the effect does not occur. These results suggest that both valvular and vascular endothelial cells involve caveolae in mechanosensing fluid flow.

In summary, we have identified lists of hundreds of genes that are regulated by shear stress in aortic and aortic valve endothelial cells. These two cell types respond to shear conditions in similar and different ways, some of which were determined using ontological categorization. The explicit roles of valvular endothelial cells in inflammatory, oxidative stress, and mechanotransduction pathways have yet to be elucidated, but this data suggests that valvular endothelial cells are important mediators of valvular function, and vascular endothelial cells may not adequately mimic these functions in a tissue engineering application. While valvular endothelial cells may not ultimately be useful as a cell source for living heart valve replacements, future study with these cells will yield more insight into appropriate valvular functions, and help develop targeted therapeutic strategies, perhaps identifying valvular pathologies before they progress beyond the limit of efficacy of non-surgical interventions.

A statistical significance level of $P<0.005$ was chosen for these studies partly because the PPV was approximately 95% for each comparison group, but also because it pared the data to a more manageable amount to mine. The blessing of reams of data in microarray experiments is also a curse. One of the consequences of this more stringent significance level is that genes whose expression may in fact be noteworthy are deemed non-significant. It is possible that by relaxing the significance level, many other genes now significantly different would be differently regulated between comparison groups. As an example, relaxing the significance level to $P<0.05$ indicates 8

genes upregulated in flow in PAVECs but downregulated in PAECs, and 4 genes regulated in the opposite way (as opposed to 2 and 0, respectively). Simply relaxing the significance level is a risky proposition however, and independent techniques should always be used to verify any genes of interest before any conclusions can be drawn.

The expression levels of example genes of interest were verified in this study using real time PCR. While this method is an independent measurement of transcript quantity, it may also have little relevance to protein levels. Many post-transcriptional modifications exist in cells, which regulate how mRNAs are transcribed to proteins, and the ratio of transcript to protein likely varies between genes. Therefore, it is critical to assess expression at both the genomic and proteomic levels. Protein quantification is also challenging, due to the many isoforms and cleavage sites that may exist, but a general method such as Western blotting should be sufficient. Other methods of protein quantification include protein chips, flow cytometry, and ELISA-based assays.

5.4: References

1. Poggianti, E., et al., *Aortic valve sclerosis is associated with systemic endothelial dysfunction.* J Am Coll Cardiol, 2003. **41**(1): p. 136-41.

2. Paranya, G., et al., *Aortic valve endothelial cells undergo transforming growth factor-beta-mediated and non-transforming growth factor-beta-mediated transdifferentiation in vitro.* Am J Pathol, 2001. **159**(4): p. 1335-43.

3. Farivar, R.S., et al., *Transcriptional profiling and growth kinetics of endothelium reveals differences between cells derived from porcine aorta versus aortic valve.* Eur J Cardiothorac Surg, 2003. **24**(4): p. 527-34.

4. McCormick, S.M., et al., *Microarray analysis of shear stressed endothelial cells.* Biorheology, 2003. **40**(1-3): p. 5-11.

5. Dekker, R.J., et al., *Prolonged fluid shear stress induces a distinct set of endothelial cell genes, most specifically lung Kruppel-like factor (KLF2).* Blood, 2002. **100**(5): p. 1689-98.

6. Chen, B.P., et al., *DNA microarray analysis of gene expression in endothelial cells in response to 24-h shear stress.* Physiol Genomics, 2001. **7**(1): p. 55-63.

7. Ranjan, V., Z. Xiao, and S.L. Diamond, *Constitutive NOS expression in cultured endothelial cells is elevated by fluid shear stress.* Am J Physiol, 1995. **269**(2 Pt 2): p. H550-5.

8. Topper, J.N., et al., *Identification of vascular endothelial genes differentially responsive to fluid mechanical stimuli: cyclooxygenase-2, manganese superoxide dismutase, and endothelial cell nitric oxide synthase are selectively up-regulated by steady laminar shear stress.* Proc Natl Acad Sci U S A, 1996. **93**(19): p. 10417-22.

9. Gan, L., et al., *Distinct regulation of vascular endothelial growth factor in intact human conduit vessels exposed to laminar fluid shear stress and pressure.* Biochem Biophys Res Commun, 2000. **272**(2): p. 490-6.

10. Zhao, Y., et al., *Improved significance test for DNA microarray data: temporal effects of shear stress on endothelial genes.* Physiol Genomics, 2002. **12**(1): p. 1-11.

11. Zeeberg, B.R., et al., *GoMiner: a resource for biological interpretation of genomic and proteomic data.* Genome Biol, 2003. **4**(4): p. R28.

12. Levesque, M.J. and R.M. Nerem, *The elongation and orientation of cultured endothelial cells in response to shear stress.* J Biomech Eng, 1985. **107**(4): p. 341-7.

13. Einav, S., et al., *Wall shear stress distribution along the cusp of a tri-leaflet prosthetic valve.* J Biomed Eng, 1990. **12**(1): p. 13-8.

14. Nandy, S. and J.M. Tarbell, *Flush mounted hot film anemometer measurement of wall shear stress distal to a tri-leaflet valve for Newtonian and non-Newtonian blood analog fluids.* Biorheology, 1987. **24**(5): p. 483-500.

15. Nygaard, H., et al., *Two-dimensional color-mapping of turbulent shear stress distribution downstream of two aortic bioprosthetic valves in vitro.* J Biomech, 1992. **25**(4): p. 429-40.

16. Stevenson, D.M., A.P. Yoganathan, and F.P. Williams, *Numerical simulation of steady turbulent flow through trileaflet aortic heart valves--II. Results on five models.* J Biomech, 1985. **18**(12): p. 909-26.

17. Walburn, F.J. and P.D. Stein, *Wall shear stress during pulsatile flow distal to a normal porcine aortic valve.* J Biomech, 1984. **17**(2): p. 97-102.

18. Weston, M.W., D.V. LaBorde, and A.P. Yoganathan, *Estimation of the shear stress on the surface of an aortic valve leaflet.* Ann Biomed Eng, 1999. **27**(4): p. 572-9.

19. Polacek, D.C., et al., *Fidelity and enhanced sensitivity of differential transcription profiles following linear amplification of nanogram amounts of endothelial mRNA.* Physiol Genomics, 2003. **13**(2): p. 147-56.

20. Davies, P.F., et al., *The convergence of haemodynamics, genomics, and endothelial structure in studies of the focal origin of atherosclerosis.* Biorheology, 2002. **39**(3-4): p. 299-306.

21. Nadon, R. and J. Shoemaker, *Statistical issues with microarrays: processing and analysis.* Trends Genet, 2002. **18**(5): p. 265-71.

22. Wu, T.D., *Analysing gene expression data from DNA microarrays to identify candidate genes.* J Pathol, 2001. **195**(1): p. 53-65.

23. Hess, K.R., et al., *Microarrays: handling the deluge of data and extracting reliable information.* Trends Biotechnol, 2001. **19**(11): p. 463-8.

24. Yang, Y.H., et al., *Normalization for cDNA microarray data: a robust composite method addressing single and multiple slide systematic variation.* Nucleic Acids Res, 2002. **30**(4): p. e15.

25. Chen, Y.J., et al., *Normalization methods for analysis of microarray gene-expression data.* J Biopharm Stat, 2003. **13**(1): p. 57-74.

26. Novak, J.P., R. Sladek, and T.J. Hudson, *Characterization of variability in large-scale gene expression data: implications for study design.* Genomics, 2002. **79**(1): p. 104-13.

27. *Agilent G2566AA Feature Extraction Software User Manual*. Fourth Edition ed. 2001, Palo Alto, CA: Agilent Technologies.

28. McCormick, S.M., et al., *DNA microarray reveals changes in gene expression of shear stressed human umbilical vein endothelial cells.* Proc Natl Acad Sci U S A, 2001. **98**(16): p. 8955-60.

29. Sokal, R. and F. Rohlf, *Biometry*. Third ed. 1995, New York: W. H. Freeman and Co. 284 - 285.

30. Eisen, M.B., et al., *Cluster analysis and display of genome-wide expression patterns.* Proc Natl Acad Sci U S A, 1998. **95**(25): p. 14863-8.

31. Sorescu, G.P., et al., *Bone morphogenic protein 4 produced in endothelial cells by oscillatory shear stress stimulates an inflammatory response.* J Biol Chem, 2003. **278**(33): p. 31128-35.

32. Hennig, B., et al., *Proinflammatory properties of coplanar PCBs: in vitro and in vivo evidence.* Toxicol Appl Pharmacol, 2002. **181**(3): p. 174-83.

33. Boyd, N.L., et al., *Chronic shear induces caveolae formation and alters ERK and Akt responses in endothelial cells.* Am J Physiol Heart Circ Physiol, 2003. **285**(3): p. H1113-22.

34. Milovanova, T., et al., *Endothelial cell proliferation associated with abrupt reduction in shear stress is dependent on reactive oxygen species.* Antioxid Redox Signal, 2004. **6**(2): p. 245-58.

35. Bao, X., C. Lu, and J.A. Frangos, *Mechanism of temporal gradients in shear-induced ERK1/2 activation and proliferation in endothelial cells.* Am J Physiol Heart Circ Physiol, 2001. **281**(1): p. H22-9.

36. Bruder, J.L., et al., *Induced cytoskeletal changes in bovine pulmonary artery endothelial cells by resveratrol and the accompanying modified responses to arterial shear stress.* BMC Cell Biol, 2001. **2**(1): p. 1.

37. Butcher, J.T., et al., *Unique morphology and focal adhesion development of valvular endothelial cells in static and fluid flow environments.* Arteriosclerosis, Thrombosis, and Vascular Biology, 2004.

38. Imberti, B., et al., *The response of endothelial cells to fluid shear stress using a co-culture model of the arterial wall.* Endothelium, 2002. **9**(1): p. 11-23.

39. Villaschi, S. and R.F. Nicosia, *Paracrine interactions between fibroblasts and endothelial cells in a serum-free coculture model. Modulation of angiogenesis and collagen gel contraction.* Lab Invest, 1994. **71**(2): p. 291-9.

40. Delot, E.C., et al., *BMP signaling is required for septation of the outflow tract of the mammalian heart.* Development, 2003. **130**(1): p. 209-20.

41. Dong, W., et al., *2,3,7,8-tetrachlorodibenzo-p-dioxin toxicity in the zebrafish embryo: local circulation failure in the dorsal midbrain is associated with increased apoptosis.* Toxicol Sci, 2002. **69**(1): p. 191-201.

42. Eskin, S.G., *Endothelial Cell Cytochrome P450 1A1 and 1B1: Up-Regulation by Shear Stress.* Endothelium, 2004. **11**.

43. Hauck, A.J., et al., *Mitral and aortic valve disease associated with ergotamine therapy for migraine. Report of two cases and review of literature.* Arch Pathol Lab Med, 1990. **114**(1): p. 62-4.

44. Chester, A.H., et al., *Influence of 5-hydroxytryptamine on aortic valve competence in vitro.* J Heart Valve Dis, 2001. **10**(6): p. 822-5; discussion 825-6.

45. Rajamannan, N.M., et al., *Localization of caveolin 1 in aortic valve endothelial cells using antigen retrieval.* J Histochem Cytochem, 2002. **50**(5): p. 617-28.

CHAPTER 6

TISSUE ENGINEERED AORTIC VALVE LEAFLET MODEL: EFFECTS OF STEADY LAMINAR SHEAR STRESS

Cardiovascular tissues perform many important biological functions while maintaining a mechanical integrity that enables blood to flow uninhibited. These include maintenance of vessel tone, preventing blood clot formation, and the transfer of mechanical and biochemical signals. Most cardiovascular pathologies begin biologically in nature, and progress to mechanical failure. A prime example of this is with heart valve disease. The four heart valves work in conjunction with the heart to maintain unidirectional blood flow through the heart, and as such must resist highly dynamic strain and flexure in addition the hemodynamic pressures. The aortic valve, situated about the right ventricle, is the most highly stressed, and as such is the valve most often replaced by prosthetic valves. Biological destruction of the aortic valve often begins with endothelial dysfunction, such as in infective endocarditis[1] or aortic valve sclerosis[2]. Cells differentiate, die, and eventually the valve loses its ability to repair local tissue microdamage, which leads to gross tissue failure. Homograft or prosthetic valve replacement is currently the only clinical solution, and can provide approximately 10-15 years of function before failing in a number of ways mainly associated with the fact that they are nonliving substitutes[3-6]. While tissue engineering shows great promise to alleviate the weaknesses of non-viability, attempts to engineer heart valve tissue have focused perhaps necessarily on the maintenance of mechanical integrity, and have used several matrices to achieve this, including biodegradable synthetic polymers[7, 8],

decellularized heart valves[9, 10], and biological matrix molecules[11]. While each method holds some promise, they have been met with limited success so far in animal trials. Research by the Mayer group over the last 10 years culminated in the development of a biodegradable polymer valve populated with autologous vascular cells implanted in the pulmonary position[12]. After 20 weeks implantation in a sheep model, these valves exhibited similar tissue structure, cell phenotype, mechanical properties, and protein levels of normal valves. While these results demonstrated feasibility of a tissue engineered valvular replacement, the valves were still mildly regurgitant even on the low pressure pulmonary side, making their clinical use in the high pressure right heart system limited. The success of heart valve tissue engineering will therefore depend ultimately on the ability of the cells populating the device to thrive within the dynamic and complex mechanical environment, remodel the tissue to repair microdamage, and prevent the loss of critical matrix molecules.

Advances in the understanding of valvular cells biology has not kept up with the understanding of valve tissue mechanics. Indeed, most tissue engineering applications have used cells isolated from blood vessels[8, 9, 13] or stem cells[14] to populate their matrices. The aortic valve leaflet is populated with interstitial cells and lined with endothelial cells. There is surprisingly little actually known about normal valvular endothelial cell function. Valvular endothelial dysfunction has been implicated as the initiator of many clinical sequellae, including inflammatory reactions, calcification, and blood clots[1, 15, 16]. Previous work in Chapters 4 has demonstrated that aortic valve endothelial cells behave very different from aortic endothelium. Aortic valve endothelial cells align perpendicular to the direction of flow, in contrast to aortic endothelial cells, which align parallel, and this morphology change may be associated with unique mechanotransduction pathways. Gene expression is also much different between the two cell types, as reported in Chapter 5, and differences in gene regulation in response

to shear flow suggests these cells may be phenotypically distinct. Most research on interstitial cells has focused on marker expression and protein synthesis in vitro. Comparison to other cell phenotypes indicates that these cells are uniquely suited to thrive within the heart valve. In vivo evidence suggests that valvular interstitial cells are highly dynamic producers of protein and glycosaminoglycans, unlike smooth muscle cells[17], and express markers that suggest a hybrid myofibroblast like phenotype[18]. In vitro experiments have largely confirmed these observations. Interstitial cells express α-smooth muscle actin to a variable degree, as well as fibroblast surface antigen, and this was not mimicked by cells from other sources. Taylor and colleagues demonstrated that interstitial cells in three dimensional culture in vitro expressed markers similar to interstitial cells in vivo, and the relative proportions of specific marker expressing cells was maintained[19]. The mechanism for this distribution was unclear, however, because no mechanical forces were applied to their constructs. The results from Chapter 3 showed that interstitial cells expressed α-smooth muscle actin in vitro to a similar degree as smooth muscle cells, desmin to a lesser degree, and that three dimensional culture also influences cell phenotype.

What has not been addressed by any of the previously mentioned studies is the influence that native valvular endothelium may exert on the underlying interstitial cells. It is well known that proper interaction between vascular endothelial and smooth muscle cells is paramount to normal vessel function. Vascular endothelial stimulation of underlying smooth muscle cells is critical for the maintenance of vessel tone and inhibition of pathological smooth muscle cell differentiation in vivo. In vitro co-culture models have shown that endothelial cells inhibit smooth muscle proliferation under flow[20, 21]. Gene expression of endothelial cells and smooth muscle cells are also altered when soluble factors are allowed to exchange between the two cells. It is likely

that interactions between valvular endothelial cells and interstitial cells are similarly important.

The objective of this study therefore was to develop a three dimensional co-culture system using native aortic valve cells in a biological matrix that can be exposed to mechanical forces. Valvular endothelial-interstitial cell co-cultures were exposed to steady laminar shear for up to 96 hours, and the results show that valvular endothelial cells modify interstitial cell synthetic response to fluid shear stress, and stimulate interstitial cell phenotype to resemble that in vivo.

6.1: Methods

Cell Isolation and Culture. Porcine aortic valve endothelial cells (PAVECs) and aortic valve interstitial cells (PAVICs) were isolated, characterized, and cultured as described in Chapters 2 and 4. Briefly, aortic valve leaflets were isolated from porcine aortic roots and subjected to short collagenase digestion, at which point the PAVECs were removed by gentle scraping. PAVECs were then plated onto dishes coated with 50 μg/ml collagen I. Once denuded, the rest of the tissue was incubated overnight in collagenase to isolate PAVICs, which were then plated onto tissue culture plastic. Both cell types were cultured in DMEM supplemented with 10% FBS, 1% Penicillin-Streptomycin, and 1% L-glutamine, and split 1:3 upon confluence. For these experiments, PAVEC were used at passage 5, while PAVICs were used between passage 5 and 8.

Co-culture model creation. Tubular molds were created using glass rods and rubber tubing as shown in Figure 6-1 and explained in greater detail in the appendix. A collagen gel suspension containing 1 million PAVICs/ml was created as described previously in Chapter 2, and 5 ml of suspension inoculated into a sterile test tube. The

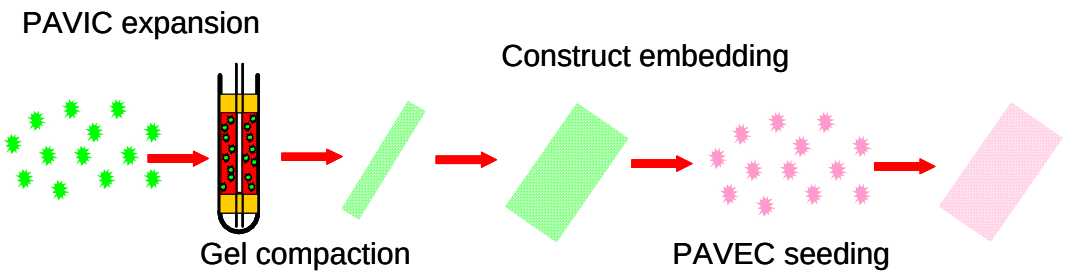

Figure 6-1: Schematic of valvular co-culture model creation

tubular molds were then inserted into the tubes, and the constructs were allowed to gel for 1 hour. The molds were then removed from the tubes and placed in a sterile dish containing 150 ml of culture media. The constructs were then allowed to compact for six days. Each construct was then gently removed from the mold and sectioned longitudinally. The surface contacting the glass mandrel was placed face down on a glass microscope slide, and any media aspirated from under the tissue to ensure a flat profile. A rectangular polycarbonate mold was placed around the construct, and 6 ml of a 3.5% agar solution at 47°C was poured over the construct and immediately sealed with another slide. The agar solidified after 1 minute at room temperature. The sandwich was flipped over and the slide covering the flat surface was removed to expose it to media. The resulting embedded construct was then placed in 35 ml of culture media. Some constructs were seeded with 50,000 PAVECs/cm^2 by aspirating enough media to expose the top surface of the construct, inoculating 200 ml of the concentrated cell suspension onto the surface, and allowing the cells to adhere for one hour. Media was then added to the embedded constructs, and the co-culture was allowed an additional two days for endothelial monolayer formation. Non PAVEC constructs followed the same procedure, except were not seeded with PAVECs.

Shear Stress Experiments. The embedded constructs were placed into a modified version of the flow chamber explained in Chapter 4. A smaller rubber spacer

was used to accommodate the glass coverslip and rectangular mold containing the embedded construct. A larger spacer was used to create the shear flow, to accommodate the increased variation in channel height due to any undulations in the construct surface. The lumenal surfaces were then exposed to 20 dynes/cm^2 steady laminar shear stress for 48 or 96 hours, with static cultures serving as controls. The actual wall shear stress on an aortic valve leaflet is much more complex and challenging to measure. Weston and colleagues estimated a maximum wall shear stress of 79 dynes/cm^2 for leaflet surfaces, but noted that the shear stress varied continuously with the valve cycle[22]. While it is important to study physiological levels of mechanical forces, those forces are often damaging to engineered tissue in vitro. The 20 dynes/cm^2 of steady laminar shear stress used in these experiments was an approximation of the mean leaflet wall shear stress, and also was the maximum shear stress that could be imposed while maintain a reasonably confluent endothelial monolayer critical to the power of the study.

Endothelial Morphology. The morphology of the endothelial cells on the construct surface was investigated using confocal microscopy using a modification of the procedure previously described in Chapter 4. Upon completion of the experiments, the constructs were removed and the agar mold cut away, leaving only a few millimeters of agar around the constructs. Co-cultures were then fixed in 3.7% paraformaldehyde overnight, then the constructs were gently peeled from the agar and placed in well of a 6-well plate in PBS. The endothelial cells were then permeablized with 0.1% Triton X-100 for 5 minutes, followed by blocking in 1% neonatal goat serum (NGS) for 1 hour. Endothelial cell phenotype was then labeled by incubation with anti-human von Willebrand Factor (Sigma F-3520, 1:100, in rabbit) for one hour, followed by rinsing, secondary antibody incubation (goat anti-rabbit, FITC, Molecular Probes A-11008, 1:100, one hour) and additional rinsing. Cells were then counterstained for f-actin

(rhodamine phalloidin, Sigma R-418, 1:400) and cell nuclei (Hoechst, Sigma F-32258, 1:1000) for 30 minutes, followed by additional rinsing and coverslipping. Constructs were then imaged using confocal microscopy. The lumenal surface of the constructs was placed face down (closest to the objective) on a glass coverslip and five representative pictures were taken of each construct. Morphological parameters were assessed as previously described in Chapter 4. Shape index and orientation angle measurements were then compared with the morphology of PAVECs monolayers on glass slides presented in Chapter 4. Two factor ANOVA was used to determine significance between cell type and condition with $P<0.05$ considered significant.

Biochemical Assays. PAVIC only constructs and co-culture models were analyzed for cell number, total protein content, and sulfated glycosaminoglycan content using the biochemical assays described in Chapter 3. Constructs were sectioned in half widthwise: half of the construct was fixed for histology, half was immediately frozen at -80°C until analyzed. Frozen constructs were then lyophilized in a vacuum centrifuge, weighed, and then digested with Proteinase-K overnight at 55°C. For cell number quantification, 10 μl of samples were added to 200 μl of buffer containing Hoechst dye at 1:10000 concentration in a 96 well plate, and plates read on a fluorometer at 385 nm. Total protein and sulfated glycosaminoglycan content was quantified using the BCA (Pierce) and Blyscan (Biocolor) assays according to the manufacturers' protocols using the proteinase K digested samples. Cell number was normalized to dry weight to account for differences in size of the samples, while matrix production was normalized to DNA content to account for slight differences in construct sizes. Additionally, all construct values were normalized by day 0 averages to account for variations between batches of constructs. Statistical significance was determined using Analysis of Variance for time duration, and T tests for differences between flow condition and cell type. $P<0.05$ was considered significant for these tests.

Cell Phenotype Characterization. PAVIC phenotype was qualitatively assessed using immunohistochemistry. Construct samples fixed overnight in 3.7% paraformaldehyde, and placed in 70% ethanol. Constructs were then paraffin embedded and sectioned at 5 μm. Immunohistochemistry was performed as described in greater detail in the appendix. Briefly, slides were deparaffinized, washed twice in PBS, and blocked in 1% bovine serum albumin (BSA) for 30 minutes. Antibodies to von Willebrand Factor (Sigma F-3520, 1:600), vimentin (Cy3 conjugate, Sigma V2228, 1:200), and α-smooth muscle actin (Cy3 conjugate, Sigma 0-6198, 1:400) were incubated singly for one hour. Before von Willebrand Factor (vWF) incubation, a brief gelatinase digestion was conducted to expose antigen. Slides were then washed, followed by incubation in secondary antibody for vWF (Molecular Probes, A-11008, 1:100) for 40 minutes. Slides were then washed twice and coverslipped with a DAPI counterstain for cell nuclei. Slides were viewed using a fluorescent microscope (Nikon E600), and several representative pictures were taken from each construct stained.

6.2: Results

Co-culture Model Development. Porcine aortic valve interstitial cells compacted the collagen hydrogels over the six day period, with a majority of the compaction occurring by day 3 (data not shown), much similar to what was shown in Chapter 3. Figure 6-2 shows an example of the compacted tubular collagen gel, which was then sectioned longitudinally to create a thin, flat three dimensional substrate entombed with interstitial cells. Imaging by polarized light showed the collagen fibril alignment through the thickness of the construct. Highly aligned fibers were concentrated near the surface of the tissue closest to the glass mandrel, and more

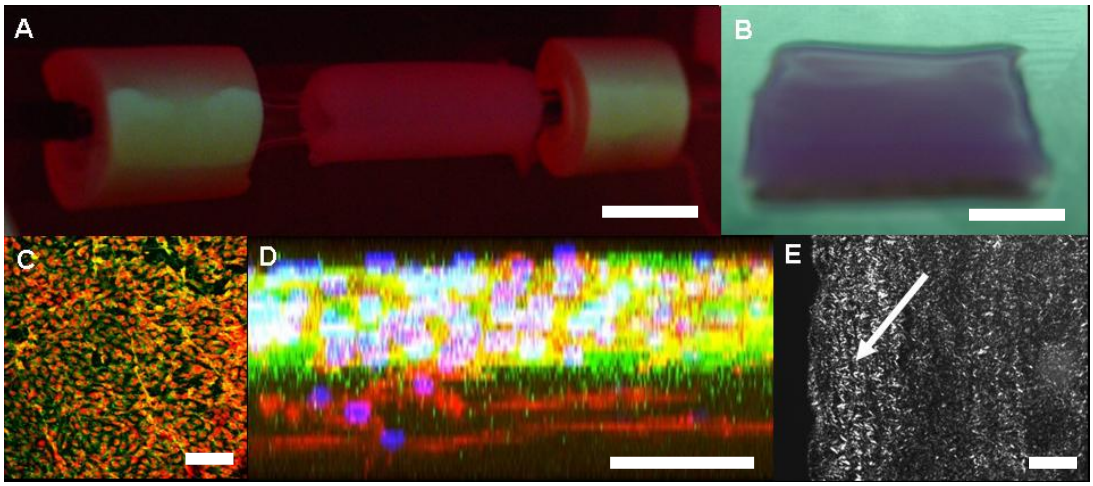

Figure 6-2: Co-culture model characterization. A: Tubular mold; B: sectioned construct; C: Confocal microscope image indicating endothelial monolayer; D: Three dimensional confocal image indicating cellular arrangement; E: Polarized light image indicating matrix alignment (bright field). Confocal staining – green (von Willebrand factor), red (f-actin), blue (cell nuclei). Scale bar = 1 cm (A,B), 100 μm (C-E).

randomly oriented near the opposite surface. This is somewhat similar to what is seen in the native valvular leaflet. It is likely the developed tissue anisotropy is due to the physical constraint placed at this surface. Cells were homogeneously distributed throughout the construct, with only slight alignment near the constrained surface.

The surface with highly aligned underlying matrix became the “lumenal” surface upon longitudinal sectioning, which was then seeded with PAVECs. Immunofluorescent staining for von Willebrand Factor indicated a reasonably confluent endothelial monolayer on the surfaces of the constructs. The entire surface of the leaflet was not completely covered with endothelial cells, but large patches like the image shown existed throughout the surface, leading us to estimate the surface approximately 70% covered with endothelial cells, with some variation between individual constructs. Z-stacked confocal microscopy showed a contact-inhibited endothelial monolayer on top of a closely apposed interstitial cell population. Some close contacts were observed

between PAVICs and PAVECs, suggesting that these cells readily interact with each other.

Endothelial Cell Alignment under Flow. It was previously shown in Chapter 4 that PAVECs in two dimensional culture align perpendicular to the direction of fluid flow. Figure 6-3 shows that on an aligned three dimensional matrix in co-culture with PAVICs, the alignment tendencies were overall not significantly different. Valvular endothelial cells in both conditions decreased their Shape Indexes from approximately 0.8 to 0.6 under flow, and changed orientation from 45° (random) to 75° (perpendicular to flow). The larger standard deviation in orientation angle for PAVECs in co-culture was due to the deviations in regional cell orientation. The PAVICs directly underneath the PAVECs gave an indication as to the matrix alignment, and some swirling patterns were observed which the endothelial cells also mimicked to a degree in their alignment. Cell alignment under flow was still predominantly perpendicular to the flow direction, and never observed to be parallel to flow direction. PAVEC morphology was different in ways undetectable by the Shape Index, however. In two dimensional culture, filamentous extensions protruded from one cell onto another, but PAVECs in three dimensional culture appeared more regularly elliptical. The protrusions increase cell perimeter without similar increases in cell area, thus compromising the effectiveness of the Shape Index in determining cell elongation. It is therefore possible that valvular endothelial cells in three dimensional co-culture were more elongated than in two dimensional culture.

Cell Organization and Proliferation. PAVEC seeded PAVIC constructs and non seeded PAVIC constructs were exposed to 20 dynes/cm^2 steady shear with static cultures of both conditions serving as controls. Figure 6-4 shows the histologically determined cellular arrangement in seeded and non-seeded constructs over time. Interstitial cells are randomly oriented within non-EC seeded constructs, with slight

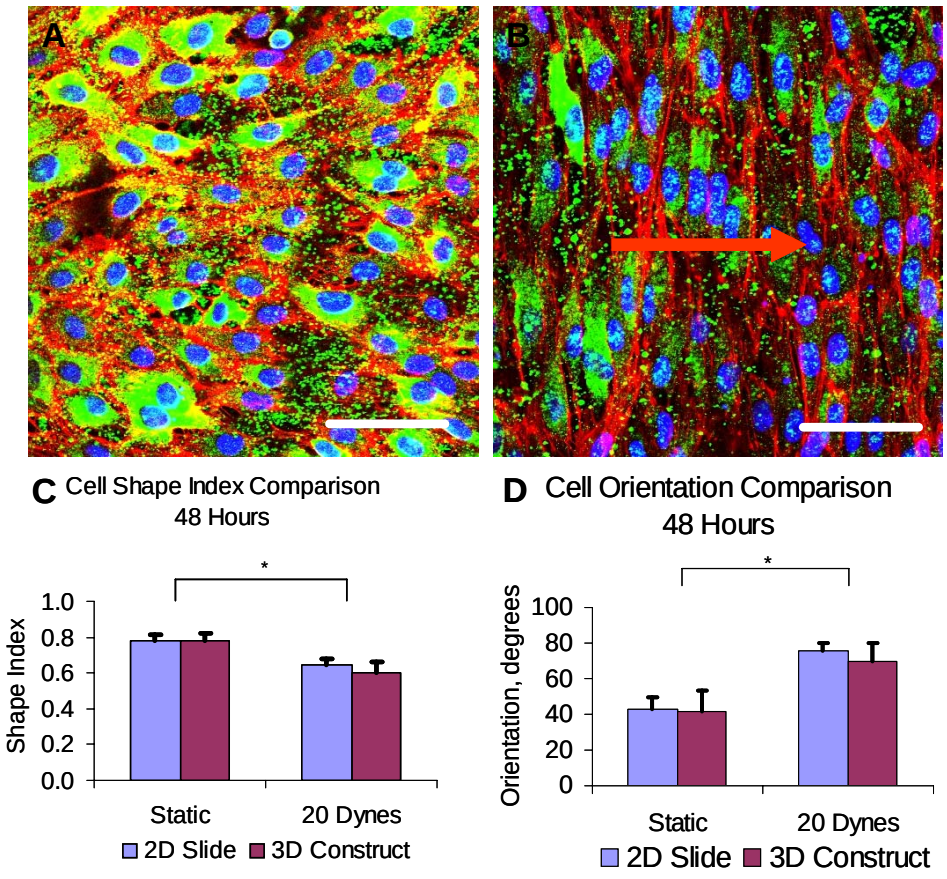

Figure 6-3: Endothelial cell alignment on valve leaflet co-culture models. A: Static culture; B: 48 hour flow (20 dynes/cm^2); C: Shape index comparison; D: Cell orientation angle comparison. Green = von Willebrand factor, red = f-actin, blue = cell nuclei. Scale bar = 50 μm.

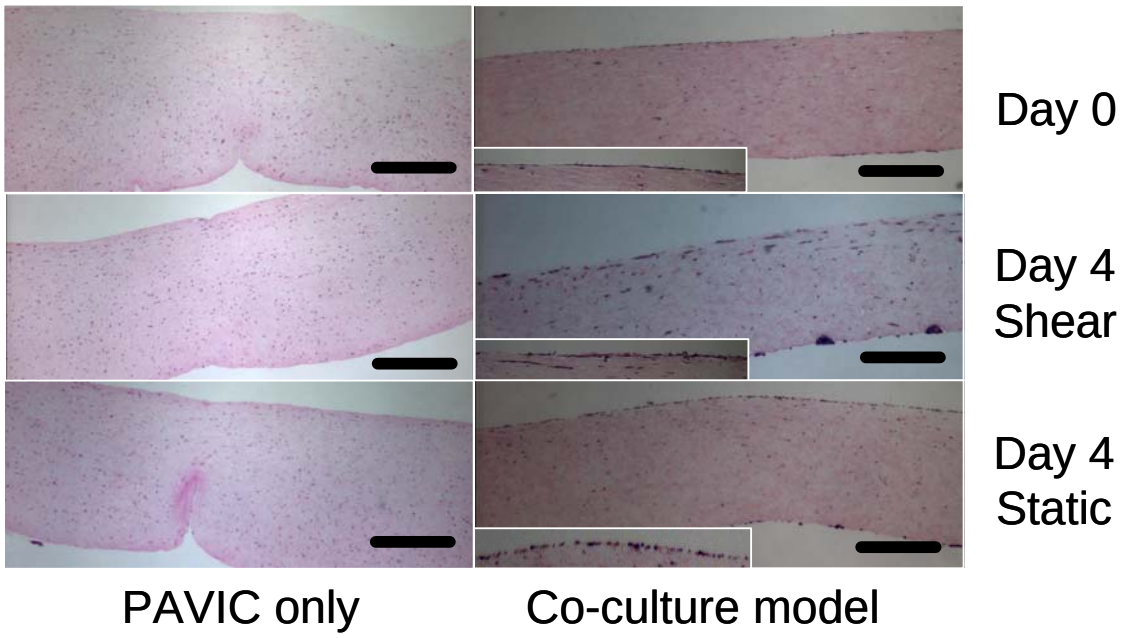

Figure 6-4: Hematoxylin and Eosin staining of constructs depicting matrix and cellular architecture. Inset depicts endothelial layer. Scale bar = 200 μm.

circumferential alignment near the lumenal surface. The application of flow enhances this alignment somewhat, but only right at the surface. Co-culture leaflet models had cells throughout the construct, but there were preferentially more cells near the lumenal surface and opposite edge of the constructs. This may be due to diffusion constraints imposed by the addition of PAVECs, limiting perfusion through the highly porous collagen matrix. Biochemical analysis of cell number (DNA content) across experimental conditions is shown in Figure 6-5A. Interstitial cell only constructs tended to increase cell number over time, with shear stress having no effect. This was in contrast to the endothelial seeded co-culture model, which maintained cell number during static culture, and decreased cell number under flow. By day four, cell content in PAVIC sheared constructs was significantly higher than sheared co-culture models.

Matrix Production. Figure 6-5B and 6-5C show the matrix production of the PAVIC constructs and PAVIC/VEC co-culture models under static and fluid flow

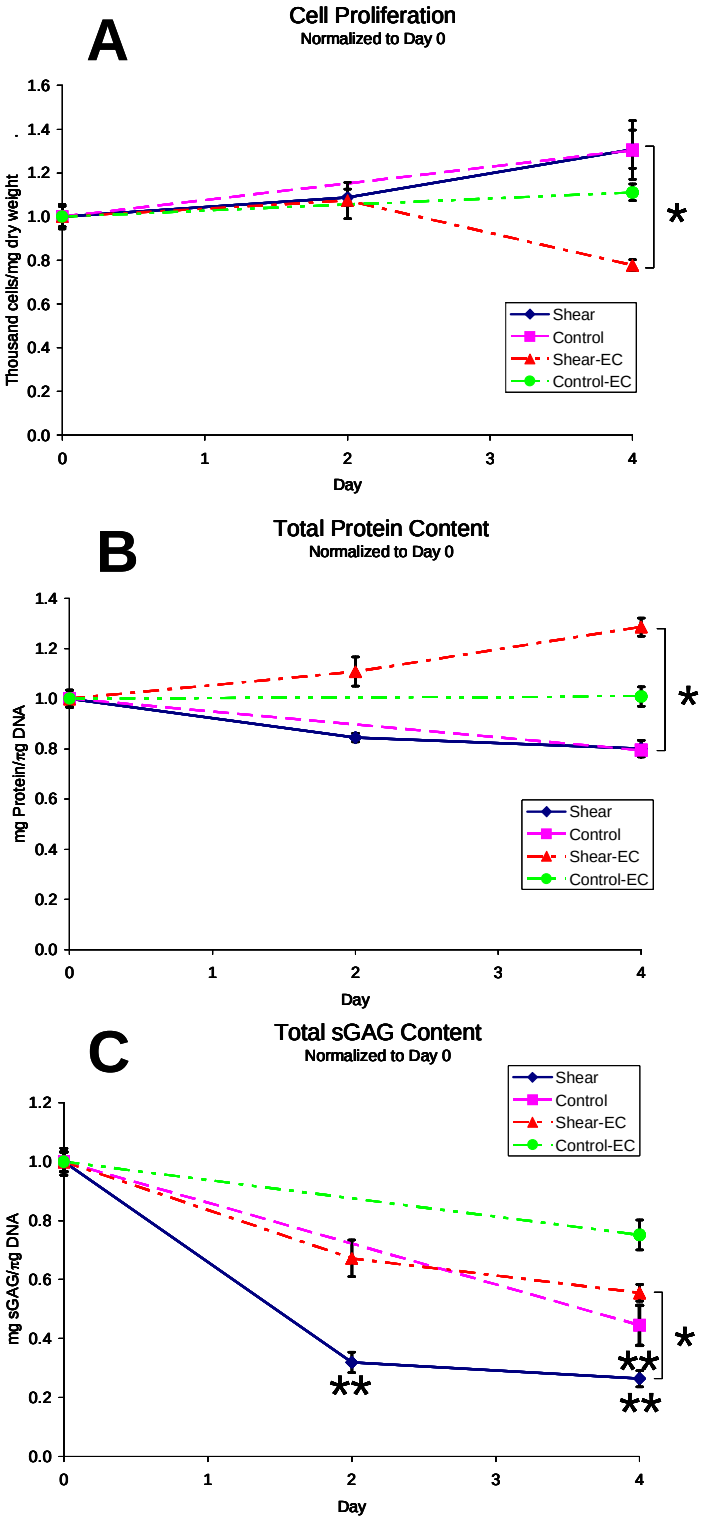

Figure 6-6: Cell content (A), Protein content (B), and sulfated glycosaminoglycan content (C) of EC and non-EC seeded constructs. Data normalized to Day 0 values and presented as mean +/- SEM. * denotes significant with respect to different condition (P<0.05), ** denotes significant with respect to Day 0 value (P<0.05)

conditions. Protein content was regulated in an opposite manner than cell content. PAVIC only constructs tended to have less protein over time, with no effects of shear. PAVIC/VEC constructs, on the other hand, tended to maintain protein content in static culture, but increase protein content under flow. At day 4, sheared PAVIC/VEC constructs have significantly more protein than PAVIC only constructs. Sulfated glycosaminoglycan (sGAG) content regulation was much different, however. sGAG content was lost in PAVIC constructs over time and with shear. Both day 2 and day 4 sheared PAVIC only constructs had significantly less sGAGs than day 0, but no significant difference between static sheared constructs at day 4. In PAVIC/VEC co-cultures, no significant difference in sGAG content was detected in static culture or under flow (P=0.055). There was significantly more sGAG content in day 4 sheared PAVIC/VEC constructs compared to sheared PAVIC only constructs, but no significant difference between statically cultured models (P=0.18).

Evolution of Interstitial Cell Phenotype. The evolution of cell phenotype was determined through the expression of vimentin, α-smooth muscle actin (α–SMA), and smooth muscle myosin. Figure 6-7 shows the vimentin expression of the PAVIC only and co-culture constructs. Vimentin expression is maintained throughout the time points investigated in both models, with little differences between flow and static culture. The cells appear more aligned after four days of flow, with vimentin expression throughout the cytoplasm. Figure 6-8 shows the expression of α-SMA in both culture models and flow conditions. In PAVIC only constructs, only a basal level of expression is observed in static culture throughout the time period investigated. The application of flow, however, increases expression of α-SMA, especially near the lumenal surface. The

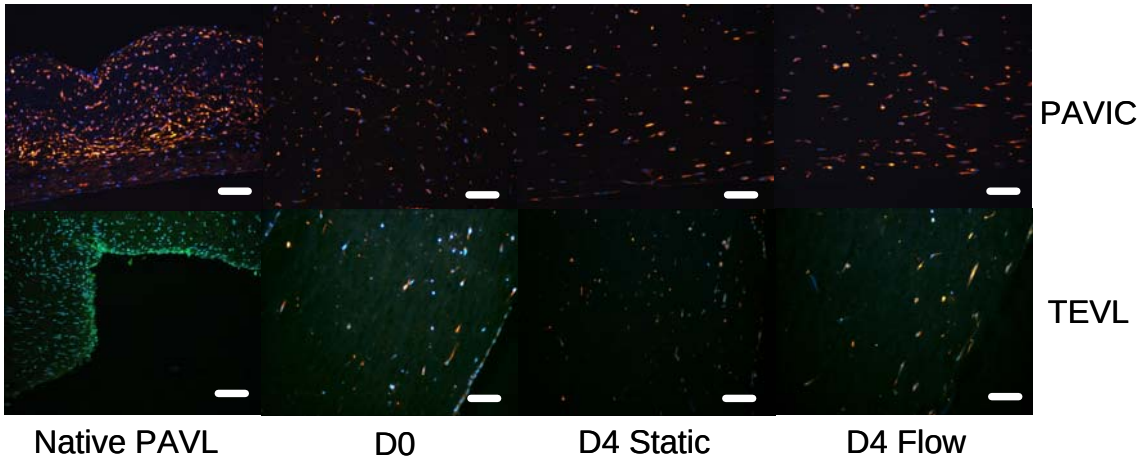

Figure 6-7: Vimentin expression in PAVIC constructs and PAVEC-Seeded co-cultures (TEVL). Counterstained for cell nuclei (blue). Bottom left panel indicates native leaflet endothelium (von Willebrand factor). Scale bar = 100 μm.

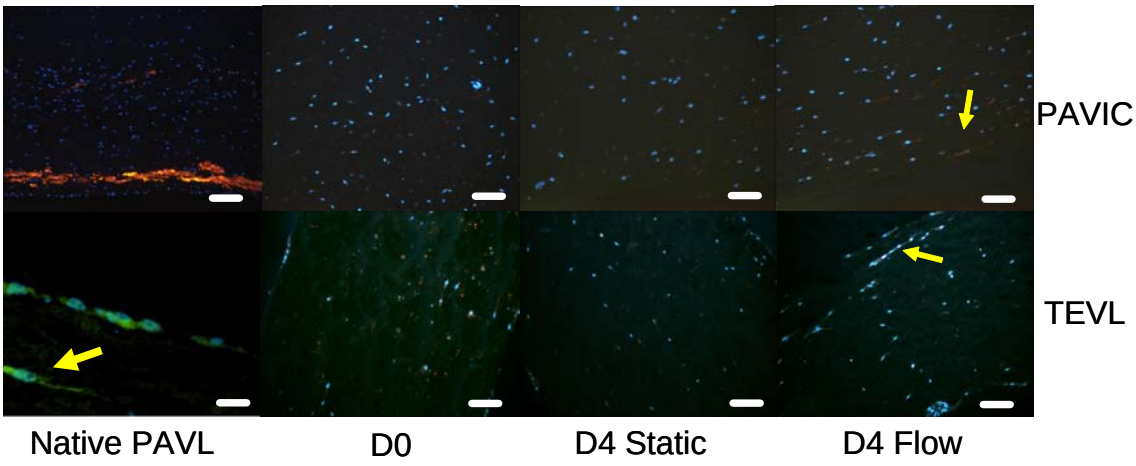

Figure 6-8: α-smooth muscle actin expression in PAVIC constructs and PAVEC-Seeded co-cultures (TEVL). Counterstained for cell nuclei (blue). Bottom left panel indicates TEVL endothelium (von Willebrand factor). Scale bar = 100 μm.

expression of α-SMA is further regulated with the addition of PAVECs. At day 0, a basal level of expression is noted, but this expression drops off during the culture period. By day 4, virtually no expression is detectable in static culture, and only slightly more with the application of flow, again in the cells closest to the lumenal surface. These results suggest that the PAVECs modulate the expression of α-smooth muscle actin in PAVICs in static and fluid flow conditions. No expression of smooth muscle myosin was observed in either model under any culture condition (data not shown). PAVEC phenotype on the lumenal surface of the co-culture models was confirmed through von Willebrand Factor (vWF) staining, as shown in the panels of figure 8-7 and 8-8. A confluent monolayer of endothelial cells was more difficult to demonstrate through immunohistochemistry, as these constructs were extremely fragile, and the handling necessary for paraffin processing likely detached some of the cells. It was interesting to note that a few cells expressing of vWF were detected in the subendothelial layers of the constructs, suggesting some migration may have occurred (arrow).

6.3: Discussion

Previous work presented in Chapters 3 and 4 and done by others have shown that valvular endothelial cells and interstitial cells behave differently in several respects from vascular cells. Valvular endothelial cells align perpendicular to fluid flow in two dimensional culture, and valvular interstitial cells express contractile markers in a different manner than smooth muscle cells. This study is the first to present a co-culture model of a valvular leaflet for in vitro study. Native aortic valve endothelial cells were placed in close proximity to valvular interstitial cells, which were homogeneously entombed in an anisotropic biological collagen matrix. This model could then be

incorporated into a steady shear flow system to investigate interactions between fluid flow, endothelial cells, and interstitial cells.

Numerous studies have demonstrated the importance of appropriate vascular endothelial-smooth muscle interactions for maintenance of blood vessel tone, and the importance of mechanical forces in regulating cell phenotype. Surprisingly, almost nothing is known about how native valvular endothelial and interstitial cells interact, or how mechanical forces influence these interactions. Rothenburger and colleagues created valvular leaflet like tissue with valvular cells co-cultured in a collagen matrix, and found that these cells synthesized collagen and proteoglycans, but did not identify any particular aspects of endothelial regulation of interstitial cell function[23]. Weston and Yoganathan developed an organ culture model of aortic valve leaflets and exposed them to shear stress for up to 48 hours[24]. They found a dramatic increase in cell number and protein and glycosaminoglycan synthesis with static incubation, but no differences with the application of any flow regimes. These results are similar in some respects and different in others in comparison with this work. Our results indicate an increase in cell content, but a decrease in protein and sGAG content for PAVIC only constructs. Weston and Yoganathan reported that their leaflet isolation protocol may have removed all viable endothelium from the leaflet surfaces, creating a model more like the PAVIC only construct, making a comparison with the co-culture model inappropriate. The native leaflet has other matrix components besides type I collagen (Christie, 1992), so some of the differences may be a result of additional matrix signals not present in these models. The static culture induced cell proliferation reported in this study may also mimic a wound healing response as has been reported by Lester et al, who showed an increase in interstitial cell proliferation with endothelial denudation[25]. Valvular interstitial cells may therefore be regulated by valvular endothelial cells to maintain cell numbers in vivo, which was mimicked by the co-culture model. In our studies, the presence of endothelial

cells caused a maintenance cell number, increase in protein synthesis, and a reduction in the loss of sGAGs induced by shear in comparison to controls. While no in vitro studies have explored these phenomena, short term studies in rat aortic valves indicated a generally more active production of proteins and GAGs in comparison to other tissues, as was reported earlier in Chapter 3. The experimental time scales were much different in our study compared to theirs, but their results suggest that the valvular endothelial – interstitial cell interactions reported by our model are somewhat similar to the in vivo condition.

Valvular endothelial cells were also shown to modulate interstitial cell phenotype in three dimensional co-culture. Contractile phenotype as determined by α-smooth muscle actin expression was reduced in co-culture, and only interstitial cells near the lumenal surface expressed the marker after four days of steady shear stress. Rabkin and colleagues have defined an “activated” interstitial cell phenotype based on among other characteristics increased α-smooth muscle actin expression[26]. This suggests that the presence of viable valvular endothelial cells helps to maintain a normal interstitial cell phenotype. In this respect, valvular endothelial cells are similar to vascular endothelial cells, which have been shown to enhance underlying cell expression of α-smooth muscle actin in a microvessel co-culture model[27]. The opposite regulation of α-smooth muscle actin induced by the different endothelial cell types suggests that each one is uniquely suited for their respective application. The presence of positive actin expression at day 0 may be due to an artificial interstitial cell activation resulting from in vitro culture, tissue handling and embedding. Previous work in Chapter 3 showed high expression of a-smooth muscle actin in two dimensional culture, which was dramatically reduced in three dimensional culture, but still positive. There were no valvular endothelial cells in those studies, however.

Mechanical forces are also very potent stimulators of cell function, including matrix remodeling, strengthening and signal transduction pathway activation. Vascular cells populating engineered valvular conduits implanted into the pulmonary circulation of sheep were able to modify their phenotype to resemble that of native interstitial cells by 20 weeks of implantation[28]. There are many sources of stimulation within animal models, including mechanical and biochemical factors, as well as the possibility of host cell growth into the conduit and immune response. It is therefore difficult to attribute causation to any specific aspect of this environment on a particular conduit response. The valvular leaflet co-culture model presented here enables the investigation of the specific effects of fluid shear stress on valvular endothelial-interstitial interactions. We have demonstrated that valvular endothelial cells align perpendicular to flow direction while in co-culture with interstitial cells in a collagen matrix, confirming our previous results in Chapter 4. Matrix alignment was predominantly circumferential, however, and a subtle influence of matrix alignment was noted. Similar constructs made with vascular endothelial cells and smooth muscle cells aligned parallel to flow regardless of matrix alignment[29], suggesting that interstitial cell-matrix alignment may influence valvular cell alignment. The actual wall shear stress on an aortic valve leaflet is much more complex and challenging to measure. Weston and colleagues estimated a maximum wall shear stress of 79 dynes/cm^2 for leaflet surfaces, but noted that the shear stress varied continuously with the valve cycle[22]. While it is important to study physiological levels of mechanical forces, those forces are often damaging to engineered tissue in vitro. The 20 dynes/cm^2 of steady laminar shear stress used in these experiments was an approximation of the mean leaflet wall shear stress, and also was the maximum shear stress that could be imposed while maintain a reasonably confluent endothelial monolayer critical to the power of the study. This level of shear stress was identical to that imposed on the monolayer studies in Chapter 4, enabling comparisons between the

two studies. The limited response of interstitial cells to steady shear suggests that this force is not important to interstitial cell function. Mechanical stimulation did have some effects on Endothelial co-culture, contributing to an increase in protein content and a reduction in the loss of glycosaminoglycans. Glycosaminoglycans perform an important lubrication function in valve leaflets, permitting internal shear between the major load bearing layers: the ventricularis and fibrosa[30]. Many glutaraldehyde-fixed bioprosthetic valve failures can be attributed to a loss of this function[31]. It is clear from these studies that fluid shear stress does not stimulate any net synthesis of glycosaminoglycans by interstitial cells, and therefore other mechanical forces may be responsible for this function.

Many serious valvular pathologies begin with the dysfunction and denudation of the endothelium, and progress through abnormal interstitial cell behavior[2]. This tissue engineered leaflet model provides an ideal system to investigate the effects of fluid forces on endothelial-interstitial cell interactions. Well controlled in vitro studies can complement more complex animal model studies to progress understanding of valvular cell biology and help develop a clinically successful living valvular replacement.

The reduction of interstitial cells within the center of some of the constructs is a concern that suggests nutrient diffusion limitations. Native valve leaflets are on the order of 500 μm thick, therefore not requiring supporting vasculature for nourishment. Only one surface of the tissue is exposed to nutrients during the six days of compaction before it is embedded in agar. It is possible that some cell loss due to starvation is occurring. The immunohistochemistry images in Figures 6 and 7 indicated that some of the engineered tissues were thinner than the native leaflet, suggesting that the collagen matrix could be compacted by the interstitial cells to a density greater than that of the native leaflet. It is interesting to note from Figure 4 that the thickness of the engineered tissue appears to be inversely proportional to the number of healthy cells within the

matrix. It is likely that both of the aforementioned factors play some role. To improve upon the diffusion limitations, the glass mandrel used in these experiments can be replaced with a porous tubular mandrel, enabling media diffusion from both sides of the leaflet.

Another limitation in this study was the lack of equal sample numbers for statistical analyses and the variability between sample batches. Each batch of interstitial cells produced between 12 and 16 constructs, which were divided into the various experimental categories. Inefficiencies in PAVEC seeding, accidental construct aspiration, and unintended leaks in the flow system eliminated constructs from this pool creating unequal sample numbers in virtually every round of experiments. Because a maximum of 8 flow loops could be used at one time due to space limitations, it sometimes occurred that no data was obtained for one experimental condition. For these reasons all data was pooled together and considered as independent experiments. While this was somewhat reasonable given the many different manipulations done independently to each construct, the variability in the data appeared to be larger between batches rather than within batches, further complicating data analysis. An improvement for the future would involve averaging data from constructs of an experimental condition from the same batch, and then using multiple batches to generate enough samples for statistical significance. A further reduction in variability could be achieved by using cells from the same isolation.

6.4: References

1. Cooper, M.D., et al., *Scanning electron microscopy studies of staphylococcal adherence to heart valve endothelial cells in organ culture: an in vitro model of acute endocarditis.* Scan Electron Microsc, 1985(Pt 3): p. 1231-7.

2. Poggianti, E., et al., *Aortic valve sclerosis is associated with systemic endothelial dysfunction.* J Am Coll Cardiol, 2003. 41(1): p. 136-41.

3. Daly, R.C., et al., *Long-term results of aortic valve replacement with nonviable homografts.* Circulation, 1991. 84(5 Suppl): p. III81-8.

4. Hammermeister, K., et al., *Outcomes 15 years after valve replacement with a mechanical versus a bioprosthetic valve: final report of the Veterans Affairs randomized trial.* J Am Coll Cardiol, 2000. 36(4): p. 1152-8.

5. Staab, M.E., et al., *Aortic valve homografts in adults: a clinical perspective.* Mayo Clin Proc, 1998. 73(3): p. 231-8.

6. North, R.A., et al., *Long-term survival and valve-related complications in young women with cardiac valve replacements.* Circulation, 1999. 99(20): p. 2669-76.

7. Shinoka, T., et al., *Tissue-engineered heart valves. Autologous valve leaflet replacement study in a lamb model.* Circulation, 1996. 94(9 Suppl): p. II164-8.

8. Kim, W.G., et al., *Tissue-engineered heart valve leaflets: an effective method for seeding autologous cells on scaffolds.* Int J Artif Organs, 2000. 23(9): p. 624-8.

9. Numata, S., et al., *Decellularized allograft valve for tissue engineering: experimental study of heart valves using decellularized cryopreserved allografts.* Heart Surg Forum, 2002. 6(1): p. 2.

10. Dohmen, P.M., et al., *Tissue engineering of an auto-xenograft pulmonary heart valve.* Asian Cardiovasc Thorac Ann, 2002. 10(1): p. 25-30.

11. Shi, Y., A. Ramamurthi, and I. Vesely, *Towards tissue engineering of a composite aortic valve.* Biomed Sci Instrum, 2002. 38: p. 35-40.

12. Hoerstrup, S.P., et al., *Functional living trileaflet heart valves grown in vitro.* Circulation, 2000. 102(19 Suppl 3): p. III44-9.

13. Stock, U.A., et al., *Tissue-engineered valved conduits in the pulmonary circulation.* J Thorac Cardiovasc Surg, 2000. 119(4 Pt 1): p. 732-40.

14. Perry, T.E., et al., *Thoracic Surgery Directors Association Award. Bone marrow as a cell source for tissue engineering heart valves.* Ann Thorac Surg, 2003. 75(3): p. 761-7; discussion 767.

15. Drake, T.A. and M. Pang, *Effects of interleukin-1, lipopolysaccharide, and streptococci on procoagulant activity of cultured human cardiac valve endothelial and stromal cells.* Infect Immun, 1989. 57(2): p. 507-12.

16. Campbell, K.M. and C.M. Johnson, *Identification of Staphylococcus aureus binding proteins on isolated porcine cardiac valve cells.* J Lab Clin Med, 1990. 115(2): p. 217-23.

17. Schneider, P.J. and J.D. Deck, *Tissue and cell renewal in the natural aortic valve of rats: an autoradiographic study.* Cardiovasc Res, 1981. 15(4): p. 181-9.

18. Filip, D.A., A. Radu, and M. Simionescu, *Interstitial cells of the heart valves possess characteristics similar to smooth muscle cells.* Circ Res, 1986. 59(3): p. 310-20.

19. Taylor, P.M., et al., *Human cardiac valve interstitial cells in collagen sponge: a biological three-dimensional matrix for tissue engineering.* J Heart Valve Dis, 2002. 11(3): p. 298-306; discussion 306-7.

20. Nackman, G.B., et al., *Flow modulates endothelial regulation of smooth muscle cell proliferation: a new model.* Surgery, 1998. 124(2): p. 353-60; discussion 360-1.

21. Ziegler, T., R.W. Alexander, and R.M. Nerem, *An endothelial cell-smooth muscle cell co-culture model for use in the investigation of flow effects on vascular biology.* Ann Biomed Eng, 1995. 23(3): p. 216-25.

22. Weston, M.W., D.V. LaBorde, and A.P. Yoganathan, *Estimation of the shear stress on the surface of an aortic valve leaflet.* Ann Biomed Eng, 1999. 27(4): p. 572-9.

23. Rothenburger, M., et al., *Tissue engineering of heart valves: formation of a three-dimensional tissue using porcine heart valve cells.* Asaio J, 2002. 48(6): p. 586-91.

24. Weston, M.W. and A.P. Yoganathan, *Biosynthetic activity in heart valve leaflets in response to in vitro flow environments.* Ann Biomed Eng, 2001. 29(9): p. 752-63.

25. Lester, W.M., et al., *Bovine mitral valve organ culture: role of interstitial cells in repair of valvular injury.* J Mol Cell Cardiol, 1992. 24(1): p. 43-53.

26. Rabkin, E., et al., *Activated interstitial myofibroblasts express catabolic enzymes and mediate matrix remodeling in myxomatous heart valves.* Circulation, 2001. 104(21): p. 2525-32.

27. Villaschi, S. and R.F. Nicosia, *Paracrine interactions between fibroblasts and endothelial cells in a serum-free coculture model. Modulation of angiogenesis and collagen gel contraction.* Lab Invest, 1994. 71(2): p. 291-9.

28. Rabkin, E., et al., *Evolution of cell phenotype and extracellular matrix in tissue-engineered heart valves during in-vitro maturation and in-vivo remodeling.* J Heart Valve Dis, 2002. 11(3): p. 308-14; discussion 314.

29. Imberti, B., et al., *The response of endothelial cells to fluid shear stress using a co-culture model of the arterial wall.* Endothelium, 2002. 9(1): p. 11-23.

30. Talman, E.A. and D.R. Boughner, *Effect of altered hydration on the internal shear properties of porcine aortic valve cusps.* Ann Thorac Surg, 2001. 71(5 Suppl): p. S375-8.

31. Talman, E.A. and D.R. Boughner, *Glutaraldehyde fixation alters the internal shear properties of porcine aortic heart valve tissue.* Ann Thorac Surg, 1995. 60(2 Suppl): p. S369-73.

CHAPTER 7

DISCUSSION

7.1: Aortic Valve Disease Treatment

The clinical data presented in Chapter 1 demonstrate the serious global problem of aortic valve disease (AVD) and its etiologies. There is a great divide between developed and underdeveloped countries as to the underlying causes of AVD, which reflects upon their relative economic status. In developed countries, great advances in medical technologies and expertise have all but eliminated rheumatic causes of AVD, yet these countries suffer from degenerative valve disorders that mimic atherosclerotic pathologies and “old age” vascular disorders. Virtually no degenerative pathology is acknowledged in these underdeveloped countries, but the eminently preventable rheumatic heart disease is severely rampant. While effective distribution of medical information and antibiotic therapy can help bridge the gap, there may be a larger issue behind this divide in terms of the direction of medical research. The cost of medical research is tremendous and time consuming, as is the cost of treating these types of diseases. The direct and indirect costs of cardiovascular disease alone were over $200 billion in the United States in 2002[1]. Many companies strive to develop therapeutic devices and drugs to target these diseases that affect over 40 million Americans. Unfortunately, it appears that a much larger global population may suffer from disease etiologies for which these novel medications and devices may not be suitable, and this population cannot afford to develop these cures themselves. While antibiotics can be

relatively inexpensive to obtain, these in general do not treat the underlying causes of these pathologies. Even in the United States, current diagnostic tools for aortic valve dysfunction relies on echocardiography, which may show a problem at a stage where it is already too late to treat non-invasively[2]. What is needed in both these situations is an effective strategy to understand the mechanistic development of these pathologies. That way diagnostic tools and targeted therapeutics can be developed for these underlying causes, effectively removing the need for any kind of prosthetic valvular replacement.

Tissue engineering technologies may provide the tools needed to achieve this goal. By combining living cells, a supportive substrate, and appropriate mechanical and/or biochemical signals, it is theoretically possible to create a living tissue substitute that can grow and remodel according to the bodies needs. Perhaps even more importantly, tissue engineering can provide more physiological models for the in vitro study of normal and pathological tissue biology in well defined chemical and mechanical environments. The paradigm for biological research in the 20th century was animal research. While having the advantage of systemic circulation, hormonal cues, and immune response, these models are very expensive, require long development times, and offer little useful mechanistic data. While animal studies are critical for the evaluation of preclinical safety and efficacy of medical drugs and devices, a significant number of animal studies could be reduced with the development of in vitro test beds that mimic physiological responses. Over the last 30 years, experimental research has developed along this line, exposing single cell layers to combinations of biochemical and mechanical cues to understand their mechanism of action and biological response. While these experiments have greatly advanced the understanding of diseases like atherosclerosis, they suffer from the potential for artificial responses due to in vitro culture. In vascular research, for example, it has been shown that statically cultured

endothelial cells actually represent a pathologically activated phenotype. With the addition of physiological mechanical cues, these cells revert to a more quiescent phenotype as is seen in vivo[3], yet still lack fundamental signals owing to a lack of neighboring smooth muscle cells and three dimensional tissue matrix. The research paradigm for the 21st century could then be the evolution of three dimensional tissue engineered models, capable of exposure to well defined mechanical and biochemical cues, so that truly mechanistic data can be obtained and properly interpreted. In the long term (and perhaps even short term), these engineered systems will shorten the time to develop promising therapeutic strategies.

7.2: Aortic Valve Biology

Almost nothing is known about aortic valve cell biology and the effects of mechanical and biochemical cues on their behavior. Techniques to isolate and culture these cells have only recently been developed, and to date only static two-dimensional culture phenotype has been assessed, and only at a surface level. In Chapter 2 of this work, detailed protocols were developed to isolate pure populations of aortic valve endothelial and interstitial cells. These cells were characterized through cytoskeletal marker expression and some functional assays, and the results compared favorably with other reports in the literature. These cells were then used to determine biological responses to mechanical forces and the effects of three dimensional culture, the results of which were discussed at the end of each chapter. The purpose of this chapter is then to combine some of the results of different chapters to gain more insight into the biological responses of valvular endothelial cells and interstitial cells to defined environments. Two prominent themes developed, and they are addressed in the following paragraphs.

Valvular Endothelial Mechanotransduction. Much has been made of the influence of mechanical signals on vascular endothelial – smooth muscle cell interactions [4-7]. Endothelial cells maintain vascular wall shear stress by maintaining vessel tone, and regulate the quiescent smooth muscle cell phenotype. Numerous experiments have been conducted in vitro to determine the mechanism of these effects, and both centralized and decentralized hypotheses have been suggested[8]. In Chapter 4, it was shown that valvular endothelial cells were also sensitive to shear forces, but in a different manner than vascular endothelial cells. Valvular endothelial cells aligned perpendicular to flow, while vascular endothelial cells aligned parallel. The perpendicular endothelial alignment is also present in vivo on aortic valve leaflets[9], suggesting that the in vitro response is similar to what is seen in vivo. This morphological change was shown to be dependent on cytoskeletal reorganization driven by changes in focal adhesion development. Focal adhesion plaques have been implicated as mechanosensors for endothelial cells[10]. It was also discussed that these differences may be related to differences in signaling pathways used by the cell. Valvular endothelial cell alignment was not disrupted by inhibition of PI 3-kinase activity, while vascular endothelial cell alignment was. Table 7-1 highlights significant gene expression differences revealed by microarray analysis that relate to shear stress response (Groups 1 and 2) from Chapter 5. Genes coding for proteases, adhesion molecules, signal pathways, and other proteins were found to change in both groups. Significant changes in genes involved with rho kinase, PI 3-kinase, and calpain were noted in valvular endothelial cells under flow. The combination of these genetic changes and the specific pathway inhibition reported in Chapter 4 strongly suggest unique mechanotransduction pathways are involved with each endothelial cell type.

A speculative hypothesis for this difference may be related to the differences in tissue strains experienced in vivo. Endothelial cells perhaps have a “memory” of their in

vivo tissue and fluid mechanical environment, and their ability to respond to these stimuli may persist in vitro. As described in Chapter 1, valvular cells are exposed to a very

Table 7-1: Flow regulated genes involved in mechanotransduction in valvular and vascular endothelial cells.

PAVEC Flow vs. PAVEC Static (Group 1)

Modulatory Adhesion Molecules/Proteases				
Gene	**Reg**	**Fold**	**Std**	**P <**
ADAM15	Up	1.26	0.12	0.005
MMP23B	Up	1.40	0.23	0.005
CD36 (thrombospondin receptor)	Down	1.30	0.09	0.001
Thrombospondin	Up	1.24	0.25	0.05
Thrombin inhibitor	Up	1.33	0.11	0.005
Thrombomodulin	Down	1.67	0.12	0.001
Prothrombin	Up	1.41	0.35	0.025
Alpah 5 integrin	Up	1.48	0.10	0.001
Beta 4 integrin binding protein	Up	1.59	0.48	0.005
Alpha 3 integrin	Down	1.15	0.05	0.05
Signal Pathways				
Gene	**Reg**	**Fold**	**Std**	**P <**
Calpain 4	Up	1.38	0.12	0.005
Calpain 1	Up	1.61	0.18	0.001
GTP-binding Rho 7	Up	2.28	0.36	0.001
Rho GDP dissociation inhibitor (DI) alpha	Up	1.41	0.23	0.025
Rho GDP DI beta	Down	1.31	0.06	0.05
Rho Guanine Nuclear Exchange factor (GNEF) 1	Up	1.40	0.08	0.005
Rho G	Up	1.47	0.55	0.05
Rac Z	Up	1.75	0.17	0.001
Rho associated coiled-coil protein kinase 1	Down	1.26	0.08	0.005
PI 3K regulatory subunit 3	Up	1.35	0.25	0.025
Activated LCAM	Down	1.48	0.30	0.005
PECAM	Up	1.30	0.30	0.05
Junction plakoglobin	Up	1.12	0.06	0.001
Connexin 50	Up	1.44	0.22	0.01
Connexin 45	Up	1.28	0.12	0.005
Endothelial Genes				
Gene	**Reg**	**Fold**	**Std**	**P <**
Human vascular endothelial growth factor (VEGF)	1	1.13	0.08	0.005
endothelial PAS domain protein 1	1	2.84	0.84	0.001
nitric oxide synthase 3 (endothelial cell)	1	1.18	0.22	0.050
platelet/endothelial cell adhesion molecule (CD31 antigen)	1	1.30	0.30	0.050
endothelin type b receptor-like protein 2	2	1.16	0.15	0.005
Human kruppel-like zinc finger protein (ZNF300)	1	1.09	0.07	0.005

Table 7-1 Continued:

PAEC Flow vs. PAEC Static (Group 2)				
Modulatory Adhesion Molecules/Proteases				
Gene	**Reg**	**Fold**	**Std**	**P <**
ADAM17	Up	1.22	0.20	0.05
MMP10	Down	1.13	0.12	0.05
MMP2	Up	3.00	0.80	0.001
Thrombospondin 1	Up	1.15	0.17	0.01
Thrombospondin 4	Up	1.40	0.46	0.05
Beta 2 integrin	Down	1.18	0.04	0.025
Alpha 5 integrin	Up	2.09	0.70	0.025
Beta 4 integrin binding protein	Up	1.79	0.43	0.025
Alpha 2B integrin	Up	1.47	0.25	0.05
Thrombomodulin precursor	Down	2.52	1.02	0.001
Thrombomodulin	Down	2.00	0.48	0.001
Prothrombin	Up	2.49	0.62	0.005
Signal Pathways				
Gene	**Reg**	**Fold**	**Std**	**P <**
Calpain 1	Up	1.64	0.57	0.01
Rho GDP DI alpha	Up	1.68	0.48	0.05
Rho GNEF 1	Up	1.19	0.12	0.025
Activated LCAM	Down	2.49	0.5	0.001
PECAM	Up	1.84	0.38	0.05
ICAM3	Up	1.19	0.08	0.025
Connexin 50	Up	1.37	0.25	0.025
Cardiac Gap Junction	Down	1.31	0.1	0.05
Connexin 37	Down	1.63	0.44	0.001
Endothelial Genes				
Gene	**Reg**	**Fold**	**Std**	**P <**
Human endothelin converting enzyme-1 (ECE-1)	1	2.20	0.79	0.001
vascular endothelial growth factor-related protein	1	1.73	0.23	0.010
Human endothelial cell protein C/APC receptor (EPCR)	1	1.63	0.45	0.005
platelet/endothelial cell adhesion molecule (CD31 antigen)	1	1.84	0.38	0.050

complex and dynamic biaxial tissue strain, in addition to fluid forces, that may also exert an influence on the endothelial cells. It has been reported that endothelial cells exposed to uniaxial stretch align perpendicular to the major axis of strain. Figure 7-1 shows a schematic of the directions and relative magnitudes of tissue strains and fluid forces. Blood vessels experience primarily circumferential strain, and the endothelial cells align perpendicular to this strain axis, which also happens to be parallel to the general flow direction. The major strain axis in valve leaflets, however, is radial, and the valvular endothelial cells align perpendicular to this, which is circumferentially along the leaflet. This alignment also happens to be perpendicular to the flow direction. Therefore, it may be possible that tissue strain is a stronger stimulus of endothelial cell alignment. An abstract presented at the 2002 EMBS-BMES Conference suggested that a 2% axial strain has the same "alignment power" as 80 dynes/cm^2 steady shear stress in a 24 hour period[11]. Additionally, Sarraf and colleagues presented a bioreactor design capable of exposing combinations of shear and strain, and their results suggest a tendency to align more with strain than flow[12]. As shown in Chapter 6, aortic valve endothelial cells aligned perpendicular to flow when cultured on top of somewhat circumferentially aligned valvular interstitial cells in a three dimensional collagen matrix. The valvular endothelial cell alignment in both cases was under the action of shear, without any strain present. It might be that endothelial cells respond to a portion of their mechanical environment (flow or strain) as if the entire environment (flow and strain) were present. As was reported in Chapter 4, valvular endothelial cells lose the ability to align to flow in later passages, suggesting that this may be a phenotypic function that can be lost with serial in vitro passaging. Data supporting the notion of a "memory" of in vivo mechanical environment does not exist currently. To truly investigate this hypothesis, experiments exposing both valvular and vascular endothelial cell responses to combinations of strain and shear stress will need to be conducted. Imberti et al demonstrated that vascular endothelial

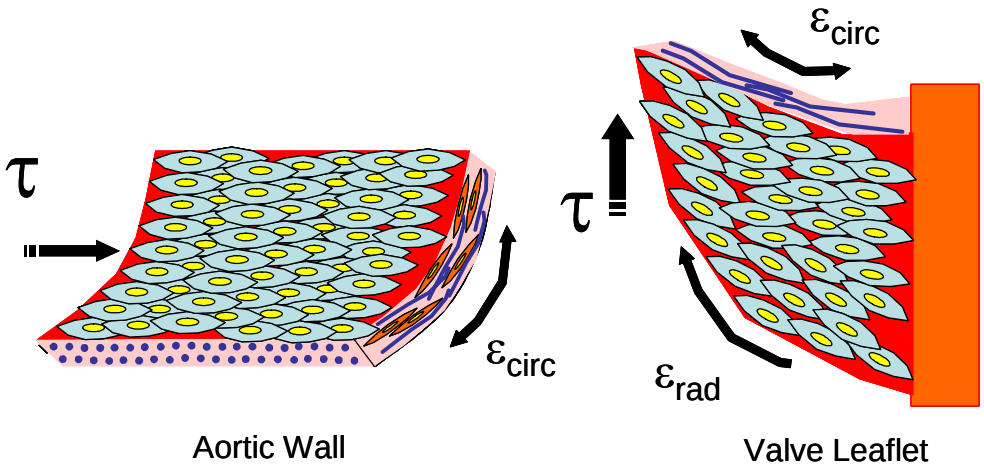

Figure 7-1: Schematic detailing the tissue strains and fluid shear stresses on aortic valve leaflets and aortas.

cells orient with the direction of mechanically aligned matrix and smooth muscle cells in static culture, but parallel to the direction of flow under shear regardless of initial orientation[7]. Due to the slight matrix effect observed in Chapter 6, it would be interesting to see if valvular endothelial cells continue to align perpendicular to flow while co-cultured on top of an oppositely (longitudinally) aligned matrix.

The more important question however is: what is the purpose for valvular endothelial mechanotransduction? There is evidence that aortic valve leaflet tissue exhibits some contractile responses to vasoactive agents, but any evidence of a vasoactive response of leaflets in vivo has yet to be reported[13]. If it is found to exist, the source of these agents must somehow be the valvular endothelial cells. In Chapter 5, the genetic profile of valvular endothelial cells in response to steady laminar shear stress was determined in the “group 1” microarray studies. A list of vasoactive agents significantly regulated by shear in valvular endothelial cells is given in Table 7-2. The presence of regulated vasoactive genes suggests that some leaflet vasoactivity may

Table 7-2: Genes coding for vasoactive agents that are sensitive to shear stress as determined by microarray analysis.

Gene	Regulation	Magnitude	P value
Nitric oxide	Up	1.18+/-0.22	0.0475
Endothelin receptor B	Down	1.16 +/- 0.15	0.0019
Angiotensin I converting enzyme	Up	1.74 +/- 0.34	0.0031
Angiotensin II receptor	Down	1.10 +/- 0.07	0.0131
Angiotensinase C	Down	1.19 +/- 0.10	0.0447
Angiotensin protease inhibitor	Down	1.26 +/- 0.11	0.0018
Somatostatin	Up	1.38 +/- 0.11	0.00004

occur, although more experiments are needed to investigate these responses. Interestingly, the somatostatin gene is upregulated in response to flow in aortic valve endothelial cells (1.38, $P<0.001$), but downregulated in aortic endothelial cells (3.24, $P<0.001$). In addition to vasoactive properties, somatostatin is an important regulator of angiogenesis[14]. The precise role of each of these agents in aortic valve biology is unclear, and without additional experiments speculation would be premature. It is certainly an interesting possibility.

Physiological vs. Pathological Valvular Cell Function. The existence of physiological and pathological phenotypes of cells is well known in vascular biology. Normal healthy vessels are characterized by a quiescent endothelial monolayer on top of a lamellar sequence of smooth muscle cells and elastic fibers. In a disease state such as in atherosclerosis, endothelial cells become activated by expressing receptors that recruit circulating monocytes, which adhere and migrate through the vessel surface into the underlying intima. The inflammatory mediators released by these cells and the endothelial cells induce smooth muscle proliferation, migration, and matrix synthesis, eventually forming the signature “atherosclerotic plaque” on the vessel[15, 16]. It has been shown that some form of atherosclerotic plaque is present on the leaflets of

diseased aortic valves, suggesting that there may be a similar pathogenesis in valvular endothelial – interstitial cell interactions[17]. Atherosclerotic progression in aortic valve leaflets in vivo is associated with the presence of inflammatory mediators, systemic endothelial dysfunction, and intra leaflet angiogenesis [18]. It is likely therefore that similar physiological and pathological phenotypes of valvular endothelial cells and interstitial cells exist.

The results from Chapters 2 through 6 suggest some possible aspects of these roles, which are listed in Table 7-3. Shear conditioned endothelial cell monolayers provided a picture of a physiological phenotype, while statically cultured cells a pathological phenotype. As shown in Chapter 4, sheared valvular endothelial cells maintain a contact inhibited monolayer, but change morphology to align perpendicular to the flow direction. It is clear from Chapter 5 that valvular endothelial cells respond to shear stress with changes in a large number of genes, a portion of which code for pro and anti-inflammatory genes. Aortic valve endothelial cells in shear appear to upregulate anti-inflammatory genes and downregulate pro-inflammatory genes, some

Table 7-3: Potential similarities and differences between aortic and aortic valve endothelial cells

Aortic vs. Aortic Valve Endothelial Cells
Similarities
Maintain non-thrombogenic barrier
Transmit nutrients and signals to underlying cells
Anti-inflammatory profile under steady laminar shear
Immunogenic
Differences
Mechanotransduction pathways
Vasoactivity (?)
Regulation of underlying cells
Bacterial adhesion properties
Calcification pathways (?)

examples of which are given in Table 7-4.

Additionally, both vascular and valvular endothelial cells may be important mediators of calcification. Both valvular and vascular endothelial cells downregulate BMP-4, a known osteogenic protein, in response to shear stress, as previously discussed in Chapter 5. Calcification is a major issue with biological and prosthetic heart

Table 7-4: Genes coding for inflammatory regulating proteins in valvular endothelial cells that are sensitive to shear stress as determined by microarray analysis.

Gene	Regulation	Magnitude	P value
Interleukin 7	Down	1.27 +/- 0.16	0.0103
Interleukin 13	Down	1.47 +/- 0.26	0.0036
Interleukin 18	Down	1.36 +/- 0.09	0.0118
Prostacyclin synthase	Up	1.26 +/- 0.07	0.0007
Leukocyte Cell Adhesion Molecule	Down	1.48 +/- 0.30	0.0015

valves, as discussed previously, and also affects the vasculature. Two genes with osteogenic properties were also differentially regulated between the two cell types, as shown in Table 7-5. It is interesting to note that one gene (OSF-2) is almost exclusively present in the vascular EC, while the other (OB-Cad) was exclusively present in the valvular endothelium. The fact that these genes are downregulated in response to flow suggests a calcification-protective endothelial phenotype. Data linking these genes to vascular and/or valvular calcification does not currently exist, but the microarray results indicate the intriguing possibility.

Table 7-5: Genes coding for bone regulating proteins in endothelial cells that are sensitive to flow.

Gene	Difference in expression between cell types in static culture	Regulation under flow in higher expressed cell type
OSF-2 (fasciclin)	444 fold higher in aorta	Down 3.13 +/- 1.52
Cadherin 11 (OB Cadherin)	113 fold higher in valve	Down 1.67 +/- 0.13

In Chapter 3, it was determined that aortic valve interstitial cells have increased α-smooth muscle actin in two dimensional culture in comparison to the more physiological three dimensional culture. Probably the best examples of phenotypic and pathological phenotypes are the two three dimensional culture models in Chapter 6. Here it is shown that aortic valve endothelial cells and interstitial cells act synergistically with steady shear stress to present a physiological tissue. Interstitial cell only constructs lack the endothelial mediated factors to maintain a physiological phenotype, thus presenting a more pathological phenotype. It was also interesting to note that non-endothelial seeded constructs had virtually change in response to flow as determined by the tests in Chapter 6, possibly suggesting an inability of interstitial cells to respond to this mechanical stimulus. Physiological valvular endothelial – interstitial cell interactions involve (1) maintenance of interstitial cell number under flow, (2) quiescent interstitial cell phenotype exhibited by decreased a-smooth muscle actin expression (except maybe immediately near the flow surface), (3) active protein synthesis, and (4) maintenance of glycosaminoglycans. Pathological conditions would be the opposite of these. These observations have been confirmed in part from research by others. Schneider and Deck showed that native leaflet cells actively produce proteins and glycosaminoglycans in vivo, and further suggested that these properties may be related to the local mechanical environments[19]. Pathological interstitial cells have also been shown to express catabolic enzymes and proteases that degrade matrix proteins, and become activated in terms of increased α-smooth muscle cell actin expression[20].

The differences in physiological and pathological valvular and vascular cell phenotype suggest a potential fundamental limitation in the use of vascular cells in repopulating tissue engineered heart valve substitutes. Rabkin and colleagues demonstrated that vascular cells resembled a physiological interstitial cell phenotype

after 20 weeks in the ovine pulmonary circulation in terms of cell phenotype and matrix synthesis[21]. One question not addressed by these researchers was whether the donor cells persisted through the 20 weeks, or if they were replaced by invading host cells, in which case they may in fact be interstitial cells. What this study does say, however, is that mechanical forces are very potent regulators of cell phenotype.

All heart valves are additionally susceptible to specific bacterial infections and genetic anomalies as detailed in Chapter 1, and it is as yet unclear how the phenotypes of cells from different valves vary. The pulmonary and aortic valves appear to be similar in terms of morphology, with the exception of the coronary ostia emanating from the aortic sinuses, and pulmonary autografts appear to function normally with the potential for growth in the aortic position[22]. The mitral and tricuspid valves are morphologically different from these two, however, and are exposed to different regimes of tissue stresses and fluid flows. The pulmonary and aortic valves both arise from the same series of endocardial cushions during development[23], in contrast to the atrio-ventricular valves[24], suggesting that these pairs of valves may share similar phenotypic traits. So far, only one study has assessed any differences between the cells from the four valves. Taylor and colleagues showed that valvular interstitial cells exhibited a more similar cytoskeletal profile to themselves than other cell sources, but that there were some differences between valves[25]. Functional differences between these cells and their consequences will undoubtedly be ascertained by future studies.

7.3: Aortic Valve Tissue Engineering

The limited success of tissue engineered heart valves to date may reflect a consideration of only a few of the many possible requirements of a functional living aortic valve replacement. These studies were primarily concerned with mechanical integrity

and matrix synthesis using vascular endothelial cells, and potential cellular functions may have been lost with their “the best available” cell source decisions. As previously discussed, the possibility of using isolated mature autologous valvular cells is probably severely limited, unless somehow healthy cells could be obtained and cultured from the damaged valve without compromising the limited function it still possesses prior to replacement. Nevertheless, because of the extremely limited understanding of valvular cell biology and valve physiology, many questions need to be addressed before this field can progress. The next few paragraphs address what is known and what needs to be known about valve biology for the purposes of tissue engineering.

Cellular Response to Mechanical Signals. The mechanical data presented in Chapter 1 indicated that valve leaflets are highly viscoelastic structures, whose cells must thrive under a variety of mechanical forces. Christie et al determined physiological stresses on the order of 400 kPa in peak systole, but the mechanical properties of the valve leaflet can withstand much higher stresses[26]. The tissue microstructure is such that it exhibits an elastic phase at low modulus, followed by an inelastic phase with a much stiffer modulus. Therefore valve leaflets are specifically designed to be very pliable at physiological stresses, but strongly resist increased distension under increased load. This is useful for creep resistance. Weston and Yoganathan determined that local shear stresses near the ventricularis are almost 80 dynes/cm^2[27], much higher than any vascular shear forces, and yet a confluent functional endothelium is present on the leaflet at all times. What is needed, therefore, is an understanding of how valvular cells respond to mechanical forces in a manner that enables them to thrive in this environment. What are the particular biological responses of valvular endothelial and interstitial cells to single defined mechanical stimuli? What are the individual effects of uniaxial strain, biaxial strain, pulsatile shear stress, and flexure on aortic valve interstitial and endothelial cell biology? Are there differences when the cells are placed in co-

culture? What are the contributing effects of three dimensional matrix? It is likely that different mechanical forces have different biological effects on valvular cells. Unlike blood vessels, however, it seems impossible to develop a device that can expose a tissue engineered aortic valve (with annulus or root) to these modes independently. It does appear possible for leaflets, but the clinical utility of a tissue engineered leaflet may be limited due to the surgical expertise required for its successful implantation.

Interfacial Dynamics of Aortic Wall and Leaflet. The aortic valve works in close cooperation with the aortic annulus and root sinuses in normal valve function. The mechanisms for the development of these unique structures are not known, but their functions have been well documented. Tissue engineered heart valves will need to address the accommodation of the native annulus and root, or strategies to mimic these in their designs. In order to do this, an understanding of the specific phenotypes that populate the sinus, sinotubular junction, and attachment regions also needs to be developed. It is likely that specific cell types regulate these areas as evidenced by the differences in tissue contraction in response to vasoactive agents. The aforementioned mechanical properties and cellular responses may also be different within these tissue regions. Apparent vasoactivity adds another level of phenotypic function that needs to be mimicked long term in a tissue engineered valvular root, but maybe just accommodated in valve leaflets.

Host Cellular Invasion and Remodeling. It was unclear whether the cells populating the engineered tissue valves in the study by Rabkin and colleagues were from the host sheep or donor sheep. Shinoka and colleagues demonstrated that autologous cells performed superior to allogeneic cells in a leaflet replacement model, suggesting that host response plays a strong role[28]. It is unclear how this could be monitored in autologous cell transfers, but Ball and colleagues successfully monitored allogeneic donor and host cell engraftment by using female (X chromosome) hosts and

Y chromosome donor cells[29]. These results suggest that some signaling exists between the donor and recipient tissue that encourages cell ingrowth. Some studies suggest that allogeneic stem cells are less immunogenic than other allogeneic cells[30]. Perhaps with these cells one can determine which cell source ultimately remains in implanted engineered valvular tissue without the risk of early failure.

Control of Tissue Remodeling. The Hoerstrup study showed that while engineered leaflets exhibited good mechanical properties and cellularity, the leaflets did not coapt properly due to leaflet shrinkage[31]. This leaflet shrinkage may be due to uncontrolled matrix compaction by the vascular cells. Matrix compaction is one of the characteristic responses when cells are embedded in engineered tissue, as evidenced by the models created in Chapters 3 and 6. In Chapter 3, valvular interstitial cells and smooth muscle cells compacted the tissue to a fixed cell density level. It is possible that this cell density is the maximum supported by engineered tissue in the contexts explored in the studies in this work. It is unclear from the Hoerstrup and Rabkin studies whether the engineered valves maintained any steady cell density, or if their constructs compacted continuously. It is therefore of critical importance to understand the matrix compaction process and how it is controlled by cells to ensure that the design of initial tissue dimensions are adequate. In this way, the cells will remodel the valve according to their own needs, but the resulting tissue will be of the right annular size with appropriately coapting leaflets.

Immune Competency. Finally, one critical issue that is particularly important for valvular tissue engineering is immunological competency. All tissue engineering utilizing allogeneic cell sources must necessarily find a way to overcome the host immune response. The fact that valvular tissues are particularly susceptible to bacterial infection makes this issue more critical. Even prosthetic valves suffer from bacterial adhesion and growth, and the invisibility of these implants to the patient's immune system makes

these infections much harder to treat. Traditional pharmacological immune suppression, although successful, carries many long term side effects that reduce patient quality of life. The ideal tissue engineered valvular substitute would therefore need to accommodate an active immune presence without rejection. This may be achievable through the design of substrates to encourage host cell ingrowth, so that the final product is devoid of allogeneic cells. This has been achieved in other applications through the use of processed extracellular matrices, which retain growth factors and matrix signals necessary for cellular recruitment[32, 33]. It is not yet known how these substances would perform in the dynamic mechanical environment of the aortic valve.

To be sure, these issues are really just a start, and more data will surely bring more questions. What is clear is that this area of biology is vastly understudied, and its functional roles are only beginning to be appreciated.

7.4: Aortic Valve Development – a Window to the Future?

One final thought about heart valve tissue engineering, and this is that the human body has been engineering heart valves out of essentially nothing since the beginning of mankind. The development of the aortic valve and cardiac outflow tract is a complex, highly regulated process that occurs in a remarkably short amount of time. The embryonic heart begins as several primitive endocardial tubes that fuse together and form a primitive single atrium and ventricle[34]. Soon after the heart tube folds upon itself, the cardiac jelly is infiltrated with differentiating mesenchymal and neural crest cells, forming cushions[35], which in turn mature into valves[23, 36, 37]. The process of cushion tissue maturation is almost completely unknown. The use of animal models, such as the zebrafish[23, 38], chick[39-41], and mouse[42-44] has greatly contributed to the understanding of cardiac development, and provide the only means of studying

these complex events in real time. Many experiments using these models have identified genes whose expression is critical to heart valve development, but most of these studies involve knockout models which develop defects or complete absences of valves that are usually not mimicked in humans. One stimulus that has only recently been investigated is mechanical force. It is known that the cardiac tube can loop while cultured *in vitro*, and at this stage in development it maintains some circulation[45]. Hove et al. have shown that complete obstruction of blood flow within the developing cardiac tube in zebrafish caused complete cessation of tube developing, including appropriate looping and valve formation[46]. Hogers et al. ligated vitelline veins in developing chick embryos, and were able to repeatedly cause a range of cardiac defects, many seen in the clinic[47]. These ligations altered the flow patterns through the heart, and specific patterns were related to an increased proportion of certain cardiac defects. While demonstrating an association between fluid flow patterns and valvular development, the exact mechanisms are still unclear. The progression from gelatinous acellular matrix to endocardial invasion to mesenchymal differentiation to matrix maturation appears to present a perfect model for tissue engineering. What is needed before this strategy can be mimicked in vitro is an understanding of how this process occurs in vivo. Specifically, what are the stimulating factors that contribute to this process? It is likely that mechanical environment plays a very prominent role. How is the matrix composition modified by the cells during development? Bioreactor schemes currently take developmental pressures and flow rates into consideration in stimulating tissue engineered heart valves in vitro, but the initial substrate is nothing like the substrate appearing in vivo. It is also possible that extracellular matrix components play a large role in cell differentiation.

In summary, the study of the specific roles of mechanical forces and extracellular matrix cues on valvular cells in both development and in adult animals can lead to the

development of an effective protocol for the generation of a clinically applicable tissue engineered heart valve, capable of growing and remodeling into the patient's own cardiovascular system. In the short term, the use of tissue engineering models of mature valvular leaflets in experiments can lead to a better understanding of the mechanistic roles of mechanical environment and extracellular matrix in physiological and pathological valvular biology. This can lead to the development of targeted therapeutic strategies that can heal the valve before disease progresses to the point of mechanical failure, reducing the need for expensive and risky interventional surgeries.

7.4: References

1. *2002 Heart and Stroke Statistical Update*. 2001, Dallas, TX: American Heart Association. 19-21.

2. Horstkotte, D., *Endocarditis: epidemiology, diagnosis and treatment.* Z Kardiol, 2000. **89 Suppl 4**: p. IV2-11.

3. Sorescu, G.P., et al., *Bone morphogenic protein 4 produced in endothelial cells by oscillatory shear stress stimulates an inflammatory response.* J Biol Chem, 2003. **278**(33): p. 31128-35.

4. Villaschi, S. and R.F. Nicosia, *Paracrine interactions between fibroblasts and endothelial cells in a serum-free coculture model. Modulation of angiogenesis and collagen gel contraction.* Lab Invest, 1994. **71**(2): p. 291-9.

5. Chiu, J.J., et al., *Shear stress inhibits adhesion molecule expression in vascular endothelial cells induced by coculture with smooth muscle cells.* Blood, 2003. **101**(7): p. 2667-74.

6. Ziegler, T., R.W. Alexander, and R.M. Nerem, *An endothelial cell-smooth muscle cell co-culture model for use in the investigation of flow effects on vascular biology.* Ann Biomed Eng, 1995. **23**(3): p. 216-25.

7. Imberti, B., et al., *The response of endothelial cells to fluid shear stress using a co-culture model of the arterial wall.* Endothelium, 2002. **9**(1): p. 11-23.

8. Davies, P.F., et al., *Spatial relationships in early signaling events of flow-mediated endothelial mechanotransduction.* Annu Rev Physiol, 1997. **59**: p. 527-49.

9. Deck, J.D., *Endothelial cell orientation on aortic valve leaflets.* Cardiovasc Res, 1986. **20**(10): p. 760-7.

10. Shyy, J.Y. and S. Chien, *Role of integrins in endothelial mechanosensing of shear stress.* Circ Res, 2002. **91**(9): p. 769-75.

11. Owatverot, T. and F. Yin. *Response of endothelial cells to combined fluid shear stress and cyclic strain*. in *Second Joint EMBS-BMES Conference*. 2002. Houston, TX: IEEE.

12. Sarraf, C.E., et al., *Heart valve and arterial tissue engineering.* Cell Prolif, 2003. **36**(5): p. 241-54.

13. Chester, A.H., M. Misfeld, and M.H. Yacoub, *Receptor-mediated contraction of aortic valve leaflets.* J Heart Valve Dis, 2000. **9**(2): p. 250-4; discussion 254-5.

14. Lawnicka, H., et al., *Effect of somatostatin and octreotide on proliferation and vascular endothelial growth factor secretion from murine endothelial cell line (HECa10) culture.* Biochem Biophys Res Commun, 2000. **268**(2): p. 567-71.

15. Schwartz, C.J., et al., *Pathophysiology of the atherogenic process.* Am J Cardiol, 1989. **64**(13): p. 23G-30G.

16. von der Thusen, J.H., et al., *Interleukins in atherosclerosis: molecular pathways and therapeutic potential.* Pharmacol Rev, 2003. **55**(1): p. 133-66.

17. Wierzbicki, A. and C. Shetty, *Aortic stenosis: an atherosclerotic disease?* J Heart Valve Dis, 1999. **8**(4): p. 416-23.

18. Poggianti, E., et al., *Aortic valve sclerosis is associated with systemic endothelial dysfunction.* J Am Coll Cardiol, 2003. **41**(1): p. 136-41.

19. Schneider, P.J. and J.D. Deck, *Tissue and cell renewal in the natural aortic valve of rats: an autoradiographic study.* Cardiovasc Res, 1981. **15**(4): p. 181-9.

20. Rabkin, E., et al., *Activated interstitial myofibroblasts express catabolic enzymes and mediate matrix remodeling in myxomatous heart valves.* Circulation, 2001. **104**(21): p. 2525-32.

21. Rabkin, E., et al., *Evolution of cell phenotype and extracellular matrix in tissue-engineered heart valves during in-vitro maturation and in-vivo remodeling.* J Heart Valve Dis, 2002. **11**(3): p. 308-14; discussion 314.

22. Lupinetti, F.M., et al., *Comparison of autograft and allograft aortic valve replacement in children.* J Thorac Cardiovasc Surg, 2003. **126**(1): p. 240-6.

23. Rothenberg, F., S.A. Fisher, and M. Watanabe, *Sculpting the cardiac outflow tract.* Birth Defects Res Part C Embryo Today, 2003. **69**(1): p. 38-45.

24. Wenink, A.C. and A.C. Gittenberger-de Groot, *Embryology of the mitral valve.* Int J Cardiol, 1986. **11**(1): p. 75-84.

25. Taylor, P.M., S.P. Allen, and M.H. Yacoub, *Phenotypic and functional characterization of interstitial cells from human heart valves, pericardium and skin.* J Heart Valve Dis, 2000. **9**(1): p. 150-8.

26. Christie, G.W., *Anatomy of aortic heart valve leaflets: the influence of glutaraldehyde fixation on function.* Eur J Cardiothorac Surg, 1992. **6 Suppl 1**: p. S25-32; discussion S33.

27. Weston, M.W., D.V. LaBorde, and A.P. Yoganathan, *Estimation of the shear stress on the surface of an aortic valve leaflet.* Ann Biomed Eng, 1999. **27**(4): p. 572-9.

28. Shinoka, T., et al., *Tissue engineering heart valves: valve leaflet replacement study in a lamb model.* Ann Thorac Surg, 1995. **60**(6 Suppl): p. S513-6.

29. Ball, S.T., et al., *Preincubation of tissue engineered constructs enhances donor cell retention.* Clin Orthop, 2004(420): p. 276-85.

30. Grinnemo, K.H., et al., *Xenoreactivity and engraftment of human mesenchymal stem cells transplanted into infarcted rat myocardium.* J Thorac Cardiovasc Surg, 2004. **127**(5): p. 1293-300.

31. Hoerstrup, S.P., et al., *Functional living trileaflet heart valves grown in vitro.* Circulation, 2000. **102**(19 Suppl 3): p. III44-9.

32. Badylak, S.F., et al., *Host protection against deliberate bacterial contamination of an extracellular matrix bioscaffold versus Dacron mesh in a dog model of orthopedic soft tissue repair.* J Biomed Mater Res, 2003. **67B**(1): p. 648-54.

33. Musahl, V., et al., *The use of porcine small intestinal submucosa to enhance the healing of the medial collateral ligament--a functional tissue engineering study in rabbits.* J Orthop Res, 2004. **22**(1): p. 214-20.

34. Phoon, C.K., *Circulatory physiology in the developing embryo.* Curr Opin Pediatr, 2001. **13**(5): p. 456-64.

35. Camenisch, T.D., et al., *Heart-valve mesenchyme formation is dependent on hyaluronan-augmented activation of ErbB2-ErbB3 receptors.* Nat Med, 2002. **8**(8): p. 850-5.

36. Abdelwahid, E., L.J. Pelliniemi, and E. Jokinen, *Cell death and differentiation in the development of the endocardial cushion of the embryonic heart.* Microsc Res Tech, 2002. **58**(5): p. 395-403.

37. Watanabe, M., A. Jafri, and S.A. Fisher, *Apoptosis is required for the proper formation of the ventriculo-arterial connections.* Dev Biol, 2001. **240**(1): p. 274-88.

38. Hurlstone, A.F., et al., *The Wnt/beta-catenin pathway regulates cardiac valve formation.* Nature, 2003. **425**(6958): p. 633-7.

39. Yoshida, H., F. Manasek, and R.A. Arcilla, *Intracardiac flow patterns in early embryonic life. A reexamination.* Circ Res, 1983. **53**(3): p. 363-71.

40. Jaffee, O.C., *The development of the arterial outflow tract in the chick embryo heart.* Anat Rec, 1967. **158**(1): p. 35-42.

41. Qayyum, S.R., et al., *Septation and valvar formation in the outflow tract of the embryonic chick heart.* Anat Rec, 2001. **264**(3): p. 273-83.

42. Dor, Y., et al., *VEGF modulates early heart valve formation.* Anat Rec, 2003. **271A**(1): p. 202-8.

43. Ji, R.P., et al., *Onset of cardiac function during early mouse embryogenesis coincides with entry of primitive erythroblasts into the embryo proper.* Circ Res, 2003. **92**(2): p. 133-5.

44. Delot, E.C., et al., *BMP signaling is required for septation of the outflow tract of the mammalian heart.* Development, 2003. **130**(1): p. 209-20.

45. Taber, L.A., *Mechanical aspects of cardiac development.* Prog Biophys Mol Biol, 1998. **69**(2-3): p. 237-55.

46. Hove, J.R., et al., *Intracardiac fluid forces are an essential epigenetic factor for embryonic cardiogenesis.* Nature, 2003. **421**(6919): p. 172-7.

47. Hogers, B., et al., *Unilateral vitelline vein ligation alters intracardiac blood flow patterns and morphogenesis in the chick embryo.* Circ Res, 1997. **80**(4): p. 473-81.

CHAPTER 8

CONCLUSIONS AND FUTURE RECCOMMENDATIONS

Aortic valve disease (AVD) is a serious clinical problem that affects the entire globe. The etiologies of AVD are different between the developed and underdeveloped world, and different research strategies will need to be pursued to meet these needs. Tissue engineering can provide an ideal solution for living heart valve replacement, including the possibilities for growth and remodeling. Tissue engineering can also be used to develop effective models for in vitro study of valvular biology and the effects of biochemical and mechanical signals on valvular cell response. A more developed understanding of valvular cell interactions in physiological conditions will help develop targeted diagnostic and therapeutic strategies that may alleviate valvular cell dysfunction before it progresses to tissue failure, potentially removing the need for valvular replacement entirely.

Pure populations of aortic valve endothelial and interstitial cells were isolated using the protocols developed in Chapter 2. Theoretically, these protocols can be applied to isolate cells from other valves, but it has yet to be tried. The cells of the mitral and pulmonary valves might be of particular interest to study: the mitral valve because of its unique morphology and function, and the pulmonary valve because of its morphological similarity to the aortic valve and ability to function well in the left heart. Ultimately, these protocols were dependent on large samples of tissue for isolation of adequate numbers of valvular endothelial cells. More powerful studies using cells from genetically modified animals, such as mice, will require different techniques to achieve

this. In the future, a more uniformly applicable, less labor intensive protocol should be pursued. Fluorescence Activated Cell Sorting (FACS) was attempted early on in this work to achieve this, but it was difficult to maintain cell viability and sterility during the sorting process. One potential technique to be used would be magnetic sorting using beads coated with endothelial specific surface markers. PECAM (CD31) is present in valvular endothelial cells, and may serve as a useful marker.

In Chapter 3 it was shown that aortic valve interstitial cells were similar to aortic smooth muscle cells in terms of contractile properties, but synthesized matrix molecules differently while in three dimensional cultures. The tissue model used in these experiments was a stress free type I collagen disk. Three important components not addressed by these studies were the effects of mechanical forces, biochemical signals, and different extracellular matrix molecules, all of which are strongly present in vivo. It is likely that additional differences will be observed between valvular and vascular cells in these environments.

In Chapter 4 it was shown that valvular endothelial cells align perpendicular to flow, which was dependent on focal adhesion and cytoskeletal rearrangement. The fact that PI 3-kinase was differentially involved in the regulation of the morphological response was intriguing, but this was only demonstrated through a cursory experiment. Additional work using genetically modified cells or gene knockdown through siRNA technology, followed by restoration of function, would be appropriate to confirm this response difference. If true, the differences in these cells would provide excellent models to study endothelial mechanotransduction. One could also investigate the response of endothelial cells from other heart valves to compare their alignment response. An additional question that needs to be addressed is the effects of flow on the endothelial cells from different sides of the leaflet. Each side of the leaflet experiences different shear forces, and the endothelial cells from each side may respond

differently. Furthermore, the steady laminar shear used in this model is only an approximation of the mean shear force, and does not model the complex pulsatile flow the leaflet experiences. More accurate flow regimes might show additional differences between these cells, including altered mechanotransduction.

In Chapter 5, microarray analysis determined hundreds of genes that were differentially expressed between valvular and vascular endothelial cells in static and fluid flow environments. These genes code for many different proteins, suggesting several functional differences between these two cell types. The results from this chapter can be taken in literally hundreds of directions, but careful consideration of each level of genomic profiling presented in this work is critical to prevent meandering down the wrong path. Genomic data mining software, like GOMiner, can provide an excellent understanding of the connections between genes. It is also critical to confirm the expression of genes of interest using other techniques, preferably at the gene and protein level, before conducting additional experiments. A particularly interesting set of genes to investigate would be fasciclin (OSF-2) and cadherin II (Cad11). These genes were differentially expressed over 100 fold in static culture, and shown to be differentially regulated under flow. While these huge expression differences could be purely artificial, if proven true they may be a window to understanding differences between vascular and valvular calcification, and how these processes are regulated by endothelial cells.

In Chapter 6 two models were presented for the study of valvular cell biology: a physiological model with both endothelial and interstitial cells in three dimensional co-culture, and a pathological model without endothelial cells. These models were exposed to steady laminar shear stress, with static cultures serving as controls, and a profile of potentially physiological and pathological responses were developed. Future experiments would involve the investigation of pulsatile flow on these models initially, followed by other mechanical modes, such as tissue strain and flexure. The synergistic

effects of strain and fluid flow could also be investigated. New bioreactor systems will ultimately need to be developed to apply these forces in an independently controlled manner. Like the tissue models in these studies, it may not be necessary to replicate exact leaflet geometries, but rather just have a three dimensional biological matrix that can accommodate close contacts between these cells.

In summary, many more questions were raised then answered by these studies, but the field of valvular biology is ripe for investigation. The clinical need is surely present, and with additional research, hopefully can be addressed in the future.

APPENDIX A: RELEVANT PROTOCOLS

PJTB01: Isolation of Porcine Valvular Cells (PVEC and PVIC) Collagenase Method

Reagnets:

Antibiotic-Antimycotic Solution — Tissue Culture Rm → Fridge
GibcoBRL, Cat. No. 15240-062
Dulbeccos Phosphate Buffered Saline (DPBS) — Tissue Culture Rm → Fridge
Gibco, Cat. No. 14190-144, no Ca or Mg
Glucose — Laboratory Rm → Shelf
SIGMA, Cat. No. G 7021, 95% α, 5% β anomer
Trypsin-EDTA: — Tissue Culture Rm → Freezr
Gibco, Cat. No. 25300-054, 0.05% Trypsin, 0.53 mM EDTA
Collagenase CLS2: — Protein Rm → Fridge
Worthington, Cat. No. 4176, ~300 U/mg
Dulbecco's Modified Eagle Medium (DMEM) (500mL) — Tissue Culture Rm → Fridge
Gibco, Cat. No. 11965-092

Solutions:

Porcine Medium (See PJTB002): — Tissue Culture Rm → Fridge

- Dulbecco's Modified Eagle Medium (DMEM) (500mL)
  Gibco, Cat. No. 11965-092
- 1% L-Glutamine added
  Mediatech Cellgro, Cat. No. 25-005-C1
- 1% HyQ Penicillin added
  MediaTech Cellgro, Cat. No. SV30010

Components:

Cooler for organ transport
Isolation utensils (Autoclave if necessary)

- Scalpels
- Forceps
- Scissors
- Surgical tray(s)
- Petri dishes precoated with paraffin
- Surgical needles
- Swabs

15 mL centrifuge tubes

Procedure :

Preparation of the Tissue Solution – PBS w/ 5x Antibiotic-Antimycotic (527.5 mL)

1. Add 27.5 mL of Antibiotic – Antimycotic solution to 500 mL of DPBS.

2. Filter to sterilize.

Preparation of the Collagenase Solution

1. Dissolve 1 mg/mL collagenase solution in DMEM without FBS (base medium).
2. Prepare 10 mL solution per valve exised.
3. Filter to sterilize.

Isolation of Heart Valve Leaflets

1. Excise heart with aorta intact aseptically from the animal as soon as possible after death.
2. Thoroughly rinse in cold DPBS, and place in a plastic bag with enough ice cold DPBS to submerge the tissue. Place the bag in the cooler and fill with ice. Transport back to the lab.
3. Upon arrival at the laboratory, place the container with the porcine heart under the sterile hood.
4. Take the heart out of the bag and quickly cut away the aorta and the lower third of the ventricles until the leaflets are exposed. Cut the leaflets about 20 percent of the length of the leaflet away from the attachment region, as that area can posess some smooth muscle cells and vascularity. Keep the tissue hydrated throughout this process using cold Tissue Solution when necessary.
5. Place the leaflets in a sterile 15 mL centrifuge tube with cold Tissue Solution. Use one tube per valve. Let incubate at room temperature for 15 minutes.

Isolation of Endothelial Layer

1. Fill 3 15 mL centrifuge tubes per valve with complete Porcine Medium.
2. Remove the tissue from the tubes, and place on a sterile (UV light) dish that has been previously coated with congealed paraffin beads to provide a surface for pin attachment.
3. Gently lay the tissue concave downwards (ventricular side upwards) on the paraffin surface. Pin the edges of the leaflet to expose the endothelial layer. All of the leaflets from a valve can be placed in the same dish and pooled together.
4. Place a few drops of cold collagenase on each upwards-facing endothelial surface. Incubate the tissue for 10 minutes at 37 C.
5. Gently swab the endothelial layer by rotating the dry, sterile swab as the endothelial surface is scraped. Place swab into one of the centrifuge tubes and gently rotate to dislodge cells. Dab the swab several times in the collagenase to dislodge cells from the fibers. Repeat this procedure two more times with fresh swabs each time.
6. Collect the collagenase/cell suspension for each valve into a separate tube.
7. Centrifuge the tubes at 1000 rpm for 10 minutes to pellet any isolated cells. Aspirate supernatant.
8. If isolating interstitial cells as well, perform that protocol while cells are centrifuged.
9. Add 3 mL Porcine Medium to the tubes and centrifuge again. Aspirate supernatant.
10. Add 5 mL Porcine Medium to the centrifuge tubes and plate the cells in a T-25 flask. Use 1 flask per centrifuge tube.
11. Culture as normal.

Isolation of Interstitial Cells

1. Fill 1 15 mL centrifuge tube with 10 mL collagenase solution per valve exised. Complete this step before isolating endothelial cells if that portion of the protocol is being followed.
2. After swabbing the leaflets, immediately place them in the appropriate tube with the collagenase solution.
3. Incubate for an appropriate amount of time (12 to 18 hours). Agitate gently if desired.
4. Centrifuge the digested tissue fragments and cells for 5 minutes at 1000 rpm, and aspirate the supernatant.
5. Centrifuge the tubes at 1000 rpm for 10 minutes. Aspirate supernatant.
6. Add 5 mL of Porcine Medium and again centrifuge tubes. Aspirate supernatant.
7. Resuspend pellet in one tube with 5 mL of Porcine Medium and add to a T-175 filled with 35 mL Porcine Media.
8. Culture as normal.

NOTES :

- Do not mix leaflets of different valves.
- Aortic root with leaflets can be isolated directly at the slaughterhouse
- Inspect endothelial cell cultures for endothelial and other developing morphology. If other cell types develop, trypsinize the cells, centrifuge them at 1000 rpm for 10 minutes, plate them back down, but change the Medium after 1 hour (can be modified based on results). Endothelial cells tend to adhere quicker than other cell types.
- Endothelial cells can also be enriched from contaminating cells using magnetic sorting with PECAM (CD31) antibody.

PJTB02: Culture of Porcine Cells

Reagents:

Dulbecco's Modified Eagle Medium (DMEM) (500 ml) Tissue Culture Rm → Fridge
Gibco, Cat. No. 11965-092
L-Glutamine (L-Glut) (100 ml) Tissue Culture Rm → Freezr
Mediatech Cellgro, Cat. No. 25-005-C1
HyQ Penicillin (PS) (100 ml) Tissue Culture Rm → Freezer
Mediatech Cellgro, Cat. No. SV30010
Fetal Bovine Serum (FBS) Heat inactivated (500 ml) Tissue Culture Rm → Freezr
Mediatech Cellgro, Cat. No. 35-011-CV
Sterile Tissue Culture Water (500 ml) Tissue Culture Rm → Shelf
Sigma, Cat. No. W3500
Collagen, Type 1 (Coll I) (100 mg) Tissue Culture Rm → Fridge
BD Biosciences, Cat. No. 354236
Trypsin-EDTA (100 ml): Tissue Culture Rm → Fridge
Gibco, Cat. No. 25300-054, 0.05% Trypsin, 0.53 mM EDTA

Components:

Tissue Culture Dishes/Flasks
Aliquot tubes

Cells:

Porcine Aortic Endothelial Cells (PAEC) (1 vial) Liquid Nitrogen Tank
Porcine Aortic Smooth Muscle Cells (PASMC) (1 vial) Liquid Nitrogen Tank
Porcine Aortic Valve Endothelial Cells (PAVEC) (1 vial) Liquid Nitrogen Tank
Porcine Aortic Valve Interstitial Cells (PAVIC) (1 vial) Liquid Nitrogen Tank

Procedure:

Aliquot of Media materials:

1. Defrost stock solutions of L-Glut, PS, and FBS
2. Divide L-Glut into 10 ml aliquots.
3. Divide PS into 10 ml aliquots (can combine with L-Glut if you want).
4. Divide FBS into 100 ml aliquots (usually done for you).
5. Make more aliquots if enough solution exists for more *complete* aliquots.
6. Place aliquots in the freezer and store at -20 C.

Dilution of Collagen I for growth substrate

1. Each bottle has a different concentration of collagen in mg/ml.
2. Make 150 ml of 50 μg/ml collagen I in Sterile Water.

Preparation of the Porcine Cell Media (1120 ml):

1. Place aliquot of L-Glut, PS, FBS, and two bottles of DMEM in the warm water bath (37 C) until they have completely thawed and/or warmed.
2. Place 1000 ml sterile filter and all reagents in the sterile hood.
3. Activate the filter by attaching the aspirating tube and turning on the vacuum pump.
4. Pour all the reagents through the sterile filter.
5. Remove the filter, cap the bottle, and label it.

Coating of Cell Culture Surface (PAVEC only)

1. Add just enough of the diluted Coll I to completely coat cell culture surface (1-2 ml/ 25 cm^2)
2. Incubate at 37 C for 1 hour.
3. Aspirate excess Coll I from dishes.

Defrosting of Cells:

1. Place the Pre-Prepared Media in the warm water bath until warmed (if needed).
2. Place the desired number of flasks into the sterile hood (usually indicated on the cryovial).
3. Add 5 ml of media/ 25 cm^2 surface area to each flask.
4. Remove the cryovials containing the appropriate cells from the Liquid Nitrogen Tank.
5. Quickly thaw the vials as quickly as possible by swirling the vials around in the bath while they are completely submerged. Remove when only a small amount of ice left in the vial(s). The rest will thaw in your hand.
6. Place an appropriate amount of cell suspension into the designated culture dishes.
7. Properly label each flask.
8. Place culture dishes in the incubator.

Feeding Cells:

Cells should be fed 24 hours after thawing or isolating, and then every 48 hours

1. Inspect flasks for adherent cells, and any contamination.
2. Place flasks with cells under sterile hood.
3. Aspirate out the old media from the opposite wall to which the cells are adhered.
4. Add 1 ml of the appropriate culture media for every 5 cm^2 of cell culture surface.
5. Place flasks back in incubator.

Splitting of Cells 1:3 according to cell culture surface area:

9. Place the Porcine Medium and the T-EDTA Solution in the warm water (37 C) bath until the reagents have completely thawed and warmed.
10. Place the dishes/flasks containing cells under the sterile hood.
11. Aspirate the current media from the opposite wall to which the cells are adhered.
12. Add 1 ml of the T-EDTA Solution for each 25 cm^2 of culture surface area to the dishes/flasks.
13. Place cells in the incubator for 3 to 5 minutes.
14. View the cells under a microscope to ensure they have released from the flask wall. If the cells have not released from the wall, lightly tap the side of the dish/flask.
15. Add 3 ml of Porcine Medium for each 25 cm^2 of culture surface area to neutralize the Trypsin.
16. Rince any adherent cells off the wall of the flask by drawing in and expelling the media from the pipette. Don't take too long though.

17. Place the cell suspension in the appropriate centrifuge tube and spin for 5 minutes at 1000 rpm.
18. While the cells are spinning add 5 ml of the appropriate media per 25 cm^2 of culture surface area.
19. Aspirate the supernatant and resuspend the pellet in a small amount of media (1 ml per flask).
20. Divide this cell suspension and plate evenly onto 3 times the original culture surface area.
21. Close and properly label each flask/dish before placing them in the incubator.
22. Feed the cells every 48 hours.

NOTES:

- DMEM is a standard medium for animal cell culture, the exact constituents can be found by consulting Gibco.
- L-Glutamine is a protein that provides a major energy source to the cells. It degrades rapidly, so the medium is supplemented with it to ensure growth.
- Penicillin and streptomycin are anti-bacterial agents.
- The molar ratios within the Porcine Medium are not exact, but it has been the standard way of making the medium at the lab.
- Diluting collagen in sterile water maintains the acidic pH to prevent precipitation.
- Trypsin is an enzyme that cleaves cell adhesion moecules. Prolonged exposure to the enzyme could disrupt normal cell function.
- EDTA removes calcium, thereby disrupting cell adhesion.
- Don't try to split too many flasks at once. The Trypsin will kill cells if not neutralized after a short amount of time.
- PAVEC culture medium can be supplemented with 50 U/ml of heparin (Sigma) to help mitigate the contamination of the culture by interstitial cells.

PJTB03: Porcine Cell Cryopreservation

Reagents:

Dimethyl Sulfoxide (DMSO) — Laboratory Rm → Shelf
J. T. Baker, Cat. No. 9224-01 (500 ml)
Fetal Bovine Serum (FBS) Heat inactivated — Tissue Culture Rm → Freezr
Mediatech Cellgro, Cat. No. 35-011-CV

Solutions:

Porcine Medium SERUM FREE (See PJTB001): — Tissue Culture Rm → Fridge

- Dulpecco's Modified Eagle Medium (DMEM)
  Gibco, Cat. No. 11965-092
- 1% L-Glutamine added
  Mediatech Cellgro, Cat. No. 25-005-C1
- 1% HyQ Penicillin added
  MediaTech Cellgro, Cat. No. SV30010

Other:

Cryovials

Cells:

Porcine Cells (PAEC, PASMC, PAVEC, PAVIC) — Tissue Culture Rm → Incbtr

Procedure :

Aliquoting FBS

1. Thaw one (of the aliquotted) bottle of FBS, and divide it into 10 ml aliquots.
2. Label and freeze for later use.

Creation of the Cryopreservation Medium

1. Make sure all reagents are sterile.
2. Do not warm reagents, merely thaw them. Do not place DMSO in refrigerator, it will freeze.
3. Cryopreservation medium is Serum Free DMEM (50%), FBS (40%), and 10% DMSO.
4. Combine the DMEM and FBS in a sterile tube. Make enough medium for 1.5 ml (total, including DMSO) per cryovial. The DMSO will be added later.

Freezing the Cells

1. Trypsinize (PJTB001) the cells to be stored.

2. Properly label the contents of the appropriate number of cryovials to be used, and place them under the sterile hood.
3. Place the cell solution in the centrifuge, and balance it with an equal amount of water in an identical tube on the opposite side of the centrifuge.
4. Run the centrifuge at 1000 rpm for 5 minutes.
5. Aspirate the supernatant, being careful not to disturb the pellet, leaving about 100μL remaining.
6. Close the tube, and flick the bottom of the tube to dislodge the pellet.
7. Add the DMEM/FBS solution to the cell pellet, and bring the cells into suspension. Make sure there are no pieces of cell pellet remaining.
8. **SLOWLY** add the DMSO to the cell solution, swirling the suspension after every few drops.
9. Place the 1.5 ml of cell solution into each cryovial.
10. Place the cryovials into the freezer storage container, and place it in the –70 C freezer for at least 24 hours, but not more than 3 days.
11. Remove the storage container from the freezer, and place the cryovials into appropriately labeled locations of the designated storage box in the nitrogen tank.
12. Close the nitrogen tank.

NOTES :

- DMSO is an agent that inhibits ice crystal formation, but also permeablizes the cell membranes, which is cytotoxic.
- Initial cell storage amounts were based on cell counting (1.5 million cells per cryovial), but subsequent storage was based on intended thawed culture. Typically cells were trypsinized from one T-175 flask (for PAVICs) or 1 T-75 flask (for PAVECs) and split into three cryovials. This was easier, more consistent, and removed the need to count cells.

PJTB04: Monolayer Flow Loop Assay

Components:

1 Fluid Reservoir Nalgene, Cat. No. DS2127-0250	Laboratory Rm → Shelf
1 Filling/Venting Caps: tubing 1/4", caps 53B Cole Parmer, Cat. No. UA-06258-10	Laboratory Rm → Shelf
1 Pressure Dampener Cole-Parmer, Cat. No. 07596-20	Laboratory Rm → Shelf
1 Flow Chamber Polycarbonate (In House Construction)	Laboratory Rm → Shelf
8' Silicone Tubing ¼" O.D. 1/8" I.D. Cole-Parmer, Cat. No. 0641167	Laboratory Rm → Shelf
8" "PharMed" (or Norprene) Tubing No. 16 Masterflex, Cat. No. 06485-16	Laboratory Rm → Shelf
Assorted tube fittings. Value Plastics, Inc. • 10 MTLL230-20 (A) • 4 SFTLL-20 (B) • 5 FTLL230-20 (C) • 1 FTLLC-6 (D)	Laboratory Rm → Shelf
4" Plastic Tie Wraps	Laboratory Rm → Shelf
Teflon Tape	Laboratory Rm → Shelf
1 Flow loop (assembled with FTLLC-6) See PJTB0005	Laboratory Rm → Shelf
1 Assembled flow block See PJTB0005	Laboratory Rm → Shelf
1 Flow chamber top plate Aluminum (In house construction)	Laboratory Rm → Shelf
1 Flow chamber bottom plate Aluminum (In house construction)	Laboratory Rm → Shelf
1 Silicone rubber gasket Stock material	Laboratory Rm → Shelf
1 Spacer (thickness important) Stock material	Laboratory Rm → Shelf
Square non-treated tissue culture dish	Tissue Culture Rm → Shelf
6 8-32 x 2" Standard head screws	Laboratory Rm → Shelf
2 Long tweezers	Laboratory Rm → Shelf
1 Standard glass slide Corning, Cat. No. 2947	Laboratory Rm → Shelf
2 Cell Scrapers Fischer Scientific, Cat. No. 08-773-2	Tissue Culture Rm → Shelf
1 Air Filter Pall Corp., Cat. No. 4192	

Solutions:

Porcine Medium (See JTB002): Tissue Culture Rm → Fridge

- Dulpecco's Modified Eagle Medium (DMEM) (1000 ml)
  Gibco, Cat. No. 11965-092
- 1% L-Glutamine added
  Mediatech Cellgro, Cat. No. 25-005-C1
- 1% HyQ Penicillin added
  MediaTech Cellgro, Cat. No. SV30010
- 10% Fetal Bovine Serum (FBS) added

Cells:

Porcine Endothelial Cells (PAEC, PAVEC) Tissue Culture Rm → Incbtr

Reagents:

Collagen, Type 1 (Coll I) (50 μg/ml) (See PJTB002) Tissue Culture Rm → Fridge

Procedure :

Assemble Flow Block

1. Tap the four holes in the flow block with a ¼-28 tap.
2. Wrap the threads of the (B) fittings with teflon tape, and twist them into the tapped holes. Be careful not to overtighten, they will break inside the holes.

Assemble Pressure Dampener

1. Use the components provided in the dampener box. Wrap the long needle-head nozzle threads with teflon and screw them into the damper holes.
2. Coat the outside of the nozzles close to the damper with silicone gasket (Pro Seal #80006). Let dry overnight.

Assemble Fluid Reservoir

1. Cut the tubing attached to the reservoir lid into a 3" and a 1" length. The 3" length will serve as the reservoir outflow port, and the other as the inflow.

Cut and Assemble Tubing:

23. Cut the Silicone tubing into 3 longer (24") pieces, and 6 shorter (6") pieces.
24. Cut an 18" piece of the Norprene tubing.
25. Using a previously constructed Flow Loop (Figure 1) as a guide, attach the appropriate fittings to the ends of the different lengths of tubing. Seal the connections by tightly wrapping a tie wrap around the tubing near the connector.
26. Assemble the flow loop components. If it is desired to keep the flow chamber separate from the loop, attach the free ends of the loop tubing to the FTLLC-6 connector. This provides a closed loop for autoclaving and/or flowing media.

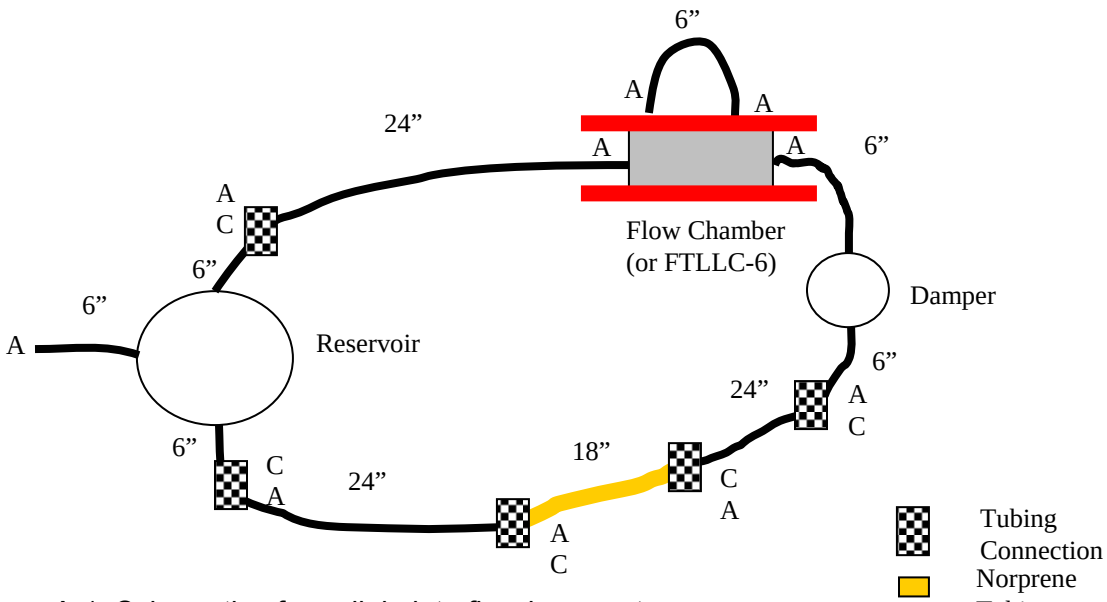

Figure A-1: Schematic of parallel plate flow loop system.

Cell Seeding

3. Autoclave glass slide and tweezers.
4. Place slide into square dish with tweezers.
5. Coat glass slide with Coll I solution (~1 ml). Spread evenly with cell scraper.
6. Incubate for 1 hour.
7. Trypsinize cells (PJTB002) into solution at a sufficient density to seed slide with 1 ml of cell solution. Typical cell densities range from 10,000 – 20,000 cells/cm^2, and are application specific. Inject solution onto slide, and spread evenly with a different cell scraper.
8. Allow 20 minutes to adhere on flat surface inside hood. Turn slide 180 degrees and let adhere for another 20 minutes. This helps to account for any unevenness of the surface.
9. Add approximately 25 ml of Porcine Medium. Cover dish.
10. Place dish into the incubator.
11. Allow 24 – 48 hours for cells to become confluent.

Autoclave Flow Loop Components

3. Place flow loop into large autoclave bag, unscrew the reservoir lid a few turns to provide air access.
4. Place the flow chamber bottom, flow block, and flow chamber top (in that order) into medium sized autoclave bag.
5. Place rubber gasket into small autoclave bag.

Sterilize Spacer

2. Sterilize the spacer according to particular requirements of that material. Placing under UV light for 45 minutes on each side works well for most materials.

Combine Flow Loop

27. Place autoclaved flow loop components, autoclaved tweezers, sterilized spacer, square dish with slide, air filter, and medium under sterile hood.
28. Open the bag with the flow chamber components and place ONLY the chamer bottom onto a tray.
29. Open the bag just enough to remove the tweezers, and use them to grab the rubber gasket, and place it in the space in the chamber.
30. Use the tweezers to grab the slide, and place it on top of the gasket.
31. Use the tweezers to grab the spacer, and place it on top of the slide.
32. Carefully place the tweezers back into its bag to maintain sterility.
33. Grab the flow block by the tubing loop, being careful not to touch the bottom surface, and place it on top of the spacer.
34. Add the flow loop chamber top, and seal the assembly with the 6 screws. Be careful to tighten uniformly, and not too tightly, so that the slide doesn't break.
35. Wipe the bottom of the slide surface showing from the chamber with an alcohol wipe.
36. Open the bag with the flow loop, and disconnect the FTLLC-6 while holding both ends of the tubing. Place the assembled flow chamber into the flow loop according to Figure 1. Twist the tubing in the opposite direction before connecting them so no stress develops in the tubing.
37. Unscrew the reservoir lid and add 125 ml of medium. Screw cap tightly.
38. Add air filter to the remaining tubing on the reservoir lid.

Running Flow Loop

1. Place a clean sheet of adsorbant paper onto one of the shelves of the large incubator.
2. Place calibrated roller pump onto shelf.
3. Carry tray with assembled flow loop to incubator, and place flow loop inside incubator.
4. Using a bracket supplied with the pump, affix the norprene tubing to the rollers.
5. Set the pump to the appropriate speed (for shear stress), and turn it on. Watch to make sure that fluid is taken from the reservoir.
6. Turn the pressure damper on its side, to allow fluid buildup inside.
7. Once the fluid builds up to the point that both ports are under the liquid line, turn the damper over again. Watch to make sure the fluid flows evenly out of the damper. Be careful not to overfill the damper.
8. Once the fluid travels back into the reservoir, add a hemostat to the loop in the flow chamber. This provides back pressure, and ensures that the flow is through the channel.
9. Let flow loop run for desired amount of time.

Removing Slides from Flow Loop System

1. Once the allotted time has passed, remove the flow cartridge from the pump and remove the hemostat from the top of the flow chamber. Disconnect tubing from either side of the flow chamber being careful not to unscrew the fittings within the flow block. Take a FTLLC-6 fitting and reconnect the tubing so media does not leak.

2. Place the flow chamber in the hood and evenly loosen the screws so the slide does not break.
3. Remove the spacer with tweezers and set aside.
4. Remove the slide of cells with tweezers and place in a square Petri dish. Add PBS (with calcium) to the dish to rinse off media and keep cells moist.
5. Thoroughly rinse out tubing and pulse dampener after use. Add bleach to media reservoir to neutralize media and rinse out. Place components on bench top to dry.

NOTES :

- Letters on Figure 1 refer to connectors used.
- When running the Flow Loop, always place the PharMed/Norprene tubing under the bracket of the roller pump.
- The Pharmed/Norprene tubing only lasts a few (~6) trials, after which longitudinal cracks will appear, so inspect it after the conclusion of each trial.
- Size 16 tubing is adequate for low and high shear of monolayers and low shear of constructs but size 25 tubing must be used for high shear of constructs due to the large spacer thickness. Construction of flow loops with size 25 tubing requires use of a 1/8 to 3/16 connector (Value Plastics part number 3050-6)
- If the holes in the non-tubular components of the Flow Loop have not already been drilled and tapped, do so now. The drill bits and tap sizes are listed below:
  - Flow Chamber: # 3 Drill, ¼ - 28 Tap, 4 holes
  - Pressure Damper: “Q” Drill, 1/8 – 27 Tap, 2 holes
- The Pharmed tubing only lasts a few (~6) trials, after which longitudinal cracks will appear, so inspect it after the conclusion of each trial.
- If block leaks from the top of the bottom chamber plate, tighten (evenly) the screws more. If it leaks from underneath the chamber, the slide has broken, and the loop should be removed so that the slide could be used as a contol.
- Slides may break several hours into the assay, so inspect regularly for leaks.

PJTB05: Immunofluorescent Staining for Confocal Microscopy

Reagents :

Formaldehyde, 20% (20 ml) Tousimis, Cat. No. #1008A	Protein Rm → Fridge
Triton-X 100 USB, Cat. No. 22686	Laboratory Rm → Shelf
Tween-20 Sigma, Cat. No. P-7949	Laboratory Rm → Shelf
Hoechst 33258 (Cell Nuclei) Molecular Probes, Cat. No. H-1398	Protein Rm → Fridge
Rhodamine Phalloidin (F-actin) Molecular Probes, Cat. No. R-415	Protein Rm → Freezer
Neonatal Goat Serum (NGS)	Tissue Culture Rm → Freezer
Non-Sterile PBS (See PJTB003)	Laboratory Rm → Shelf
Deionized Water (dH_20)	Tissue Culture Rm → Sink
Mounting Media Dako, Cat. No. S3205	Laboratory Rm → Shelf

Procedure :

Preparation of 0.1% Triton-X 100

39. Add 1 ml of Triton into 1 L of non-sterile PBS.
40. Vortex for 30 minutes.

Preparation of 1% NGS Blocking Buffer

1. Add 5 ml NGS into 500 ml non-sterile PBS.

Preparation of 3.7% Paraformaldehyde Solution

1. Add 10 ml of 20% formaldehyde into 44 ml non-sterile PBS.

Staining Cells

1. Fix the cells in 3.7% paraformaldehyde for 5 minutes.
2. Rinse 2 times with PBS.
3. Permeabilize the cells in cold 0.1% triton-X 100 for 5 minutes.
4. Rinse 2 times with PBS.
5. Incubate in 1% NGS Blocking Buffer for 1 hour at 37 C.
6. Incubate in primary antibody, diluted to the proper concentration with Blocking Buffer, for 40 minutes at 37 C.
7. Rinse 2 times with PBS.
8. Incubate in secondary antibody diluted to the appropriate concentration in Blocking Buffer for 40 minutes at 37 C. Many fluorophores used in secondary antibodies are sensititve to light, so cover them with an opaque container.
9. Rinse 2 times with PBS.

10. Incubate in Hoechst and Rhodamine Phalloidin (counterstains) diluted to the appropriate concentrations for 20 minutes at 37 C. Again, cover the slides during this process.
11. Rinse twice with PBS.
12. Rinse once in dH_20.
13. Place a drop of Mounting Media on the slide or coverslip to be sealed.
14. Place a coverslip over the drop, and press firmly but evenly on the coverslip to remove the air bubbles. Be careful not to slide the coverslip across the slide.
15. Seal the coverslip with nail polish.
16. Wrap slides in a paper towel, and place in the refridgerator until it is time to image slides.
17. Keep slides covered while transporting them, so contrast is not lost due to light exposure.

Table A-1: Antibody sources and dilutions used in experiments.

Primary antibodies and dilutions used with success				
Antibody	*Host Imm/Fluor.*	*Company*	*Cat. Number*	*Dilution*
Rhod. Phalloidin	N/A Tex Red Conj.	Molecular Probes	R-415	10 U/ml
Hoechst 553	N/A Dapi Conj.	Molecular Probes	H-1398	1:100
Anti-Vinculin	Mouse Mono IgG	Upstate Biotech.	05-386	1:100
Anti-α Actinin	Mouse Mono IgM	Sigma	A5044	1:100
Anti-α5 integrin	Rabbit Poly IgG	Chemicon	AB1928	1:100
von Willebrand factor	Rabbit Mono IgG	Sigma	F-3520	1:100
Talin	Mouse IgG	Sigma	T-3287	1:100
Desmin	Mouse IgG	Sigma	D-1033	1:100
β_3 Integrin	Rabbit IgG	Chemicon	AB1932	1:100
Focal Adhesion Kinase	Rabbit IgG	Upstate Biotech	06-543	1:100
α-Smooth muscle actin	Mouse/Cy 3	Sigma	0-6198	1:100
vimentin	Mouse/Cy 3	Sigma	V2258	1:100
β_1 Integrin	Mouse Mono IgG	Chemicon	MAB2000	1:100

Secondary antibodies used with success				
Antibody	*Host Imm/Fluor.*	*Company*	*Cat. Number*	*Dilution*
Anti-mouse IgG	Goat/FITC	Sigma	F 0257	1:100
Anti-Rabbit IgG	Sheep/FITC	Sigma	F7512	1:100
Anti-Mouse IgM	Unknown/FITC	Dr. Andres Garcia		1:100
Anti-Rabbit IgG	Goat/AF 488	Molecular Probes	A-11008	1:100

Approximate amounts of diluted antibody for various surfaces		
Surface	*Area, cm^2*	*Fluid volume, μl*
Glass slide	28.5	125
25mm circle coverslip	4.9	25

PJTB06: Preparation of Three-Dimensional Collagen Type I Constructs

Reagents:

Porcine Medium (See JTB002): Tissue Culture Rm → Fridge

- Dulpecco's Modified Eagle Medium (DMEM) (1000 ml)
  Gibco, Cat. No. 11965-092
- 1% L-Glutamine added
  Mediatech Cellgro, Cat. No. 25-005-C1
- 1% HyQ Penicillin added
  MediaTech Cellgro, Cat. No. SV30010
- 10% Fetal Bovine Serum (FBS) added

Collagen, Type 1 (Coll I) (100 mg) Tissue Culture Rm → Fridge
BD Biosciences, Cat. No. 354236

Trypsin-EDTA (100 ml): Tissue Culture Rm → Fridge
Gibco, Cat. No. 25300-054, 0.05% Trypsin, 0.53 mM EDTA

Fetal Bovine Serum (FBS) Heat inactivated (500 ml) Tissue Culture Rm → Freezer
Mediatech Cellgro, Cat. No. 35-011-CV

DMEM Powder Back Wall of 1D → Fridge
Sigma, Cat. No. D1152

Chemicals

Sodium Bicarbonate Laboratory Rm → Shelf
Sigma, Cat. No. S-6014

Sodium Hydroxide (NaOH) Laboratory Rm → Shelf
VWR, Cat. No. VW5749-4 (1 N)

Sulfuric Acid (H_2SO_4) Flammable Cab → Shelf
VWR, Cat. No. VW3259-1 (10 N)

Components

Silicone Tubing Laboratory Rm → Shelf

Note: For disk constructs, the molds to be used are the 35 mm diameter wells of a 6-well plate (non-tissue culture treated). For tubular constructs, the mold consists of a test tube and inner mandrel assembly (see diagram). Tubular constructs are molded onto a silicone sleeve that is coated with collagen.

Preparation of Silicone Sleeves (for tubular constructs only)

1. Cut sleeves into 3.81 cm (1.5") lengths.

2. Under a fume hood and wearing proper protection, transfer approximately 30 mL of 10 N sulfuric acid to a centrifuge tube. Put the sleeves in the sulfuric acid in order to etch the surface. Allow the sleeves to sit in the acid for 45-90 min. Separate sleeves from each other so that the entire surface is etched.

3. Carefully remove the sleeves from the sulfuric acid and rinse WELL (6-8 times) with fresh distilled water. The sulfuric acid can be re-used.

4. Autoclave sleeves. Also autoclave glass mandrels, stoppers, test tubes, caps and instruments at the same time.

5. Prepare 50 µg/mL collagen Type I from rat tail in sterile tissue culture water.

6. Transfer ~30 mL of the stock collagen solution to a 50 mL centrifuge tube. Immerse etched and autoclaved silicone sleeves into the ECM and allow to sit for 12-24 h at 4 ˚C.

7. Arrange sleeves in a sterile Petri dish. Using sterile forceps, slide silicone sleeves onto sterile glass mandrels. It may help to pre-wet the mandrel with the ECM in the lumen of the sleeve; this provides lubrication for the sleeve to slide onto the mandrel. Place rubber stoppers on mandrels in appropriate positions for preparation of constructs (i.e. sleeves will provide 1.5" gap between stoppers).

8. Allow sleeves on mandrels to dry for at least 1 h.

Preparation of Collagen Gel Reagents

1. Dilute 1 N NaOH to 0.1 N in dH_2O. Filter to sterilize. Approximately 50 mL of 0.1 N NaOH is sufficient for the creation of 100 constructs.
2. Prepare 5X concentrated DMEM. Dissolve powder in 200 mL of dH_2O. Add 3.7g sodium bicarbonate. Filter sterilize. Separate into 10 ml aliquots and store at -20°C until use.

Preparation of Cell-Collagen Suspension

Appropriate volumes of the following reagents should be ready and kept on ice:
(use attached worksheet to determine appropriate volumes)

5X concentrated DMEM: (Volume of FBS, NaOH, and Collagen)*0.25
Fetal Bovine Serum: (Total Suspension Vol)*0.10
Extra DMEM: Added extra to ensure proper total volume
0.1 M NaOH: (Collagen Vol.)*(0.02)/(NaOH Conc.)
Type I Collagen from Rat Tail: (Total Suspension Vol.)*(2 mg/ml)/(Stock Coll. Conc.)

1. Use trypsin to detach cells to be used from their culture surface. Collect cells in an appropriate tube and remove a sample for cell counting. Wash cells once in medium and centrifuge for 5 min @ 1000 rpm to obtain a cell pellet.

2. Count cell sample using Coulter Counter. Resuspend pellet of collected cells and transfer number of cells required to make constructs to a 50 mL centrifuge tube (allows up to 50 mL of cell-collagen suspension to be made).
3. Centrifuge cell suspension for 5 min @ 1000 rpm to obtain a pellet. Aspirate supernatant and place tube on ice.
4. To tube containing cell pellet, add required volumes of complete culture medium, 5X concentrated DMEM and Fetal Bovine Serum. Use a pipetor to gently resuspend cells.

5. Add required volume of 0.1 M NaOH and mix. The next steps should be done quickly but carefully to avoid prolonged contact of cell with high pH solution, while avoiding premature gelation of cell-collagen suspension.
6. Add required volume of acid-solubilized Type I collagen from rat tail and mix thoroughly. Solution is viscous, so mixing is difficult. Tube can be capped and inverted if required, taking car to create as few bubbles into the solution as possible. Once collagen component has been added, keep cool to prevent gelling, and pour mixed solution into molds as soon as possible.
7. Use a pipettor to transfer the required volume of cell-collagen suspension to each of the molds.
   For disk constructs → Add 3.0 mL of cell-collagen suspension to 35 mm wells of a non-tissue culture treated 6-well plate. Gently swirl plate to distribute suspension evenly in the wells. Put cover on plate.
   For tube constructs → First add 5.0 mL of cell-collagen suspension to glass test tubes. Then immediately insert a mandrel-sleeve-stopper assembly into the test tube, ensuring that there is no air trapped in the annular space that will form the tubular construct. Cover test tubes with a cap.
8. Immediately place mold in a cell culture incubator at 37 °C. Allow to sit undisturbed for 30-60 min, until gelation is visibly complete.

9. For disk constructs → leave in cell culture incubator for 24 h.
10. For tubular constructs → Remove molds from cell culture incubator and place in laminar flow hood. Remove caps and aspirate gelled material from lumen of glass mandrels. Be careful not to aspirate too much material (i.e. do not aspirate part of construct, only excess material in lumen of mandrel). Use ridged forceps to carefully remove mandrel assembly and gelled constructs from test tubes, and place in a 150 mm Petri dish containing ~130 ml of warm culture medium. Place constructs in cell culture incubator at 37 °C.

11. Allow constructs to incubate for 24 h undisturbed. After this period, release constructs from mold to allow further gel compaction.
    For disk constructs → Use a sterile small spatula or pipette tip to release constructs from sides and floor of culture well. If wells are non-tissue culture treated, the construct will not re-adhere and will compact unconstrained.
    For tube constructs → Use sterile scissors and forceps to cut the construct free from the rubber stoppers at the end of the mold. There will be some excess material outside the stoppers. Remove this and discard.

NOTES:

- This protocol is for use with acid solubilized Type I rat tail collagen. It may need to be modified for other collagen types.
- The attached printout of an Excel spreadsheet shows the information needed to prepare 8 standard tubular constructs. The calculation used to determine the amount of 0.1 M NaOH needed to neutralize the collagen solution is based on the information given in the manufacturer's Product Specification sheet.
- 3.5 mg/mL is minimum collagen concentration that can be used to get a final collagen concentration of 2.0 mg/mL. Higher collagen concentrations (3.8 – 4.5 mg/mL) are desirable for their improved gelling qualities.
- Constructs have been made with and without silicone sleeves. While using sleeves aids greatly in construct handling, no differences in compaction or viability have been noted.

PJTB07: Flow Cytometry for Cells in Three Dimensional Constructs

Reagents :

Glycine — Laboratory Rm → Shelf

Sodium Chloride (NaCl, — Laboratory Rm → Shelf

Normal Goat Serum — Tissue Culture Rm → Freezer

3.7% Paraformaldehyde (see JTBP05) — Protein Rm → Fridge
Tousimis Cat. No. #1008A

Sucrose — Laboratory Rm → Shelf

Triton X-100 — Laboratory Rm → Shelf
Sigma X-100

Trizma Pre-Set Crystals — Laboratory Rm → Shelf
Sigma # T-4753

Tween-20 — Laboratory Rm → Shelf

Collagenase CLS2: — Protein Rm → Fridge
Worthington, Cat. No. 4176, ~300 U/mg

Solutions :

Dulbeccos Phosphate Buffered Saline (DPBS) — Tissue Culture Rm → Fridge
Gibco, Cat. No. 14190-144, no Ca or Mg

Porcine Medium (See PJTB002): — Tissue Culture Rm → Fridge

- Dulbecco's Modified Eagle Medium (DMEM) (500mL)
  Gibco, Cat. No. 11965-092
- 1% L-Glutamine added
  Mediatech Cellgro, Cat. No. 25-005-C1
- 1% HyQ Penicillin added
  MediaTech Cellgro, Cat. No. SV30010

Tween-20 Stock Solution : 0.1 %

Tween-20	100 μL

Add Tween-20 to 100 mL of dH20 and mix well.

Tris-Buffered Saline with Tween (TTBS)

Trizma Pre-Set Crystals	14.2 g
NaCl	11.7 g
Tween-20 Stock	10 mL

Dissolve the Trizma Crystals and NaCl in 990 mL dH20 and add 10 mL of 0.1% Tween stock (to give a final concentration of 0.001 % Tween). Mix well. Adjust pH to ~8.0 using Tris-Base/Tris-Cl at RT.

Glycine : 20 mM

Add 0.15 g of glycine to 100 mL of TTBS and mix to dissolve. Adjust pH to 2-3 for use in protocol.

Blocking buffer : 5% NGS

Add 5 mL of NGS to 95 mL of TTBS.

Coating buffer : 1% NGS

Add 1 mL of NGS to 99 mL of TTBS.

Fixation buffer : Paraformaldehyde (for 20 mL final solution)

3.7% paraformaldehyde (dilute from 20%)

Dilute Tousimis formaldehyde (stored under nitrogen) to desired concentration in DPBS. Add appropriate amount of sucrose and allow to dissolve. Solution can be kept up to 1 month at 4 ˚C.

Triton X-100 Stock Solution : 10 %

Triton X-100 10 mL

Add Triton X-100 to 90 mL of dH20 and put on stir plate with stir bar. Will take ~30-60 minutes to fully dissolve.

Permeabilization buffer :

Add 1 mL of Triton X-100 Stock to 99 mL of TTBS (for final concentration of 0.1% Triton X-100) and mix well.

- higher concentrations of Triton can also be used (e.g. 0.2 %, 0.5 %)

Procedure :

1. Cells should be in a suspension in DMEM to begin protocol. If cells are from monolayer culture they must be trypsinized to bring into suspension (PJTB02). If cells are from 3D construct, the construct must be digested to bring cells into suspension (PJTB01).
   a. Incubate constructs in 600 U/ml collagenase in serum free DMEM for 1 hour, vortexing frequently.
   b. Once all the collagen is digested, centrifuge the suspension for 5 minutes at ~200g (1000 rpm).
2. Wash cells gently once with TTBS (or DPBS). For each wash, suspend the cells in TTBS (or DPBS) and agitate gently, then spin down at 1000 rpm for 3 min and aspirate supernatant.
3. Add 0.5 mL of 3.7% paraformaldehyde (PF) in DPBS and mix well with light vortexing. Let fix for 5 min at room temperature.
4. Wash cells gently once in TTBS (or DPBS).
5. Incubate the cells in 20 mM glycine solution solution for 15 min at room temperature. This will neutralize the charges caused by PF fixation.
6. Wash cells gently once in TTBS (or DPBS). Cells can be stored at 4 °C at this point in fresh TTBS (or PBS) if desired.
7. Permeabilize cells in Permeabilization buffer for 5 min at room temperature.

8. Wash cells gently twice in TTBS.
9. Block nonspecific binding with 5% normal goat serum (diluted in TTBS or PBS) for 1 hr at 37°C or overnight (12-15 hr) at 4 °C.
10. Centrifuge at 1000rpm for 3 min and remove blocking medium: do not wash off, merely drain.
11. In order to perform a flow cytometric analysis, three types of samples will be necessary : 1] an unstained sample of cells, 2] a sample stained with the appropriate isotype control antibody (or secondary only), and 3] a sample stained for the marker of interest.
12. Briefly spin down thawed primary antibody aliquot and isotype control aliquot to bring any crystals to bottom of tube. Add antibody to tubes, vortex gently and incubate at 37 °C for 60 min.
13. Wash samples gently 2 times in TTBS or PBS.
14. Add 100µL of blocking buffer (5% NGS) to each tube prior to adding secondary antibody.
15. Briefly spin down secondary antibody aliquot to bring any crystals to bottom of tube. Add secondary antibody to tubes, vortex gently and incubate samples with secondary antibody for 30min at 37°C.
16. Wash samples gently 2 times in TTBS or PBS. Resuspend in 500 µL PBS for flow cytometry analysis.

NOTES :

- use of 1.7 mL non-stick centrifuge tubes is recommended to avoid loss of cells.
- TTBS has the potential advantage that the low concentration of mild detergent (Tween) may keep cells from sticking to each other and to the wash tubes. Also, TBS is reported to be better at maintaining physiological pH during temperature changes.
- Pre-coat centrifuge tubes or plates to be used with 1% NGS to prevent cells from sticking to sides of tubes. This prevents loss of cells during the multiple washing steps.
    - pre-coat for 1 h @ 37 ºC, or 4 h @ RT, or overnight @ 4 ºC
    - pre-coating optional if “non-stick” centrifuge tubes are used

PJTB08: Modification to the Flow Loop Assay to Accommodate Three Dimensional Constructs

Solutions:

Agar — Laboratory Rm → Shelf
Sigma, Cat. No. A-9915

Porcine Medium (See JTB002): — Tissue Culture Rm → Fridge

- Dulpecco's Modified Eagle Medium (DMEM) (1000 ml)
  Gibco, Cat. No. 11965-092
- 1% L-Glutamine added
  Mediatech Cellgro, Cat. No. 25-005-C1
- 1% HyQ Penicillin added
  MediaTech Cellgro, Cat. No. SV30010
- 10% Fetal Bovine Serum (FBS) added

Instruments:

Instrument tray: — Laboratory Rm
- Mandrel grabbers
- Section lifter (spatula)
- Smooth angled forceps
- Serrated angled forceps
- Flat tweezers
- Angled scissors
- # 4 Scalpel with No.20 blade

Glass microscope slides
Embedding molds

Square Petri dishes — Laboratory Rm → Shelf

Samples:

Tubular constructs cultured to day 6 — Tissue Culture Rm → Incbtr

All procedures should be performed in a biological safety cabinet using aseptic techniques to prevent microbial contamination

Embedding Constructs

Preparation of Materials and Instruments

1. Immediately before embedding constructs, create 3.5% agar solution (w/v in dH_2O) in a 125 ml bottle.
2. Autoclave agar solution and 50 ml glass centrifuge tubes to melt agar.
3. While hot, transfer agar solution to a hot water bath at 48°C to keep liquid.
4. Prepare tray of instruments on paper towel. Autoclave new glass slides, used glass slides, molds and tray of instruments in advance.

Preparation of Constructs

Steps can be done for all constructs at once.

1. Place one autoclaved new glass slide in a square cell culture dish and set aside.
2. Remove dish of constructs from incubator and place in sterile cell culture hood.
3. Remove rubber stopper from mandrel end and slide constructs on sleeves off the mandrel. Remove mandrels and rubber stoppers from dish.
4. Holding silicone sleeve with angled forceps slowly cut sleeve and construct along the long axis with angled scissors. Then remove the silicone sleeve from the construct.

Embedding Procedure

Steps should be done to only two constructs at a time to prevent drying and cell death.

1. Using smooth angled forceps grab one corner of the construct and slide onto spatula with the lumen down. Transfer construct onto new glass slide in square dish keeping the lumen down.
2. Using a scalpel, cut away ragged ends of construct and remove excess material. Center the construct on the glass slide with forceps.
3. Aspirate excess fluid off the slide being careful not to aspirate the construct but remove all fluid from around it to ensure a good agar seal.
4. Place mold over slide with hole over construct. Quickly remove agar from hot water bath and add 7 ml over construct. Quickly place used glass slide over agar and press hard with mandrel grabbers and flat tweezers until the agar solidifies to ensure a good seal.
5. After the agar has cooled, remove excess from the sides of the mold and discard. Add 35 ml of flow media to the dish. Using flat tweezers flip the slide/mold/slide combination over and carefully slide off the top slide to expose the lumen.
6. Place the dishes of embedded construct into the incubator at 37°C and 5% CO_2.

Construct Flow Loop Assay

1. Follow steps identical to PJTB04, except use the glass slide/embedded construct instead of the glass slide.
2. For this modification, a thinner rubber substrate is required to accommodate the added thickness of the mold.
3. Use a thicker spacer to create the channel height needed for the appropriate shear stress to account for undulations on the construct surface, and adjust the pump rate accordingly.

PJTB09: Quantitation of Cellular DNA Content Using Hoechst 33258 Dye

Reagents :

Proteinase K

Tris-HCl
Sigma T-4753
EDTA

Sodium Chloride (NaCl) — Laboratory Rm → Shelf
Sigma, Cat. No. S-7653
Sodium Doecytl Sulfate — Laboratory Rm → Shelf
US Biochemicals, Cat. No. 21651
Hoechst 33258 Dye — Protein Fridge → Shelf
Sigma, Cat. No. 33258
Calf Thymus DNA Standard Solution
Bio-Rad Laboratories
dH_2O

Solutions :

Proteinase K Solution: — For 500 mL

- Buffer 1 :
  - dH_2O — 475 mL
  - 50 mM Tris-HCl — 25 mL of 1 M stock
  - 0.1 M EDTA — 18.6 g
  - 0.2 M NaCl — 5.84 g
- pH to 7.4
- Aliqout out volume required (1 mL per construct)
- Add :
  - 0.5 mg/mL Proteinase K
  - 0.1 mg/mL SDS
- dissolve and freeze excess aliquots

Hoechst 33258 Dye Solution :

- Buffer 2 :
  - 10 mM Tris
  - 1 mM EDTA $Na_2.2H_20$
  - 0.2 M NaCl
- pH to 7.4
- Add :
  - 0.1 µg/mL Hoechst 33258 dye
  - stock is at 10,000X, shake well before using
    - stock soln is made up in H2O (Sigma protocol)
- PROTECT FROM EXPOSURE TO LIGHT.

DNA Standards :

- dilute standard solution (1 mg/mL) to 30 ug/mL in Buffer 1

Procedure :

Digestion of Constructs :

1. Cut desired amount of material from construct. Rinse 3X in PBS to remove medium.
2. Lyophilize constructs using Speed-Vac for 4 – 8 h (until vacuum pressure is constant). Take dry weight of sample (if desired),
3. Put construct sample in tube with 1 mL of Proteinase K solution per ~1 M cells (keep track of precise Proteinase K volume in order to determine absolute amount of DNA later). Vortex to mix thoroughly.
4. Incubate construct in Proteinase K solution for 12-16 h at 55 ˚C, shaking (vortex) occasionally.
5. At end of incubation, visually inspect sample to ensure that construct is fully digested.
6. Freeze sample once, then use in assay.
7. For **blanks**, load 10 µL of Buffer 1 (used for Proteinase K solution) into each of 4 wells.
8. For **DNA Standards**, prepare 4 microcentrifuge tubes containing 200 µL of Buffer 1 each.
   a. Add 200 µL of DNA Standard Solution (30 µg/mL) to the first tube and mix well to yield a 15 µg/mL solution.
   b. Repeat serial dilution to get solutions of 30, 15, 7.5, 3.75, and 1.88 µg/mL.
   c. Load 10 µL of each standard solution into 96-well plate, in duplicate.
9. For **cell standards**, prepare 4 microcentrifuge tubes containing 500 µL of Buffer 1 each.
   a. Add 200 µL of Cell Standard Solution (1000 K cells/mL) to the first tube and mix well to yield a 500 K cells/mL.
   b. Repeat serial dilution to get solutions of 1000, 500, 250, 125 and 62.5 K cells/mL.
   c. Load 10 µL of each standard solution into 96-well plate, in duplicate.
10. Vortex vigorously to ensure that samples are well mixed. Draw through a 25G needle to fully mix and break up debris. Centrifuge 2 min at 2000 rpm to remove any large debris from supernatant.
11. Load samples into 96-well plate in duplicate. Aim to have ~0.5 – 1.0 M cells per mL of sample solution being analyzed (to be well in linear region of standard curve).
12. Add 200 µL of Hoechst 33258 Dye solution to every well in plate. Protect entire plate from light in order to minimize fading of fluorochrome.
13. Incubate for 15 min @ RT in the dark, then read on fluorometer.
    a. Excitation 365 nm, Emission 458 nm.
    b. Cutoff at 455 nm.

NOTES :

- Modified from Jan Stegemann, adapted from Kim B-S, Mooney DJ, “Engineering Smooth Muscle Tissue with a Predefined Structure”, *J Biomed Mater Res*, 41, pp. 322-332, 1998 and Topher Hunter’s protocol.
- USE **BLACK** 96-well plates for best results (though clear ones can also be used).
- For total protein (Pierce BCA) assay, Proteinase K buffer 1 will need to be diluted 10:1 in dH_2O to lower concentrations of SDS and EDTA under the assay thresholds. Then use 5 µl of sample in 50 µl of buffer in the 96 well plate assay.

Western Blotting for Focal Adhesion Proteins
With Optional Immunoprecipitation

Day 0: Prepare stock buffers and gels

Preparing the polyacrylamide gel:

- prepare the following stock solutions
  - A: 50% acrylamide/BIS (29:1)
    - 4.3 g acrylamide
    - 1.7 g BIS

    OR
    - 50 g 29:1 BisAcrylamide
    - bring to 100 ml with water
    - store at 4°C covered with foil (for 2 months)
  - B: separating gel buffer (1M Tris-HCl pH 8.8)
    - add 30.3 g Tris to about 150 ml water; adjust pH to 8.8 with HCl
    - bring to 250 ml with water
  - C: 10% SDS
    - 10 g SDS
    - bring to 100 ml with water
  - D: stacking gel buffer (0.375 M Tris HCl pH 6.8)
    - add 11.4 g Tris to about 150 ml water; adjust pH to 6.8 with HCl
    - bring to 250 ml with water
  - E: catalyst (make fresh on the day of use)
    - 100 mg ammonium persulfate in 2 ml of water
  - F: 50% sucrose
    - 50 g sucrose
    - bring to 100 ml with water
- prepare the separating gels (2)
  - 7% separating gel
    - A: 3.5 ml
    - B: 9.4 ml
    - C: 250 μl
    - F: 4 ml
    - Water: 7.3 ml
    - E: 625 μl (add last and mix well
    - TEMED: 6.25 μl (add last and mix well)
  - fill cassette to the second from top line and overlay with water to the top
  - polymerize for 1 hour
- prepare the stacking gels (2)
  - 4% stacking gel
    - A: 500 μl
    - D: 2.1 ml
    - C: 62.5 μl
    - Water: 3.15 ml
    - E: 0.5 ml (add last and mix well)
    - TEMED: 2.5 μl (add last and mix well)

    - pour out the overlay solution completely and fill to the top with the stacking gel solution
    - insert the comb and polymerize for 30 min

Preparing 6x Protein Loading Buffer:

- make 4x Tris-HCl SDS buffer, pH 6.8
    - 6.05 g Tris + 40 ml water → pH to 6.8 with HCl
    - bring up to 100 ml with water
    - filter in 0.45 μm filter
    - add 0.4 g SDS
- make 6x protein loading buffer
    - 7 ml 4x Tris-HCl SDS, 3.8 g glycerol, 1 g SDS, 0.93 g DTT, 1.2 mg bromphenol blue
    - bring up to 10ml with water

Preparing 10x Running Buffer:

- make 240 mM Tris (base), 1.92 M glycine, 1% SDS in water
    - 29 g Tris (base), 144 g glycine, 10 g SDS
    - bring up to 1 L with water

Preparing 10x Tris-Glycine (for Transfer Buffer):

- 30.3 g Tris (base), 144.1 g glycine
- bring up to 1 L with water

Preparing 1M Tris-HCl, pH 7.6 (for TBS-Tween):

- 31.52 g Tris-HCl
- bring up to 200 ml with water → pH to 7.6

Preparing RIPA Lysis Buffer:

- make 150 mM NaCl, 1% Triton X-100, 1% deoxycholate, 0.1% SDS, 150mM Tris, pH 7.2
    - 15 ml 1 M Tris-HCl→ pH to 7.2
    - 0.88 g NaCl
    - 1 ml Triton X-100
    - 1 ml 10% SDS
    - 1 g deoxycholate (DOC)
    - bring up to 100 ml with water

Day 1: Preparing Cell Lysate, Immunoprecipitation

Preparing Cell Lysates:

1. After experiments, place one or two glass microscope slides into a square Petri dish.
2. wash the monolayer once with room temp PBS with Ca, Mg
3. Prepare cold RIPA lysis buffer containing 1mM Na_3VO_4 and add fresh protease inhibitors

   a. 100 μl for each slide.
   b. RIPA lysis buffer: 150 mM NaCl, 1% Triton X-100, 1% deoxycholate, 0.1% SDS, 150mM Tris, pH 7.2
   c. Add protease inhibitors: 350 μg/ml PMSF, 10 μg/ml leupeptin, 10 μg/ml aprotinin
      i. → 2.5 ml RIPA + 1 mg Na_3VO_4 + 25 μl PMSF (57 mM) + 25 μl leupeptin + 25 μl
         (1) aprotinin (both are 1 mg/ml)
4. incubate at room temp. for 10-20 min (optional: 4°C with occasional rocking)
5. scrape the cells from the dishes and transfer to a 0.65 ml microcentrifuge tube
6. pipette up and down ~25 times to shear DNA with the R-100 pipette
7. spin the tube for 10 min at 10,000g
8. keep supernatant - transfer to a clean tube (can keep pellet if want to assay it)
9. spin again if necessary

Protein Quantification

1. Run μ-BCA Assay
2. Run IP on same amount of total protein

Immunoprecipitation (Optional):

1. Pre-clear with serum, if necessary
2. add 5 μg (5 μl) anti-FAK (rabbit polyclonal IgG) to 65 μl of the cell lysate (save some lysate to load as a positive control)
3. incubate at 4°C for 60 min, fix tubes to orbital rocker to shake
4. add 10 μl protein A beads (10% vol/vol in lysis buffer); use the R-20 pipette, trim the tip to accommodate the slurry
5. incubate at 4°C for 60 min, fix tubes to orbital rocker to shake
6. collect protein A beads by centrifugation at 10,000g for 3 min
7. aspirate with a pipette tip and save the supernatent (4°C)
8. wash the beads three times with lysis buffer and aspirate completely with a 23-gauge bent needle (insert the needle directly into the beads to remove the remaining wash buffer)
9. resuspend the beads in 20 μl 6x protein loading buffer
10. boil the samples for 10 min and spin the tubes for 10 min at 10,000g
11. transfer the supernatant to clean tubes

Day 2: SDS-PAGE, Transfer

1. prepare protein marker and cell lysate positive control
2. boil samples for 10 min
3. make running buffer or dilute 10x running buffer in dH_2O (make 500 ml)
4. assemble the gel box (cassettes face inward)
   a. fill middle channel with running buffer
   b. fill outer channel at least halfway with running buffer
5. load samples into the gel
6. run the electrophoresis
   a. 90 V in stacking gel (~30 min)

b. 115 V in separating gel (few hours)

Protein Transfer:

1. prepare the transfer buffer
   a. transfer buffer: 100 ml 10x Tris-glycine, 2.5 ml 10% SDS, 150 ml methanol, water up to 1 L
2. prepare the transfer membrane and filter paper
   a. cut PVDF or nitrocellulose transfer membrane to the dimensions of the gel (do not handle, use tweezers)
   b. pre-wet PVDF transfer membrane in methanol for 30 seconds (do NOT pre-wet nitrocellulose), rinse in deionized water, soak in 50-100 ml of transfer buffer for several minutes
   c. cut filter paper to the dimensions of the gel and soak in transfer buffer briefly prior to use
3. prepare the blotting pads
   a. soak blotting pads in transfer buffer until saturated
   b. remove air pockets and bubbles by squeezing pads while they are submerged in buffer
4. load the blot module assembly
   a. place 2 saturated blotting pads on the electrode of the cathode core (deeper and darker gray)
   b. place the filter paper on the top of the blotting pads
   c. place the first gel on top of the filter paper, making sure no air bubbles are trapped beneath the gel
      i. make sure that the protein transfers to the membrane in the same orientation as it was loaded
   d. wet the surface of the gel with several milliliters of transfer buffer and place the transfer membrane on the gel; remove air bubbles
   e. place the filter paper on the top of the membrane; remove air bubbles
   f. repeat for the second gel
   g. place the anode core on the top of the gel/membrane sandwiches

For 2 membranes:

anode core (+)
blotting pad
blotting pad
filter paper
transfer membrane
2^{nd} gel
filter paper
blotting pad
filter paper
transfer membrane
1^{st} gel
filter paper
blotting pad
blotting pad
cathode core (-)

1. hold the blot module together at the top and slide it into the guide rails on the lower buffer chamber
2. places the wedges
3. fill the blot module with transfer buffer until the gel/membrane sandwich is covered in transfer buffer (approximately 200 ml)
4. fill the lower buffer chamber with transfer buffer in the gap between the front of the blot module and the front of the lower buffer chamber (the water level should be approx. 2 cm from the top of the lower buffer chamber)
5. place the lid on the unit and plug the leads into the power supply
6. turn the power supply on and set to the appropriate voltage (30 V, 90 min)
7. prepare blotto/Tween blocking buffer
    a. Blocking buffer: 5% non-fat dry milk in PBS w/o Ca^{2+}/Mg^{2+} + 0.02% azide + 0.2% Tween 20
        i. For 100 ml: 5 g non-fat dry milk, 2 ml azide (1%), 200 □l Tween 20, bring to 100 ml with PBS w/o Ca^{2+}/Mg^{2+}
8. dry the transfer membrane on a paper towel for 5 min (protein facing up)
9. mark the ladder with a pencil
10. rewet the membrane with methanol
11. rinse the membrane several times with water
12. block in blotto/Tween blocking buffer overnight at 4°C

Day 3: Antibody Blotting, ECF Imaging

Antibody Blotting

1. cut the membrane in half, if necessary (based on size of the protein)
2. incubate the primary antibodies at room temp for 1 hour, rocking (use 12 ml per membrane)
3. prepare TBS-Tween for washing
    a. TBS-T: 20 mM Tris-HCL + 137 mM NaCl + 0.1% Tween-20
        i. For 1 L: 20 ml 1M Tris-HCl (pH 7.6), 8 g NaCl, 1 ml Tween-20, bring to 1 L with water
4. wash the membrane twice with TBS-T
5. rock with TBS-T for 15 min, then rock with TBS-T twice for 5 min each
6. incubate the secondary antibody at room temp for 1 hour, rocking (use 12 ml per membrane)
    a. alkaline phosphatase-conjugated donkey anti-rabbit or mouse IgG, 1:10,000 dilution
        i. 12 ml blocking buffer + 1.2 μl secondary (per membrane)
7. wash the membrane twice with TBS-T
8. rock with TBS-T for 15 min, then rock with TBS-T twice for 5 min each

ECF Imaging

1. ECF substrate is stored in the –80C (stock is 0.6 mg/ml)
2. use 1 ml ECF per membrane
3. spread 1 ml ECF evenly on a transparency
4. allow excess buffer to drip off the membrane

5. lay the membrane face down on the ECF, starting with an edge; make sure no bubbles are trapped and that the membrane doesn't move after it touches the ECF
6. react for 5+ min.
7. dry the membranes on a paper towel
8. Fuji Film PhosphoImager:
   a. use the FLA Fluor State 2340
   b. place the membrane face down on the stage in the upper left-hand corner
   c. lay a transparency over the membrane to flatten
9. Image Reader Software
   a. Sample Mode: Fluor 473, Filter Y520
   b. 16 bit gradation, 50 resolution, F10 sensitivity

Notes:

Table A-2: Antibody concentrations used in Western blotting.

Antibody (species)	Company	Catalog No.	Concentration for WB	Protein Size (kDa)	Protein Loaded (μg)	Reducing Buffer Needed?
β1 Integrin (mouse)	Chemicon	MAB2000	1:500	130	15	Yes
Vinculin (mouse)	Upstate Bio	05-386	1:500	117	10	Yes
FAK (rabbit)	Upstate Bio	06-543	1:1000	126	15	Yes

- Secondary antibodies are biotin anti-(species) at 1:10,000 dilution.

PJTB11: Immunohistochemistry Assay

Reagents and Solutions

10X PBS
Boehringer Mannheim #1666789

1%BSA/PBS
Dissolve 1g fraction V BSA (Sigma #A2153 kept on fridge door) in 100ml 1X PBS. Mix until fully dissolved. Aliquot into 5ml volumes and store at -20 C.

1% Gelatin/PBS
Dissolve 1g of gelatin powder in 100ml 1X PBS using gentle heat.
Aliquot into 5ml volumes and store at –20 C.

Biotinylated Secondary antibody and normal animal serum
Vector Laboratories, Inc.:
Biotinylated horse anti-mouse IgG #
Normal horse serum #
Biotinylated goat anti-rabbit IgG #
Normal goat serum #

Avidin D, Fluorochrome conjugated
Vector Laboratories, Inc.:
Texas red #A-2006, Fluoroscein #A-2001

Vectashield Mountant with DAPI
Vector Laboratories #H-1500

Antibodies
Monoclonal mouse anti-alpha sma-cy3
Sigma #C6198 Clone 1A4 (1:400)
Monoclonal mouse anti-vimentin-cy3
Sigma #C9080 Clone V9 (1:200)
Monoclonal Rabbit anti-von Willebrand Factor
Sigma #F3520 (1:600)

Protease
Sigma #8083
Stock 100mg/ml
Working 100ug/ml

1. Fixed paraffin embedded tissue is deparaffinized, and rehydrated in descending grades of alcohol. This can be done using the Leica Autostainer.
2. Sections are washed in 1X PBS 4min.
3. Coverslip autofluorescnce control slides with Vector hardset/DAPI mountant (for nuclear counterstain).

4. Sections that will be stained with vWF require antigen retrieval using 100ug/ml protease pretreatment of the tissue for 10 min., rt. Dilute 50ul of 100mg/ml stock in 50ml PBS.
5. Wash slides in 1X PBS twice for 4 min. each, rt.
6. Block tissue using 1% gelatin/PBS mixture for 20 min. rt.
7. Prepare primary antibodies in 1%BSA/PBS:
    a. Mouse anti-SMA-Cy3 at 1:400
    b. Mouse anti-VIM-Cy3 at 1:200
    c. Rabbit anti-vWF at 1:600
    d. BSA/PBS only (vWF secondary control)
8. Blot off the gelatin/PBS and apply the primary antibody. Incubate sections in a humid chamber for 1h at rt in the dark.
9. Blot off excess antibody and wash slides in 1X PBS twice for 4 min. each, rt in the dark. Coverslip finished slides as per step 1.
10. Prepare 1:400 working dilution of the biotinylated goat anti-rabbit IgG secondary antibody in 1%BSA/ PBS, and add 2% normal goat serum. Apply antibody and incubate 30 min. at rt in a humid chamber in the dark.
11. Blot off excess antibody and wash slides in 1X PBS twice for 4 min. each, rt in the dark.
12. Incubate sections with a 1:100 dilution of fluorescein conjugated avidin D in 1%BSA/PBS for 30 minutes in the dark.
13. Blot off excess solution and wash slides in 1X PBS for 4 minutes, twice in the dark. Coverslip slide #3 and 4 as per step 1.
14. Apply second batch of primary antibodies and incubate for 1 hour at rt in the dark.
    i. Anti-SMA-Cy3 at 1:400
    ii. Anti-VIM-Cy3 at 1:200
15. Blot off excess antibody and wash slides in 1X PBS twice for 4 min. each at rt in the dark.
16. Mount completed slides as per step 1.

Controls:
The following control slides are subjected to the same experimental conditions including blocking solution, washes, etc. The differences are noted below.

1. No primary antibody aka secondary antibody control: This primary antibody is omitted from this slide. Incubate this slide with the diluent of the primary antibody. This slide is treated the same as all other slides after this step. Purpose: Determines the specificity of the primary antibody. Ensure there is no nonspecific staining resulting from the secondary antibody.

2. Autofluorescence control: This slide is subjected to diluents of antibodies and reagents only. It is not exposed to the primary, secondary or avidin solutions. Purpose: Confirms specificity of the primary antibody. Detection of autofluorescence or background fluorescence that may be present in the tissue under study.

Notes:

- Positive von Willebrand Factor staining was also demonstrated using goat anti-rabbit Alexa Fluor 488 (Molecular Probes #A-11008, 1:100)
- For extended storage of samples, protect stained sections from light and keep refrigerated.

PJTB12: Isolation and Quantification of RNA

Equipment:

RNEasy kit
Qiagen, Cat. No. 74104
RNAse free DNAse
Qiagen, Cat. No. 79254
Homogenizer (Qiashredder)
Qiagen, Cat. No. 79654
RNAse free sterile tips
Fisherbrand: 10 μl, 20 μl, 200 μl, 1000 μl
UV Cuvettes
RNA 6000 Nano LabChip Kit
Agilent, Cat. No. 5065-4476

Reagents:

Dulbecco's Phosphate Buffered Saline (DPBS)
Gibco, with Ca, Mg
β-Mercaptoethanol (B-ME)
Sigma, Cat. No. M-3148 Molecular biology grade
Ethanol
Aldrich, Cat. No. E702-3 Molecular biology grade
DEPC Water
ResGen, Cat. No. 750024

Procedure:

RNA Isolation Solution Preparation

Lysis Buffer

1. 10 ml RLT buffer with 100 μl B-ME.
2. Protect from light and store for up to one month

DNAse

1. Mix DNAse and Qiagen water from kit, aliquot into 100 μl units, store at 20C.
2. Add 10 μl DNAse to 70 μl RDD (in kit) for 80 μl per sample. Use fresh.

70% Ethanol

1. Mix Ethanol (7 ml) with DEPC water (3 ml) and store at room temp.

RNA Isolation

NOTE: This process can only be done on a few samples at a time. RNA changes w/in 1 hour.

1. For shear experiments, place two slides in a square Petri dish filled with DPBS.
2. Aspirate DPBS and trypsinze cells with 1mL per slide for 3 mins at rt. Place in 15 ml tube.
3. Centrifuge at ~200g (1000 rpm) for 5 minutes and COMPLETELY remove supernatant.
4. Add 350 μl lysis buffer to each tube. Homogenize sample with either a 20 gauge needle (5-10 times) or with the Qiashredder (10,000 rpm for 2 minutes).

Samples can be stored at -20C at this point if desired. Thaw at 37C for 10 minutes before continuing.

5. Add 350 μl 70% ethanol to each tube. Mix well by pipetting.
6. Transfer the 700 μl solution to an RNEasy Mini column placed in a 2 ml collection tube. Centrifuge at 10,000 rpm for 30 sec.
7. Pipette supernatant back into top of column, repeat centrifugation and discard effluent. Make sure no fluid remains on top of the column.
8. Add 350 μl of RW1 solution (from kit) to each RNEasy column. Centrifuge at 10,000 rpm for 30 sec. and discard effluent.
9. Add 80 μl DNAse mix to each column and incubate for 15 min. at rt.
10. Repeat step 8.
11. Replace the collection tubes with new ones and add 500 μl RPE buffer to each column. Centrifuge at 10,000 rpm for 30 sec. and discard effluent.
12. Add 500 μl RPE and centrifuge at MAX rpm for 2 minutes. Make sure no fluid remains at the top of the column.
13. Label 1.5 ml collection tubes (in kit) and aliquot some RNAse free water into a small tube.
14. Transfer the RNEasy columns to the labeled tubes. Add 25 μl of RNAse free water and incubate for 1 minute. Centrifuge at MAX speed for 1 minute, and discard the RNEasy column.
15. Place the collection tube on ice

Samples can be stored at -20C for up to 1 month at this point if desired. Thaw at 37C for 10 minutes before using.

RNA Quality Assessment and Quantification

RNA quantity is determined using UV Spectrometry.

1. Label small eppendorf tubes and add 99 μl RNAse free water to each tube (may be different for each spectrometer).
2. Add 1 μl of RNA solution to each tube. Can use 2 μl (in 98 μl water) if sample is dilute.
3. Place the 100 μl solution in a UV-Vis cuvette.
4. Follow protocol for particular Spectrometer. Optimal values for UV-Vis are 1.8-2.1.
5. Record RNA concentration (ng/μl).

RNA quality is assessed using the Agilent RNA 6000 Nano LabChip on the Agilent Bioanalyzer.

1. For total RNA, the RNA 6000 Nano Assay quantitative range is 50-500 ng/μl.
2. Prepare Gel-Dye mix. Put 400 ml of RNA gel matrix in to spin filter and centrifuge at 1500 g for 10 min. Use within 4 weeks.
3. Mix 130 μl of filtered RNA gel matrix with 2 μl RNA dye in a 1.5 ml RNAse free tube. Vortex well and store at 4C for up to 1 week.
4. Place new RNA chip on the chip priming station. Pipette 9.0 μl of gel-dye mix into well marked "G". Close priming station and press plunger until held by the clip.
5. Release the clip after exactly 30 seconds, and inspect the chip for air bubbles.
6. Pipette 9.0 μl of gel-dye mix in wells marked "G"
7. Pipette 5.0 μl of RNA 6000 Nano Marker in each of 12 sample wells and ladder well.
8. Pipette 1.0 μl of an RNA sample into each sample well. Place 1 μl of RNA 6000 Nano Marker in each well not used.
9. Vortex chip for 1 min. at set point of the IKA-Vortexer.
10. Run the chip in the Agilent 2100 Bioanalyzer for 5 min.
11. Remove chip and discard. Clean bioanalyzer with water chip.
12. Optimal peak ratio is 1.8 – 2.1 with no additional peaks, blunted peaks, or smears.

PJTB13: Real Time PCR Quantification of RNA Using Roche Light Cycler

Equipment:

Roche Light Cycler
Light Cycler capillaries
    Roche, Cat. No. 1909339
Cold block
Siliconized tubes
    PGC Scientifics, Cat. No. 505-201

Reagents:

Invitrogen recombinant Taq kit
    Invitrogen, Cat. No. 10342-020
Taq start antibody
    Clonetech (BD)
dNTPs (100 mM)
    Invitrogen, Cat. No. 10216-018, 10219-012, 10218-014, 10217-016
Agarose
    Invitrogen, Cat. No. 15510-027
Ethidium Bromide
    Fisher Biotech
DTT
RNAse OUT
SuperScript II reverse transcriptase
RNAse H
SYBR green

Procedure:

Reverse Transcription of RNA to cDNA.

1. From UV spectrometer, determine amount of RNA sample (μl) that contains 4 μg RNA.
2. For first strand synthesis of each RNA sample, add the following components at rt:
    a. 1 μl random primers
    b. 4 μg RNA (in μl).
    c. 1 μl of dNTP mix (each 10 mM)
    d. Enough milliQ water to reach 12 μl.
3. Heat mixture to 65C for 5 min. then chill on ice. Briefly centrifuge.
4. Add the following reagents while tube is on ice:
    a. 4 μl of 5X first strand buffer
    b. 2 μl 0.1 M DTT
    c. 1 μl RNAse OUT (40 U/μl)
5. Mix contents gently and incubate at 42C for 2 min.
6. Add 1 μl of SuperScript II and mix gently by pipetting.
7. Incubate for 50 min. at 42C.
8. Inactivate the reaction by heating at 70C for 15 min.

9. Add 1 ml of RNAse H (Ecoli) and incubate at 37C for 20 min to purify the cDNA (optional).
10. Samples can be stored at -20C until used.

Real time PCR Amplification of cDNA

1. Assemble all reagents and samples on ice.
2. Use a siliconized tube for the master mix (prevents mix loss).
3. While on ice, add the following reagents (multiplied by number of samples) to a different tube.
   a. 0.75 μl Taq Antibody (working dilution)
   b. 0.15 μl Taq polymerase
4. Let the reaction progress for 5 min. on ice. Mix by pipetting gently.
5. While this reaction is occurring, add the following reagents to the siliconized tube as fast as possible.
   a. MilliQ water – enough to ensure 14 μl total sample volume per reaction – calculate first!)
   b. 1.5 ml 10X PCR buffer – buffer for the PCR reaction
   c. 1.2 μl $MgCl_2$ – activates reaction (50 mM)
   d. 0.5 μl BSA – random blocking agent
   e. 0.3 dNTPs – nucleotide building blocks
   f. 0.3 μl forward primer – designed for RNA of interest
   g. 0.3 μl reverse primer – designed for RNA of interest
   h. 0.16 μl SYBR Green – fluorescent dye for quantification. Keep covered or in dark.
6. Once the 5 min. have passed, add the Taq – Ab mix to the siliconized tube and continue adding reagents until complete.
7. Mix master mix by vortexing very lightly, then briefly spin down.
8. Aliquot 14 μl of mix to each capillary tube while tubes are in the cold block.
9. Add 1 μl of Milli Q water to blank tube and immediately cover.
10. Add 1 μl of RNA sample to each sample capillary tube. Pipette several times to ensure mixing.
11. Add 1 μl of standard RNA to each standard tube.
12. Cover all tubes, place the capillary cassettes in the microcentrifuge, and spin briefly (stop once 2000 rpm is reached).
13. Replace cassettes into the cold block, and transfer the cold block to the Light Cycler.
14. Adjust settings on the machine for the proper cycling temperatures and times.
15. Add capillaries to machine and begin cycle. Retain amplified samples when completed.

Confirmation of Specific Amplification through DNA Gel Electrophoresis

1. Make a 2% agarose gel (for small gel, 100 ml TAE buffer and 2 g agarose in glass beaker).
2. Microwave until solution begins to bubble. Add 7 ml Ethidium Bromide to gel solution.
3. Pour solution into a DNA gel dedicated electrophoresis unit (because of ethidium) under the fume hood. Add sample well mold. Let solidify at rt.
4. Uncover and invert capillary sample tubes in labeled 1.5 ml tubes, and centrifuge briefly.

5. Fill electrophoresis box with TAE buffer.
6. Once gel has solidified, pre-run (before adding samples) the gel at 100 V for one hour.
7. Add 20 μl DNA ladder to the first well, followed by 15 μl of samples in subsequent wells.
8. Run the gel at 80 V until ladder separates enabling the distinction of appropriate band length.
9. Stop voltage, remove gel and image using UV camera.
10. Inspect ladder and sample bands to confirm appropriate band is present without contaminating bands. Adjust protocol and cycling parameters if unsatisfactory results occur.

APPENDIX B: DERIVATION OF WALL SHEAR STRESS IN PARALLEL PLATE FLOW

Navier-Stokes Equations (Cartesian coordinates):

$$\rho(\partial u/\partial t + u\partial u/\partial x + v\partial u/\partial y + w\partial u/\partial z) = f_x - \partial P/\partial x + \mu(\partial^2 u/\partial x^2 + \partial d^2 v/\partial dy^2 + \partial^2 w/\partial z^2)$$

Continuity:

$$\partial\rho/\partial t + \rho(\partial u/\partial x + \partial v/\partial y + \partial w/\partial z) = 0$$

Assumptions: steady state, fully developed, incompressible, parallel plate, unidirectional flow.

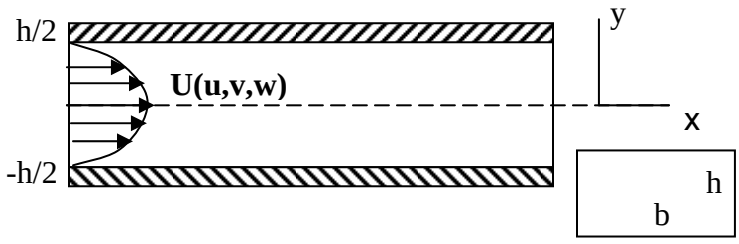

Equations reduce to:

$$dP/dx = \mu(\partial^2 u/\partial y^2)$$

Parabolic velocity profile

$u(y) = (1/\mu)(dP/dx)(y^2/2) + c_1 y + c_2$ boundary conditions: $u(h/2) = u(-h/2) = 0$

$$u(y) = -(1/8\mu)(dP/dx)(h^2 - 4y^2)$$

Velocity – Flow rate relationship:

$Q = V = \int u \cdot n dA = u_{ave} A_{cs}$ $u_{ave} = (-2/3)(h^2/8\mu)(dP/dx)$

$Q = -(bh^3/12\mu)(dP/dx)$ $dP/dx = -12\mu Q/bh^3$

Wall shear stress:

$\tau_w = \mu(du/dy)$ $du/dy = (1/\mu)(dP/dx)y$

$\tau_w = -12\mu Qy/bh^3$ at $y = -h/2$ $\boxed{\tau_w = 6\mu Q/bh^2}$

APPENDIX C: AGILENT MICROARRAY FEATURE EXTRACTION AND PROCESSING

The following is a summary of how the features on the microarrays were extracted and processed using the Agilent G2566AA Feature Extraction Software, located at the Cardiovascular Research Institute at the Morehouse School of Medicine in Atlanta, GA. The microarrays were processed by technicians at the Institute, with my sincere appreciation for their assistance. More detailed information can be found in the software User's Manual. Table C-1 shows the Feature Extraction filter criteria used in these experiments, with each step explained in greater detail below.

Feature Identification

All data processing is conducted on an extremely high resolution image taken of the microarray by the Microarray Scanner. The extraction software first brackets the microarray image by locating bright fields placed at the corners of the arrays, and then makes a sweep across the image to locate the intense spots. Since most of the array features should have a high intensity with respect to background, the software can easily develop a grid using the found features, across which it then passes once more to identify weaker features. The spots are identified with an ellipse (usually a circle) centered over the feature centroid. Sometimes, spots are located off the originally designed grid, which the software can usually find; otherwise they can be selected for manually.

Table C-1: Agilent Feature Extraction Software filter criteria used for the microarray experiments presented in this thesis.

Agilent Feature Filter Criteria	**Value**	**Interpretation**
ControlType	0	Data point was not a control
rSurrogateUsed	0	No surrogate value was used
gSurrogateUsed	0	No surrogate value was used
gIsFound	1	Green signal is present in spot
rIsFound	1	Red signal is present in spot
gIsSaturated	0	<50% pixels above saturation threshold
rIsSaturated	0	<50% pixels above saturation threshold
gIsFeatNonUnifOL	0	Green pixel noise not non uniform outlier
rIsFeatNonUnifOL	0	Red pixel noise not non uniform outlier
gIsBGNonUnifOL	0	Same with local green background pixel noise
rIsBGNonUnifOL	0	Same with local red background pixel noise
gIsFeatPopnOL	0	Green feature not a population outlier (IQR)
rIsFeatPopnOL	0	Red feature not a population outlier (IQR)
gIsBGPopnOL	0	Green background not population outlier (IQR)
rIsBGPopnOL	0	Red background not population outlier (IQR)
IsManualFlag	0	Not flagged by user upon manual inspection
rIsPosAndSignif	1	Red BG subtracted signal > Red BG (T test, P<0.01)
gIsPosAndSignif	1	Green BG subtracted signal > Green BG (T test, P<0.01)
rIsWellAboveBG	1	Red signal > 2.6*StDev of Red BG signal
gIsWellAboveBG	1	Green signal > 2.6*StDev of Green BG signal
rPValFeatEqBG	<0.01	Red mean signal significance over red BG
gPValFeatEqBG	<0.01	Green mean signal significance over green BG
gProcessedSignal	Value	Processed Red intensity used for statistics
rProcessedSignal	Value	Processed Green intensity used for statistics

Feature Processing

The pixels within the ellipse were used to calculate feature data values. The software also calculates a local background in the immediate vicinity of the ellipse. From these pixels, feature mean signal, standard deviation, and number of pixels were determined for each color. The extraction software then performed pixel outlier rejection

to eliminate extreme intensity values (high or low) based on population statistics. The final statistics were then calculated for each color of every feature and its local background. The pixel correlation (between the two colors) was also calculated. Local background is determined by placing two sequentially larger ellipses concentric with the first one: the space between the first ellipse and the second was an “exclusion zone”, while the space between the second and third ellipses was the “background zone”. Background for each feature was then determined by measuring the red and green channels in the portions of the background zones not overlapped by other exclusion zones.

Outlier Rejection. Pixel outlier rejection was determined for every pixel within the ellipse after the initial statistics were determined. Outlier pixels were determined based on their intensity values being greater than 1.42 times the interquartile range (IQR). For normally distributed pixel intensities, values outside this range were outside a 99% confidence interval of the mean (>2.6 times the standard deviation). If a pixel was an outlier in one color, the pixel was removed in both colors. It is also possible that entire features are outliers because the presence of some corruption on the array or a contaminating fiber that shows up in the scanner as a highly fluorescent smear. To account for this, a noise model was applied to the entire array to identify feature and local background pattern expressions that significantly deviated from a baseline. The model is a polynomial equation made up of three variables: the intensity dependent variance (square of the coefficient of variation percentage), variance due to the Poisson distributed noise, and variance due to signal independent background noise (i.e. scanner noise). Additionally, the Agilent Human cDNA 1 microarray has 100 replicate features, whose expression levels can be compared to determine a noise distribution within the array spots using the same model. The same level of 1.42*IQR is used to flag the feature or local background as outliers.

Feature Saturation. Pixel saturation was defined as a signal at the maximum allowed intensity value as determined by the scanner. If more than 50% of all pixels remaining after outlier rejection are saturated in one color, then the feature is marked as saturated.

Background Subtraction. It is very important to subtract background measurements from the raw feature signals to account for systematic biases in the data arising from sources such as substrate fluorescence, non-specific binding to the substrate, or the scanning process. Background can also vary differently for each color channel. The feature extraction software has a multitude of global background level determinations, but local background for each individual feature was subtracted from the features in these experiments.

Dye Normalization. After background subtraction, it is common to have a green or red color bias at the low end of the signal range. In a self-self array (same target labeled by both red and green channels) one would expect to see a linear plot of red vs. green signal. Bias at the low end will cause the signal to "hook" towards one axis. Agilent's background adjustment algorithm corrects for this bias in two steps: first it finds the central tendency of the data set, and then estimates the best adjustments in the red and green channels that would create a linear relationship. In these microarray experiments, the normalization features (features which followed the central tendency) were selected using a Rank Consistency Filter, which selects features that fall within consistent trends of the red and green channels with no assumption of the underlying tendency of the data. Only the features that passed the previous criteria were considered for this normalization. Once this dataset was determined, the data was normalized according to the well known LOWESS method, a locally weighted linear regression curve fit. This method assumes that dye bias is intensity dependent, and therefore the background subtracted signal is multiplied by a value that is a function of

the feature intensity. The normalization dataset was used to determine these functions, which were then applied to all of the applicable features.

Significance Determination. Once the data have been normalized, significant expression can now be determined. Two factors are important in determining significance: the log ratio and the measured error. The Agilent software calculates error based on two models: the propagated error based on pixel statistics, and a Universal Error Model. For these experiments, the most conservative error model (one that results in the higher P<value) was used. Using the available pixels on all applicable spots, sample statistics were calculated based on underlying normally distributed populations (T tests) to determine significant expression. Only sample for which each channel was significantly expressed above background ($P<0.01$) were used in subsequent analyses, and the processed signal intensity values (red and green) were then used as the data points.

Statistics Using Multiple Microarrays

The Agilent Feature Extraction Software also has the capability to determine significantly changed expression by measuring the differences in intensity of the red and green channels. Each pixel is counted as an independent data point, thus creating a large sample number as an estimator of the population. T tests are conducted on this data, and usually $P<0.01$ is considered significant. While this method is simple and accommodated by the software, its utility breaks down when considering multiple microarrays. It appears that the variability between microarray hybridizations is larger than the variability within the arrays. If this were not so, then only a single array would be needed for any study, just using multiple spots for each cDNA profiled. Furthermore, differences in sample batches, hybridization efficiencies, and random variations in the

entire process can lead to extensive variation in microarray intensities. An example of several genes whose expression varies tremendously between arrays is shown in Figure A3-1. These genes were all significantly expressed within each array (P<0.01), had fold changes larger than 2.0 within these arrays, yet between the arrays varied wildly, even to the point of significant expression in the opposite direction.

Two Factor Analysis of Variance. It was therefore decided early on to design the microarray experiments to accommodate high-powered statistical analyses. Multifactor Analysis of Variance is a powerful statistical tool that partitions experimental variation into bins, therefore reducing the variance used for a specific test. As shown in Table C-2, the mean squared error associated with the treatment effect (shear or cell type) can be separated and used in determining significant expression. A two factor mixed ANOVA was therefore applied to all the microarray expression data presented in

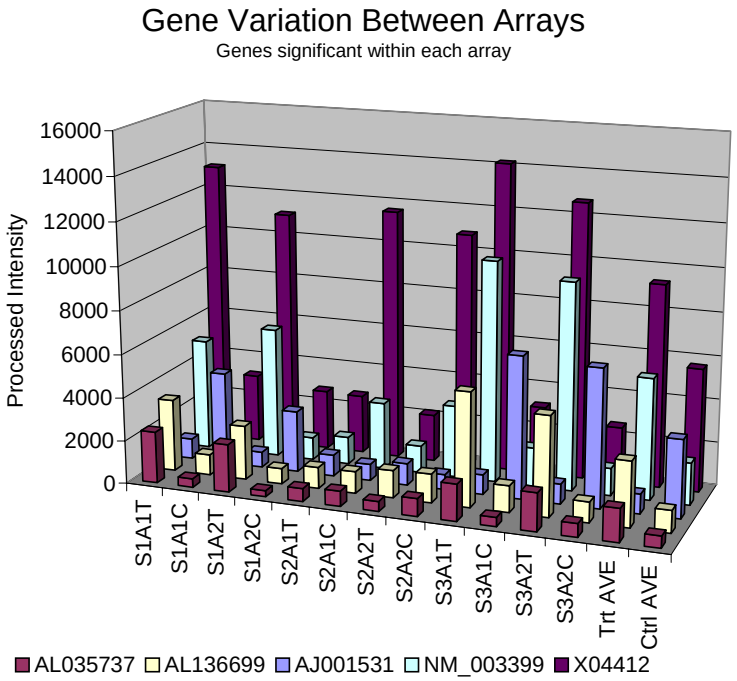

Figure C-1: Example genes with significant expression as determined by single array feature extraction software (P<0.01) yet wildly varying expression between arrays.

Table C-2: Mixed ANOVA model (A fixed, B random). Statistical Model is:

$$Y_{ijk} = \mu + \alpha_i + \beta_j + (\alpha\beta)_{ij} + \varepsilon_{ijk}$$

Source of Variation	Degrees of Freedom (DF)	Expected Mean Squared Error (MSE)
A (fixed)	a-1	$\sigma^2 + n\sigma^2_{AB} + [(nb)/(a-1)]\Sigma\alpha^2$
B (random)	b-1	$\sigma^2 + na\sigma^2_B$
AxB (interaction)	(a-1)(b-1)	$\sigma^2 + n\sigma^2_{AB}$
Within Subgroups	ab(n-1)	σ^2
Total	abn-1	

this work. Cell type or shear stress was the treatment effect, while slide number was the random effect. Since each slide contained two identical array areas, each hybridized at the same time with the same samples, each spot present in both arrays could be considered as replicates. Three microarray slides were used for each experiment, creating an N=3, n=2 arrangement.

To highlight the improved sensitivity of the two factor ANOVA, a comparison was made between this method and other statistical methods for which assumptions could reasonably be made to satisfy their criteria, including non-parametric analyses and paired statistical analyses, the results are shown in Figure A3-2. The mixed ANOVA was much more sensitive than other models, with hundreds of genes determined significant at the $P<0.001$ level, in contrast to the single factor ANOVA, where only 4 genes were deemed significant. Other methods were not capable of determining significance at more conservative P values because the sample numbers required were larger than those available from these experiments.

While the increased sensitivity improved the Positive Predictive Value in these experiments at increasingly more conservative P values, it was unclear whether these methods were actually excluding non-significant expression. Although much less critical

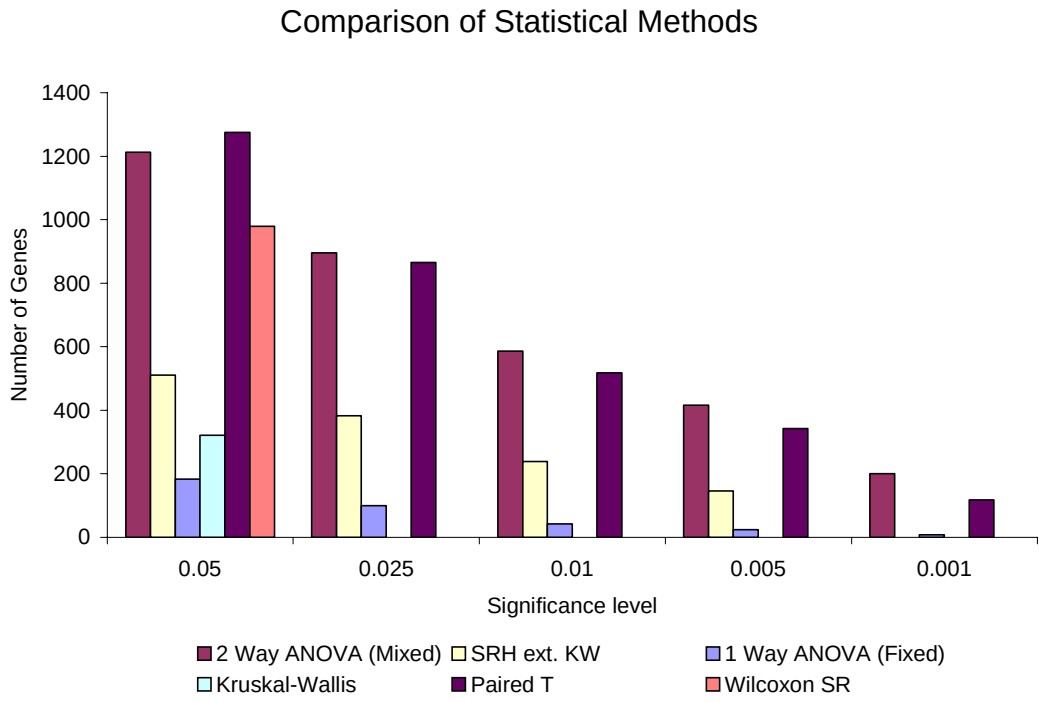

Figure C-2: Comparison of significantly changed genes as determined by relevant statistical models based on different underlying assumptions on population and sample distributions.

than equal sample sizes, two factor ANOVA presupposes an underlying normal sample distribution. To compare the potential confounding effects of non-normal distributions and very conservative P values, a comparison of “smallest fold accepted” (SFA) genes and “largest fold rejected” (LFR) genes at different significance levels. Figure A3-3 shows some examples of these. From these figures it is clear that the large variations in intensity levels between arrays pose a problem for using a “fold change” cutoff in determining significant gene expression using multiple arrays. What remains unclear, however, is which statistical level is best. Arguments can be made to use less conservative P values based on the LFR method, but more conservative values based on the SFA method. Both methods, however, seem to converge upon $P<0.005$ as being the most reasonable. Regardless of what level of significance is chosen, it is critical to confirm any interesting expression results with independent methods. As shown in

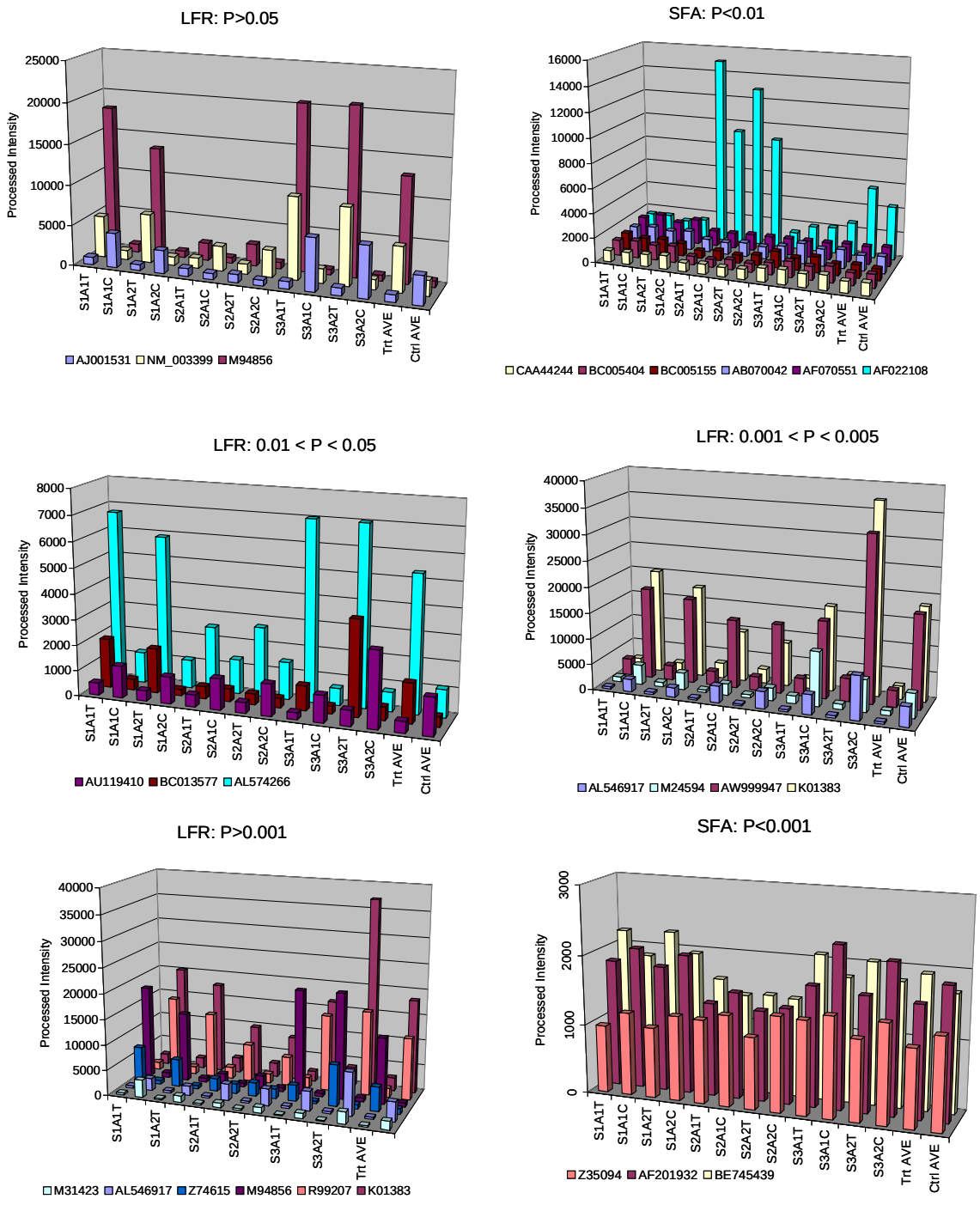

Figure C-3: Comparison of Largest Fold Rejection (LFR) and Smallest Fold Accepted (SFA) genes at different significance levels.

Figure 5-8 of this thesis, microarray data does not necessarily compare 1:1 to other methods, and further differences may be seen at the protein level.

APPENDIX D: ONTOLOGICAL CATEGORIZATION OF GENE EXPRESSION

Group 1: PAVEC 20 48 vs. PAVEC C 48
GOMiner Gene Ontology Summary

Enriched 88
Depleted 52

Rank	Gene Category	No. Genes	No. Under	No. Over	No. Genes	P-Under	P-Over	P-Chngd	Reg.
1	biosynthesis	567	29	66	95	0.134	1E-04	0	Enrchd
2	cytoskeleton	390	21	51	72	0.128	0	0	Enrchd
3	cytoplasm	2062	84	200	284	0.603	0	0	Enrchd
4	microtubule cytoskeleton organization and biogenesis	30	7	6	13	2E-04	0.02	0	Dpltd
5	cell organization and biogenesis	516	35	50	85	0.002	0.023	0.0002	Dpltd
6	cytoplasm organization and biogenesis	335	21	39	60	0.037	0.002	0.0002	Enrchd
7	transferase activity, transferring pentosyl groups	10	4	2	6	5E-04	0.164	0.0003	Dpltd
8	motor activity	82	11	10	21	5E-04	0.076	0.0003	Dpltd
9	microtubule cytoskeleton	156	12	21	33	0.028	0.005	0.0003	Enrchd
10	M-phase specific microtubule process	18	6	2	8	1E-04	0.385	0.0004	Dpltd
11	actin cytoskeleton	159	7	26	33	0.491	1E-04	0.0004	Enrchd
12	cytoskeleton organization and biogenesis	221	14	28	42	0.074	0.003	0.0006	Enrchd
13	microtubule associated complex	100	8	15	23	0.055	0.006	0.0007	Enrchd
14	intracellular	3499	163	277	440	0.009	0.02	0.0007	Dpltd
15	mitotic cell cycle	272	34	15	49	0	0.908	0.0007	Dpltd

16	establishment of cell polarity (sensu Fungi)	5	0	4	4	1	1E-04	0.0008	Enrchd
17	establishment and/or maintenance of cell polarity (sensu Fungi)	5	0	4	4	1	1E-04	0.0008	Enrchd
18	establishment and/or maintenance of cell polarity (sensu Saccharomyces)	5	0	4	4	1	1E-04	0.0008	Enrchd
19	establishment of cell polarity	5	0	4	4	1	1E-04	0.0008	Enrchd
20	establishment of cell polarity (sensu Saccharomyces)	5	0	4	4	1	1E-04	0.0008	Enrchd
21	microtubule-based process	84	10	10	20	0.002	0.086	0.001	Dpltd
22	organelle organization and biogenesis	278	15	34	49	0.177	0.002	0.0012	Enrchd
23	amino acid activation	25	1	8	9	0.654	3E-04	0.0012	Enrchd
24	ligase activity, forming aminoacyl-tRNA and related compounds	25	1	8	9	0.654	3E-04	0.0012	Enrchd
25	ligase activity, forming carbon-oxygen bonds	25	1	8	9	0.654	3E-04	0.0012	Enrchd
26	tRNA ligase activity	25	1	8	9	0.654	3E-04	0.0012	Enrchd
27	cyclin catabolism	3	3	0	3	1E-04	1	0.0015	Dpltd
28	DNA replication and chromosome cycle	157	23	8	31	0	0.9	0.0016	Dpltd
29	RNA ligase activity	26	1	8	9	0.668	4E-04	0.0017	Enrchd
30	cell cycle	566	47	40	87	0	0.628	0.0019	Dpltd
31	Rho guanyl-nucleotide exchange factor activity	6	2	2	4	0.023	0.066	0.0021	Dpltd

32	synaptic vesicle endocytosis	6	2	2	4	0.023	0.066	0.0021	Dpltd
33	ligase activity, forming phosphoric ester bonds	28	1	8	9	0.695	7E-04	0.003	Enrchd
34	synaptic vesicle transport	10	2	3	5	0.062	0.032	0.003	Enrchd
35	mitotic spindle assembly	14	5	1	6	2E-04	0.656	0.003	Dpltd
36	phosphoric diester hydrolase activity	45	4	8	12	0.115	0.015	0.0038	Enrchd
37	M phase	153	16	13	29	5E-04	0.332	0.0041	Dpltd
38	spindle assembly	15	5	1	6	3E-04	0.682	0.0045	Dpltd
39	vacuole	95	0	20	20	1	0	0.0048	Enrchd
40	polyamine metabolism	4	1	2	3	0.156	0.029	0.0055	Enrchd
41	tRNA binding	4	0	3	3	1	0.002	0.0055	Enrchd
42	amino acid and derivative metabolism	103	5	16	21	0.425	0.003	0.0058	Enrchd
43	kinesin complex	72	7	9	16	0.029	0.079	0.0065	Dpltd
44	carboxylic acid metabolism	193	7	27	34	0.696	8E-04	0.0066	Enrchd
45	spindle	26	6	2	8	5E-04	0.579	0.0069	Dpltd
46	structural constituent of muscle	26	2	6	8	0.293	0.01	0.0069	Enrchd
47	organic acid metabolism	194	7	27	34	0.701	8E-04	0.0072	Enrchd
48	myosin II	14	1	4	5	0.447	0.016	0.0162	Enrchd
49	actin filament	19	2	4	6	0.185	0.046	0.0163	Enrchd
50	replication fork	30	8	0	8	0	1	0.017	Dpltd
51	enzyme regulator activity	310	24	24	48	0.002	0.422	0.0173	Dpltd
52	kinase regulator activity	36	3	6	9	0.186	0.045	0.0178	Enrchd
53	response to endogenous stimulus	171	19	10	29	1E-04	0.816	0.0192	Dpltd
54	lysosome	81	0	16	16	1	2E-04	0.0201	Enrchd

55	protein kinase inhibitor activity	10	1	3	4	0.345	0.032	0.0205	Enrchd
56	DNA polymerase complex	10	4	0	4	5E-04	1	0.0205	Dpltd
57	kinase inhibitor activity	10	1	3	4	0.345	0.032	0.0205	Enrchd
58	mitotic chromosome condensation	10	1	3	4	0.345	0.032	0.0205	Enrchd
59	telomere maintenance	10	3	1	4	0.007	0.534	0.0205	Dpltd
60	mitotic prophase	10	1	3	4	0.345	0.032	0.0205	Enrchd
61	response to DNA damage stimulus	165	19	9	28	0	0.865	0.021	Dpltd
62	enzyme binding	20	3	3	6	0.048	0.178	0.0211	Dpltd
63	DNA-directed DNA polymerase activity	20	6	0	6	1E-04	1	0.0211	Dpltd
64	response to temperature	37	0	9	9	1	0.001	0.0212	Enrchd
65	DNA replication	130	20	3	23	0	0.997	0.022	Dpltd
66	regulation of gene expression, epigenetic	15	3	2	5	0.022	0.303	0.0221	Dpltd
67	oxidoreductase activity, acting on the CH-NH group of donors	6	0	3	3	1	0.007	0.0231	Enrchd
68	cortical actin cytoskeleton	6	0	3	3	1	0.007	0.0231	Enrchd
69	cortical cytoskeleton	6	0	3	3	1	0.007	0.0231	Enrchd
70	telomerase-dependent telomere maintenance	6	2	1	3	0.023	0.367	0.0231	Dpltd
71	mitotic anaphase	6	3	0	3	0.001	1	0.0231	Dpltd
72	voltage-dependent ion-selective channel activity	6	0	3	3	1	0.007	0.0231	Enrchd
73	hydrolase activity, hydrolyzing O-glycosyl compounds	44	3	7	10	0.274	0.039	0.0246	Enrchd

74	isomerase activity	70	3	11	14	0.56	0.012	0.0258	Enrchd
75	chromatin	70	10	4	14	5E-04	0.766	0.0258	Dpltd
76	S phase of mitotic cell cycle	132	20	3	23	0	0.997	0.026	Dpltd
77	cell	4532	192	348	540	0.28	0.032	0.0265	Enrchd
78	nuclear membrane	51	3	8	11	0.355	0.031	0.0273	Enrchd
79	amino acid derivative metabolism	27	1	6	7	0.682	0.012	0.029	Enrchd
80	oxidoreductase activity, acting on the CH-CH group of donors	27	1	6	7	0.682	0.012	0.029	Enrchd
81	intramolecular isomerase activity	11	0	4	4	1	0.006	0.0293	Enrchd
82	endoplasmic reticulum lumen	11	1	3	4	0.372	0.042	0.0293	Enrchd
83	response to heat	33	0	8	8	1	0.002	0.0297	Enrchd
84	carbohydrate metabolism	252	8	31	39	0.829	0.003	0.0302	Enrchd
85	nucleotidyltransferase activity	65	9	4	13	0.001	0.713	0.0311	Dpltd
86	DNA dependent DNA replication	72	11	3	14	2E-04	0.907	0.0323	Dpltd
87	extrachromosomal DNA	46	3	7	10	0.297	0.048	0.0329	Enrchd
88	regulation of CDK activity	22	4	2	6	0.012	0.488	0.0334	Dpltd
89	chromosome organization and biogenesis (sensu Eukarya)	121	14	7	21	4E-04	0.795	0.0337	Dpltd
90	enzyme activator activity	93	8	9	17	0.038	0.241	0.034	Dpltd
91	oxidoreductase activity, acting on paired donors, with incorporation or reduction of molecular oxygen	34	0	8	8	1	0.003	0.035	Enrchd

92	G2/M transition of mitotic cell cycle	34	6	2	8	0.002	0.724	0.035	Dpltd
93	small protein conjugating enzyme activity	34	5	3	8	0.012	0.46	0.035	Dpltd
94	membrane lipid metabolism	53	0	11	11	1	0.001	0.0355	Enrchd
95	transferase activity	844	49	64	113	0.007	0.406	0.036	Dpltd
96	L-cystine transporter activity	3	0	2	2	1	0.015	0.0365	Enrchd
97	bile acid transporter activity	3	0	2	2	1	0.015	0.0365	Enrchd
98	NADPH regeneration	3	0	2	2	1	0.015	0.0365	Enrchd
99	glycine metabolism	3	0	2	2	1	0.015	0.0365	Enrchd
100	pentose-phosphate shunt	3	0	2	2	1	0.015	0.0365	Enrchd
101	regulation of catabolism	3	0	2	2	1	0.015	0.0365	Enrchd
102	response to auxin stimulus	3	0	2	2	1	0.015	0.0365	Enrchd
103	pteridine and derivative biosynthesis	3	2	0	2	0.005	1	0.0365	Dpltd
104	cation-transporting ATPase activity	3	0	2	2	1	0.015	0.0365	Enrchd
105	mitotic metaphase/anaphase transition	3	2	0	2	0.005	1	0.0365	Dpltd
106	plasma membrane fusion	3	0	2	2	1	0.015	0.0365	Enrchd
107	anaphase-promoting complex	3	2	0	2	0.005	1	0.0365	Dpltd
108	protein kinase C binding	3	0	2	2	1	0.015	0.0365	Enrchd
109	nuclear ubiquitin ligase complex	3	2	0	2	0.005	1	0.0365	Dpltd
110	sulfur amino acid transporter activity	3	0	2	2	1	0.015	0.0365	Enrchd
111	acyl-CoA dehydrogenase activity	3	0	2	2	1	0.015	0.0365	Enrchd

112	permease activity	3	0	2	2	1	0.015	0.0365	Enrchd
113	uptake permease activity	3	0	2	2	1	0.015	0.0365	Enrchd
114	ABC-type uptake permease activity	3	0	2	2	1	0.015	0.0365	Enrchd
115	mRNA localization, intracellular	3	0	2	2	1	0.015	0.0365	Enrchd
116	spectrin	3	0	2	2	1	0.015	0.0365	Enrchd
117	response to extracellular stimulus	7	0	3	3	1	0.011	0.037	Enrchd
118	other isomerase activity	7	2	1	3	0.031	0.414	0.037	Dpltd
119	oxidoreductase activity, acting on paired donors, with incorporation or reduction of molecular oxygen, miscellaneous	7	0	3	3	1	0.011	0.037	Enrchd
120	response to nutrients	7	0	3	3	1	0.011	0.037	Enrchd
121	DNA topoisomerase activity	7	2	1	3	0.031	0.414	0.037	Dpltd
122	amino acid permease activity	7	0	3	3	1	0.011	0.037	Enrchd
123	coenzyme metabolism	60	1	11	12	0.922	0.004	0.0374	Enrchd
124	ligase activity, forming carbon-nitrogen bonds	60	6	6	12	0.037	0.276	0.0374	Dpltd
125	mitochondrion organization and biogenesis	17	0	5	5	1	0.006	0.0375	Enrchd
126	metabolism	3481	159	262	421	0.027	0.267	0.0393	Dpltd
127	establishment and/or maintenance of cell polarity	12	0	4	4	1	0.009	0.0401	Enrchd
128	membrane fusion	23	1	5	6	0.623	0.023	0.0409	Enrchd

129	G1/S transition of mitotic cell cycle	35	6	2	8	0.003	0.739	0.041	Dpltd
130	amine metabolism	117	5	15	20	0.537	0.023	0.0432	Enrchd
131	intracellular transport	305	12	33	45	0.618	0.015	0.0435	Enrchd
132	organic acid transporter activity	42	1	8	9	0.832	0.01	0.0454	Enrchd
133	carboxylic acid transporter activity	42	1	8	9	0.832	0.01	0.0454	Enrchd
134	morphogenesis	624	26	59	85	0.52	0.022	0.0459	Enrchd
135	organogenesis	552	24	52	76	0.433	0.033	0.0468	Enrchd
136	intracellular transporter activity	18	1	4	5	0.534	0.038	0.0472	Enrchd
137	nucleosome	30	4	3	7	0.034	0.38	0.0492	Dpltd
138	microtubule motor activity	30	4	3	7	0.034	0.38	0.0492	Dpltd
139	nuclear organization and biogenesis	126	14	7	21	7E-04	0.828	0.0494	Dpltd
140	anion channel activity	24	0	6	6	1	0.007	0.0495	Enrchd

Group 2: PAEC 20 48 vs. PAEC C 48
GOMiner Gene Ontology Summary

Enriched 97
Depleted 20

Rank	Gene Category	No. Genes	No. Under	No. Over	No. Genes	P-Under	P-Over	P-Chngd	Reg.
1	extracellular space	479	21	64	85	0.198	0	0	Enrchd
2	extracellular	557	27	71	98	0.06	1E-04	0	Enrchd
3	actin cytoskeleton	80	4	18	22	0.329	1E-04	0.0001	Enrchd
4	cytoskeleton	214	12	31	43	0.083	0.002	0.0003	Enrchd
5	extracellular matrix structural constituent	37	4	8	12	0.043	0.01	0.0009	Enrchd
6	extracellular matrix	101	9	14	23	0.01	0.042	0.0015	Dpltd
7	nonselective vesicle docking	3	0	3	3	1	6E-04	0.0017	Enrchd
8	superoxide metabolism	3	0	3	3	1	6E-04	0.0017	Enrchd
9	collagen fibril organization	3	0	3	3	1	6E-04	0.0017	Enrchd
10	structural molecule activity	217	13	28	41	0.047	0.013	0.0017	Enrchd
11	calcium ion binding	179	13	22	35	0.011	0.043	0.002	Dpltd
12	regulation of cell migration	9	2	3	5	0.04	0.034	0.0021	Enrchd
13	pigmentation	17	2	5	7	0.124	0.011	0.0023	Enrchd
14	ferric iron binding	6	0	4	4	1	6E-04	0.0026	Enrchd
15	membrane	1020	37	110	147	0.531	8E-04	0.0032	Enrchd
16	actin filament	10	0	5	5	1	7E-04	0.0037	Enrchd
17	vacuole	54	0	14	14	1	1E-04	0.0037	Enrchd
18	iron ion binding	10	0	5	5	1	7E-04	0.0037	Enrchd
19	striated muscle thin filament	7	2	2	4	0.024	0.112	0.0054	Dpltd
20	cellular process	1732	73	159	232	0.028	0.053	0.0057	Dpltd
21	enzyme inhibitor activity	87	3	16	19	0.618	0.002	0.0063	Enrchd
22	purine ribonucleoside triphosphate biosynthesis	25	1	7	8	0.604	0.004	0.007	Enrchd
23	ribonucleoside triphosphate biosynthesis	25	1	7	8	0.604	0.004	0.007	Enrchd

24	purine nucleoside triphosphate biosynthesis	25	1	7	8	0.604	0.004	0.007	Enrchd
25	secretion	25	1	7	8	0.604	0.004	0.007	Enrchd
26	pigment metabolism	16	1	5	6	0.447	0.008	0.0082	Enrchd
27	P-P-bond-hydrolysis-driven transporter activity	71	4	12	16	0.255	0.014	0.0087	Enrchd
28	cellular defense response	26	1	7	8	0.618	0.005	0.0091	Enrchd
29	oxidoreductase activity, acting on paired donors, with incorporation or reduction of molecular oxygen	26	1	7	8	0.618	0.005	0.0091	Enrchd
30	purine ribonucleoside triphosphate metabolism	26	1	7	8	0.618	0.005	0.0091	Enrchd
31	ribonucleoside triphosphate metabolism	26	1	7	8	0.618	0.005	0.0091	Enrchd
32	purine nucleoside triphosphate metabolism	26	1	7	8	0.618	0.005	0.0091	Enrchd
33	nucleoside triphosphate biosynthesis	26	1	7	8	0.618	0.005	0.0091	Enrchd
34	cytoskeleton organization and biogenesis	135	3	23	26	0.876	7E-04	0.0091	Enrchd
35	porphyrin metabolism	12	1	4	5	0.358	0.014	0.0096	Enrchd
36	hydrolase activity, acting on acid anhydrides, catalyzing transmembrane movement of substances	66	4	11	15	0.215	0.02	0.0101	Enrchd
37	ATPase activity, coupled to transmembrane movement of substances	66	4	11	15	0.215	0.02	0.0101	Enrchd

38	carbohydrate binding	32	4	5	9	0.027	0.127	0.0108	Dpltd
39	ATP-binding cassette (ABC) transporter activity	27	1	7	8	0.632	0.006	0.0116	Enrchd
40	defense/immunity protein activity	44	3	8	11	0.212	0.028	0.0129	Enrchd
41	purine ribonucleotide biosynthesis	33	1	8	9	0.706	0.005	0.0134	Enrchd
42	polysaccharide biosynthesis	13	0	5	5	1	0.003	0.014	Enrchd
43	organelle organization and biogenesis	181	4	28	32	0.903	9E-04	0.0144	Enrchd
44	nonselective vesicle exocytosis	5	0	3	3	1	0.005	0.0144	Enrchd
45	coenzymes and prosthetic group catabolism	2	0	2	2	1	0.007	0.0145	Enrchd
46	anti-apoptosis	28	1	7	8	0.646	0.007	0.0145	Enrchd
47	porphyrin catabolism	2	0	2	2	1	0.007	0.0145	Enrchd
48	copper, zinc superoxide dismutase activity	2	0	2	2	1	0.007	0.0145	Enrchd
49	superoxide dismutase activity	2	0	2	2	1	0.007	0.0145	Enrchd
50	oxidoreductase activity, acting on superoxide radicals as acceptor	2	0	2	2	1	0.007	0.0145	Enrchd
51	nucleoside triphosphate metabolism	28	1	7	8	0.646	0.007	0.0145	Enrchd
52	synaptic vesicle coating	2	0	2	2	1	0.007	0.0145	Enrchd
53	negative regulation of lymphocyte differentiation	2	0	2	2	1	0.007	0.0145	Enrchd
54	dynactin complex	2	0	2	2	1	0.007	0.0145	Enrchd
55	interleukin-8 receptor binding	2	0	2	2	1	0.007	0.0145	Enrchd
56	acetate kinase activity	2	0	2	2	1	0.007	0.0145	Enrchd
57	ferritin complex	2	0	2	2	1	0.007	0.0145	Enrchd
58	lysosome	45	0	11	11	1	9E-04	0.0153	Enrchd

59	muscle fiber	23	3	4	7	0.048	0.123	0.0154	Dpltd
60	transition metal ion transport	18	1	5	6	0.486	0.014	0.0154	Enrchd
61	endopeptidase inhibitor activity	51	3	9	12	0.281	0.025	0.0156	Enrchd
62	protease inhibitor activity	51	3	9	12	0.281	0.025	0.0156	Enrchd
63	lytic vacuole	51	0	12	12	1	8E-04	0.0156	Enrchd
64	iron ion transport	9	0	4	4	1	0.004	0.016	Enrchd
65	glucan biosynthesis	9	0	4	4	1	0.004	0.016	Enrchd
66	mitotic spindle assembly	9	3	1	4	0.003	0.548	0.016	Dpltd
67	circulation	34	2	7	9	0.351	0.021	0.0163	Enrchd
68	hydrolase activity, hydrolyzing O-glycosyl compounds	34	1	8	9	0.717	0.006	0.0163	Enrchd
69	purine ribonucleotide metabolism	34	1	8	9	0.717	0.006	0.0163	Enrchd
70	carbohydrate metabolism	156	4	24	28	0.827	0.002	0.0177	Enrchd
71	transmembrane receptor activity	184	13	19	32	0.014	0.205	0.0182	Dpltd
72	hydrolase activity, acting on glycosyl bonds	41	1	9	10	0.782	0.006	0.0206	Enrchd
73	purine nucleotide biosynthesis	36	1	8	9	0.737	0.009	0.0236	Enrchd
74	ribonucleotide biosynthesis	36	1	8	9	0.737	0.009	0.0236	Enrchd
75	cysteine protease inhibitor activity	10	2	2	4	0.048	0.204	0.0241	Dpltd
76	muscle development	54	5	7	12	0.044	0.166	0.0241	Dpltd
77	kinase inhibitor activity	10	0	4	4	1	0.007	0.0241	Enrchd
78	spindle assembly	10	3	1	4	0.005	0.586	0.0241	Dpltd
79	DNA-directed DNA polymerase activity	10	4	0	4	3E-04	1	0.0241	Dpltd
80	cytoplasm organization and biogenesis	210	7	28	35	0.648	0.009	0.0255	Enrchd
81	regulation of angiogenesis	6	0	3	3	1	0.01	0.0263	Enrchd

82	glycogen biosynthesis	6	0	3	3	1	0.01	0.0263	Enrchd
83	delta DNA polymerase complex	6	3	0	3	9E-04	1	0.0263	Dpltd
84	Golgi membrane	15	3	2	5	0.015	0.365	0.0267	Dpltd
85	ribonucleotide metabolism	37	1	8	9	0.747	0.01	0.0279	Enrchd
86	motor activity	43	1	9	10	0.798	0.008	0.0283	Enrchd
87	coenzymes and prosthetic group metabolism	68	3	11	14	0.45	0.025	0.0292	Enrchd
88	development	596	31	55	86	0.018	0.243	0.03	Dpltd
89	polysaccharide metabolism	26	0	7	7	1	0.005	0.03	Enrchd
90	synaptic vesicle transport	11	0	4	4	1	0.01	0.0344	Enrchd
91	cell motility	130	11	12	23	0.007	0.417	0.035	Dpltd
92	ATP biosynthesis	16	1	4	5	0.447	0.04	0.0351	Enrchd
93	nucleoside phosphate metabolism	16	1	4	5	0.447	0.04	0.0351	Enrchd
94	extracellular matrix structural constituent conferring tensile strength activity	16	0	5	5	1	0.008	0.0351	Enrchd
95	nucleotide biosynthesis	51	2	9	11	0.558	0.025	0.037	Enrchd
96	phospholipase D activity	3	0	2	2	1	0.02	0.04	Enrchd
97	alpha-amylase activity	3	0	2	2	1	0.02	0.04	Enrchd
98	hydrogen-translocating V-type ATPase complex	3	0	2	2	1	0.02	0.04	Enrchd
99	oxygen binding	3	0	2	2	1	0.02	0.04	Enrchd
100	calcium-mediated signaling	3	0	2	2	1	0.02	0.04	Enrchd
101	regulation of lymphocyte differentiation	3	0	2	2	1	0.02	0.04	Enrchd
102	microvillus	3	0	2	2	1	0.02	0.04	Enrchd
103	muscle thin filament tropomyosin	3	2	0	2	0.004	1	0.04	Dpltd
104	mitotic spindle elongation	3	2	0	2	0.004	1	0.04	Dpltd
105	hormone secretion	3	0	2	2	1	0.02	0.04	Enrchd

106	myosin ATPase activity	3	0	2	2	1	0.02	0.04	Enrchd
107	group transfer coenzyme metabolism	22	1	5	6	0.557	0.033	0.041	Enrchd
108	transferase activity, transferring sulfur-containing groups	7	0	3	3	1	0.016	0.042	Enrchd
109	DNA polymerase complex	7	3	0	3	0.002	1	0.042	Dpltd
110	vacuolar membrane	7	0	3	3	1	0.016	0.042	Enrchd
111	purine nucleotide metabolism	40	1	8	9	0.774	0.016	0.0444	Enrchd
112	integral to membrane	740	27	76	103	0.519	0.026	0.0445	Enrchd
113	enzyme regulator activity	190	12	19	31	0.04	0.247	0.0445	Dpltd
114	ATP metabolism	17	1	4	5	0.467	0.049	0.0449	Enrchd
115	collagen	17	0	5	5	1	0.011	0.0449	Enrchd
116	synaptic vesicle	12	0	4	4	1	0.014	0.0468	Enrchd
117	neurotransmitter secretion	12	0	4	4	1	0.014	0.0468	Enrchd

Group 3: PAVEC C 48 vs. PAEC C 48
GOMiner Gene Ontology Summary

Enriched 36
Depleted 25

Rank	Gene Category	No. Genes	No. Under	No. Over	No. Genes	P-Under	P-Over	P-Chngd	Reg.
1	regulation of cell migration	14	2	6	5	0.039	1E-04	0	Enrchd
2	copper ion binding	30	7	0	7	0	1	0.0006	Dpltd
3	response to reactive oxygen species	2	0	2	2	1	0.003	0.0025	Enrchd
4	tetrapyrrole binding	2	1	2	2	0.045	0.003	0.0025	Enrchd
5	multidrug transporter activity	2	2	0	2	5E-04	1	0.0025	Dpltd
6	blood vessel development	49	2	10	8	0.309	3E-04	0.0028	Enrchd
7	cell-cell signaling	279	16	16	25	6E-04	0.478	0.0035	Dpltd
8	nucleobase, nucleoside, nucleotide and nucleic acid transport	22	1	6	5	0.399	0.001	0.0041	Enrchd
9	phosphorylase activity	14	2	4	4	0.039	0.006	0.0043	Enrchd
10	cadmium ion binding	8	3	0	3	6E-04	1	0.0059	Dpltd
11	cell motility	263	10	24	23	0.078	0.01	0.0068	Enrchd
12	cell communication	1660	51	88	103	0.009	0.703	0.0082	Dpltd
13	structural molecule activity	426	10	35	33	0.513	0.011	0.0084	Enrchd
14	cellular morphogenesis	59	3	10	8	0.152	0.001	0.009	Enrchd
15	mRNA-nucleus export	18	0	6	4	1	3E-04	0.0111	Enrchd
16	response to external stimulus	790	32	22	54	7E-04	1	0.0111	Dpltd
17	regulation of angiogenesis	10	1	4	3	0.207	0.002	0.0117	Enrchd
18	gap-junction forming channel activity	10	1	3	3	0.207	0.015	0.0117	Enrchd

19	connexon channel activity	10	1	3	3	0.207	0.015	0.0117	Enrchd
20	cell migration	76	2	13	9	0.522	2E-04	0.0138	Enrchd
21	ATP-gated cation channel activity	4	2	0	2	0.003	1	0.0143	Dpltd
22	interleukin-8 receptor binding	4	1	2	2	0.088	0.017	0.0143	Enrchd
23	acetate kinase activity	4	0	4	2	1	0	0.0143	Enrchd
24	DNA clamp loader activity	4	0	4	2	1	0	0.0143	Enrchd
25	drug transporter activity	4	2	0	2	0.003	1	0.0143	Dpltd
26	RNA-nucleus export	20	0	6	4	1	5E-04	0.0163	Enrchd
27	chromatin	20	0	4	4	1	0.022	0.0163	Enrchd
28	RNA transport	20	0	6	4	1	5E-04	0.0163	Enrchd
29	nucleic acid transport	20	0	6	4	1	5E-04	0.0163	Enrchd
30	synaptic transmission	119	8	8	12	0.006	0.337	0.0165	Dpltd
31	transmission of nerve impulse	119	8	8	12	0.006	0.337	0.0165	Dpltd
32	folic acid binding	12	2	2	3	0.03	0.14	0.02	Dpltd
33	excitatory extracellular ligand-gated ion channel activity	12	3	0	3	0.002	1	0.02	Dpltd
34	alpha-type channel activity	139	7	8	13	0.039	0.506	0.0228	Dpltd
35	response to metal ion	5	2	0	2	0.005	1	0.023	Dpltd
36	angiogenesis	45	2	7	6	0.275	0.011	0.0244	Enrchd
37	chromosome condensation	13	0	6	3	1	0	0.025	Enrchd
38	imaginal disc metamorphosis	13	2	2	3	0.034	0.159	0.025	Dpltd
39	cell adhesion	381	12	29	28	0.161	0.048	0.0277	Enrchd
40	enzyme regulator activity	350	15	21	26	0.013	0.38	0.0296	Dpltd
41	ligand-gated ion channel activity	35	5	0	5	0.001	1	0.0297	Dpltd
42	extracellular ligand-gated ion channel activity	24	4	0	4	0.002	1	0.0305	Dpltd
43	viral life cycle	14	2	1	3	0.039	0.549	0.0307	Dpltd

44	viral infectious cycle	14	2	1	3	0.039	0.549	0.0307	Dpltd
45	regulation of cell shape	14	1	4	3	0.277	0.006	0.0307	Enrchd
46	response to abiotic stimulus	319	16	8	24	0.002	0.998	0.0314	Dpltd
47	copper ion homeostasis	6	2	0	2	0.007	1	0.0333	Dpltd
48	cell fate specification	6	1	2	2	0.13	0.039	0.0333	Enrchd
49	pre-replicative complex formation and maintenance	6	0	3	2	1	0.003	0.0333	Enrchd
50	phosphotransferase activity, carboxyl group as acceptor	6	0	4	2	1	1E-04	0.0333	Enrchd
51	negative regulation of angiogenesis	6	1	2	2	0.13	0.039	0.0333	Enrchd
52	establishment of tissue polarity	6	0	3	2	1	0.003	0.0333	Enrchd
53	sister chromatid cohesion	6	0	4	2	1	1E-04	0.0333	Enrchd
54	microvillus	6	0	2	2	1	0.039	0.0333	Enrchd
55	alpha-N-acetylneuraminate alpha-2,8-sialyltransferase activity	6	1	2	2	0.13	0.039	0.0333	Enrchd
56	RNA localization	26	0	6	4	1	0.003	0.0396	Enrchd
57	transition metal ion homeostasis	26	4	0	4	0.003	1	0.0396	Dpltd
58	response to chemical substance	153	10	3	13	0.003	0.992	0.0449	Dpltd
59	coreceptor activity	7	0	3	2	1	0.005	0.0451	Enrchd
60	mesoderm cell fate commitment	7	2	0	2	0.01	1	0.0451	Dpltd
61	post-embryonic morphogenesis	7	0	4	2	1	3E-04	0.0451	Enrchd

PAVEC 20 48 vs. PAEC 20 48
GOMiner Gene Ontology Summary

Enriched 34
Depleted 11

Rank	Gene Category	No. Genes	No. Under	No. Over	No. Genes	P-Under	P-Over	P-Chngd	Reg.
1	copper ion binding	14	8	1	9	0	0.86	0.002	Dpltd
2	intramolecular transferase activity, phosphotransferases	4	1	3	4	0.39	0.01	0.0038	Enrchd
3	phosphotransferase activity, carboxyl group as acceptor	4	0	4	4	1	0	0.0038	Enrchd
4	calcium ion storage activity	4	3	1	4	0.006	0.43	0.0038	Dpltd
5	isomerase activity	47	7	13	20	0.301	0.01	0.0055	Enrchd
6	cytoskeletal protein binding	122	21	22	43	0.039	0.08	0.0057	Dpltd
7	cell	2716	323	376	699	0.179	0.02	0.0087	Enrchd
8	carbohydrate metabolism	170	18	38	56	0.702	0	0.0089	Enrchd
9	nucleolus	40	1	16	17	0.993	0	0.0103	Enrchd
11	nucleotide-sugar metabolism	12	4	3	7	0.042	0.2	0.0135	Dpltd
12	chromosome condensation	12	1	6	7	0.773	0	0.0135	Enrchd
13	NADPH regeneration	5	0	4	4	1	0	0.0151	Enrchd
14	pentose-phosphate shunt	5	0	4	4	1	0	0.0151	Enrchd
15	intramolecular transferase activity	5	1	3	4	0.461	0.02	0.0151	Enrchd
16	collagen type IV	5	1	3	4	0.461	0.02	0.0151	Enrchd
17	RNA elongation from Pol II promoter	3	1	2	3	0.31	0.05	0.0152	Enrchd
18	UDP-N-acetylglucosamine metabolism	3	3	0	3	0.002	1	0.0152	Dpltd
19	sterol O-acyltransferase activity	3	2	1	3	0.037	0.35	0.0152	Dpltd
20	neuron differentiation	3	2	1	3	0.037	0.35	0.0152	Dpltd

21	regulation of mitotic cell cycle	3	1	2	3	0.31	0.05	0.0152	Enrchd
22	regulation of S phase of mitotic cell cycle	3	1	2	3	0.31	0.05	0.0152	Enrchd
23	cadmium ion binding	3	3	0	3	0.002	1	0.0152	Dpltd
24	carbohydrate biosynthesis	48	7	12	19	0.32	0.02	0.0163	Enrchd
26	extracellular matrix structural constituent	40	6	10	16	0.317	0.03	0.0238	Enrchd
27	intracellular	2096	229	316	545	0.946	0	0.0243	Enrchd
28	oxygen and reactive oxygen species metabolism	37	6	9	15	0.254	0.05	0.0249	Enrchd
30	nuclear body	8	0	5	5	1	0	0.0263	Enrchd
31	regulation of cell migration	8	4	1	5	0.009	0.68	0.0263	Dpltd
32	viral nucleocapsid	19	1	8	9	0.905	0	0.0271	Enrchd
33	viral capsid (sensu Retroviridae)	19	1	8	9	0.905	0	0.0271	Enrchd
34	viral capsid	28	2	10	12	0.854	0	0.0273	Enrchd
35	energy pathways	123	15	25	40	0.462	0.02	0.0306	Enrchd
36	chromatin	11	1	5	6	0.743	0.01	0.0329	Enrchd
37	structural molecule activity	225	21	47	68	0.89	0	0.0331	Enrchd
40	nicotinamide metabolism	6	0	4	4	1	0	0.0365	Enrchd
41	NADPH metabolism	6	0	4	4	1	0	0.0365	Enrchd
42	DNA strand elongation	6	1	3	4	0.523	0.03	0.0365	Enrchd
43	pyridine nucleotide metabolism	6	0	4	4	1	0	0.0365	Enrchd
44	DNA replication factor C complex	6	1	3	4	0.523	0.03	0.0365	Enrchd
45	phospholipid transporter activity	6	1	3	4	0.523	0.03	0.0365	Enrchd
46	morphogenesis	433	72	51	123	5E-04	0.84	0.0378	Dpltd
49	GTPase regulator activity	76	15	11	26	0.026	0.42	0.0405	Dpltd
52	carbohydrate catabolism	36	4	10	14	0.616	0.02	0.0427	Enrchd
56	virion	30	2	10	12	0.879	0	0.0473	Enrchd
57	superoxide metabolism	4	0	3	3	1	0.01	0.0496	Enrchd

63	mannosyl-oligosaccharide 1,2-alpha-mannosidase activity	4	3	0	3	0.006	1	0.0496	Dpltd
70	protein translocase activity	4	0	3	3	1	0.01	0.0496	Enrchd
72	electron transporter activity	127	16	24	40	0.404	0.04	0.0498	Enrchd
73	cytoplasm	1235	134	193	327	0.864	0	0.05	Enrchd

APPENDIX E: K-MEANS CLUSTERING OF GENE ARRAY DATA

Agilent Feature #	Gene ID	Gene Name/Description	Grp1 Ave	Grp2 Ave	Grp3 Ave	Grp4 Ave
9443	AJ292757	Human TUBB1 gene for Human beta tubulin 1, class VI.	1.141	1.141	0.672	1.298
12860	D14582	Human mRNA for epimorphin.	0.863	1.030	0.735	1.039
6599	AF195657	Human DNA mismatch repair protein (MLH3) mRNA, complete cds.	1.093	1.419	0.443	0.825
14262	AF243527	Human serine protease gene cluster, complete sequence.	0.787	1.028	0.717	0.941
3648	D83402	Human gene for prostacyclin synthase, exon 10 and complete cds.	1.000	1.033	0.518	0.999
6455	M75110	Human H,K-ATPase beta subunit mRNA, complete cds.	1.010	0.597	0.011	0.767
14372	D13388	Human mRNA for DnaJ protein homolog, complete cds.	1.042	1.371	0.470	1.292
5556	D01038	integrin, alpha 3 (antigen CD49C, alpha 3 subunit of VLA-3 receptor)	1.004	1.038	0.062	0.994
8386	M36860	Human elastin mRNA, complete cds.	0.894	1.467	0.537	1.157
15945	AL136761	Human mRNA; cDNA DKFZp434I0515 (from clone DKFZp434I0515); complete cds.	1.051	1.023	0.663	0.918
12204	AF071771	zinc finger protein 143 (clone pHZ-1)	1.108	1.477	0.433	0.850
3779	AF049090	Human casein kinase I gamma 3L (CSNK1G3L) mRNA, complete cds.	0.927	1.042	0.686	0.969
11470	AB037786	Human mRNA for KIAA1365 protein, partial cds.	0.922	1.168	0.612	0.959
7537	AI962856	Putative prostate cancer tumor suppressor	0.947	1.002	0.653	1.094
7816	AK022927	Human cDNA FLJ12865 fis, clone NT2RP2003643, moderately similar to Mouse (Mus musculus) mRNA for CMP-N-acetylneuraminic acid synthetase.	1.117	1.002	0.577	1.062
16573	AI299518	ESTs, Highly similar to 2208307A PNG gene [H.sapiens]	0.865	1.523	0.482	1.181
13444	NM_006896	homeo box A7	1.207	1.021	0.645	1.171
9552	M76423	Human carbonic anhydrase VII (CA VII) gene, exons 4,5,6, and 7, and complete cds.	1.024	1.014	0.572	1.034
8972	AI207650	APEX nuclease (multifunctional DNA repair enzyme)	1.058	1.018	0.743	0.806
9864	BC009208	Human, clone MGC:16169 IMAGE:3634845, mRNA, complete cds.	0.849	1.349	0.661	0.832
13458	AI927764	phosphomannomutase 2	0.882	0.696	0.232	1.026
17262	AF195766	Human ZHX1 protein (ZHX1) mRNA, complete cds.	1.063	1.556	0.582	0.652
8626	AL578299	aminoacylase 1	1.097	1.183	0.118	0.951
14383	U45325	Human Kruppel-related 3 (HKR3) gene, exons 4-11, and complete cds.	1.147	1.198	0.687	0.894

11025	BC003394	Human, heterogeneous nuclear ribonucleoprotein C (C1/C2), clone MGC:5418 IMAGE:3447724, mRNA, complete cds.	1.000	1.115	0.530	0.771
10181	AF060568	Human promyelocytic leukemia zinc finger protein (PLZF) gene, complete cds.	0.929	1.179	0.738	0.951
3207	BC000266	Human, NADH dehydrogenase (ubiquinone) 1 alpha subcomplex, 1 (7.5kD, MWFE), clone MGC:2066 IMAGE:3352028, mRNA, complete cds.	0.881	1.211	0.605	0.960
6959	AK021796	Human cDNA FLJ11734 fis, clone HEMBA1005443.	0.979	0.678	0.398	0.907
14092	AK026204	Human cDNA: FLJ22551 fis, clone HSI00804.	0.931	1.174	0.635	0.916
9879	M94859	Human calnexin mRNA, complete cds.	1.075	1.211	0.660	1.322
13263	AY014180	Human E3 ubiquitin ligase Smurf2 mRNA, complete cds.	1.076	1.092	0.483	0.964
6267	U03493	Human connexin45 gene, complete cds.	1.273	1.093	0.575	0.653
5440	L12398	Human dopamine D4 receptor (DRD4) mRNA (D4.7) sequence.	0.782	1.323	0.623	0.997
14143	AF060568	Human promyelocytic leukemia zinc finger protein (PLZF) gene, complete cds.	1.013	1.086	0.642	0.923
11004	U03911	Human mutator gene (hMSH2) mRNA, complete cds.	0.960	1.083	0.724	0.957
10532	AI347985	matrix metalloproteinase 23B	1.379	1.285	0.659	0.693
9529	AF124432	Human HOM-TES-103 tumor antigen mRNA, complete sequence.	0.976	1.281	0.701	0.955
14693	AP000577	Human genomic DNA, chromosome 11q, clone:CMB9-51L7.	0.986	1.263	0.746	0.856
9863	BC003564	Human, ATPase, H+ transporting, lysosomal (vacuolar proton pump), member J, clone MGC:1970 IMAGE:3546257, mRNA, complete cds.	1.057	1.088	0.709	1.070
15845	AB037831	Human mRNA for KIAA1410 protein, partial cds.	0.995	1.089	0.436	0.741
11488	L12168	Human adenylyl cyclase-associated protein (CAP) mRNA, complete cds.	0.945	1.555	0.503	1.012
4021	AV714317	TGFB inducible early growth response	1.173	0.799	0.317	0.773
12967	L32140	Human afamin mRNA, complete cds.	1.064	0.724	0.195	1.272
3524	AB051544	Human mRNA for KIAA1757 protein, partial cds.	0.951	0.947	0.722	0.899
11128	U11276	Human hNKR-P1a protein (NKR-P1A) mRNA, complete cds.	0.958	0.952	0.355	1.116
12049	AK026690	Homo sapiens cDNA: FLJ23037 fis, clone LNG02036, highly similar to HSU68019 Homo sapiens mad protein homolog (hMAD-3) mRNA	1.282	0.848	0.547	1.292
3635	AJ003147	Human complete genomic sequence between D16S3070 and D16S3275, containing Familial Mediterranean Fever gene disease.	0.972	1.774	0.490	0.924
5969	BE780960	phosphofructokinase, muscle	1.260	0.950	0.721	0.914
11303	D82345	Human mRNA for NB thymosin beta, complete cds.	1.341	0.949	0.602	0.878

13842	AA489676	BCE-1 protein	0.966	0.899	0.344	0.957
9523	U50871	Human familial Alzheimer's disease (STM2) gene, complete cds.	0.974	0.922	0.252	1.466
5751	L76703	protein phosphatase 2, regulatory subunit B (B56), epsilon isoform	0.824	0.997	0.154	0.902
14689	AF044323	Human cytochrome c oxidase assembly protein COX15 (COX15) mRNA, complete cds.	0.922	0.768	0.243	0.830
10512	U09825	zinc finger protein 173	1.200	0.904	0.294	1.089
8286	U63963	Human CSF-1 receptor (FMS) gene, complete cds, and (SMF) gene, partial cds.	0.959	0.927	0.612	0.812
10392	BI835373	signal sequence receptor, delta (translocon-associated protein delta)	1.122	2.081	0.026	0.910
13340	M84326	Human ADP-ribosylation factor 1 mRNA, complete cds.	1.179	0.955	0.212	0.512
11909	AW965948	NADH dehydrogenase (ubiquinone) 1, subcomplex unknown, 1 (6kD, KFYI)	0.808	0.844	0.607	0.973
10360	AW972560	chaperonin containing TCP1, subunit 4 (delta)	1.015	0.920	0.715	0.947
2917	F07456	methionine adenosyltransferase II, alpha	0.950	0.976	0.561	1.099
3876	AB021644	Human GIOT-4 mRNA for gonadotropin inducible transcription repressor-4, complete cds.	0.897	0.977	0.390	0.926
15062	BG495228	low molecular mass ubiquinone-binding protein (9.5kD)	0.988	0.817	0.637	1.273
8500	J03745	Human endonexin II mRNA, complete cds.	0.982	0.822	0.202	1.129
3951	H15124	RAB35, member RAS oncogene family	1.030	0.959	0.431	0.926
10643	BI054765	insulin-like growth factor 1 receptor	0.915	0.836	0.549	0.905
16238	AY008372	Human oxysterol binding protein-related protein 3 (ORP3) mRNA, complete cds.	0.877	0.986	0.340	0.934
18327	AL542973	cyclin-dependent kinase inhibitor 1A (p21, Cip1)	1.839	0.837	0.493	1.336
3714	AB032957	Human mRNA for KIAA1131 protein, partial cds.	0.815	0.803	0.398	0.801
9551	U09117	Human phospholipase c delta 1 mRNA, complete cds.	1.139	0.970	0.444	1.227
10395	BE168491	major histocompatibility complex, class I, C	1.195	0.963	0.721	1.243
9105	NM_003052	solute carrier family 34 (sodium phosphate), member 1	0.879	0.986	0.614	1.078
16313	M87339	Human replication factor C, 37-kDa subunit mRNA, complete cds.	0.584	0.876	1.601	0.766
17268	D38305	Human mRNA for Tob, complete cds.	0.791	0.913	1.106	0.699
14438	AL132665	Human mRNA; cDNA DKFZp566E034 (from clone DKFZp566E034); complete cds.	0.864	0.767	1.561	0.494
11902	BF034561	G-rich RNA sequence binding factor 1	0.750	1.111	1.238	0.875
4179	BC007951	SRY (sex determining region Y)-box 9 (campomelic dysplasia, autosomal sex-reversal)	0.899	1.101	1.356	0.626
5654	BC005883	hypothetical protein	0.897	0.938	1.343	0.682
16737	AL048242	methylthioadenosine phosphorylase	0.643	0.926	0.956	0.681

13765	BG618998	CDC28 protein kinase 2	0.476	0.970	1.163	1.046
2920	AI033892	ESTs, Highly similar to B Chain B, Crystal Structure Of The Human Cdk2 Kinase Complex With Cell Cycle-Regulatory Protein Ckshs1 [H.sapiens]	0.708	1.020	1.264	0.785
4417	BC000335	nucleoporin 88kD	0.901	0.977	1.545	0.631
14595	AK001696	Human cDNA FLJ10834 fis, clone NT2RP4001207.	0.782	1.014	0.952	0.714
12219	AI536671	hypothetical protein PRO1489	0.606	0.957	1.211	0.426
16245	U15128	Human beta-1,2-N-acetylglucosaminyltransferase II (MGAT2) gene, complete cds.	0.930	1.002	1.270	0.686
9416	AK001362	Human cDNA FLJ10500 fis, clone NT2RP2000369.	0.875	0.970	1.086	0.700
14581	U43328	Human link protein mRNA, complete cds.	0.785	1.030	1.139	0.687
12815	AF008915	Human EVI5 homolog mRNA, complete cds.	0.885	1.027	1.033	0.713
9152	BC008328	PAX transcription activation domain interacting protein 1 like	0.803	1.082	1.089	0.744
8749	BG619195	KIAA0528 gene product	0.731	1.077	1.331	0.731
8833	AI051628	v-jun avian sarcoma virus 17 oncogene homolog	0.732	0.932	1.311	0.805
3789	AP000427	Human genomic DNA, chromosome 8q23, clone:KB1171G1.	0.761	1.060	0.838	0.708
4311	BG572762	caspase 4, apoptosis-related cysteine protease	0.738	1.067	1.073	0.819
8282	AB005666	Human mRNA for GTPase-activating protein, complete cds.	0.959	1.039	1.026	0.731
5589	AL531502	serine (or cysteine) proteinase inhibitor, clade G (C1 inhibitor), member 1	0.716	0.941	1.115	0.644
4265	BG433239	smg GDS-ASSOCIATED PROTEIN	0.748	1.005	1.099	0.917
9117	BF690275	pyruvate kinase, muscle	0.802	0.803	1.303	0.653
13320	BG289736	protein phosphatase 1, catalytic subunit, gamma isoform	0.652	1.163	1.243	0.823
12723	D14497	Human mRNA for proto-oncogene protein, complete cds.	0.899	1.451	1.284	0.661
11894	AL580466	protein phosphatase 3 (formerly 2B), regulatory subunit B (19kD), alpha isoform (calcineurin B, type I)	0.703	1.192	0.853	0.702
13316	AL571008	baculoviral IAP repeat-containing 5 (survivin)	0.577	1.363	1.235	1.027
14254	AF260225	Human TESTIN 2 and TESTIN 3 genes, complete cds, alternatively spliced.	0.698	1.336	1.085	0.810
7368	BG107450	KIAA0256 gene product	0.533	1.335	1.287	0.903
12811	D14134	Human mRNA for RAD51, complete cds.	0.669	1.324	1.005	0.963
6923	M74091	Human cyclin mRNA.	0.680	1.277	1.051	0.812
13441	BE702316	eukaryotic translation initiation factor 4B	0.772	1.309	1.434	0.677
12493	AF132811	Human nectin-like protein 2 (NECL2) mRNA, complete cds.	0.604	1.177	0.983	0.544
16571	BI908492	unc119 (C.elegans) homolog	1.293	1.613	0.609	1.222
6755	D38555	Human mRNA for KIAA0079 gene, complete cds.	1.075	1.564	0.962	0.945

8676	AI275084	transcription factor AP-2 beta (activating enhancer-binding protein 2 beta)	1.090	1.560	0.875	1.074
16468	AF062332	catenin (cadherin-associated protein), delta 1	1.121	1.704	0.858	0.988
4753	BC011519	Human, angiotensinogen (serine (or cysteine) protease inhibitor, clade A (alpha-1 antiprotease, antitrypsin), member 8), clone MGC:17092 IMAGE:4213559, mRNA, complete cds.	0.797	1.976	0.867	0.978
13485	AL571444	LIS1-interacting protein NUDEL; endooligopeptidase A	1.216	1.527	1.128	1.159
15087	BF793662	FERM, RhoGEF (ARHGEF) and pleckstrin domain protein 1 (chondrocyte-derived)	1.085	2.001	0.784	1.031
14288	AL117468	Human mRNA; cDNA DKFZp586N1922 (from clone DKFZp586N1922); partial cds.	1.197	1.525	0.948	1.256
2447	AL529959	eukaryotic translation initiation factor 3, subunit 8 (110kD)	1.130	1.518	0.929	1.401
6364	AK026157	Human cDNA: FLJ22504 fis, clone HRC11430.	1.234	1.516	0.871	0.932
10503	AI619551	nuclear cap binding protein subunit 2, 20kD	0.905	1.514	0.908	1.245
9439	L02547	Human (clone pZ50-19) cleavage stimulation factor 50kDa subunit, complete cds.	1.053	1.735	0.793	1.537
15187	BC004467	KIAA0171 gene product	1.023	1.570	0.857	1.180
4842	BC005968	Human, ATP binding protein associated with cell differentiation, clone MGC:14620 IMAGE:4073821, mRNA, complete cds.	0.785	1.607	0.696	0.870
2460	NM_005529	heparan sulfate proteoglycan 2 (perlecan)	1.150	1.878	0.894	1.131
13619	AI698095	KIAA0699 protein	1.066	1.784	0.772	0.870
9731	M94166	Human heregulin-beta1 gene, complete cds.	0.779	1.804	0.948	1.208
16463	BC001832	Human, eukaryotic translation initiation factor 5A, clone MGC:4130 IMAGE:2961296, mRNA, complete cds.	1.402	1.603	0.624	1.227
15341	BG675712	calmodulin 2 (phosphorylase kinase, delta)	1.000	1.591	0.940	1.078
8683	L06133	Human putative Cu++-transporting P-type ATPase mRNA, complete cds.	1.083	1.635	1.100	1.583
10516	AV650019	nuclear factor of kappa light polypeptide gene enhancer in B-cells inhibitor-like 2	0.729	1.752	0.786	1.292
16890	BE410539	KIAA0304 gene product	1.047	1.584	1.003	1.559
9385	BAB23193	putative	0.956	1.507	1.023	1.310
12988	AF108765	Human testis 6-phosphofructo-2-kinase/fructose 2,6-bisphosphatase (PFKFB4) mRNA, complete cds.	0.988	1.896	0.870	0.980
12103	NM_014214	inositol(myo)-1(or 4)-monophosphatase 2	1.134	1.583	0.809	0.972
8779	L38951	karyopherin (importin) beta 1	0.826	8.971	0.813	1.590
3618	BC004108	Human, clone IMAGE:3687782, mRNA, partial cds.	0.943	2.066	0.971	0.972

16011	D78130	Human mRNA for squalene epoxidase, complete cds.	1.140	1.507	0.922	1.047
4120	AU135575	villin 2 (ezrin)	1.230	1.504	0.834	1.273
6263	M36711	Human sequence-specific DNA-binding protein (AP-2) mRNA, complete cds.	0.957	2.743	0.673	0.945
2296	BC005133	Human, clone MGC:11134 IMAGE:3836683, mRNA, complete cds.	0.966	2.351	0.919	1.148
9079	BE909056	clathrin, light polypeptide (Lca)	0.927	2.411	0.929	1.191
12274	BG252978	membrane component, chromosome 11, surface marker 1	1.148	2.438	0.863	0.896
10098	AB062981	Macaque brain cDNA clone:QmoA-10634, full insert sequence.	0.954	3.079	0.902	1.050
11864	AW296083	Homo sapiens cDNA: FLJ21897 fis, clone HEP03447, highly similar to AF052178 Homo sapiens clone 24523 mRNA sequence	0.829	2.302	0.911	1.148
14096	M64925	Human palmitoylated erythrocyte membrane protein (MPP1) mRNA, complete cds.	1.450	3.104	0.270	1.126
9124	NM_003359	UDP-glucose dehydrogenase	1.380	3.147	0.939	0.937
12866	CAA44244	formin, isoform IV	1.041	4.698	0.944	1.511
10200	L06862	collagen, type VII, alpha 1 (epidermolysis bullosa, dystrophic, dominant and recessive)	0.979	2.005	0.929	1.030
7051	BG746580	mitochondrial ribosomal protein S27	1.071	1.284	0.715	1.048
6894	U24166	Human EB1 mRNA, complete cds.	1.606	2.194	0.933	1.016
11589	AJ243972	Human mRNA for 6-phosphogluconolactonase (6PGL gene).	1.008	2.073	0.918	1.004
3366	AB019602	Human IDN3-B mRNA, complete cds.	0.965	1.399	0.720	1.050
8340	AK027542	Human cDNA FLJ14636 fis, clone NT2RP2001233, weakly similar to ZINC FINGER PROTEIN 91.	0.949	1.701	0.863	1.161
17874	AF009802	Human homeodomain protein (BAPX1) gene, complete cds.	1.011	2.072	0.666	1.258
11269	AF025529	Human leucocyte Ig-like receptor-6b (LIR-6) mRNA, complete cds.	1.008	2.087	0.812	1.009
13644	AA582575	intersectin 1 (SH3 domain protein)	0.855	1.655	0.712	1.269
16576	BG569292	angiogenin, ribonuclease, RNase A family, 5	0.882	2.134	0.703	1.003
7590	BG718906	ESTs, Weakly similar to I38022 hypothetical protein [H.sapiens]	0.710	2.125	0.926	0.929
12566	AB033035	Human mRNA for KIAA1209 protein, partial cds.	1.611	0.947	1.044	1.176
6002	AL525317	delta sleep inducing peptide, immunoreactor	1.933	0.903	1.129	1.213
5642	BF340474	hypothetical protein FLJ11560	1.633	0.819	1.042	1.120
16276	L20852	Human leukemia virus receptor 2 (GLVR2) mRNA, complete cds.	1.657	0.915	1.084	1.688
16146	BC000429	Human, chromosome 14 open reading frame 2, clone MGC:8356 IMAGE:2819801, mRNA, complete cds.	1.919	0.883	0.865	1.119
5563	BC012195	Human, Similar to valosin-containing protein, clone MGC:4053 IMAGE:2822943, mRNA, complete cds.	1.621	0.845	0.804	1.093

10945	BC004967	Human, putative glialblastoma cell differentiation-related, clone MGC:2352 IMAGE:3535682, mRNA, complete cds.	1.750	0.978	0.864	1.153
4315	BG831512	DiGeorge syndrome critical region gene DGSI; likely ortholog of mouse expressed sequence 2 embryonic lethal	1.570	0.961	1.183	1.022
8959	AI554560	GTP-binding protein Rho7	2.256	1.099	0.974	1.074
14300	J03746	Human glutathione S-transferase mRNA, complete cds.	1.653	1.312	0.915	1.090
8905	AW303586	transforming growth factor, beta 2	2.815	1.082	0.967	1.368
13749	BF681347	actin, alpha 2, smooth muscle, aorta	1.803	1.265	0.885	1.288
8171	AF252872	Human cystine/glutamate transporter xCT mRNA, complete cds.	4.021	1.251	0.882	1.059
16936	BG498371	clones 23667 and 23775 zinc finger protein	1.513	1.216	1.009	0.952
11403	U76549	Human cytokeratin 8 mRNA, complete cds.	1.352	1.105	0.733	1.246
5961	AF073362	meiotic recombination (S. cerevisiae) 11 homolog A	3.327	1.198	0.984	1.640
16115	AF063594	Human brain my036 protein mRNA, complete cds.	1.553	1.337	1.057	1.198
2757	BG612479	adenine phosphoribosyltransferase	1.670	1.184	0.792	1.105
5727	BF309422	DNA fragmentation factor, 45 kD, alpha polypeptide	1.570	1.120	0.924	1.067
6023	BF795451	tryptophanyl-tRNA synthetase	1.944	1.128	0.831	2.465
2745	BC004390	phosphatidylserine synthase 1	1.678	1.130	0.826	1.050
7047	BF305705	histone deacetylase 5	1.890	1.136	0.916	1.127
12523	AL117413	Human mRNA; cDNA DKFZp566M051 (from clone DKFZp566M051).	1.534	1.330	1.159	1.072
16436	AF024636	serine/threonine kinase 24 (Ste20, yeast homolog)	1.509	1.368	0.858	1.134
8647	BI862079	peroxiredoxin 2	1.588	1.040	1.057	1.422
6647	AB053450	Human mRNA for KIAA1776 protein (fibrillin3), complete cds.	1.780	0.964	1.029	1.244
8820	NM_000157	glucosidase, beta; acid (includes glucosylceramidase)	1.858	0.977	0.978	1.517
2928	K03191	cytochrome P450, subfamily I (aromatic compound-inducible), polypeptide 1	8.300	0.966	0.920	1.254
8346	U20734	Human transcription factor junB (junB) gene, 5' region and complete cds.	1.704	0.967	0.871	1.187
13837	BF984053	proteasome (prosome, macropain) subunit, beta type, 6	1.346	0.973	0.834	1.525
14767	M10036	Human triosephosphate isomerase mRNA, complete cds.	2.172	0.975	0.920	1.513
4491	AL538660	heterogeneous nuclear ribonucleoprotein R	2.031	0.975	0.892	0.992
5535	BC010693	Human, Similar to hypothetical protein FLJ10883, clone IMAGE:3855861, mRNA, partial cds.	1.466	1.536	1.045	1.303
10171	BI088564	upstream binding transcription factor, RNA polymerase I	1.961	1.140	0.911	1.586
16774	AL543484	Ras association (RalGDS/AF-6) domain family 1	1.898	1.372	1.029	1.234
7286	AU118354	ATP-binding cassette, sub-family G (WHITE), member 2	1.733	1.534	1.236	1.732

7289	AB007890	KIAA0430 gene product	1.560	1.409	0.919	0.940
18362	BG722759	phytanoyl-CoA hydroxylase (Refsum disease)	1.591	1.398	0.771	1.529
12094	L07956	glucan (1,4-alpha-), branching enzyme 1 (glycogen branching enzyme, Andersen disease, glycogen storage disease type IV)	2.548	1.031	0.909	0.964
7441	AW250734	NADH dehydrogenase (ubiquinone) flavoprotein 1 (51kD)	2.005	1.032	1.333	2.063
8059	AAD43813	Na,K-ATPase alpha-4 subunit	1.653	1.168	0.914	0.993
12695	AF220490	Human group III secreted phospholipase A2 mRNA, complete cds.	1.776	1.013	0.853	1.702
16401	BC011741	Human, clone MGC:19671 IMAGE:3352603, mRNA, complete cds.	1.778	0.749	0.916	1.507
10684	AB011173	KIAA0601 protein	0.968	0.687	0.955	1.115
14597	U39657	Human MAP kinase kinase 6 (MKK6) mRNA, complete cds.	0.949	0.571	0.916	0.890
14161	U12535	Human epidermal growth factor receptor kinase substrate (Eps8) mRNA, complete cds.	0.593	0.704	0.816	0.659
16746	AA523974	hypothetical protein MGC14139	0.911	0.597	0.868	0.746
4243	L01042	TATA element modulatory factor 1	0.827	0.589	0.789	1.049
3397	AJ002535	Human mRNA for obscurin (OBSCN gene).	0.827	0.709	0.872	0.756
12085	BG821629	phosphomannomutase 2	0.897	0.710	0.858	1.000
7341	AI952550	MADS box transcription enhancer factor 2, polypeptide A (myocyte enhancer factor 2A)	0.680	0.698	1.335	1.084
13215	AB014569	Human mRNA for KIAA0669 protein, complete cds.	0.692	0.711	0.981	1.297
9782	AB023161	Human mRNA for KIAA0944 protein, partial cds.	0.945	0.550	0.937	0.933
3841	BAB47481	KIAA1852 protein	0.826	0.546	0.998	0.948
16743	L33075	IQ motif containing GTPase activating protein 1	0.611	0.545	0.947	1.041
7284	BG390232	reticulocalbin 2, EF-hand calcium binding domain	0.953	0.716	1.048	1.043
12047	AW778997	transforming, acidic coiled-coil containing protein 1	1.058	0.609	0.767	0.965
16707	AA534580	serine/threonine kinase with Dbl- and pleckstrin homology domains	0.865	0.638	0.808	0.828
9596	BC001765	Human, Similar to stromal antigen 2, clone MGC:1282 IMAGE:3352347, mRNA, complete cds.	0.748	0.638	0.864	0.910
18326	AI858946	KIAA0295 protein	0.857	0.530	0.886	1.128
13754	AI299309	inhibitor of DNA binding 2, dominant negative helix-loop-helix protein	1.050	0.668	0.849	1.119
15089	U54617	pyruvate dehydrogenase kinase, isoenzyme 4	1.244	0.676	0.660	0.985
11431	AK024923	Human cDNA: FLJ21270 fis, clone COL01749.	0.870	0.679	0.812	1.085
13643	AI050952	activated leucocyte cell adhesion molecule	0.688	0.673	0.841	0.933

11627	AF279372	Human inositol 3,4,5,6 tetrakisphosphate 1-kinase/inositol 1,3,4-trisphosphate 5/6-kinase mRNA, complete cds.	1.023	0.767	0.736	0.912
8921	BF310946	ribosomal protein L35	0.805	0.685	1.019	0.866
10378	AI125923	H2B histone family, member B	0.876	0.663	0.935	1.096
14094	AF113127	Human S1R protein (S1R) mRNA, complete cds.	1.170	0.694	0.832	0.799
5716	AI823889	purinergic receptor (family A group 5)	0.952	0.691	0.950	1.122
14398	AF151900	Human CGI-142 protein mRNA, complete cds.	0.665	0.772	0.931	0.839
4938	AF385084	Human heat shock protein mRNA, complete cds.	0.900	0.655	1.055	0.871
8805	D87743	solute carrier family 9 (sodium/hydrogen exchanger), isoform 6	0.976	0.647	0.930	0.819
5489	AI992137	hepatocellular carcinoma-associated antigen 58	0.903	0.772	0.683	1.076
16937	AI885852	H2A histone family, member O	0.676	0.717	0.852	1.350
7112	AL552252	GTP-binding protein homologous to Saccharomyces cerevisiae SEC4	1.042	0.679	0.726	1.438
15183	NM_013416	neutrophil cytosolic factor 4 (40kD)	1.045	0.514	0.795	1.077
14123	AF179896	Human TALE homeobox protein Meis2b mRNA, complete cds.	0.607	0.465	0.925	0.940
14566	AP000504	Human genomic DNA, chromosome 6p21.3, HLA Class I region, section 3/20.	0.926	0.500	0.435	1.075
6496	BAB30461	putative	0.746	0.743	0.743	0.786
13596	U10990	nuclear receptor subfamily 2, group C, member 2	0.820	0.733	0.966	1.095
16452	AA453425	seven transmembrane domain protein	1.017	0.729	1.063	0.769
8526	AF153605	Human androgen induced protein (AIG-1) mRNA, complete cds.	0.982	0.496	0.892	1.156
13210	M36821	Human cytokine (GRO-gamma) mRNA, complete cds.	1.021	0.722	0.787	0.862
10005	M65131	Human methylmalonyl-CoA mutase (MCM) mRNA, complete cds.	0.691	0.421	0.742	1.217
5532	AU119325	protein tyrosine phosphatase, non-receptor type 2	0.797	0.747	0.934	1.138
4104	BG620669	actin related protein 2/3 complex, subunit 3 (21 kD)	1.055	0.738	0.748	1.077
11620	AB016068	Human mRNA for Ste24p, complete cds.	0.922	0.741	0.773	0.895
4271	AA521448	ESTs, Weakly similar to T22587 hypothetical protein F53F8.5 - Caenorhabditis elegans [C.elegans]	0.963	0.718	0.783	0.823
16766	AA031914	KIAA0143 protein	0.600	0.736	0.841	0.627
12682	U54996	Human protein ZW10 homolog (HZW10) mRNA, complete cds.	0.959	0.501	0.838	0.906
17531	AF309033	Human tankyrase-2 (TNKS-2) mRNA, complete cds.	1.047	0.924	1.506	1.100
13014	D21205	Human mRNA for estrogen responsive finger protein, complete cds.	0.932	0.981	2.118	1.551

11163	BC001731	Human, membrane component, chromosome 11, surface marker 1, clone MGC:1378 IMAGE:3355481, mRNA, complete cds.	0.905	0.924	2.127	0.873
14447	AK026623	Human cDNA: FLJ22970 fis, clone KAT10766, highly similar to HUMCOXNE Human nuclear-encoded mitochondrial cytochrome c oxidase Va subunit mRNA.	0.808	1.268	1.808	1.064
11481	AF073482	Human myotubularin related protein 7 mRNA, partial cds.	0.700	1.308	1.070	1.362
1350	BI962886	U2 small nuclear ribonucleoprotein auxiliary factor (65kD)	0.599	0.955	1.299	1.056
9522	U58334	Human Bcl2, p53 binding protein Bbp/53BP2 (BBP/53BP2) mRNA, complete cds.	0.765	0.823	1.790	1.303
9070	F28484	ribosomal protein L18a	0.810	1.173	1.770	1.176
5652	D89976	5-aminoimidazole-4-carboxamide ribonucleotide formyltransferase/IMP cyclohydrolase	0.604	0.923	1.315	1.477
16428	M62925	Human transglutaminase K enzyme mRNA, complete cds.	1.101	0.967	1.571	1.122
15961	AB011089	Human mRNA for KIAA0517 protein, partial cds.	1.039	1.113	1.507	1.099
16892	BF589570	hypothetical protein FLJ20277	0.833	1.152	1.512	0.988
11924	BG563075	translational inhibitor protein p14.5	0.978	0.894	1.524	1.051
8142	D26361	Human mRNA for KIAA0042 gene, complete cds.	1.002	1.096	1.894	0.902
4123	BC007007	interleukin 18 (interferon-gamma-inducing factor)	0.736	0.761	1.367	1.465
11939	BG740338	acetyl-Coenzyme A acetyltransferase 1 (acetoacetyl Coenzyme A thiolase)	1.016	1.015	1.510	1.439
9377	AF029777	Human histone acetyltransferase (GCN5) mRNA, partial cds.	0.995	1.090	1.283	1.599
3617	BC006285	Human, clone MGC:10315 IMAGE:3960073, mRNA, complete cds.	0.923	0.992	1.617	1.140
15029	F25690	ESTs, Weakly similar to TELT_HUMAN TELETHONIN [H.sapiens]	0.964	1.034	1.786	1.635
7190	NM_001767	CD2 antigen (p50), sheep red blood cell receptor	0.944	0.930	1.824	0.803
10651	R01051	ATP-binding cassette, sub-family A (ABC1), member 1	0.863	1.527	1.293	1.580
6555	CAA73251	Pro-Pol-dUTPase polyprotein	1.035	1.418	1.480	1.613
5360	BC001362	Human, 2',3'-cyclic nucleotide 3' phosphodiesterase, clone MGC:2262 IMAGE:3051112, mRNA, complete cds.	1.035	1.005	1.801	1.071
6410	AL080202	Human mRNA; cDNA DKFZp434F172 (from clone DKFZp434F172).	1.024	0.700	1.280	2.109
4112	AL558909	protein tyrosine phosphatase, non-receptor type 18 (brain-derived)	1.070	1.011	1.642	1.127
16738	BF726950	H2A histone family, member L	0.621	1.438	1.485	1.496
15057	AL571972	Fc fragment of IgG, receptor, transporter, alpha	0.932	1.521	1.301	1.126
5023	AB060914	Macaque brain cDNA clone:QtrA-14537, full insert sequence.	0.854	0.831	1.145	1.742

10975	AF064854	Human map 17q24; 5.13cR from GATA41C05 repeat region, complete sequence.	0.954	1.045	1.522	1.123
5985	D89618	karyopherin alpha 3 (importin alpha 4)	0.856	1.045	1.438	1.544
6888	D28480	Human mRNA for hMCM2, complete cds.	0.666	1.369	1.282	1.189
7523	AV726230	myelin-associated oligodendrocyte basic protein	0.667	0.933	0.925	1.392
13671	R42895	serine dehydratase	1.055	1.020	1.670	1.505
8934	AI417964	calcium channel, voltage-dependent, L type, alpha 1S subunit	0.897	1.011	1.578	1.341
13493	BG469316	H1 histone family, member X	1.200	1.014	1.414	1.713
5965	AA825544	peroxisomal long-chain acyl-coA thioesterase	0.918	0.940	1.505	0.929
12060	U30894	N-sulfoglucosamine sulfohydrolase (sulfamidase)	1.081	0.961	2.275	0.993
8620	BC000833	mitogen-activated protein kinase-activated protein kinase 5	0.900	0.914	1.989	1.044
10068	AK026968	Human cDNA: FLJ23315 fis, clone HEP12021.	1.001	0.961	1.600	1.188
4896	AB070089	Macaque testis cDNA clone:QtsA-13272, full insert sequence.	0.846	0.946	1.978	1.102
2912	M80629	cell division cycle 2-like 5 (cholinesterase-related cell division controller)	0.752	1.014	1.872	0.894
15948	BC011904	Human, Similar to putative sialoglycoprotease type 2, clone MGC:20293 IMAGE:4121450, mRNA, complete cds.	1.003	1.072	2.163	0.852
10374	BE935831	microtubule-associated protein 1B	1.244	1.124	5.744	0.904
4955	M32284	Human glucocorticoid receptor gene, partial.	0.902	0.947	1.512	0.988
4118	AL583224	CAT56 protein	1.096	1.002	1.685	1.220
13524	M74547	retinoblastoma-like 1 (p107)	0.765	0.927	2.299	1.407
14396	AF129756	Human MSH55 gene, partial cds; and CLIC1, DDAH, G6b, G6c, G5b, G6d, G6e, G6f, BAT5, G5b, CSK2B, BAT4, G4, Apo M, BAT3, BAT2, AIF-1, 1C7, LST-1, LTB, TNF, and LTA genes, complete cds.	0.930	0.725	2.950	0.877
6819	AF052224	Human neuronal double zinc finger protein (ZNF231) mRNA, complete cds.	1.438	0.925	1.855	0.879
12095	L04284	myeloid/lymphoid or mixed-lineage leukemia (trithorax (Drosophila) homolog)	0.902	1.043	1.686	1.030
4233	AL559849	histone deacetylase 1	1.079	0.923	1.588	1.125
12524	AF062072	Human zinc finger protein 216 (ZNF216) gene, complete cds.	1.332	1.095	10.363	1.266
15992	AJ001612	Human mRNA for L-3-phosphoserine-phosphatase homologue.	1.334	0.936	1.595	0.925
11006	D17530	Human mRNA for drebrin E, complete cds.	1.151	1.081	87.630	1.747
11317	AF132963	Human CGI-29 protein mRNA, complete cds.	0.884	0.978	1.522	1.190
10618	AI915504	KIAA0652 gene product	0.794	0.956	4.167	0.934

5631	AW082035	keratin 16 (focal non-epidermolytic palmoplantar keratoderma)	1.009	1.076	6.600	1.669
16239	AL133080	Human mRNA; cDNA DKFZp434A0727 (from clone DKFZp434A0727).	1.014	0.738	2.521	0.798
4014	AW409924	chromosome 19 open reading frame 3	1.320	1.126	2.847	1.776
10201	D78333	chaperonin containing TCP1, subunit 6B (zeta 2)	1.071	0.678	1.529	0.982
8468	BC010100	Human, clone MGC:19693 IMAGE:3506451, mRNA, complete cds.	0.899	1.209	1.829	1.421
10036	AF295368	Human G-protein coupled receptor GPR86 (GPR86) mRNA, complete cds.	0.950	0.661	2.048	0.828
13594	BC006103	CDC-like kinase 3	1.067	0.788	1.655	1.005
6454	AJ251026	Human mRNA for putative odorant binding protein b-a (OBPIIb gene).	1.016	0.853	1.534	0.785
4077	AU099021	membrane-bound transcription factor protease, site 2	0.782	0.883	3.807	0.870
18516	AA010378	integral membrane protein 2A	0.664	0.507	3.156	2.764
10073	AB011542	Human mRNA for MEGF9, partial cds.	1.021	0.813	1.679	1.141
7272	AV763549	ATP synthase, H+ transporting, mitochondrial F1 complex, gamma polypeptide 1	1.032	0.791	1.555	0.754
18012	BG033362	adaptor-related protein complex 2, mu 1 subunit	1.543	0.869	1.682	0.790
6046	AI765830	biliverdin reductase A	1.493	0.632	1.651	1.034
5484	AP000529	Human genomic DNA, chromosome 22q11.2, Cat Eye Syndrome region, clone:c3G11.	0.867	1.149	1.966	0.875
9106	U49957	LIM domain-containing preferred translocation partner in lipoma	0.844	0.904	1.583	1.193
9055	BG704884	translin-associated factor X	1.116	1.156	2.361	0.904
9846	AK027494	Human cDNA FLJ14588 fis, clone NT2RM4001819, highly similar to Human p58/GTA (galactosyltransferase associated protein kinase) mRNA.	1.206	0.667	1.564	0.775
10069	U64998	Human ribonuclease k6 precursor gene, complete cds.	1.030	0.894	1.945	0.796
8899	AI884541	surfeit 5	1.054	0.459	0.928	1.001
10246	BE410528	DNA-damage-inducible transcript 3	1.236	0.458	0.980	1.020
13617	AL109778	phosphodiesterase 8A	1.291	0.722	0.982	0.903
3681	BC001791	Human, clone MGC:2663 IMAGE:3543910, mRNA, complete cds.	1.116	0.474	1.190	1.041
15362	BE620977	electron-transfer-flavoprotein, alpha polypeptide (glutaric aciduria II)	1.077	0.459	0.943	0.894
4942	D88152	Human mRNA for acetyl-coenzyme A transporter, complete cds.	1.365	0.496	1.350	1.170
2612	NM_025228	hypothetical protein dJ434O14.3	1.109	0.497	1.151	1.055
12206	AL524757	ARP1 (actin-related protein 1, yeast) homolog A (centractin alpha)	1.637	0.319	0.899	0.642
14472	M29474	Human recombination activating protein (RAG-1) gene, complete cds.	1.000	0.424	1.053	1.029
11291	M93651	Human set gene, complete cds.	0.889	0.468	0.898	0.946
15051	NM_005113	golgi autoantigen, golgin subfamily a, 5	1.342	0.474	1.670	2.311
5379	AK025256	Human cDNA: FLJ21603 fis, clone COL07238.	1.000	0.720	1.011	0.986

4941	AL136699	Human mRNA; cDNA DKFZp564I1782 (from clone DKFZp564I1782); complete cds.	1.291	0.426	1.580	1.028
18158	BG387891	enoyl Coenzyme A hydratase, short chain, 1, mitochondrial	1.068	0.730	0.870	1.215
15225	BG261319	transducer of ERBB2, 1	1.145	0.410	1.629	1.057
5222	AF037447	Human ribosomal S6 protein kinase mRNA, complete cds.	1.681	0.349	0.823	0.880
11116	AL136721	Human mRNA; cDNA DKFZp566K1946 (from clone DKFZp566K1946); complete cds.	1.156	0.738	0.903	1.010
7199	AL556984	transmembrane 7 superfamily member 2	1.196	0.326	0.546	1.076
11628	S56805	preproendothelin 1 {alternatively transcribed} [Human, placenta, mRNA, 1251 nt].	1.033	0.338	1.384	1.232
11599	AF041432	Human bet3 (BET3) mRNA, complete cds.	1.026	0.345	1.116	0.868
7913	BAB23139	putative	1.188	0.736	1.021	0.906
15238	AB044807	PDZ domain protein (Drosophila inaD-like)	0.982	0.733	0.936	1.037
11338	BAA07650	sulfate transporter	0.787	0.356	0.998	0.895
14594	BC011568	Human, endoplasmic reticulum chaperone SIL1, homolog of Yeast, clone MGC:20202 IMAGE:4640182, mRNA, complete cds.	1.220	0.729	0.892	1.086
13435	BG257096	adenosine deaminase	0.903	0.731	1.233	1.187
8615	AK024146	Human cDNA FLJ14084 fis, clone HEMBB1002383.	1.388	0.367	1.247	0.858
16319	AB028971	Human mRNA for KIAA1048 protein, complete cds.	0.973	0.389	0.796	1.374
3625	BAB22250	putative	0.945	0.408	0.930	1.041
17834	AJ293866	Human mRNA for FNK serine/threonine protein kinase.	1.109	0.408	0.765	0.833
2776	U46571	DnaJ (Hsp40) homolog, subfamily C, member 7	1.087	0.500	1.020	2.711
13010	AL137370	Human mRNA; cDNA DKFZp434H2226 (from clone DKFZp434H2226); partial cds.	1.177	0.714	1.108	0.863
9549	M38258	Human retinoic acid receptor gamma 1 mRNA, complete cds.	0.908	0.513	1.242	0.927
14939	AA737180	cofactor required for Sp1 transcriptional activation, subunit 2 (150kD)	0.952	0.519	1.012	2.102
5218	AF182423	Human MDS024 (MDS024) mRNA, complete cds.	0.980	0.695	1.102	0.921
10332	L38935	Homo sapiens GT212 mRNA	1.239	0.639	1.004	0.942
6264	U48296	Human protein tyrosine phosphatase PTPCAAX1 (hPTPCAAX1) mRNA, complete cds.	1.041	0.635	0.906	1.090
13509	BE812844	transcription elongation factor A (SII), 1	0.897	0.637	1.343	1.287
5722	NM_004906	Wilms' tumour 1-associating protein	0.889	0.694	1.169	1.936
9481	AJ302068	Human HSPB9 gene for small heat shock protein B9.	0.954	0.697	1.220	0.887
16001	J03870	Human cystatin SA-I mRNA, complete cds.	1.327	0.694	0.783	1.235

14555	AAH07256	Unknown (protein for MGC:15514)	1.178	0.647	1.057	0.850
8831	BG258940	phosphotidylinositol transfer protein, beta	1.057	0.628	0.993	1.178
12871	AB022017	Human mRNA for AMP-activated protein kinase alpha-1, complete cds.	0.918	0.663	1.020	0.958
7193	BG768698	homeo box A4	1.053	0.670	1.089	0.940
13763	U22512	conserved helix-loop-helix ubiquitous kinase	1.055	0.692	0.875	1.104
16751	AU121122	suppressor of Ty (S.cerevisiae) 6 homolog	1.321	0.691	0.840	1.243
10102	AB007856	Human KIAA0396 mRNA, partial cds.	1.148	0.652	1.187	0.974
5803	AB044947	NDRG family, member 4	1.210	0.657	0.966	0.911
6728	D30756	Human mRNA for KIAA0049 gene, complete cds.	1.241	0.633	0.966	1.541
5726	AI968278	peroxisome proliferative activated receptor, delta	0.918	0.628	0.972	0.921
3209	AF035606	Human calcium binding protein (ALG-2) mRNA, complete cds.	1.011	0.538	0.899	0.986
4416	AB033823	tektin 2 (testicular)	1.056	0.677	1.079	1.007
7079	NM_014003	pre-mRNA splicing factor similar to S. cerevisiae Prp16	1.226	0.556	1.325	1.076
7518	M58459	ribosomal protein S4, Y-linked	0.938	0.544	1.245	0.870
11109	AF135794	Human AKT3 protein kinase mRNA, complete cds.	1.305	0.554	1.103	0.885
8932	BC001746	protein tyrosine phosphatase, non-receptor type 7	0.819	0.574	1.299	1.145
10471	AW150631	stem-loop (histone) binding protein	1.238	0.542	1.012	1.094
8157	AAF03128	F-box protein FBL2	0.853	0.557	1.197	1.104
7371	AF068266	core-binding factor, runt domain, alpha subunit 2; translocated to, 2	1.177	0.575	0.927	1.172
4249	BG765209	ring finger protein 10	1.044	0.628	1.438	0.750
6349	AB055286	Macaque brain cDNA, clone:QflA-11789.	1.461	0.626	0.904	1.791
14408	AK025398	Human cDNA: FLJ21745 fis, clone COLF5038.	1.160	0.699	1.178	1.346
12814	AB018271	Human mRNA for KIAA0728 protein, partial cds.	1.265	0.613	0.913	1.462
10999	S85655	prohibitin [Human, mRNA, 1043 nt].	1.261	0.622	1.150	0.999
11619	J03077	Human co-beta glucosidase (proactivator) mRNA, complete cds.	1.199	0.585	1.179	1.135
8606	AI422208	SH3 domain binding glutamic acid-rich protein	1.330	0.601	0.909	1.135
9853	AF007189	Human claudin 3 (CLDN3) gene, complete cds.	1.121	0.669	0.956	1.421
3520	BAB47409	MEGF10 protein (KIAA1780)	1.014	0.180	1.031	0.712
16600	BG236381	NADH dehydrogenase (ubiquinone) 1 alpha subcomplex, 9 (39kD)	0.974	0.747	1.129	1.247
6355	M74099	Human displacement protein (CCAAT) mRNA.	1.182	0.745	0.936	1.125
15684	D67029	Human SEC14L mRNA, complete cds.	1.088	0.748	0.848	1.129
11286	L48722	Human (clone hh18) protein tyrosine phosphatase (ptp-IV1r) gene, 5' end of cds.	0.882	0.749	0.888	1.105

6711	AL136626	Human mRNA; cDNA DKFZp564C012 (from clone DKFZp564C012); complete cds.	1.164	0.743	1.027	1.162
7195	AK027886	CGI-01 protein	1.128	1.771	1.030	1.219
6261	D29641	Human mRNA for KIAA0052 protein, partial cds.	1.192	1.737	1.314	0.838
9869	AF089745	Human FK506-binding protein (FKBP63) mRNA, partial cds.	2.117	1.995	0.804	0.980
4784	BC003698	Human, clone MGC:5601 IMAGE:3461017, mRNA, complete cds.	1.037	1.552	1.084	0.975
5672	BC004151	tyrosyl-tRNA synthetase	1.742	1.518	1.047	1.057
7037	AL570066	fibulin 5	1.766	1.955	0.970	0.731
18004	BC009345	Human, clone MGC:16749 IMAGE:4130844, mRNA, complete cds.	1.198	2.314	1.425	1.311
10486	BG763361	gelsolin (amyloidosis, Finnish type)	1.405	2.608	1.331	0.958
13382	BG697126	calpain 1, (mu/I) large subunit	1.605	1.477	1.146	0.868
7192	BE892211	putative glialblastoma cell differentiation-related	1.564	1.306	0.938	1.045
14267	AJ245599	Human mRNA for putative secreted ligand (fjx1 gene homologue).	1.355	2.292	1.378	0.822
13831	BE730977	low density lipoprotein-related protein-associated protein 1 (alpha-2-macroglobulin receptor-associated protein 1)	1.646	1.740	0.995	1.009
11651	CAC28982	bA243J16.9 (novel protein similar to Interferon regulatory factor (transcriptional regulator))	1.234	1.760	1.095	0.937
16167	AB037799	Human mRNA for KIAA1378 protein, partial cds.	1.039	2.113	1.174	0.959
16759	BI825951	zyxin	1.524	1.459	1.079	1.150
14124	AB056806	Macaque brain cDNA clone:QflA-13812, full insert sequence.	1.512	1.579	0.998	1.057
3213	BC001118	Human, Similar to seven transmembrane domain protein, clone MGC:1936 IMAGE:2989840, mRNA, complete cds.	1.124	2.214	1.499	0.880
11918	BC001636	ATP-binding cassette, sub-family C (CFTR/MRP), member 1	1.924	1.672	1.688	0.758
5102	BC002862	Human, Similar to aldo-keto reductase, clone MGC:10612 IMAGE:3941289, mRNA, complete cds.	0.982	1.740	1.120	0.769
3474	BC004821	Human, diaphorase (NADH) (cytochrome b-5 reductase), clone MGC:5150 IMAGE:3450773, mRNA, complete cds.	1.911	1.766	0.687	0.999
12199	BF868865	erythrocyte membrane protein band 4.1 (elliptocytosis 1, RH-linked)	1.256	1.673	0.852	1.040
10666	J03210	matrix metalloproteinase 2 (gelatinase A, 72kD gelatinase, 72kD type IV collagenase)	2.297	1.794	1.171	1.145
5827	BF725116	SEX gene	2.238	1.609	0.985	1.142
11424	CAC41174	unnamed protein product	1.069	2.650	1.201	0.900
12235	AB002323	dynein, cytoplasmic, heavy polypeptide 1	2.584	2.663	0.999	1.049
10245	BG260215	KIAA0013 gene product	1.048	1.574	1.016	0.949

14895	AP000503	Human genomic DNA, chromosome 6p21.3, HLA Class I region, section 2/20.	1.340	1.672	1.166	1.031
5801	BM008239	DEAD/H (Asp-Glu-Ala-Asp/His) box polypeptide 24	1.206	1.695	1.354	0.867
7428	BG431313	stromal cell-derived factor 2	1.560	1.557	1.133	0.912
8161	M12128	Human cytoskeletal tropomyosin isoform (2.5 kb) mRNA, 3' end.	1.381	1.538	1.259	1.151
5596	AB002806	Human OS-9 mRNA, complete cds.	1.880	1.847	1.048	1.060
12061	BG741096	nitric oxide synthase 3 (endothelial cell)	1.166	4.081	1.158	0.895
11460	AP003113	Human genomic DNA, chromosome 8q23, clone:KB1747F8.	1.873	1.861	1.692	0.992
11884	BC003575	mannosyl (alpha-1,3-)-glycoprotein beta-1,2-N-acetylglucosaminyltransferase	1.334	1.600	1.031	0.906
4414	BI822721	gp25L2 protein	1.657	1.841	0.888	1.098
6037	BE798151	guanine nucleotide binding protein-like 1	1.259	1.814	0.974	1.476
4428	BF671958	malate dehydrogenase 1, NAD (soluble)	1.007	1.713	0.887	1.186
18175	U24576	LIM domain only 4	1.520	1.382	0.907	0.985
10994	BC006313	Human, musculin (activated B-cell factor-1), clone MGC:12624 IMAGE:4123825, mRNA, complete cds.	1.357	1.525	0.886	1.023
14257	BC004868	Human, clone MGC:10702 IMAGE:3833242, mRNA, complete cds.	1.157	1.560	0.933	0.842
10473	BC008813	annexin A8	1.136	1.545	1.010	1.208
14417	AJ007610	Human mRNA for protocadherin alpha 9 (PCDHA9 gene).	0.892	0.432	1.325	0.847
4095	N92498	Homo sapiens mRNA; cDNA DKFZp564H2416 (from clone DKFZp564H2416)	0.657	0.629	0.773	1.249
8181	AB014547	Human mRNA for KIAA0647 protein, partial cds.	0.777	0.677	1.712	0.852
12198	AW968138	seven in absentia (Drosophila) homolog 1	0.897	0.696	1.700	0.904
3485	AB070098	Macaque testis cDNA clone:QtsA-13672, full insert sequence.	0.679	0.647	1.091	0.950
17529	M68956	Human myristoylated alanine-rich C-kinase substrate mRNA, complete cds.	0.587	0.879	1.479	1.155
8638	BG766412	replication factor C (activator 1) 5 (36.5kD)	0.672	0.873	1.169	0.917
7607	BI818571	suppression of tumorigenicity 7	0.733	0.861	1.150	0.923
10204	U13695	Human homolog of Yeast mutL (hPMS1) gene, complete cds.	0.680	0.806	0.910	1.042
14909	NM_003968	ubiquitin-activating enzyme E1C (homologous to yeast UBA3)	1.054	0.633	1.322	0.866
11099	AK027344	Human cDNA FLJ14438 fis, clone HEMBB1000317, weakly similar to FIBULIN-1, ISOFORM D PRECURSOR.	0.694	0.710	1.380	0.966
11957	BG676784	CDK2-associated protein 1	1.187	0.658	1.170	1.134
6914	BC007655	Human, protein phosphatase 1, regulatory (inhibitor) subunit 2, clone MGC:1327 IMAGE:3346573, mRNA, complete cds.	1.029	0.700	1.069	1.122

4107	BG251495	splicing factor proline/glutamine rich (polypyrimidine tract-binding protein-associated)	0.889	0.652	1.285	1.011
16781	AI022747	hypothetical protein MGC12904	0.932	0.707	1.065	0.865
14277	AF112219	Human esterase D mRNA, complete cds.	0.709	0.684	1.116	0.935
15342	AA523378	proliferating cell nuclear antigen	0.550	0.687	1.105	0.775
12703	AK001559	Human cDNA FLJ10697 fis, clone NT2RP3000527, weakly similar to ZINC FINGER PROTEIN 43.	0.739	0.626	1.494	1.193
4405	BG333934	replication protein A2 (32kD)	0.771	0.620	0.997	1.130
13419	BG765030	ribosomal protein S16	0.868	0.526	1.126	0.688
14266	AL133047	Human mRNA; cDNA DKFZp434D0215 (from clone DKFZp434D0215); partial cds.	0.695	0.813	1.300	0.900
11907	BG939578	ubiquitin carboxyl-terminal esterase L3 (ubiquitin thiolesterase)	0.727	0.703	1.225	0.861
9886	J05096	Human Na,K-ATPase subunit alpha 2 (ATP1A2) gene, complete cds.	0.940	0.662	1.249	0.891
16607	U53445	downregulated in ovarian cancer 1	0.720	0.818	1.079	1.127
2517	D90277	carcinoembryonic antigen-related cell adhesion molecule 3	1.034	0.742	1.268	0.744
11798	AK023133	Human cDNA FLJ13071 fis, clone NT2RP3001792, moderately similar to HETEROGENEOUS NUCLEAR RIBONUCLEOPROTEIN M.	0.802	0.653	1.887	0.627
9555	BC000859	Human, clone IMAGE:3459481, mRNA, partial cds.	0.841	0.735	1.102	0.962
13825	AB011125	KIAA0553 protein	0.783	0.570	1.327	0.937
5019	U37688	Human RATS1 mRNA, complete cds.	0.729	0.782	1.214	1.188
8777	BF797654	chromosome 21 open reading frame 4	1.132	0.569	1.573	1.043
1032	BE253911	H2A histone family, member N	0.647	0.901	1.245	0.950
5562	AK023160	hypothetical protein FLJ10509	0.897	0.587	1.402	0.963
13174	AF309033	Human tankyrase-2 (TNKS-2) mRNA, complete cds.	0.737	0.769	1.240	0.940
16008	M60315	Human transforming growth factor-beta BMP protein (tgf-beta) mRNA, complete cds.	0.747	0.511	1.294	0.643
3933	BC014621	asparagine synthetase	0.742	0.969	1.138	0.984
7440	NM_014725	KIAA0189 gene product	0.917	0.741	1.279	1.070
5025	D10583	Human mRNA for IgE receptor beta subunit, complete cds.	0.979	1.532	0.921	0.858
13674	BG775483	junction plakoglobin	1.116	1.645	1.561	0.772
10013	D25545	Human mRNA for PIMT isozyme I, complete cds.	1.048	1.890	1.230	0.529
12987	AAF51854	CG11367 gene product	1.261	1.490	0.981	0.733
16591	AF006513	chromodomain helicase DNA binding protein 1	0.718	1.393	0.874	0.770
11920	AF241850	ret finger protein 2	0.793	1.779	0.946	0.697
15337	NM_006643	serologically defined colon cancer antigen 3	1.394	1.913	0.885	0.830
11775	L34209	Human clone DMPC-HFF1-1415B prostaglandin synthase-2 (PGHS-2) gene, promoter region.	1.019	1.873	1.008	0.607
15966	AAF47301	BcDNA:GH03108 gene product	1.160	1.364	0.921	0.608

11246	M93650	Human paired box gene (PAX6) homologue, complete cds.	1.138	2.662	0.917	0.484
10383	BG169146	ribosomal protein S14	1.111	1.716	0.983	0.814
5720	AL574109	procollagen-proline, 2-oxoglutarate 4-dioxygenase (proline 4-hydroxylase), alpha polypeptide I	0.955	1.797	0.668	0.680
10302	AF064087	cullin 3	1.031	1.797	0.914	0.720
13824	BF796127	vacuolar protein sorting 45B (yeast homolog)	1.334	1.253	0.693	0.703
15004	NM_014693	KIAA0604 gene product	0.836	1.528	1.253	0.894
7516	BM009356	general transcription factor IIF, polypeptide 1 (74kD subunit)	0.852	1.589	1.182	0.810
11906	BF808164	SWI/SNF related, matrix associated, actin dependent regulator of chromatin, subfamily f, member 1	1.029	1.525	0.946	0.599
13321	AW969737	basic leucine zipper nuclear factor 1 (JEM-1)	0.950	1.516	1.317	0.703
6026	U15782	cleavage stimulation factor, 3' pre-RNA, subunit 3, 77kD	1.234	1.561	0.898	0.909
11192	AB035207	Human mRNA for Tob2, complete cds.	0.978	1.823	0.935	0.893
7504	D14533	xeroderma pigmentosum, complementation group A	1.240	1.987	0.917	0.782
9789	AF189251	Human cytomegalovirus partial fusion receptor mRNA, partial cds.	0.916	1.588	0.760	0.837
16734	BE644965	ESTs, Weakly similar to JC5314 CDC28/cdc2-like kinase associating arginine-serine cyclophilin [H.sapiens]	0.766	1.668	1.004	0.846
16601	AV705674	synaptosomal-associated protein, 23kD	1.039	1.543	1.059	0.791
10060	D28235	Human PTGS2 gene for prostaglandin endoperoxide synthase-2, complete cds.	0.954	2.071	1.088	0.814
43	AAC84147	tuftelin	1.062	1.745	0.863	0.814
4173	BG338004	ubiquinol-cytochrome c reductase (6.4kD) subunit	1.114	3.374	0.948	0.695
14238	AF205075	Human organic anion transporter polypeptide-related protein 4 (OATPRP4) mRNA, complete cds.	1.010	1.508	1.225	0.938
5958	AI110630	myeloid/lymphoid or mixed-lineage leukemia (trithorax (Drosophila) homolog); translocated to, 3	0.881	1.544	1.377	0.792
6892	BC002775	Human, Similar to CG9602 gene product, clone MGC:3733 IMAGE:3619626, mRNA, complete cds.	0.755	1.852	1.121	0.879
15223	AL535015	ubiquinol-cytochrome c reductase core protein II	0.926	1.757	0.936	0.887
8485	AP003480	Human genomic DNA, chromosome 8q23, clone: KB1970H2.	1.172	1.212	1.030	0.734
12032	BI333047	Human D9 splice variant A mRNA, complete cds	0.934	1.548	0.917	0.878
4427	BC005127	adipose differentiation-related protein	0.884	2.161	0.902	0.822
10168	AA122155	kinesin family member 3C	1.341	1.571	0.722	0.594
13615	BE538296	cytochrome c oxidase subunit Va	0.816	1.536	0.890	0.910
11260	U72245	Human phospholemman chloride channel mRNA, complete cds.	1.096	1.807	1.081	0.752

10100	AL136888	Human mRNA; cDNA DKFZp434P1672 (from clone DKFZp434P1672); complete cds.	1.311	1.343	0.779	0.697
8477	M58342	Human iduronate 2-sulfatase mRNA, complete cds.	1.146	1.356	0.915	0.747
13207	AB049054	Human BRAL1 mRNA for brain link protein-1, complete cds.	0.972	1.308	0.891	0.706
8800	BC002390	etoposide-induced mRNA	0.795	2.380	0.893	0.635
12693	AB020880	Human mRNA for squamous cell carcinoma antigen SART-3, complete cds.	0.967	2.311	1.428	0.652
7448	BI911036	tumor necrosis factor receptor superfamily, member 14 (herpesvirus entry mediator)	1.164	2.240	0.973	0.654
17838	AF112227	Human TDE homolog mRNA, complete cds.	1.275	1.583	0.954	0.898
14111	AL050144	Human mRNA; cDNA DKFZp586C1620 (from clone DKFZp586C1620); partial cds.	0.769	1.863	0.734	0.755
7595	BG762583	protein tyrosine phosphatase, non-receptor type substrate 1	1.017	1.540	0.875	0.894
11467	BC002466	Human, v-raf murine sarcoma 3611 viral oncogene homolog 1, clone MGC:2356 IMAGE:3347509, mRNA, complete cds.	1.254	2.041	0.909	0.862
11745	BF110337	low density lipoprotein receptor-related protein 8, apolipoprotein e receptor	1.610	2.240	1.175	0.854
5329	AF112210	Human heat shock protein hsp70-related protein mRNA, complete cds.	0.748	0.922	0.930	1.088
7842	AP001670	Human genomic DNA, chromosome 21q, section 14/105.	0.703	1.155	0.931	0.994
7398	AW514303	ESTs, Highly similar to I51803 TAXREB107 [H.sapiens]	0.671	0.921	0.992	1.030
16274	BC003554	Human, ubiquitin-conjugating enzyme E2E 3 (homologous to Yeast UBC4/5), clone MGC:1316 IMAGE:3537280, mRNA, complete cds.	0.626	0.865	0.867	0.835
17241	AK001106	Human cDNA FLJ10244 fis, clone HEMBB1000632, weakly similar to GUANINE NUCLEOTIDE RELEASING PROTEIN.	0.648	1.281	1.172	1.088
13315	M86699	TTK protein kinase	0.533	0.903	0.915	1.072
6507	J04111	Human c-jun proto oncogene (JUN), complete cds, clone hCJ-1.	0.555	0.906	0.544	0.985
8791	BG574227	H-2K binding factor-2	0.718	1.080	0.952	0.968
13012	BC004975	Human, cyclin I, clone MGC:3795 IMAGE:2957878, mRNA, complete cds.	0.732	1.145	0.882	1.284
3962	BI492241	ESTs, Highly similar to TBCA_HUMAN TUBULIN-SPECIFIC CHAPERONE A [H.sapiens]	0.692	1.179	0.946	0.916
12801	AF032862	Human intracellular hyaluronic acid binding protein (IHABP) mRNA, complete cds.	0.423	1.144	0.908	0.988
2782	BF795918	topoisomerase (DNA) II alpha (170kD)	0.436	1.119	1.004	1.367
4067	AW779701	aquaporin 7	0.718	1.263	0.972	1.343

10161	AF199339	Human lens epithelium-derived growth factor gene, alternatively spliced, complete cds.	0.683	1.160	1.197	1.098
13583	NM_014000	vinculin	0.512	1.106	0.828	0.632
15652	AF334735	Human sperm protein 17 mRNA, complete cds.	0.721	1.103	0.946	1.015
16575	AC004969	six transmembrane epithelial antigen of the prostate	0.697	0.820	0.886	1.121
15780	BC000474	Human, quinone oxidoreductase homolog, clone MGC:8642 IMAGE:2961571, mRNA, complete cds.	0.567	0.903	0.815	0.822
17497	AK023115	Human cDNA FLJ13053 fis, clone NT2RP3001459.	0.606	1.116	1.185	0.905
9127	BG198322	brain and reproductive organ-expressed (TNFRSF1A modulator)	0.724	1.260	0.779	0.902
10335	AI478561	dual specificity phosphatase 11 (RNA/RNP complex 1-interacting)	0.698	0.887	0.950	0.920
16922	BE739599	peroxiredoxin 3	0.732	1.038	0.927	1.211
13457	AI042585	S-adenosylmethionine decarboxylase 1	0.662	1.171	1.066	0.871
13835	AY007110	putative human HLA class II associated protein I	0.543	1.029	0.945	0.948
8839	AB014522	CLIP-associating protein 1	0.712	0.992	0.733	1.004
13481	AI687946	PDZ and LIM domain 1 (elfin)	0.436	0.945	0.848	0.931
8368	AK024809	Human cDNA: FLJ21156 fis, clone CAS09878.	0.307	1.171	0.910	1.875
9941	U78027	Human Bruton's tyrosine kinase (BTK), alpha-D-galactosidase A (GLA), L44-like ribosomal protein (L44L) and FTP3 (FTP3) genes, complete cds.	0.669	1.030	1.003	1.238
12196	NM_014736	KIAA0101 gene product	0.445	1.574	0.904	1.155
1340	AB011166	KIAA0594 protein	0.659	0.939	0.868	1.051
10397	AI925424	calcium/calmodulin-dependent protein kinase kinase 2, beta	0.652	0.791	1.011	1.140
13776	BC001350	arginase, type II	0.580	1.005	0.859	0.962
10644	BC000418	ectodermal-neural cortex (with BTB-like domain)	0.354	1.026	1.034	0.932
7046	AA738354	cleavage and polyadenylation specific factor 5, 25 kD subunit	0.700	1.012	0.871	1.284
14263	BC000633	Human, TTK protein kinase, clone MGC:865 IMAGE:3343925, mRNA, complete cds.	0.550	0.826	0.886	1.313
181	D00210	Human gene for thrombomodulin precursor, complete cds.	0.600	0.943	0.823	1.077
1197	BF183143	serine/threonine kinase 12	0.692	0.952	0.948	1.036
3798	AF264785	Human hairy (HRY) mRNA, complete cds.	0.746	0.879	0.920	1.204
11934	AL520473	cell division cycle 2, G1 to S and G2 to M	0.380	0.844	0.915	0.929
3946	AU152618	DEK oncogene (DNA binding)	0.537	1.347	0.978	1.649
15222	AA724155	Homo sapiens cDNA: FLJ23324 fis, clone HEP12482, highly similar to HUMMYOHCB Human nonmuscle myosin heavy chain-B (MYH10) mRNA	0.604	0.742	0.918	0.910
7362	NM_002188	interleukin 13	0.689	0.932	1.074	0.920
12234	AI636026	leukotriene A4 hydrolase	0.628	0.953	0.801	0.995

13801	BF977892	SWI/SNF related, matrix associated, actin dependent regulator of chromatin, subfamily b, member 1	0.679	1.076	0.839	1.110
6456	AJ006266	Human mRNA for AND-1 protein.	0.689	0.861	0.879	0.892
6881	AF046001	Human zinc finger transcription factor (ZNF207) mRNA, complete cds.	0.649	0.970	0.918	1.175
9572	AF294842	Human ubiquitin UBF-fl mRNA, complete cds.	0.627	0.982	0.878	1.002
4931	U56387	Human protease PC6 isoform A (PCSK5) mRNA, complete cds.	0.747	1.071	1.076	1.001
10188	AB020863	Human genomic DNA of 8p21.3-p22 anti-oncogene of hepatocellular colorectal and non-small cell lung cancer , segment 6/11.	2.398	0.893	1.146	0.974
3460	D90279	Human mRNA for collagen alpha 1(V) chain, complete cds.	1.601	1.006	0.957	0.907
11239	AK000753	Human cDNA FLJ20746 fis, clone HEP06040.	1.560	1.007	0.926	0.767
14871	BG777366	interleukin 8	5.622	1.469	0.851	0.144
6712	BC002735	Human, dihydrolipoamide S-succinyltransferase (E2 component of 2-oxo-glutarate complex), clone MGC:3898 IMAGE:3627724, mRNA, complete cds.	1.720	1.013	0.957	0.675
16028	BC007063	Human, peroxiredoxin 1, clone MGC:12514 IMAGE:3961375, mRNA, complete cds.	4.178	1.462	0.819	0.586
16118	M21533	Human MHC class I lymphocyte antigen (HLA-E) (HLA-6.2) gene, complete cds.	2.748	0.989	0.987	0.474
13025	BC000452	Human, Similar to thioredoxin peroxidase 1, clone MGC:8456 IMAGE:2821457, mRNA, complete cds.	1.939	0.767	0.867	0.866
16109	U60644	Human HU-K4 mRNA, complete cds.	1.538	0.788	0.837	0.918
9131	AL567017	solute carrier family 3 (activators of dibasic and neutral amino acid transport), member 2	1.320	0.799	1.032	0.689
15056	BG424817	heat shock 70kD protein 9B (mortalin-2)	1.654	0.774	0.912	0.853
4759	BC000693	Human, ARP1 (actin-related protein 1, Yeast) homolog A (centractin alpha), clone MGC:2357 IMAGE:3347881, mRNA, complete cds.	1.715	0.648	0.787	0.965
10522	BG699149	myosin, heavy polypeptide 9, non-muscle	2.108	0.980	0.901	0.726
9121	AL552738	tumor differentially expressed 1	1.813	1.148	0.907	0.894
7279	BC012746	mesoderm development candidate 2	1.387	0.721	0.959	0.714
12033	BI908045	integrin beta 4 binding protein	1.519	1.242	0.922	0.905
10525	AU132321	guanine nucleotide binding protein (G protein), alpha inhibiting activity polypeptide 1	1.681	1.002	1.021	0.953
4078	BI553471	isocitrate dehydrogenase 3 (NAD+) beta	1.502	0.994	1.002	0.792
4258	BG708735	ras homolog gene family, member C	2.286	0.753	1.030	1.017
16178	AF068863	Human oligodendrocyte-specific protein (OSP) mRNA, complete cds.	2.415	1.078	0.881	0.694

10514	U76368	solute carrier family 7 (cationic amino acid transporter, y+ system), member 2	2.460	1.056	1.159	0.879
9557	M94345	Human macrophage capping protein mRNA, complete cds.	2.100	0.915	0.969	0.801
13597	AB007851	phosphoribosyl pyrophosphate synthetase-associated protein 2	1.677	0.916	1.269	0.815
16116	AB032261	Human Scd mRNA for stearoyl-CoA desaturase, complete cds.	1.777	0.934	0.958	0.643
7345	AU139931	core promoter element binding protein	2.195	0.660	1.053	0.887
3392	L35263	Human CSaids binding protein (CSBP1) mRNA, complete cds.	1.593	0.807	0.921	0.909
14759	AAC25584	aortic carboxypeptidase-like protein ACLP	2.591	1.190	0.911	0.473
12202	BF981829	myosin, light polypeptide 1, alkali; skeletal, fast	1.969	0.763	0.970	0.945
11913	BC006169	SH3-domain binding protein 5 (BTK-associated)	1.647	1.330	0.744	0.845
15052	BE790900	palmitoyl-protein thioesterase 2	1.576	1.087	1.139	0.879
6905	AF225896	Human tensin mRNA, complete cds.	1.420	1.072	0.874	0.650
14079	AK027263	Human cDNA FLJ14357 fis, clone HEMBA1000005, highly similar to DNAJ PROTEIN HOMOLOG MTJ1.	1.546	0.928	0.978	0.746
16764	AL530764	RAB4, member RAS oncogene family	1.399	0.935	0.900	0.746
14580	BC009384	Human, Similar to chromogranin A (parathyroid secretory protein 1), clone IMAGE:4127895, mRNA, partial cds.	1.624	1.039	0.955	0.956
6281	AB002313	Human mRNA for KIAA0315 gene, partial cds.	1.895	1.121	1.211	0.781
10336	AB014606	kinesin family member 1C	1.660	0.754	0.841	0.724
15392	BF689926	electron-transfer-flavoprotein, beta polypeptide	1.684	0.867	1.202	0.882
11800	AU121423	serine threonine protein kinase	2.592	0.939	0.674	0.937
4327	NM_000543	sphingomyelin phosphodiesterase 1, acid lysosomal (acid sphingomyelinase)	1.514	1.208	0.829	0.711
3321	AB054881	Human mRNA for Soluble-type polypeptide FZD4S, complete cds.	1.839	1.111	1.006	0.950
14743	AF061970	Human paired related homeobox protein (PRX2) mRNA, complete cds.	1.589	0.763	0.934	0.940
11749	BI596354	heme oxygenase (decycling) 1	2.851	1.250	0.728	0.917
7355	BC002502	putative breast adenocarcinoma marker (32kD)	1.526	0.927	0.921	0.818
12666	U29460	Human cytochrome b561 gene, exon 1.	1.405	0.912	0.725	0.926
1975	BC006247	Human, Similar to KRAB-zinc finger protein SZF1-1, clone IMAGE:3945618, mRNA, partial cds.	1.396	0.708	0.919	0.862
4002	AB006713	dihydropyrimidinase-like 4	1.551	0.936	1.011	0.750
6956	AF100759	Human transmembrane 4 superfamily protein mRNA, complete cds.	1.293	0.940	0.951	0.726
13295	M58018	Human beta-myosin heavy chain (MYH7) mRNA, complete cds.	1.355	1.657	1.983	0.916
12680	U28281	Human secretin receptor mRNA, complete cds.	0.971	1.258	1.688	1.119
16614	BG385746	pyrroline-5-carboxylate reductase 1	1.217	1.186	1.536	0.909

10622	AL574829	farnesyltransferase, CAAX box, alpha	1.049	1.598	1.266	1.729
9136	NM_003605	O-linked N-acetylglucosamine (GlcNAc) transferase (UDP-N-acetylglucosamine:polypeptide-N-acetylglucosaminyl transferase)	1.296	1.265	1.514	0.989
9727	D31885	Human mRNA for KIAA0069 gene, partial cds.	1.139	1.399	2.125	1.248
5422	D14710	Human mRNA for ATP synthase alpha subunit, complete cds.	1.039	1.715	1.412	1.047
16730	BG255394	prefoldin 4	0.781	1.388	1.602	0.942
7131	C06042	carcinoembryonic antigen-related cell adhesion molecule 7	0.982	1.955	1.497	1.303
11472	AP000009	Human genomic DNA of 21q22.2 Down Syndrome region, segment 2/13.	1.070	2.039	1.726	0.961
13667	AV756387	ribosomal protein L3	1.197	1.900	1.497	1.544
8829	BE926667	thousand and one amino acid protein kinase	1.026	1.574	1.327	1.075
12042	AL549846	TGFB-induced factor (TALE family homeobox)	1.263	1.509	1.760	0.945
12180	BG169279	G protein pathway suppressor 1	1.348	2.387	2.727	1.425
12977	AF286904	Human enhancer of polycomb 1 (EPC1) mRNA, complete cds.	1.177	1.929	1.866	0.983
14745	U77085	Human epithelial membrane protein (CL-20) mRNA, complete cds.	0.787	1.222	1.593	1.438
11871	BG575020	thyroid hormone receptor interactor 10	1.415	1.320	1.881	1.597
15988	CAA30534	cytokeratin 4 (408 AA)	0.930	1.751	1.488	1.022
13755	AL598805	Homo sapiens, clone MGC:12401 IMAGE:3933998, mRNA, complete cds	1.332	1.122	1.677	1.173
11474	AK001159	Human cDNA FLJ10297 fis, clone NT2RM1001074.	1.215	1.268	2.147	0.884
10961	BC009001	Human, 3-oxoacid CoA transferase, clone MGC:17088 IMAGE:4148643, mRNA, complete cds.	0.976	1.264	1.193	1.587
9888	AF061832	Human M4 protein deletion mutant mRNA, complete cds.	0.945	0.777	1.107	1.607
5725	BG779717	Homo sapiens cDNA: FLJ21814 fis, clone HEP01068	1.105	0.848	1.271	1.579
2624	AW025893	lymphotoxin beta (TNF superfamily, member 3)	0.929	1.437	1.151	1.817
13634	AL557298	serine hydroxymethyltransferase 2 (mitochondrial)	1.372	1.411	0.965	1.877
7496	BG183465	proteasome (prosome, macropain) subunit, alpha type, 1	0.883	1.248	1.080	2.256
10034	BC001380	Human, succinate dehydrogenase complex, subunit A, flavoprotein (Fp), clone MGC:1484 IMAGE:3051442, mRNA, complete cds.	1.012	1.407	0.773	2.145
13775	NM_002470	myosin, heavy polypeptide 3, skeletal muscle, embryonic	1.203	0.858	1.099	1.790
6422	AB027233	Human mRNA for membrane protein FOAP-12, complete cds.	1.060	0.871	1.353	1.816
10324	BG745129	KDEL (Lys-Asp-Glu-Leu) endoplasmic reticulum protein retention receptor 1	1.151	0.856	0.861	1.835
8297	AL137687	Human mRNA; cDNA DKFZp434M152 (from clone DKFZp434M152).	0.567	1.279	1.179	2.174

11768	BC011978	Human, Similar to RIKEN cDNA 1110018J12 gene, clone IMAGE:3865164, mRNA, partial cds.	1.518	1.293	1.624	2.068
8007	AL136919	Human mRNA; cDNA DKFZp586J1119 (from clone DKFZp586J1119); complete cds.	1.012	0.877	1.067	1.679
3766	U03272	Human fibrillin-2 mRNA, complete cds.	1.167	1.596	0.975	1.800
10370	AL544102	chromosome 11 open reading frame 13	1.052	1.122	1.002	1.567
6035	BE619835	growth arrest-specific 1	1.092	1.242	0.854	1.523
17697	AP000501	Human genomic DNA, chromosome 8p11.2, clone:91h23 to 9-41.	1.007	1.215	1.066	1.606
10183	BE266628	BCL2-antagonist of cell death	1.074	1.039	1.121	1.917
9847	AL117607	Human mRNA; cDNA DKFZp564N0763 (from clone DKFZp564N0763).	1.156	0.803	1.015	2.043
14276	AF003924	Human zinc finger protein ANC_2H01 mRNA, complete cds.	0.713	0.720	1.242	1.669
10981	L47345	Human elongin A mRNA, complete cds.	0.817	1.027	1.102	1.569
10472	AL519675	arsA (bacterial) arsenite transporter, ATP-binding, homolog 1	1.432	0.936	1.181	1.866
10682	BI870489	nidogen (enactin)	1.116	0.935	1.745	2.573
17233	M77171	Human zinc finger protein gene, partial cds.	1.225	1.010	1.136	1.629
13683	NM_005414	SKI-like	1.433	1.054	1.173	1.535
14158	AK000160	Human cDNA FLJ20153 fis, clone COL08656, highly similar to AJ001381 Human incomplete cDNA for a mutated allele.	1.111	1.086	1.122	1.684
8909	AL536237	tubulin, beta, 5	1.154	0.924	1.409	1.567
11936	AU131934	origin recognition complex, subunit 4 (yeast homolog)-like	0.904	0.761	1.377	1.818
9068	BE741277	protein with polyglutamine repeat; calcium (ca2+) homeostasis endoplasmic reticulum protein	1.009	1.013	1.238	1.538
3399	AF308285	Human serologically defined breast cancer antigen NY-BR-16 mRNA, complete cds.	1.375	1.006	1.148	1.623
3704	BC001348	Human, heterogeneous nuclear ribonucleoprotein H1 (H), clone MGC:8619 IMAGE:2961378, mRNA, complete cds.	0.949	0.836	1.398	1.593
4490	D76444	zinc finger protein homologous to Zfp103 in mouse	1.180	0.956	0.957	2.323
8023	U33635	Human colon carcinoma kinase-4 (CCK4) mRNA, complete cds.	1.231	0.968	0.959	1.636
8448	U23851	Human atrophin-1 mRNA, complete cds.	1.123	0.962	1.147	2.405
15312	BG163551	cerebral cavernous malformations 1	0.720	0.787	1.390	1.895
2742	AK027480	zinc finger protein 266	1.175	0.977	1.121	1.836
14847	NM_001393	extracellular matrix protein 2, female organ and adipocyte specific	1.295	0.980	1.148	1.603
12077	AW469468	palmitoyl-protein thioesterase 2	0.995	1.005	1.148	2.728
16590	NM_000097	coproporphyrinogen oxidase (coproporphyria, harderoporphyria)	0.644	0.790	1.480	3.169
7285	AI088306	hypothetical protein FLJ23306	1.747	0.955	1.025	2.475

9528	AP000350	Human genomic DNA, chromosome 22q11.2, clone KB1125A3.	0.989	0.951	1.563	2.752
4464	NM_014459	protocadherin 17	0.940	0.950	1.504	1.841
11598	D86967	Human mRNA for KIAA0212 gene, complete cds.	1.071	0.912	1.027	2.864
4246	AB011085	KIAA0513 gene product	1.137	0.785	1.212	1.606
6032	BG825129	glypican 1	1.241	1.760	0.889	2.122
8968	BC015345	homeo box B7	1.117	1.149	1.123	1.892
13362	NM_016614	TRAF and TNF receptor-associated protein	1.245	1.698	1.140	2.304
17683	D85429	Human gene for heat shock protein 40, complete cds.	1.221	1.164	1.248	1.592
2924	BG506029	translocase of inner mitochondrial membrane 17 (yeast) homolog A	1.707	1.700	1.128	4.045
5719	BE217961	ets variant gene 6 (TEL oncogene)	0.836	1.127	1.199	2.005
17693	L00974	Human SP40,40 gene, exons 5-9.	1.270	0.892	1.217	1.729
14090	AB043587	Human gcp60 mRNA for golgi resident protein GCP60, complete cds.	0.764	1.201	1.308	1.618
16138	BC000612	Human, Similar to katanin p60 (ATPase-containing) subunit A 1, clone MGC:2599 IMAGE:3347282, mRNA, complete cds.	1.254	0.946	1.527	0.533
14750	M31211	Human myosin light chain 1 slow a (MLC1sa) mRNA, complete cds.	2.050	1.035	1.564	0.453
1355	AL532086	group-specific component (vitamin D binding protein)	1.204	1.460	1.116	0.592
16180	AK000852	Human cDNA FLJ20845 fis, clone ADKA01901.	1.528	1.153	1.449	0.829
3365	AF068755	Human sec7 domain family member (GBF1) mRNA, complete cds.	1.149	1.438	1.491	0.632
18032	AA641722	protein kinase C, alpha binding protein	0.996	1.019	1.204	0.668
13652	BE791502	clathrin, light polypeptide (Lcb)	1.769	1.267	1.065	0.782
882	BG824361	putative protein similar to nessy (Drosophila)	1.489	0.711	0.966	0.683
14237	BC001691	Human, holocytochrome c synthase (cytochrome c heme-lyase), clone MGC:1443 IMAGE:3030501, mRNA, complete cds.	1.794	1.156	1.405	0.876
10685	AW960243	neural precursor cell expressed, developmentally down-regulated 8	1.372	1.043	1.220	0.749
15398	BE856759	KIAA0138 gene product	1.559	1.173	1.327	0.804
13373	AL556109	mitogen-activated protein kinase kinase kinase 11	1.261	0.836	1.235	0.609
18461	D88674	ornithine decarboxylase antizyme inhibitor	1.375	0.965	1.527	0.899
12994	BC010155	Human, Similar to RIKEN cDNA B230118G17 gene, clone MGC:19604 IMAGE:3622817, mRNA, complete cds.	1.657	1.202	1.677	0.726
2826	AJ004832	neuropathy target esterase	1.356	0.975	0.970	0.596
7292	AL521557	p53-induced protein	1.220	1.188	0.897	0.693
14426	BC001900	Human, Similar to branched chain aminotransferase 2, mitochondrial, clone MGC:2082 IMAGE:3537603, mRNA, complete cds.	1.101	1.198	1.001	0.726
18485	AL546458	serine protease inhibitor, Kunitz type, 2	1.251	1.207	1.126	0.648

5797	NM_000702	ATPase, Na+/K+ transporting, alpha 2 (+) polypeptide	1.795	0.992	1.143	0.447
16611	BG674956	selenophosphate synthetase 2	1.245	1.001	1.390	0.740
6817	L06237	Human microtubule-associated protein 1B (MAP1B) gene, complete cds.	1.265	1.505	1.344	0.698
9945	AK000826	Human cDNA FLJ20819 fis, clone ADSE00511.	1.156	0.935	0.877	0.748
14941	AL548337	Homo sapiens cDNA FLJ10229 fis, clone HEMBB1000136	1.567	1.434	1.115	0.467
9902	AF265208	Human SWI-SNF complex protein p270 mRNA, partial cds.	1.540	0.815	1.202	0.707
10629	AL544994	myeloid/lymphoid or mixed-lineage leukemia (trithorax (Drosophila) homolog); translocated to, 7	1.679	1.360	1.181	0.748
5990	AL553335	N-ethylmaleimide-sensitive factor attachment protein, alpha	1.418	1.067	2.000	0.761
16309	BC000819	Human, Similar to CG6950 gene product, clone MGC:5114 IMAGE:3453829, mRNA, complete cds.	1.092	1.060	0.852	0.743
3141	AB014773	Human mRNA for MOP-4, complete cds.	2.039	1.296	1.055	0.630
11746	NM_019848	Protein P3	1.315	1.076	1.759	0.811
1195	BG283735	hypothetical protein	1.183	1.271	1.292	0.707
18009	AAA28530	fat protein	1.044	1.049	1.804	0.735
8985	BI713774	somatostatin	1.381	1.365	1.271	0.574
5570	L04284	Human germline HRX mRNA, complete cds.	0.854	1.751	1.084	0.881
11752	AL537232	hypothetical protein A-211C6.1	0.697	2.865	0.961	1.692
14382	D31883	Human mRNA for KIAA0059 gene, complete cds.	1.105	1.657	1.064	1.437
15227	AI924594	tetraspan 2	0.799	1.609	0.823	1.005
4017	BI859947	protein kinase, AMP-activated, gamma 1 non-catalytic subunit	0.931	2.441	1.100	0.837
9370	AB032957	Human mRNA for KIAA1131 protein, partial cds.	0.823	2.532	1.338	0.902
5959	AI656717	ESTs, Weakly similar to ubiquitous TPR motif, Y isoform [H.sapiens]	0.899	1.516	0.895	1.046
10467	BG165773	succinate dehydrogenase complex, subunit B, iron sulfur (Ip)	0.803	1.798	1.511	0.819
10186	BI496977	protein phosphatase 2, regulatory subunit B (B56), epsilon isoform	0.757	2.424	1.075	1.085
18311	AK001450	exostoses (multiple)-like 2	0.744	1.525	1.034	0.846
17875	U65090	Human carboxypeptidase D mRNA, complete cds.	0.846	2.384	1.081	0.968
7183	U67733	phosphodiesterase 2A, cGMP-stimulated	0.705	1.763	1.323	0.962
11277	AB058599	Human arpp mRNA for ankyrin-repeat protein, complete cds.	0.676	1.793	0.848	0.919
13778	AL558308	CD3E antigen, epsilon polypeptide (TiT3 complex)	0.893	3.488	1.019	0.792
9834	BC009200	Human, Rho GDP dissociation inhibitor (GDI) beta, clone MGC:15348 IMAGE:3621138, mRNA, complete cds.	0.767	4.369	1.148	0.934
4377	NM_021724	nuclear receptor subfamily 1, group D, member 1	0.760	1.669	0.957	1.011
7070	AL571412	RNA helicase-related protein	0.898	1.768	1.260	0.812

11183	AAC52262	neural cell adhesion protein BIG-2 precursor	0.885	1.768	0.919	0.971
3237	D38550	Human mRNA for KIAA0075 gene, partial cds.	0.868	1.538	1.009	1.014
10711	BI761480	laminin, alpha 2 (merosin, congenital muscular dystrophy)	0.864	2.955	1.370	0.822
8167	M27394	Human B-lymphocyte cell-surface antigen B1 (CD20).	1.038	1.675	0.970	1.127
8652	BF943707	RNA binding motif protein 14	0.767	1.665	1.320	0.978
3788	M28372	Human sterol regulatory element-binding protein (CNBP) mRNA, complete cds.	0.975	1.701	1.029	1.189
5561	AV649527	aldehyde dehydrogenase 1 family, member A1	0.856	1.802	0.996	1.310
12051	BG032793	ribosomal protein L37	0.744	2.165	1.036	1.059
18520	AL526053	cAMP responsive element modulator	0.710	2.166	0.941	1.078
7348	BC007831	phosphodiesterase 6D, cGMP-specific, rod, delta	0.617	1.329	1.290	1.155
10665	AL122062	chromosome 2 open reading frame 6	0.703	1.403	1.124	1.050
10343	AL079635	RNA polymerase II transcriptional regulation mediator (Med6, S. cerevisiae, homolog of)	0.767	1.580	0.930	0.938
6356	L23320	Human replication factor C large subunit mRNA, complete cds.	0.681	1.866	1.073	1.393
11959	BF676785	S-adenosylmethionine decarboxylase 1	0.747	2.042	1.129	0.889
11590	AF080157	Human IkB kinase-a (IKK-alpha) mRNA, complete cds.	0.952	1.904	1.015	1.103
3372	BC000697	Human, Similar to Male-specific RNA 84Dd, clone MGC:3092 IMAGE:3349383, mRNA, complete cds.	0.699	1.815	1.336	1.123
4419	BC012063	retinoid X receptor, gamma	0.783	1.964	0.976	0.950
8769	BG483858	actin related protein 2/3 complex, subunit 3 (21 kD)	1.007	1.945	1.243	1.034
7370	BI602406	3-hydroxyanthranilate 3,4-dioxygenase	1.034	1.942	0.913	1.446
16316	U67615	Human beige protein homolog (chs) mRNA, complete cds.	0.816	1.599	1.223	1.252
7555	BI756567	phosphodiesterase 3B, cGMP-inhibited	0.516	1.651	1.156	0.861
5812	L13858	son of sevenless (Drosophilia) homolog 2	0.926	1.710	0.970	1.203
5162	AF279370	Human DZIP3 mRNA, partial cds.	0.745	1.333	0.891	0.862
16422	D26350	Human mRNA for inositol 1,4,5-trisphosphate receptor type 2, complete cds.	1.005	2.133	1.245	1.775
2780	BF439351	hypothetical gene CG018	0.955	1.813	1.029	1.407
15831	BC005330	Human, tissue factor pathway inhibitor 2, clone MGC:12416 IMAGE:3929933, mRNA, complete cds.	0.948	1.501	1.225	1.355
12832	U76713	Human apobec-1 binding protein 1 mRNA, complete cds.	0.850	1.504	1.170	0.906
12838	BC001178	Human, ATP synthase, H+ transporting, mitochondrial F0 complex, subunit F6, clone MGC:2243 IMAGE:3357779, mRNA, complete cds.	0.803	1.614	1.255	1.282

17567	AF264014	Human scavenger receptor cysteine-rich type 1 protein M160 precursor, mRNA, complete cds, alternatively spliced.	0.899	0.824	0.811	0.718
3945	AI884353	mitochondrial translational release factor 1	0.855	0.807	0.963	0.728
13187	AF092905	Human protein phosphatase type-1 catalytic subunit delta isoform (PPCS1D) mRNA, complete cds.	0.877	0.802	0.922	0.573
8930	AF053755	solute carrier family 4, sodium bicarbonate cotransporter, member 7	0.807	0.816	1.144	0.678
8000	U17714	Human putative tumor suppressor ST13 (ST13) mRNA, complete cds.	0.874	0.536	0.951	0.240
11110	AK001364	Human cDNA FLJ10502 fis, clone NT2RP2000414, highly similar to Human HnRNP F protein mRNA.	0.766	0.788	0.890	0.645
13052	AF193612	Human fringe protein mRNA, partial cds.	1.046	0.804	0.867	0.681
12252	AI922645	origin recognition complex, subunit 2 (yeast homolog)-like	0.931	0.781	0.928	0.735
7583	M17754	BN51 (BHK21) temperature sensitivity complementing	0.915	0.833	0.883	0.638
11098	BAB22284	putative	1.026	0.825	1.036	0.343
6891	AL137751	Human mRNA; cDNA DKFZp434I0812 (from clone DKFZp434I0812); partial cds.	1.132	0.780	0.928	0.692
3774	AF117233	Human znf-xp protein mRNA, complete cds.	0.917	0.878	0.849	0.643
5050	AF251295	Human DC22 mRNA, complete cds.	1.024	1.026	0.957	0.538
11866	BC007506	checkpoint suppressor 1	0.895	1.187	0.998	0.550
3147	AJ278314	Human mRNA for phospholipase C-beta-1b (PLCB1 gene).	1.070	0.785	0.915	0.659
15690	AK024054	Human cDNA FLJ13992 fis, clone Y79AA1002139, weakly similar to DNAJ PROTEIN HOMOLOG 1.	0.965	1.028	1.044	0.620
16406	BG575502	phosphorylase, glycogen; brain	1.257	1.027	1.067	0.631
10502	U52828	catenin (cadherin-associated protein), delta 2 (neural plakophilin-related arm-repeat protein)	1.001	0.981	0.911	0.737
10222	U72518	Human destrin-2 pseudogene mRNA, complete cds.	1.081	0.883	0.804	0.736
6648	M13003	Human metallothionein (MT)I-F gene, complete cds.	1.001	1.202	0.919	0.742
5377	BAB01579	unnamed protein product	0.872	1.069	0.904	0.705
9560	L33881	Human protein kinase C iota isoform, complete cds.	0.752	1.170	1.195	0.197
16773	AB005659	ATP-binding cassette, sub-family C (CFTR/MRP), member 5	1.045	1.097	0.886	0.680
14120	BC000905	Human, RAB1, member RAS oncogene family, clone MGC:5233 IMAGE:2900705, mRNA, complete cds.	1.213	1.210	0.864	0.660
14245	AF103796	Human placenta-specific ATP-binding cassette transporter (ABCP) mRNA, complete cds.	1.247	1.230	1.069	0.226
12672	AK001148	Human cDNA FLJ10286 fis, clone HEMBB1001384, highly similar to Human COP9 complex subunit 4 mRNA.	0.834	1.021	0.924	0.489

9108	BE566830	sperm associated antigen 9	1.126	1.250	1.067	0.730
12251	BG829032	eukaryotic translation initiation factor 3, subunit 7 (zeta, 66/67kD)	1.328	1.172	0.925	0.555
10941	L44140	Human chromosome X region from filamin (FLN) gene to glucose-6-phosphate dehydrogenase (G6PD) gene, complete cds's.	1.284	0.986	1.063	0.553
10511	BE466436	KIAA1340 protein	1.170	0.966	0.857	0.539
7213	BG211331	gamma-aminobutyric acid (GABA) A receptor, alpha 6	0.808	1.129	0.988	0.453
6358	M57892	Human carbonic anhydrase isozyme VI (CA6) mRNA, complete cds.	0.857	1.047	0.952	0.587
16477	AB020650	Human mRNA for KIAA0843 protein, complete cds.	1.062	1.043	1.280	0.463
17836	AJ278245	Human mRNA for LanC-like protein 2 (lancl2 gene).	0.993	0.908	0.903	0.732
9696	BC007947	Human, clone IMAGE:4299555, mRNA, partial cds.	1.150	1.127	0.914	0.584
7365	AA479280	Sjogren syndrome antigen B (autoantigen La)	0.725	0.906	0.908	0.741
17202	BC000382	Human, interleukin enhancer binding factor 2, 45kD, clone MGC:8391 IMAGE:2820505, mRNA, complete cds.	0.868	1.135	0.792	0.373
15982	M21389	Human keratin type II (58 kD) mRNA, complete cds.	1.147	0.990	0.970	0.378
5260	M23077	Human pepsinogen gene, exon 9, clone PCG401.	0.955	0.902	0.865	0.613
11935	BE463542	phosphatidylinositol glycan, class H	0.999	1.059	1.078	0.397
6612	BC005145	Human, GDP dissociation inhibitor 2, clone MGC:2027 IMAGE:3504736, mRNA, complete cds.	1.162	1.148	1.141	0.704
4183	AI989900	glioblastoma amplified sequence	0.818	0.903	0.921	0.727
14848	AW249865	ATPase, H+ transporting, lysosomal (vacuolar proton pump) membrane sector associated protein M8-9	1.010	1.151	0.943	0.679
6886	BC010457	Human, clone IMAGE:4156419, mRNA, partial cds.	0.749	1.152	1.134	0.740
14787	BC009490	Human, clone IMAGE:3936863, mRNA, partial cds.	0.815	1.250	0.995	0.576
11106	U20759	Human parathyroid cell calcium-sensing receptor mRNA, complete cds.	0.898	1.263	0.879	0.532
11890	AI741847	KIAA0076 gene product	0.873	1.052	0.768	0.747
14440	AF142571	Tamarin (Saguinus oedipus) intracellular vitamin D binding protein 1 (IDBP1) mRNA, complete cds.	1.004	0.988	1.123	0.486
9453	AF094481	Human trinucleotide repeat DNA binding protein p20-CGGBP (CGGBP) gene, complete cds.	1.151	0.855	0.762	0.695
9716	AB037788	Human mRNA for KIAA1367 protein, partial cds.	0.957	0.854	0.927	0.738
14711	AB018290	Human mRNA for KIAA0747 protein, partial cds.	1.035	0.987	0.852	0.718
11636	M64347	Human novel growth factor receptor mRNA, 3' cds.	1.013	0.854	1.145	0.699
8765	D87075	solute carrier family 23 (nucleobase transporters), member 1	0.920	0.772	0.774	0.623

7914	U13879	Human neuron-restrictive silencer factor mRNA, partial cds.	0.941	0.773	1.075	0.241
15381	AI802091	deoxyribonuclease I	0.874	0.948	1.011	0.467
11630	BC003019	Human, peroxisomal short-chain alcohol dehydrogenase, clone MGC:4052 IMAGE:2822884, mRNA, complete cds.	1.048	0.971	0.853	0.361
17975	AF043906	Human T245 protein (T245) mRNA, complete cds.	0.906	1.077	1.267	0.515
11563	L03411	Human RD protein (RD) mRNA, complete cds.	1.068	0.843	1.159	0.611
17842	AK002022	Human cDNA FLJ11160 fis, clone PLACE1007014, weakly similar to 36 KD NUCLEOLAR PROTEIN HNP36.	0.853	1.000	0.941	0.216
6756	U09368	Human zinc finger protein ZNF140.	1.045	0.992	1.141	0.733
5262	BAB08217	embryonic serine protease-2	0.900	0.929	1.029	0.625
3176	AF218313	Human putative helicase RUVBL mRNA, complete cds.	0.801	0.924	0.893	0.718
3178	AK001393	Human cDNA FLJ10531 fis, clone NT2RP2001036.	0.923	1.062	1.099	0.592
9588	AB049842	Macaque brain cDNA, clone:QnpA-17571.	0.911	1.047	0.990	0.615
13774	AV740966	ESTs, Highly similar to R5HU7 ribosomal protein L7, cytosolic [H.sapiens]	0.692	0.866	0.929	0.649
16561	AA130458	lectin, galactoside-binding, soluble, 4 (galectin 4)	1.314	0.989	0.761	0.661
16604	BG258011	S-adenosylhomocysteine hydrolase	0.801	1.266	0.751	0.625
9097	AI632238	peanut (Drosophila)-like 2	1.208	1.091	0.920	0.523
5583	BI711468	integral membrane protein 2B	1.240	0.992	0.898	0.500
11422	BC001380	Human, succinate dehydrogenase complex, subunit A, flavoprotein (Fp), clone MGC:1484 IMAGE:3051442, mRNA, complete cds.	1.176	1.091	0.983	0.107
16243	BC001971	Human, Similar to cyclin-dependent kinase inhibitor 1B (p27, Kip1), clone MGC:5304 IMAGE:3458141, mRNA, complete cds.	1.099	0.960	1.015	0.712
11315	AB016243	Human gene for regulatory factor 2 of sodium/hydrogen exchanger isoform A3, complete cds.	0.952	0.948	0.753	0.693
9419	AK000679	Human cDNA FLJ20672 fis, clone KAIA4492, highly similar to M95549 Human sodium/glucose cotransporter-like protein.	0.989	0.962	0.910	0.419
11240	D63486	Human mRNA for KIAA0152 gene, complete cds.	0.886	0.987	0.720	0.440
16731	BG775549	ESTs, Highly similar to A31233 ribosomal protein RS.40K, cytosolic [H.sapiens]	0.994	0.976	1.037	0.603
13439	AJ009610	autoimmune regulator (automimmune polyendocrinopathy candidiasis ectodermal dystrophy)	1.006	1.337	0.760	0.541
16263	AY029486	Human G-protein gamma subunit 13 mRNA, complete cds.	0.989	0.961	0.904	0.641
1273	M10058	asialoglycoprotein receptor 1	0.717	0.482	1.049	2.386

10099	L14754	Human DNA-binding protein (SMBP2) mRNA, complete cds.	1.065	0.990	0.894	2.043
5277	AF109135	Human archvillin (SVIL) mRNA, complete cds.	0.940	0.997	0.874	1.768
14295	M25629	Human kallikrein mRNA, complete cds, clone clone phKK25.	0.802	1.058	0.908	1.636
14297	AJ238520	Human mRNA for putative transcription factor-like nuclear regulator (TFNR gene).	0.684	1.033	0.908	3.361
8212	D83664	Human mRNA for CAAF1 (calcium-binding protein in amniotic fluid 1), complete cds.	0.948	0.797	0.785	1.554
6042	AW245149	siah binding protein 1; FBP interacting repressor; pyrimidine tract binding splicing factor; Ro ribonucleoprotein-binding protein 1	1.032	0.992	0.873	1.683
7360	M74047	steroid-5-alpha-reductase, alpha polypeptide 2 (3-oxo-5 alpha-steroid delta 4-dehydrogenase alpha 2)	1.147	1.001	0.970	1.641
16736	BG537655	ribosomal protein S4, X-linked	0.939	1.006	0.750	1.362
10063	AF260728	Human lipocalin-interacting protein mRNA, complete cds.	1.074	0.946	0.901	1.706
2611	AI193222	hypothetical protein LOC55565	1.010	0.998	0.863	1.602
18359	AA487463	HYA22 protein	0.675	1.009	0.870	1.431
7128	AU159460	LIM and SH3 protein 1	0.753	0.945	0.753	1.538
5491	AB022659	KIAA0470 gene product	0.709	1.030	1.161	1.968
8916	BG761337	carbamoyl-phosphate synthetase 1, mitochondrial	0.897	0.804	1.085	1.506
11157	BC006286	Human, dual specificity phosphatase 12, clone MGC:10337 IMAGE:3958403, mRNA, complete cds.	1.027	1.030	0.963	2.634
10067	BC007065	Human, glutathione S-transferase theta 1, clone MGC:12516 IMAGE:3995846, mRNA, complete cds.	0.973	0.716	0.777	3.213
8502	AF373036	Human ZNFPHEX133 protein (ZNFPHEX133) mRNA, complete cds.	0.997	1.020	0.955	1.703
13517	N62961	synaptosomal-associated protein, 91 kDa (mouse) homolog	0.813	0.781	0.974	1.539
7113	BC005861	integrin, beta 2 (antigen CD18 (p95), lymphocyte function-associated antigen 1; macrophage antigen 1 (mac-1) beta subunit)	1.031	1.016	0.952	1.638
2913	BG033340	similar to ubiquitin binding protein	0.940	1.064	1.338	1.787
11159	BAB23372	putative	1.024	0.912	0.837	1.541
15233	BE729850	enhancer of zeste (Drosophila) homolog 2	0.618	1.069	0.899	1.593
4487	AL046515	vimentin	0.844	1.069	1.071	1.589
6879	U05040	Human FUSE binding protein mRNA, complete cds.	0.662	0.877	0.892	1.545
17217	AAC59868	MAM domain protein	1.028	1.272	0.701	1.689
12796	AB058685	Human mRNA for KIAA1782 protein, partial cds.	0.877	1.265	0.952	1.734
6874	BC000692	Human, Similar to hyaluronoglucosaminidase 2, clone MGC:1922 IMAGE:3347760, mRNA, complete cds.	1.154	1.265	0.750	1.701

6420	AF002715	Human MAP kinase kinase kinase (MTK1) mRNA, complete cds.	1.030	0.868	0.977	2.247
11439	AF322916	Human uveal autoantigen mRNA, complete cds.	0.602	0.729	0.932	1.636
5251	U62631	Human B-cell receptor CD22-B isoform and alternatively spliced B-cell receptor CD22-A isoform (CD22) gene, complete cds.	1.182	1.273	0.991	1.930
13214	L25270	Human XE169 mRNA, complete cds.	0.957	1.366	0.739	1.499
4444	AW327435	ESTs, Highly similar to SR72_HUMAN SIGNAL RECOGNITION PARTICLE 72 KD PROTEIN [H.sapiens]	0.857	0.882	0.910	1.522
9883	AJ250915	Human p10 gene for chaperonin 10 (Hsp10 protein) and p60 gene for chaperonin 60 (Hsp60 protein).	0.721	0.854	0.767	1.765
5553	AW439814	Homo sapiens cDNA FLJ13092 fis, clone NT2RP3002147	0.989	0.847	1.135	1.569
17532	BAB26282	putative	1.005	0.786	0.835	1.587
6576	AB029488	Human C11orf21 mRNA, complete cds.	1.049	0.840	0.961	1.649
10174	BF229298	UDP-Gal:betaGlcNAc beta 1,4-galactosyltransferase, polypeptide 5	1.193	0.857	0.886	2.047
3959	BI259169	KIAA0052 protein	0.790	0.857	1.092	1.860
14531	AB051551	Human mRNA for KIAA1764 protein, partial cds.	0.772	0.757	1.128	1.593
5800	AV713821	S100 calcium-binding protein A4 (calcium protein, calvasculin, metastasin, murine placental homolog)	0.884	0.780	0.838	1.666
2385	AL560352	STIP1 homology and U-Box containing protein 1	1.521	0.659	1.011	2.391
16242	AK001355	Human cDNA FLJ10493 fis, clone NT2RP2000274.	0.915	0.739	1.156	1.829
6962	BAA91104	unnamed protein product	1.141	1.096	0.889	1.914
10944	BC000508	Human, proteasome (prosome, macropain) subunit, beta type, 1, clone MGC:8505 IMAGE:2822268, mRNA, complete cds.	1.173	0.816	0.979	2.849
14908	BF224187	natriuretic peptide receptor C/guanylate cyclase C (atrionatriuretic peptide receptor C)	0.652	1.091	0.682	2.614
10365	AL533518	UDP-glucose pyrophosphorylase 2	0.842	1.095	0.824	1.617
4429	U46024	myotubular myopathy 1	0.847	0.913	0.939	2.215
8794	BC006297	chromosome 1 open reading frame 2	1.214	1.086	0.833	1.835
7215	AA404652	interferon-stimulated transcription factor 3, gamma (48kD)	0.866	0.984	0.848	2.210
10079	BC000113	Human, clone IMAGE:3352566, mRNA, partial cds.	1.248	1.116	0.839	1.633
3633	AB021663	Human mRNA for leucine-zipper protein, complete cds.	0.964	0.891	0.721	2.396
13342	K00842	Human beta-tubulin pseudogene, clone 7-beta.	0.705	1.163	0.981	1.540
2904	S46622	protein phosphatase 3 (formerly 2B), catalytic subunit, gamma isoform (calcineurin A gamma)	1.115	1.706	0.502	2.411
16114	AF177198	Human talin mRNA, complete cds.	0.896	0.833	1.155	1.514
6898	AF098534	Human RAD17 isoform 4 (RAD17) mRNA, complete cds.	0.869	1.147	0.707	1.506

7369	N94350	Thy-1 cell surface antigen	0.641	1.119	0.826	1.688
17211	U78181	Human sodium channel 2 (hBNaC2) mRNA, complete cds.	0.875	0.952	0.785	1.525
7350	BF913759	uroporphyrinogen III synthase (congenital erythropoietic porphyria)	1.234	0.847	0.619	2.150
8907	AF009674	axin	1.558	0.794	0.956	1.133
14600	AK001111	Human cDNA FLJ10249 fis, clone HEMBB1000725, highly similar to Rattus norvegicus GTPase Rab8b mRNA.	1.306	0.971	0.918	1.848
15787	AAH11294	ectonucleotide pyrophosphatase/phosphodiesterase 5	2.108	0.992	1.408	2.084
15782	AB037819	Human mRNA for KIAA1398 protein, partial cds.	1.750	0.983	0.817	1.021
13056	U31501	Human fragile X mental retardation syndrome related protein (FXR2) mRNA, complete cds.	1.656	0.777	1.115	1.235
12246	BG211824	malic enzyme 1, NADP(+)-dependent, cytosolic	1.979	1.090	1.185	1.013
14623	AB017169	Human mRNA for Slit-3 protein, complete cds.	1.943	0.997	1.110	1.003
5494	BE271496	anchor attachment protein 1 (Gaa1p, yeast) homolog	1.870	0.861	0.986	1.137
11493	BC008881	Human, kinesin 2 (60-70kD), clone MGC:15245 IMAGE:4301579, mRNA, complete cds.	1.753	0.889	1.176	1.173
2588	AA314436	chaperonin containing TCP1, subunit 7 (eta)	1.965	1.249	1.116	1.442
2673	AL545741	solute carrier family 1 (neutral amino acid transporter), member 5	2.014	1.321	1.138	1.403
9623	D31767	Human mRNA for KIAA0058 gene, complete cds.	1.360	0.866	1.316	1.856
10567	BG674024	heat shock 70kD protein 1A	2.221	0.861	1.450	1.483
12896	CAB05006	contains similarity to Pfam domain: PF00207 (Alpha-2-macroglobulin family), Score=377.3, E-value=1.1e-113, N=1; PF01835 (Alpha-2-macroglobulin family N-terminal region), Score=157.5, E-value=2.1e-46, N=2~cDNA EST yk41d7.3 comes fr	1.804	1.111	1.170	0.967
5537	BC006332	Human, clathrin, light polypeptide (Lcb), clone MGC:12930 IMAGE:4299637, mRNA, complete cds.	1.799	1.398	1.108	1.524
13029	AB002347	Human mRNA for KIAA0349 gene, partial cds.	1.597	0.620	0.995	1.013
4310	U62966	solute carrier family 28 (sodium-coupled nucleoside transporter), member 1	1.605	0.826	1.188	0.898
14844	M80899	Human novel protein AHNAK mRNA, partial sequence.	1.339	0.839	1.103	1.521
13165	BC001778	Human, Similar to uroporphyrinogen decarboxylase, clone MGC:1856 IMAGE:3542421, mRNA, complete cds.	1.729	1.134	1.066	1.352
6751	J04988	Human 90 kD heat shock protein gene, complete cds.	1.777	1.105	1.241	1.022

14626	AF196481	Human RING finger protein (FXY2) mRNA, complete cds.	1.890	0.999	1.310	1.170
16887	AA528133	Homo sapiens 14q32 Jagged2 gene, complete cds; and unknown gene	1.574	1.026	0.893	1.355
3927	NM_004785	solute carrier family 9 (sodium/hydrogen exchanger), isoform 3 regulatory factor 2	1.798	1.006	1.590	1.330
5559	BF726634	crystallin, alpha B	1.633	0.800	1.174	0.981
12183	BE876028	tropomyosin 2 (beta)	1.842	1.009	0.951	0.995
11592	BC012085	Human, Similar to serine/threonine protein kinase, clone MGC:20014 IMAGE:4554884, mRNA, complete cds.	1.958	0.944	1.276	1.155
5488	BF968460	3-hydroxy-3-methylglutaryl-Coenzyme A synthase 1 (soluble)	2.379	0.936	1.350	1.168
17702	D88674	Human mRNA for antizyme inhibitor, complete cds.	1.556	0.777	0.978	1.284
15839	AK026573	Human cDNA: FLJ22920 fis, clone KAT06686, highly similar to HSU29175 Human transcriptional activator (BRG1) mRNA.	1.635	0.934	1.210	0.934
5715	AL545227	synaptogyrin 2	1.584	1.062	1.046	1.193
4091	BE787478	thioredoxin reductase 1	3.381	0.757	1.048	1.172
16765	D87071	KIAA0233 gene product	1.686	0.760	1.188	1.155
9067	NM_002222	inositol 1,4,5-triphosphate receptor, type 1	1.528	0.967	0.979	0.952

APPENDIX F: CDNA MICROARRAY RESULTS

Genes Significantly (P<0.005) Upregulated By Shear Stress in PAVEC
Group 1 Up

Agilent Feature #	Gene Name/Description	Count 545		Fold STD
		Gene ID	Fold AVE	
2928	cytochrome P450, subfamily I (aromatic compound-inducible), polypeptide 1	K03191	8.38	1.27
2518	carboxylesterase 1 (monocyte/macrophage serine esterase 1)	L07765	6.66	2.59
14871	interleukin 8	BG777366	5.85	1.77
8171	Human cystine/glutamate transporter xCT mRNA, complete cds.	AF252872	4.46	2.29
2435	aldo-keto reductase family 1, member C1 (dihydrodiol dehydrogenase 1; 20-alpha (3-alpha)-hydroxysteroid dehydrogenase)	BI759009	4.36	1.65
16028	Human, peroxiredoxin 1, clone MGC:12514 IMAGE:3961375, mRNA, complete cds.	BC007063	4.23	0.70
4091	thioredoxin reductase 1	BE787478	3.52	1.00
15436	secretory leukocyte protease inhibitor (antileukoproteinase)	BG533465	3.42	0.48
5961	meiotic recombination (S. cerevisiae) 11 homolog A	AF073362	3.39	0.71
6425	Human E2IG1 (E2IG1) mRNA, complete cds.	AF191017	3.22	0.86
7857	Human full length insert cDNA YH92E12.	AF074995	3.15	1.65
11212	Human, Similar to ubiquitin carboxy-terminal hydrolase L1, clone MGC:8524 IMAGE:2822541, mRNA, complete cds.	BC000332	3.05	0.65
6011	procollagen-proline, 2-oxoglutarate 4-dioxygenase (proline 4-hydroxylase), beta polypeptide (protein disulfide isomerase; thyroid hormone binding protein p55)	BG744516	2.88	0.75
11749	heme oxygenase (decycling) 1	BI596354	2.86	0.18
4415	endothelial PAS domain protein 1	AW377189	2.84	0.84
16118	Human MHC class I lymphocyte antigen (HLA-E) (HLA-6.2) gene, complete cds.	M21533	2.83	0.78
8905	transforming growth factor, beta 2	AW303586	2.83	0.32
18356	FOS-like antigen 2	X16706	2.82	1.25
12235	dynein, cytoplasmic, heavy polypeptide 1	AB002323	2.73	0.91
16878	2,3-bisphosphoglycerate mutase	X04327	2.70	0.40
10233	enolase 2, (gamma, neuronal)	BG169625	2.68	0.65
10220	Human mRNA for fibrillin.	X63556	2.67	0.45
12094	glucan (1,4-alpha-), branching enzyme 1 (glycogen branching enzyme, Andersen disease, glycogen storage disease type IV)	L07956	2.66	0.85
15034	cysteine-rich protein 2	AL515731	2.65	0.54

16417	voltage-dependent anion channel 3	AI492354	2.62	1.77
11800	serine threonine protein kinase	AU121423	2.61	0.32
14759	aortic carboxypeptidase-like protein ACLP	AAC25584	2.60	0.25
11977	FK506-binding protein 9 (63 kD)	AL555732	2.56	0.45
5488	3-hydroxy-3-methylglutaryl-Coenzyme A synthase 1 (soluble)	BF968460	2.54	1.08
16899	solute carrier family 6 (neurotransmitter transporter, L-proline), member 7	NM_014228	2.54	0.63
10115	Human SP-40,40 mRNA for complement-associated protein SP-40,40 alpha-1 and beta-1 chain.	X14723	2.53	0.55
12902	Human HK2 mRNA for hexokinase II.	Z46376	2.50	0.72
10514	solute carrier family 7 (cationic amino acid transporter, y+ system), member 2	U76368	2.50	0.49
16413	G protein-coupled receptor 3	U18550	2.47	0.59
15033	dickkopf (Xenopus laevis) homolog 3	AB034203	2.45	0.54
16475	potassium inwardly-rectifying channel,subfamily J, member 13	AJ006128	2.45	0.57
16178	Human oligodendrocyte-specific protein (OSP) mRNA, complete cds.	AF068863	2.44	0.36
15024	HCGII-7 protein	X81001	2.42	0.56
10188	Human genomic DNA of 8p21.3-p22 anti-oncogene of hepatocellular colorectal and non-small cell lung cancer , segment 6/11.	AB020863	2.41	0.28
5827	SEX gene	BF725116	2.39	0.87
12595	Human mRNA for Tec protein-tyrosine kinase, complete cds.	D29767	2.39	0.85
13782	chitinase 3-like 1 (cartilage glycoprotein-39)	AL035737	2.39	0.57
8279	Human MHC class I HLA-B13 chain gene (Aw68.2,30; B13,51), complete cds.	M24041	2.38	0.51
15787	ectonucleotide pyrophosphatase/phosphodiesterase 5	AAH11294	2.37	1.29
11748	Human, clone IMAGE:2905327, mRNA, partial cds.	BC002991	2.34	0.43
4266	hexosaminidase A (alpha polypeptide)	BG686397	2.31	0.51
4258	ras homolog gene family, member C	BG708735	2.30	0.30
9787	Human proto-oncogene Bcd orf1 and orf2 mRNA, complete cds.	U51869	2.29	0.44
3624	Human mitochondrial glutathione reductase (GRD1) mRNA, complete cds; nuclear gene for mitochondrial product.	AF228704	2.28	0.27
8959	GTP-binding protein Rho7	AI554560	2.28	0.36
18203	hexabrachion (tenascin C, cytotactin)	BG679767	2.27	0.53
14484	Human, CDC37 (cell division cycle 37, S. cerevisiae, homolog), clone MGC:3241 IMAGE:3505011, mRNA, complete cds.	BC000083	2.25	0.42
6470	Human, ATPase, H+ transporting, lysosomal (vacuolar proton pump) 21kD, clone MGC:4498 IMAGE:2964510, mRNA, complete cds.	BC005876	2.25	0.50
10567	heat shock 70kD protein 1A	BG674024	2.24	0.33
14767	Human triosephosphate isomerase mRNA, complete cds.	M10036	2.23	0.56
10522	myosin, heavy polypeptide 9, non-muscle	BG699149	2.23	0.73

7345	core promoter element binding protein	AU139931	2.22	0.35
6642	Human, 3-hydroxy-3-methylglutaryl-Coenzyme A synthase 1 (soluble), clone MGC:8344 IMAGE:2819708, mRNA, complete cds.	BC000297	2.21	0.73
9557	Human macrophage capping protein mRNA, complete cds.	M94345	2.17	0.66
959	phosphorylase, glycogen; muscle (McArdle syndrome, glycogen storage disease type V)	BI759873	2.16	0.66
9869	Human FK506-binding protein (FKBP63) mRNA, partial cds.	AF089745	2.15	0.44
16969	heat shock 70kD protein 8	BG504802	2.14	0.48
5906	CD151 antigen	BE787930	2.12	0.49
14750	Human myosin light chain 1 slow a (MLC1sa) mRNA, complete cds.	M31211	2.09	0.48
2925	ATPase, H+ transporting, lysosomal (vacuolar proton pump) 21kD	BG108730	2.08	0.32
8380	Human triosephosphate isomerase mRNA, complete cds.	M10036	2.08	0.48
4491	heterogeneous nuclear ribonucleoprotein R	AL538660	2.08	0.45
3141	Human mRNA for MOP-4, complete cds.	AB014773	2.06	0.34
7572	protein tyrosine phosphatase, receptor type, U	U73727	2.06	0.16
16148	Human mRNA for diacylglycerol kinase.	X62535	2.06	0.14
14791	Human cathepsin B mRNA, 3' UTR with a stem-loop structure providing mRNA stability.	L22569	2.03	0.73
2588	chaperonin containing TCP1, subunit 7 (eta)	AA314436	2.02	0.53
16267	Human follistatin gene, exons 1-5.	M19480	2.02	0.62
6440	Human hepatocellular carcinoma associated protein (JCL-1) mRNA, complete cds.	U92544	2.02	0.39
7441	NADH dehydrogenase (ubiquinone) flavoprotein 1 (51kD)	AW250734	2.02	0.30
16671	ubiquitin-conjugating enzyme E2H (homologous to yeast UBC8)	AW206129	2.02	0.55
10615	ALL1-fused gene from chromosome 1q	BG498770	2.02	0.37
2673	solute carrier family 1 (neutral amino acid transporter), member 5	AL545741	2.02	0.14
8692	plexin B2	BC004542	1.99	0.52
10171	upstream binding transcription factor, RNA polymerase I	BI088564	1.98	0.34
12202	myosin, light polypeptide 1, alkali; skeletal, fast	BF981829	1.98	0.25
12246	malic enzyme 1, NADP(+)-dependent, cytosolic	BG211824	1.98	0.12
10555	calcium channel, voltage-dependent, beta 3 subunit	AL565681	1.98	0.26
11592	Human, Similar to serine/threonine protein kinase, clone MGC:20014 IMAGE:4554884, mRNA, complete cds.	BC012085	1.97	0.25
13025	Human, Similar to thioredoxin peroxidase 1, clone MGC:8456 IMAGE:2821457, mRNA, complete cds.	BC000452	1.96	0.35
7592	collagen, type IV, alpha 1	NM_001845	1.96	0.46
16146	Human, chromosome 14 open reading frame 2, clone MGC:8356 IMAGE:2819801, mRNA, complete cds.	BC000429	1.96	0.43
6023	tryptophanyl-tRNA synthetase	BF795451	1.96	0.22

11918	ATP-binding cassette, sub-family C (CFTR/MRP), member 1	BC001636	1.95	0.33
3474	Human, diaphorase (NADH) (cytochrome b-5 reductase), clone MGC:5150 IMAGE:3450773, mRNA, complete cds.	BC004821	1.94	0.41
6002	delta sleep inducing peptide, immunoreactor	AL525317	1.94	0.19
14882	hexokinase 2	BI257175	1.94	0.18
6281	Human mRNA for KIAA0315 gene, partial cds.	AB002313	1.93	0.40
18327	cyclin-dependent kinase inhibitor 1A (p21, Cip1)	AL542973	1.93	0.68
11460	Human genomic DNA, chromosome 8q23, clone:KB1747F8.	AP003113	1.93	0.51
3321	Human mRNA for Soluble-type polypeptide FZD4S, complete cds.	AB054881	1.93	0.64
13169	Human mRNA for plasma gelsolin.	X04412	1.92	0.67
16774	Ras association (RalGDS/AF-6) domain family 1	AL543484	1.92	0.33
14626	Human RING finger protein (FXY2) mRNA, complete cds.	AF196481	1.92	0.39
10426	KIAA0088 protein	BI760656	1.92	0.38
8820	glucosidase, beta; acid (includes glucosylceramidase)	NM_000157	1.92	0.54
12553	Human, pleckstrin 2 (Mouse) homolog, clone MGC:4867 IMAGE:3457876, mRNA, complete cds.	BC001226	1.91	0.37
5494	anchor attachment protein 1 (Gaa1p, yeast) homolog	BE271496	1.91	0.40
5596	Human OS-9 mRNA, complete cds.	AB002806	1.90	0.31
7047	histone deacetylase 5	BF305705	1.90	0.22
17843	Human cathepsin L (CTSL) gene, exon 1, intron 1, and exon 2 including 5' end of cds.	L06426	1.89	0.24
4263	tyrosine kinase with immunoglobulin and epidermal growth factor homology domains	X60957	1.88	0.39
12183	tropomyosin 2 (beta)	BE876028	1.88	0.41
12906	Human T-cell receptor zeta-chain mRNA, complete cds.	J04132	1.88	0.41
5852	protein tyrosine phosphatase, receptor type, T	NM_007050	1.88	0.16
9126	creatine kinase, mitochondrial 1 (ubiquitous)	BG680747	1.88	0.35
12896	contains similarity to Pfam domain: PF00207 (Alpha-2-macroglobulin family), Score=377.3, E-value=1.1e-113, N=1; PF01835 (Alpha-2-macroglobulin family N-terminal region), Score=157.5, E-value=2.1e-46, N=2~cDNA EST yk41d7.3 comes fr	CAB05006	1.87	0.56
10745	lectin, galactoside-binding, soluble, 1 (galectin 1)	BF979102	1.85	0.28
13749	actin, alpha 2, smooth muscle, aorta	BF681347	1.85	0.46
5537	Human, clathrin, light polypeptide (Lcb), clone MGC:12930 IMAGE:4299637, mRNA, complete cds.	BC006332	1.83	0.37
3927	solute carrier family 9 (sodium/hydrogen exchanger), isoform 3 regulatory factor 2	NM_004785	1.83	0.33
15877	Human MAP1 light chain 3-like protein 1 mRNA, complete cds.	AF276658	1.82	0.36

9121	tumor differentially expressed 1	AL552738	1.82	0.21
16656	excision repair cross-complementing rodent repair deficiency, complementation group 4	NM_005236	1.82	0.26
15338	protease, cysteine, 1 (legumain)	Y09862	1.82	0.49
11493	Human, kinesin 2 (60-70kD), clone MGC:15245 IMAGE:4301579, mRNA, complete cds.	BC008881	1.82	0.52
4880	Human cDNA: FLJ22163 fis, clone HRC00430.	AK025816	1.82	0.33
5797	ATPase, Na+/K+ transporting, alpha 2 (+) polypeptide	NM_000702	1.81	0.29
15343	cystinosis, nephropathic	BG392867	1.81	0.14
16401	Human, clone MGC:19671 IMAGE:3352603, mRNA, complete cds.	BC011741	1.81	0.36
6751	Human 90 kD heat shock protein gene, complete cds.	J04988	1.81	0.35
16116	Human Scd mRNA for stearoyl-CoA desaturase, complete cds.	AB032261	1.81	0.36
10945	Human, putative glialblastoma cell differentiation-related, clone MGC:2352 IMAGE:3535682, mRNA, complete cds.	BC004967	1.80	0.46
6647	Human mRNA for KIAA1776 protein (fibrillin3), complete cds.	AB053450	1.80	0.31
14237	Human, holocytochrome c synthase (cytochrome c heme-lyase), clone MGC:1443 IMAGE:3030501, mRNA, complete cds.	BC001691	1.80	0.16
7285	hypothetical protein FLJ23306	AI088306	1.80	0.50
13652	clathrin, light polypeptide (Lcb)	BE791502	1.80	0.34
15108	syntaxin 6	AI339089	1.79	0.40
10727	stress-induced-phosphoprotein 1 (Hsp70/Hsp90-organizing protein)	BG721124	1.79	0.14
12695	Human group III secreted phospholipase A2 mRNA, complete cds.	AF220490	1.79	0.20
7286	ATP-binding cassette, sub-family G (WHITE), member 2	AU118354	1.78	0.44
18376	cyclin D3	AI803460	1.78	0.48
5933	microsomal glutathione S-transferase 1	BF037095	1.78	0.12
14752	Human plasma membrane calcium ATPase (hPMCA4) mRNA, complete cds.	M25874	1.77	0.22
16672	bridging integrator 1	BG250172	1.77	0.13
7037	fibulin 5	AL570066	1.77	0.15
15782	Human mRNA for KIAA1398 protein, partial cds.	AB037819	1.77	0.29
5672	tyrosyl-tRNA synthetase	BC004151	1.77	0.34
6916	Human cDNA: FLJ20866 fis, clone ADKA02201.	AK024519	1.77	0.34
13788	hematopoietic cell-specific Lyn substrate 1	X16663	1.76	0.36
9006	nucleoside phosphorylase	BE266250	1.76	0.40
10754	KIAA0202 protein	AL532971	1.76	0.25
9969	Human, tubulin, beta polypeptide, clone MGC:8685 IMAGE:2964590, mRNA, complete cds.	BC001352	1.75	0.40
12289	ras-related C3 botulinum toxin substrate 2 (rho family, small GTP binding protein Rac2)	BG684065	1.75	0.17

18360	v-Ha-ras Harvey rat sarcoma viral oncogene homolog	BG419155	1.75	0.24
4964	Human Bmx mRNA for cytoplasmic tyrosine kinase.	X83107	1.75	0.13
4759	Human, ARP1 (actin-related protein 1, Yeast) homolog A (centractin alpha), clone MGC:2357 IMAGE:3347881, mRNA, complete cds.	BC000693	1.74	0.35
18361	peptidylprolyl isomerase B (cyclophilin B)	BE868117	1.74	0.21
499	Human, transmembrane 4 superfamily member (tetraspan NET-7), clone MGC:4120 IMAGE:2958221, mRNA, complete cds.	BC003157	1.74	0.34
10561	adenylate cyclase 7	D25538	1.74	0.19
13200	Human gamma-filamin (FLNC) gene, complete cds.	AF252549	1.74	0.23
6712	Human, dihydrolipoamide S-succinyltransferase (E2 component of 2-oxo-glutarate complex), clone MGC:3898 IMAGE:3627724, mRNA, complete cds.	BC002735	1.73	0.23
2924	translocase of inner mitochondrial membrane 17 (yeast) homolog A	BG506029	1.73	0.32
16765	KIAA0233 gene product	D87071	1.73	0.41
15410	spectrin, beta, non-erythrocytic 1	BI758140	1.73	0.46
16663	phosphofructokinase, platelet	BE378739	1.73	0.42
10629	myeloid/lymphoid or mixed-lineage leukemia (trithorax (Drosophila) homolog); translocated to, 7	AL544994	1.72	0.43
16791	microtubule-associated protein 1A	NM_002373	1.72	0.26
9881	Human mRNA for enteric smooth muscle gamma-actin.	X16940	1.72	0.40
10525	guanine nucleotide binding protein (G protein), alpha inhibiting activity polypeptide 1	AU132321	1.72	0.39
8346	Human transcription factor junB (junB) gene, 5' region and complete cds.	U20734	1.72	0.22
8992	phospholipase C, delta 1	BI489731	1.71	0.27
7335	myosin, light polypeptide 6, alkali, smooth muscle and non-muscle	AV716792	1.71	0.29
12994	Human, Similar to RIKEN cDNA B230118G17 gene, clone MGC:19604 IMAGE:3622817, mRNA, complete cds.	BC010155	1.70	0.43
10090	Human RLIP76 protein mRNA, complete cds.	L42542	1.70	0.21
9162	hypothetical protein FLJ20277	BE501346	1.70	0.15
14743	Human paired related homeobox protein (PRX2) mRNA, complete cds.	AF061970	1.70	0.61
2745	phosphatidylserine synthase 1	BC004390	1.70	0.28
16410	hematopoietic PBX-interacting protein	BI754234	1.70	0.11
11913	SH3-domain binding protein 5 (BTK-associated)	BC006169	1.69	0.41
15038	KIAA0562 gene product	AB011134	1.69	0.30
2757	adenine phosphoribosyltransferase	BG612479	1.69	0.28
3939	collagen, type IV, alpha 4	Y17397	1.69	0.18
5222	Human ribosomal S6 protein kinase mRNA, complete cds.	AF037447	1.69	0.15
12983	Human cAMP-specific phosphodiesterase 8B (PDE8B) mRNA, partial cds.	AF079529	1.69	0.34

8618	discs, large (Drosophila) homolog 5	NM_004747	1.68	0.14
5438	Human mRNA for glutathione peroxidase, complete cds.	D00632	1.68	0.66
13597	phosphoribosyl pyrophosphate synthetase-associated protein 2	AB007851	1.68	0.11
13552	actin related protein 2/3 complex, subunit 5 (16 kD)	AL560125	1.68	0.37
4414	gp25L2 protein	BI822721	1.68	0.27
12829	Human mRNA; cDNA DKFZp762G216 (from clone DKFZp762G216).	AL512709	1.68	0.30
10088	Human testis-specific PGK-2 gene for phosphoglycerate kinase (ATP:3-phospho-D-glycerate 1-phosphotransferase, EC 2.7.2.3).	X05246	1.67	0.19
15056	heat shock 70kD protein 9B (mortalin-2)	BG424817	1.67	0.28
16970	calumenin	AW614911	1.67	0.32
13655	P450 (cytochrome) oxidoreductase	AF258341	1.67	0.24
16276	Human leukemia virus receptor 2 (GLVR2) mRNA, complete cds.	L20852	1.67	0.22
12913	Human carnitine octanoyltransferase mRNA, complete cds.	AF073770	1.67	0.16
10336	kinesin family member 1C	AB014606	1.67	0.17
14156	Human cDNA FLJ11937 fis, clone HEMBB1000556, weakly similar to Human mRNA for KIAA0750 protein.	AK021999	1.67	0.18
8059	Na,K-ATPase alpha-4 subunit	AAD43813	1.66	0.20
13056	Human fragile X mental retardation syndrome related protein (FXR2) mRNA, complete cds.	U31501	1.66	0.16
14300	Human glutathione S-transferase mRNA, complete cds.	J03746	1.66	0.17
14617	Human, clone MGC:15351 IMAGE:4126712, mRNA, complete cds.	BC008861	1.66	0.36
11972	Niemann-Pick disease, type C2 gene	BG397837	1.65	0.25
5559	crystallin, alpha B	BF726634	1.65	0.27
3460	Human mRNA for collagen alpha 1(V) chain, complete cds.	D90279	1.65	0.42
7501	phosphatidylinositol 4-kinase, catalytic, beta polypeptide	BG025389	1.65	0.27
16652	coronin, actin-binding protein, 1A	BG758313	1.65	0.27
18073	Human, Similar to biliverdin reductase A, clone MGC:14491 IMAGE:4282476, mRNA, complete cds.	BC005902	1.65	0.35
5642	hypothetical protein FLJ11560	BF340474	1.65	0.23
951	oxygen regulated protein (150kD)	AW450554	1.64	0.20
12206	ARP1 (actin-related protein 1, yeast) homolog A (centractin alpha)	AL524757	1.64	0.16
5715	synaptogyrin 2	AL545227	1.64	0.51
4310	solute carrier family 28 (sodium-coupled nucleoside transporter), member 1	U62966	1.64	0.35
10712	hypothetical protein ET	AL545372	1.64	0.22
13445	protein C (inactivator of coagulation factors Va and VIIIa)	M11228	1.63	0.35
337	Human myelodysplasia/myeloid leukemia factor 2 (MLF2) mRNA, complete cds.	U57342	1.63	0.27
12492	Human isopeptidase T-3 (ISOT-3) mRNA, complete cds.	U75362	1.63	0.19

5563	Human, Similar to valosin-containing protein, clone MGC:4053 IMAGE:2822943, mRNA, complete cds.	BC012195	1.62	0.12
12566	Human mRNA for KIAA1209 protein, partial cds.	AB033035	1.62	0.21
11270	Human, clone MGC:2827 IMAGE:2964565, mRNA, complete cds.	BC001087	1.62	0.45
6894	Human EB1 mRNA, complete cds.	U24166	1.62	0.21
271	Human tie mRNA for putative receptor tyrosine kinase.	X60957	1.62	0.47
8154	Human choroideremia mRNA.	X78121	1.62	0.33
3392	Human CSaids binding protein (CSBP1) mRNA, complete cds.	L35263	1.62	0.29
8647	peroxiredoxin 2	BI862079	1.62	0.31
10268	dual specificity phosphatase 3 (vaccinia virus phosphatase VH1-related)	AL555009	1.62	0.22
9007	spectrin, alpha, non-erythrocytic 1 (alpha-fodrin)	U83867	1.61	0.34
13382	calpain 1, (mu/I) large subunit	BG697126	1.61	0.18
9902	Human SWI-SNF complex protein p270 mRNA, partial cds.	AF265208	1.61	0.54
13029	Human mRNA for KIAA0349 gene, partial cds.	AB002347	1.61	0.20
9947	Human LPS-Induced TNF-Alpha Factor (LITAF) mRNA, complete cds.	U77396	1.61	0.23
12071	procollagen-lysine, 2-oxoglutarate 5-dioxygenase (lysine hydroxylase) 2	U84573	1.60	0.10
18362	phytanoyl-CoA hydroxylase (Refsum disease)	BG722759	1.60	0.22
14546	Human MHC class I HLA-C-alpha-2 chain and alternative mRNA, complete cds, clones 4 and 10.	M24097	1.60	0.21
9410	Human HOK-2 mRNA for zinc finger protein.	X82125	1.60	0.23
16317	Human mRNA for KIAA0834 protein, complete cds.	AB020641	1.60	0.36
8786	latent transforming growth factor beta binding protein 1	M34057	1.60	0.56
7192	putative glialblastoma cell differentiation-related	BE892211	1.60	0.34
16759	zyxin	BI825951	1.59	0.54
422	Human cDNA FLJ14781 fis, clone NT2RP4000455, weakly similar to TRANS-ACTING TRANSCRIPTIONAL PROTEIN ICP0.	AK027687	1.59	0.44
4315	DiGeorge syndrome critical region gene DGSI; likely ortholog of mouse expressed sequence 2 embryonic lethal	BG831512	1.59	0.27
12033	integrin beta 4 binding protein	BI908045	1.59	0.48
16887	Homo sapiens 14q32 Jagged2 gene, complete cds; and unknown gene	AA528133	1.59	0.22
9660	Human 6-O-methylguanine-DNA methyltransferase (MGMT) mRNA, complete cds.	M29971	1.59	0.59
7428	stromal cell-derived factor 2	BG431313	1.58	0.29
5727	DNA fragmentation factor, 45 kD, alpha polypeptide	BF309422	1.58	0.21

13065	Human, ubiquitin B, clone MGC:8385 IMAGE:2820408, mRNA, complete cds.	BC000379	1.58	0.16
15052	palmitoyl-protein thioesterase 2	BE790900	1.58	0.08
13795	glutaminyl-tRNA synthetase	BG179717	1.58	0.23
14941	Homo sapiens cDNA FLJ10229 fis, clone HEMBB1000136	AL548337	1.58	0.18
13233	CG3104 gene product	AAF51192	1.58	0.20
12523	Human mRNA; cDNA DKFZp566M051 (from clone DKFZp566M051).	AL117413	1.58	0.42
7361	desmoglein 2	AU124258	1.57	0.39
17702	Human mRNA for antizyme inhibitor, complete cds.	D88674	1.57	0.24
10229	KIAA0130 gene product	D50920	1.57	0.28
15398	KIAA0138 gene product	BE856759	1.57	0.20
16367	Human serum response factor (SRF) mRNA, complete cds.	J03161	1.57	0.16
11729	calcitonin/calcitonin-related polypeptide, alpha	X03662	1.57	0.20
5850	aconitase 2, mitochondrial	BC014092	1.57	0.19
7289	KIAA0430 gene product	AB007890	1.57	0.16
14079	Human cDNA FLJ14357 fis, clone HEMBA1000005, highly similar to DNAJ PROTEIN HOMOLOG MTJ1.	AK027263	1.57	0.26
4002	dihydropyrimidinase-like 4	AB006713	1.57	0.24
8907	axin	AF009674	1.56	0.15
11239	Human cDNA FLJ20746 fis, clone HEP06040.	AK000753	1.56	0.10
11827	Human, RNA binding motif protein 4, clone MGC:8418 IMAGE:2820928, mRNA, complete cds.	BC000307	1.56	0.15
4325	integrin, alpha 5 (fibronectin receptor, alpha polypeptide)	M13918	1.56	0.18
8803	squalene epoxidase	AF098865	1.56	0.38
6019	cysteine-rich protein 1 (intestinal)	BI222747	1.56	0.21
16115	Human brain my036 protein mRNA, complete cds.	AF063594	1.56	0.13
6784	Human mRNA for KIAA1206 protein, partial cds.	AB033032	1.56	0.30
16356	Human ADP-ribosylation factor 1 mRNA, complete cds.	M84326	1.56	0.25
4103	amphiregulin (schwannoma-derived growth factor)	AL546917	1.55	0.30
7355	putative breast adenocarcinoma marker (32kD)	BC002502	1.55	0.30
15959	Human phosphatidylinositol polyphosphate 5-phosphatase type IV mRNA, complete cds.	AF187891	1.55	0.20
18012	adaptor-related protein complex 2, mu 1 subunit	BG033362	1.55	0.13
15252	Homo sapiens cDNA: FLJ21339 fis, clone COL02601, highly similar to AF007152 Homo sapiens clone 23649 and 23755 unknown mRNA	AF007152	1.55	0.10
740	Human cytosolic inhibitor of NRF2 (INRF2) mRNA, complete cds.	AF361886	1.55	0.21
4327	sphingomyelin phosphodiesterase 1, acid lysosomal (acid sphingomyelinase)	NM_000543	1.54	0.33

15031	procollagen-lysine, 2-oxoglutarate 5-dioxygenase 3	AL544817	1.54	0.13
15809	Human eukaryotic initiation factor 2B-epsilon mRNA, partial cds.	U23028	1.54	0.15
12026	lipase A, lysosomal acid, cholesterol esterase (Wolman disease)	AU141268	1.54	0.42
9778	Human RET ligand 2 (RETL2) mRNA, complete cds.	U97145	1.54	0.33
9067	inositol 1,4,5-triphosphate receptor, type 1	NM_002222	1.53	0.14
16180	Human cDNA FLJ20845 fis, clone ADKA01901.	AK000852	1.53	0.10
13807	GTP-binding protein overexpressed in skeletal muscle	AW297828	1.53	0.29
18175	LIM domain only 4	U24576	1.53	0.20
12291	carnitine acetyltransferase	X78706	1.53	0.27
16936	clones 23667 and 23775 zinc finger protein	BG498371	1.53	0.21
7534	chloride intracellular channel 1	AA291390	1.53	0.27
12135	LIM and senescent cell antigen-like domains 1	U09284	1.52	0.15
14768	Human mRNA PLSTIRE for serine/threonine protein kinase.	X66365	1.52	0.39
10722	nucleoporin 62kD	BG822825	1.52	0.26
11768	Human, Similar to RIKEN cDNA 1110018J12 gene, clone IMAGE:3865164, mRNA, partial cds.	BC011978	1.52	0.12
4078	isocitrate dehydrogenase 3 (NAD+) beta	BI553471	1.52	0.26
3999	guanylate cyclase 1, soluble, beta 3	X66533	1.52	0.17
14124	Macaque brain cDNA clone:QflA-13812, full insert sequence.	AB056806	1.52	0.16
17690	Human, LIM domain only 4, clone MGC:872 IMAGE:3355972, mRNA, complete cds.	BC003600	1.52	0.23
10982	Human mRNA for NOTCH4, partial cds.	D63395	1.51	0.44
15858	Human ALK-1 mRNA.	Z22533	1.51	0.42
13616	similar to vaccinia virus HindIII K4L ORF	BE743194	1.51	0.31
13442	glutamate receptor, metabotropic 4	NM_000841	1.51	0.23
9376	Human mRNA for apolipoprotein E receptor 2, complete cds.	D50678	1.51	0.20
9010	keratin 15	AU122673	1.51	0.19
8034	Human, clone MGC:13090 IMAGE:3938680, mRNA, complete cds.	BC006143	1.51	0.27
13732	lysosomal-associated membrane protein 2	BI549272	1.50	0.14
882	putative protein similar to nessy (Drosophila)	BG824361	1.50	0.22
6044	absent in melanoma 1	AU139521	1.50	0.35
9896	Human cDNA FLJ14871 fis, clone PLACE1002591, moderately similar to CORONIN-LIKE PROTEIN P57.	AK027777	1.50	0.29
10678	glutathione S-transferase A4	BI597618	1.50	0.27
9386	Human mRNA for phenylalkylamine binding protein.	Z37986	1.50	0.43
2156	Human DNA for apoER2, complete cds, and exon 19.	D86407	1.50	0.18
9402	Human myosin heavy chain 12 (MYO5A) mRNA, complete cds.	U90942	1.50	0.24
6349	Macaque brain cDNA, clone:QflA-11789.	AB055286	1.50	0.35

16173	Human mRNA for putative phospholipase, complete cds.	AB019435	1.49	0.17
9772	Human caldesmon mRNA, complete cds.	M64110	1.49	0.30
6666	Human cDNA FLJ14937 fis, clone PLACE1010231, weakly similar to CELL SURFACE GLYCOPROTEIN EMR1 PRECURSOR.	AK027843	1.49	0.17
12230	ELL-RELATED RNA POLYMERASE II, ELONGATION FACTOR	U88629	1.49	0.54
6978	Human beta-glucuronidase mRNA, complete cds.	M15182	1.49	0.20
570	Human, secretory carrier membrane protein 2, clone MGC:1284 IMAGE:3050527, mRNA, complete cds.	BC001376	1.49	0.18
16197	Human mRNA for zinc finger protein (clone 647).	X16282	1.48	0.10
13184	Human mRNA for Mel-18 protein, complete cds.	D13969	1.48	0.45
3403	Human, integrin, alpha 5 (fibronectin receptor, alpha polypeptide), clone MGC:3697 IMAGE:3629647, mRNA, complete cds.	BC008786	1.48	0.10
15234	ATPase, H+ transporting, lysosomal (vacuolar proton pump) 9kD	BG779549	1.48	0.21
86	Human pyruvate dehydrogenase kinase isoenzyme 1 (PDK1) mRNA, complete cds.	L42450	1.48	0.40
4422	nuclear factor of kappa light polypeptide gene enhancer in B-cells 2 (p49/p100)	BC002844	1.47	0.19
5535	Human, Similar to hypothetical protein FLJ10883, clone IMAGE:3855861, mRNA, partial cds.	BC010693	1.47	0.13
4445	RAE1 (RNA export 1, S.pombe) homolog	BG107329	1.47	0.11
7099	hypothetical protein	BG180936	1.47	0.24
14537	Human elongation factor G1 (EFG1) mRNA, complete cds; nuclear gene for mitochondrial product.	AF367998	1.47	0.19
6785	Human centrosomal Nek2-associated protein 1 (C-NAP1) mRNA, complete cds.	AF049105	1.47	0.16
4965	Human mRNA for cathepsin C.	X87212	1.46	0.14
9873	Human mRNA for EDF-1 protein.	AJ005259	1.46	0.14
16285	Human mRNA for KIAA0356 protein, partial cds.	AB002354	1.46	0.26
14096	Human palmitoylated erythrocyte membrane protein (MPP1) mRNA, complete cds.	M64925	1.46	0.17
13683	SKI-like	NM_005414	1.45	0.28
9535	Human cDNA: FLJ23436 fis, clone HRC12692.	AK027089	1.45	0.30
6502	Human, fatty acid desaturase 3, clone MGC:4158 IMAGE:3532219, mRNA, complete cds.	BC004901	1.45	0.24
6819	Human neuronal double zinc finger protein (ZNF231) mRNA, complete cds.	AF052224	1.45	0.21
13861	mitogen-activated protein kinase 3	BC013992	1.45	0.13
5113	Human mRNA for HKR1, partial cds.	AB013897	1.45	0.37
12819	Human mRNA for copine VI protein.	AJ133798	1.45	0.25
13709	electron-transferring-flavoprotein dehydrogenase	AL551954	1.45	0.30

4399	3'-phosphoadenosine 5'-phosphosulfate synthase 1	AF016496	1.45	0.17
196	Human, Similar to CG5057 gene product, clone MGC:5309 IMAGE:2899986, mRNA, complete cds.	BC003353	1.45	0.16
15218	tyrosine 3-monooxygenase/tryptophan 5-monooxygenase activation protein, eta polypeptide	BI458375	1.44	0.12
5738	HS1 binding protein	BI261559	1.44	0.24
11087	Human mRNA for lysosomal sialoglycoprotein, complete cds.	D12676	1.44	0.32
13048	Human mRNA for KIAA0093 gene, partial cds.	D42055	1.44	0.26
5990	N-ethylmaleimide-sensitive factor attachment protein, alpha	AL553335	1.44	0.31
4858	epithelial protein lost in neoplasm alpha	AAF23756	1.44	0.30
2608	fibrillin 1 (Marfan syndrome)	NM_000138	1.44	0.09
9943	type II cytokeratin	BAA85657	1.44	0.17
7883	Human liver glycogen phosphorylase mRNA, complete cds.	M14636	1.44	0.19
7274	protein phosphatase 2, regulatory subunit B (B56), beta isoform	AV708790	1.44	0.18
12591	Human mitochondrial outer membrane protein (TOM40) mRNA, nuclear gene encoding mitochondrial protein, complete cds.	AF043250	1.43	0.25
3935	Human mRNA for KIAA1285 protein, partial cds.	AB033111	1.43	0.29
9381	Human PRM1, PRM2, PRM3, TNP2 and SOCS-1 genes.	Z46940	1.43	0.40
9758	cystathionine gamma-lyase [Human, liver, mRNA, 1326 nt].	S52784	1.43	0.31
5013	Human cDNA FLJ14456 fis, clone HEMBB1001915, moderately similar to UBIQUITIN CARBOXYL-TERMINAL HYDROLASE 64E (EC 3.1.2.15).	AK027362	1.43	0.23
18174	protein tyrosine phosphatase, non-receptor type 9	BC010863	1.43	0.20
5733	Homo sapiens clone 23763 unknown mRNA, partial cds	BG743005	1.43	0.17
2821	COP9 homolog	BG540353	1.43	0.23
5639	KIAA0121 gene product	D50911	1.42	0.19
16205	Human tuberin (TSC2) gene, intron 36.	AF020094	1.42	0.13
12210	KIAA0326 protein	AB002324	1.42	0.17
12539	Human PWP1-interacting protein 4 mRNA, complete cds.	AF277317	1.42	0.13
16612	adaptor-related protein complex 4, mu 1 subunit	AW170559	1.42	0.14
8981	cysteine-rich, angiogenic inducer, 61	AL549837	1.42	0.26
10626	ubiquitin B	BG546472	1.42	0.09
3926	annexin A7	NM_004034	1.42	0.11
13840	ilvB (bacterial acetolactate synthase)-like	AC003956	1.42	0.18
10650	cathepsin H	BI752945	1.42	0.11
18382	RAE1 (RNA export 1, S.pombe) homolog	AW590594	1.42	0.15
16947	cysteinyl-tRNA synthetase	BF000138	1.41	0.28
16764	RAB4, member RAS oncogene family	AL530764	1.41	0.18

16325	Human mRNA for KIAA0272 gene, partial cds.	D87462	1.41	0.13
17910	Human clone IMAGE:2141030, mRNA sequence.	AF339792	1.41	0.19
4480	EphB3	X75208	1.41	0.21
16951	nuclear receptor subfamily 1, group H, member 3	BF570118	1.41	0.11
16159	Human, heterogeneous nuclear ribonucleoprotein U (scaffold attachment factor A), clone MGC:1992 IMAGE:2966453, mRNA, complete cds.	BC003621	1.41	0.14
11885	phosphorylase, glycogen; liver (Hers disease, glycogen storage disease type VI)	BE884737	1.40	0.11
1975	Human, Similar to KRAB-zinc finger protein SZF1-1, clone IMAGE:3945618, mRNA, partial cds.	BC006247	1.40	0.16
16463	Human, eukaryotic translation initiation factor 5A, clone MGC:4130 IMAGE:2961296, mRNA, complete cds.	BC001832	1.40	0.07
7881	putative	BAB24631	1.40	0.21
15353	tubulin, beta polypeptide	BE729764	1.40	0.30
10470	protein tyrosine kinase 9-like (A6-related protein)	BF220316	1.40	0.14
9157	heat shock 70kD protein 5 (glucose-regulated protein, 78kD)	BI560455	1.40	0.26
7279	mesoderm development candidate 2	BC012746	1.40	0.19
15093	Rho guanine nucleotide exchange factor (GEF) 1	BE397399	1.40	0.08
5512	low density lipoprotein-related protein 1 (alpha-2-macroglobulin receptor)	BE838269	1.40	0.23
13869	BRCA1 associated protein-1 (ubiquitin carboxy-terminal hydrolase)	BG109611	1.40	0.21
8302	Human sno oncogene mRNA for snoN protein, ski-related.	X15219	1.40	0.27
9929	Human calmodulin-I (CALM1) mRNA, 3'UTR, partial sequence.	U16850	1.40	0.14
10532	matrix metalloproteinase 23B	AI347985	1.40	0.23
16940	transformer-2 alpha (htra-2 alpha)	BG250879	1.39	0.04
12766	Human septin 2-like cell division control protein mRNA, complete cds.	AF146760	1.39	0.21
13526	dystrobrevin, beta	AL562339	1.39	0.16
15361	hydroxysteroid (17-beta) dehydrogenase 4	AU125131	1.39	0.20
13158	Human, Similar to KIAA0174 gene product, clone MGC:3110 IMAGE:3350789, mRNA, complete cds.	BC000116	1.39	0.10
15355	heat shock protein 75	BE901723	1.39	0.18
16061	Human mRNA for NuMA protein.	Z11583	1.39	0.11
5588	acetyl-Coenzyme A transporter	D88152	1.39	0.08
8985	somatostatin	BI713774	1.38	0.11
9124	UDP-glucose dehydrogenase	NM_003359	1.38	0.10
17619	Human, calpain 4, small subunit (30K), clone MGC:1790 IMAGE:3347146, mRNA, complete cds.	BC000592	1.38	0.12
2443	Human Fanconi anaemia group A gene, exons 39, 40, 41, 42 and 43.	Z83095	1.38	0.19

13546	protective protein for beta-galactosidase (galactosialidosis)	AL562902	1.38	0.39
554	Human mRNA; cDNA DKFZp434H0923 (from clone DKFZp434H0923).	AL137712	1.38	0.14
13634	serine hydroxymethyltransferase 2 (mitochondrial)	AL557298	1.38	0.10
12711	Human CGI-10 protein mRNA, complete cds.	AF132944	1.37	0.15
10082	Human clone 24863 mRNA sequence.	AF131806	1.37	0.46
4942	Human mRNA for acetyl-coenzyme A transporter, complete cds.	D88152	1.37	0.15
16931	keratin 6A	BG681462	1.37	0.29
5883	phospholipase D1, phophatidylcholine-specific	U38545	1.37	0.24
4430	galactosidase, alpha	X16889	1.36	0.02
13295	Human beta-myosin heavy chain (MYH7) mRNA, complete cds.	M58018	1.36	0.18
14769	Human C4-sterol methyl oxidase homolog (DESP4) mRNA, complete cds.	U93162	1.36	0.22
2450	Human glia-derived nexin (GDN) mRNA, 5' end.	M17783	1.36	0.40
6038	ATPase, Class I, type 8B, member 1	NM_005603	1.36	0.18
8911	golgi SNAP receptor complex member 2	BE729362	1.36	0.17
12180	G protein pathway suppressor 1	BG169279	1.36	0.18
7121	aldehyde dehydrogenase 3 family, member B1	U10868	1.36	0.10
8606	SH3 domain binding glutamic acid-rich protein	AI422208	1.36	0.30
5511	Homo sapiens cDNA FLJ13847 fis, clone THYRO1000852, highly similar to Human branched-chain amino acid aminotransferase (ECA40) mRNA	AL558311	1.36	0.16
10339	kinesin family member 1C	AB014606	1.35	0.15
13837	proteasome (prosome, macropain) subunit, beta type, 6	BF984053	1.35	0.16
10190	similar to S. cerevisiae Sec6p and R. norvegicus rsec6	AF055006	1.35	0.17
16907	ribophorin I	BE780549	1.35	0.09
18230	myosin, light polypeptide 5, regulatory	L03785	1.35	0.19
17872	Human cDNA: FLJ23249 fis, clone COL04196.	AK026902	1.35	0.19
14844	Human novel protein AHNAK mRNA, partial sequence.	M80899	1.35	0.22
17575	Human mRNA for peptide transporter 3, complete cds.	AB020598	1.35	0.25
5178	Human DNA topoisomerase III mRNA, complete cds.	U43431	1.35	0.17
7854	Human SWI/SNF complex 170 KDa subunit (BAF170) mRNA, complete cds.	U66616	1.35	0.19
1968	Human mRNA for ring-IBR-ring domain containing protein Dorfin, complete cds.	AB029316	1.35	0.12
15051	golgi autoantigen, golgin subfamily a, 5	NM_005113	1.35	0.12
12251	eukaryotic translation initiation factor 3, subunit 7 (zeta, 66/67kD)	BG829032	1.35	0.23
13824	vacuolar protein sorting 45B (yeast homolog)	BF796127	1.35	0.20
5834	ATPase, Na+/K+ transporting, beta 3 polypeptide	AU151263	1.35	0.08

17232	Human, Similar to RIKEN cDNA 2300002L21 gene, clone MGC:17528 IMAGE:3458906, mRNA, complete cds.	BC010541	1.34	0.07
4014	chromosome 19 open reading frame 3	AW409924	1.34	0.27
14895	Human genomic DNA, chromosome 6p21.3, HLA Class I region, section 2/20.	AP000503	1.34	0.13
13346	Human urokinase-type plasminogen receptor, exon 7.	U09937	1.34	0.15
11559	Human mRNA for rat HREV107-like protein.	X92814	1.34	0.08
11335	Human cDNA FLJ11848 fis, clone HEMBA1006708, weakly similar to HYPOTHETICAL 46.4 KD TRP-ASP REPEATS CONTAINING PROTEIN IN PMC1-TFG2 INTERGENIC REGION.	AK021910	1.34	0.18
2605	tumor necrosis factor receptor superfamily, member 21	NM_014452	1.34	0.16
5510	phenylalanine-tRNA synthetase-like	AD000092	1.34	0.12
5977	D123 gene product	BE792735	1.34	0.19
6564	Novel Human mRNA from chromosome 20, similar to SW:GOLI_DROME Q06003 GOLIATH PROTEIN.	AL096778	1.33	0.34
11007	Human DiGeorge syndrome critical region, centromeric end.	L77570	1.33	0.22
6441	Human cDNA: FLJ23330 fis, clone HEP12654.	AK026983	1.33	0.09
10559	neuronal PAS domain protein 2	U77970	1.33	0.19
2820	CD44 antigen (homing function and Indian blood group system)	BG822701	1.33	0.32
14955	putative mitochondrial outer membrane protein import receptor	BF509900	1.33	0.14
13080	thrombin inhibitor	BAA19875	1.33	0.11
2448	KIAA0515 protein	AB011087	1.33	0.22
948	heat shock transcription factor 1	BG473635	1.32	0.08
16968	dynactin 2 (p50)	U50733	1.32	0.17
4941	Human mRNA; cDNA DKFZp564I1782 (from clone DKFZp564I1782); complete cds.	AL136699	1.32	0.29
11746	Protein P3	NM_019848	1.32	0.06
4410	proteasome (prosome, macropain) 26S subunit, non-ATPase, 1	AU118540	1.32	0.03
14559	Human, 3 beta-hydroxy-delta 5-C27-steroid oxidoreductase, clone MGC:10497 IMAGE:3626629, mRNA, complete cds.	BC004929	1.31	0.15
4307	cytochrome c oxidase subunit IV	BF726186	1.31	0.16
16809	myosin, light polypeptide kinase	AW951177	1.31	0.15
6940	Human cDNA: FLJ23306 fis, clone HEP11541.	AK026959	1.31	0.11
10236	mitogen-activated protein kinase 4	AV707392	1.31	0.17
14906	Human keratin 18 (KRT18) gene, complete cds.	AF179904	1.31	0.20
14600	Human cDNA FLJ10249 fis, clone HEMBB1000725, highly similar to Rattus norvegicus GTPase Rab8b mRNA.	AK001111	1.31	0.10
12657	Human voltage-gated chloride ion channel CLCN5.	X91906	1.31	0.11
6973	Human mRNA for putative ATPase, partial.	AJ006268	1.31	0.16

5809	ATP-binding cassette, sub-family B (MDR/TAP), member 10	AW949716	1.31	0.17
14847	extracellular matrix protein 2, female organ and adipocyte specific	NM_001393	1.30	0.17
13191	Human, Similar to ribophorin I, clone MGC:5072 IMAGE:3461167, mRNA, complete cds.	BC010839	1.30	0.11
4015	Human mRNA; cDNA DKFZp761F0324 (from clone DKFZp761F0324).	AL136595	1.30	0.17
9136	O-linked N-acetylglucosamine (GlcNAc) transferase (UDP-N-acetylglucosamine:polypeptide-N-acetylglucosaminyl transferase)	NM_003605	1.30	0.12
14584	Human mitochondrial benzodiazepine receptor (MBR) gene, complete cds.	U12421	1.30	0.19
5724	diptheria toxin resistance protein required for diphthamide biosynthesis (Saccharomyces)-like 2	BI521245	1.30	0.15
14582	Human ERK3 mRNA.	X80692	1.30	0.08
8294	Human, RIKEN cDNA 2610511F20 gene, clone MGC:15482 IMAGE:2987858, mRNA, complete cds.	BC007557	1.30	0.17
15960	Human mRNA; cDNA DKFZp761E129 (from clone DKFZp761E129); partial cds.	AL137453	1.30	0.16
10941	Human chromosome X region from filamin (FLN) gene to glucose-6-phosphate dehydrogenase (G6PD) gene, complete cds's.	L44140	1.29	0.11
7818	Human cDNA FLJ10762 fis, clone NT2RP4000008, moderately similar to CHLORINE CHANNEL PROTEIN P64.	AK001624	1.29	0.10
14616	Human, nucleobindin 1, clone MGC:8479 IMAGE:2821805, mRNA, complete cds.	BC002356	1.29	0.04
7251	sushi-repeat-containing protein, X chromosome	U78093	1.29	0.08
15203	cystatin B (stefin B)	BG283058	1.29	0.37
9968	Human mRNA for KIAA0996 protein, complete cds.	AB023213	1.28	0.18
8688	cytoplasmic FMRP interacting protein 1	BI522540	1.28	0.13
7206	immunoglobulin heavy constant mu	BM008087	1.28	0.11
1668	Human, MpV17 transgene, murine homolog, glomerulosclerosis, clone MGC:1703 IMAGE:2967261, mRNA, complete cds.	BC001115	1.28	0.28
12868	Human mRNA; cDNA DKFZp761P2414 (from clone DKFZp761P2414); complete cds.	AL161976	1.28	0.07
6267	Human connexin45 gene, complete cds.	U03493	1.28	0.12
3708	Human, tubulin alpha 1, clone MGC:16616 IMAGE:4111591, mRNA, complete cds.	BC009314	1.28	0.21
5405	Human gene encoding retina-specific guanylyl cyclase.	AJ222657	1.27	0.11
13733	zinc finger protein 263	AC004232	1.27	0.13
4237	zinc finger protein 151 (pHZ-67)	BG326594	1.27	0.20
13366	hypothetical protein 24432	AI379916	1.27	0.17
10687	eukaryotic translation initiation factor 2B, subunit 5 (epsilon, 82kD)	U23028	1.27	0.06
10084	Human bcr mRNA (break point cluster gene).	Y00061	1.27	0.12
6817	Human microtubule-associated protein 1B (MAP1B) gene, complete cds.	L06237	1.27	0.09
15843	Human nuclear orphan receptor LXR-alpha mRNA, complete cds.	U22662	1.27	0.10

11458	Human protein phosphatase 2C alpha 2 mRNA, complete cds.	AF070670	1.27	0.10
3953	insulin-like growth factor binding protein-2 [Human, placenta, Genomic, 1342 nt, segment 4 of 4].	S37730	1.26	0.20
11964	prostaglandin I2 (prostacyclin) synthase	D38145	1.26	0.07
13818	tissue specific transplantation antigen P35B	BG750166	1.26	0.35
2513	a disintegrin and metalloproteinase domain 15 (metargidin)	BG766668	1.26	0.12
9115	ELK3, ETS-domain protein (SRF accessory protein 2)	BI767724	1.26	0.14
13218	Human preprothyrotropin-releasing hormone gene, exon 3 and thyrotropin-releasing hormone, complete cds.	M63582	1.26	0.08
13362	TRAF and TNF receptor-associated protein	NM_016614	1.26	0.18
6807	Human CpG island DNA genomic Mse1 fragment, clone 186c1, reverse read cpg186c1.rt1b.	Z55026	1.25	0.06
16772	NBR2	U88573	1.25	0.15
10374	microtubule-associated protein 1B	BE935831	1.25	0.10
8359	Human mRNA; cDNA DKFZp564K2478 (from clone DKFZp564K2478); complete cds.	AL136690	1.25	0.10
16611	selenophosphate synthetase 2	BG674956	1.25	0.05
9134	transmembrane 9 superfamily member 2	AU131084	1.24	0.07
10246	DNA-damage-inducible transcript 3	BE410528	1.24	0.09
15404	COP9 (constitutive photomorphogenic, Arabidopsis, homolog) subunit 3	AA287305	1.24	0.11
11001	Human mRNA for KIAA0820 protein, partial cds.	AB020627	1.23	0.11
7418	catenin (cadherin-associated protein), alpha 1 (102kD)	AW250105	1.23	0.10
7292	p53-induced protein	AL521557	1.22	0.09
12846	bA346K17.2 (A novel protein similar to the cell division control protein 91 (CDC91, YLR459W or L9122.2) from Yeast)	CAC14080	1.22	0.10
7110	heat shock 70kD protein 9B (mortalin-2)	BG427082	1.22	0.14
13855	for protein disulfide isomerase-related	D49490	1.22	0.10
12136	guanine nucleotide binding protein (G protein), alpha inhibiting activity polypeptide 2	BC014627	1.22	0.09
14799	Human HALPHA44 gene for alpha-tubulin, exons 1-3.	X06956	1.21	0.24
13865	prostate tumor over expressed gene 1	BG764153	1.21	0.09
7424	tight junction protein 2 (zona occludens 2)	L27476	1.21	0.15
6950	Human, Similar to UDP-galactose transporter related, clone MGC:20043 IMAGE:3832062, mRNA, complete cds.	BC011888	1.21	0.08
15824	Human encoding vasodilator-stimulated phosphoprotein (VASP).	Z46389	1.21	0.19

11405	Human DMAHP gene.	X84813	1.21	0.09
13075	Human oncomodulin gene, exon 5.	L20348	1.20	0.09
14288	Human mRNA; cDNA DKFZp586N1922 (from clone DKFZp586N1922); partial cds.	AL117468	1.20	0.08
44	Human mRNA for KET protein.	Y16961	1.20	0.36
14751	Human esophageal cancer related gene 4 protein (ECRG4) mRNA, complete cds.	AF325503	1.20	0.08
1809	Human mRNA for ubiquitin-like protein, complete cds.	D23662	1.19	0.12
10405	PTD008 protein	AA315771	1.19	0.15
7913	putative	BAB23139	1.19	0.08
5560	galactose-1-phosphate uridylyltransferase	BG741575	1.18	0.06
8672	radixin	BF194976	1.17	0.07
7122	Rac/Cdc42 guanine exchange factor (GEF) 6	D13631	1.17	0.09
4253	KIAA0670 protein/acinus	AF124727	1.17	0.12
12109	NADH dehydrogenase (ubiquinone) 1 beta subcomplex, 7 (18kD, B18)	BI835169	1.16	0.14
16011	Human mRNA for squalene epoxidase, complete cds.	D78130	1.15	0.20
15081	myosin, light polypeptide, regulatory, non-sarcomeric (20kD)	AA345289	1.15	0.12
16785	karyopherin (importin) beta 2	U72069	1.14	0.08
2447	eukaryotic translation initiation factor 3, subunit 8 (110kD)	AL529959	1.13	0.07
6951	Human, clone MGC:15765 IMAGE:3501642, mRNA, complete cds.	BC009434	1.13	0.24
6789	Human vascular endothelial growth factor (VEGF) mRNA, 3'UTR.	AF024710	1.13	0.08
13674	junction plakoglobin	BG775483	1.12	0.06
14611	Human kruppel-like zinc finger protein (ZNF300) mRNA, complete cds.	AF395541	1.09	0.07

Genes Significantly (P<0.005) Downregulated By Shear Stress in PAVEC
Group 1 Down

Agilent Feature #	Gene Name/Description	Count 311		
		Gene ID	Fold AVE	Fold STD
8368	Human cDNA: FLJ21156 fis, clone CAS09878.	AK024809	4.16	3.27
16488	kinesin-like 4	NM_007317	3.02	1.99
10644	ectodermal-neural cortex (with BTB-like domain)	BC000418	2.95	0.96
11934	cell division cycle 2, G1 to S and G2 to M	AL520473	2.65	0.34
14388	Human cDNA FLJ12587 fis, clone NT2RM4001217, moderately similar to Mouse (Mus musculus) actin-binding protein (ENC-1) mRNA.	AK022649	2.62	0.66
11654	Human cyclin-selective ubiquitin carrier protein mRNA, complete cds.	U73379	2.57	0.30
8825	caveolin 1, caveolae protein, 22kD	NM_001753	2.55	0.79
9932	Human caveolin 1 (CAV1) gene, exon 3 and partial cds.	AF125348	2.52	0.79
9622	Human cell cycle control gene CDC2.	Y00272	2.51	0.35
13481	PDZ and LIM domain 1 (elfin)	AI687946	2.33	0.46
2782	topoisomerase (DNA) II alpha (170kD)	BF795918	2.31	0.28
12196	KIAA0101 gene product	NM_014736	2.26	0.24
11882	polymerase (DNA directed), epsilon 2	AF036899	2.20	0.34
10544	kinesin-like 1	X85137	2.19	0.28
14857	v-myc avian myelocytomatosis viral related oncogene, neuroblastoma derived	BF313082	2.12	0.92
11506	Human BRCA1, Rho7 and vatI genes, complete cds, and ipf35 gene, partial cds.	L78833	2.10	0.21
13765	CDC28 protein kinase 2	BG618998	2.10	0.13
5847	thymopoietin	U09088	2.10	0.25
9094	amylase, alpha 2B; pancreatic	NM_020978	2.09	0.69
11142	Human mRNA encoding the c-myc oncogene.	V00568	2.05	0.37
17894	Human, Similar to cyclin B1, related sequence 1, clone MGC:2548 IMAGE:2963100, mRNA, complete cds.	BC006510	2.03	0.18
16273	Human nuclear factor I-B2 (NFIB2) mRNA, complete cds.	U85193	2.02	0.16
9541	Human, PDZ and LIM domain 1 (elfin), clone MGC:5344 IMAGE:2985229, mRNA, complete cds.	BC000915	2.01	0.36
13503	chromosome condensation-related SMC-associated protein 1	BE793681	2.00	0.43
4408	ESTs, Highly similar to A38712 fibrillarin [H.sapiens]	AI199605	2.00	0.50
8941	highly expressed in cancer, rich in leucine heptad repeats	AA878068	1.99	0.38
7555	phosphodiesterase 3B, cGMP-inhibited	BI756567	1.98	0.44
6942	Human dek mRNA.	X64229	1.95	0.20
2619	paternally expressed 10	AF038197	1.95	0.36

3348	Human histone acetyltransferase 1 mRNA, complete cds.	AF030424	1.93	0.21
251	Human ubiquitin-specific protease (UBP) mRNA, complete cds.	AF117386	1.91	0.30
13815	glia maturation factor, gamma	AA279067	1.89	0.12
2292	Human mRNA for KIAA0949 protein, partial cds.	AB023166	1.89	0.19
7368	KIAA0256 gene product	BG107450	1.89	0.27
13315	TTK protein kinase	M86699	1.88	0.17
3946	DEK oncogene (DNA binding)	AU152618	1.87	0.20
10641	kinesin-like 5 (mitotic kinesin-like protein 1)	BM014478	1.87	0.16
16260	Human cDNA FLJ10633 fis, clone NT2RP2005640.	AK001495	1.87	0.64
8531	similar to mouse olfactory receptor 13; similar to P34984 (PID:g464305)	AAD05193	1.87	0.25
2515	CHK1 (checkpoint, S.pombe) homolog	AF016582	1.86	0.24
203	Human replication protein A 14kDa subunit (RPA) mRNA, complete cds.	L07493	1.85	0.86
1345	serine (or cysteine) proteinase inhibitor, clade I (neuroserpin), member 1	BI915951	1.85	0.16
13835	putative human HLA class II associated protein I	AY007110	1.85	0.12
15342	proliferating cell nuclear antigen	AA523378	1.83	0.19
6507	Human c-jun proto oncogene (JUN), complete cds, clone hCJ-1.	J04111	1.81	0.15
8297	Human mRNA; cDNA DKFZp434M152 (from clone DKFZp434M152).	AL137687	1.80	0.39
13316	baculoviral IAP repeat-containing 5 (survivin)	AL571008	1.79	0.50
5465	vaccinia related kinase 1	AA312869	1.78	0.16
3167	Human, Similar to gene rich cluster, C8 gene, clone MGC:2577 IMAGE:3138951, mRNA, complete cds.	BC002551	1.77	0.36
15978	Human cDNA: FLJ21715 fis, clone COL10287, highly similar to AF071569 Human multifunctional calcium/calmodulin-dependent protein kinase II delta2 isoform mRNA.	AK025368	1.77	0.19
13776	arginase, type II	BC001350	1.75	0.31
12827	Human early B-cell transcription factor (EBF) mRNA, partial cds.	AF208502	1.72	0.17
16313	Human replication factor C, 37-kDa subunit mRNA, complete cds.	M87339	1.72	0.09
8842	fasciculation and elongation protein zeta 2 (zygin II)	AF113124	1.70	0.12
11439	Human uveal autoantigen mRNA, complete cds.	AF322916	1.69	0.33
12219	hypothetical protein PRO1489	AI536671	1.68	0.36
1350	U2 small nuclear ribonucleoprotein auxiliary factor (65kD)	BI962886	1.68	0.20
12551	Human mRNA for transferrin receptor.	X01060	1.67	0.47
181	Human gene for thrombomodulin precursor, complete cds.	D00210	1.67	0.12
13806	cadherin 11, type 2, OB-cadherin (osteoblast)	BI766088	1.67	0.13
8740	dCMP deaminase	AA101974	1.67	0.17
5976	serum-inducible kinase	BG677879	1.67	0.60

3326	Human cDNA FLJ10470 fis, clone NT2RP2000032, weakly similar to RAS SUPPRESSOR PROTEIN 1.	AK001332	1.66	0.60
12882	Human, CDC20 (cell division cycle 20, S. cerevisiae, homolog), clone MGC:15276 IMAGE:2959596, mRNA, complete cds.	BC009426	1.66	0.28
5652	5-aminoimidazole-4-carboxamide ribonucleotide formyltransferase/IMP cyclohydrolase	D89976	1.66	0.17
16895	BRCA1 associated RING domain 1	AW002440	1.66	0.22
15222	Homo sapiens cDNA: FLJ23324 fis, clone HEP12482, highly similar to HUMMYOHCB Human nonmuscle myosin heavy chain-B (MYH10) mRNA	AA724155	1.66	0.10
9014	EphA4	L36645	1.66	0.56
14123	Human TALE homeobox protein Meis2b mRNA, complete cds.	AF179896	1.66	0.20
7348	phosphodiesterase 6D, cGMP-specific, rod, delta	BC007831	1.65	0.34
10501	exonuclease 1	AC004783	1.64	0.36
16640	hypoxia-inducible factor 1, alpha subunit (basic helix-loop-helix transcription factor)	AU154668	1.63	0.11
11671	Human H1.2 gene for histone H1.	X57129	1.63	0.48
15233	enhancer of zeste (Drosophila) homolog 2	BE729850	1.62	0.13
1985	Human Trio isoform mRNA, complete cds.	AF091395	1.62	0.19
15044	inhibitor of growth family, member 3	BG574907	1.61	0.22
4446	KIAA0603 gene product	BI906891	1.60	0.22
16274	Human, ubiquitin-conjugating enzyme E2E 3 (homologous to Yeast UBC4/5), clone MGC:1316 IMAGE:3537280, mRNA, complete cds.	BC003554	1.60	0.17
4421	insulin-like growth factor 1 (somatomedin C)	M11568	1.60	0.20
6008	Homo sapiens cDNA: FLJ21930 fis, clone HEP04301, highly similar to HSU90916 Human clone 23815 mRNA sequence	U90916	1.60	0.29
12707	Human TRIP7-like protein mRNA, complete cds.	AY043282	1.60	0.14
11255	Human mRNA; cDNA DKFZp761C121 (from clone DKFZp761C121); complete cds.	AL136560	1.59	0.35
7533	ataxia telangiectasia and Rad3 related	U49844	1.59	0.40
14908	natriuretic peptide receptor C/guanylate cyclase C (atrionatriuretic peptide receptor C)	BF224187	1.59	0.48
8747	ribosomal protein L23a	AA857067	1.59	0.31
13679	myosin, heavy polypeptide 8, skeletal muscle, perinatal	Z38133	1.59	0.16
2462	hypothetical protein	AI792005	1.58	0.10
3373	Human, hypothetical protein, clone MGC:3375 IMAGE:3609357, mRNA, complete cds.	BC002677	1.58	0.32
1032	H2A histone family, member N	BE253911	1.58	0.37
12532	Human PBX3 mRNA.	X59841	1.57	0.17
17241	Human cDNA FLJ10244 fis, clone HEMBB1000632, weakly similar to GUANINE NUCLEOTIDE RELEASING PROTEIN.	AK001106	1.57	0.32

11284	Human (clones HGPCD2 and HGPCD15) pterin-4a-carbinolamine dehydratase (PCBD) gene, complete cds.	L41560	1.57	0.26
10588	minichromosome maintenance deficient (S. cerevisiae) 7	AI285101	1.57	0.28
7369	Thy-1 cell surface antigen	N94350	1.57	0.13
16737	methylthioadenosine phosphorylase	AL048242	1.56	0.16
16590	coproporphyrinogen oxidase (coproporphyria, harderoporphyria)	NM_000097	1.56	0.12
7065	heterogeneous nuclear ribonucleoprotein H3 (2H9)	BG574659	1.56	0.32
14618	Human, Similar to advillin, clone MGC:1461 IMAGE:2961396, mRNA, complete cds.	BC004134	1.56	0.58
4719	Human 1-8D gene from interferon-inducible gene family.	X57351	1.55	0.36
10275	hypothetical protein MGC19556	BG830088	1.55	0.18
9113	primase, polypeptide 2A (58kD)	X74331	1.55	0.38
16328	Human H2B.2 and H2A.1 genes for Histone H2A and H2B.	X57138	1.55	0.34
6881	Human zinc finger transcription factor (ZNF207) mRNA, complete cds.	AF046001	1.54	0.10
8053	Human mRNA for MEMD protein.	Y10183	1.54	0.21
185	Human, Similar to heterogeneous nuclear ribonucleoprotein A3, clone MGC:20045 IMAGE:4661041, mRNA, complete cds.	BC012090	1.54	0.25
10397	calcium/calmodulin-dependent protein kinase kinase 2, beta	AI925424	1.54	0.15
56	Human hypoxanthine phosphoribosyltransferase (HPRT) mRNA, complete cds.	M31642	1.54	0.27
16799	ovo (Drosophila) homolog-like 1	AF016045	1.53	0.10
13320	protein phosphatase 1, catalytic subunit, gamma isoform	BG289736	1.53	0.08
9169	neurogranin (protein kinase C substrate, RC3)	BF948983	1.53	0.29
4994	Human zinc finger protein 277 (ZNF277) mRNA, complete cds.	AF209198	1.53	0.25
7578	ATP synthase, H+ transporting, mitochondrial F0 complex, subunit b, isoform 1	AA527110	1.53	0.13
6888	Human mRNA for hMCM2, complete cds.	D28480	1.53	0.32
5129	bA149I18.1 (novel protein)	CAC16127	1.53	0.42
10462	mal, T-cell differentiation protein	NM_022439	1.53	0.25
4242	interferon induced transmembrane protein 1 (9-27)	BG506643	1.53	0.31
4095	Homo sapiens mRNA; cDNA DKFZp564H2416 (from clone DKFZp564H2416)	N92498	1.53	0.14
746	Human CAAX box protein TIMAP mRNA, complete cds.	AF362910	1.52	0.35
13543	ESTs, Highly similar to JC4662 ribosomal protein S3a, cytosolic [H.sapiens]	BF663467	1.52	0.28
6879	Human FUSE binding protein mRNA, complete cds.	U05040	1.52	0.13
13457	S-adenosylmethionine decarboxylase 1	AI042585	1.51	0.07
5267	Human cDNA FLJ13287 fis, clone OVARC1001161.	AK023349	1.51	0.30

15022	interferon induced transmembrane protein 3 (1-8U)	BE886918	1.51	0.25
14398	Human CGI-142 protein mRNA, complete cds.	AF151900	1.51	0.15
11359	Human putative transcriptional regulator ENX-1 mRNA, complete cds.	U52965	1.51	0.06
13166	Human mRNA for KIAA1226 protein, partial cds.	AB033052	1.50	0.25
7398	ESTs, Highly similar to I51803 TAXREB107 [H.sapiens]	AW514303	1.50	0.23
10005	Human methylmalonyl-CoA mutase (MCM) mRNA, complete cds.	M65131	1.50	0.41
4703	Human mRNA for SET-binding protein (SEB), complete cds.	AB022660	1.50	0.16
3485	Macaque testis cDNA clone:QtsA-13672, full insert sequence.	AB070098	1.50	0.30
14705	Human genomic DNA, chromosome 21q22.1, D21S226-AML region, clone:T604.	AP000303	1.49	0.14
18359	HYA22 protein	AA487463	1.49	0.20
2903	methylmalonyl Coenzyme A mutase	AA702733	1.49	0.40
11277	Human arpp mRNA for ankyrin-repeat protein, complete cds.	AB058599	1.49	0.23
900	polymerase (DNA directed), delta 3	D26018	1.49	0.07
8510	Human 5T4 oncofetal trophoblast glycoprotein gene.	AJ012159	1.49	0.14
3753	Human mRNA for protein kinase PAK5, complete cds.	AB040812	1.49	0.18
10204	Human homolog of Yeast mutL (hPMS1) gene, complete cds.	U13695	1.49	0.25
1675	Human CUG-binding protein LYLQ isoform mRNA, complete cds.	AF267533	1.48	0.08
15656	Human Ste-20 related kinase SPAK mRNA, complete cds.	AF099989	1.48	0.14
3797	Human, secretory granule, neuroendocrine protein 1 (7B2 protein), clone MGC:12446 IMAGE:3949961, mRNA, complete cds.	BC005349	1.48	0.12
13643	activated leucocyte cell adhesion molecule	AI050952	1.48	0.30
8915	hypothetical protein FLJ11149	BI752967	1.48	0.31
10307	A kinase (PRKA) anchor protein (yotiao) 9	NM_005751	1.48	0.15
13801	SWI/SNF related, matrix associated, actin dependent regulator of chromatin, subfamily b, member 1	BF977892	1.47	0.09
10161	Human lens epithelium-derived growth factor gene, alternatively spliced, complete cds.	AF199339	1.47	0.18
6356	Human replication factor C large subunit mRNA, complete cds.	L23320	1.47	0.11
7362	interleukin 13	NM_002188	1.47	0.26
14297	Human mRNA for putative transcription factor-like nuclear regulator (TFNR gene).	AJ238520	1.46	0.11
14266	Human mRNA; cDNA DKFZp434D0215 (from clone DKFZp434D0215); partial cds.	AL133047	1.46	0.24
13774	ESTs, Highly similar to R5HU7 ribosomal protein L7, cytosolic [H.sapiens]	AV740966	1.45	0.17
13174	Human tankyrase-2 (TNKS-2) mRNA, complete cds.	AF309033	1.45	0.59
8978	centaurin, beta 2	BC014843	1.45	0.28

14406	Human NADH-ubiquinone oxidoreductase subunit CI-SGDH mRNA, complete cds.	AF047181	1.45	0.31
3962	ESTs, Highly similar to TBCA_HUMAN TUBULIN-SPECIFIC CHAPERONE A [H.sapiens]	BI492241	1.45	0.07
14254	Human TESTIN 2 and TESTIN 3 genes, complete cds, alternatively spliced.	AF260225	1.44	0.18
16950	HIV-1 rev binding protein 2	AW974533	1.43	0.16
8857	H2B histone family, member A	AV759568	1.43	0.21
8535	Human mRNA; cDNA DKFZp564J2222 (from clone DKFZp564J2222); complete cds.	AL136608	1.43	0.10
7046	cleavage and polyadenylation specific factor 5, 25 kD subunit	AA738354	1.43	0.06
7183	phosphodiesterase 2A, cGMP-stimulated	U67733	1.43	0.19
10665	chromosome 2 open reading frame 6	AL122062	1.43	0.12
7842	Human genomic DNA, chromosome 21q, section 14/105.	AP001670	1.42	0.08
5503	RAS p21 protein activator (GTPase activating protein) 1	NM_022650	1.42	0.11
13197	Human myocyte-specific enhancer factor 2A (MEF2A) gene, last coding exon, and complete cds.	U49020	1.42	0.06
5420	Human nuclear antigen H731-like protein mRNA, complete cds.	U96628	1.42	0.06
8839	CLIP-associating protein 1	AB014522	1.42	0.22
13342	Human beta-tubulin pseudogene, clone 7-beta.	K00842	1.42	0.07
2920	ESTs, Highly similar to B Chain B, Crystal Structure Of The Human Cdk2 Kinase Complex With Cell Cycle-Regulatory Protein Ckshs1 [H.sapiens]	AI033892	1.42	0.14
14276	Human zinc finger protein ANC_2H01 mRNA, complete cds.	AF003924	1.41	0.19
14277	Human esterase D mRNA, complete cds.	AF112219	1.41	0.10
5491	KIAA0470 gene product	AB022659	1.41	0.09
10299	Homo sapiens clone 24711 mRNA sequence	AF055029	1.41	0.17
15813	Human death associated protein 4 (DAP4) mRNA, complete cds.	AF081567	1.41	0.13
7590	ESTs, Weakly similar to I38022 hypothetical protein [H.sapiens]	BG718906	1.41	0.07
7967	thymosin beta-10 [Human, metastatic melanoma cell line, mRNA, 453 nt].	S54005	1.40	0.20
1368	membrane-bound transcription factor protease, site 1	AL133583	1.40	0.15
16591	chromodomain helicase DNA binding protein 1	AF006513	1.40	0.18
15091	putative DNA binding protein	BC010013	1.40	0.05
14744	Human mRNA for p cadherin.	X63629	1.40	0.17
5589	serine (or cysteine) proteinase inhibitor, clade G (C1 inhibitor), member 1	AL531502	1.40	0.13
16726	retinoblastoma-binding protein 4	BC015123	1.40	0.16
8791	H-2K binding factor-2	BG574227	1.40	0.14
15312	cerebral cavernous malformations 1	BG163551	1.40	0.17
14704	Human programmed cell death 9 (PDCD9) mRNA, complete cds.	AF146192	1.40	0.11
4272	hypothetical protein	W74196	1.40	0.15

497	Human, tyrosine 3-monooxygenase/tryptophan 5-monooxygenase activation protein, epsilon polypeptide, clone MGC:1250 IMAGE:3139004, mRNA, complete cds.	BC001440	1.40	0.15
12287	zinc finger protein 197	NM_006991	1.39	0.37
15652	Human sperm protein 17 mRNA, complete cds.	AF334735	1.39	0.16
16607	downregulated in ovarian cancer 1	U53445	1.39	0.09
6885	Human monocytic leukaemia zinc finger protein (MOZ) mRNA, complete cds.	U47742	1.39	0.07
13347	Human cDNA FLJ10655 fis, clone NT2RP2005933, weakly similar to NUCLEOPORIN NUP57.	AK001517	1.39	0.08
16462	Human apolipoprotein AI regulatory protein-1/chicken ovalbumin upstream promoter transcription factor II (TFCOUP2) gene, complete cds.	U60477	1.38	0.05
9127	brain and reproductive organ-expressed (TNFRSF1A modulator)	BG198322	1.38	0.09
13216	Human mRNA for KIAA1296 protein, partial cds.	AB037717	1.38	0.09
11940	RAP1A, member of RAS oncogene family	BI856433	1.38	0.12
2816	KIAA0301 protein	N24059	1.38	0.16
7365	Sjogren syndrome antigen B (autoantigen La)	AA479280	1.38	0.06
8749	KIAA0528 gene product	BG619195	1.38	0.19
254	Human cDNA FLJ20403 fis, clone KAT01539.	AK000410	1.38	0.22
5874	interferon-induced protein with tetratricopeptide repeats 1	M24594	1.38	0.55
3798	Human hairy (HRY) mRNA, complete cds.	AF264785	1.37	0.34
7607	suppression of tumorigenicity 7	BI818571	1.37	0.16
10327	dUTP pyrophosphatase	AW276291	1.37	0.12
8833	v-jun avian sarcoma virus 17 oncogene homolog	AI051628	1.37	0.09
8588	Human cDNA FLJ11341 fis, clone PLACE1010786.	AK002203	1.36	0.15
3933	asparagine synthetase	BC014621	1.36	0.22
6631	Human mRNA for KIAA0636 protein, complete cds.	AB014536	1.36	0.11
11969	pleckstrin homology, Sec7 and coiled/coil domains 1(cytohesin 1)	NM_017456	1.36	0.10
2591	Homo sapiens, Similar to RNA binding motif protein, X chromosome, clone MGC:9398 IMAGE:3875565, mRNA, complete cds	BG167309	1.35	0.06
11902	G-rich RNA sequence binding factor 1	BF034561	1.35	0.23
12051	ribosomal protein L37	BG032793	1.35	0.11
11185	Human mRNA for myb-related gene A-myb 5'-region.	X13294	1.35	0.10
8443	Human, ribosomal protein S24, clone MGC:3989 IMAGE:2958303, mRNA, complete cds.	BC003149	1.35	0.15
11959	S-adenosylmethionine decarboxylase 1	BF676785	1.34	0.14
4265	smg GDS-ASSOCIATED PROTEIN	BG433239	1.34	0.16
10697	nuclear receptor subfamily 3, group C, member 1	X03225	1.34	0.26

9596	Human, Similar to stromal antigen 2, clone MGC:1282 IMAGE:3352347, mRNA, complete cds.	BC001765	1.34	0.12
9560	Human protein kinase C iota isoform, complete cds.	L33881	1.34	0.19
5329	Human heat shock protein hsp70-related protein mRNA, complete cds.	AF112210	1.34	0.10
13785	ESTs, Highly similar to ROA3_HUMAN HETEROGENEOUS NUCLEAR RIBONUCLEOPROTEIN A3 [H.sapiens]	AW976907	1.34	0.08
13139	Human, Williams-Beuren syndrome chromosome region 1 homolog (Human), clone MGC:19645 IMAGE:2960402, mRNA, complete cds.	BC010021	1.34	0.06
3455	Human cDNA FLJ12082 fis, clone HEMBB1002492.	AK022144	1.34	0.11
8838	ADP-ribosyltransferase 3	AI201027	1.34	0.13
6886	Human, clone IMAGE:4156419, mRNA, partial cds.	BC010457	1.34	0.05
1969	Human Bruton's tyrosine kinase (BTK), alpha-D-galactosidase A (GLA), L44-like ribosomal protein (L44L) and FTP3 (FTP3) genes, complete cds.	U78027	1.33	0.17
6892	Human, Similar to CG9602 gene product, clone MGC:3733 IMAGE:3619626, mRNA, complete cds.	BC002775	1.33	0.16
738	Human protocadherin-beta15 (PCDHB15) mRNA, complete cds.	AF217742	1.33	0.06
13305	M-phase phosphoprotein 10 (U3 small nucleolar ribonucleoprotein)	X98494	1.33	0.29
10186	protein phosphatase 2, regulatory subunit B (B56), epsilon isoform	BI496977	1.33	0.13
5413	Human, Similar to RIKEN cDNA 1200013F24 gene, clone MGC:12197 IMAGE:3997840, mRNA, complete cds.	BC006982	1.32	0.05
14090	Human gcp60 mRNA for golgi resident protein GCP60, complete cds.	AB043587	1.32	0.16
9522	Human Bcl2, p53 binding protein Bbp/53BP2 (BBP/53BP2) mRNA, complete cds.	U58334	1.31	0.14
12702	Macaque brain cDNA clone:QmoA-10711, full insert sequence.	AB062987	1.31	0.12
13524	retinoblastoma-like 1 (p107)	M74547	1.31	0.13
16734	ESTs, Weakly similar to JC5314 CDC28/cdc2-like kinase associating arginine-serine cyclophilin [H.sapiens]	BE644965	1.31	0.13
8652	RNA binding motif protein 14	BF943707	1.31	0.13
10343	RNA polymerase II transcriptional regulation mediator (Med6, S. cerevisiae, homolog of)	AL079635	1.31	0.11
5970	proliferation-associated 2G4, 38kD	BI088072	1.31	0.13
4419	retinoid X receptor, gamma	BC012063	1.31	0.31
425	Human, Similar to caspase 2, clone MGC:2181 IMAGE:3346279, mRNA, complete cds.	BC002427	1.30	0.20
15186	pre-mRNA splicing factor 17	NM_015891	1.30	0.06
15359	SFRS protein kinase 1	AW958364	1.30	0.08
4461	guanine nucleotide binding protein 11	BF115554	1.30	0.03

10015	Human mRNA; cDNA DKFZp434F1016 (from clone DKFZp434F1016); partial cds.	AL137287	1.30	0.23
8677	Human cDNA FLJ11367 fis, clone HEMBA1000303, highly similar to Mouse (Mus musculus) Plenty of SH3s (POSH) mRNA.	AK021429	1.30	0.09
15628	Human, activated RNA polymerase II transcription cofactor 4, clone MGC:17295 IMAGE:3457167, mRNA, complete cds.	BC010537	1.30	0.07
7574	CD36 antigen (collagen type I receptor, thrombospondin receptor)-like 2 (lysosomal integral membrane protein II)	D12676	1.30	0.09
6027	complement component 3a receptor 1	NM_004054	1.29	0.19
8789	cullin 5	X81882	1.29	0.20
9077	splicing factor, arginine/serine-rich (transformer 2 Drosophila homolog) 10	BC000160	1.29	0.10
7132	activator of S phase kinase	AI289307	1.29	0.06
116	Human cDNA FLJ20268 fis, clone HEP01005, highly similar to U48251 Human protein kinase C-binding protein RACK7.	AK000275	1.29	0.16
14581	Human link protein mRNA, complete cds.	U43328	1.28	0.16
13286	REV3 (yeast homolog)-like, catalytic subunit of DNA polymerase zeta	AL096744	1.28	0.16
16654	apolipoprotein C-III	X01388	1.28	0.06
8439	Human mRNA (clone p5) for archain.	X81198	1.28	0.11
8336	Human cDNA FLJ20342 fis, clone HEP13572.	AK000349	1.28	0.05
11899	ribosomal protein L12	BG471683	1.28	0.20
16830	polymerase (RNA) II (DNA directed) polypeptide D	AA598900	1.27	0.17
12573	Human, heterogeneous nuclear ribonucleoprotein R, clone MGC:2039 IMAGE:3139052, mRNA, complete cds.	BC001449	1.27	0.28
8372	Human, clone MGC:16644 IMAGE:4123062, mRNA, complete cds.	BC009294	1.27	0.13
647	Human protocadherin 43 gene, exon 1.	AF052683	1.27	0.07
12863	Human mRNA for KIAA0551 protein, partial cds.	AB011123	1.26	0.17
16642	Kell blood group precursor (McLeod phenotype)	NM_021083	1.26	0.05
10074	Human PR-domain zinc-finger protein PFM1 mRNA, complete cds.	AF144757	1.26	0.25
15323	Rho-associated, coiled-coil containing protein kinase 1	U43195	1.26	0.08
4753	Human, angiotensinogen (serine (or cysteine) protease inhibitor, clade A (alpha-1 antiprotease, antitrypsin), member 8), clone MGC:17092 IMAGE:4213559, mRNA, complete cds.	BC011519	1.26	0.11
16251	Human mRNA for KIAA1225 protein, partial cds.	AB033051	1.26	0.06
16310	Human histone acetyltransferase (HBOa) mRNA, complete cds.	AF140360	1.25	0.09
7536	mitogen-activated protein kinase kinase kinase 7	BE080188	1.25	0.15
7416	vascular cell adhesion molecule 1	AL037831	1.25	0.24
7278	KIAA0710 gene product	BE177965	1.25	0.12

6004	centromere protein C 1	NM_001812	1.25	0.13
9152	PAX transcription activation domain interacting protein 1 like	BC008328	1.25	0.05
14294	Human mRNA for annexin A13 (ANXA13 gene), isoform b.	AJ306450	1.25	0.22
6330	Human mRNA; cDNA DKFZp586H1719 (from clone DKFZp586H1719); complete cds.	AL136918	1.24	0.06
12677	Human, synaptosomal-associated protein, 23kD, clone MGC:5155 IMAGE:3461227, mRNA, complete cds.	BC003686	1.24	0.16
15075	methyl-CpG binding domain protein 4	AI634868	1.24	0.17
16156	Human mRNA; cDNA DKFZp434F1016 (from clone DKFZp434F1016); partial cds.	AL137287	1.24	0.30
15803	Human mRNA; cDNA DKFZp761F0324 (from clone DKFZp761F0324).	AL136595	1.23	0.06
9581	Human mRNA for hSNF2H, complete cds.	AB010882	1.23	0.06
16305	Human signal transducing adaptor molecule STAM mRNA, complete cds.	U43899	1.23	0.10
8514	Human, Similar to GATA-binding protein 2, clone MGC:2306 IMAGE:3139044, mRNA, complete cds.	BC002557	1.23	0.10
6976	Human chondroitin sulfate proteoglycan versican V0 splice-variant precursor peptide mRNA, complete cds.	U16306	1.23	0.10
18033	KIAA0903 protein	AI022927	1.22	0.17
5539	immunoglobulin (CD79A) binding protein 1	Y08915	1.22	0.09
3836	Human, regulator of G-protein signalling 4, clone MGC:2124 IMAGE:3510260, mRNA, complete cds.	BC000737	1.22	0.08
10252	katanin p60 (ATPase-containing) subunit A 1	AI220473	1.21	0.08
13188	Human mRNA; cDNA DKFZp434H0413 (from clone DKFZp434H0413); partial cds.	AL137261	1.21	0.33
232	Human mRNA for KIAA0259 gene, partial cds.	D87448	1.21	0.08
135	Human DNA for 3-ketoacyl-CoA thiolase beta-subunit of mitochondrial trifunctional protein, complete cds, exon 16, partial sequence.	D86850	1.20	0.07
2744	transcription factor-like 1	AL534715	1.20	0.06
46	Human, menage a trois 1 (CAK assembly factor), clone MGC:5154 IMAGE:3453943, mRNA, complete cds.	BC000820	1.20	0.06
14613	Human PTS gene for 6-pyruvoyltetrahydropterin synthase, complete cds.	AB042297	1.20	0.06
5719	ets variant gene 6 (TEL oncogene)	BE217961	1.20	0.07
8501	Human HT032 mRNA, complete cds.	AF261138	1.20	0.05
4429	myotubular myopathy 1	U46024	1.19	0.21
10365	UDP-glucose pyrophosphorylase 2	AL533518	1.19	0.13
9570	Human B-cell receptor-associated protein BAP37 mRNA, complete cds.	AF126021	1.19	0.15
11741	Human mRNA for KIAA0827 protein, complete cds.	AB020634	1.19	0.11
12064	kinectin 1 (kinesin receptor)	Z22551	1.19	0.10
8505	Human, cyclin L ania-6a, clone MGC:14615 IMAGE:4066376, mRNA, complete cds.	BC007081	1.19	0.11
15867	Human mRNA for protein phosphatase 6.	X92972	1.18	0.04

10553	ubiquitin-conjugating enzyme E2I (homologous to yeast UBC9)	AW365112	1.18	0.08
6658	Human, clone MGC:5302 IMAGE:3456869, mRNA, complete cds.	BC001297	1.17	0.14
3945	mitochondrial translational release factor 1	AI884353	1.17	0.07
7178	endothelin type b receptor-like protein 2	NM_004767	1.16	0.15
739	Human mRNA; cDNA DKFZp586I1918 (from clone DKFZp586I1918); complete cds.	AL136911	1.16	0.02
5108	Human AF5q31 protein (AF5q31) mRNA, complete cds.	AF197927	1.16	0.06
13213	Human sodium-hydrogen exchanger 6 (NHE-6) mRNA, nuclear gene encoding mitochondrial protein, complete cds.	AF030409	1.15	0.09

Genes Significantly (P<0.005) Upregulated By Shear Stress in PAEC
Group 2 Up

Agilent Feature #	Gene Name/Description	Count 324		
		Gene ID	Fold AVE	Fold STD
2928	cytochrome P450, subfamily I (aromatic compound-inducible), polypeptide 1	K03191	9.33	2.87
2409	Human mRNA for interleukin-1 precursor (pre IL-1).	X02851	6.45	3.79
11749	heme oxygenase (decycling) 1	BI596354	5.45	3.29
14871	interleukin 8	BG777366	5.29	2.87
2450	Human glia-derived nexin (GDN) mRNA, 5' end.	M17783	5.06	2.22
16028	Human, peroxiredoxin 1, clone MGC:12514 IMAGE:3961375, mRNA, complete cds.	BC007063	4.51	1.04
4091	thioredoxin reductase 1	BE787478	4.38	1.44
8171	Human cystine/glutamate transporter xCT mRNA, complete cds.	AF252872	4.31	1.73
1123	peroxiredoxin 1	BG432135	4.26	1.16
9047	serine (or cysteine) proteinase inhibitor, clade E (nexin, plasminogen activator inhibitor type 1), member 1	BG829624	4.03	2.07
4290	major histocompatibility complex, class I, B	AL537877	3.82	1.60
471	Macaque dd-4 gene for 3(20)alpha-hydroxysteroid/dihydrodiol dehydrogenase, complete cds.	AB070211	3.78	1.58
16118	Human MHC class I lymphocyte antigen (HLA-E) (HLA-6.2) gene, complete cds.	M21533	3.54	1.36
8279	Human MHC class I HLA-B13 chain gene (Aw68.2,30; B13,51), complete cds.	M24041	3.41	1.41
9557	Human macrophage capping protein mRNA, complete cds.	M94345	3.37	1.30
10133	Human, phosphogluconate dehydrogenase, clone MGC:8331 IMAGE:2819330, mRNA, complete cds.	BC000368	3.25	0.80
12173	superoxide dismutase 2, mitochondrial	BG773219	3.23	1.38
15034	cysteine-rich protein 2	AL515731	3.19	1.40
4137	capping protein (actin filament), gelsolin-like	BF978545	3.18	1.19
4165	amphiregulin (schwannoma-derived growth factor)	AL546917	3.09	0.78
5908	immediate early response 3	AI911657	3.08	1.46
10666	matrix metalloproteinase 2 (gelatinase A, 72kD gelatinase, 72kD type IV collagenase)	J03210	3.00	0.80
11212	Human, Similar to ubiquitin carboxy-terminal hydrolase L1, clone MGC:8524 IMAGE:2822541, mRNA, complete cds.	BC000332	2.91	0.63
12235	dynein, cytoplasmic, heavy polypeptide 1	AB002323	2.90	1.15
12094	glucan (1,4-alpha-), branching enzyme 1 (glycogen branching enzyme, Andersen disease, glycogen storage disease type IV)	L07956	2.81	0.94
1067	accessory proteins BAP31/BAP29	BI756994	2.73	0.70

9508	Human partial ARNT gene for aryl hydrocarbon receptor nuclear translocator, exons 14-22.	AJ251863	2.71	0.96
10171	upstream binding transcription factor, RNA polymerase I	BI088564	2.67	1.10
12902	Human HK2 mRNA for hexokinase II.	Z46376	2.65	0.97
10514	solute carrier family 7 (cationic amino acid transporter, y+ system), member 2	U76368	2.64	0.94
16774	Ras association (RalGDS/AF-6) domain family 1	AL543484	2.60	0.89
15152	cytidine deaminase	AV649252	2.60	1.09
4258	ras homolog gene family, member C	BG708735	2.59	0.93
16116	Human Scd mRNA for stearoyl-CoA desaturase, complete cds.	AB032261	2.54	0.27
5827	SEX gene	BF725116	2.54	0.70
12553	Human, pleckstrin 2 (Mouse) homolog, clone MGC:4867 IMAGE:3457876, mRNA, complete cds.	BC001226	2.53	0.95
15338	protease, cysteine, 1 (legumain)	Y09862	2.53	0.66
3342	Human abnormal beta-hexosaminidase alpha chain (HEXA) mRNA, partial cds.	J04178	2.51	0.41
9006	nucleoside phosphorylase	BE266250	2.49	1.24
9536	Human mRNA encoding prothrombin.	V00595	2.49	0.62
10188	Human genomic DNA of 8p21.3-p22 anti-oncogene of hepatocellular colorectal and non-small cell lung cancer , segment 6/11.	AB020863	2.48	0.97
13025	Human, Similar to thioredoxin peroxidase 1, clone MGC:8456 IMAGE:2821457, mRNA, complete cds.	BC000452	2.45	0.64
10295	desmuslin	AB002351	2.44	1.00
16961	ferritin, light polypeptide	BE394443	2.43	0.30
441	Human, ras homolog gene family, member C, clone MGC:15462 IMAGE:2966676, mRNA, complete cds.	BC007245	2.42	0.74
10745	lectin, galactoside-binding, soluble, 1 (galectin 1)	BF979102	2.41	0.57
2156	Human DNA for apoER2, complete cds, and exon 19.	D86407	2.41	0.89
16413	G protein-coupled receptor 3	U18550	2.40	0.36
523	Human, clone MGC:3977 IMAGE:2821990, mRNA, complete cds.	BC003000	2.38	0.39
14998	cathepsin C	AV717480	2.36	0.34
16899	solute carrier family 6 (neurotransmitter transporter, L-proline), member 7	NM_014228	2.36	0.32
2588	chaperonin containing TCP1, subunit 7 (eta)	AA314436	2.35	0.90
13466	prostaglandin-endoperoxide synthase 1 (prostaglandin G/H synthase and cyclooxygenase)	S36219	2.35	0.92
16475	potassium inwardly-rectifying channel,subfamily J, member 13	AJ006128	2.32	0.38
16146	Human, chromosome 14 open reading frame 2, clone MGC:8356 IMAGE:2819801, mRNA, complete cds.	BC000429	2.31	0.68
15024	HCGII-7 protein	X81001	2.29	0.33

4325	integrin, alpha 5 (fibronectin receptor, alpha polypeptide)	M13918	2.28	0.90
2758	transaldolase 1	BE538166	2.28	0.43
5672	tyrosyl-tRNA synthetase	BC004151	2.25	0.69
14981	membrane protein of cholinergic synaptic vesicles	BG760616	2.24	0.74
2164	Human heparin-binding EGF-like growth factor mRNA, complete cds.	M60278	2.24	0.74
882	putative protein similar to nessy (Drosophila)	BG824361	2.23	0.21
5792	holocytochrome c synthase (cytochrome c heme-lyase)	AL561481	2.22	0.79
15358	cytochrome P450, subfamily I (dioxin-inducible), polypeptide 1 (glaucoma 3, primary infantile)	BG939664	2.21	0.78
11745	low density lipoprotein receptor-related protein 8, apolipoprotein e receptor	BF110337	2.21	0.48
13655	P450 (cytochrome) oxidoreductase	AF258341	2.20	0.65
3345	Human endothelin converting enzyme-1 (ECE-1) gene, exon 19, partial cds.	AF018034	2.20	0.79
13640	growth arrest-specific 11	AL561072	2.19	0.83
11748	Human, clone IMAGE:2905327, mRNA, partial cds.	BC002991	2.17	0.27
11587	Human dioxin-inducible cytochrome P450 (CYP1B1) mRNA, complete cds.	U03688	2.17	0.69
11460	Human genomic DNA, chromosome 8q23, clone:KB1747F8.	AP003113	2.17	0.83
827	Human, dimethylarginine dimethylaminohydrolase 2, clone MGC:1351 IMAGE:3138832, mRNA, complete cds.	BC001435	2.15	0.57
1128	glutathione-S-transferase like; glutathione transferase omega	BI858997	2.15	0.28
13609	guanine nucleotide binding protein (G protein), beta polypeptide 2	BG251149	2.13	0.76
14060	Human GP36b glycoprotein mRNA, complete cds.	U10362	2.13	0.71
14580	Human, Similar to chromogranin A (parathyroid secretory protein 1), clone IMAGE:4127895, mRNA, partial cds.	BC009384	2.12	0.84
13029	Human mRNA for KIAA0349 gene, partial cds.	AB002347	2.12	0.33
15396	annexin A1	AU139496	2.12	0.46
8647	peroxiredoxin 2	BI862079	2.11	0.44
4263	tyrosine kinase with immunoglobulin and epidermal growth factor homology domains	X60957	2.10	0.49
8613	phosphoglycerate mutase 2 (muscle)	BE264368	2.10	0.70
9386	Human mRNA for phenylalkylamine binding protein.	Z37986	2.10	0.42
13652	clathrin, light polypeptide (Lcb)	BE791502	2.10	0.48
13113	Human lactate dehydrogenase A mRNA, complete cds.	AY009108	2.09	0.52
14880	stanniocalcin 2	BC013958	2.09	1.00
16765	KIAA0233 gene product	D87071	2.05	0.45
15383	thiosulfate sulfurtransferase (rhodanese)	BI820468	2.05	0.51
1156	actin, gamma 2, smooth muscle, enteric	X16940	2.04	1.01
8672	radixin	BF194976	2.04	0.26
1227	ferritin, heavy polypeptide 1	BE878314	2.03	0.38

9881	Human mRNA for enteric smooth muscle gamma-actin.	X16940	2.02	1.03
3321	Human mRNA for Soluble-type polypeptide FZD4S, complete cds.	AB054881	2.02	1.10
7086	BTG family, member 2	BG750101	2.01	0.53
2540	melanoma-associated antigen recognised by cytotoxic T lymphocytes	BC000507	2.01	0.67
4327	sphingomyelin phosphodiesterase 1, acid lysosomal (acid sphingomyelinase)	NM_000543	1.99	0.57
563	Human mitochondrial inner membrane preprotein translocase Tim17a mRNA, nuclear gene encoding mitochondrial protein, complete cds.	AF106622	1.98	0.59
15033	dickkopf (Xenopus laevis) homolog 3	AB034203	1.98	0.83
602	Human alpha-2 type XI collagen mRNA (COL11A2).	J04974	1.98	0.71
7155	calcium channel, voltage-dependent, alpha 2/delta subunit 2	NM_006030	1.97	0.55
4120	villin 2 (ezrin)	AU135575	1.97	0.55
10470	protein tyrosine kinase 9-like (A6-related protein)	BF220316	1.96	0.54
14546	Human MHC class I HLA-C-alpha-2 chain and alternative mRNA, complete cds, clones 4 and 10.	M24097	1.96	0.43
15353	tubulin, beta polypeptide	BE729764	1.96	0.80
13597	phosphoribosyl pyrophosphate synthetase-associated protein 2	AB007851	1.95	0.55
2925	ATPase, H+ transporting, lysosomal (vacuolar proton pump) 21kD	BG108730	1.95	0.17
12206	ARP1 (actin-related protein 1, yeast) homolog A (centractin alpha)	AL524757	1.95	0.75
12896	contains similarity to Pfam domain: PF00207 (Alpha-2-macroglobulin family), Score=377.3, E-value=1.1e-113, N=1; PF01835 (Alpha-2-macroglobulin family N-terminal region), Score=157.5, E-value=2.1e-46, N=2~cDNA EST yk41d7.3 comes fr	CAB05006	1.95	0.30
16869	HNK-1 sulfotransferase	AW956276	1.95	0.87
91	Human Bcl-2-interacting protein beclin mRNA, complete cds.	AF077301	1.94	0.38
3474	Human, diaphorase (NADH) (cytochrome b-5 reductase), clone MGC:5150 IMAGE:3450773, mRNA, complete cds.	BC004821	1.94	0.79
12994	Human, Similar to RIKEN cDNA B230118G17 gene, clone MGC:19604 IMAGE:3622817, mRNA, complete cds.	BC010155	1.93	0.39
9846	Human cDNA FLJ14588 fis, clone NT2RM4001819, highly similar to Human p58/GTA (galactosyltransferase associated protein kinase) mRNA.	AK027494	1.92	0.49
837	sperm associated antigen 7	BI858087	1.92	0.38
8964	tumor necrosis factor receptor superfamily, member 5	X60592	1.92	0.74
3338	Human putative tRNA synthetase-like protein mRNA, complete cds.	U07424	1.91	0.49
1053	calpain, small subunit 1	BG831069	1.91	0.50

14617	Human, clone MGC:15351 IMAGE:4126712, mRNA, complete cds.	BC008861	1.90	0.40
10336	kinesin family member 1C	AB014606	1.90	0.52
12174	cytochrome b-245, alpha polypeptide	BG751568	1.89	0.84
8820	glucosidase, beta; acid (includes glucosylceramidase)	NM_000157	1.89	0.28
2385	STIP1 homology and U-Box containing protein 1	AL560352	1.89	0.39
570	Human, secretory carrier membrane protein 2, clone MGC:1284 IMAGE:3050527, mRNA, complete cds.	BC001376	1.89	0.28
1135	hyaluronoglucosaminidase 2	AU137033	1.89	0.27
2867	macrophage stimulating 1 receptor (c-met-related tyrosine kinase)	X70040	1.88	0.26
13028	Human lymphocyte activation antigen 4F2 large subunit mRNA, complete cds.	J03569	1.87	0.17
13786	protease, serine, 15	BC000235	1.87	0.48
14759	aortic carboxypeptidase-like protein ACLP	AAC25584	1.87	0.62
14769	Human C4-sterol methyl oxidase homolog (DESP4) mRNA, complete cds.	U93162	1.86	0.35
11918	ATP-binding cassette, sub-family C (CFTR/MRP), member 1	BC001636	1.86	0.15
1309	pM5 protein	X57398	1.85	0.36
2237	Human tenascin-X (XA) mRNA, complete cds.	U24488	1.84	0.40
13749	actin, alpha 2, smooth muscle, aorta	BF681347	1.84	0.92
14905	hypothetical protein FLJ10305	BM012099	1.84	0.60
12946	Human cDNA: FLJ20986 fis, clone CAE01156.	AK024639	1.84	0.29
1103	dual specificity phosphatase 4	BC002671	1.84	0.47
3973	colony stimulating factor 2 (granulocyte-macrophage)	BE669962	1.83	0.82
12695	Human group III secreted phospholipase A2 mRNA, complete cds.	AF220490	1.83	0.43
1386	ubiquitin specific protease 5 (isopeptidase T)	BE019497	1.82	0.52
14750	Human myosin light chain 1 slow a (MLC1sa) mRNA, complete cds.	M31211	1.81	0.51
8959	GTP-binding protein Rho7	AI554560	1.81	0.30
8346	Human transcription factor junB (junB) gene, 5' region and complete cds.	U20734	1.80	0.41
1622	Human sky mRNA for Sky, complete cds.	D17517	1.80	0.30
10982	Human mRNA for NOTCH4, partial cds.	D63395	1.80	0.15
6002	delta sleep inducing peptide, immunoreactor	AL525317	1.80	0.53
2235	Human mRNA; cDNA DKFZp586O0222 (from clone DKFZp586O0222); complete cds.	AL136935	1.79	0.31
12202	myosin, light polypeptide 1, alkali; skeletal, fast	BF981829	1.79	0.54
13788	hematopoietic cell-specific Lyn substrate 1	X16663	1.78	0.39
1276	xeroderma pigmentosum, complementation group C	X65024	1.78	0.52
15052	palmitoyl-protein thioesterase 2	BE790900	1.78	0.48
14941	Homo sapiens cDNA FLJ10229 fis, clone HEMBB1000136	AL548337	1.77	0.15
11410	Human cDNA: FLJ21665 fis, clone COL08913.	AK025318	1.77	0.74
13169	Human mRNA for plasma gelsolin.	X04412	1.77	0.73
2246	Human mRNA for p115, complete cds.	D86326	1.77	0.34

14745	Human epithelial membrane protein (CL-20) mRNA, complete cds.	U77085	1.76	0.56
13056	Human fragile X mental retardation syndrome related protein (FXR2) mRNA, complete cds.	U31501	1.75	0.60
337	Human myelodysplasia/myeloid leukemia factor 2 (MLF2) mRNA, complete cds.	U57342	1.75	0.51
8618	discs, large (Drosophila) homolog 5	NM_004747	1.74	0.38
2233	Human ETL protein (ETL) mRNA, complete cds.	AF192403	1.74	0.49
15218	tyrosine 3-monooxygenase/tryptophan 5-monooxygenase activation protein, eta polypeptide	BI458375	1.74	0.38
10176	Human 180 kDa bullous pemphigoid antigen 2/type XVII collagen (BPAG2/COL17A1) gene, exon 23.	U76585	1.74	0.65
15031	procollagen-lysine, 2-oxoglutarate 5-dioxygenase 3	AL544817	1.73	0.46
10655	activated p21cdc42Hs kinase	BG742978	1.733	0.37
13795	glutaminyl-tRNA synthetase	BG179717	1.73	0.34
10220	Human mRNA for fibrillin.	X63556	1.73	0.88
6299	Human ASM-2 mRNA for sphingomyelin phosphodiesterase (EC 3.1.4.12).	X52679	1.73	0.23
2757	adenine phosphoribosyltransferase	BG612479	1.72	0.61
12722	Human receptor protein-tyrosine kinase (TEK) mRNA, complete cds.	L06139	1.72	0.16
7286	ATP-binding cassette, sub-family G (WHITE), member 2	AU118354	1.71	0.26
1132	TNF receptor-associated factor 3	U19260	1.70	0.27
15179	solute carrier family 25 (mitochondrial carrier; adenine nucleotide translocator), member 6	AL527028	1.70	0.40
5727	DNA fragmentation factor, 45 kD, alpha polypeptide	BF309422	1.69	0.36
14844	Human novel protein AHNAK mRNA, partial sequence.	M80899	1.69	0.51
12233	cAMP responsive element binding protein-like 1	U89337	1.69	0.65
13288	LIM domain only 6	AI017508	1.69	0.34
14906	Human keratin 18 (KRT18) gene, complete cds.	AF179904	1.68	0.48
13743	cartilage oligomeric matrix protein (pseudoachondroplasia, epiphyseal dysplasia 1, multiple)	L32137	1.68	0.63
15203	cystatin B (stefin B)	BG283058	1.68	0.35
740	Human cytosolic inhibitor of NRF2 (INRF2) mRNA, complete cds.	AF361886	1.68	0.27
15241	class I cytokine receptor	AF265242	1.67	0.48
11885	phosphorylase, glycogen; liver (Hers disease, glycogen storage disease type VI)	BE884737	1.67	0.49
11913	SH3-domain binding protein 5 (BTK-associated)	BC006169	1.66	0.59
4343	nucleobindin 1	BG288969	1.65	0.45
14910	keratin 8	BI255878	1.65	0.41
4487	vimentin	AL046515	1.65	0.50
15038	KIAA0562 gene product	AB011134	1.63	0.21

6906	Human, Similar to keratin 7, clone MGC:3625 IMAGE:3610347, mRNA, complete cds.	BC002700	1.63	0.35
3512	Human endothelial cell protein C/APC receptor (EPCR) mRNA, complete cds.	L35545	1.63	0.45
915	myosin, light polypeptide 4, alkali; atrial, embryonic	BI832777	1.62	0.40
13319	serine (or cysteine) proteinase inhibitor, clade B (ovalbumin), member 6	BG196819	1.62	0.42
6046	biliverdin reductase A	AI765830	1.62	0.20
4003	Human HES-related repressor protein 2 HERP2 mRNA, complete cds.	AF232239	1.62	0.43
7129	Human, clone IMAGE:3446372, mRNA, partial cds.	BC000987	1.62	0.23
8646	troponin T2, cardiac	BC002653	1.62	0.41
9410	Human HOK-2 mRNA for zinc finger protein.	X82125	1.61	0.28
9402	Human myosin heavy chain 12 (MYO5A) mRNA, complete cds.	U90942	1.60	0.64
6956	Human transmembrane 4 superfamily protein mRNA, complete cds.	AF100759	1.60	0.23
5684	interferon gamma receptor 2 (interferon gamma transducer 1)	U05877	1.59	0.35
422	Human cDNA FLJ14781 fis, clone NT2RP4000455, weakly similar to TRANS-ACTING TRANSCRIPTIONAL PROTEIN ICP0.	AK027687	1.59	0.22
14584	Human mitochondrial benzodiazepine receptor (MBR) gene, complete cds.	U12421	1.59	0.24
1824	Human collagen type XII alpha-1 precursor (COL12A1) mRNA.	U73778	1.59	0.59
14589	Human genes for S100E calcium binding protein, CAPL, and S100D calcium binding protein EF-Hand (partial).	Z18950	1.58	0.39
8633	Human basic transcription factor 2 p44 (btf2p44) gene, partial cds, neuronal apoptosis inhibitory protein (naip) and survival motor neuron protein (smn) genes, complete cds.	U80017	1.58	0.27
2743	tenascin XB	NM_019105	1.57	0.20
11916	S100 calcium-binding protein A5	AW090645	1.57	0.36
13299	actin, beta	BG481840	1.57	0.67
12541	Human ASCL3 gene, CEGP1 gene, C11orf14 gene, C11orf15 gene, C11orf16 gene and C11orf17 gene.	AJ400877	1.56	0.33
2572	Homer, neuronal immediate early gene, 3	AL162099	1.55	0.38
7486	amyloid beta (A4) precursor protein-binding, family B, member 1 (Fe65)	BG699532	1.55	0.41
3223	Human chloride channel ABP mRNA, complete cds.	AF034607	1.54	0.30
1826	Human hXBP-1 transcription factor DNA.	L13850	1.54	0.25
744	CG14353 gene product	AAF49284	1.53	0.26
2571	mitogen-activated protein kinase 11	AI394426	1.53	0.25
3699	Human osteonectin gene, exon 7.	M25743	1.53	0.36
13184	Human mRNA for Mel-18 protein, complete cds.	D13969	1.53	0.28
1080	KIAA0853 protein	NM_015070	1.53	0.34

14096	Human palmitoylated erythrocyte membrane protein (MPP1) mRNA, complete cds.	M64925	1.53	0.34
14375	Human, clone MGC:14836 IMAGE:4286914, mRNA, complete cds.	BC008500	1.53	0.14
14925	KIAA0225 protein	D86978	1.52	0.23
4315	DiGeorge syndrome critical region gene DGSI; likely ortholog of mouse expressed sequence 2 embryonic lethal	BG831512	1.52	0.44
1975	Human, Similar to KRAB-zinc finger protein SZF1-1, clone IMAGE:3945618, mRNA, partial cds.	BC006247	1.52	0.24
820	T-cell, immune regulator 1	NM_006053	1.52	0.22
1062	iduronate 2-sulfatase (Hunter syndrome)	AI042325	1.51	0.60
499	Human, transmembrane 4 superfamily member (tetraspan NET-7), clone MGC:4120 IMAGE:2958221, mRNA, complete cds.	BC003157	1.51	0.16
13616	similar to vaccinia virus HindIII K4L ORF	BE743194	1.50	0.47
16134	Human leucocyte Ig-like receptor-3 (LIR-3) mRNA, complete cds.	AF025533	1.50	0.14
1115	autocrine motility factor receptor	AA582146	1.50	0.09
2910	Down syndrome critical region gene 1	BG287042	1.50	0.30
12199	erythrocyte membrane protein band 4.1 (elliptocytosis 1, RH-linked)	BF868865	1.49	0.18
2723	keratin 7	BI094014	1.49	0.38
6666	Human cDNA FLJ14937 fis, clone PLACE1010231, weakly similar to CELL SURFACE GLYCOPROTEIN EMR1 PRECURSOR.	AK027843	1.49	0.25
13515	HLA-G histocompatibility antigen, class I, G	AF071019	1.48	0.17
12996	Human chromosome 21 segment HS21C052.	AL163252	1.48	0.28
12633	Human cell cycle-regulated factor p78 mRNA, complete cds.	AF068007	1.48	0.38
12237	collagen, type VIII, alpha 1	BC013581	1.48	0.73
15303	heat shock transcription factor 4	AI741735	1.48	0.14
5113	Human mRNA for HKR1, partial cds.	AB013897	1.48	0.20
12074	zinc finger protein 239	BF972810	1.47	0.18
7390	cerebellar degeneration-related protein (62kD)	BI869500	1.47	0.20
12833	Human ets homologous factor (EHF) mRNA, complete cds.	AF170583	1.47	0.23
12856	Human guanine nucleotide-binding protein (Gi) alpha subunit mRNA, complete cds.	M27543	1.46	0.32
3987	Human genomic DNA, chromosome 8q23, clone:KB1107E3.	AP000426	1.46	0.29
508	Human chromosome 21 segment HS21C004.	AL163204	1.46	0.09
3201	Human mRNA for KIAA0671 protein, complete cds.	AB014571	1.46	0.46
13562	non-metastatic cells 3, protein expressed in	BC000250	1.46	0.44
13840	ilvB (bacterial acetolactate synthase)-like	AC003956	1.45	0.24
13324	Human cDNA FLJ12298 fis, clone MAMMA1001837, weakly similar to ZINC FINGER PROTEIN 29.	AK022360	1.45	0.30
2565	ATPase, H+ transporting, lysosomal (vacuolar proton pump), subunit 1	BE252259	1.45	0.23

669	Human, hypothetical protein, clone MGC:816 IMAGE:3357388, mRNA, complete cds.	BC000244	1.45	0.13
11419	Human zinc finger protein ZNF133.	U09366	1.45	0.13
10190	similar to S. cerevisiae Sec6p and R. norvegicus rsec6	AF055006	1.45	0.10
5591	Human, Similar to claudin 15, clone MGC:19536 IMAGE:3677931, mRNA, complete cds.	BC010160	1.44	0.19
14612	Human mRNA for TTF-I.	X83973	1.44	0.12
11422	Human, succinate dehydrogenase complex, subunit A, flavoprotein (Fp), clone MGC:1484 IMAGE:3051442, mRNA, complete cds.	BC001380	1.44	0.22
2558	KIAA0435 gene product	AB007895	1.44	0.30
13478	thymidine kinase 1, soluble	AL520356	1.43	0.48
15036	non-metastatic cells 2, protein (NM23B) expressed in	BI599403	1.43	0.15
14992	2',3'-cyclic nucleotide 3' phosphodiesterase	NM_033133	1.42	0.38
13493	H1 histone family, member X	BG469316	1.42	0.44
14616	Human, nucleobindin 1, clone MGC:8479 IMAGE:2821805, mRNA, complete cds.	BC002356	1.42	0.34
6603	Human, KIAA1049 protein, clone MGC:19865 IMAGE:3678670, mRNA, complete cds.	BC011884	1.41	0.39
1763	Human alkali myosin light chain 1 mRNA, complete cds.	M20642	1.41	0.29
12210	KIAA0326 protein	AB002324	1.41	0.26
8328	Human cDNA: FLJ22528 fis, clone HRC12825.	AK026181	1.41	0.18
1201	mannosidase, alpha, class 1A, member 1	NM_005907	1.41	0.32
13464	NADH dehydrogenase (ubiquinone) Fe-S protein 7 (20kD) (NADH-coenzyme Q reductase)	AV698517	1.40	0.18
12542	aortic carboxypeptidase-like protein ACLP	AAC25584	1.40	0.29
515	Human phospholipid transfer protein mRNA, complete cds.	L26232	1.40	0.28
2295	Human copper chaperone for superoxide dismutase (CCS) mRNA, complete cds.	AF002210	1.40	0.14
8689	Human spinster-like protein mRNA, complete cds.	AF212371	1.39	0.19
6979	Human ASCL3 gene, CEGP1 gene, C11orf14 gene, C11orf15 gene, C11orf16 gene and C11orf17 gene.	AJ400877	1.39	0.17
4013	Notch (Drosophila) homolog 4	D63395	1.39	0.04
987	sulfotransferase, estrogen-preferring	NM_005420	1.39	0.14
14682	Human PRR2 mRNA.	X80038	1.39	0.26
10218	pvt-1 (murine) oncogene homolog, MYC activator	AI498125	1.38	0.22
13087	Human cDNA: FLJ22950 fis, clone KAT09618, highly similar to HUMCDA24A Human CD24 signal transducer mRNA.	AK026603	1.38	0.11
16180	Human cDNA FLJ20845 fis, clone ADKA01901.	AK000852	1.38	0.15
677	Human mRNA for ribonuclease/angiogenin inhibitor (RAI).	X13973	1.37	0.15
807	protein phosphatase 4, regulatory subunit 1	AW865929	1.37	0.13
13614	IMP (inosine monophosphate) dehydrogenase 1	AL525547	1.37	0.40

13373	mitogen-activated protein kinase kinase kinase 11	AL556109	1.37	0.32
13775	myosin, heavy polypeptide 3, skeletal muscle, embryonic	NM_002470	1.37	0.20
12097	KIAA0339 gene product	AB002337	1.37	0.32
2069	Human phosphomannomutase mRNA, complete cds.	U86070	1.36	0.14
4141	erythropoietin receptor	S45332	1.36	0.18
764	Human prostaglandin transporter hPGT mRNA, complete cds.	U70867	1.36	0.17
6612	Human, GDP dissociation inhibitor 2, clone MGC:2027 IMAGE:3504736, mRNA, complete cds.	BC005145	1.35	0.11
11274	Human NF-kappa-B transcription factor p65 subunit mRNA, complete cds.	L19067	1.34	0.36
904	testican 3	BC000460	1.34	0.19
8802	immediate early protein	BG255669	1.34	0.10
11597	Human ALAS1 (ALASH) mRNA for delta-aminolevulinate synthase (housekeeping) (EC 2.3.1.37).	X56351	1.34	0.08
2561	TAR (HIV) RNA-binding protein 2	BC005860	1.33	0.09
1358	Ts translation elongation factor, mitochondrial	AU143121	1.33	0.17
12079	karyopherin beta 2b, transportin	AF019039	1.33	0.28
1577	Human, Similar to vesicle-associated membrane protein 3, clone MGC:2110 IMAGE:3544610, mRNA, complete cds.	BC003570	1.33	0.09
6758	Human mRNA for KIAA1092 protein, partial cds.	AB029015	1.32	0.29
1230	phosphofructokinase, liver	AL041002	1.32	0.14
14594	Human, endoplasmic reticulum chaperone SIL1, homolog of Yeast, clone MGC:20202 IMAGE:4640182, mRNA, complete cds.	BC011568	1.32	0.13
7548	Nef-associated factor 1	NM_006058	1.32	0.07
10339	kinesin family member 1C	AB014606	1.32	0.25
554	Human mRNA; cDNA DKFZp434H0923 (from clone DKFZp434H0923).	AL137712	1.32	0.11
2410	Human multiple endocrine neoplasia type 1 candidate protein number 18 (HSPF2) mRNA, complete cds.	AF036874	1.30	0.23
366	Human TLH29 protein precursor (TLH29) mRNA, complete cds.	AF208232	1.30	0.19
12812	unnamed protein product	CAC51188	1.30	0.09
5397	Human mRNA for DREAM protein.	AJ131730	1.29	0.13
14711	Human mRNA for KIAA0747 protein, partial cds.	AB018290	1.29	0.20
4015	Human mRNA; cDNA DKFZp761F0324 (from clone DKFZp761F0324).	AL136595	1.29	0.14
604	Human, Similar to RIKEN cDNA 4930500C14 gene, clone MGC:9341 IMAGE:3456620, mRNA, complete cds.	BC008981	1.29	0.11
11619	Human co-beta glucosidase (proactivator) mRNA, complete cds.	J03077	1.28	0.06
897	tissue factor pathway inhibitor 2	BG621010	1.28	0.10
11435	GTPase activating protein SynGAP-c	AAC40082	1.28	0.15

14574	Human, clone MGC:10520 IMAGE:3938462, mRNA, complete cds.	BC004480	1.28	0.09
7237	ATP-binding cassette, sub-family B (MDR/TAP), member 4	X06181	1.27	0.19
924	Human activin beta-A subunit (exon 2).	X57579	1.27	0.36
10200	collagen, type VII, alpha 1 (epidermolysis bullosa, dystrophic, dominant and recessive)	L06862	1.26	0.11
13142	embryonic poly(A) binding protein	AAK29408	1.24	0.17
11428	Human, distal-less homeo box 5, clone MGC:10672 IMAGE:3941691, mRNA, complete cds.	BC006226	1.23	0.18
10350	dynamin 2	BE277949	1.23	0.08
10348	CD34 antigen	BG696256	1.23	0.20
10212	interleukin 2 receptor, beta	M26062	1.22	0.06
7844	Human transcription factor IL-4 Stat mRNA, complete cds.	U16031	1.22	0.11
3229	Human CpG island DNA genomic Mse1 fragment, clone 71f4, forward read cpg71f4.ft1a.	Z55905	1.20	0.16
11629	Human cDNA: FLJ21512 fis, clone COL05769.	AK025165	1.18	0.11
711	Human mitochondrial carrier homolog 1 isoform b (MTCH1) mRNA, partial cds; nuclear gene for mitochondrial product.	AF192559	1.16	0.11
15371	butyrophilin, subfamily 3, member A3	U90548	1.14	0.09

Genes Significantly (P<0.005) Downregulated By Shear Stress in PAEC
Group 2

Agilent Feature #	Gene Name/Description	Count 157		
		Gene ID	Fold AVE	Fold STD
15769	Macaque somatostatin I mRNA, complete cds.	M19318	6.91	3.10
3508	Human, matrix Gla protein, clone MGC:12316 IMAGE:3930143, mRNA, complete cds.	BC005272	5.86	2.47
2397	matrix Gla protein	AW999947	5.75	1.82
10644	ectodermal-neural cortex (with BTB-like domain)	BC000418	3.56	1.10
2692	reelin	NM_005045	3.41	1.66
13133	Human reelin (RELN) mRNA, complete cds.	U79716	3.35	1.32
8297	Human mRNA; cDNA DKFZp434M152 (from clone DKFZp434M152).	AL137687	3.27	1.01
8985	somatostatin	BI713774	3.24	1.05
12801	Human intracellular hyaluronic acid binding protein (IHABP) mRNA, complete cds.	AF032862	3.18	1.56
1232	stathmin-like 2	AL535825	3.15	0.74
11934	cell division cycle 2, G1 to S and G2 to M	AL520473	3.15	1.88
1196	osteoblast specific factor 2 (fasciclin I-like)	AW608422	3.13	1.52
2619	paternally expressed 10	AF038197	3.11	1.34
8368	Human cDNA: FLJ21156 fis, clone CAS09878.	AK024809	3.08	1.66
12631	Human butyrylcholinesterase, mRNA, complete cds.	M16541	3.07	1.54
79	Human FZD8 mRNA for seven-transmembrane receptor Frizzled-8, complete cds.	AB043703	2.95	1.35
14388	Human cDNA FLJ12587 fis, clone NT2RM4001217, moderately similar to Mouse (Mus musculus) actin-binding protein (ENC-1) mRNA.	AK022649	2.84	0.89
11100	Human mRNA for KIAA1057 protein, partial cds.	AB028980	2.70	0.94
2782	topoisomerase (DNA) II alpha (170kD)	BF795918	2.67	1.26
16390	pituitary tumor-transforming 1	AW957275	2.66	1.16
14302	Human factor I (C3b/C4b inactivator) mRNA, complete cds.	J02770	2.64	0.62
4121	lumican	AU137979	2.62	0.54
10641	kinesin-like 5 (mitotic kinesin-like protein 1)	BM014478	2.62	0.59
1214	neuro-oncological ventral antigen 1	NM_006489	2.59	1.11
2374	inositol polyphosphate-4-phosphatase, type II, 105kD	U96922	2.59	1.15
868	KIAA0022 gene product	D14664	2.53	1.20
181	Human gene for thrombomodulin precursor, complete cds.	D00210	2.52	1.02
2219	Human mRNA for caldesmon, 3' UTR.	AJ223812	2.50	0.49
13643	activated leucocyte cell adhesion molecule	AI050952	2.49	0.50

15978	Human cDNA: FLJ21715 fis, clone COL10287, highly similar to AF071569 Human multifunctional calcium/calmodulin-dependent protein kinase II delta2 isoform mRNA.	AK025368	2.48	0.60
3322	Human mRNA for mitotic kinesin-like protein-1 (MKLP-1 gene).	X67155	2.47	0.61
8053	Human mRNA for MEMD protein.	Y10183	2.44	0.38
13583	vinculin	NM_014000	2.39	0.34
78	Human mRNA; cDNA DKFZp564F1016 (from clone DKFZp564F1016).	AL110174	2.36	0.31
11089	Human mRNA for Slit-2 protein, complete cds.	AB017168	2.34	0.41
8941	highly expressed in cancer, rich in leucine heptad repeats	AA878068	2.32	1.15
2878	dystrophin (muscular dystrophy, Duchenne and Becker types), includes DXS142, DXS164, DXS206, DXS230, DXS239, DXS268, DXS269, DXS270, DXS272	AA889832	2.30	0.88
5248	Human CpG island DNA genomic Mse1 fragment, clone 25c6, reverse read cpg25c6.rt1b.	Z65191	2.29	0.91
5517	homeo box B6	NM_018952	2.28	0.32
13481	PDZ and LIM domain 1 (elfin)	AI687946	2.24	0.54
203	Human replication protein A 14kDa subunit (RPA) mRNA, complete cds.	L07493	2.18	0.74
11119	Human protein kinase (SGK3) mRNA, complete cds.	AF169035	2.17	0.30
299	Human cDNA FLJ20271 fis, clone HEP01715.	AK000278	2.16	0.35
331	Human mRNA for lipophilin B.	AJ224172	2.15	0.45
15082	interferon-induced, hepatitis C-associated microtubular aggregate protein (44kD)	NM_006417	2.12	0.79
12035	EphA5	L36644	2.10	0.66
12259	bone morphogenetic protein 4	NM_001202	2.07	0.91
13316	baculoviral IAP repeat-containing 5 (survivin)	AL571008	2.05	0.47
5526	secretogranin II (chromogranin C)	NM_003469	2.04	0.41
463	Human adapter protein CMS mRNA, complete cds.	AF146277	2.02	0.19
14161	Human epidermal growth factor receptor kinase substrate (Eps8) mRNA, complete cds.	U12535	2.01	0.25
14263	Human, TTK protein kinase, clone MGC:865 IMAGE:3343925, mRNA, complete cds.	BC000633	2.01	0.59
9192	thrombomodulin	M16552	2.00	0.48
2460	heparan sulfate proteoglycan 2 (perlecan)	NM_005529	2.00	0.66
17270	Human interferon-inducible protein 9-27 mRNA, complete cds.	J04164	1.98	0.70
12532	Human PBX3 mRNA.	X59841	1.94	0.50
13800	KIAA0483 protein	AI690717	1.91	0.25
14266	Human mRNA; cDNA DKFZp434D0215 (from clone DKFZp434D0215); partial cds.	AL133047	1.91	0.28
2292	Human mRNA for KIAA0949 protein, partial cds.	AB023166	1.88	0.46
4931	Human protease PC6 isoform A (PCSK5) mRNA, complete cds.	U56387	1.87	0.47
15022	interferon induced transmembrane protein 3 (1-8U)	BE886918	1.85	0.58

14847	extracellular matrix protein 2, female organ and adipocyte specific	NM_001393	1.82	0.33
15146	ribosomal protein S29	AA827393	1.82	0.29
12863	Human mRNA for KIAA0551 protein, partial cds.	AB011123	1.81	0.48
12707	Human TRIP7-like protein mRNA, complete cds.	AY043282	1.81	0.45
4446	KIAA0603 gene product	BI906891	1.79	0.33
13754	inhibitor of DNA binding 2, dominant negative helix-loop-helix protein	AI299309	1.78	0.35
4001	phospholipid scramblase 1	NM_021105	1.77	0.39
11141	Human, clone MGC:5585 IMAGE:3459639, mRNA, complete cds.	BC000861	1.76	0.28
12703	Human cDNA FLJ10697 fis, clone NT2RP3000527, weakly similar to ZINC FINGER PROTEIN 43.	AK001559	1.75	0.48
10759	mannose receptor, C type 1	X55635	1.75	0.50
3221	Human, ATPase, Na+/K+ transporting, beta 1 polypeptide, clone MGC:1798 IMAGE:3506311, mRNA, complete cds.	BC000006	1.74	0.56
12882	Human, CDC20 (cell division cycle 20, S. cerevisiae, homolog), clone MGC:15276 IMAGE:2959596, mRNA, complete cds.	BC009426	1.74	0.77
4133	ribosomal protein S15a	BG285655	1.74	0.36
11155	Human alpha-catenin-like protein mRNA, complete cds.	U97067	1.72	0.35
16461	Human lysyl oxidase-like 3 protein (LOXL3) mRNA, complete cds.	AF311313	1.72	0.34
710	Human, Similar to plastin 3 (T isoform), clone IMAGE:3447893, mRNA, partial cds.	BC008588	1.68	0.19
13850	fibromodulin	AI249821	1.67	0.19
512	Human KIAA0405 mRNA, complete cds.	AB007865	1.65	0.63
7859	Human connexin 37 (GJA4) mRNA, complete cds.	M96789	1.63	0.44
13247	Human lysyl hydroxylase isoform 2 (PLOD2) mRNA, complete cds.	U84573	1.60	0.38
7590	ESTs, Weakly similar to I38022 hypothetical protein [H.sapiens]	BG718906	1.59	0.20
1233	neuropeptide Y	K01911	1.59	0.32
15342	proliferating cell nuclear antigen	AA523378	1.59	0.31
12509	Human, ring finger protein 13, clone MGC:13487 IMAGE:3683407, mRNA, complete cds.	BC009781	1.59	0.32
11593	Human mRNA for KIAA1309 protein, partial cds.	AB037730	1.59	0.58
3190	Human mRNA for fibroblast tropomyosin TM30 (pl).	X05276	1.59	0.16
741	Human putative secretory protein precursor, mRNA, complete cds.	AF142573	1.58	0.46
1144	cyclin G1	BC000196	1.58	0.37
4944	Human cDNA FLJ11756 fis, clone HEMBA1005595, weakly similar to DYNEIN HEAVY CHAIN, CYTOSOLIC.	AK021818	1.58	0.23
12702	Macaque brain cDNA clone:QmoA-10711, full insert sequence.	AB062987	1.58	0.35

8147	Unknown (protein for MGC:15514)	AAH07256	1.57	0.32
3379	Human striated muscle contraction regulatory protein (Id2B) mRNA, complete cds.	M96843	1.57	0.28
106	Human mRNA for PDGF receptor beta-like tumor suppressor (PRLTS), complete cds.	D37965	1.56	0.26
5597	Human homolog of Yeast mutL (hPMS1) gene, complete cds.	U13695	1.55	0.35
14090	Human gcp60 mRNA for golgi resident protein GCP60, complete cds.	AB043587	1.53	0.19
12787	Human genomic DNA, chromosome 1q22-q23, CD1 region, section 2/4.	AP002533	1.52	0.17
1350	U2 small nuclear ribonucleoprotein auxiliary factor (65kD)	BI962886	1.52	0.36
9412	Human mRNA for UDP-N-acetylglucosamine transporter, complete cds.	AB021981	1.51	0.14
12931	Human cDNA: FLJ22903 fis, clone KAT05624.	AK026556	1.51	0.22
1383	CGG triplet repeat binding protein 1	AA225329	1.50	0.18
1059	anti-Mullerian hormone receptor, type II	AF172932	1.49	0.41
14744	Human mRNA for p cadherin.	X63629	1.49	0.26
14276	Human zinc finger protein ANC_2H01 mRNA, complete cds.	AF003924	1.49	0.21
7220	acid-inducible phosphoprotein	AK027723	1.47	0.35
3355	Human 3-methylcrotonyl-CoA carboxylase biotin-containing subunit (MCCA) mRNA, complete cds.	AF297332	1.46	0.51
2462	hypothetical protein	AI792005	1.46	0.27
9106	LIM domain-containing preferred translocation partner in lipoma	U49957	1.44	0.12
13801	SWI/SNF related, matrix associated, actin dependent regulator of chromatin, subfamily b, member 1	BF977892	1.43	0.37
14256	laminin A-chain	AAA39406	1.43	0.21
12007	Rho-associated, coiled-coil containing protein kinase 2	D87931	1.43	0.20
2300	Human HNOEL-iso (HNOEL-iso) mRNA, complete cds.	AF201945	1.40	0.32
1000	CDC45 (cell division cycle 45, S.cerevisiae, homolog)-like	BC010022	1.39	0.31
1197	serine/threonine kinase 12	BF183143	1.39	0.41
9122	reproduction 8	AW474066	1.39	0.25
13255	Human neuronatin alpha and neuronatin beta genes, complete cds.	U31767	1.38	0.25
12788	Human regulator of G-protein signaling 7 (RGS7) mRNA, complete cds.	AF090116	1.37	0.28
4004	Human mRNA; cDNA DKFZp761K102 (from clone DKFZp761K102); complete cds.	AL136593	1.37	0.39
1357	KIAA0355 gene product	AB002353	1.37	0.31
4932	Human mRNA; cDNA DKFZp586A1519 (from clone DKFZp586A1519); partial cds.	AL050095	1.36	0.16
14294	Human mRNA for annexin A13 (ANXA13 gene), isoform b.	AJ306450	1.36	0.09
1680	Human atrial natriuretic peptide clearance receptor (ANP C receptor) mRNA, complete cds.	M59305	1.35	0.19

3164	Human genomic DNA of 21q22.2 Down Syndrome region, segment 11/13.	AP000020	1.35	0.17
13342	Human beta-tubulin pseudogene, clone 7-beta.	K00842	1.34	0.22
1032	H2A histone family, member N	BE253911	1.33	0.20
3256	similar to wee1-like protein kinase; similar to P30291 (PID:g1351419)	AAD04726	1.33	0.15
8003	Human two pore domain K+ channel (TASK-2) mRNA, complete cds.	AF084830	1.33	0.20
14522	Human cDNA FLJ13812 fis, clone THYRO1000327, highly similar to Human autocrine motility factor receptor (AMFR) mRNA.	AK023874	1.32	0.20
3543	Human cDNA FLJ20073 fis, clone COL02320.	AK000080	1.32	0.12
1667	Human mRNA for Sec23A isoform, 2748bp.	X97064	1.32	0.21
4011	myotubularin related protein 8	AW601612	1.31	0.26
11624	Human mRNA; cDNA DKFZp564M182 (from clone DKFZp564M182); partial cds.	AL049999	1.31	0.13
1845	Human chromosome 3, olfactory receptor pseudogene cluster 1, complete sequence, and myosin light chain kinase (MLCK) pseudogene, partial sequence.	AF042089	1.31	0.10
12090	adenylate cyclase 2 (brain)	AI160340	1.30	0.06
4036	Human, S-adenosylhomocysteine hydrolase-like 1, clone MGC:15558 IMAGE:3139729, mRNA, complete cds.	BC007576	1.30	0.18
4272	hypothetical protein	W74196	1.30	0.15
913	ubiquitin carboxyl extension protein [Human, mRNA, 540 nt].	S79522	1.29	0.20
746	Human CAAX box protein TIMAP mRNA, complete cds.	AF362910	1.28	0.05
5440	Human dopamine D4 receptor (DRD4) mRNA (D4.7) sequence.	L12398	1.28	0.12
6027	complement component 3a receptor 1	NM_004054	1.27	0.25
900	polymerase (DNA directed), delta 3	D26018	1.27	0.19
7132	activator of S phase kinase	AI289307	1.23	0.11
13785	ESTs, Highly similar to ROA3_HUMAN HETEROGENEOUS NUCLEAR RIBONUCLEOPROTEIN A3 [H.sapiens]	AW976907	1.22	0.04
6031	KIAA0328 protein	AB002326	1.22	0.08
1308	cytochrome c oxidase subunit VIII	AW009404	1.21	0.24
12556	Human type-I T-cell cytokine receptor mRNA, complete cds.	AF265242	1.20	0.15
6976	Human chondroitin sulfate proteoglycan versican V0 splice-variant precursor peptide mRNA, complete cds.	U16306	1.20	0.07
304	Human glutathione S-transferase A4-4 (GSTA4) mRNA, complete cds.	AF025887	1.20	0.14
104	Human alpha mannosidase II mRNA, complete cds.	U31520	1.19	0.10
13644	intersectin 1 (SH3 domain protein)	AA582575	1.19	0.08
10665	chromosome 2 open reading frame 6	AL122062	1.18	0.13
4786	Human sorting nexin 8 (SNX8) mRNA, complete cds.	AF121858	1.18	0.15

2239	Human pancreatic phospholipase A-2 (PLA-2) gene, exons 1 to 3.	M22970	1.17	0.10
2301	Human, serum amyloid A1, clone MGC:12369 IMAGE:4071612, mRNA, complete cds.	BC007022	1.16	0.12
14406	Human NADH-ubiquinone oxidoreductase subunit CI-SGDH mRNA, complete cds.	AF047181	1.16	0.11
13146	Human mRNA; cDNA DKFZp434N1235 (from clone DKFZp434N1235); complete cds.	AL136857	1.15	0.07
9503	alpha,-antitrypsin-like protein	BAA24419	1.11	0.07

Genes Significantly (P<0.005) Abundant In PAVEC In comparison to PAEC in static culture Group 3

Agilent Feature #	Gene Name/Description	Count 236		
		Gene ID	Fold AVE	Fold STD
13806	cadherin 11, type 2, OB-cadherin (osteoblast)	BI766088	113.16	66.59
16271	Human short form transcription factor C-MAF (c-maf) mRNA, complete cds.	AF055376	10.77	3.23
18283	adducin 3 (gamma)	AU134494	7.11	2.67
10719	HIV-1 rev binding protein 2	BE380146	5.89	1.42
15139	neural cell adhesion molecule 1	BI493304	4.51	0.96
12201	fibrinogen-like 2	AI796353	4.24	0.88
7859	Human connexin 37 (GJA4) mRNA, complete cds.	M96789	3.95	1.14
7437	transmembrane 4 superfamily member 2	AL568153	3.85	0.60
13220	Human (clone CCG-B7) mRNA sequence.	L10373	3.49	1.14
2290	Human chondroadherin mRNA, complete cds.	AF371328	3.47	1.71
6891	Human mRNA; cDNA DKFZp434I0812 (from clone DKFZp434I0812); partial cds.	AL137751	3.35	0.52
5567	P311 protein	AF119859	3.30	1.54
18516	integral membrane protein 2A	AA010378	3.21	0.60
8672	radixin	BF194976	3.04	0.46
12595	Human mRNA for Tec protein-tyrosine kinase, complete cds.	D29767	2.98	2.11
5800	S100 calcium-binding protein A4 (calcium protein, calvasculin, metastasin, murine placental homolog)	AV713821	2.96	0.92
13133	Human reelin (RELN) mRNA, complete cds.	U79716	2.93	0.92
16178	Human oligodendrocyte-specific protein (OSP) mRNA, complete cds.	AF068863	2.86	1.42
14857	v-myc avian myelocytomatosis viral related oncogene, neuroblastoma derived	BF313082	2.85	0.95
7592	collagen, type IV, alpha 1	NM_001845	2.82	1.39
14791	Human cathepsin B mRNA, 3' UTR with a stem-loop structure providing mRNA stability.	L22569	2.60	1.75
16548	v-kit Hardy-Zuckerman 4 feline sarcoma viral oncogene homolog	X06182	2.59	0.51
17356	Human mRNA for purine nucleoside phosphorylase (PNP; EC 2.4.2.1).	X00737	2.53	1.15
2407	Rho GDP dissociation inhibitor (GDI) beta	BG388517	2.45	0.68
14723	Human ARTS protein (PNUTL2) mRNA, complete cds; nuclear gene for mitochondrial product.	AF176379	2.39	0.74
9115	ELK3, ETS-domain protein (SRF accessory protein 2)	BI767724	2.38	1.17
2450	Human glia-derived nexin (GDN) mRNA, 5' end.	M17783	2.37	0.60

10654	sialyltransferase 8 (alpha-2, 8-polysialytransferase) D	L41680	2.33	0.50
18517	glutathione peroxidase 1	BI908630	2.32	0.92
4120	villin 2 (ezrin)	AU135575	2.31	0.79
3862	Human mRNA; cDNA DKFZp564E227 (from clone DKFZp564E227); complete cds.	AL136693	2.30	1.50
14553	Human, clone IMAGE:4183312, mRNA, partial cds.	BC008099	2.29	0.80
9834	Human, Rho GDP dissociation inhibitor (GDI) beta, clone MGC:15348 IMAGE:3621138, mRNA, complete cds.	BC009200	2.28	0.73
2376	Human mRNA for KIAA1095 protein, partial cds.	AB029018	2.27	0.57
12906	Human T-cell receptor zeta-chain mRNA, complete cds.	J04132	2.25	1.15
4179	SRY (sex determining region Y)-box 9 (campomelic dysplasia, autosomal sex-reversal)	BC007951	2.21	1.10
4263	tyrosine kinase with immunoglobulin and epidermal growth factor homology domains	X60957	2.21	1.18
12722	Human receptor protein-tyrosine kinase (TEK) mRNA, complete cds.	L06139	2.20	0.63
6782	Human cDNA FLJ11312 fis, clone PLACE1010105, weakly similar to RING CANAL PROTEIN.	AK002174	2.20	1.11
17977	CD3Z antigen, zeta polypeptide (TiT3 complex)	AL557555	2.20	1.00
13158	Human, Similar to KIAA0174 gene product, clone MGC:3110 IMAGE:3350789, mRNA, complete cds.	BC000116	2.17	0.95
3414	Human vascular endothelial cell growth factor 165 receptor/neuropilin (VEGF165) mRNA, complete cds.	AF016050	2.13	0.42
1367	myosin, heavy polypeptide 11, smooth muscle	NM_002474	2.12	1.28
13589	5'-nucleotidase (purine), cytosolic type B	D38524	2.10	1.11
14254	Human TESTIN 2 and TESTIN 3 genes, complete cds, alternatively spliced.	AF260225	2.08	0.38
1803	Human mRNA; cDNA DKFZp586F2423 (from clone DKFZp586F2423).	AL080209	2.07	0.87
7303	heterogeneous nuclear ribonucleoprotein H1 (H)	BE296051	2.06	0.91
8682	sialyltransferase	U14550	2.04	0.71
11814	adaptor-related protein complex 4, mu 1 subunit	BG831341	2.03	1.02
14060	Human GP36b glycoprotein mRNA, complete cds.	U10362	2.03	0.96
3363	Human mRNA for KIAA1816 protein, partial cds.	AB058719	2.03	0.46
14096	Human palmitoylated erythrocyte membrane protein (MPP1) mRNA, complete cds.	M64925	2.03	0.94
6968	fat protein	AAA28530	2.02	0.72
5797	ATPase, Na+/K+ transporting, alpha 2 (+) polypeptide	NM_000702	2.01	0.95
13216	Human mRNA for KIAA1296 protein, partial cds.	AB037717	1.97	0.74

5672	tyrosyl-tRNA synthetase	BC004151	1.96	1.06
8506	Human transcriptional coactivator ALY mRNA, partial cds.	AF047002	1.96	0.66
12704	Human c-kit proto-oncogene mRNA.	X06182	1.96	0.32
14281	Human, clone IMAGE:3604332, mRNA, partial cds.	BC003659	1.96	0.94
5498	flap structure-specific endonuclease 1	BG773958	1.94	1.03
18464	Sec23 (S. cerevisiae) homolog B	BI460300	1.93	1.34
9557	Human macrophage capping protein mRNA, complete cds.	M94345	1.89	0.87
6002	delta sleep inducing peptide, immunoreactor	AL525317	1.89	0.70
10655	activated p21cdc42Hs kinase	BG742978	1.881	0.73
14100	antiquitin=26g turgor protein homolog [Human, kidney, mRNA, 1809 nt].	S74728	1.88	0.76
5193	Human genomic DNA, chromosome 6p21.3, HLA Class I region, section 2/20.	AP000503	1.87	0.82
16612	adaptor-related protein complex 4, mu 1 subunit	AW170559	1.87	0.80
11972	Niemann-Pick disease, type C2 gene	BG397837	1.83	1.08
7857	Human full length insert cDNA YH92E12.	AF074995	1.82	1.12
13348	non-POU-domain-containing, octamer-binding	BI254716	1.81	0.49
10166	tubulin, alpha 1 (testis specific)	BE742772	1.81	0.66
10555	calcium channel, voltage-dependent, beta 3 subunit	AL565681	1.80	0.69
16772	NBR2	U88573	1.80	0.64
3708	Human, tubulin alpha 1, clone MGC:16616 IMAGE:4111591, mRNA, complete cds.	BC009314	1.80	0.77
6467	Human, Similar to gene rich cluster, C10 gene, clone MGC:4750 IMAGE:3537206, mRNA, complete cds.	BC009925	1.79	0.21
16165	Human protein kinase HIPK2 mRNA, complete cds.	AF208291	1.77	0.97
4137	capping protein (actin filament), gelsolin-like	BF978545	1.76	0.79
10684	KIAA0601 protein	AB011173	1.75	0.44
3392	Human CSaids binding protein (CSBP1) mRNA, complete cds.	L35263	1.75	1.01
15333	receptor (calcitonin) activity modifying protein 2	AL548945	1.72	0.40
9580	Human transforming growth factor-beta 1 binding protein mRNA, complete cds.	M34057	1.72	0.23
15398	KIAA0138 gene product	BE856759	1.72	0.69
1642	Human ornithine aminotransferase (OAT) gene, exon 6 and partial cds.	M88760	1.71	0.41
6302	Human, Similar to threonyl-tRNA synthetase, clone MGC:3031 IMAGE:3163506, mRNA, complete cds.	BC000541	1.71	0.32
14854	KIAA0172 protein	D79994	1.71	0.31
12042	TGFB-induced factor (TALE family homeobox)	AL549846	1.71	0.36
9112	Friend leukemia virus integration 1	X67001	1.71	0.67
16731	ESTs, Highly similar to A31233 ribosomal protein RS.40K, cytosolic [H.sapiens]	BG775549	1.71	0.89
7047	histone deacetylase 5	BF305705	1.70	0.76

18361	peptidylprolyl isomerase B (cyclophilin B)	BE868117	1.68	0.80
16714	adenylosuccinate lyase	AL022238	1.67	0.61
11800	serine threonine protein kinase	AU121423	1.67	0.68
11262	Human EF-1delta gene encoding Human elongation factor-1-delta.	Z21507	1.67	0.42
13200	Human gamma-filamin (FLNC) gene, complete cds.	AF252549	1.66	0.81
13743	cartilage oligomeric matrix protein (pseudoachondroplasia, epiphyseal dysplasia 1, multiple)	L32137	1.66	0.89
13026	Human, Similar to S-adenosylhomocysteine hydrolase, clone MGC:2319 IMAGE:3139231, mRNA, complete cds.	BC011606	1.66	0.74
9410	Human HOK-2 mRNA for zinc finger protein.	X82125	1.65	0.51
16737	methylthioadenosine phosphorylase	AL048242	1.65	0.20
13855	for protein disulfide isomerase-related	D49490	1.65	0.89
11040	Human cytoplasmic protein mRNA, complete cds.	AF177377	1.64	0.79
8631	catenin (cadherin-associated protein), alpha-like 1	BF793401	1.64	0.21
5965	peroxisomal long-chain acyl-coA thioesterase	AA825544	1.64	0.40
2432	cathepsin Z	AI913006	1.63	0.37
9709	Human mRNA for smooth muscle myosin.	X69292	1.63	0.56
8059	Na,K-ATPase alpha-4 subunit	AAD43813	1.63	0.68
9882	Human mitochondrial 2,4-dienoyl-CoA reductase mRNA, complete cds.	L26050	1.62	0.45
11626	Human mRNA for stabilin-1 (stab1 gene).	AJ275213	1.62	0.40
15962	Human mRNA; cDNA DKFZp564C053 (from clone DKFZp564C053).	AL049246	1.61	0.83
11303	Human mRNA for NB thymosin beta, complete cds.	D82345	1.61	0.25
18009	fat protein	AAA28530	1.60	0.58
1975	Human, Similar to KRAB-zinc finger protein SZF1-1, clone IMAGE:3945618, mRNA, partial cds.	BC006247	1.60	0.45
11336	Human mRNA for HKR1, partial cds.	AB013897	1.59	0.33
5251	Human B-cell receptor CD22-B isoform and alternatively spliced B-cell receptor CD22-A isoform (CD22) gene, complete cds.	U62631	1.58	0.67
17233	Human zinc finger protein gene, partial cds.	M77171	1.58	0.46
16557	thymosin, beta, identified in neuroblastoma cells	BG531641	1.57	0.20
5572	U2(RNU2) small nuclear RNA auxillary factor 1 (non-standard symbol)	BF968650	1.57	0.33
11450	Human mitogen inducible gene mig-2, complete cds.	Z24725	1.56	0.17
7294	signal sequence receptor, beta (translocon-associated protein beta)	BE887942	1.56	0.86
9535	Human cDNA: FLJ23436 fis, clone HRC12692.	AK027089	1.56	0.64
3700	Human PHD-finger protein (GRC5) mRNA, complete cds.	AF043725	1.55	0.67
17966	KIAA1796 protein	AB058699	1.54	0.38

9846	Human cDNA FLJ14588 fis, clone NT2RM4001819, highly similar to Human p58/GTA (galactosyltransferase associated protein kinase) mRNA.	AK027494	1.54	0.23
7830	Human can mRNA.	X64228	1.53	0.68
7976	Human SH2-containing protein Nsp3 mRNA, complete cds.	AF124251	1.53	0.16
13733	zinc finger protein 263	AC004232	1.52	0.51
5802	dihydropyrimidinase-like 3	AU133750	1.52	0.21
14743	Human paired related homeobox protein (PRX2) mRNA, complete cds.	AF061970	1.52	0.30
6398	Human hCENP-B gene for centromere autoantigen B (CENP-B).	X55039	1.51	0.25
1799	Human mRNA for ADP ribosylation factor-like protein, complete cds.	AB016811	1.51	0.66
9608	Human nonclathrin coat protein gamma2-COP mRNA, complete cds.	AF157833	1.51	0.35
4250	ESTs, Highly similar to I59087 ISG-K54 [H.sapiens]	AI609624	1.50	0.47
6035	growth arrest-specific 1	BE619835	1.50	0.10
13519	replication factor C (activator 1) 2 (40kD)	BE295474	1.49	0.29
12530	Human, hydroxymethylbilane synthase, clone MGC:8561 IMAGE:2822949, mRNA, complete cds.	BC000520	1.49	0.17
16785	karyopherin (importin) beta 2	U72069	1.49	0.62
16738	H2A histone family, member L	BF726950	1.49	0.12
12848	Human histone H2A.1 (H2A) gene, complete cds.	M60752	1.48	0.17
7438	T54 protein	AL580887	1.48	0.14
9453	Human trinucleotide repeat DNA binding protein p20-CGGBP (CGGBP) gene, complete cds.	AF094481	1.48	0.43
6888	Human mRNA for hMCM2, complete cds.	D28480	1.47	0.37
16937	H2A histone family, member O	AI885852	1.47	0.17
16468	catenin (cadherin-associated protein), delta 1	AF062332	1.46	0.64
9406	Human mRNA for DB1, complete cds.	D28118	1.46	0.40
15218	tyrosine 3-monooxygenase/tryptophan 5-monooxygenase activation protein, eta polypeptide	BI458375	1.46	0.48
2742	zinc finger protein 266	AK027480	1.46	0.31
6806	Human cDNA FLJ11321 fis, clone PLACE1010324.	AK002183	1.46	0.46
15306	serine palmitoyltransferase, long chain base subunit 2	AF111168	1.46	0.35
13617	phosphodiesterase 8A	AL109778	1.45	0.36
14711	Human mRNA for KIAA0747 protein, partial cds.	AB018290	1.45	0.31
14388	Human cDNA FLJ12587 fis, clone NT2RM4001217, moderately similar to Mouse (Mus musculus) actin-binding protein (ENC-1) mRNA.	AK022649	1.45	0.18
16936	clones 23667 and 23775 zinc finger protein	BG498371	1.45	0.58
6890	Human gas1 gene, complete cds.	L13698	1.44	0.23

12977	Human enhancer of polycomb 1 (EPC1) mRNA, complete cds.	AF286904	1.44	0.38
1377	zinc finger protein 184 (Kruppel-like)	BG254958	1.44	0.30
14574	Human, clone MGC:10520 IMAGE:3938462, mRNA, complete cds.	BC004480	1.44	0.34
14611	Human kruppel-like zinc finger protein (ZNF300) mRNA, complete cds.	AF395541	1.44	0.34
15308	Bcl-2 binding component 3	BG258126	1.44	0.23
1195	hypothetical protein	BG283735	1.44	0.13
14906	Human keratin 18 (KRT18) gene, complete cds.	AF179904	1.44	0.63
7557	RAD54 (S.cerevisiae)-like	BG763599	1.44	0.31
10493	cyclin D1 (PRAD1: parathyroid adenomatosis 1)	X59798	1.43	0.27
3631	Human, nuclear RNA export factor 1, clone MGC:4612 IMAGE:3504065, mRNA, complete cds.	BC004904	1.43	0.12
5972	immature colon carcinoma transcript 1	BC015335	1.43	0.13
14257	Human, clone MGC:10702 IMAGE:3833242, mRNA, complete cds.	BC004868	1.41	0.39
15198	ATPase, Ca++ transporting, plasma membrane 4	AI885833	1.41	0.34
14717	Human zinc finger protein mRNA.	M80583	1.41	0.50
16782	pumilio (Drosophila) homolog 1	BC013398	1.41	0.57
15100	moesin	NM_002444	1.41	0.57
14514	Human zinc finger protein zfp31 (zf31) mRNA, partial cds.	U71600	1.40	0.27
10506	catalase	BG287806	1.40	0.21
6261	Human mRNA for KIAA0052 protein, partial cds.	D29641	1.40	0.42
10503	nuclear cap binding protein subunit 2, 20kD	AI619551	1.40	0.32
14436	Human translation initiation factor eIF-2 gamma subunit mRNA, complete cds.	L19161	1.39	0.50
6019	cysteine-rich protein 1 (intestinal)	BI222747	1.38	0.22
12033	integrin beta 4 binding protein	BI908045	1.38	0.48
5068	p59fyn(T)=OKT3-induced calcium influx regulator [Human, Jurkat J6 T-cell line, mRNA Partial, 1605 nt].	S74774	1.38	0.13
16727	zinc finger protein 184 (Kruppel-like)	N80080	1.38	0.41
12654	Human, clone IMAGE:2989556, mRNA, partial cds.	BC001699	1.38	0.13
16289	Human, ATP synthase, H+ transporting, mitochondrial F1 complex, gamma polypeptide 1, clone MGC:5380 IMAGE:3445817, mRNA, complete cds.	BC000931	1.37	0.37
7521	MAX protein	BC003525	1.37	0.31
8229	Human cDNA FLJ13300 fis, clone OVARC1001342, highly similar to 40S RIBOSOMAL PROTEIN S8.	AK023362	1.37	0.15
8330	Human guanylate cyclase activating protein (GCAP) gene exons 1-4, complete cds.	L36861	1.36	0.18
8638	replication factor C (activator 1) 5 (36.5kD)	BG766412	1.36	0.23
9100	KIAA1688 protein	AW207595	1.36	0.39
1032	H2A histone family, member N	BE253911	1.36	0.22

10490	cell division cycle 25B	BF976307	1.36	0.30
14382	Human mRNA for KIAA0059 gene, complete cds.	D31883	1.35	0.35
6756	Human zinc finger protein ZNF140.	U09368	1.35	0.26
10309	vesicle-associated membrane protein 3 (cellubrevin)	BE379661	1.35	0.27
11099	Human cDNA FLJ14438 fis, clone HEMBB1000317, weakly similar to FIBULIN-1, ISOFORM D PRECURSOR.	AK027344	1.35	0.15
5997	acidic 82 kDa protein mRNA	BG697006	1.34	0.23
6874	Human, Similar to hyaluronoglucosaminidase 2, clone MGC:1922 IMAGE:3347760, mRNA, complete cds.	BC000692	1.34	0.35
3223	Human chloride channel ABP mRNA, complete cds.	AF034607	1.34	0.46
6037	guanine nucleotide binding protein-like 1	BE798151	1.34	0.31
6333	Human, nucleolar protein 1 (120kD), clone MGC:3093 IMAGE:3349415, mRNA, complete cds.	BC000656	1.33	0.17
15330	ribosomal protein S15	BG477036	1.33	0.30
3681	Human, clone MGC:2663 IMAGE:3543910, mRNA, complete cds.	BC001791	1.33	0.28
13502	DEAD/H (Asp-Glu-Ala-Asp/His) box polypeptide 18 (Myc-regulated)	BG613100	1.33	0.15
15192	Homo sapiens PAK2 mRNA, complete cds	AF092132	1.32	0.40
15982	Human keratin type II (58 kD) mRNA, complete cds.	M21389	1.32	0.25
14681	Human, BCS1 (Yeast homolog)-like, clone MGC:8631 IMAGE:2961496, mRNA, complete cds.	BC000416	1.32	0.21
4161	KIAA0246 protein	NM_015136	1.32	0.11
12693	Human mRNA for squamous cell carcinoma antigen SART-3, complete cds.	AB020880	1.31	0.26
14519	Human mRNA for KIAA1338 protein, partial cds.	AB037759	1.31	0.21
9888	Human M4 protein deletion mutant mRNA, complete cds.	AF061832	1.31	0.10
10999	prohibitin [Human, mRNA, 1043 nt].	S85655	1.30	0.16
9848	Human, keratin 8, clone MGC:1711 IMAGE:3349233, mRNA, complete cds.	BC000654	1.30	0.04
16104	Human cDNA: FLJ23506 fis, clone LNG03055.	AK027159	1.30	0.08
11584	Human mRNA for CHD5 protein.	Y12478	1.30	0.22
10974	Human mRNA for frizzled-2, complete cds.	AB017364	1.30	0.24
9081	tumor necrosis factor (TNF superfamily, member 2)	NM_000594	1.30	0.36
17357	Human, aldo-keto reductase family 1, member A1 (aldehyde reductase), clone MGC:12529 IMAGE:4051944, mRNA, complete cds.	BC005394	1.29	0.09
16424	Mouse Mammary Turmor Virus Receptor homolog	AI280835	1.29	0.18
7233	nuclear matrix protein p84	AV713026	1.29	0.15

8039	Human, laminin receptor 1 (67kD, ribosomal protein SA), clone MGC:12521 IMAGE:3997019, mRNA, complete cds.	BC005391	1.28	0.23
14057	Human cDNA FLJ11018 fis, clone PLACE1003602, highly similar to Human mRNA expressed in placenta.	AK001880	1.28	0.22
13499	minichromosome maintenance deficient (S. cerevisiae) 3	AU124152	1.28	0.14
15361	hydroxysteroid (17-beta) dehydrogenase 4	AU125131	1.28	0.33
12666	Human cytochrome b561 gene, exon 1.	U29460	1.28	0.09
14925	KIAA0225 protein	D86978	1.27	0.35
2108	Human general transcription factor 2-I (GTF2I) mRNA, alternatively spliced product, complete cds.	AF038968	1.27	0.11
10063	Human lipocalin-interacting protein mRNA, complete cds.	AF260728	1.27	0.18
11481	Human myotubularin related protein 7 mRNA, partial cds.	AF073482	1.26	0.13
14753	Human protein phosphatase 2A beta subunit mRNA, complete cds.	M64930	1.26	0.30
14719	Human Nit protein 2 (NIT2) mRNA, complete cds.	AF284574	1.24	0.42
15326	vesicle-associated membrane protein 8 (endobrevin)	AV716151	1.23	0.23
9554	Human, eukaryotic translation initiation factor 4E binding protein 2, clone MGC:12944 IMAGE:2823322, mRNA, complete cds.	BC005057	1.23	0.25
14994	synaptojanin 1	BF677649	1.22	0.13
5052	Human gene for ribosomal protein S2, partial cds.	AB007147	1.21	0.27
2273	Human cDNA: FLJ21675 fis, clone COL09090, highly similar to AF119857 Human PRO1855 mRNA.	AK025328	1.21	0.11
6625	Human acidic ribosomal phosphoprotein P2 mRNA, complete cds.	M17887	1.18	0.11
11422	Human, succinate dehydrogenase complex, subunit A, flavoprotein (Fp), clone MGC:1484 IMAGE:3051442, mRNA, complete cds.	BC001380	1.16	0.19
7390	cerebellar degeneration-related protein (62kD)	BI869500	1.15	0.22
4156	sulfotransferase family, cytosolic, 1A, phenol-preferring, member 3	BE745439	1.13	0.06
7450	peroxisomal farnesylated protein	AL571857	1.13	0.10
8801	protein phosphatase 1, regulatory subunit 7	Z50749	1.11	0.10

Genes Significantly (P<0.005) Abundant In PAEC
In comparison to PAVEC in static culture
Group 3

Agilent Feature #	Gene Name/Description	Count 180		
		Gene ID	Fold AVE	Fold STD
1196	osteoblast specific factor 2 (fasciclin I-like)	AW608422	444.02	294.72
15769	Macaque somatostatin I mRNA, complete cds.	M19318	107.50	50.03
14871	interleukin 8	BG777366	40.93	18.28
8985	somatostatin	BI713774	16.45	3.27
4103	amphiregulin (schwannoma-derived growth factor)	AL546917	9.57	5.48
504	Human metallothionein-I-A gene, complete coding sequence.	K01383	7.26	3.24
4183	glioblastoma amplified sequence	AI989900	6.84	2.20
14728	Human mRNA for pro-alpha-1 type 3 collagen.	X14420	6.70	3.93
17499	Human mRNA for metallothionein isoform 1R.	X97261	6.45	2.95
9935	Human cDNA FLJ20129 fis, clone COL06190.	AK000136	6.09	3.58
18197	metallothionein 1E (functional)	H72532	5.66	2.38
10676	interferon-stimulated protein, 15 kDa	AI739106	5.61	1.71
2397	matrix Gla protein	AW999947	5.48	0.96
11616	Human mRNA for phospholipase C, complete cds.	D42108	5.22	1.95
5874	interferon-induced protein with tetratricopeptide repeats 1	M24594	4.85	1.35
10569	growth arrest and DNA-damage-inducible, alpha	AI814872	4.58	1.58
3456	Human CD39L3 (CD39L3) mRNA, complete cds.	AF039917	4.28	1.23
17864	Human mRNA for cardiac gap junction protein.	X52947	4.19	1.64
3221	Human, ATPase, Na+/K+ transporting, beta 1 polypeptide, clone MGC:1798 IMAGE:3506311, mRNA, complete cds.	BC000006	4.17	1.88
1214	neuro-oncological ventral antigen 1	NM_006489	4.10	2.49
6648	Human metallothionein (MT)I-F gene, complete cds.	M13003	3.92	1.34
5561	aldehyde dehydrogenase 1 family, member A1	AV649527	3.91	1.69
18467	gap junction protein, alpha 1, 43kD (connexin 43)	X52947	3.83	1.22
11122	KIAA0412	BAA24842	3.48	1.74
13850	fibromodulin	AI249821	3.36	1.55
17217	MAM domain protein	AAC59868	3.32	0.91
10465	neuronatin	AI638471	3.30	1.53
10091	Human leukemogenic homolog protein (MEIS1) mRNA, complete cds.	U85707	3.12	1.06

17584	Human mRNA for soluble guanylyl cyclase.	Y15723	3.07	1.09
10982	Human mRNA for NOTCH4, partial cds.	D63395	3.05	0.44
10539	myxovirus (influenza) resistance 1, homolog of murine (interferon-inducible protein p78)	AA477235	2.99	0.85
4964	Human Bmx mRNA for cytoplasmic tyrosine kinase.	X83107	2.97	0.64
13807	GTP-binding protein overexpressed in skeletal muscle	AW297828	2.94	0.18
13444	homeo box A7	NM_006896	2.91	0.84
16809	myosin, light polypeptide kinase	AW951177	2.85	0.75
9994	Human Apo-2 ligand mRNA, complete cds.	U57059	2.83	0.33
4311	caspase 4, apoptosis-related cysteine protease	BG572762	2.78	0.60
14759	aortic carboxypeptidase-like protein ACLP	AAC25584	2.72	2.37
16296	Human mRNA for cyclin-E binding protein 1, complete cds.	AB027289	2.69	1.07
4796	Human mRNA for KIAA0762 protein, partial cds.	AB018305	2.68	0.96
11439	Human uveal autoantigen mRNA, complete cds.	AF322916	2.65	0.83
2768	very low density lipoprotein receptor	BG028841	2.65	0.80
5958	myeloid/lymphoid or mixed-lineage leukemia (trithorax (Drosophila) homolog); translocated to, 3	AI110630	2.61	0.34
2460	heparan sulfate proteoglycan 2 (perlecan)	NM_005529	2.58	1.49
9416	Human cDNA FLJ10500 fis, clone NT2RP2000369.	AK001362	2.56	0.55
6842	Human mRNA; cDNA DKFZp586B1817 (from clone DKFZp586B1817).	AL050088	2.56	0.51
18061	ATP-binding cassette, sub-family G (WHITE), member 2	BI497116	2.54	0.35
18492	PTH-responsive osteosarcoma B1 protein	AA002033	2.51	0.16
12071	procollagen-lysine, 2-oxoglutarate 5-dioxygenase (lysine hydroxylase) 2	U84573	2.49	0.62
8681	glycogen synthase 1 (muscle)	AL556228	2.39	0.69
16426	tetraspan 5	AF065389	2.34	0.41
17663	Human mRNA for neurexin I-alpha protein, complete cds.	AB035356	2.31	0.30
17241	Human cDNA FLJ10244 fis, clone HEMBB1000632, weakly similar to GUANINE NUCLEOTIDE RELEASING PROTEIN.	AK001106	2.26	0.47
7286	ATP-binding cassette, sub-family G (WHITE), member 2	AU118354	2.25	0.37
8983	immunoglobulin superfamily containing leucine-rich repeat	AB003184	2.22	0.47
13537	Human (clone CTG-A4) mRNA sequence	AL530945	2.19	0.59
11598	Human mRNA for KIAA0212 gene, complete cds.	D86967	2.13	0.76

8037	Human mRNA; cDNA DKFZp667P184 (from clone DKFZp667P184).	AL512742	2.11	0.69
14079	Human cDNA FLJ14357 fis, clone HEMBA1000005, highly similar to DNAJ PROTEIN HOMOLOG MTJ1.	AK027263	2.09	0.66
11486	Human mRNA for KIAA0705 protein, complete cds.	AB014605	2.08	0.43
6781	Human G-protein gamma-10 subunit mRNA, complete cds.	U31383	2.08	0.55
4753	Human, angiotensinogen (serine (or cysteine) protease inhibitor, clade A (alpha-1 antiprotease, antitrypsin), member 8), clone MGC:17092 IMAGE:4213559, mRNA, complete cds.	BC011519	2.07	0.86
15227	tetraspan 2	AI924594	2.06	0.28
18357	SWI/SNF related, matrix associated, actin dependent regulator of chromatin, subfamily a, member 1	NM_003069	2.05	0.53
13215	Human mRNA for KIAA0669 protein, complete cds.	AB014569	2.02	0.19
9695	Human, glutathione S-transferase M3 (brain), clone MGC:3310 IMAGE:3509784, mRNA, complete cds.	BC000088	1.98	0.17
7886	Human mRNA for NADP dependent leukotriene b4 12-hydroxydehydrogenase, partial cds.	D49387	1.96	0.69
4013	Notch (Drosophila) homolog 4	D63395	1.93	0.26
5589	serine (or cysteine) proteinase inhibitor, clade G (C1 inhibitor), member 1	AL531502	1.92	0.63
15978	Human cDNA: FLJ21715 fis, clone COL10287, highly similar to AF071569 Human multifunctional calcium/calmodulin-dependent protein kinase II delta2 isoform mRNA.	AK025368	1.90	0.54
7499	ESTs	AA233775	1.90	0.81
3543	Human cDNA FLJ20073 fis, clone COL02320.	AK000080	1.89	0.77
16461	Human lysyl oxidase-like 3 protein (LOXL3) mRNA, complete cds.	AF311313	1.87	0.37
7810	Human mRNA for HLA class-I (HLA-A26) heavy chain, complete cds (clone cMIY-1).	D32129	1.84	0.50
14372	Human mRNA for DnaJ protein homolog, complete cds.	D13388	1.83	0.84
14589	Human genes for S100E calcium binding protein, CAPL, and S100D calcium binding protein EF-Hand (partial).	Z18950	1.81	0.31
8361	Human mRNA for KIAK0002 gene, complete cds.	D13639	1.81	0.86
11916	S100 calcium-binding protein A5	AW090645	1.81	0.19
14522	Human cDNA FLJ13812 fis, clone THYRO1000327, highly similar to Human autocrine motility factor receptor (AMFR) mRNA.	AK023874	1.79	0.55
16905	KIAA0368 protein	AB002366	1.79	0.39

11907	ubiquitin carboxyl-terminal esterase L3 (ubiquitin thiolesterase)	BG939578	1.78	0.73
16267	Human follistatin gene, exons 1-5.	M19480	1.77	0.32
6038	ATPase, Class I, type 8B, member 1	NM_005603	1.77	0.35
12230	ELL-RELATED RNA POLYMERASE II, ELONGATION FACTOR	U88629	1.77	0.45
3496	Human nectin 3 mRNA, complete cds.	AF282874	1.76	0.70
13583	vinculin	NM_014000	1.74	0.50
5682	retinoblastoma 1 (including osteosarcoma)	BI092056	1.73	0.63
12259	bone morphogenetic protein 4	NM_001202	1.73	0.34
10395	major histocompatibility complex, class I, C	BE168491	1.73	0.28
15097	cholinergic receptor, nicotinic, delta polypeptide	BF306695	1.72	0.59
4719	Human 1-8D gene from interferon-inducible gene family.	X57351	1.70	0.39
4310	solute carrier family 28 (sodium-coupled nucleoside transporter), member 1	U62966	1.70	0.27
4296	KIAA0212 gene product	D86967	1.69	0.55
11431	Human cDNA: FLJ21270 fis, clone COL01749.	AK024923	1.68	0.73
11260	Human phospholemman chloride channel mRNA, complete cds.	U72245	1.66	0.43
16607	downregulated in ovarian cancer 1	U53445	1.66	0.28
7075	neuronatin	AW161393	1.66	0.19
13676	glutaminase	BI764185	1.65	0.59
8826	troponin I, skeletal, slow	AL596761	1.65	0.12
7362	interleukin 13	NM_002188	1.64	0.38
8671	GRO1 oncogene (melanoma growth stimulating activity, alpha)	BG753792	1.63	0.26
3859	Human angiopoietin-like protein PP1158 mRNA, complete cds.	AF202636	1.62	0.33
17539	Human partial mRNA for putative nuclear factor.	AJ276691	1.61	0.54
17560	Human transcription factor ISGF-3 mRNA, complete cds.	M97935	1.60	0.46
14546	Human MHC class I HLA-C-alpha-2 chain and alternative mRNA, complete cds, clones 4 and 10.	M24097	1.60	0.70
5686	ras-like protein	AA043151	1.58	0.16
6972	Human mRNA for TL132.	AJ012755	1.58	0.54
8497	Human hepatocellular carcinoma-associated antigen 67 (HCA67) mRNA, complete cds.	AF243495	1.56	0.19
5971	Homo sapiens clone DT1P1B6 mRNA, CAG repeat region	BI868318	1.55	0.44
9058	ATPase, H+ transporting, lysosomal (vacuolar proton pump) 42kD	N75606	1.55	0.47
7590	ESTs, Weakly similar to I38022 hypothetical protein [H.sapiens]	BG718906	1.53	0.60
11788	metaxin 2	AW237281	1.53	0.64
16283	Human RAR-responsive (TIG1) mRNA, complete cds.	U27185	1.53	0.35

5973	receptor-interacting serine-threonine kinase 2	BG170405	1.53	0.40
15961	Human mRNA for KIAA0517 protein, partial cds.	AB011089	1.52	0.39
6040	ESTs	AI869879	1.50	0.36
9863	Human, ATPase, H+ transporting, lysosomal (vacuolar proton pump), member J, clone MGC:1970 IMAGE:3546257, mRNA, complete cds.	BC003564	1.49	0.43
7408	RAS protein activator like 2	NM_004841	1.49	0.23
8219	Human forkhead-related transcription factor FREAC-10 (FKHL18) mRNA, partial cds.	AF042831	1.49	0.33
9788	LPRP=pHL E1F1 [Human, lacrimal gland, mRNA Partial, 507 nt].	S79048	1.48	0.41
3825	Human SH2-containing protein Nsp2 mRNA, complete cds.	AF124250	1.46	0.60
14288	Human mRNA; cDNA DKFZp586N1922 (from clone DKFZp586N1922); partial cds.	AL117468	1.46	0.14
13178	C33 antigen=type III integral membrane protein [human, T cell line MOLT-4, Peptide, 267 aa]	AAB23825	1.45	0.29
8168	Human mRNA for KIAA0769 protein, complete cds.	AB018312	1.44	0.42
4003	Human HES-related repressor protein 2 HERP2 mRNA, complete cds.	AF232239	1.44	0.22
10232	collagen, type V, alpha 2	AU117484	1.42	0.18
11893	LIM domain kinase 2	NM_016733	1.42	0.15
1337	ceruloplasmin (ferroxidase)	M13699	1.41	0.45
15843	Human nuclear orphan receptor LXR-alpha mRNA, complete cds.	U22662	1.38	0.27
10416	KIAA0573 protein	AB011145	1.38	0.26
17186	Human homeobox 1.4 protein mRNA, complete cds.	M74297	1.38	0.24
11565	Human 10kD protein (BC10) mRNA, complete cds.	AF053470	1.38	0.25
11752	hypothetical protein A-211C6.1	AL537232	1.37	0.51
9549	Human retinoic acid receptor gamma 1 mRNA, complete cds.	M38258	1.37	0.17
7366	ubiquitin-conjugating enzyme E2L 6	AW976741	1.36	0.25
9069	serine (or cysteine) proteinase inhibitor, clade F (alpha-2 antiplasmin, pigment epithelium derived factor), member 1	AL541945	1.36	0.14
15386	protein tyrosine phosphatase, receptor type, C-associated protein	BG397566	1.34	0.38
15378	phospholipase A2, group IVA (cytosolic, calcium-dependent)	AI627464	1.34	0.37
16773	ATP-binding cassette, sub-family C (CFTR/MRP), member 5	AB005659	1.34	0.32
16556	phosphotriesterase related	BG170397	1.34	0.13
10532	matrix metalloproteinase 23B	AI347985	1.33	0.07
14888	Human nGAP mRNA, complete cds.	AF047711	1.33	0.17
9912	Human mRNA for NADP+-dependent malic enzyme.	X79440	1.33	0.31

14126	Human genomic DNA, chromosome 21q, section 96/105.	AP001752	1.33	0.10
13446	alpha2,8-sialyltransferase	U91641	1.33	0.38
13622	nerve growth factor, beta polypeptide	X52599	1.33	0.18
4173	ubiquinol-cytochrome c reductase (6.4kD) subunit	BG338004	1.32	0.16
1818	Human, crystallin, alpha B, clone MGC:12326 IMAGE:3933748, mRNA, complete cds.	BC007008	1.32	0.16
15024	HCGII-7 protein	X81001	1.31	0.24
5720	procollagen-proline, 2-oxoglutarate 4-dioxygenase (proline 4-hydroxylase), alpha polypeptide I	AL574109	1.31	0.22
6914	Human, protein phosphatase 1, regulatory (inhibitor) subunit 2, clone MGC:1327 IMAGE:3346573, mRNA, complete cds.	BC007655	1.31	0.18
5998	gene with multiple splice variants near HD locus on 4p16.3	AB000460	1.30	0.09
16422	Human mRNA for inositol 1,4,5-trisphosphate receptor type 2, complete cds.	D26350	1.30	0.17
16961	ferritin, light polypeptide	BE394443	1.29	0.16
2733	transducer of ERBB2, 2	AI554661	1.28	0.31
16899	solute carrier family 6 (neurotransmitter transporter, L-proline), member 7	NM_014228	1.28	0.16
14068	Human mRNA for KIAA1249 protein, partial cds.	AB033075	1.28	0.32
3968	Human mRNA for alpha-actinin, partial cds.	X55187	1.26	0.14
17500	Human factor XIII subunit a mRNA, 3' end.	M14539	1.25	0.08
14543	Human RNA polymerase II elongation factor SIII, p15 subunit mRNA, complete cds.	L34587	1.24	0.25
11890	KIAA0076 gene product	AI741847	1.23	0.21
14594	Human, endoplasmic reticulum chaperone SIL1, homolog of Yeast, clone MGC:20202 IMAGE:4640182, mRNA, complete cds.	BC011568	1.23	0.16
12689	Human mRNA for KIAA0085 gene, partial cds.	D42042	1.23	0.16
5487	f-box and leucine-rich repeat protein 5	AA768000	1.22	0.15
6460	Human, clone MGC:14993 IMAGE:3613406, mRNA, complete cds.	BC010420	1.22	0.15
15851	Human P2X4 purinoreceptor mRNA, complete cds.	U83993	1.21	0.38
12110	GRO3 oncogene	X53800	1.21	0.19
8621	Human, melanoma inhibitory activity, clone MGC:14503 IMAGE:4333499, mRNA, complete cds.	BC005910	1.21	0.16
15057	Fc fragment of IgG, receptor, transporter, alpha	AL571972	1.20	0.20
14584	Human mitochondrial benzodiazepine receptor (MBR) gene, complete cds.	U12421	1.20	0.15

14890	bM106N23.1 (novel protein kinase (ortholog of human dJ272L16.1 and rat Ca2+/calmodulin dependent protein kinase))	CAC41379	1.19	0.10
13023	Human mRNA for SURF-2.	Z35094	1.19	0.10
6493	Human DC10 (DC10) mRNA, complete cds.	AF201932	1.18	0.12
3800	pN44=prostate secretory protein [Human, prostate tissue, mRNA, 475 nt].	S67815	1.17	0.20
3882	Human Kruppel-like zinc finger protein GLIS2 mRNA, complete cds.	AF325914	1.17	0.19
17661	Human P2x1 receptor mRNA, complete cds.	U45448	1.15	0.11
12988	Human testis 6-phosphofructo-2-kinase/fructose 2,6-bisphosphatase (PFKFB4) mRNA, complete cds.	AF108765	1.15	0.09
15799	Human mRNA; cDNA DKFZp586A181 (from clone DKFZp586A181); partial cds.	AL050391	1.11	0.09
13752	guanylate cyclase 2D, membrane (retina-specific)	NM_000180	1.11	0.11
15168	SGC32445 protein	AF070551	1.09	0.12

Genes Significantly (P<0.005) Abundant In PAVEC In comparison to PAEC in shear Group 4

Agilent Feature #	Gene Name/Description	Count 424		
		Gene ID	Fold AVE	Fold STD
9463	Human fatty acid binding protein homologue (PA-FABP) mRNA, complete cds.	M94856	25.36	11.71
16178	Human oligodendrocyte-specific protein (OSP) mRNA, complete cds.	AF068863	5.33	2.70
12201	fibrinogen-like 2	AI796353	5.08	0.72
8954	gap junction protein, alpha 4, 37kD (connexin 37)	AL574266	4.61	0.74
8756	X-prolyl aminopeptidase (aminopeptidase P) 2, membrane-bound	NM_003399	4.24	2.22
10719	HIV-1 rev binding protein 2	BE380146	4.07	0.52
15139	neural cell adhesion molecule 1	BI493304	3.47	0.29
4250	ESTs, Highly similar to I59087 ISG-K54 [H.sapiens]	AI609624	3.45	0.81
16906	HLA class II region expressed gene KE4	BC000645	3.41	1.29
16557	thymosin, beta, identified in neuroblastoma cells	BG531641	3.28	1.25
10522	myosin, heavy polypeptide 9, non-muscle	BG699149	3.23	1.53
7009	Human transketolase (tk) mRNA, complete cds.	L12711	3.09	0.45
9580	Human transforming growth factor-beta 1 binding protein mRNA, complete cds.	M34057	3.07	1.49
1367	myosin, heavy polypeptide 11, smooth muscle	NM_002474	3.04	1.28
18517	glutathione peroxidase 1	BI908630	2.96	0.51
2928	cytochrome P450, subfamily I (aromatic compound-inducible), polypeptide 1	K03191	2.89	0.55
18516	integral membrane protein 2A	AA010378	2.86	0.75
7437	transmembrane 4 superfamily member 2	AL568153	2.78	0.63
13782	chitinase 3-like 1 (cartilage glycoprotein-39)	AL035737	2.78	1.48
5567	P311 protein	AF119859	2.69	1.07
4290	major histocompatibility complex, class I, B	AL537877	2.68	1.07
7592	collagen, type IV, alpha 1	NM_001845	2.66	0.50
7348	phosphodiesterase 6D, cGMP-specific, rod, delta	BC007831	2.65	0.49
10644	ectodermal-neural cortex (with BTB-like domain)	BC000418	2.65	0.27
9156	transcriptional coactivator	AI088790	2.63	0.20
13200	Human gamma-filamin (FLNC) gene, complete cds.	AF252549	2.58	0.78
5797	ATPase, Na+/K+ transporting, alpha 2 (+) polypeptide	NM_000702	2.58	0.75
16118	Human MHC class I lymphocyte antigen (HLA-E) (HLA-6.2) gene, complete cds.	M21533	2.57	1.04
78	Human mRNA; cDNA DKFZp564F1016 (from clone DKFZp564F1016).	AL110174	2.50	0.82

13466	prostaglandin-endoperoxide synthase 1 (prostaglandin G/H synthase and cyclooxygenase)	S36219	2.50	0.66
14791	Human cathepsin B mRNA, 3' UTR with a stem-loop structure providing mRNA stability.	L22569	2.49	0.65
9869	Human FK506-binding protein (FKBP63) mRNA, partial cds.	AF089745	2.48	1.08
9834	Human, Rho GDP dissociation inhibitor (GDI) beta, clone MGC:15348 IMAGE:3621138, mRNA, complete cds.	BC009200	2.47	0.20
16878	2,3-bisphosphoglycerate mutase	X04327	2.47	0.87
859	biglycan	BG111541	2.45	0.84
1799	Human mRNA for ADP ribosylation factor-like protein, complete cds.	AB016811	2.45	0.58
2588	chaperonin containing TCP1, subunit 7 (eta)	AA314436	2.42	1.01
10567	heat shock 70kD protein 1A	BG674024	2.42	0.79
5596	Human OS-9 mRNA, complete cds.	AB002806	2.41	0.67
5908	immediate early response 3	AI911657	2.40	0.14
4730	Human heparan sulfate proteoglycan (HSPG) core protein, 3' end.	J04621	2.40	0.78
16643	deleted in liver cancer 1	NM_006094	2.38	0.91
13220	Human (clone CCG-B7) mRNA sequence.	L10373	2.34	0.47
10486	gelsolin (amyloidosis, Finnish type)	BG763361	2.32	0.67
7155	calcium channel, voltage-dependent, alpha 2/delta subunit 2	NM_006030	2.32	0.59
9557	Human macrophage capping protein mRNA, complete cds.	M94345	2.31	0.67
2435	aldo-keto reductase family 1, member C1 (dihydrodiol dehydrogenase 1; 20-alpha (3-alpha)-hydroxysteroid dehydrogenase)	BI759009	2.29	0.26
11964	prostaglandin I2 (prostacyclin) synthase	D38145	2.29	0.64
9006	nucleoside phosphorylase	BE266250	2.29	0.42
18356	FOS-like antigen 2	X16706	2.28	0.86
11977	FK506-binding protein 9 (63 kD)	AL555732	2.27	0.97
4921	Human MacGAP mRNA, complete cds.	AB053293	2.27	0.31
17659	Human 26-kDa cell surface protein TAPA-1 mRNA, complete cds.	M33680	2.26	0.46
7441	NADH dehydrogenase (ubiquinone) flavoprotein 1 (51kD)	AW250734	2.26	0.74
6440	Human hepatocellular carcinoma associated protein (JCL-1) mRNA, complete cds.	U92544	2.25	0.35
3460	Human mRNA for collagen alpha 1(V) chain, complete cds.	D90279	2.25	0.77
17356	Human mRNA for purine nucleoside phosphorylase (PNP; EC 2.4.2.1).	X00737	2.24	0.32
2757	adenine phosphoribosyltransferase	BG612479	2.23	0.47
2697	LIM domain only 2 (rhombotin-like 1)	X61118	2.21	0.94
4356	enolase 3, (beta, muscle)	X51957	2.19	0.68
8415	nonmuscle myosin heavy chain	AAA48988	2.19	0.82
499	Human, transmembrane 4 superfamily member (tetraspan NET-7), clone MGC:4120 IMAGE:2958221, mRNA, complete cds.	BC003157	2.17	0.71
4137	capping protein (actin filament), gelsolin-like	BF978545	2.15	0.55
7047	histone deacetylase 5	BF305705	2.15	0.39

280	Human cDNA FLJ14035 fis, clone HEMBA1004638.	AK024097	2.15	0.47
8059	Na,K-ATPase alpha-4 subunit	AAD43813	2.15	0.55
8992	phospholipase C, delta 1	BI489731	2.12	0.61
9787	Human proto-oncogene Bcd orf1 and orf2 mRNA, complete cds.	U51869	2.11	0.20
5160	Human, clone MGC:14256 IMAGE:4129368, mRNA, complete cds.	BC007847	2.09	0.46
14096	Human palmitoylated erythrocyte membrane protein (MPP1) mRNA, complete cds.	M64925	2.07	0.37
17481	Human, clone MGC:10986 IMAGE:3636469, mRNA, complete cds.	BC004400	2.07	0.53
15398	KIAA0138 gene product	BE856759	2.06	0.37
6349	Macaque brain cDNA, clone:QflA-11789.	AB055286	2.05	0.93
10171	upstream binding transcription factor, RNA polymerase I	BI088564	2.03	0.71
4932	Human mRNA; cDNA DKFZp586A1519 (from clone DKFZp586A1519); partial cds.	AL050095	2.03	0.64
7430	nuclear factor I/X (CCAAT-binding transcription factor)	D51465	2.02	0.18
8346	Human transcription factor junB (junB) gene, 5' region and complete cds.	U20734	2.02	0.23
5672	tyrosyl-tRNA synthetase	BC004151	2.02	0.73
3708	Human, tubulin alpha 1, clone MGC:16616 IMAGE:4111591, mRNA, complete cds.	BC009314	2.02	0.29
11972	Niemann-Pick disease, type C2 gene	BG397837	2.01	0.54
14060	Human GP36b glycoprotein mRNA, complete cds.	U10362	2.01	0.51
16772	NBR2	U88573	2.01	0.18
16410	hematopoietic PBX-interacting protein	BI754234	2.01	0.76
12173	superoxide dismutase 2, mitochondrial	BG773219	1.99	0.39
11460	Human genomic DNA, chromosome 8q23, clone:KB1747F8.	AP003113	1.99	0.59
14998	cathepsin C	AV717480	1.98	0.38
3338	Human putative tRNA synthetase-like protein mRNA, complete cds.	U07424	1.96	0.60
17654	N-RAP	AAC53323	1.96	0.48
6996	Human cDNA FLJ20299 fis, clone HEP06342, highly similar to AB023137 Human mRNA for KIAA0920 protein.	AK000306	1.96	0.59
837	sperm associated antigen 7	BI858087	1.94	0.21
7808	Human cDNA: FLJ21343 fis, clone COL02679.	AK024996	1.93	0.63
9535	Human cDNA: FLJ23436 fis, clone HRC12692.	AK027089	1.92	0.48
10654	sialyltransferase 8 (alpha-2, 8-polysialytransferase) D	L41680	1.92	0.46
8991	nuclear RNA helicase, DECD variant of DEAD box family	BC010455	1.92	0.34
5572	U2(RNU2) small nuclear RNA auxillary factor 1 (non-standard symbol)	BF968650	1.89	0.21
7534	chloride intracellular channel 1	AA291390	1.88	0.34
7192	putative glialblastoma cell differentiation-related	BE892211	1.88	0.43
1776	Human mRNA for KIAA0615 protein, complete cds.	AB014515	1.88	0.42

16146	Human, chromosome 14 open reading frame 2, clone MGC:8356 IMAGE:2819801, mRNA, complete cds.	BC000429	1.88	0.40
1925	Human, Similar to src homology 3 domain-containing protein HIP-55, clone MGC:15142 IMAGE:4299867, mRNA, complete cds.	BC011677	1.87	0.59
12722	Human receptor protein-tyrosine kinase (TEK) mRNA, complete cds.	L06139	1.86	0.33
14156	Human cDNA FLJ11937 fis, clone HEMBB1000556, weakly similar to Human mRNA for KIAA0750 protein.	AK021999	1.86	0.31
12829	Human mRNA; cDNA DKFZp762G216 (from clone DKFZp762G216).	AL512709	1.86	0.40
14300	Human glutathione S-transferase mRNA, complete cds.	J03746	1.85	0.11
13352	ornithine aminotransferase (gyrate atrophy)	BG577287	1.85	0.72
14750	Human myosin light chain 1 slow a (MLC1sa) mRNA, complete cds.	M31211	1.85	0.76
10470	protein tyrosine kinase 9-like (A6-related protein)	BF220316	1.85	0.17
3700	Human PHD-finger protein (GRC5) mRNA, complete cds.	AF043725	1.85	0.31
11001	Human mRNA for KIAA0820 protein, partial cds.	AB020627	1.85	0.35
2432	cathepsin Z	AI913006	1.84	0.24
14621	Human, splicing factor 3b, subunit 2, 145kD, clone IMAGE:2822659, mRNA, partial cds.	BC000401	1.83	0.32
7159	Human alpha-2,8-polysialyltransferase (PST) gene, complete cds.	L41680	1.83	0.37
6871	Human, eukaryotic translation elongation factor 1 delta (guanine nucleotide exchange protein), clone MGC:2544 IMAGE:2961609, mRNA, complete cds.	BC009907	1.82	0.27
4113	heat shock 27kD protein 2	D89617	1.82	0.36
9709	Human mRNA for smooth muscle myosin.	X69292	1.82	0.31
1571	Human U1-snRNP binding protein homolog mRNA, complete cds.	U44799	1.82	0.42
14237	Human, holocytochrome c synthase (cytochrome c heme-lyase), clone MGC:1443 IMAGE:3030501, mRNA, complete cds.	BC001691	1.81	0.29
7935	Human mRNA for Mn superoxide dismutase (EC 1.15.1.1.).	Y00472	1.81	0.34
10166	tubulin, alpha 1 (testis specific)	BE742772	1.81	0.27
2924	translocase of inner mitochondrial membrane 17 (yeast) homolog A	BG506029	1.81	0.43
9097	peanut (Drosophila)-like 2	AI632238	1.80	0.37
6849	Human, DR1-associated protein 1 (negative cofactor 2 alpha), clone MGC:19653 IMAGE:3029273, mRNA, complete cds.	BC010025	1.80	0.19
9138	ESTs, Highly similar to ITF2_HUMAN TRANSCRIPTION FACTOR 4 [H.sapiens]	AA936434	1.80	0.68
16774	Ras association (RalGDS/AF-6) domain family 1	AL543484	1.80	0.24
6302	Human, Similar to threonyl-tRNA synthetase, clone MGC:3031 IMAGE:3163506, mRNA, complete cds.	BC000541	1.79	0.20

9546	Human cDNA: FLJ21971 fis, clone HEP05790.	AK025624	1.79	0.25
201	Human replication factor C, 40-kDa subunit (A1) mRNA, complete cds.	M87338	1.79	0.15
16115	Human brain my036 protein mRNA, complete cds.	AF063594	1.78	0.25
4466	small nuclear ribonucleoprotein polypeptides B and B1	BE535667	1.78	0.38
15877	Human MAP1 light chain 3-like protein 1 mRNA, complete cds.	AF276658	1.77	0.19
4073	ribose 5-phosphate isomerase A (ribose 5-phosphate epimerase)	BG571262	1.77	0.38
10514	solute carrier family 7 (cationic amino acid transporter, y+ system), member 2	U76368	1.76	0.50
4889	Human iroquois homeobox protein 4 (IRX4) mRNA, complete cds.	AF124733	1.76	0.12
9010	keratin 15	AU122673	1.76	0.37
15241	class I cytokine receptor	AF265242	1.75	0.41
6891	Human mRNA; cDNA DKFZp434I0812 (from clone DKFZp434I0812); partial cds.	AL137751	1.75	0.24
16907	ribophorin I	BE780549	1.74	0.10
1601	Human zinc finger protein ZNF224 mRNA, complete cds.	AF187990	1.74	0.38
3624	Human mitochondrial glutathione reductase (GRD1) mRNA, complete cds; nuclear gene for mitochondrial product.	AF228704	1.74	0.37
4078	isocitrate dehydrogenase 3 (NAD+) beta	BI553471	1.74	0.55
13667	ribosomal protein L3	AV756387	1.73	0.36
6035	growth arrest-specific 1	BE619835	1.73	0.19
2345	fusion, derived from t(12;16) malignant liposarcoma	AL549027	1.73	0.22
5374	Human zinc finger protein (ZNF154) mRNA, partial cds.	U20648	1.72	0.53
6534	Human cDNA FLJ11773 fis, clone HEMBA1005852.	AK021835	1.72	0.20
6603	Human, KIAA1049 protein, clone MGC:19865 IMAGE:3678670, mRNA, complete cds.	BC011884	1.72	0.39
3414	Human vascular endothelial cell growth factor 165 receptor/neuropilin (VEGF165) mRNA, complete cds.	AF016050	1.72	0.18
420	Human mRNA for rap2b gene.	X52987	1.72	0.32
14854	KIAA0172 protein	D79994	1.72	0.33
11262	Human EF-1delta gene encoding Human elongation factor-1-delta.	Z21507	1.71	0.13
3150	Human ARF GTPase-activating protein GIT1 mRNA, complete cds.	AF124490	1.71	0.11
17484	Human mRNA for RNA polymerase II associated protein RAP74.	X64037	1.71	0.17
4447	nucleolar and coiled-body phosphprotein 1	AL553791	1.70	0.25
10493	cyclin D1 (PRAD1: parathyroid adenomatosis 1)	X59798	1.70	0.12
1135	hyaluronoglucosaminidase 2	AU137033	1.70	0.52
6728	Human mRNA for KIAA0049 gene, complete cds.	D30756	1.70	0.54
18026	Human, clone MGC:2491 IMAGE:3353174, mRNA, complete cds.	BC000262	1.70	0.25

6002	delta sleep inducing peptide, immunoreactor	AL525317	1.70	0.42
6046	biliverdin reductase A	AI765830	1.69	0.18
10188	Human genomic DNA of 8p21.3-p22 anti-oncogene of hepatocellular colorectal and non-small cell lung cancer , segment 6/11.	AB020863	1.69	0.38
16652	coronin, actin-binding protein, 1A	BG758313	1.69	0.42
2858	cyclin-dependent kinase 9 (CDC2-related kinase)	BM009991	1.68	0.41
9410	Human HOK-2 mRNA for zinc finger protein.	X82125	1.68	0.29
2227	cytoplasmic antiprotease=38 kda intracellular serine protease inhibitor [Human, placenta, mRNA, 1465 nt].	S69272	1.67	0.54
393	Human cation-chloride cotransporter-interacting protein mRNA, complete cds.	AF284422	1.67	0.21
10365	UDP-glucose pyrophosphorylase 2	AL533518	1.67	0.08
6751	Human 90 kD heat shock protein gene, complete cds.	J04988	1.66	0.36
16597	serum response factor (c-fos serum response element-binding transcription factor)	BG744841	1.66	0.19
16805	disabled (Drosophila) homolog 2 (mitogen-responsive phosphoprotein)	U39050	1.66	0.45
16940	transformer-2 alpha (htra-2 alpha)	BG250879	1.66	0.22
54	Human (clone pAT 464) potential lymphokine/cytokine mRNA, complete cds.	M25315	1.65	0.54
9383	Human apoptosis-associated nuclear protein PHLDA1 (PHLDA1) mRNA, partial cds.	AF220656	1.65	0.24
10512	zinc finger protein 173	U09825	1.65	0.17
13191	Human, Similar to ribophorin I, clone MGC:5072 IMAGE:3461167, mRNA, complete cds.	BC010839	1.65	0.13
17630	Human, aldo-keto reductase family 1, member B1 (aldose reductase), clone MGC:1804 IMAGE:3357652, mRNA, complete cds.	BC000260	1.65	0.19
12591	Human mitochondrial outer membrane protein (TOM40) mRNA, nuclear gene encoding mitochondrial protein, complete cds.	AF043250	1.65	0.16
10383	ribosomal protein S14	BG169146	1.65	0.08
15308	Bcl-2 binding component 3	BG258126	1.64	0.18
422	Human cDNA FLJ14781 fis, clone NT2RP4000455, weakly similar to TRANS-ACTING TRANSCRIPTIONAL PROTEIN ICP0.	AK027687	1.64	0.29
12566	Human mRNA for KIAA1209 protein, partial cds.	AB033035	1.63	0.25
17690	Human, LIM domain only 4, clone MGC:872 IMAGE:3355972, mRNA, complete cds.	BC003600	1.63	0.39
13290	nucleolin	AV724878	1.63	0.23
6566	Human mRNA; cDNA DKFZp434K0220 (from clone DKFZp434K0220); complete cds.	AL136801	1.62	0.26
5697	v-maf musculoaponeurotic fibrosarcoma (avian) oncogene homolog	AF055376	1.62	0.17
16565	major histocompatibility complex, class II, DQ beta 1	U83582	1.62	0.14
16491	eukaryotic translation initiation factor 3, subunit 5 (epsilon, 47kD)	BG258493	1.62	0.18

5748	GCN1 (general control of amino-acid synthesis 1, yeast)-like 1	BI259893	1.62	0.41
15763	Human mRNA for integrin beta(4)subunit.	X51841	1.62	0.30
911	Human cDNA FLJ12993 fis, clone NT2RP3000197.	AK023055	1.61	0.31
3139	Human beta-tubulin (TUB4q) mRNA, complete cds.	U83110	1.61	0.29
10945	Human, putative glialblastoma cell differentiation-related, clone MGC:2352 IMAGE:3535682, mRNA, complete cds.	BC004967	1.61	0.41
16612	adaptor-related protein complex 4, mu 1 subunit	AW170559	1.61	0.37
14925	KIAA0225 protein	D86978	1.61	0.16
9853	Human claudin 3 (CLDN3) gene, complete cds.	AF007189	1.61	0.34
14254	Human TESTIN 2 and TESTIN 3 genes, complete cds, alternatively spliced.	AF260225	1.61	0.31
6635	Human Na K-ATPase beta-3 subunit (atp1b3) gene, exon 7 and complete cds.	AF005896	1.61	0.19
11130	Human transcription factor (CBFB) mRNA, 3' end.	L20298	1.61	0.32
9443	Human TUBB1 gene for Human beta tubulin 1, class VI.	AJ292757	1.61	0.33
17830	Human mRNA for KIAA1308 protein, partial cds.	AB037729	1.61	0.23
3223	Human chloride channel ABP mRNA, complete cds.	AF034607	1.61	0.08
15232	death-associated protein 6	AL549502	1.61	0.24
2758	transaldolase 1	BE538166	1.61	0.18
7086	BTG family, member 2	BG750101	1.61	0.48
12654	Human, clone IMAGE:2989556, mRNA, partial cds.	BC001699	1.60	0.25
872	angio-associated, migratory cell protein	BI091422	1.60	0.23
18175	LIM domain only 4	U24576	1.60	0.37
16714	adenylosuccinate lyase	AL022238	1.59	0.30
8672	radixin	BF194976	1.59	0.15
2540	melanoma-associated antigen recognised by cytotoxic T lymphocytes	BC000507	1.58	0.35
17249	Human poly(ADP-ribose) polymerase mRNA, complete cds.	M32721	1.57	0.16
6267	Human connexin45 gene, complete cds.	U03493	1.57	0.11
2385	STIP1 homology and U-Box containing protein 1	AL560352	1.57	0.39
4006	LIM domain kinase 1	D26309	1.57	0.37
13216	Human mRNA for KIAA1296 protein, partial cds.	AB037717	1.57	0.13
7121	aldehyde dehydrogenase 3 family, member B1	U10868	1.56	0.34
5733	Homo sapiens clone 23763 unknown mRNA, partial cds	BG743005	1.56	0.18
6319	Human, putative receptor protein, clone MGC:12310 IMAGE:4051155, mRNA, complete cds.	BC005268	1.56	0.10
5707	zinc finger protein 22 (KOX 15)	AL528233	1.56	0.27

740	Human cytosolic inhibitor of NRF2 (INRF2) mRNA, complete cds.	AF361886	1.56	0.12
7532	slit (Drosophila) homolog 3	BF061381	1.56	0.23
3648	Human gene for prostacyclin synthase, exon 10 and complete cds.	D83402	1.55	0.35
6470	Human, ATPase, H+ transporting, lysosomal (vacuolar proton pump) 21kD, clone MGC:4498 IMAGE:2964510, mRNA, complete cds.	BC005876	1.55	0.32
4913	Human complement-c1q tumor necrosis factor-related protein (CTRP6) mRNA, complete cds.	AF329842	1.55	0.26
211	Human genomic DNA, chromosome 22q11.2, BCRL2 region, clone:KB1440D3.	AP000553	1.55	0.38
4229	cyclin-dependent kinase inhibitor 1C (p57, Kip2)	BF055303	1.55	0.34
916	Human unknown mRNA.	AF058918	1.55	0.37
5196	Human mRNA for neurite outgrowth-promoting protein.	X55110	1.54	0.14
7937	Human SBBI26 mRNA, complete cds.	AF111113	1.54	0.26
523	Human, clone MGC:3977 IMAGE:2821990, mRNA, complete cds.	BC003000	1.54	0.34
14382	Human mRNA for KIAA0059 gene, complete cds.	D31883	1.53	0.20
3704	Human, heterogeneous nuclear ribonucleoprotein H1 (H), clone MGC:8619 IMAGE:2961378, mRNA, complete cds.	BC001348	1.53	0.19
3382	Human cDNA FLJ12566 fis, clone NT2RM4000852.	AK022628	1.53	0.27
5965	peroxisomal long-chain acyl-coA thioesterase	AA825544	1.53	0.25
5743	structure specific recognition protein 1	M86737	1.53	0.12
901	H3 histone, family 3B (H3.3B)	BG338936	1.53	0.24
16276	Human leukemia virus receptor 2 (GLVR2) mRNA, complete cds.	L20852	1.53	0.28
17865	Human, farnesyl diphosphate synthase (farnesyl pyrophosphate synthetase, dimethylallyltranstransferase, geranyltranstransferase), clone MGC:15352 IMAGE:4132071, mRNA, complete cds.	BC010004	1.53	0.04
9112	Friend leukemia virus integration 1	X67001	1.52	0.32
6270	Human blood plasma glutamate carboxypeptidase precursor (PGCP) mRNA, complete cds.	AF119386	1.52	0.12
6532	Human cDNA: FLJ22405 fis, clone HRC08294.	AK026058	1.52	0.21
16604	S-adenosylhomocysteine hydrolase	BG258011	1.52	0.23
7294	signal sequence receptor, beta (translocon-associated protein beta)	BE887942	1.52	0.33
4414	gp25L2 protein	BI822721	1.52	0.11
8783	Homo sapiens SRp46 splicing factor transcribed retropseudogene	AF031165	1.51	0.12
13786	protease, serine, 15	BC000235	1.51	0.30
2371	hypothetical protein F23149_1	BE562607	1.51	0.17
586	Human platelet-derived growth factor A chain (PDGFA) gene, exons only.	M83575	1.51	0.13

6874	Human, Similar to hyaluronoglucosaminidase 2, clone MGC:1922 IMAGE:3347760, mRNA, complete cds.	BC000692	1.51	0.18
810	carcinoembryonic antigen-related cell adhesion molecule 5	AW951446	1.50	0.19
16034	Human, tubulin, beta 5, clone MGC:15683 IMAGE:3350604, mRNA, complete cds.	BC007605	1.50	0.22
12638	Human macrophage-specific colony-stimulating factor (CSF-1) mRNA, complete cds.	M37435	1.50	0.38
4927	Human, Similar to RIKEN cDNA 1500041N16 gene, clone MGC:4238 IMAGE:2961616, mRNA, complete cds.	BC005870	1.50	0.19
7302	bridging integrator 1	BF529230	1.50	0.17
1590	Human high mobility group box (SSRP1) mRNA, complete cds.	M86737	1.50	0.24
7974	Human mRNA for KIAA0664 protein, partial cds.	AB014564	1.50	0.32
12042	TGFB-induced factor (TALE family homeobox)	AL549846	1.50	0.17
4403	N-methylpurine-DNA glycosylase	AL530962	1.49	0.31
10655	activated p21cdc42Hs kinase	BG742978	1.49	0.26
6050	v-Ki-ras2 Kirsten rat sarcoma 2 viral oncogene homolog	AI740449	1.49	0.28
5802	dihydropyrimidinase-like 3	AU133750	1.49	0.22
13067	Human, profilin 1, clone MGC:5227 IMAGE:2900010, mRNA, complete cds.	BC006768	1.48	0.17
4075	guanylate kinase 1	T36282	1.48	0.31
5052	Human gene for ribosomal protein S2, partial cds.	AB007147	1.48	0.15
4344	adenosine monophosphate deaminase 2 (isoform L)	BF894450	1.47	0.30
12126	RNA binding motif protein 10	BI115686	1.47	0.19
2101	Human mRNA for TIP49, complete cds.	AB012122	1.47	0.17
9888	Human M4 protein deletion mutant mRNA, complete cds.	AF061832	1.47	0.22
4783	Human mRNA for FLJ00083 protein, partial cds.	AK024484	1.47	0.20
12530	Human, hydroxymethylbilane synthase, clone MGC:8561 IMAGE:2822949, mRNA, complete cds.	BC000520	1.47	0.26
571	Human integrin alpha 10 subunit (ITGA10) mRNA, complete cds.	AF112345	1.46	0.19
351	Human mRNA for DNA replication licensing factor (huMCM5), complete cds.	D83986	1.46	0.26
9155	bleomycin hydrolase	AA044158	1.46	0.10
1576	Human, F-box only protein 7, clone MGC:16046 IMAGE:3611049, mRNA, complete cds.	BC008361	1.46	0.21
6332	Human clone CDABP0155 mRNA sequence.	AY007163	1.46	0.31
8743	Kelch-like ECH-associated protein 1	BC002417	1.46	0.11
13348	non-POU-domain-containing, octamer-binding	BI254716	1.46	0.20
6973	Human mRNA for putative ATPase, partial.	AJ006268	1.45	0.27
4786	Human sorting nexin 8 (SNX8) mRNA, complete cds.	AF121858	1.45	0.33

7050	ribosomal protein S6 kinase, 90kD, polypeptide 1	BG878337	1.45	0.18
13633	proteasome (prosome, macropain) activator subunit 1 (PA28 alpha)	BE879690	1.45	0.19
4858	epithelial protein lost in neoplasm alpha	AAF23756	1.45	0.11
4253	KIAA0670 protein/acinus	AF124727	1.45	0.20
6742	Human CTP:phosphocholine cytidyltransferase mRNA, complete cds.	L28957	1.45	0.27
8359	Human mRNA; cDNA DKFZp564K2478 (from clone DKFZp564K2478); complete cds.	AL136690	1.45	0.29
8229	Human cDNA FLJ13300 fis, clone OVARC1001342, highly similar to 40S RIBOSOMAL PROTEIN S8.	AK023362	1.44	0.14
10684	KIAA0601 protein	AB011173	1.44	0.32
2571	mitogen-activated protein kinase 11	AI394426	1.44	0.21
16936	clones 23667 and 23775 zinc finger protein	BG498371	1.44	0.27
16095	Human clone ID 193225 NAD (H)-specific isocitrate dehydrogenase gamma subunit mRNA, alternatively spliced, partial cds.	U69268	1.44	0.24
17202	Human, interleukin enhancer binding factor 2, 45kD, clone MGC:8391 IMAGE:2820505, mRNA, complete cds.	BC000382	1.44	0.12
14249	Human cysteine protease CPP32 isoform alpha mRNA, complete cds.	U13737	1.43	0.22
4307	cytochrome c oxidase subunit IV	BF726186	1.43	0.12
7279	mesoderm development candidate 2	BC012746	1.43	0.13
7355	putative breast adenocarcinoma marker (32kD)	BC002502	1.43	0.17
8772	MYC-associated zinc finger protein (purine-binding transcription factor)	BG260604	1.43	0.13
8920	splicing factor, arginine/serine-rich 4	BF855449	1.43	0.23
1642	Human ornithine aminotransferase (OAT) gene, exon 6 and partial cds.	M88760	1.42	0.10
9778	Human RET ligand 2 (RETL2) mRNA, complete cds.	U97145	1.42	0.06
5977	D123 gene product	BE792735	1.42	0.24
13519	replication factor C (activator 1) 2 (40kD)	BE295474	1.42	0.29
13587	hypothetical protein	AW006162	1.42	0.20
2731	glucosaminyl (N-acetyl) transferase 1, core 2 (beta-1,6-N-acetylglucosaminyltransferase)	AL555400	1.42	0.14
18019	activating transcription factor 3	BI834286	1.42	0.21
5384	Human, ornithine aminotransferase (gyrate atrophy), clone MGC:5182 IMAGE:3449883, mRNA, complete cds.	BC000964	1.42	0.18
3229	Human CpG island DNA genomic Mse1 fragment, clone 71f4, forward read cpg71f4.ft1a.	Z55905	1.41	0.28
15631	Human thioredoxin mRNA, nuclear gene encoding mitochondrial protein, complete cds.	U78678	1.41	0.18
16737	methylthioadenosine phosphorylase	AL048242	1.41	0.15
2271	Human alphaCP-4 (PCBP4) mRNA, complete cds.	AF176330	1.41	0.15
17633	Human histidine-rich calcium binding protein (HRC) mRNA, complete cds.	M60052	1.41	0.07

6569	Human full length insert cDNA clone ZD48C09.	AF086289	1.41	0.17
16575	six transmembrane epithelial antigen of the prostate	AC004969	1.40	0.25
5387	Human, Similar to RIKEN cDNA 9430029K10 gene, clone IMAGE:3534558, mRNA, partial cds.	BC007644	1.40	0.16
16180	Human cDNA FLJ20845 fis, clone ADKA01901.	AK000852	1.40	0.23
8688	cytoplasmic FMRP interacting protein 1	BI522540	1.40	0.23
3697	Human clone 23600 cytochrome c oxidase subunit IV mRNA, complete cds.	U90915	1.39	0.10
11129	Human lysosomal membrane glycoprotein CD63 mRNA.	M58485	1.39	0.26
1965	cellular repressor of E1A-stimulated genes	AAH08628	1.39	0.18
6538	Human guanine nucleotide exchange factor mss4 mRNA, complete cds.	U74324	1.39	0.21
6846	Human CST gene for cerebroside sulfotransferase, exon 1, 2, 3, 4, 5.	AB029900	1.39	0.08
7469	IMP (inosine monophosphate) dehydrogenase 2	BI223795	1.39	0.17
6909	Human, hydroxyacyl-Coenzyme A dehydrogenase/3-ketoacyl-Coenzyme A thiolase/enoyl-Coenzyme A hydratase (trifunctional protein), alpha subunit, clone MGC:1728 IMAGE:2966432, mRNA, complete cds.	BC009235	1.38	0.22
6415	Human mRNA for KIAA0842 protein, partial cds.	AB020649	1.38	0.17
16616	nucleolar and coiled-body phosphprotein 1	Z34289	1.38	0.12
12072	PHD finger protein 1	BF342325	1.38	0.11
5405	Human gene encoding retina-specific guanylyl cyclase.	AJ222657	1.38	0.23
5667	H1 histone family, member 2	AW316807	1.38	0.25
16727	zinc finger protein 184 (Kruppel-like)	N80080	1.38	0.15
10505	ubiquitin-protein ligase NEDD4-like	BE391083	1.37	0.20
5351	Human, NADH dehydrogenase (ubiquinone) 1 alpha subcomplex, 10 (42kD), clone MGC:5103 IMAGE:3451514, mRNA, complete cds.	BC003417	1.37	0.20
13515	HLA-G histocompatibility antigen, class I, G	AF071019	1.37	0.17
3681	Human, clone MGC:2663 IMAGE:3543910, mRNA, complete cds.	BC001791	1.37	0.15
5061	Human mRNA for GCP170, complete cds.	D63997	1.37	0.20
6037	guanine nucleotide binding protein-like 1	BE798151	1.37	0.07
31	Human Golgi membrane sialoglycoprotein MG160 (GLG1) mRNA, complete cds.	U64791	1.37	0.08
62	Human SM22 alpha gene, 5' flanking region.	D84344	1.37	0.19
4014	chromosome 19 open reading frame 3	AW409924	1.36	0.20
12875	Human NJAC protein (NJAC) mRNA, complete cds.	AF144103	1.36	0.26
2295	Human copper chaperone for superoxide dismutase (CCS) mRNA, complete cds.	AF002210	1.36	0.20

15624	Human, procollagen-proline, 2-oxoglutarate 4-dioxygenase (proline 4-hydroxylase), beta polypeptide (protein disulfide isomerase; thyroid hormone binding protein p55), clone MGC:9192 IMAGE:3879411, mRNA, complete cds.	BC010859	1.36	0.15
9077	splicing factor, arginine/serine-rich (transformer 2 Drosophila homolog) 10	BC000160	1.36	0.15
8615	Human cDNA FLJ14084 fis, clone HEMBB1002383.	AK024146	1.36	0.22
4739	Human cDNA FLJ10162 fis, clone HEMBA1003560, highly similar to GUANINE NUCLEOTIDE-BINDING PROTEIN G(I)/G(S)/G(O) GAMMA-2 SUBUNIT.	AK001024	1.36	0.18
8972	APEX nuclease (multifunctional DNA repair enzyme)	AI207650	1.36	0.13
4754	Human cDNA FLJ14493 fis, clone MAMMA1002972.	AK027399	1.36	0.16
1963	Human mRNA for Cdc42-interacting protein 4 (CIP4).	AJ000414	1.35	0.20
14562	Human pcnp mRNA for PEST-containing nuclear protein, complete cds.	AB037675	1.35	0.20
10685	neural precursor cell expressed, developmentally down-regulated 8	AW960243	1.35	0.10
7195	CGI-01 protein	AK027886	1.35	0.23
4692	Human cDNA FLJ12255 fis, clone MAMMA1001476, highly similar to URIDINE KINASE (EC 2.7.1.48).	AK022317	1.35	0.20
10170	ring finger protein 1	AL576514	1.35	0.15
13295	Human beta-myosin heavy chain (MYH7) mRNA, complete cds.	M58018	1.35	0.18
15982	Human keratin type II (58 kD) mRNA, complete cds.	M21389	1.35	0.09
4179	SRY (sex determining region Y)-box 9 (campomelic dysplasia, autosomal sex-reversal)	BC007951	1.34	0.16
2447	eukaryotic translation initiation factor 3, subunit 8 (110kD)	AL529959	1.34	0.17
3662	zinc finger protein	AAC60294	1.34	0.14
6327	Human mRNA for Ig kappa light chain, anti-RhD, therad 7.	AJ010442	1.34	0.17
7871	Human bone morphogenetic protein 2A (BMP-2A) mRNA.	M22489	1.34	0.20
14611	Human kruppel-like zinc finger protein (ZNF300) mRNA, complete cds.	AF395541	1.34	0.16
2925	ATPase, H+ transporting, lysosomal (vacuolar proton pump) 21kD	BG108730	1.33	0.19
10332	Homo sapiens GT212 mRNA	L38935	1.33	0.14
3201	Human mRNA for KIAA0671 protein, complete cds.	AB014571	1.33	0.12
807	protein phosphatase 4, regulatory subunit 1	AW865929	1.33	0.18
6042	siah binding protein 1; FBP interacting repressor; pyrimidine tract binding splicing factor; Ro ribonucleoprotein-binding protein 1	AW245149	1.33	0.20
206	Human mRNA for KIAA1290 protein, partial cds.	AB033116	1.33	0.23

18317	ESTs, Highly similar to DDP_HUMAN X-LINKED DEAFNESS DYSTONIA PROTEIN [H.sapiens]	BG612847	1.33	0.19
7281	non-histone chromosome protein 2 (S. cerevisiae)-like 1	BE748666	1.32	0.08
4090	tubby like protein 1	AI344222	1.32	0.14
11291	Human set gene, complete cds.	M93651	1.32	0.06
11939	acetyl-Coenzyme A acetyltransferase 1 (acetoacetyl Coenzyme A thiolase)	BG740338	1.32	0.11
6472	Human, thioredoxin-like, clone MGC:12349 IMAGE:3686411, mRNA, complete cds.	BC005289	1.32	0.20
7976	Human SH2-containing protein Nsp3 mRNA, complete cds.	AF124251	1.32	0.13
3507	Human, replication factor C (activator 1) 5 (36.5kD), clone MGC:1155 IMAGE:3544137, mRNA, complete cds.	BC001866	1.31	0.10
6807	Human CpG island DNA genomic Mse1 fragment, clone 186c1, reverse read cpg186c1.rt1b.	Z55026	1.31	0.13
11012	Human plectin (PLEC1) mRNA, complete cds.	U53204	1.31	0.11
7507	apolipoprotein B mRNA editing enzyme, catalytic polypeptide 1	AI380263	1.31	0.28
3161	Human serum amyloid A protein mRNA, complete cds.	M81349	1.30	0.19
4156	sulfotransferase family, cytosolic, 1A, phenol-preferring, member 3	BE745439	1.30	0.09
1668	Human, MpV17 transgene, murine homolog, glomerulosclerosis, clone MGC:1703 IMAGE:2967261, mRNA, complete cds.	BC001115	1.30	0.21
2103	Human cysteine sulfinic acid decarboxylase-related protein 1 (CSAD) mRNA, complete cds.	AF116545	1.30	0.12
16028	Human, peroxiredoxin 1, clone MGC:12514 IMAGE:3961375, mRNA, complete cds.	BC007063	1.30	0.10
12074	zinc finger protein 239	BF972810	1.30	0.20
4724	Human mRNA; cDNA DKFZp434F054 (from clone DKFZp434F054); complete cds.	AL136863	1.30	0.08
6019	cysteine-rich protein 1 (intestinal)	BI222747	1.29	0.19
7051	mitochondrial ribosomal protein S27	BG746580	1.29	0.14
3230	Human mRNA for transcription factor.	AJ012463	1.28	0.18
3291	Human DAZ associated protein 1 (DAZAP1) mRNA, complete cds.	AF181719	1.28	0.06
3374	Human dematin (HRD1) mRNA, complete cds.	L19713	1.28	0.05
10079	Human, clone IMAGE:3352566, mRNA, partial cds.	BC000113	1.28	0.13
13758	acetyl-Coenzyme A acyltransferase 1 (peroxisomal 3-oxoacyl-Coenzyme A thiolase)	BC011977	1.27	0.16
6666	Human cDNA FLJ14937 fis, clone PLACE1010231, weakly similar to CELL SURFACE GLYCOPROTEIN EMR1 PRECURSOR.	AK027843	1.27	0.09
14436	Human translation initiation factor eIF-2 gamma subunit mRNA, complete cds.	L19161	1.27	0.15
3933	asparagine synthetase	BC014621	1.27	0.10

3860	Human, N-acetylneuraminic acid phosphate synthase; sialic acid synthase, clone MGC:934 IMAGE:3505324, mRNA, complete cds.	BC000008	1.27	0.06
6812	Human mRNA for KIAA1798 protein, partial cds.	AB058701	1.26	0.14
15326	vesicle-associated membrane protein 8 (endobrevin)	AV716151	1.26	0.10
3541	Human sodium channel beta-1 subunit (SCN1B) mRNA, complete cds.	L10338	1.26	0.09
15966	BcDNA:GH03108 gene product	AAF47301	1.26	0.08
356	Human HT025 mRNA, complete cds.	AF245436	1.26	0.14
6813	Human cDNA: FLJ22923 fis, clone KAT06970, highly similar to HSP6973 Human mRNA for TOM1 protein.	AK026576	1.26	0.12
1671	Human helicase-like protein (HLP) mRNA, complete cds.	U09877	1.26	0.16
10201	chaperonin containing TCP1, subunit 6B (zeta 2)	D78333	1.25	0.11
3146	Human, cysteine-rich protein 1 (intestinal), clone MGC:3888 IMAGE:3631097, mRNA, complete cds.	BC002738	1.25	0.16
3657	Human mRNA; cDNA DKFZp434B1272 (from clone DKFZp434B1272); partial cds.	AL162032	1.25	0.12
18299	hypothetical protein MGC3101	BF196967	1.25	0.10
7844	Human transcription factor IL-4 Stat mRNA, complete cds.	U16031	1.25	0.10
6522	Human creatine transporter mRNA, complete cds.	L31409	1.25	0.14
1947	Human udulin 2 mRNA, 3' end.	M64109	1.24	0.15
4464	protocadherin 17	NM_014459	1.24	0.11
2379	ribonuclease HI, large subunit	BE045964	1.24	0.13
10660	B-cell translocation gene 1, anti-proliferative	AA807633	1.24	0.14
10088	Human testis-specific PGK-2 gene for phosphoglycerate kinase (ATP:3-phospho-D-glycerate 1-phosphotransferase, EC 2.7.2.3).	X05246	1.23	0.09
1972	Human mRNA for KIAA0575 protein, complete cds.	AB011147	1.22	0.16
4441	KIAA0998 protein	AV687594	1.20	0.10
596	Human antigen CD9 gene, exon 4.	L08121	1.20	0.16
6480	Human, Similar to RIKEN cDNA 2610100E10 gene, clone MGC:2404 IMAGE:2821736, mRNA, complete cds.	BC006505	1.20	0.11
5833	SELENOPHOSPHATE SYNTHETASE ; Human selenium donor protein	BG574707	1.20	0.03
1120	NADH dehydrogenase (ubiquinone) Fe-S protein 8 (23kD) (NADH-coenzyme Q reductase)	NM_002496	1.19	0.14
7518	ribosomal protein S4, Y-linked	M58459	1.19	0.11
16138	Human, Similar to katanin p60 (ATPase-containing) subunit A 1, clone MGC:2599 IMAGE:3347282, mRNA, complete cds.	BC000612	1.19	0.12
7237	ATP-binding cassette, sub-family B (MDR/TAP), member 4	X06181	1.17	0.09
12836	Human putative transcription factor (WBSCR12) mRNA, complete cds.	AF156489	1.16	0.11

8328	Human cDNA: FLJ22528 fis, clone HRC12825.	AK026181	1.15	0.07
7132	activator of S phase kinase	AI289307	1.14	0.04
2046	Human insulin-like growth factor binding protein-4 (IGFBP4) gene, promoter and complete cds.	U20982	1.09	0.05

Genes Significantly (P<0.005) Abundant In PAEC
In comparison to PAVEC in shear
Group 4

Agilent Feature #	Gene Name/Description	Count 511		
		Gene ID	Fold AVE	Fold STD
18199	slit (Drosophila) homolog 2	AW263423	9.43	1.39
1676	Human aldehyde dehydrogenase 6 mRNA, complete cds.	U07919	8.85	1.85
15264	ESTs, Highly similar to AF078844 1 hqp0376 protein [H.sapiens]	BG165945	7.42	2.07
16812	metallothionein 1X	BF130769	7.24	2.11
14302	Human factor I (C3b/C4b inactivator) mRNA, complete cds.	J02770	6.60	1.60
5731	ankyrin-like with transmembrane domains 1	NM_007332	6.22	1.77
504	Human metallothionein-I-A gene, complete coding sequence.	K01383	5.97	1.17
11089	Human mRNA for Slit-2 protein, complete cds.	AB017168	5.77	1.38
8985	somatostatin	BI713774	5.20	1.30
18197	metallothionein 1E (functional)	H72532	4.88	1.25
18437	protease, serine, 12 (neurotrypsin, motopsin)	AJ001531	4.72	1.05
9935	Human cDNA FLJ20129 fis, clone COL06190.	AK000136	4.54	0.40
9768	Translation may initiate at the ATG codon at nucleotides 40-42 or the ATG at nucleotides 43-45	CAC32434	4.42	1.25
9369	Human GABAA receptor subunit alpha4 mRNA, complete cds.	U30461	4.33	0.94
18292	cerebellar degeneration-related protein (34kD)	M16965	4.28	1.06
6907	Human, cathepsin S, clone MGC:3886 IMAGE:3610589, mRNA, complete cds.	BC002642	4.26	1.11
6648	Human metallothionein (MT)I-F gene, complete cds.	M13003	4.19	0.56
11616	Human mRNA for phospholipase C, complete cds.	D42108	4.02	0.65
18467	gap junction protein, alpha 1, 43kD (connexin 43)	X52947	3.84	0.47
1214	neuro-oncological ventral antigen 1	NM_006489	3.70	0.51
17723	Human onconeural ventral antigen-1 (Nova-1) mRNA, complete cds.	U04840	3.49	0.84
4864	Human transmembrane protein Jagged mRNA, partial cds.	U77720	3.40	0.52
6749	Human mRNA full length insert cDNA clone EUROIMAGE 345330.	AL079274	3.25	1.20
3456	Human CD39L3 (CD39L3) mRNA, complete cds.	AF039917	3.22	1.37
12929	Human mRNA for neurotrypsin.	AJ001531	3.03	0.70
8774	mannosidase, alpha, class 1A, member 1	AU119410	2.97	0.60
13807	GTP-binding protein overexpressed in skeletal muscle	AW297828	2.96	0.29
18492	PTH-responsive osteosarcoma B1 protein	AA002033	2.92	0.28
5561	aldehyde dehydrogenase 1 family, member A1	AV649527	2.92	1.36

14142	Human cerebellar-degeneration-related antigen (CDR34) gene, complete cds.	M31423	2.87	1.11
1201	mannosidase, alpha, class 1A, member 1	NM_005907	2.83	1.14
3902	Human mRNA for GRIP1 protein.	AJ133439	2.82	0.67
2397	matrix Gla protein	AW999947	2.82	0.55
10091	Human leukemogenic homolog protein (MEIS1) mRNA, complete cds.	U85707	2.82	0.67
16607	downregulated in ovarian cancer 1	U53445	2.80	0.28
13852	acid sphingomyelinase-like phosphodiesterase	Y08136	2.75	0.42
12071	procollagen-lysine, 2-oxoglutarate 5-dioxygenase (lysine hydroxylase) 2	U84573	2.74	1.28
10571	Rho GTPase activating protein 5	U17032	2.69	0.61
5696	fibroblast growth factor 13	NM_033642	2.69	0.54
5786	Ewing sarcoma breakpoint region 1	BI871381	2.68	0.53
9932	Human caveolin 1 (CAV1) gene, exon 3 and partial cds.	AF125348	2.63	0.39
10982	Human mRNA for NOTCH4, partial cds.	D63395	2.61	0.30
7555	phosphodiesterase 3B, cGMP-inhibited	BI756567	2.61	0.42
8825	caveolin 1, caveolae protein, 22kD	NM_001753	2.58	0.36
3508	Human, matrix Gla protein, clone MGC:12316 IMAGE:3930143, mRNA, complete cds.	BC005272	2.54	0.34
14123	Human TALE homeobox protein Meis2b mRNA, complete cds.	AF179896	2.42	0.33
17217	MAM domain protein	AAC59868	2.41	1.08
5503	RAS p21 protein activator (GTPase activating protein) 1	NM_022650	2.39	0.23
10569	growth arrest and DNA-damage-inducible, alpha	AI814872	2.39	0.12
13676	glutaminase	BI764185	2.39	0.22
11439	Human uveal autoantigen mRNA, complete cds.	AF322916	2.38	0.43
16905	KIAA0368 protein	AB002366	2.37	0.31
1069	UDP-glucose ceramide glucosyltransferase	AI609116	2.35	0.64
897	tissue factor pathway inhibitor 2	BG621010	2.35	0.69
16721	interleukin 9 receptor	NM_002186	2.33	0.32
4346	caspase 5, apoptosis-related cysteine protease	NM_004347	2.32	1.00
12259	bone morphogenetic protein 4	NM_001202	2.30	0.83
13444	homeo box A7	NM_006896	2.30	0.81
14079	Human cDNA FLJ14357 fis, clone HEMBA1000005, highly similar to DNAJ PROTEIN HOMOLOG MTJ1.	AK027263	2.28	0.56
9416	Human cDNA FLJ10500 fis, clone NT2RP2000369.	AK001362	2.26	0.30
13583	vinculin	NM_014000	2.26	0.68
11598	Human mRNA for KIAA0212 gene, complete cds.	D86967	2.25	0.27
11655	dJ12G14.2 (novel protein similar to predicted chicken protein)	CAB88112	2.24	0.43

4753	Human, angiotensinogen (serine (or cysteine) protease inhibitor, clade A (alpha-1 antiprotease, antitrypsin), member 8), clone MGC:17092 IMAGE:4213559, mRNA, complete cds.	BC011519	2.23	0.30
4827	Human mRNA for KIAA0369 gene, complete cds.	AB002367	2.21	0.57
3763	Human G-protein-coupled receptor 48 (GPR48) mRNA, complete cds.	AF257182	2.21	0.23
16409	hypothetical protein DKFZp564F013	AA215791	2.20	0.35
11486	Human mRNA for KIAA0705 protein, complete cds.	AB014605	2.19	0.39
5958	myeloid/lymphoid or mixed-lineage leukemia (trithorax (Drosophila) homolog); translocated to, 3	AI110630	2.19	0.59
7055	Human glioma amplified on chromosome 1 protein (GAC1) mRNA, complete cds.	AF030435	2.16	0.65
2878	dystrophin (muscular dystrophy, Duchenne and Becker types), includes DXS142, DXS164, DXS206, DXS230, DXS239, DXS268, DXS269, DXS270, DXS272	AA889832	2.16	0.47
6842	Human mRNA; cDNA DKFZp586B1817 (from clone DKFZp586B1817).	AL050088	2.16	0.31
17663	Human mRNA for neurexin I-alpha protein, complete cds.	AB035356	2.15	0.32
5854	integrin, alpha M (complement component receptor 3, alpha; also known as CD11b (p170), macrophage antigen alpha polypeptide)	NM_000632	2.15	0.21
13316	baculoviral IAP repeat-containing 5 (survivin)	AL571008	2.14	0.47
11625	Human histidine decarboxylase (HDC) mRNA, complete cds.	M60445	2.14	0.36
4114	hydroxy-delta-5-steroid dehydrogenase, 3 beta- and steroid delta-isomerase 1	AL541089	2.13	0.53
4446	KIAA0603 gene product	BI906891	2.13	0.29
7886	Human mRNA for NADP dependent leukotriene b4 12-hydroxydehydrogenase, partial cds.	D49387	2.12	0.48
2687	proteoglycan 1, secretory granule	BG489803	2.10	0.30
14245	Human placenta-specific ATP-binding cassette transporter (ABCP) mRNA, complete cds.	AF103796	2.09	0.43
14051	Human mRNA for KIAA0106 gene, complete cds.	D14662	2.09	0.25
4964	Human Bmx mRNA for cytoplasmic tyrosine kinase.	X83107	2.08	0.16
2768	very low density lipoprotein receptor	BG028841	2.07	0.33
4310	solute carrier family 28 (sodium-coupled nucleoside transporter), member 1	U62966	2.07	0.67
11978	vascular endothelial growth factor	AI887978	2.06	0.27
3487	Human receptor protein-tyrosine kinase (HEK8) mRNA, complete cds.	L36645	2.05	0.58
18152	chimerin (chimaerin) 1	BF940950	2.05	0.50
4013	Notch (Drosophila) homolog 4	D63395	2.04	0.37
13850	fibromodulin	AI249821	2.04	0.40
4311	caspase 4, apoptosis-related cysteine protease	BG572762	2.03	0.78

5645	secretory carrier membrane protein 1	BG613898	2.01	0.40
16498	RYK receptor-like tyrosine kinase	BG740085	2.01	0.23
17268	Human mRNA for Tob, complete cds.	D38305	1.97	0.28
4063	glycine receptor, beta	AF094755	1.97	0.48
13215	Human mRNA for KIAA0669 protein, complete cds.	AB014569	1.97	0.43
6789	Human vascular endothelial growth factor (VEGF) mRNA, 3'UTR.	AF024710	1.96	0.30
3140	Human insulin-stimulated protein kinase 1 (ISPK-1) mRNA, complete cds.	U08316	1.96	0.20
13263	Human E3 ubiquitin ligase Smurf2 mRNA, complete cds.	AY014180	1.95	0.43
2875	KIAA0161 gene product	AW172840	1.95	0.36
4395	cyclin H	BC005280	1.93	0.68
746	Human CAAX box protein TIMAP mRNA, complete cds.	AF362910	1.93	0.28
6008	Homo sapiens cDNA: FLJ21930 fis, clone HEP04301, highly similar to HSU90916 Human clone 23815 mRNA sequence	U90916	1.92	0.36
892	profilin 2	AV724105	1.90	0.33
4265	smg GDS-ASSOCIATED PROTEIN	BG433239	1.90	0.19
5971	Homo sapiens clone DT1P1B6 mRNA, CAG repeat region	BI868318	1.90	0.22
12987	CG11367 gene product	AAF51854	1.88	0.78
4064	interleukin 13 receptor, alpha 1	AL600856	1.88	0.51
1985	Human Trio isoform mRNA, complete cds.	AF091395	1.87	0.37
12219	hypothetical protein PRO1489	AI536671	1.87	0.29
17799	Human fibromodulin mRNA, partial cds.	U05291	1.85	0.37
6781	Human G-protein gamma-10 subunit mRNA, complete cds.	U31383	1.85	0.11
8681	glycogen synthase 1 (muscle)	AL556228	1.85	0.59
8037	Human mRNA; cDNA DKFZp667P184 (from clone DKFZp667P184).	AL512742	1.85	0.31
3496	Human nectin 3 mRNA, complete cds.	AF282874	1.85	0.10
181	Human gene for thrombomodulin precursor, complete cds.	D00210	1.85	0.35
10322	regulator of differentiation (in S. pombe) 1	NM_005156	1.83	0.13
6965	Human mRNA full length insert cDNA clone EUROIMAGE 248114.	AL079279	1.83	0.13
3221	Human, ATPase, Na+/K+ transporting, beta 1 polypeptide, clone MGC:1798 IMAGE:3506311, mRNA, complete cds.	BC000006	1.83	0.56
15234	ATPase, H+ transporting, lysosomal (vacuolar proton pump) 9kD	BG779549	1.83	0.14
46	Human, menage a trois 1 (CAK assembly factor), clone MGC:5154 IMAGE:3453943, mRNA, complete cds.	BC000820	1.83	0.17
4376	fibroblast growth factor receptor 1 (fms-related tyrosine kinase 2, Pfeiffer syndrome)	BI766434	1.82	0.23
12553	Human, pleckstrin 2 (Mouse) homolog, clone MGC:4867 IMAGE:3457876, mRNA, complete cds.	BC001226	1.82	0.71
2843	microsomal glutathione S-transferase 2	W73858	1.82	0.22

15097	cholinergic receptor, nicotinic, delta polypeptide	BF306695	1.82	0.25
8053	Human mRNA for MEMD protein.	Y10183	1.81	0.08
3725	Human elastin (ELN) gene, partial cds.	U62292	1.81	0.51
4304	tumor necrosis factor (ligand) superfamily, member 10	AW022060	1.79	0.18
11260	Human phospholemman chloride channel mRNA, complete cds.	U72245	1.79	0.31
4726	Human, protein phosphatase 5, catalytic subunit, clone MGC:5260 IMAGE:3459309, mRNA, complete cds.	BC001970	1.78	0.45
5663	regulator of G-protein signalling 7	AL566862	1.78	0.36
18061	ATP-binding cassette, sub-family G (WHITE), member 2	BI497116	1.78	0.16
10648	glioma tumor suppressor candidate region gene 1	AA290865	1.77	0.39
2593	ectonucleotide pyrophosphatase/phosphodiesterase 2 (autotaxin)	L35594	1.77	0.19
18033	KIAA0903 protein	AI022927	1.76	0.14
9058	ATPase, H+ transporting, lysosomal (vacuolar proton pump) 42kD	N75606	1.76	0.24
4825	Human mRNA for hFat protein.	X87241	1.75	0.40
4876	Human metaxin 2 (MTX2) mRNA, nuclear gene encoding mitochondrial protein, complete cds.	AF053551	1.75	0.18
11463	Human nicotinic acetylcholine receptor alpha3 subunit precursor, mRNA, complete cds.	U62432	1.75	0.36
18311	exostoses (multiple)-like 2	AK001450	1.75	0.46
8141	Human cDNA FLJ14753 fis, clone NT2RP3003101, weakly similar to Mouse mRNA for tetracycline transporter-like protein.	AK027659	1.74	0.47
15652	Human sperm protein 17 mRNA, complete cds.	AF334735	1.74	0.38
9169	neurogranin (protein kinase C substrate, RC3)	BF948983	1.74	0.05
8605	Human mRNA for vacuolar proton-ATPase subunit M9.2.	Y15286	1.74	0.14
7368	KIAA0256 gene product	BG107450	1.74	0.13
6507	Human c-jun proto oncogene (JUN), complete cds, clone hCJ-1.	J04111	1.74	0.14
5162	Human DZIP3 mRNA, partial cds.	AF279370	1.73	0.22
8951	toll-like receptor 2	NM_003264	1.73	0.16
14316	Human zinc finger protein ZNF191 (ZNF191) gene, complete cds.	AF016052	1.73	0.17
8510	Human 5T4 oncofetal trophoblast glycoprotein gene.	AJ012159	1.73	0.24
15861	Human 14 kDa beta-galactoside-binding lectin (ll4) gene, complete cds.	M57678	1.73	0.29
639	Human, growth factor receptor-bound protein 2, clone MGC:1737 IMAGE:3345524, mRNA, complete cds.	BC000631	1.73	0.29
7504	xeroderma pigmentosum, complementation group A	D14533	1.72	0.26
18483	Human BAC clone RG083M05 from 7q21-7q22	AC000064	1.72	0.11
8983	immunoglobulin superfamily containing leucine-rich repeat	AB003184	1.71	0.19
8900	target of myb1 (chicken) homolog-like 1	AI921588	1.70	0.22

271	Human tie mRNA for putative receptor tyrosine kinase.	X60957	1.70	0.23
7161	myosin X	AU151619	1.70	0.31
6003	spinocerebellar ataxia 2 (olivopontocerebellar ataxia 2, autosomal dominant, ataxin 2)	U70323	1.70	0.31
8806	hypothetical protein A-211C6.1	BG108225	1.70	0.32
15879	Human, Similar to RIKEN cDNA 0610013E23 gene, clone MGC:12169 IMAGE:3930310, mRNA, complete cds.	BC006971	1.69	0.19
15969	Human pancreatic lipase related protein 1 (PLRP1) mRNA, complete cds.	M93283	1.69	0.14
4301	hypothetical protein FLJ11175	AI469703	1.69	0.21
5287	Human ATP synthase beta subunit (ATPSB) gene, complete cds.	M27132	1.68	0.09
8826	troponin I, skeletal, slow	AL596761	1.68	0.25
7967	thymosin beta-10 [Human, metastatic melanoma cell line, mRNA, 453 nt].	S54005	1.68	0.15
5948	old astrocyte specifically induced substance	NM_052854	1.68	0.40
4335	v-rel avian reticuloendotheliosis viral oncogene homolog	X75042	1.68	0.27
14320	Human host cell factor 2 (HCF-2) mRNA, complete cds.	AF117210	1.68	0.13
7386	sarcoglycan, epsilon	AJ000534	1.68	0.35
16177	Human thioredoxin mRNA, complete cds.	AF313911	1.68	0.47
18219	trophoblast glycoprotein	Z29083	1.68	0.16
10343	RNA polymerase II transcriptional regulation mediator (Med6, S. cerevisiae, homolog of)	AL079635	1.67	0.32
3147	Human mRNA for phospholipase C-beta-1b (PLCB1 gene).	AJ278314	1.66	0.21
13759	pregnancy specific beta-1-glycoprotein 4	M20881	1.66	0.19
13178	C33 antigen=type III integral membrane protein [human, T cell line MOLT-4, Peptide, 267 aa]	AAB23825	1.66	0.23
11907	ubiquitin carboxyl-terminal esterase L3 (ubiquitin thiolesterase)	BG939578	1.66	0.29
8915	hypothetical protein FLJ11149	BI752967	1.66	0.18
7902	Human clone 23742 mRNA, partial cds.	AF035287	1.65	0.27
18468	glutamate-cysteine ligase, modifier subunit	L35546	1.65	0.38
6040	ESTs	AI869879	1.65	0.21
1345	serine (or cysteine) proteinase inhibitor, clade I (neuroserpin), member 1	BI915951	1.64	0.16
4141	erythropoietin receptor	S45332	1.64	0.31
2834	Human SH3 domain-containing protein SH3P18 mRNA, complete cds	BE708457	1.63	0.25
10007	Human cDNA FLJ14690 fis, clone NT2RP2005270.	AK027596	1.63	0.57
16640	hypoxia-inducible factor 1, alpha subunit (basic helix-loop-helix transcription factor)	AU154668	1.62	0.37
7286	ATP-binding cassette, sub-family G (WHITE), member 2	AU118354	1.62	0.29
10416	KIAA0573 protein	AB011145	1.62	0.36
14948	hypothetical protein MGC4701	AF040964	1.62	0.36
4815	Human, Similar to protein phosphatase 2 (formerly 2A), catalytic subunit, beta isoform, clone MGC:21354 IMAGE:4454972, mRNA, complete cds.	BC012022	1.62	0.25

17592	Human activin beta-A subunit (exon 2).	X57579	1.62	0.32
8607	KIAA0759 protein	AA527389	1.61	0.18
15146	ribosomal protein S29	AA827393	1.61	0.24
7590	ESTs, Weakly similar to I38022 hypothetical protein [H.sapiens]	BG718906	1.61	0.12
11927	KIAA1441 protein	BI859994	1.61	0.40
12035	EphA5	L36644	1.61	0.47
17539	Human partial mRNA for putative nuclear factor.	AJ276691	1.61	0.22
5896	protein kinase C, mu	X75756	1.61	0.28
5517	homeo box B6	NM_018952	1.60	0.25
14618	Human, Similar to advillin, clone MGC:1461 IMAGE:2961396, mRNA, complete cds.	BC004134	1.60	0.15
4504	RAB5A, member RAS oncogene family	BC001267	1.60	0.12
15855	Human fibroblast growth factor receptor (FGFr) transmembrane form mRNA, complete cds.	M34185	1.60	0.23
14090	Human gcp60 mRNA for golgi resident protein GCP60, complete cds.	AB043587	1.60	0.16
7843	Human fetal brain adenylyl cyclase mRNA, 3' end.	L05500	1.60	0.26
13615	cytochrome c oxidase subunit Va	BE538296	1.60	0.23
1357	KIAA0355 gene product	AB002353	1.60	0.08
10341	eyes absent (Drosophila) homolog 2	U69178	1.60	0.60
6631	Human mRNA for KIAA0636 protein, complete cds.	AB014536	1.59	0.36
2908	predicted osteoblast protein	AI491952	1.59	0.19
12702	Macaque brain cDNA clone:QmoA-10711, full insert sequence.	AB062987	1.59	0.10
5973	receptor-interacting serine-threonine kinase 2	BG170405	1.59	0.34
16815	A kinase (PRKA) anchor protein (yotiao) 9	NM_005751	1.59	0.20
6975	Human nidogen mRNA, complete cds.	M30269	1.59	0.28
7499	ESTs	AA233775	1.59	0.41
10232	collagen, type V, alpha 2	AU117484	1.58	0.19
1800	Human cDNA FLJ14494 fis, clone MAMMA1003035, weakly similar to RIBOSOMAL LARGE SUBUNIT PSEUDOURIDINE SYNTHASE C (EC 4.2.1.70).	AK027400	1.58	0.30
2212	Human cDNA FLJ10783 fis, clone NT2RP4000417, weakly similar to MANNOSYL-OLIGOSACCHARIDE ALPHA-1,2-MANNOSIDASE (EC 3.2.1.113).	AK001645	1.58	0.22
16970	calumenin	AW614911	1.58	0.11
9412	Human mRNA for UDP-N-acetylglucosamine transporter, complete cds.	AB021981	1.58	0.27
2829	quinone oxidoreductase homolog	BF058741	1.57	0.29
13188	Human mRNA; cDNA DKFZp434H0413 (from clone DKFZp434H0413); partial cds.	AL137261	1.57	0.24
4316	UDP-N-acteylglucosamine pyrophosphorylase 1	AL520091	1.56	0.37
710	Human, Similar to plastin 3 (T isoform), clone IMAGE:3447893, mRNA, partial cds.	BC008588	1.56	0.13
11752	hypothetical protein A-211C6.1	AL537232	1.56	0.25
11473	Human MARK (MARK) mRNA, complete cds.	AF154845	1.55	0.36

5994	frizzled (Drosophila) homolog 6	BG180759	1.55	0.29
262	Human MAGUK protein VAM-1 mRNA, complete cds.	AF162130	1.55	0.21
1784	Human calumein (Calu) mRNA, complete cds.	AF013759	1.55	0.14
11969	pleckstrin homology, Sec7 and coiled/coil domains 1(cytohesin 1)	NM_017456	1.55	0.21
1349	ESTs	AA973023	1.55	0.17
11620	Human mRNA for Ste24p, complete cds.	AB016068	1.55	0.24
8407	Human (clone Q-2OD3) interferon receptor (IFNAR2) gene, exon 1.	L42237	1.54	0.21
5660	erythrocyte membrane protein band 4.1-like 1	AB002336	1.54	0.08
4094	adaptor-related protein complex 3, sigma 1 subunit	BF032683	1.54	0.08
9438	Human orphan hormone nuclear receptor RORalpha1 mRNA, complete cds.	U04897	1.54	0.19
1110	membrane-spanning 4-domains, subfamily A, member 2 (Fc fragment of IgE, high affinity I, receptor for; beta polypeptide)	NM_000139	1.54	0.19
8374	Human, reticulocalbin 2, EF-hand calcium binding domain, clone MGC:1650 IMAGE:3505241, mRNA, complete cds.	BC004892	1.53	0.19
4412	Homo sapiens cDNA: FLJ22044 fis, clone HEP09141	AW058438	1.53	0.25
2099	Human hox11 proto-oncogene, exons 1 to 3 and hug-1 gene.	AJ009794	1.53	0.21
7453	nuclear transcription factor, X-box binding 1	BG327231	1.53	0.23
13456	aryl hydrocarbon receptor	AA844153	1.53	0.12
7284	reticulocalbin 2, EF-hand calcium binding domain	BG390232	1.53	0.22
13197	Human myocyte-specific enhancer factor 2A (MEF2A) gene, last coding exon, and complete cds.	U49020	1.52	0.29
16983	Janus kinase 1 (a protein tyrosine kinase)	AA131737	1.52	0.20
16398	Human mRNA for cytokine inducible nuclear protein.	X83703	1.52	0.24
4429	myotubular myopathy 1	U46024	1.52	0.21
11097	Human mRNA; cDNA DKFZp586D0724 (from clone DKFZp586D0724).	AL110150	1.52	0.15
963	growth hormone receptor	X06562	1.51	0.23
6007	capping protein (actin filament) muscle Z-line, alpha 2	BC005338	1.50	0.05
797	G protein-coupled receptor 56	BF593277	1.50	0.28
12838	Human, ATP synthase, H+ transporting, mitochondrial F0 complex, subunit F6, clone MGC:2243 IMAGE:3357779, mRNA, complete cds.	BC001178	1.50	0.13
6295	Human, clone MGC:14796 IMAGE:4050837, mRNA, complete cds.	BC005993	1.50	0.27
11431	Human cDNA: FLJ21270 fis, clone COL01749.	AK024923	1.49	0.39
8839	CLIP-associating protein 1	AB014522	1.49	0.22
18323	kinesin 2 (60-70kD)	AW963252	1.49	0.18
12064	kinectin 1 (kinesin receptor)	Z22551	1.49	0.21
2519	KIAA0284 protein	AK025023	1.49	0.27
2457	MAGUK protein p55T; Protein Associated with Lins 2	NM_016447	1.49	0.21

18142	paired mesoderm homeo box 1	NM_022716	1.49	0.23
4691	Human ERGIC-53 mRNA.	X71661	1.49	0.26
12803	Human transcription factor HOXA13 (HOXA13) gene, complete cds.	U82827	1.49	0.22
15028	selectin L (lymphocyte adhesion molecule 1)	X17519	1.48	0.23
3415	Human Rho-associated, coiled-coil containing protein kinase p160ROCK mRNA, complete cds.	U43195	1.48	0.19
14709	Human serine-threonine protein kinase NKIAMRE (NKIAMRE) mRNA, complete cds.	AF130372	1.48	0.22
7600	FSHD region gene 1	T41211	1.48	0.31
17497	Human cDNA FLJ13053 fis, clone NT2RP3001459.	AK023115	1.48	0.21
1368	membrane-bound transcription factor protease, site 1	AL133583	1.48	0.18
11565	Human 10kD protein (BC10) mRNA, complete cds.	AF053470	1.48	0.16
1684	Human cDNA FLJ14393 fis, clone HEMBA1003222.	AK027299	1.47	0.37
1365	hypothetical protein DKFZp547M136 similar to widely-interspaced zinc finger motifs	BF062131	1.47	0.25
16591	chromodomain helicase DNA binding protein 1	AF006513	1.47	0.31
6355	Human displacement protein (CCAAT) mRNA.	M74099	1.47	0.12
1337	ceruloplasmin (ferroxidase)	M13699	1.47	0.20
13582	argininosuccinate synthetase	BF305206	1.47	0.10
4230	NCK adaptor protein 1	AI591085	1.47	0.24
7373	solute carrier family 16 (monocarboxylic acid transporters), member 1	AI565092	1.46	0.30
10618	KIAA0652 gene product	AI915504	1.46	0.38
13754	inhibitor of DNA binding 2, dominant negative helix-loop-helix protein	AI299309	1.46	0.15
2910	Down syndrome critical region gene 1	BG287042	1.46	0.26
3779	Human casein kinase I gamma 3L (CSNK1G3L) mRNA, complete cds.	AF049090	1.46	0.19
11313	Human cDNA FLJ11028 fis, clone PLACE1004128, highly similar to GUANINE NUCLEOTIDE-BINDING PROTEIN BETA SUBUNIT 4.	AK001890	1.46	0.30
5947	CDC14 (cell division cycle 14, S. cerevisiae) homolog A	AF000367	1.46	0.11
56	Human hypoxanthine phosphoribosyltransferase (HPRT) mRNA, complete cds.	M31642	1.46	0.10
15324	inositol 1,4,5-triphosphate receptor, type 2	D26350	1.46	0.28
14447	Human cDNA: FLJ22970 fis, clone KAT10766, highly similar to HUMCOXNE Human nuclear-encoded mitochondrial cytochrome c oxidase Va subunit mRNA.	AK026623	1.46	0.19
1340	KIAA0594 protein	AB011166	1.46	0.22
6252	Human mRNA for connective tissue growth factor.	X78947	1.45	0.26
3313	Human homeobox B7 (HOXB7) gene, partial cds; and homeobox B6 (HOXB6), homeobox B5 (HOXB5), homeobox B4 (HOXB4), and homeobox B3 (HOXB3) genes, complete cds.	AF287967	1.45	0.15

10335	dual specificity phosphatase 11 (RNA/RNP complex 1-interacting)	AI478561	1.45	0.30
5853	zinc finger protein 187	BC013951	1.45	0.16
541	Human ELP-1 mRNA sequence.	M88458	1.45	0.21
12772	Human cDNA: FLJ22135 fis, clone HEP20858.	AK025788	1.44	0.17
17945	sushi-repeat protein	NM_014467	1.44	0.28
16881	core-binding factor, runt domain, alpha subunit 2; translocated to, 1; cyclin D-related	D43638	1.44	0.27
2293	Human h-Sp1 mRNA.	X68194	1.44	0.12
5720	procollagen-proline, 2-oxoglutarate 4-dioxygenase (proline 4-hydroxylase), alpha polypeptide I	AL574109	1.44	0.14
3789	Human genomic DNA, chromosome 8q23, clone:KB1171G1.	AP000427	1.44	0.21
5682	retinoblastoma 1 (including osteosarcoma)	BI092056	1.44	0.10
8129	Human phosphoinositide-specific phospholipase C PLC-epsilon mRNA, complete cds.	AF190642	1.44	0.28
5182	Human beta 3-endonexin mRNA, long form and short form, complete cds.	U37139	1.43	0.19
5689	adaptor-related protein complex 3, beta 1 subunit	U81504	1.43	0.18
18435	acyl-Coenzyme A oxidase 2, branched chain	BG545036	1.43	0.04
6910	Human FUSE binding protein 3 (FBP3) mRNA, partial cds.	U69127	1.43	0.17
16918	cathepsin K (pycnodysostosis)	AL544409	1.43	0.24
731	Human mRNA for KIAA1665 protein, partial cds.	AB051452	1.43	0.19
8168	Human mRNA for KIAA0769 protein, complete cds.	AB018312	1.43	0.13
8074	Human, Similar to glucosamine-phosphate N-acetyltransferase, clone MGC:20441 IMAGE:4661046, mRNA, complete cds.	BC012179	1.43	0.22
16894	B-factor, properdin	AF349679	1.43	0.26
12176	tousled-like kinase 1	AA701891	1.43	0.21
14068	Human mRNA for KIAA1249 protein, partial cds.	AB033075	1.43	0.17
6892	Human, Similar to CG9602 gene product, clone MGC:3733 IMAGE:3619626, mRNA, complete cds.	BC002775	1.42	0.13
13128	Human, argininosuccinate synthetase, clone MGC:3634 IMAGE:3010137, mRNA, complete cds.	BC009243	1.42	0.10
4407	tRNA isopentenylpyrophosphate transferase	BE156258	1.42	0.21
15323	Rho-associated, coiled-coil containing protein kinase 1	U43195	1.42	0.20
13177	Human cDNA FLJ14929 fis, clone PLACE1009130, weakly similar to UBIQUITIN-PROTEIN LIGASE E3A (EC 6.3.2.-).	AK027835	1.42	0.11
2774	sialyltransferase 4C (beta-galactosidase alpha-2,3-sialytransferase)	AA453813	1.42	0.28
12190	hypothetical protein FLJ20366	AW976023	1.42	0.20
12091	fms-related tyrosine kinase 1 (vascular endothelial growth factor/vascular permeability factor receptor)	X51602	1.42	0.36

16951	nuclear receptor subfamily 1, group H, member 3	BF570118	1.42	0.11
6500	Human, general transcription factor IIA, 2 (12kD subunit), clone MGC:3613 IMAGE:2819215, mRNA, complete cds.	BC001919	1.42	0.16
12244	general transcription factor IIH, polypeptide 2 (44kD subunit)	AF078847	1.41	0.17
13761	calmegin	D86322	1.41	0.15
9863	Human, ATPase, H+ transporting, lysosomal (vacuolar proton pump), member J, clone MGC:1970 IMAGE:3546257, mRNA, complete cds.	BC003564	1.41	0.21
10384	SPARC-like 1 (mast9, hevin)	X82157	1.41	0.23
7128	LIM and SH3 protein 1	AU159460	1.41	0.12
6471	Human casein kinase I gamma 3L (CSNK1G3L) mRNA, complete cds.	AF049090	1.41	0.38
13187	Human protein phosphatase type-1 catalytic subunit delta isoform (PPCS1D) mRNA, complete cds.	AF092905	1.41	0.12
1350	U2 small nuclear ribonucleoprotein auxiliary factor (65kD)	BI962886	1.41	0.18
3568	unnamed protein product	CAC38896	1.41	0.15
10397	calcium/calmodulin-dependent protein kinase kinase 2, beta	AI925424	1.41	0.25
3373	Human, hypothetical protein, clone MGC:3375 IMAGE:3609357, mRNA, complete cds.	BC002677	1.41	0.17
16809	myosin, light polypeptide kinase	AW951177	1.41	0.23
11284	Human (clones HGPCD2 and HGPCD15) pterin-4a-carbinolamine dehydratase (PCBD) gene, complete cds.	L41560	1.41	0.17
9938	Human pephBGT-1 betaine-GABA transporter mRNA, complete cds.	U27699	1.40	0.26
3917	Homo sapiens cDNA: FLJ23197 fis, clone REC00917	AI079280	1.40	0.13
12842	Human sushi-repeat protein (SRPUL) mRNA, complete cds.	AF060567	1.40	0.25
9415	Human mRNA for KIAA0048 gene, complete cds.	D28588	1.39	0.16
16461	Human lysyl oxidase-like 3 protein (LOXL3) mRNA, complete cds.	AF311313	1.39	0.25
18022	Human mRNA for AP-2 beta transcription factor.	X95694	1.39	0.35
11878	KIAA0155 gene product	D63875	1.38	0.16
9851	Human genes TAP1, TAP2, LMP2, LMP7 and DOB.	X66401	1.38	0.14
9737	Human ubiquitous alpha-2,3-sialyltransferase VI mRNA, complete cds.	AF119391	1.38	0.16
14755	Human mRNA; cDNA DKFZp434B105 (from clone DKFZp434B105); partial cds.	AL117626	1.38	0.21
663	Human excision repair protein ERCC6 mRNA, complete cds.	L04791	1.38	0.24
14979	KIAA0781 protein	BF984909	1.38	0.26
2459	cyclin-dependent kinase 5, regulatory subunit 1 (p35)	BE797921	1.38	0.11
10665	chromosome 2 open reading frame 6	AL122062	1.38	0.20
13455	KIAA0645 gene product	BE646437	1.38	0.18

5485	Human BRCA1, Rho7 and vatI genes, complete cds, and ipf35 gene, partial cds.	L78833	1.38	0.22
7341	MADS box transcription enhancer factor 2, polypeptide A (myocyte enhancer factor 2A)	AI952550	1.37	0.21
8926	FK506-binding protein 1B (12.6 kD)	BC002614	1.37	0.25
15843	Human nuclear orphan receptor LXR-alpha mRNA, complete cds.	U22662	1.37	0.03
5501	Sob protein	AAC47282	1.37	0.18
12498	Human mRNA for KIAA0338 gene, partial cds.	AB002336	1.37	0.10
2560	branched chain keto acid dehydrogenase E1, beta polypeptide (maple syrup urine disease)	M55575	1.37	0.22
7057	ISL1 transcription factor, LIM/homeodomain, (islet-1)	U07559	1.37	0.11
9549	Human retinoic acid receptor gamma 1 mRNA, complete cds.	M38258	1.37	0.21
7530	EphA2	AI568135	1.37	0.18
5496	Human normal mucosa of esophagus specific 1 (NMES1) mRNA, complete cds.	AF228422	1.37	0.18
9158	M-phase phosphoprotein 9	AA843678	1.37	0.14
16334	Human mRNA for KIAA0696 protein, partial cds.	AB014596	1.37	0.19
7215	interferon-stimulated transcription factor 3, gamma (48kD)	AA404652	1.36	0.19
3821	Human tubulin-folding cofactor C mRNA, complete cds.	U61234	1.36	0.21
2366	myosin ID	BE502669	1.36	0.19
5644	phosphoribosylformylglycinamidine synthase (FGAR amidotransferase)	AB002359	1.35	0.26
2551	phosphorylase kinase, beta	AL079451	1.35	0.19
1937	Human mRNA for semaphorin sem2, complete cds.	AB029496	1.35	0.11
11111	Human LDLC mRNA.	Z34975	1.35	0.20
7298	ESTs, Moderately similar to KIAA0696 protein [H.sapiens]	AA436684	1.35	0.18
5998	gene with multiple splice variants near HD locus on 4p16.3	AB000460	1.35	0.13
15846	Human cDNA FLJ20731 fis, clone HEP10272.	AK000738	1.35	0.13
7243	FK506-binding protein 1A (12kD)	BF971255	1.35	0.11
16700	archain 1	AI700509	1.35	0.09
4944	Human cDNA FLJ11756 fis, clone HEMBA1005595, weakly similar to DYNEIN HEAVY CHAIN, CYTOSOLIC.	AK021818	1.35	0.14
16879	replication factor C (activator 1) 4 (37kD)	BF062845	1.35	0.19
12043	KIAA0107 gene product	NM_014814	1.34	0.14
15796	Human cathepsin O (CTSO) mRNA, complete cds.	U13665	1.34	0.18
17186	Human homeobox 1.4 protein mRNA, complete cds.	M74297	1.34	0.18
9069	serine (or cysteine) proteinase inhibitor, clade F (alpha-2 antiplasmin, pigment epithelium derived factor), member 1	AL541945	1.34	0.21
16748	hippocalcin-like 1	AI566904	1.34	0.12
10073	Human mRNA for MEGF9, partial cds.	AB011542	1.34	0.19
10651	ATP-binding cassette, sub-family A (ABC1), member 1	R01051	1.34	0.15

5831	adenomatosis polyposis coli	AA621432	1.34	0.12
8848	low density lipoprotein receptor defect C complementing	AW299301	1.34	0.25
3501	Human cDNA FLJ10976 fis, clone PLACE1001399.	AK001838	1.34	0.12
5489	hepatocellular carcinoma-associated antigen 58	AI992137	1.34	0.13
3760	Human mRNA for KIAA0271 gene, complete cds.	D87461	1.33	0.11
232	Human mRNA for KIAA0259 gene, partial cds.	D87448	1.33	0.12
8474	Human mRNA; cDNA DKFZp564L023 (from clone DKFZp564L023); complete cds.	AL136643	1.33	0.09
3798	Human hairy (HRY) mRNA, complete cds.	AF264785	1.33	0.13
497	Human, tyrosine 3-monooxygenase/tryptophan 5-monooxygenase activation protein, epsilon polypeptide, clone MGC:1250 IMAGE:3139004, mRNA, complete cds.	BC001440	1.33	0.11
16556	phosphotriesterase related	BG170397	1.33	0.15
17950	ubiquitin-conjugating enzyme E2E 1 (homologous to yeast UBC4/5)	BI523924	1.33	0.14
6473	Human mRNA for KIAA0483 protein, partial cds.	AB007952	1.33	0.10
14674	Human cellular co-factor (RAB) gene, complete cds.	L42025	1.32	0.19
11583	Human Rab-related GTP-binding protein mRNA, complete cds.	AF235022	1.32	0.15
13620	calcium channel, voltage-dependent, alpha 2/delta subunit 1	AC006145	1.32	0.22
3672	Human type IV collagen alpha 5 chain (COL4A5) gene, exon 51 and complete cds, alternatively spliced.	U04520	1.32	0.16
952	solute carrier family 25 (mitochondrial carrier; Graves disease autoantigen), member 16	AL574883	1.32	0.09
12246	malic enzyme 1, NADP(+)-dependent, cytosolic	BG211824	1.32	0.08
1892	Human nucleolysin TIAR mRNA, complete cds.	M96954	1.32	0.11
14398	Human CGI-142 protein mRNA, complete cds.	AF151900	1.32	0.13
8788	JM4 protein	BI818455	1.32	0.20
5350	Human RCC1-like G exchanging factor RLG mRNA, complete cds.	AF060219	1.31	0.13
14297	Human mRNA for putative transcription factor-like nuclear regulator (TFNR gene).	AJ238520	1.31	0.10
7583	BN51 (BHK21) temperature sensitivity complementing	M17754	1.31	0.18
7519	RAN binding protein 2-like 1	AI859613	1.31	0.17
6433	Human subunit of coatomer complex.	X70476	1.31	0.08
17277	Human mRNA for phosphatidylinositol transfer protein (PI-TPbeta), complete cds.	D30037	1.31	0.17
14280	Human, voltage-dependent anion channel 3, clone MGC:1966 IMAGE:3343379, mRNA, complete cds.	BC002456	1.31	0.12
11561	Human tumor-related protein (PDRC2) mRNA, complete cds.	AF081497	1.31	0.22
12260	interleukin 15 receptor, alpha	U31628	1.31	0.18

7408	RAS protein activator like 2	NM_004841	1.31	0.10
1286	R3H domain (binds single-stranded nucleic acids) containing	AW973355	1.31	0.15
17335	Human mRNA for phospholipase C-beta-1a (PLCB1 gene).	AJ278313	1.31	0.17
4292	glutathione synthetase	AL573289	1.31	0.17
14094	Human S1R protein (S1R) mRNA, complete cds.	AF113127	1.31	0.17
13747	TATA box binding protein (TBP)-associated factor, RNA polymerase II, J, 20kD	AI681931	1.30	0.16
7275	ESTs, Highly similar to Unknown gene product [H.sapiens]	N51995	1.30	0.12
13517	synaptosomal-associated protein, 91 kDa (mouse) homolog	N62961	1.30	0.09
179	Human mRNA; cDNA DKFZp434F0272 (from clone DKFZp434F0272).	AL137330	1.30	0.15
5651	RAD51 (S. cerevisiae) homolog C	BC000667	1.30	0.08
12720	Human HSKM-B (HSKM-B) mRNA, complete cds.	AF226053	1.30	0.20
16278	Human mRNA for five-lipoxygenase activating protein (FLAP).	X52195	1.30	0.11
5225	Human asialoglycoprotein receptor H1 mRNA, complete cds.	M10058	1.29	0.20
3455	Human cDNA FLJ12082 fis, clone HEMBB1002492.	AK022144	1.29	0.12
7024	actin filament associated protein	D25248	1.29	0.09
7434	prolactin	BG393056	1.29	0.20
7344	formin-like	BG235961	1.29	0.11
15953	Human, clone IMAGE:3957484, mRNA.	BC006415	1.28	0.13
5282	Human mRNA for growth hormone receptor.	X06562	1.28	0.18
7510	stromal interaction molecule 1	U52426	1.28	0.07
12211	epithelial membrane protein 1	AW265568	1.28	0.17
12187	putative nucleic acid binding protein RY-1	AI358942	1.28	0.14
10647	DKFZP434P1750 protein	AI634733	1.28	0.13
9594	Human mRNA for proteasome subunit HsC10-II, complete cds.	D26598	1.28	0.14
11920	ret finger protein 2	AF241850	1.28	0.12
11746	Protein P3	NM_019848	1.28	0.20
16326	Human mRNA; cDNA DKFZp586C1622 (from clone DKFZp586C1622); partial cds.	AL050164	1.28	0.13
5552	ESTs, Moderately similar to JG0186 vesicle-associated membrane protein-associated protein B [H.sapiens]	N38854	1.28	0.14
1259	Homo sapiens cDNA FLJ11904 fis, clone HEMBB1000048	AI908481	1.28	0.16
1796	Human cDNA FLJ10679 fis, clone NT2RP2006565, moderately similar to Sus scrofa mRNA for SCAMP1 protein.	AK001541	1.28	0.11
7369	Thy-1 cell surface antigen	N94350	1.28	0.17
7247	chromosome 1 open reading frame 9	BE466870	1.27	0.14
12221	pancreatitis-associated protein	NM_002580	1.27	0.19
12110	GRO3 oncogene	X53800	1.27	0.15
8075	Human mRNA for TBX18 protein, partial.	AJ010278	1.27	0.14
13643	activated leucocyte cell adhesion molecule	AI050952	1.27	0.12

4100	phosphoserine phosphatase	Y10275	1.27	0.09
2622	succinate dehydrogenase complex, subunit D, integral membrane protein	AB006202	1.27	0.10
9064	acylphosphatase 1, erythrocyte (common) type	AW958424	1.27	0.14
12915	Human neurocan (CSPG3) mRNA, complete cds.	AF026547	1.26	0.19
5822	potassium large conductance calcium-activated channel, subfamily M, alpha member 1	BI084703	1.26	0.14
11434	Human HOX3D gene for homeoprotein HOX3D.	X61755	1.26	0.18
11892	B melanoma antigen	NM_001187	1.26	0.11
12984	Human putative protein kinase NY-REN-64 antigen mRNA, complete cds.	AF155118	1.26	0.07
5899	ATPase, Ca++ transporting, cardiac muscle, slow twitch 2	AI620652	1.26	0.11
14441	Human clone cDSC1 Down syndrome cell adhesion molecule (DSCAM) mRNA, complete cds.	AF217525	1.26	0.14
6529	Human mRNA for ATP synthase subunit e, complete cds.	D50371	1.26	0.14
2428	KIAA0831 protein	AW662896	1.26	0.10
13458	phosphomannomutase 2	AI927764	1.25	0.17
10103	Human G-protein-coupled receptor APJ gene, complete cds.	U03642	1.25	0.10
11890	KIAA0076 gene product	AI741847	1.24	0.13
2906	TRAF family member-associated NFKB activator	BF439429	1.24	0.12
535	Human chromosome 21 segment HS21C003.	AL163203	1.24	0.09
7213	gamma-aminobutyric acid (GABA) A receptor, alpha 6	BG211331	1.24	0.12
696	Human cDNA FLJ13093 fis, clone NT2RP3002151, highly similar to G1 TO S PHASE TRANSITION PROTEIN 1 HOMOLOG.	AK023155	1.24	0.09
12834	Human mRNA for DNA polymerase beta, complete cds.	D29013	1.24	0.15
5963	corticotropin releasing hormone	AW513199	1.24	0.06
16923	protein kinase C, iota	AA969093	1.24	0.09
3193	Human, clone IMAGE:3355813, mRNA, partial cds.	BC000282	1.24	0.13
6469	Human, clone MGC:16924 IMAGE:3855040, mRNA, complete cds.	BC010627	1.23	0.14
9879	Human calnexin mRNA, complete cds.	M94859	1.23	0.09
3603	Human Bruton's tyrosine kinase (BTK), alpha-D-galactosidase A (GLA), L44-like ribosomal protein (L44L) and FTP3 (FTP3) genes, complete cds.	U78027	1.23	0.10
5632	D-dopachrome tautomerase	BG478996	1.23	0.11
6571	Human mRNA for Nop10p, complete cds.	AB043104	1.23	0.10
11910	replication factor C (activator 1) 1 (145kD)	AW840383	1.23	0.11
5412	Human cDNA FLJ11191 fis, clone PLACE1007598, weakly similar to ZINC FINGER PROTEIN 184.	AK002053	1.23	0.14
2739	coronin, actin-binding protein, 2A	BC000010	1.22	0.11

4071	interferon consensus sequence binding protein 1	AW964220	1.22	0.14
979	cytoplasmic FMRP interacting protein 1	AA430381	1.22	0.08
3551	Human mRNA for steroid receptor coactivator 1a.	AJ000881	1.22	0.11
8500	Human endonexin II mRNA, complete cds.	J03745	1.21	0.08
14876	Homo sapiens clone 24400 mRNA sequence	AF052145	1.21	0.09
5508	Human cDNA: FLJ22269 fis, clone HRC03179.	AK025922	1.21	0.05
14685	Human mRNA for KIAA0959 protein, partial cds.	AB023176	1.21	0.12
13222	Human mRNA for epsilon isoform of 61kDa regulatory subunit of PP2A.	Z69029	1.21	0.13
15871	Human cDNA FLJ12469 fis, clone NT2RM1000874, highly similar to Human death effector domain-containing testicular molecule mRNA.	AK022531	1.20	0.10
10344	ESTs, Highly similar to I58410 Erg-3 [H.sapiens]	BI712083	1.20	0.06
5882	amiloride-sensitive cation channel 2, neuronal	NM_020039	1.20	0.10
2503	sema domain, immunoglobulin domain (Ig), short basic domain, secreted, (semaphorin) 3C	BG938585	1.19	0.14
8621	Human, melanoma inhibitory activity, clone MGC:14503 IMAGE:4333499, mRNA, complete cds.	BC005910	1.18	0.06
13435	adenosine deaminase	BG257096	1.18	0.14
4239	ESTs, Weakly similar to CA18 MOUSE COLLAGEN ALPHA 1(VIII) CHAIN PRECURSOR [M.musculus]	AW275800	1.18	0.10
3400	Human, transforming growth factor beta-stimulated protein TSC-22, clone MGC:8464 IMAGE:2821602, mRNA, complete cds.	BC000456	1.17	0.09
5719	ets variant gene 6 (TEL oncogene)	BE217961	1.17	0.07
1587	Human cDNA FLJ11830 fis, clone HEMBA1006559, moderately similar to Mouse (Mus musculus) PRAJA1 (Praja1) mRNA.	AK021892	1.17	0.07
12686	Human mRNA for frizzled-7, complete cds.	AB017365	1.17	0.06
3489	Human two-pore potassium channel TPKC1 mRNA, complete cds.	AF004711	1.17	0.09
8191	Human cyclophilin-related processed pseudogene.	X52855	1.16	0.05
2104	Human mRNA for ryudocan core protein.	D13292	1.16	0.09
5500	glutathione S-transferase M3 (brain)	AA623012	1.16	0.06
5108	Human AF5q31 protein (AF5q31) mRNA, complete cds.	AF197927	1.16	0.05
3644	Human complete genomic sequence between D16S3070 and D16S3275, containing Familial Mediterranean Fever gene disease.	AJ003147	1.16	0.05
13644	intersectin 1 (SH3 domain protein)	AA582575	1.15	0.09
17842	Human cDNA FLJ11160 fis, clone PLACE1007014, weakly similar to 36 KD NUCLEOLAR PROTEIN HNP36.	AK002022	1.15	0.09
5979	EST	AI025099	1.15	0.07
3800	pN44=prostate secretory protein [Human, prostate tissue, mRNA, 475 nt].	S67815	1.15	0.08

16562	laminin, gamma 2 (nicein (100kD), kalinin (105kD), BM600 (100kD), Herlitz junctional epidermolysis bullosa))	AA677534	1.14	0.08
18161	KIAA0690 protein	BF843103	1.14	0.10
16941	bone morphogenetic protein 6	AA426586	1.13	0.10

VITA

Jonathan was born October 20, 1976 in Danvers, Massachusetts, the son of Dana Gordon Butcher and Deborah Marie Hinckley. He grew up not too far away in Ipswich MA, known for its old house, fantastic beach, and excellent seafood. Jonathan attended public schools all his life, and entertained a career in the Navy before opting to go to the University of Virginia to study mechanical engineering. He graduated in 2000 with a Bachelor's and Masters degree in mechanical engineering, and his research there was focused on developing a footwell intrusion simulation system for automobile crash sled testing. Georgia Tech provided a completely new area of research for him in where he could contribute to saving people's lives from debilitating diseases through living technologies. While at Virginia, Jonathan met his future wife Christine Meaney, and they were married in July 2001. Jonathan and Christine have a black Labrador retriever named Lucy. The next chapter in their life will be in Charleston, SC, where Jonathan has a postdoctoral position in cardiovascular developmental biology with Dr. Roger Markwald.